Geochemistry and Chemistry of Oil Shales

Geochemistry and Chemistry of Oil Shales

Francis P. Miknis, EDITOR
U.S. Department of Energy

John F. McKay, EDITOR
U.S. Department of Energy

Based on a symposium sponsored
by the ACS Divisions
of Geochemistry, Fuel Chemistry,
and Petroleum Chemistry
at the 185th Meeting
of the American Chemical Society,
Seattle, Washington,
March 20–25, 1983

ACS SYMPOSIUM SERIES **230**

ACS Symposium Series

M. Joan Comstock, *Series Editor*

FOREWORD

The ACS SYMPOSIUM SERIES was founded in 1974 to provide a medium for publishing symposia quickly in book form. The format of the Series parallels that of the continuing ADVANCES IN CHEMISTRY SERIES except that in order to save time the papers are not typeset but are reproduced as they are submitted by the authors in camera-ready form. Papers are reviewed under the supervision of the Editors with the assistance of the Series Advisory Board and are selected to maintain the integrity of the symposia; however, verbatim reproductions of previously published papers are not accepted. Both reviews and reports of research are acceptable since symposia may embrace both types of presentation.

PREFACE

THE DEVELOPMENT OF A SHALE OIL INDUSTRY has been limited by the commercial reality that petroleum can be produced less expensively than shale oil. Until that time when petroleum becomes unavailable or too expensive, there will be little or no profit in producing synthetic fuels, and therefore a synthetic fuel industry will not be developed. In addition to being tied to the price of petroleum, shale oil has a second problem, a scientific problem. Oil shales are complex mixtures of organic and inorganic components that require a special technology to recover, upgrade, and refine to usable organic and inorganic products. The tasks of chemists and engineers are to minimize the cost of each of these steps. Through an understanding of the geochemistry and chemistry of the resource and the recovery, upgrading, and refining processes, it may be possible to produce shale oil less expensively. Only then can we begin to tap the earth for this enormous energy resource.

Oil shales occur worldwide and span the spectrum of geologic time. *Oil shale* is a misnomer, used mainly in the economic rather than the geologic sense. There is very little oil in oil shale and often the rock is not a true shale (e.g., the Green River Formation "oil shales"). However, upon heating, the *kerogen* (insoluble organic matter) in the rock produces liquid products that can be upgraded and refined to useful products. Whether an oil shale deposit represents a viable potential source of synthetic liquid fuel depends both on the quantity of organic matter in the sediment and on the quality or nature of its chemical composition. The chemical composition largely determines the fate of the organic matter during heating. Because oil shales are diverse in their compositions, lithologies, and genesis, it can be expected that their behavior on heating will also be different. It was with this in mind that the symposium on geochemistry and chemistry of oil shales was held.

In this symposium we have attempted to bring together a large number of scientists from around the world to learn about the geochemistry of shales in various countries and how they are similar and how they differ. In addition, the symposium included discussions by leading shale oil chemists concerning their work to define the chemical nature of shales, to define the chemistry involved in shale oil production, and to develop new or improved recovery processes. Papers on the inorganic chemistry of oil shale were solicited for the symposium because we recognized that the inorganic chemistry of oil shale is important to the total chemistry of oil shale recovery processes.

Many of the papers presented at this symposium have been revised and updated for inclusion in the present volume and we thank all the contributors for their cooperation and efforts. We are grateful to the ACS Divisions of Fuel, Geochemistry, and Petroleum for their support. Acknowledgment is made to the Donors of the Petroleum Research Fund, administered by the American Chemical Society for partial support of this symposium.

On a sad note, Dr. Irving A. Breger, one of the founders of the Geochemistry Division of the ACS, died on October 13, 1982. The symposium in Seattle was held in his memory.

FRANCIS P. MIKNIS
JOHN F. MCKAY
University of Wyoming Research Corporation,
formerly Laramie Energy Technology Center,
U.S. Department of Energy
Laramie, Wyoming

May 16, 1983

x

In Geochemistry and Chemistry of Oil Shales; Miknis, F., el al.;
ACS Symposium Series; American Chemical Society: Washington, DC, 1983.

Geochemistry and Pyrolysis of Oil Shales

B. P. TISSOT and M. VANDENBROUCKE

Institut Français du Pétrole, BP 311, 92506, Rueil-Malmaison, France

Oil shales are defined according to economic criteria :
they are rocks yielding commercial amounts of liquid
hydrocarbons upon destructive distillation. They contain
an organic matter (kerogen) similar to that of petroleum
source-rocks. Specific geochemical characteristics of oil
shales, as compared to petroleum source-rocks are pre-
sented hereunder : low natural thermal evolution, high
carbon content, high hydrogen amount of the organic mat-
ter. The evolution of some geochemical parameters during
pyrolysis is shown for different oil shales. Finally,
specific features of the composition of shale oils compa-
red to that of natural petroleums are indicated : presen-
ce of unsaturated hydrocarbons, higher amount of hetero-
atomic compounds.

There is no geological or chemical definition of an oil shale.
Any rock yielding oil in commercial amount upon pyrolysis may be
considered as an oil shale. The composition of the inorganic frac-
tion may vary from a shale where clay minerals are predominant,
such as the Lower Jurassic shales of Western Europe (particularly
France and West Germany.), to carbonates with subordinate amounts
of clay and other minerals, such as the Green River shales of Co-
lorado, Utah and Wyoming.
    The organic fraction is mainly an insoluble solid material,
kerogen, which is entirely comparable to the organic matter present
in many petroleum source rocks (1-2). Figure 1 shows the elemental
composition of the Green River shales, the Lower Toarcian shales
of the Paris Basin and W. Germany and also various oil shales from
different origins. A large number of core samples from the Green
River and the Paris Basin shales was taken at various burial
depths. They cover the diagenesis, catagenesis and metagenesis sta-
ges of thermal evolution (1) (the latter stage was available from
the Green River shales only). The diagram shows that these two
shales series constitute typical evolution paths of type I and
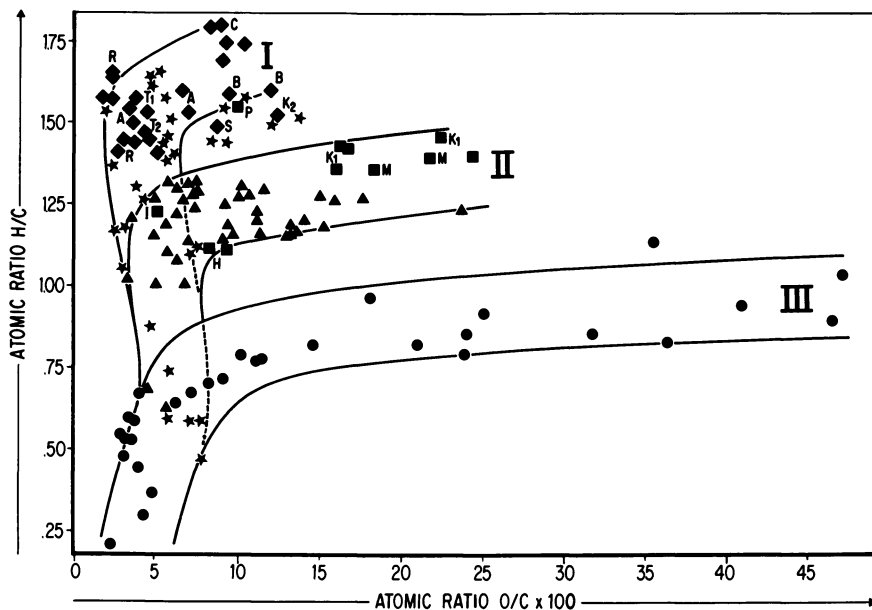
Figure 1. Van Krevelen diagram showing the elemental composition of oil shale kerogens. The organic constituents of the Green River shales (★) and the Toarcian shales (▲) of the Paris Basin are typical kerogens of Types I and II, respectively. Other oil shales belong to either Type I (◆) or II (■). Key: A, Autun boghead, Permian, France; B, Moscow boghead, Permian, USSR; C, Coorongite, recent, Australia; H, Marahunite, Tertiary, Brazil; I, Irati shales, Permian, Brazil; K_1 and K_2, Kukersite, Paleozoic, USSR; M, Messel shale, Eocene, W. Germany; R, Kerosene shale, Permian, Australia; S, Tasmanite, Permian, Australia; T_1, torbanite, Carboniferous, Scotland; and T_2, torbanite, Permian, Australia. The evolution path of humic coals (Type III) (●) is shown for comparison.

type II kerogens according to the definition of Tissot et al (3).
Furthermore, other oil shale kerogens belong either to type I,
such as coorongite and kerosen shales (Australia), torbanite (Sco-
tland and S. Africa) and bogheads ; or to type II, such as kuker-
site (USSR), Irati (Brazil) and Messel (W. Germany) shales ; tas-
manite (Australia) shows an intermediate elemental composition.
The evolution path of humic coals is also shown in Figure 1 for
comparison. It has obviously a lower hydrogen content than any of
the oil shale kerogens, unless they have been deeply altered by
thermal evolution.

Infrared spectroscopy (Figure 2 and Table I) of the kerogens
(4) from oil shales shows that all of them are rich in aliphatic
bands at 2900 and 1450 cm^{-1} related to chainlike and cyclic sa-
turated material. However, kerogens of type I, such as Green River
shales and torbanite, contain a larger proportion of long alipha-
tic chains, marked by the absorption bands at 720 cm^{-1}.

Table I : Relative importance of aliphatic bands in infrared spec-
troscopy of some kerogens from selected oil shales
(arbitrary units).

Type	Sample	IR Aliphatic bands (cm^{-1})			
		K_{2900} C-H	K_{1450} CH_2+CH_3	K_{1375} CH_3	K_{720} $(CH_2)_n$ n$\geqslant$4
I	Green River sh. Torbanite	136.6 105.3	11.2 10.8	1.5 2.1	1.3 1.1
II	Toarcian shales Kukersite Messel shales	73.0 72.7 76.0	10.0 11.5 9.6	2.5 2.8 3.7	0. 0.4 0.2

The total oil yield obtained from the shale upon pyrolysis is
usually measured by the standard Fisher assay. However, it is pos-
sible to obtain a fast and accurate measurement of the oil yield
by using the Rock Eval source rock analyzer (5), which operates
on small quantities of rock, such as 50 or 100 mg. Figure 3 shows
the comparison between the value obtained from the Rock Eval pyro-
lysis and the yield of the Fisher assay on the Toarcian shales of
the Paris Basin.

A series of experiments has been carried out to observe the
generation of the different classes of oil constituents. Aliquots
of two kerogens from the Green River Shale (type I) (6) and the
Lower Toarcian shales of the Paris Basin (type II) (7) where hea-
ted at a constant heating rate of 4°C min^{-1} to different final
temperatures ranging from 375°C to 550°C. A humic coal from Indo-
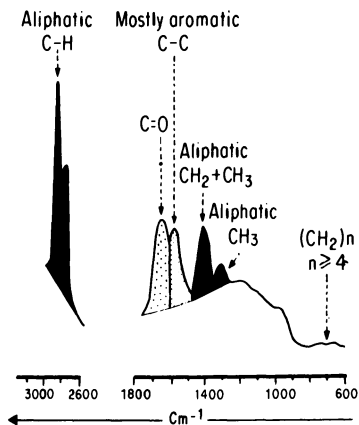nesia (type III) was also used for comparison (8). These various

Figure 2. *Typical IR spectrum of the kerogen isolated from lower Toarcian shales of the Paris Basin.*
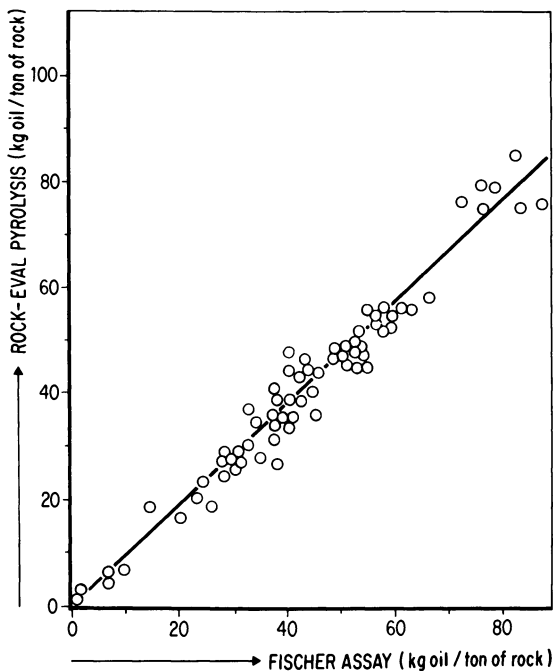

Figure 3. *Correlation between oil content obtained by the Fischer assay and by the Rock–Eval pyrolysis.*

samples have experienced a comparable thermal history in geologi-
cal conditions : they belong to the final stage of diagenesis (1)
(vitrinite reflectance between 0.4 and 0.5%). The mass balance of
the organic fraction is shown in Figure 4 as a function of the
final temperature. At 375°C, most of the organic material is still
made of kerogen. With increasing final temperature an increasingly
large fraction is converted to oil which condensates in a cold
trap, leaving a solid residue or char. The non-recovered fraction
is assumed to be mainly carbon dioxide, water and light hydrocar-
bons non condensable in the cold trap.

A somewhat different behaviour is observed according to the ty-
pe of kerogen : the Green River shale (type I) requires higher
temperatures, as the maximum rate of conversion occurs ca. 475°,
versus 425-450°C for the Paris Basin shale (type II) and the humic
coal (type III). Furthermore the conversion ratio and the compo-
sition of the products are different : the total conversion ratio
(condensate plus non-recovered products) decreases from over 80%
for type I, to 55% for type II and 35% only for coal. The amount
of oil (condensate) generated is relatively high in kerogens from
oil shales : 62% for type I and 37% for type II, whereas it is
low (less than 12%) for coal. This is partly due to an important
generation of carbon dioxide and water from humic coals. The
relative proportion of hydrocarbons (saturated, unsaturated, aro-
matics) compared to N,S,O - compounds also decreases from type I
to type III.

The total amount and composition of the hydrocarbons generated
is shown in Figure 5. The Green River oil shale (type I) produces
mainly linear or branched hydrocarbons, whereas the Paris Basin
shale (type II) generates mainly cyclic - particularly aromatic -
hydrocarbons. The percentage of aromatics is also important in
coal pyrolysis, but the absolute amount is much smaller. The
bottom part of Figure 6 shows the distribution of n-alkanes in
shale oils : it is regularly decreasing from C_{17} to C_{30} in the
oil derived from type II kerogen, which is a fluid synthetic oil ;
it is relatively flat up to C_{30} (type I) or even increasing towards
a C_{25}-C_{29} maximum (type III) in the two other synthetic oils which
have a waxy character. Furthermore, a slight predominance of the
odd-numbered molecules (C_{25}, C_{27}, C_{29}) noted in the oil derived
from humic coal points to a contribution of natural waxes from
higher plants to the organic material.

A direct pyrolysis-gas chromatography of the kerogens was also
performed and is presented in Figure 7 (9). The chromatograms
taken at pyrolysis temperature of 475°C show the total distribu-
tion of hydrocarbons, with the relative importance of long-chain
molecules up to C_{30} in types I and III. It also shows the impor-
tance of low-boiling aromatics (B : benzene ; T : toluene ;
X : xylenes) generated from humic coal (type III) as compared to
those generated from oil shales (types I and II).

Composition of the solid organic residue of pyrolysis was
also analyzed in order to follow the progressive change from the
immature kerogen to the final char. Figure 8 presents the elemen-
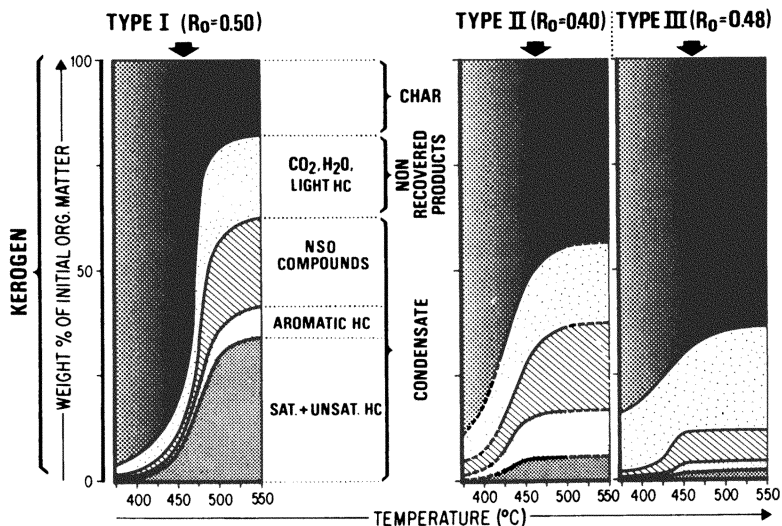
Figure 4. *Pyrolysis of kerogens at a standard heating rate of 4 °C min⁻¹ up to various final temperatures. Mass balance is of recovered and nonrecovered products plus residual char.*
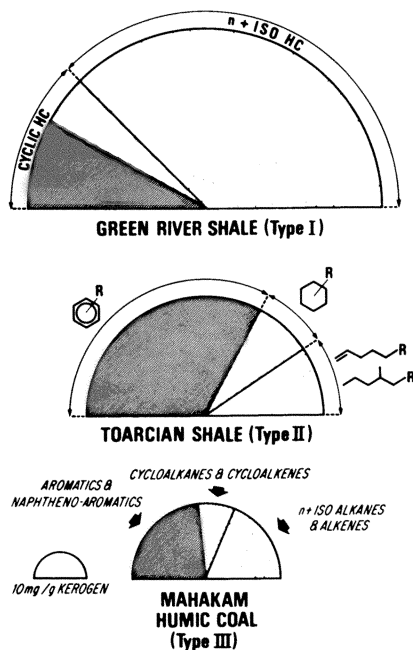
Figure 5. *Hydrocarbons generated from the two main types of oil shales by pyrolysis at 4 °C min⁻¹ rate up to 500 °C. Hydrocarbons generated from a humic coal (Type III) are shown for comparison.*
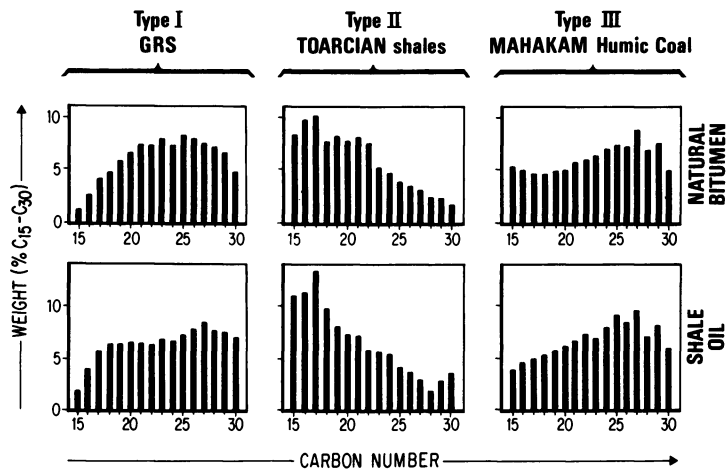
Figure 6. Comparison of the normal alkane distribution in shale oil generated by pyrolysis and in bitumen from geological samples with an equivalent stage of thermal evolution.
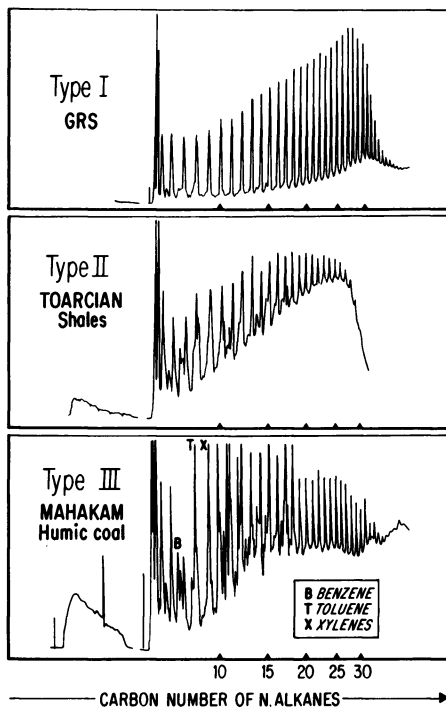
Figure 7. Pyrolysis–GC at 475 °C. The chromatogram shows total hydrocarbons.
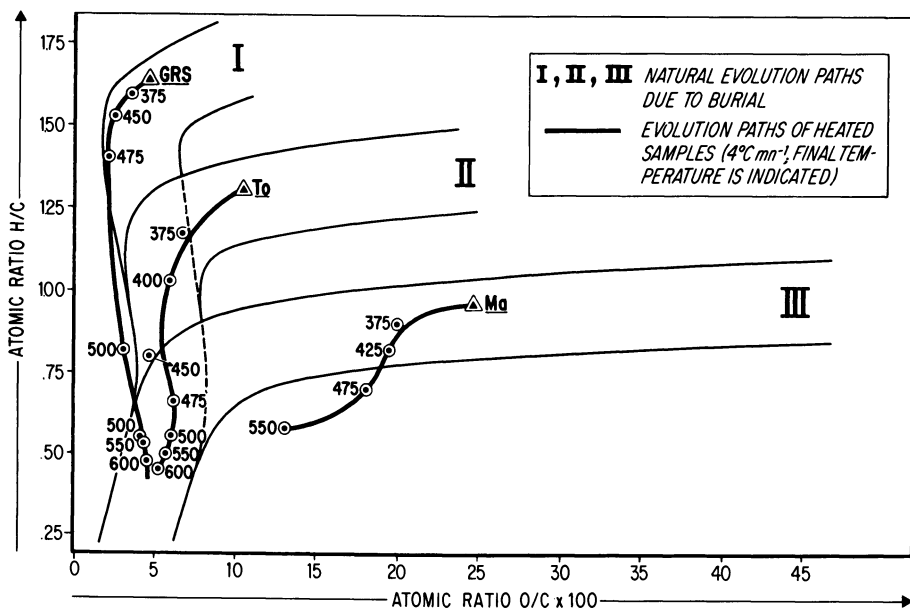
Figure 8. *Evolution paths of heated samples compared to natural evolution paths of Series I, II, and III.*

tal composition of the solid organic fraction corresponding to the experiments reported in Figure 4. Artificial evolution of the two types of oil shale kerogen and the humic coal is represented by the elemental composition and the final temperature of pyrolysis. The artificial evolution paths corresponding to types I and II are reasonably comparable to the natural evolution paths observed in geological situation (10 - 11), where the Green River and Paris Basin shales are buried at depth (this path is marked by bands I and II, respectively, in Figure 8). The major loss of hydrogen occurs ca. 475-500°C for type I and ca. 400-475°C for type II kerogen ; this remark is in agreement with a comparable delay in their respective conversion ratio reported in Figure 4. The behaviour of coal is somewhat different from that of oil shale kerogen : its artifical evolution does not duplicate the natural evolution path of humic coals. This is possibly due to the higher oxygen content of the initial sample and to its preferential elimination as water (a hydrogen consuming process) during pyrolysis, as compared to geological situations, where oxygen is mostly eliminated as carbon dioxide.

A confirmation of the inadequacy of pyrolysis to simulate the natural evolution of coal is provided in Figure 9, where two parameters of the Rock Eval pyrolysis are presented. The hydrogen index (5) is plotted as a function of a thermal evolution parameter T_{max} (temperature of pyrolysis corresponding to the maximum rate of release of organic compounds). The hatched bands marked I, II and III correspond to the natural evolution paths (under burial in geological situation) of the Green River Shales (10) , the Paris Basin and W. Germany Toarcian shales (11), and humic coals (12), respectively. Again, the artificial evolution paths of type I and type II oil shale kerogens are reasonably comparable to the natural evolution paths, whereas the deviation is important for coal. The graph points to an early loss of hydrogen, possibly used for oxygen elimination through water generation : thus the hydrogen index, which measures the potential for further hydrocarbon generation, is lowered at an early stage of thermal evolution as compared to its behaviour in geological situation.

Another aspect of the comparison between pyrolysis and natural evolution of the organic matter is shown in Figure 10. In the Paris Basin, Lower Jurassic shales have been mined as oil shales where they are outcropping, whereas in the central part of the basin they were submitted to sufficient burial to generate bitumen in large amounts (11) ; in turn, a small fraction of that bitumen migrated to form small oil fields. Figure 10 presents the global composition of i) shale oil generated by laboratory pyrolysis, ii) natural bitumen generated at depth in the shale acting as a source rock, and iii) crude oil accumulated in a small field. The global composition of shale oil (non-aromatic hydrocarbons, aromatic hydrocarbons, N,S,O - compounds) shows some similarities with that of natural bitumen, especially the high content of N,S, O - compounds, as compared to the content in pooled oil. This si-
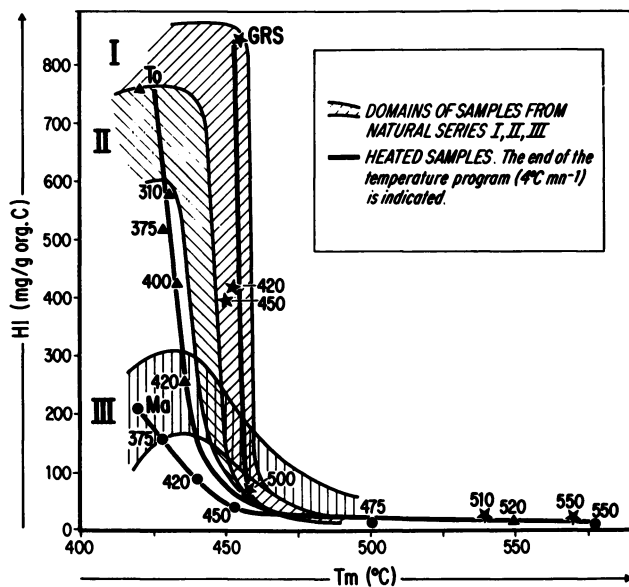
Figure 9. Evolution of hydrogen index vs. T_{max} of Rock–Eval pyrolysis in natural Series I, II, and III (hatched) and in heated samples (identified by final temperature of pyrolysis). Key: ★, Green River shales (GRS); ▲, Toarcian shales (To); and ●, humic coals (Ma).

Type II
ORGANIC MATTER

H NSO COMPOUNDS   U UNSATURATES
A AROMATICS   S SATURATES

SHALE OIL   NATURAL BITUMEN   POOLED OIL
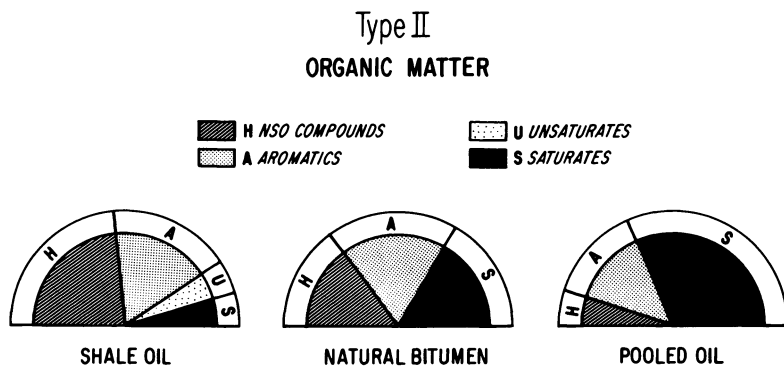
Figure 10. Composition of shale oil, natural bitumen present at depth, and pooled oil, which are all derived from lower Jurassic shales, Paris Basin.

milarity is also observed in Figure 6 where the n-alkanes dis-
tribution of three shale oils is compared with that of three
natural bitumens of comparable stage of thermal evolution.

   There are two major causes for the differences observed bet-
ween shale oil and crude oil. One is due to generation by pyroly-
sis of compounds unusual in natural bitumens and crude oils, such
as unsaturated hydrocarbons (olefins) : Figure 10. Nitrogen hete-
ro-compounds are also much more abundant than they are in natural
bitumen or crude oils. The other difference is due to the migra-
ted character of pooled oil which results in a preferential
migration of hydrocarbons, especially saturates, and a retention
of most of the N,S,O - compounds in the source rock (1) . Thus
natural bitumen has an intermediate composition, separated from
shale oil by the conditions of pyrolysis and from pooled oil by
migration across sedimentary beds.

Literature Cited

 1. Tissot,B.P. ; Welte, D.H., "Petroleum formation and occurren-
    ce", Springer-Verlag : Berlin, Heidelberg, New-York, 1978.
 2. Durand B. in "Kerogen, Insoluble organic matter from sedimen-
    tary rocks", Durand B. Ed. ; Editions Technip Paris, 1980,
    p. 13,113.
 3. Tissot, B. ; Durand, B. ; Espitalié, J. ; Combaz, A., Am. As-
    soc. Petrol. Geol. Bull. 1974, 58, 499.
 4. Rouxhet, P.G. ; Robin, P.L.; Nicaise, G., in "Kerogen",
    Durand, B. Ed.; Editions Technip : Paris, 1980 ; p. 163.
 5. Espitalié, J.; Madec, M.; Tissot B.; Mennig, J.J.; Leplat,P.,
    Offshore Technology conference, Preprint OTC 2935,(1977), 439.
 6. Vandenbroucke, M.; Durand, B.; Hood, A.; in Proc. 8th Inter-
    national Meeting on Organic Geochemistry, Moscow, 1977, in
    press.
 7. Huc, A.Y., Thesis, University of Strasbourg, 1978.
 8. Monin, J.C.; Durand, B.; Vandenbroucke, M.; Huc, A.Y.; in
    "Advances in Organic Geochemistry 1979" ; Douglas, A.G. and
    Maxwell, J.R. Eds; Pergamon Press : Oxford, 1980 ; p. 517.
 9. Saint-Paul, C.; Monin, J.C.; Durand, B, Rev. Inst. Fr. Pétrole
    1980, XXXV-6, 1065.
10. Tissot, B.; Deroo, G.; Hood, A., Geochim. et Cosmochim. Acta.
    1978, 42, 1469.
11. Tissot, B.; Califet-Debyser, Y.; Deroo, G.; Oudin, J.L., Am.
    Assoc. Petrol. Geol. Bull. 1971, 55-12, 2177.
12. Durand, B.; Nicaise, G.; Roucaché, J.; Vandenbroucke, M.;
    Hagemann, H.W., in "Advances in Organic Geochemistry 1975,
    Campos, R. and Goni, J. Eds.; Enadimsa : Madrid, 1977, p.601.

Geochemistry of Brazilian Oil Shales

CLAUDIO COSTA NETO

Universidade Federal do Rio de Janeiro, Instituto de Química, Rio de Janeiro, Brazil

A definition of geochemistry of oil shales (o.s.) is
proposed in order to systematize the presentation of
the subject. A general view of the chief Brazilian o.
s. reserves is made prior to discussing information
on their chemical composition (organic and inorganic).
Geochemical aspects of Stratigraphic Functions are
stressed and a Correlation Matrix for elements in a
stratigraphic column of Irati Formation (F.) is dis-
cussed. The analytical methods of Solid Phase Extrac-
tion and Functional Group Marker developed for the a-
nalysis of bitumens and kerogens and the results ob-
tained from the application of these methods to Bra-
zilian o.s. is discussed. The geochemical aspects in-
volved with a large diabase intrusion in the Irati is
particularly stressed; results on the phylogenetic
studies on hydrocarbon chains of Irati o.s. are also
presented. A critical discussion on the role of a
Theoretical Organic Geochemistry is presented. The
paper ends with a brief description of a comprehen-
sive Analytical Bibliography on Brazilian o.s. prepar
ed to serve as a data base for these organites.

The bibliography on Brazilian oil shales amounts today to ap-
proximately 850 papers. No more than 250 deal with chemistry and
the number of documents discussing its geochemistry is rather small.
Many conclusions can be drawn from this statement. For instance,
that oil shales do not appear to have been considered, as yet, an
important subject in the Brazilian Science and Society (the rele-
vance of oil shales to the Brazilian Society has been widely dis-
cussed by Costa Neto (1)). If it is looked at from a technical view
point, a question may be posed: which were (or should be) the bound
aries chosen for geochemistry whithin the universe of information
on the chemistry of oil shales? Judging from what is published in
the literature an answer to this question may be that these "bound

aries", if they exist, are "fuzzy" and very "relative" (that is, they will vary according to whom is making the selection). But, indeed, "boundaries" can be given to any subject if they are well "defined" - that is to say what it tries to describe, and what are the purposes and objectives. If the definition is imaginative e- nough, it may go even further estimulating questions on points that may have not yet been discussed and, in many ways, directing the work to new lines of research in the field (this point will be dis cussed later on). This presentation will then start with a defini- tion for the geochemistry of oil shales.

Definitions

Chemistry deals with the nature (structure) and transformations of substances. Geochemistry deals with the nature (structure) and transformations of substances proper to the geosphere. Geochemistry of oil shales deals with the nature (structure) and the natural trans formations of oil shales. This is a very general definition. If we go further, looking for the fundamental objectives of the geochem istry of oil shales, we can say that they are:

1. to know, at the molecular level, the materia actuale of oil shales (the matter of oil shales as it stands today) i.e. the chem ical nature of the organic and inorganic phases that constitute oil shales seeking to establish their structure (geometrical relation- ships among atoms and molecules).

2. to define the natural transformations of the materia prima into the materia actuale, through modeling from the knowledge of the chemical constituents of the materia actuale and further sim- ulations (theoretical and experimental) of the processes.

3. to infer, from what is known from the materia actuale, the possible nature of the materia prima, i.e. the matter that gave or igin to oil shales.

These objectives can be correlated according to fig. 1.
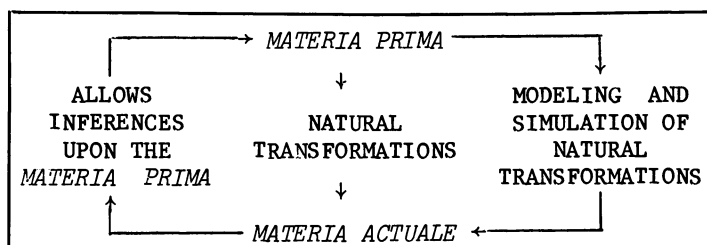

Figure 1. Purposes of the geochemistry of oil shales.

Indeed, it becomes easier to recognise the boundaries of geochem istry within the chemistry of oil shales if one presents the whole universe of information on the chemistry of oil shales (see fig. 2). In this diagram three main sets of substances (materials) are rec- ognized: the materia prima, the materia actuale (already presented

in fig. 1) and a new set, the <u>materia transformada,</u> i.e. substances produced by transformation of oil shales by man. Two sets of processes exist: the natural one - described before - and the one representing the man-produced transformations. The geochemistry dominium, within the general chemistry of oil shales, may be, then, easily recognised.

```
┌─────────────────────────────────────────────────────────────┐
│                                                               │
│      MATERIA PRIMA                        ↰                    │
│            ↓                              │                    │
│  NATURAL TRANSFORMATIONS            GEOCHEMISTRY               │
│            ↓                         DOMINIUM                  │
│                                                               │
│      MATERIA ACTUALE                      │                    │
│            ↓                              ↲                    │
│                                           │                    │
│     MAN  PRODUCED                  FUNDAMENTAL CHEMISTRY/       │
│    TRANSFORMATIONS                    TECHNOLOGY                │
│            ↓                          DOMINIUM                 │
│  MATERIA  TRANSFORMADA                    ↲                    │
│                                                               │
└─────────────────────────────────────────────────────────────┘
```
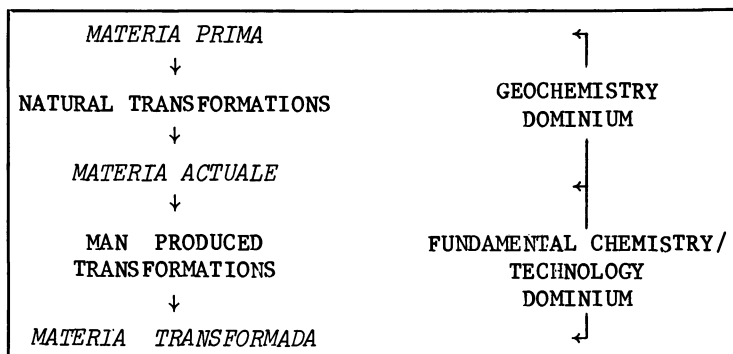
Figure 2. General dominion of the chemistry of oil shales (Xistoquimica).

The greatest amount of information we have nowadays on the geochemistry of oil shales is related to the chemical composition of the materia actuale, but restricted to the identification of organic and inorganic species.

The materia actuale should be looked upon as a highly complex tridimensional network of atoms. To determine the nature of these atoms, the relationship among them as well as their geometrical arrangement in space constitute the geochemistry of the materia actuale.

The direct determination of the structure or organites has not yet been achieved. The physical relationship among the various molecules in the material has not yet been considered and near to nothing is known concerning the stereostructures of organites (the term Organite (2) will be used to designate any geological system containing organic matter associated - in any proportion - to an inorganic matrix).

It is utopic to think to define the "structure" of an oil shale. At most we will be able to define the structure of microuniverses within the oil shale material, where one expects a chosen reaction to occur (this point will be stressed later, when we deal with the chemical reactions occurring in the bulk of the rock).

Nevertheless, a systematic "ideal" approach toward the goal of establishing a "structure" for organites would start with the determination of the knots of the network, that is, the elemental composition (qualitative and quantitative) of the oil shales.

The second stage would involve the determination of the conectivities among these elements, established as molecular moieties

(functional groups, hydrocarbon chains), molecules, crystals etc. This can be said to define the topological structure of oil shales. This relationship can be seen under two main aspects; a chemical one - where the relationship among the various elements can be characterized as chemical bonds - and a physical one - where the various compounds are "bound" together forming the material itself.

A partial characterization of the organic matter may be made - specially for the highly complicated macromolecules present in or- ganites, like the kerogen - through the characterization of func- tional groups.

The final stage aims at the characterization of the stereostruc- ture - the geometrical arrangement of the molecules - of (or wi- thin) oil shales.

Most of the geochemistry of the materia actuale of organites has reached the point of characterizing their organic molecules and inorganic minerals as isolated species.

But, in order to be give a "good" geochemical description for an oil shale, one must bear in mind that the composition of oil shales varies within the same reserve according to depth and local. So, the geochemical study of a given oil shale formation comprises, more than determining the chemical composition of a given isolated sample, of the determination of Geochemical Functions of Distribu- tion of a given element or molecule in the geological formation, that is, along the longitudinal stratigraphic axis - a longitudinal stratigraphic function - and along a same horizon in the formation: a transversal stratigraphic function. To be taken as true geochem- ical data the results of the composition of a materia actuale must be displayed as distribution functions along the formation (and not only as the common results of analysis of sparse samples). Most of what is called in the literature "data on geochemistry of organ- ites" are mere exercises of analytical chemistry on geological sam- ples. Correlation indexes between pairs, trios etc. of chemical elements or molecules along the formation will complement the geo- chemical structural data. The distribution functions will reflect the effect of temperature, pressure, time and structure on the geo- chemical transformations of the materia prima into the materia ac- tuale.

The Brazilian Irati Formation (Permian) is a good example to illustrate most of what was said: first, what is known about this oil shale comes from samples obtained from a narrow belt that con- stituted the border of the Paraná Basin. Going west, these forma- tions deepen to 2-3 thousand meters; the materia actuale of this part may be quite different from that which outcrops. Second, a hot diabase intrusion is known to have occurred in the Irati forma- tion. Temperature effects change considerably the nature of the or- ganic matter so that a variation on the nature of the organic mat- ter of the materia actuale is to be expected in the regions of dif- ferent temperatures. Third, there are neat differences regarding many aspects when one goes from North to South in the Formation: 1. The sulfur content increases, going from pratically zero at São

Paulo to up to 5-7% in São Gabriel (frontier with Uruguai).   The
inorganic phase is mainly carbonates in São Paulo while in the South
it is mainly clays. Even the characteristic fossil of the   Irati
Formation changes from the Stereosternum tumidum in São Paulo, pro
per to fresh, limpid water to the Mesosaurus braziliensis, in   the
South, more adapted to brackish water. What would then be the chem-
ical composition of the Irati Formation if not a distribution func
tion?

Before going into the discussion of the available data on the
geochemistry of Brazilian oil shales, insights into the   existing
Brazilian oil shale reserves will be given, so that the reader can
feel the importance of these organites to Brazil.

Occurrences of Oil Shales in Brazil

Oil shales are abundant in Brazil. Occurrences are known over
almost all the Brazilian territory: the main deposits are shown in
fig. 3. A comprehensive survey of the sites where occurrences have
been registred was published by Costa Neto (1). Nevertheless, only
a few of these deposits are really known, and certainly   not   many
will become economically significant.

Oil shales represent to Brazil a ponderable fraction of the fos
sil organic matter the country counts upon. Table I shows the lat-
est official numbers for the reserves of organites.

Table I. Fossil organic matter reserves of Brazil (3).

Organite	Unities	Measured	Estimated	Total	Equivalent in 1000teP[1]
Petroleum	$10^3 m^3$	237700	–	237700	199660
Natural gas	$10^3 m^3$	60287	–	60287	54861
Shale Oil	$10^3 m^3$	465000[2]	207000	672000	565000
Coal	10^3 ton	6460000	16150000	22160000	4270000
Peat	10^3 ton	–	3154000	3154000	240000

1. tEP = tons equivalent to petroleum.
2. These numbers refer to the oil shale reserves that have   been
studied by Petrobras, passible to be processed by the PETROSIX proc
ess.

The main oil shale resources known in Brazil today are: the
IRATI FORMATION, by far the largest, which extends from the state
of São Paulo to the frontier with Uruguai. The very   conservative
numbers shown in Table II are meant to represent the measured re-
serves processable by the Petrosix process developed by Petrobras
to retort oil shales. These restrictions are mainly related to min
ing variables, carbon content, brittleness etc. Indeed, they repre
sent only a small fraction (the border) of the Paraná Basin.

The Vale do Paraíba oil shale, with a known reserve of 1.3 bil

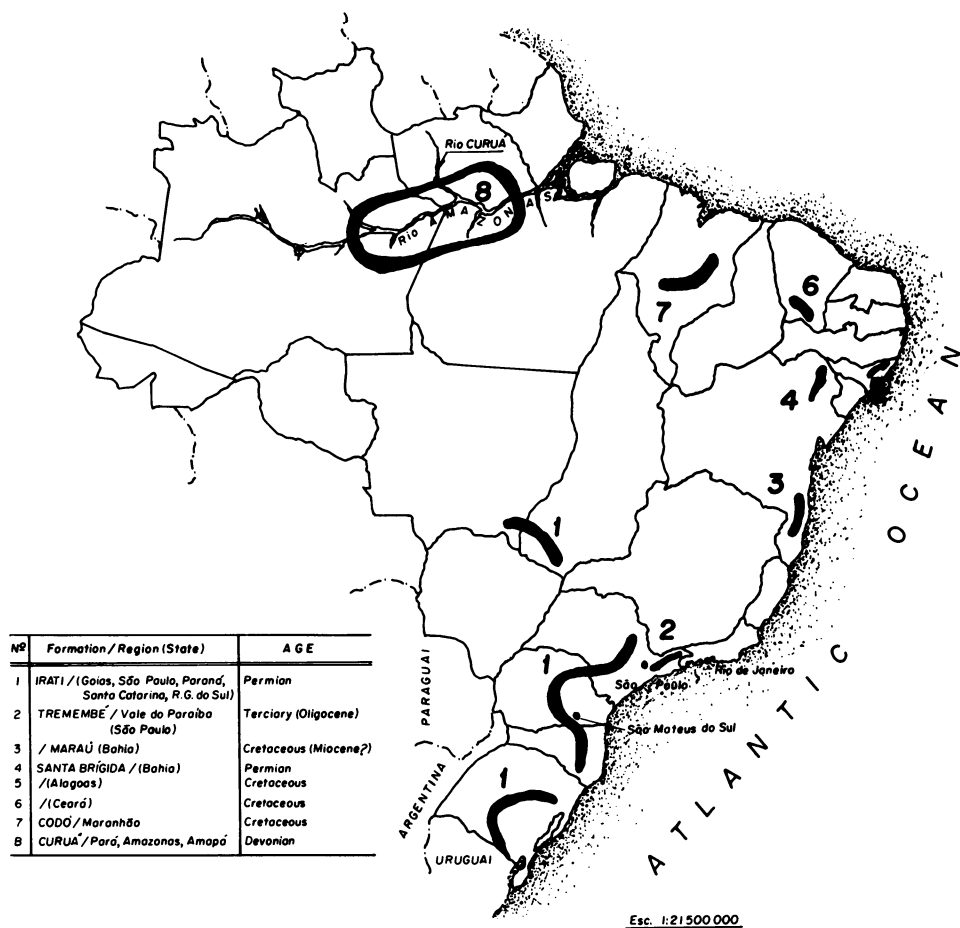| Nº	Formation / Region (State)	AGE
I	IRATI / (Goias, São Paulo, Paraná, Santa Catarina, R.G. do Sul)	Permian
2	TREMEMBÉ / Vale do Paraiba (São Paulo)	Terciary (Oligocene)
3	/ MARAÚ (Bahia)	Cretaceous (Miocene?)
4	SANTA BRÍGIDA / (Bahia)	Permian
5	/(Alagoas)	Cretaceous
6	/(Ceará)	Cretaceous
7	CODÓ / Maranhão	Cretaceous
8	CURUÁ / Pará, Amazonas, Amapá	Devonian

Figure 3. Main oil shale occurrences in Brazil.

lion bbl, is located between the cities of Rio de Janeiro and São Paulo. The average oil content is, nevertheless, low (4-5%), although in one of the facies of this oil shale, the so called "papiráceo" (paper-like), the oil content can go as high as 25%. Less important is the Maraú Formation in Bahia state with a reserve of only 4.8 million tons.

Table II. Main Brazilian oil shale reserves.

RESERVE	CAPACITY (10^6 bbl oil)	REFERENCE
IRATI	(945000)	4
	20000	5
Paraná	11200	6
São Mateus do Sul	647	7
Rio Grande do Sul		
Don Pedrito	350	7
São Gabriel	150	7
VALE DO PARAÍBA	5000	8
Tremembé-Taubaté- -Pindamonhangaba	2000	9
MARAÚ	4.8	10
João Branco	0.13	10

More details on the geology, economics etc. of these reserves can be found in Bigarella (11) and Moreira (12). The Brazilian Oil Shale Bibliography (13) should be consulted for exaustive surveys.

A lot has been said in the Brazilian literature about the end uses of oil shales. In Brazil, oil shales are looked at by most scientists, government agencies and the public in general as a source of synfuels, consequently as an alternative source of energy, since the known reserves of petroleum are not to be considered as very significant. Other line of thoughts (14) considers oil shales as raw material (feedstock) for the chemical industry, with the specific goal of producing materials and health goods.

It is interesting to quote that the oldest known reference in the literature to Brazilian oil shales was made in 1865, by Archer (15) concerning "A new bituminous substance imported under the name of coal from Brazil". Also that in the celebrated series of papers published by Treibs (16), where be defined the organic origin of petroleum, the Brazilian oil shale from Maraú was one of the materials he used to show the presence of porphyrins in organites.

Despite the economic significance of oil shales to Brazil they have not yet had the due attention they deserve, specially regarding their geochemistry.

This paper will not be restricted to a description of geochemical features of Brazilian oil shales, since, as it was mentioned before, they are rather scarce. It will be, indeed, more of a critical discussion of Geochemistry on (using) Brazilian oil shales.

Elemental Composition of Brazilian Oil Shales

    The first step toward establishing a structure for oil shales
is to determine its elemental composition. The data available   in
the literature on the elemental composition of Brazilian oil shales
is quite meagre in respect to geochemical meaning.   Nevertheless,
the available data will be presented for the main reserves, in or-
der to give, at least, an indication of its composition. An   ex-
haustive survey of the carbon, hydrogen, oxygen & nitrogen and sul
phur composition of Brazilian oil shales was presented by Costa Ne
to (1). Most of the data showed in this paper refer to sparse sam-
ples.
    Carbon, hydrogen and oxygen occur in oil shales in both organic
and inorganic parts. The carbon content of oil shales is   directly
associated to the most important parameter for its utilization, i.
e., oil production by pyrolysis (shale oil). The distinction   be-
tween organic and inorganic carbon (carbonates) is very easy to be
made by analytical methods. But, the distinction between   hydrogen
or oxygen derived from the organic matter, and that   originating
from the inorganic matrix does not have any trivial solution   in
Brazilian oil shales as the constitutional water of the clays   can
only be liberated at high temperatures (> 500ºC) and clays are ve
ry intimately associated to the organic matter of oil shales to an
extend that it is practically impossible to get the organic matter
free of clay (see further discussions on the subject below).

Average Values vs. Stratigraphic Distribution Functions. When the
commercial production of shale oil from a given reserve is consid-
ered, the average carbon (oil) content is the parameter looked at.
For geochemistry, nevertheless, this value has not a very   great
meaning and stratigraphic distribution functions are the ones   to
be used. A good example of this can be given by the Brazilian Vale
do Paraiba oil shale (Tremembé Formation): thin layers of an   or-
ganic rich material (the "papiráceo" = paper like facies)   alter-
nate with a different facies, the so called "conchoidal" ("shell-
-like" fracture: in portuguese concha = shell). These   two   facies
are rather different, not only regarding the macroscopic   aspect
but also the carbon content (the "papiráceo" facies can reach 25%
of carbon while the "conchoidal" one has 13%). Fossils are found
pratically only in the "papiráceo"; the complete column alternates
these two facies with clay layers down to 150m deep. The proposed
(17) economic column for commercial exploration of this reserve sug
gests the utilization of a 30m column with an average 4% of   oil
production.
    A stratigraphic distribution functions for elements in an Ira-
ti Column (CERI-1) at São Mateus do Sul was described and discus-
sed by Costa Neto (18). In general terms one can say that the Ira-
ti F. is composed of two well defined layers, the first with 5,5m

and the second with 3,5m (average thickness), separated by an intermediate layer of 10m. In the Southern part of the formation the first layer has been eroded off so that only the second layer exists.

The presence of sulphur in oil shales has direct geochemical implications as well as direct economic significance.

The distribution of sulphur along the North-South axis in the Irati F. is informative about the paleogeography of the Paraná basin. At the Irati F. the sulphur content docreases from = 7,5% at Don Pedrito (near the Uruguai border), to 3-4% at São Mateus do Sul (Paraná), to practically zero at Rio Claro (São Paulo). It has been shown that this sulphur is present as pyrite (19). This distribution suggests the existence of a link of the Paraná "lake" (?) to the sea at the South (probably through the Rio da Prata). Thus, south of the basin, a marine environment may have predominated. As one goes north, a salinity gradient (negative) is established as the contribution from fresh water (rivers etc.) to the water mass of the lake increases, lowering, consequently, the sulphur content.

The association of sulphur with metals, a matter also of geochemical significance, will be treated later when the elemental correlation matrix is discussed.

The high sulphur content of the Irati F. at São Mateus do Sul is an important (economic and strategic) feature in the commercial exploration of oil shales in Brazil, since it is considered, nowadays, as the most important reserve of pyritic sulphur in a country that still imports 95% of the (elemental) sulphur it consumes.

The macro-constituents present in the inorganic matrix define the two major classes in which oil shales can be classified: argillaceous and carbonatic. In the first, clays constitute the major part of the inorganic matrix, while in the second, calcite or dolomite are the predominant inorganic species.

The Irati F. presents both, the argillaceous base, in the South and the carbonatic at São Paulo (Rio Claro). The Vale do Paraíba and Marau oil shales have argillaceous matrices, while the Codó oil shale has a carbonatic one.

The knowledge of the presence of minor elements in oil shale represents an important group of informations for geochemistry (see e.g. Keith and Degens (20) and Lerman (21)) and also of significance in the commercial exploration of oil shales; this is the case of uranium (see Swanson (41) for a review on the geochemistry of uranium in black shales) that in many places (the Swedish oil shale is known for the high uranium content of 0,02%) occur associated to the organic matter of sediments.

Stratigraphic elemental distribution functions for an Irati column (CERI-1) were determined (22) for 21 elements (C,S,B,Ba,Be, Ce,Co,Cu,Cr,Fe,La,Mg,Mn,Mo,Ni,Pb,V,Y,Zr,Sr and U). Pair-correlation studies between these elements were made using the corresponding (linear) correlation coefficients (δ) determined from the composition stratigraphic functions.

Main correlations ($\delta > 0.8$) were found for the pairs Mg-Mn (0.97), Ca-Mg (0.92), Cu-Fe (0.91), Ca-Mn (0.90), S-Fe (0.84) and S-Cu (0.82). Carbon correlates more weakly (0.6 < δ < 0.8) with sulphur (0.68), vanadium (0.73) and uranium (0.6).

Molecular Composition of Brazilian oil shales. Oil shales may be considered as composed of two main (chemical) phases: an inorganic phase, constituted of mineral species (crystaline and/or amorphous) and an organic phase that, in its turn, can be divided into two other (sub) phases: the bitumen, the soluble (in organic solvents) fraction and the kerogen defined as the insoluble organic matter of organic.

A detailed analysis (18) of the inorganic matrix of a stratigraphy column (CERI-1) of the Irati F., based on infrared and X-ray spectrometry, showed that the clays are mainly Kaolinite and Illite, intimately associated to the organic matter. There is no record in the literature where a complete separation between these two phases has been accomplished for this oil shale. It should be noted that a chemical bond between the silicate matrix and the kerogen has been suggested (23). Montmorilonite has been detected as inserts in the column but never directly associated with the organic matter.

The exact characterization of the clays present in oil shales as well as their physical relationship (stereostructure) with the organic matter are items of major importance to geochemistry at the point one intends to describe mechanisms for geochemical transformations of oil shales.

Another major mineral present in Irati column CERI-1 is pyrite. Dolomite can be found, significantly, only in the interlayer.

Chemical Composition of the organic phase of Brazilian oil shales
Bitumens

The use of conventional procedures for the analysis of bitumens has led mainly to the identification of hydrocarbons, carboxylic acids and porphyrins due to the ease with which these classes of compounds can be isolated.

For the Irati oil shale carboxylic acids and hydrocarbons total together 30% of the bitumen (porphyrins are present in very small amounts). Still, 70% of the bitumen remains to be characterized.

A separation approach based on a fractionation according to functional groups became the basis for the SOLID PHASE EXTRACTION METHOD (24) developed for fractionating the bitumen into sets of compounds possessing a same functional (organic) group (isofunctional set of compounds), through reaction between the bitumen and a specific functional reagent bound to a solid phase. As an example, diphenylethylenediamine bound to a polystyrene matrix, was used to "fish" the aldehydes out of a bitumen. In a further step, the aldehydes were regenerated from the solid phase and, in the next step, separated and identified by GC-MS. A pictoric representation of the method is shown in fig. 4.
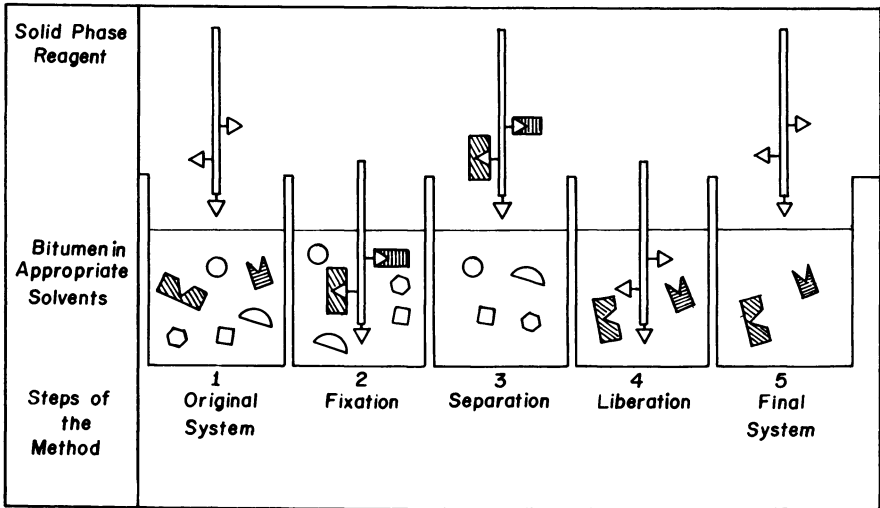
Figure 4. Pictorial representation of the solid phase extraction method.

This method allowed, for the first time, the separation of al-
dehydes and of ketones from an organite as groups of substances;
moreover, many of the aldehydes and ketones were, for the first
time, isolated from oil shales.

The use of the Solid Phase Extraction Method has been concen-
trated mainly in the study of aldehydes and ketones of bitumens.
Benzaldehydes, naphtaldehydes, fenilacetaldehydes, acetophenones,
acetonaphtones, indanones, tetralones and aliphatic ketones were
isolated from the Irati oil shale by using this method (24, 26).

It must be said that, in these cases the recovery of aldehydes
and ketones was shown to be complete (Spot Tests (25) were used to
detect aldehydes and ketones in the fractions); we know today that
resins in which the functional group reagents are bound directly to
the solid matrix discriminate products of large molecular volume,
as for instance, steroidal ketones, although the isoprenoid methyl
ketone in C_{18} was isolated from the Maraú oil shale as the major
product. New resins in which the functional group reagents are lo-
cated further away from the solid matrix are being presently engi-
neered in order to avoid this discrimination.

A very comprehensive analysis of hydrocarbons (linear, acyclic
and cyclic - steranes, hopanes etc.- isoprenoids) carboxylic ac-
ids, aldehydes, ketones and amines of the Vale do Paraíba and Ma-
raú oil shales was made by Chicarelli (27). An extremely careful
quantitative and qualitative analysis of hydrocarbons (n-, iso-
and anteiso-paraffins, isoprenoids, steranes and triterpanes) and
carboxylic acids of Irati oil shale was presented by Carvalhaes
(28). Nooner & Oro (29) also reported data on the hydrocarbons pres
ent in the Irati Formation. Polycyclic aromatic hydrocarbons in I-
rati were determined by Youngblood & Blumer (40).

Kerogens

Two main approaches have been used toward the chemical charac-
terization of kerogens of Brazilian oil shales:

1. Direct determination of functional groups by the Functional
Group Marker Method.

2. Degradation to soluble molecules mainly by permanganate oxi
dation to carboxylic acids.

The Functional Marker Method (26) was developed with the spe-
cific goal to determining directly and specifically organic func-
tional groups in kerogens.

In this method, specific functional groups reagents containing
a marker - halogens, radioactive isotopes, fluorescent moieties
etc. - are made to react with kerogens, in which, after thorough
washings, the marker is determined; the value found is a direct
measure (minimum value) of that functional group content of the ke
rogen. Figure 5 gives a pictorial representation of the Functional
Markers Method in a more complete version of the original one (26).
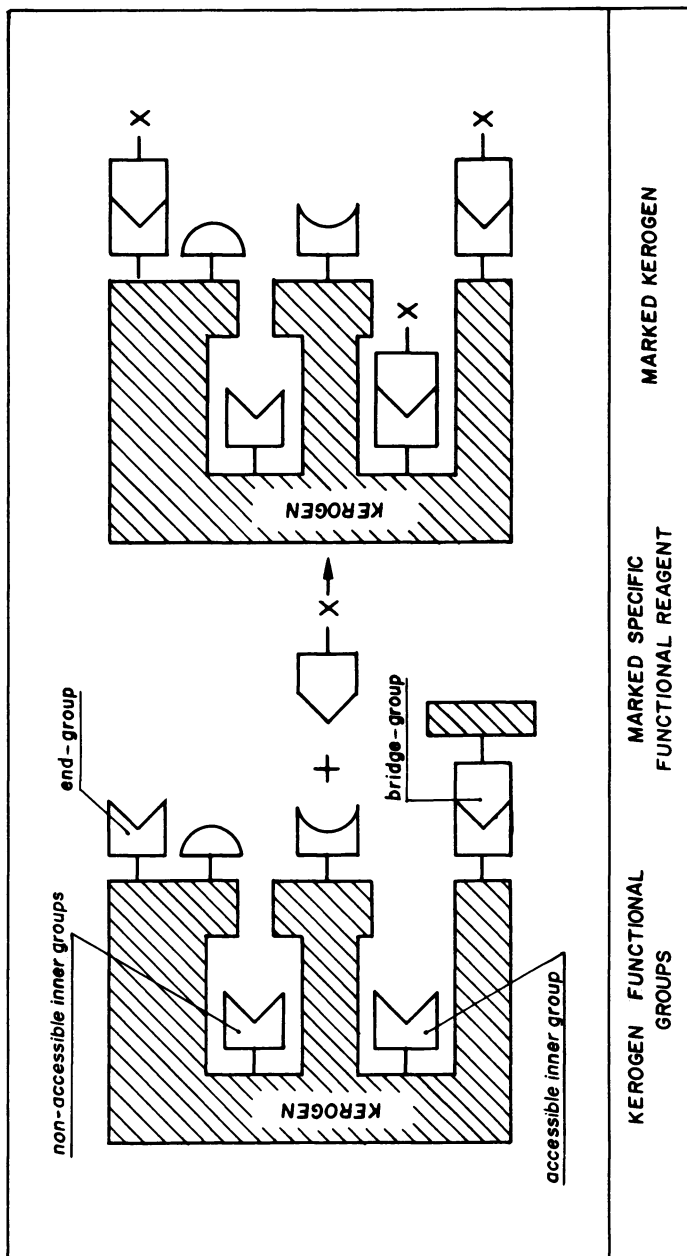It tries to show that it is expected that not all groups in kero-

Figure 5. Pictorial representation of the functional markers method.

gen may be reached by the specific functional reagent, so that the content of functional group in kerogen determined by this method should be taken as the minimum content.

This method was used to determine the content of various organic functional groups (amines, alcohols, phenols, aldehydes, ketones, carboxyl, insaturation, allylic/benzylic sites) in kerogens of Brazilian oil shales. The results (26) indicate the Tremembé Formation as being the most functionatized while Irati is the least. This is in accordance with the accepted trend that functionalizations correlates with maturity.

The use of marked functional reagents may also help on the morphological description of oil shales; by using a correct pair marker/method the physical location of groups or clusters of groups on the kerogen surface may be achieved. So, by using fluorescent markers/fluorescence microscope or markers containing a heavy metal/ion microprobe it may be possible to map the organic functional groups at the surface of kerogens.

As it was mentioned in the general definition of the objectives of the Geochemistry of oil shales the final goal in the study of the materia actuale is to determine its stereostructure. In this particular case, the Functional Marker Method may be of help in trying to locate relative positions of functional groups in microuniverses of the tridimensional network.

The method used most for the chemical characterization of kerogen involves oxidative degradation, achieved mainly thorough the permanganic oxidation (for a comprehensive discussion of the method see Vitorovic (30)). From this oxidation carboxylic acids are produced and, from these, the nature and length of the hydrocarbon chains of kerogens are defined. This method does not allow one to know the nature of the functional groups originally present in the kerogens.

A modified alkaline permanganate oxidation in which the kerogen has been previously treated by N-bromo succinimide has been applied to some Brazilian oil shales (31). The idea behind this modifications is to halogenate benzylic and allylic positions so that when this modified kerogen is treated with alkali a hydroxyl group is exchanged with the halogen making these positions easily oxidizable by the permanganate reagent. The results obtained by alkaline permanganate oxidation on both modified and unmodified Irati oil shale kerogen showed that almost twice as much carboxylic acids can be obtained from the modified kerogen. An increase in the relative amount of aromatic and dicarboxylic aliphatic acids was also observed.

Natural transformations of Oil Shales

Very little - not to say nothing - is known about the pathways followed by the materia prima in the process of being transformed into the materia actuale.

The lack of good formulations to describe the transformations

of the geolipids under geological conditions makes the task of writing a chapter on geochemical transformations of oil shales much more a proposition for the future than a record of known facts and proved theories.

Four are the main parameters involved in geochemical transformations of oil shales: temperature, pressure, time and stereostructure (in this respect one is mainly thinking of the relative position of the organic and inorganic phases and, consequently, on a possible catalytic role that the inorganic phase may play in the transformations of the organic matter).

Regarding Brazilian oil shales, there is no record in the literature about their stereostructure. The effect of pressure is not very strong since all Brazilian oil shales studied are not deep (< 150m) – at this depth pressure reaches values of approximately 30kgf/m^2. Brazilian oil shales vary in age – time is a most distinct variable in geochemical processes – from the Oligocene (Vale do Paraíba) to the Devonian (Curuá F.). Dating of these oil shales have been made entirely through paleontology (on fig. 3 it is presented the ages of the main oil shale Formations in Brazil).

Temperature is the main "driving force" of the geochemical processes to a point that a thermal alteration index (an indication of the maximum temperature the sample has reached) can be used to say if the organic matter is mature to produce oil or gas.

Maturation is, nevertheless, a product of the effect of all these parameters combined on the organic matter of oil shales. We shall give now the values of some of the indexes used to define maturation in respect to Brazilian oil shales.

Carbon Preference Index (32). This index, devised by Bray and Evans to be used as a maturity index decreases as the sediment increases maturation to a limit of one. Carvalhaes (28) showed that an Irati sample submitted to a maximum of 50°C in its thermal history, presented a CPI of 1.58 indicating it to be a reasonably mature sediment. Nooner & Oro (29) gave the values of 1.05 for this Formation.

The CPI determination as a stratigraphic function (33) in the Irati Formation led to the characterization of a most important phenomenum that occurred in this region, a diabase intrusion with important implications to organic geochemistry. In this stratigraphic column, the CPI varied from 1.07 at the bottom of the first layer (8.8m depth) to 1.21 at the bottom of the lower layer (21.4m depth). The completely anomalous behaviour of the CPI as a stratigraphic function in this column led to the characterization of the above mentioned heat effect caused by the diabase intrusion.

Thermal Alteration Index. This index, of a very empiric nature, tries to define the maximum temperature reached by the rock in terms of color and preservation of the sample (for more details see e.g. Correia (34)). The use of this index has been very useful in studies with the Irati F. to detect temperature effects due to the diabase intrusion. Used as a stratigraphic function in the column CERI-1 it was possible to detect a heat effect on the top of the lower

layer (105ºC) while most of the column was in the range 70-80ºC. The implications of this effect will be discussed later in this paper.

Pristane/Phytane Index. The data obtained for the stratigraphic column CERI-1 (33) say that the ratio pristane/phytane varies from 1.1 (at the top of the 1st layer) to 2.0 (2m below the previous point). It keeps approximately constant at 1.5 for the rest of the column. Carvalhaes (23) found the value 1.94 for a sample of the same formation. In all samples so far analysed from the Irati F. the ratio is greater than one.

Epimers Ratio Index. Chiral centers occur in the materia prima in one definite configuration. The degree of epimerization of these centers in the materia actuale have been interpreted as a measure of the degree of maturation of the sediments.

Patience et al. (35) discussed the racemization of the chiral centers of pristane from an Irati sample concluding that it is a mature sediment based on the 50:50 ratio formed for the stereoisomers RS and RR (or SS). The ratio of the $17\beta H, 21\beta H$ to $17\alpha H, 21\beta H$ isomers of hopanes have also been used as an index for the maturation of the organic matter (see e.g. Seifert & Moldowan (36)). Chicarelli (27) showed that for the Vale do Paraíba oil shale there is a clear predominance of the configuration $\beta\beta$ while for the Marau the ratio tends to one. This indicates that the Vale do Paraíba oil shale is rather immature and that the Marau one, although not very mature is, nevertheless, more than the Vale do Paraíba one. For the Irati F. there is a definite epimerization at the 17 and 21 position (35).

The functionality of an oil shale is generally related (inversely) to its maturation. One can see from the three Brazilian oil shales compared (26) in functional groups content that the Vale do Paraíba oil shale is the most functionalized corroborating the above results that say it to be the less mature. Although no numerical correlations have yet been established in this respect, one can antecipate that indexes can be derived to correlate maturation with the decaying of functional groups.

The diabase intrusion in the Irati Formation. A natural laboratory for the study of the influence of heat in geochemical reactions

Temperature is a fundamental parameter that definitely influences the maturation of sediments. This has been shown empiricaly and laboratory simulations use it as the "driving force" to induce maturation. In this way, the use of the thermal alteration index in geological materials allows one to qualify (37) source rocks as imature (temperature below 60ºC), mature (able to produce oil if the sediment reached temperatures of 60-150ºC) and senile - able to produce gas if the temperature surpassed 150ºC. It must be always kept in mind that these transformations occurred along millions of years, and, consequently, all tentatives to simulate these processes in laboratory suffer a severe criticism of their validity.

The study of effect of temperature on the maturation of the organic matter of sediments has been inferred mainly on the basis of the study of variations of the nature of the organic matter (CPI, for instance) with depth, in long stratigraphic columns. The temperature gradient considered corresponds to the geothermal gradient and the influence of deposition time and pressure are generally neglected.

The deposition time could, indeed, be neglected, if it is small compared to the age of the formation - it is practically so in thin (hundreds of meters) deposits - although it would not be the same with the pressure effect. In these thin deposits the variation in quality of the organic matter is not very well defined.

So, the data obtained from the study of long, "normal", stratigraphic columns are not very conclusive in respect to the influence of temperature as an isolated parameter since it, indeed, reflects the combined effects of temperature, pressure and time.

Fortunately, it is know that a hot diabase intrusion occurred at the Irati F. due to an intense volcanism that occurred southwest of Brazil during the Triassic (approximately 150 million year after Irati has been formed).

These intrusions were selective in the Irati F. that is, some regions were strongly hit, others were not and still others were only partially affected by the heat. It is obvious that the cases where the oil shale was totality hit by the molten rock nothing remained of the organic matter. The region where no intrusion occured is the best for oil shale exploration and can be used as a (geochemical) reference material. The partially hit region is the one that interests most for geochemical studies (and not so much to the exploration people since a good deal of the organic matter has been destroyed) since it is possible to define regions where a complete gradient of temperature - from a total carbonization level to a zero effect - can be found at a same stratigraphic level, that is, under the same pressure and time of formation. One can have then - in natural conditions - means to study the effect of temperature independently of the effects of pressure and time and check models designed to describe the effect of temperature in the geochemistry of oil shales.

The effect of this hot intrusion on an Irati stratigraphic column showed (33) that the carbon preference index and the ratio light/heavy n-alcanes could be correlated with data of thermal alteration index (paleotemperature) and the results interpreted as a temperature effect on C-C bond breakage. To these data it should be added that the values of a phenol index (a measure of the degree of aromatization) also determined (38) for this stratigraphic column (both for the bitumen and the kerogen) showed no correlation with the paleotemperatures. An explanation for this difference in behavior can be given based on different temperature breakpoints for different reactions - in this case the reactions are the aliphatic C-C bond breakage and the aromatization of chains containing an oxygen atom.

Phylogeny of Hydrocarbon Chains. An important chapter in the geochemistry of oil shales is the one dealing with the "genealogy" of the final products - the hydrocarbons. The results (28) of the phylogenetic study of the serie carboxylic acids → aldehydes → alcohols → hydrocarbons from the bitumen of a sample from the Irati F. showed no correlation between n-acids (C_n) (C_{11}-C_{35}) and n-hydrocarbons (C_{n-1}) (the linear correlation coefficient δ = 0,15). Between n-carboxylic acids (C_n) and normal carbonyl/hydroxy compounds (C_{n-1}) the value of δ was even lower (0.07) for the low molecular weight fraction (C_{11}-C_{20}), but reached a reasonable value of 0.71 for the fraction C_{23}-C_{35}. The correlation was also very poor for n-hydrocarbons (C_n) and normal carbonyl/hydroxyl (C_n) compounds. These results indicate that it was not possible to find any correlation among the hydrocarbon chains in the series carboxylic acid → carbonyl/hydroxy compounds → hydrocarbons in the bitumen of Irati oil shale. Nevertheless these results should not be taken as conclusive regarding the lack of any correlation between these chains, since the major part of the organic matter of the materia prima has been incorporated to kerogen.

Aldehydes as geochemical markers. One of the most important reactions in organic geochemistry is reduction (hydrogenation) where hydrocarbons (petroleum) are formed from oxygenated (mainly) substances. Reductions are endothermic reactions. So, any reaction path way model designed to explain reduction in the bulk of the sediment will have to deal with both the energy source and the energy transfer mechanism for these reactions. So far, no good models exist in either case.

The functional group aldehyde is a very reactive one. Aldehydes are strong reductants and, consequently, can only survive in strong reducing medium. This characteristic may promote the aldehyde group to an important geochemical marker since it can define the levels of oxi-reduction of the sediments and be used as reactions path indicators for reactions taking place in the bulk of the geological mass.

The aldehydes isolated from Irati F. belong to the series of benzaldehydes, naftaldehydes and phenylacetaldehydes. In respect to the ketones, aliphatic ketones, acetophenones, acetonaphtones, indanones and tetralones could be identified. What would be the geochemical meaning of the existence of these aldehydes and ketones found in the rock? Were these groups originally present in the materia prima and during all the diagenetic processes or were they produced in the diagenesis? If so, how were they produced in the sediment? What is the chemical environment for these compounds in the bulk of the material (stereostructure of the oil shale)?

Theoretical Organic Geochemistry

The characterization of the geochemical reactions are quite fundamentally distinct from those of the conventional chemistry:

The main trend of the geochemical reactions is toward reduction (de
functionalization) that is, they follow a path in a reductive   a-
xis. Their time scale is millions of years and most of these reac-
tions occur in solid phase. The reactions take place,   generally,
at high pressures, although temperatures very seldom surpass 150°C.
As a consequence of this set of conditions (and the proper   "rea-
gents") the main (final) product of these reactions are hydrocar-
bons. By the same reasons, the universe of laws that rule geochem-
istry is quite different from the ones that rule conventional chem
istry. We can think, indeed, that it is, as far from conventional
chemistry as this is, e.g., from excited state chemistry.

All tentatives to explain the mechanisms of geochemical trans-
formations have been made trying to paralel them to the   reactions
occurring in the laboratory, i.e. those of the "conventional" chem
istry: breakage of bonds leading to reactive intermediates as free
ions. Laboratory simulations have been used to "prove" the   sug-
gested processes and also the nature of possible precursors. How-
ever, these simulations can be questioned from the very begining:
in the laboratory simulations of geochemical reactions the   long
time effect of the natural process is substituted by a high tempe-
rature one in the laboratory. This point is critical in any discus
sion of the validity of the method of laboratory simulation. More-
over, the lack of care in reproducing the geometry of the   natural
system is very common, especially with regard to the relative posi
tions of the organic and inorganic phases. In this way the   data
obtained in most of the laboratory simulations may be very distant
from a reproduction of the natural processes, and thus loosing all
the validity as a simulation for geochemistry.

All these arguments lead us to consider that THEORETICAL SI-
MULATIONS are the ones most indicated to test models for geochem-
ical transformations.

Modeling may include tests on the steric arrangement of   com-
pounds in oil shales, a most difficult experimental feature to be
determined, or reproduced.

In theoretical simulation it is possible to use the   natural
parameters of the geochemical transformations as e.g. reaction time
(impossible to be reproduced in an experimental simulation)   and
consequently to really simulate the natural process.

The study of the mechanism of a reaction implies that we know
reagents and products and the conditions in which the reaction ta-
kes place. "Reagents" and reaction conditions are generally unknown
in geochemical processes. Nevertheless, one reaction is known   in
which part (at least) of the reagents is known: that is the epime-
rization of optically active centers in geolipids. It is reasonable
to consider that the chiral centers of the materia prima have the
same configuration as those of a known existing natural specie. This
is the case, e.g., of phytol from chlorophyl of the present   day
plants that can be taken as a base for the primordial configuration
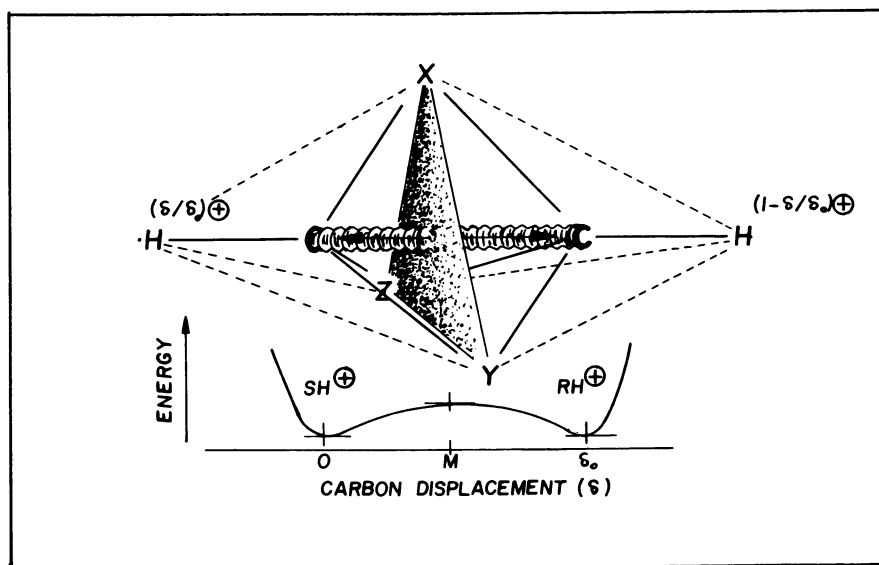of phytol and derivatives (phytane and pristane) found in sediments.

Figure 6. Schematic diagram for the epimerization model using the charge-assisted vibrational displacement mechanism.

The degree of epimerization of the hydrocarbon centers have been related to the degree of maturation of the organic matter of the sediment. Moreover any mechanism proposed to explain this reaction, must have in mind that it takes place in the bulk of the rock, i.e., in solid phase.

In 1981 Costa Neto proposed (2) the so called "charge assisted vibrational displacement mechanism" trying to respect all geochemical parameters for the particular reaction of epimerization of the chiral centers of hydrocarbons in sediments. In this model a "rigid" microuniverse composed of a protonic center (from the clay) and an optically active center of the geolipid would lead to the epimerization by displacement of one of the carbon atoms of the network (fig. 6) in a "vibrating lattice". Even the effect of pressure, particularly important in geochemical reactions but often neglected in laboratory simulations, could be taken into account through the influence of the distance between the associated proton (from the silicate matrix) and the chiral center. The "vibrating lattice" model may be equally useful for understanding the breakage of the C-C bonds and also of multiple atom transfer, particularly those in which the hydride ion transfer occur with consequent reduction of the acceptor structure.

An Information System for Brazilian Oil Shales

The literature on Brazilian oil shales is relatively small. From the 850 documents registered at the library of the Projeto Xistoquimica today, covering all areas related to oil shales, abstracts were produced which allowed, through a KWIC/KWOC format that a data base were developed for Brazilian oil shales.

This system contains, presently, four main files: one that arranges chromologically the references of all documents containing an abstract. A second relating historical facts regarding Brazilian oil shales; a third containing a geographical record of the places the oil shales were found; and the fourth, a substance index, in which all substances isolated from Brazilian oil shales are described. All these files are produced in three main indexes: a chronological, an author and a subject index.

These files combined produce the Information System for Brazilian Oil Shales. The details for this system were described by Costa Neto et al. (39).

Literature Cited

1. Costa Neto, C. Quim. Nova 1980, 3, 64-104.
2. Costa Neto, C. in "Advances in Organic Geochemistry", Bjorøy, M. Ed. Pergamon, London (in press).
3. Brasil. Ministério das Minas e Energia "Balanço Energético Nacional", MME, Brasília D.F., 1982; p.80.
4. Brasil. Departamento Nacional da Produção Mineral, Brasil, DNPM, Publ. Espec. 1970, 10, 1-111.

5. Brasil. Conselho Nacional do Petróleo, Atual. Cons. Nac. Petrol. 1974, 4, 70.
6. Mesquita, H.C. Rev. Admin. Pub. 1978, 12, 103-19.
7. Bruni, C.E.; Padula, V.T. An. Congr. Brasil. Geol. 1974, 28, 103-19.
8. Froes Abreu, S. "A situação do problema do xisto betuminoso no Brasil" 24p. (unpublished paper).
9. Campos, J.M. Eng. Mineração, Met. 1955, 22, 1941-2.
10. Tesch, N.A.; Moraes Filho, O.; Silva, P.E.L. "Projeto Maraui-to; prospecção de rochas oleígenas e barita". Secret. Minas e Energia Bahia, Salvador, 1976.
11. Bigarella, J.J. in "Simpósio sobre Ciência e Tecnologia do Xis to", Costa Neto, C. ed. Acad. Brasil. Cienc., Rio de Janeiro, 1975, p.1-79.
12. Moreira, H.B. in "Anais Simpósio sobre aproveitamento do xis-to", Acad. Cienc. Est. São Paulo, 1981; p.64-111.
13. Costa Neto, C.; Califfa, L.M.; Santos, E.T.G.; Montá, M.V.M.; Castro, C.M.A.; Calaza, N.M.; Rego, E.S. "Brazilian Oil Shale Analytical Bibliography", Projeto Xistoquímica - Univ. Fed. Rio de Janeiro, Rio de Janeiro, 1978 (in portuguese).
14. Costa Neto, C. "Perspectives for the utilization of oil shales in Brazil", Projeto Xistoquímica - Univ. Fed. Rio de Janeiro, Rio de Janeiro, 1978 (in portuguese).
15. Archer, T.C. Proc. Roy. Soc. Edimburgh 1865, 5, 364-5.
16. Treibs, A. Justus Liebigs Ann. Chem. 1935, 517, 172-96.
17. Campos, J.M. Eng. Mineração Met. 1952, 16, 417-21.
18. Costa Neto, C.; Nakayama, H.T.; Scofield, A.L.; Alencastro, R. B. An. Acad. Brasil. Cienc. 1977, 49, 127-38.
19. Costa Neto, C.; Cardoso, J.N.; Nakayama, H.T. An. Acad. Brasil. Cienc. 1969, 41, 367-73.
20. Keith, M.L.; Degens, E.T. in "Researches in Geochemistry", A-belson, P.H.Ed., J. Wiley, New York, 1959; p.38-61.
21. Lerman, A. Sedimentology 1966, 6, 267-86.
22. Costa Neto, C.; d'Avila, L.A.; Martin, P.S. An. Acad. Brasil. Cienc. 1983 (in press).
23. Costa Neto, C.; Costa Neto, A.; Nakayama, H.T.; Alencastro, R. B.; Andrade, J.M.V. An. Acad. Brasil. Cienc. 1969, 41, 357-66.
24. Costa Neto, C.; Pinto, R.C.P.; Maçaira, A.M.P. in "Oil Sand and Oil Shale Chemistry", Strausz, O.P.; Lowen, E.Eds. Verlag-Chemie, New York, 1978; p.345-58.
25. Feigl, F. "Spot Tests in Organic Analysis" 7th Ed. Elsevier, Amsterdam, 1966.
26. Costa Neto, C.; Maçaira, A.M.P.; Pinto, R.C.P.; Nakayama, H.T.; Cardoso, J.N. in "Advances in Organic Geochemistry", Maxwell, J.R., Douglas, A. Eds. Pergamon, London, 1980, p.249-63.
27. Chicarelli, M.I. M.Sc. Thesis, Univ. Fed. Rio de Janeiro (Bra-sil) 1982.
28. Carvalhaes, S.F. Ph.D. Thesis, Univ. Fed. Rio de Janeiro (Bra-sil) 1979.
29. Nooner, D.W.; Oro, J. in "Chemical evolution of the Early Pre-

cambrian", Ponamperuma, C.Ed., Academic, New York, 1977; p.69-79.

30. Vitorovic, D.K. in "Kerogen: Insoluble Organic Matter from Sedimentary Rocks", Durand, B. Ed., Technip, Paris, 1980. p.301-38.
31. Lachter, E.R. M.Sc. Thesis, Univ. Fed. Rio de Janeiro (Brasil) 1982.
32. Bray, C.E.; Evans, E.D. Geochem. Cosmochim. Acta 1961, 22, 2-15.
33. Costa Neto, C.; Furtado, E.G.; Concha, F.J.M.; Cardoso, J.N.; Quadros, L.P. Chem. Geol. 1978, 23, 1981-92.
34. Correia, M. Rev. Inst. Fr. Petrole 1969, 24, 1417-54.
35. Patience, R.L.; Rowland, S.J.; Maxwell, J.R. Geochim. Cosmochim. Acta 1978, 42, 1871-5.
36. Seifert, W.K.; Moldowan, J.M. Geochim. Cosmochim. Acta 1978, 42, 77-95.
37. Quadros, L.P. Bol. Tec. Petrobrás 1975, 18, 3-11.
38. Nakayama, H.T. Ph.D. Thesis, Univ. Fed. Rio de Janeiro (Brasil) 1980.
39. Costa Neto, C.; Califfa, L.M.; Santos, E.T.G.; Montá, M.V.M.; Castro, C.M.A.; Calaza, N.M.; Rego, E.S. An. Reunião Brasil. Cienc. Inf. 1979; p.514-64.
40. Youngblood, W.W.; Blumer, M. Geochim. Cosmochim. Acta 1975, 39, 1303-14.
41. Swanson, V.E. U.S. Geol. Surv. Prof. Papers, 1961 (356-C), 67-112.

Geolipids in Aleksinac Oil Shale

D. VITOROVIC and MIRJANA SABAN

University of Belgrade, Department of Chemistry, P.O. Box 550, 11001 Belgrade, Yugoslavia

This paper presents data on isolation and identifica-
tion of the following types of geolipids from the
Aleksinac oil shale, a Miocene lake sediment: n-al-
kanes, iso- and/or anteiso-alkanes, aliphatic iso-
prenoid alkanes, polycyclic isoprenoid alkanes, aro-
matic hydrocarbons, saturated unbranched, aliphatic
isoprenoid, hopanoic, and aromatic mono- and poly-
carboxylic acids, fatty acid methyl esters, aliphat-
ic γ- and δ-lactones, cyclic γ-lactones, aliphatic
methyl- and isoprenoid ketones, and the triterpenoid
ketone adiantone. Possible origin of the identified
compound classes is discussed, particularly of those
which had not been identified previously as geolipids.

The oil shale from Aleksinac (Yugoslavia) is a lacustrine
sediment of Miocene age. Both the soluble portion of the organic
matter, the bitumen, and the insoluble kerogen of this shale have
been studied extensively. In this paper isolation and identifica-
tion of various types of geolipids from the Aleksinac shale, car-
ried out in the last few years, will be reviewed. A thorough ex-
amination of the bitumen was expected to give additional data on
the origin of the organic matter and on the sedimentation condi-
tions and postburial changes, as well as to serve as a basis for
structural correlations between the bitumen constituents and the
kerogen.

Experimental Procedures

The shale sample contained 20.4% organic matter (1). It was
powdered to -100 mesh (Tyler). In most cases the bitumen was iso-
lated by 100 hr Soxhlet extraction either with benzene or with a
mixture of benzene and methanol (1:1).
　　Various schemes for isolation of different fractions and var-
ious separation techniques were used, such as the usual chemical

preparative method, chromatographic techniques, molecular sieving and clathration.

   Identifications were made by gas chromatography involving co-injection of internal standards, or by combinations of gas chromatography, mass spectrometry and computer processing.

Results and Discussion

   The yields of the benzene- and the benzene-methanol soluble bitumens were approximately 1% and 4%, respectively. The composition of the bitumens depended on the extraction procedure. Generally, the extracts consisted mainly of neutral components. One typical example is given in Table I (2).

Table I. Composition of the Aleksinac Shale Bitumens

Components	% of the Benzene Soluble Bitumen	% of the Benzene-Methanol Soluble Bitumen
Neutral	81.36	53.48
Acids	6.51	31.46
Phenols	7.28	8.18
Basic	0.21	0.17

n-Alkanes. The n-alkane fraction of the benzene soluble bitumen was found to consist of a C_{13}-C_{37} homologous series (Figure 1) with a predominance of the odd-carbon-numbered members in the C_{25}-C_{37} range (3). The Carbon Preference Index (CPI) was 1.46 and 1.75, for the n-alkanes from the benzene- and benzene-methanol soluble bitumens, respectively. The range of identified n-alkanes suggested a mixed origin of these hydrocarbons. The CPI values obtained for the n-alkanes, having at the same time in mind their possible mixed origin, may be interpreted as a sign of immaturity of the organic matter of Aleksinac oil shale.

   The differences found in the yields and compositions of the benzene- and the benzene-methanol soluble bitumens, as well as in the CPI values of the corresponding n-alkane fractions, suggest that standardization of bitumen extraction procedures is necessary if meaningful comparison of the composition of materials isolated from sediments of different ages and origins is to be made.

Branched Alkanes. 2,6,10,14-Tetramethyl-hexadecane (phytane) and 2,6,10,14-tetramethyl-pentadecane (pristane) were found in considerable amounts (3). The dominance of phytane over pristane was observed. Other aliphatic isoprenoid alkanes: C_{15} (2,6,10-trimethyl-dodecane, farnesane), C_{16} (2,6,10-trimethyl-tridecane), and C_{18} (2,6,10-trimethyl-pentadecane) were also identified (4). In the thiourea adduct of the branched-cyclic fraction, a homologous
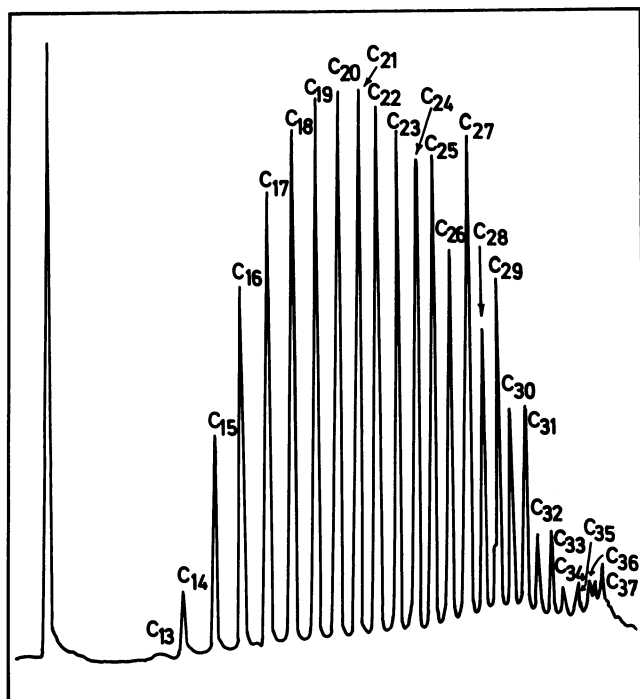
Figure 1. Chromatogram of the n-alkane fraction of the benzene soluble bitumen.

C_{18}–C_{28} series of _iso_- or _anteiso_-alkanes was suggested by gas
chromatography involving coinjection of five standards of _iso_-al-
kanes (_2,3_). Two nonidentified homologous series, containing 7 and
9 members, were also indicated in the thiourea adduct of the
branched-cyclic fraction by a diagram of log t_r (retention time)
VS number of C-atoms (_2_).

Cyclic Alkanes. In the cyclic fraction the following polycyclic
isoprenoid compounds were identified (_4_): C_{27}–C_{29} steranes,
methyl-C_{29} sterane, C_{27}–C_{32} pentacyclic triterpanes of hopane
type (except C_{28}), and the bicyclic tetraterpane perhydro-β-caro-
tane (Table II).

Table II. Isoprenoid Alkanes Found in the Aleksinac Shale Bitumen

Aliphatic	C_{15}	C_{16}	C_{18}	C_{19}	C_{20}	
Steranes	C_{27}	C_{28}	C_{28}	C_{29}	C_{29}	C_{29}
5 H	α	α+β	?	α	α	α
14 H	α+β	β	α+β	β	α+β	α
Triterpanes	C_{27}	C_{27}	C_{29}	C_{29}	C_{30}(4)*	C_{31}(3)* C_{32}
17 H	α	?	α	?	?	? α
Tetraterpane	C_{40}					

* Number of isomers

The mass spectrometric differentiation between various ste-
rane isomers was based on intensity ratios of fragmentation ions
m/z 151 and 149 (A/B rings) and intensity ratios of fragmentation
ions m/z 217 and 218 (C/D rings)(_5-7_). The identification of indi-
vidual triterpane stereoisomers was based on the known fact (_8_)
that in the mass spectra of isomers with all rings in _trans_ posi-
tions (biolipid isomers), fragmentation ion _m_ (m/z = 149, 177, 205
and 219 for C_{27}, C_{29}, C_{31} and C_{32}, respectively) is of a higher
intensity than the fragmentation ion _n_ (m/z = 191), while for the
17αH isomers the ratio _n/m_ is greater than 1.
       The finding of a number of C_{28} and C_{29} steranes in Aleksinac
shale bitumen is not surprising because it is known (_7,9_) that in
addition to relatively stable steranes having a configuration of
biological precursors, in ancient sediments thermodynamically more
stable isomers may be found. In the sterane gas chromatogram of
Aleksinac shale bitumen, three peaks contained a mixture of 14βH
and 14αH isomers (m/z 218/217 = 0.76-0.83), while two peaks con-
tained only 14βH isomers of C_{28} and C_{29} steranes (m/z 218/217 =
1.21 and 1.40, respectively). One 14βH isomer of both C_{28} and C_{29}
steranes had a shorter retention time than the 14αH isomer, which

agreed with earlier findings (7) that isomers having configura-
tions of precursor biolipid molecules do have the longest reten-
tion times. Except in one gas chromatographic peak, which con-
tained a mixture of 5αH and 5βH isomers, 5βH sterane isomers were
not identified. This may be easily explained by the fact that 5βH
isomers are more rarely found in biolipids than the 5αH isomers.
Moreover, 5αH isomers are thermodynamically more stable.

Only one methyl-sterane, $C_{30}H_{54}$, was identified. 4-Methyl-
steranes have been identified earlier in the Messel shale (10).

According to the results of GC-MS analysis, the triterpane
fraction consisted of two C_{27} and C_{29} isomers, four C_{30} isomers,
three C_{31} isomers, and one C_{32} isomer. Thermodynamically stable
17αH,21βH stereoisomers have been found in many crude oils and
ancient sediments (8,11,12) and therefore they could be called
geolipid triterpanes and may be used as diagenetic-maturation in-
dicators.

By the methods used it was not possible to determine the con-
figuration of the rings D/E for several triterpanes (C_{27}, C_{29},
C_{31}) because of the presence of other compounds in the same GC
peaks producing the same fragmentation ions.

Four isomers of the triterpane C_{30} suggested that in addition
to the less stable 17βH,21βH hopane isomer, and more stable 17αH,
21βH hopane and 17βH,21αH moretane, one more C_{30} pentacyclic tri-
terpane was present, such as lupane, whose mass spectrum did not
differ much from mass spectra of compounds of the hopane series.
However, for a more reliable identification of these four C_{30} tri-
terpanes a more efficient GC separation plus authentic compounds
for GC comparison would be necessary.

According to the identified tetraterpane, the Aleksinac shale
is more like the Eocene Green River shale, which also contained
perhydro-β-carotene (5,13), than like the Miocene Messel shale in
which acyclic lycopane has been identified (10). These differences
probably originate from different participation of various carot-
enoids in the biolipids whose remains were precipitated with the
sediments.

All identified compounds are known to be bitumen constituents
of other shales. However, the identified steranes confirm a high-
er plant origin of at least one part of the organic matter of
Aleksinac shale. On the other hand, a certain number of triter-
panes of the hopane type may have originated from lower procary-
otic organisms in which hopane oxygen compounds have been recently
identified (8). Procaryotic organisms may have taken part in early
diagenetic microbiological transformations of the sedimented or-
ganic matter.

The presence of thermodynamically stable stereoisomers of
steranes and triterpanes, nonspecific for biological molecules,
such as 14βH cholestane, ergostane and sitostane, 17αH,21βH nor-
hopane, trisnorhopane, and bishomohopane, suggests diagenetic and
maturational changes of the organic matter of Aleksinac shale.
was in the range of the members in the homologous series.

Aromatic Hydrocarbons. A few classes of aromatic hydrocarbons: C_nH_{2n-14} (biphenyls) and C_nH_{2n-18} (anthracenes and/or phenanthrenes) were isolated and identified in the 5% ether in petroleum ether eluate of the benzene soluble bitumen (14). The following compounds were identified: biphenyl, methyl-biphenyl (2 isomers), dimethyl- and trimethyl-biphenyl, anthracene, methyl-, dimethyl- and trimethyl-anthracene or phenanthrene. From the mass spectra, it was not possible to determine the position of the methyl groups in the substituted biphenyls, nor was it possible to decide whether the compounds of general formula C_nH_{2n-18} (with the exception of anthracene itself) had an anthracene or a phenanthrene nucleus.

The identified aromatic hydrocarbons are presumably products of maturational changes characteristic of most ancient sediments.

Acids. A review of various acids identified in the Aleksinac shale is given in Table III.

The organic acid components were isolated from the benzene- and the benzene-methanol soluble bitumens according to the usual chemical method (15). The yields of ether soluble acids were different, 7.55% and 20.75% of the bitumen, i.e., 0.10% and 0.95% of the shale, respectively. The range of identified acids differed as well. The benzene-methanol soluble bitumen contained a number of more polar acids which were not identified in the benzene soluble bitumen.

By chromatographic separation of the benzene soluble bitumen, followed by chemical separation of the methanol eluate, a fraction of weak acids was obtained. In this fraction, in addition to C_{11}-C_{24} saturated unbranched monocarboxylic acids, C_{11}-C_{21} saturated unbranched dicarboxylic acids, and C_{14} to C_{19} (except C_{17} and C_{18}) isoprenoid acids, three polycyclic acids of hopane type were identified in the form of their methyl esters (16): C_{31} (17βH,21βH), C_{32} (17αH,21βH), and C_{32} (17βH,21βH) hopanoic acids (Figure 2). Mass spectrometric determination of the configurations was based on relative intensities of fragmentation ions m/z 191 and 249 (or m/z 263)(17). Mass spectra of the corresponding methyl esters are shown in Figure 3.

Hopanoic acids have been found in many recent and ancient sediments (12,18). The polycyclic acids found in the bitumen of Aleksinac shale may have originated from bacterial hopanes (19), and may serve as evidence of bacterial or abiogenic oxidation processes occurring during diagenesis of organic matter in Aleksinac shale.

As already mentioned, isoprenoid acids were found only recently, in the same fraction of the weak acids in which hopanoic acids were identified.

From Table III it is obvious that similar types of aliphatic acids were found in the benzene soluble and the benzene-methanol soluble bitumens as well as in the extract of demineralized shale and in the kerogen hydrolysis product (20). The only difference

Table III. Acids Identified in the Aleksinac Oil Shale

Products Identified	Free Acids — Extracted		Bound Acids (20) — Extracted	
	as salts with water from raw and bitumen-free shale	with benzene or benzene-methanol from raw shale	from kerogen hydrolysis product	after removal of mineral portion
Aliphatic Acids				
Saturated unbranched				
Monocarboxylic	–	C_6–C_{24}	C_6–C_{33}	C_5–C_{32}
Dicarboxylic	C_6–C_{15}	C_7–C_{21}	C_3–C_{30}	C_3–C_{28}
Isoprenoid	–	C_{14}–C_{16}, C_{19}	–	–
Hopanoic Acids	–	C_{31}, C_{32} (2)*	–	–
Aromatic Acids				
Monocarboxylic	Benzoic	Benzoic	Benzoic	
		Me-benzoic (2)	Me-benzoic	
		di-Me-benzoic (4)		
		tri-Me-benzoic		
	Hydroxy-benzoic	Hydroxy-benzoic (2)		
	Me-hydroxy-benzoic			
	Methoxy-benzoic	Methoxy-benzoic		
		Naphthoic (2)		
	Me-naphthoic	Me-naphthoic		
Dicarboxylic	Benzene (2)	Benzene		
	Me-benzene	Me-benzene (2)		
	Hydroxy-benzene			
	Me-hydroxy-benzene			
	Naphthalene (4)	Naphthalene		
Tricarboxylic	Benzene (3)	Benzene		
	Naphthalene (4)			

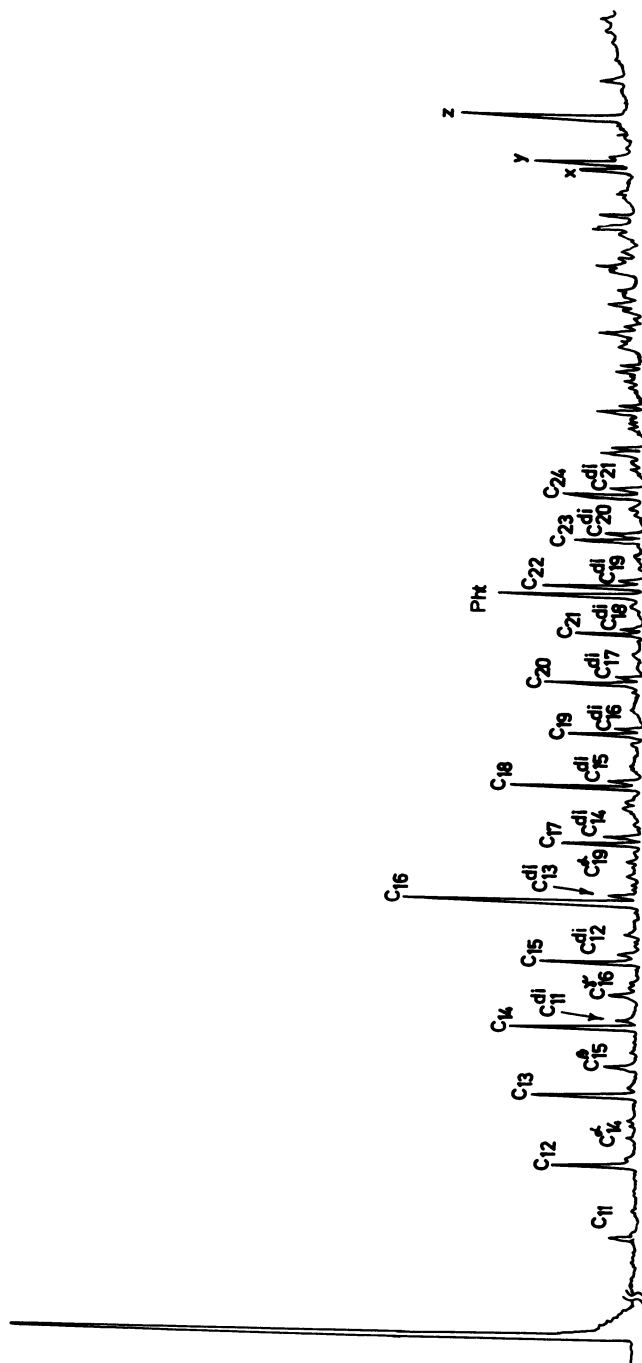* Numbers in parentheses indicate the number of isomers

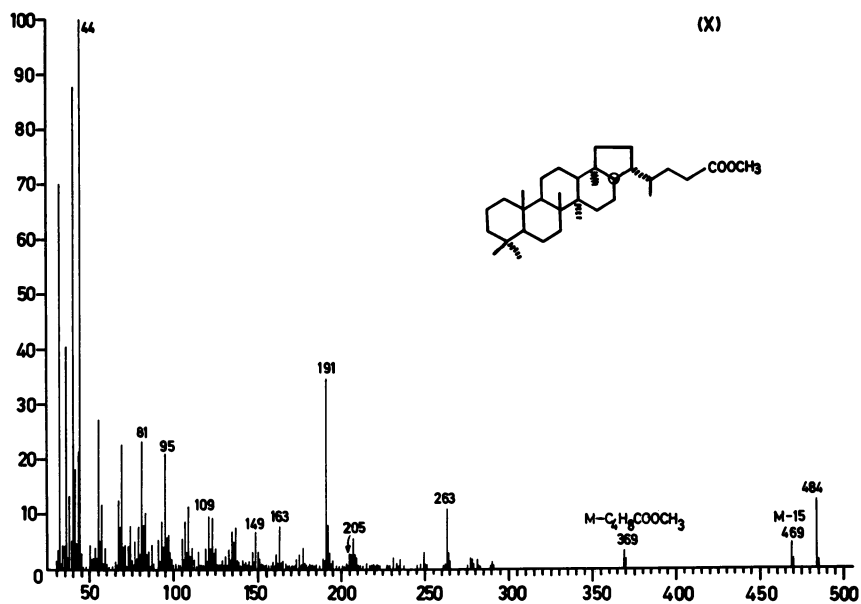*Figure 2. Gas chromatogram of the weak acids in the form of methyl esters.*

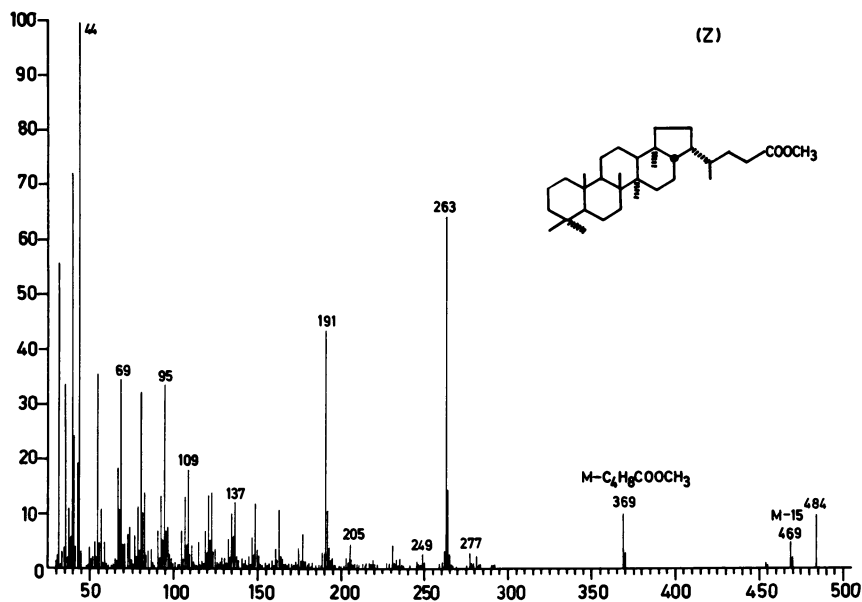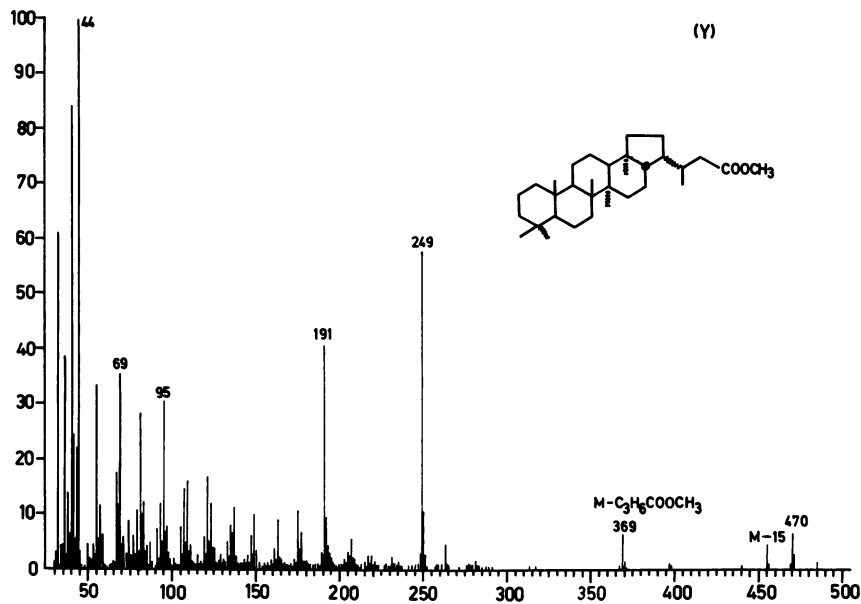*Figure 3a. Mass spectrum of peak X from the gas chromatogram of Figure 2.*

Figure 3b. Mass spectra of peaks Y and Z from the gas chromatogram of Figure 2.

The list of acids isolated from aqueous extracts of the shale is given for comparison. These acids were identified in the water extracts from raw Aleksinac shale as well as from bitumen-free shale, i.e., before and after the extraction of the bitumen (21). Mass spectrometric identifications of various isomers were based on comparison of the relative intensities of molecular ions and their corresponding base peak ions. The compounds extracted with water from the bitumen-free shale were very similar to the compounds isolated from the raw shale. The findings suggest that the acids were present as salts in both instances. In the aqueous extracts aromatic and dicarboxylic acids predominated, while aliphatic monocarboxylic acids were absent. Comparison of the chemical nature of water extractable acids with the acids obtained from the bitumen of the same shale showed a similarity in the type and range of aromatic and saturated unbranched dicarboxylic acids.

Fatty Acid Methyl Esters. In one of the eluates of the benzene soluble bitumen, obtained with 5% ether in petroleum ether, the presence of an oxygenated series $C_nH_{2n}O_2$ was indicated by high resolution mass spectrometry. This series was found to consist of C_4-C_{25} fatty acid methyl esters (except for C_9, C_{10} and C_{12}) (14). As far as we know, fatty acid methyl esters had not been found earlier as biolipids or geolipids. If their existence in various shale bitumens should be confirmed, their appearance could be explained either by diagenetic transformation of some precursor biological aliphatic molecules, or they might originate from biolipids so far unknown.

Aliphatic γ- and δ-Lactones. One of the most interesting findings in one of the first investigations of the acidic fraction of Aleksinac shale bitumen (15) was the identification of a homologous C_7-C_{15} series of γ-lactones (Figure 4). It was surprising to find in the acidic fraction a homologous series of components whose mass spectra had only one significant peak at m/z 85 (Figure 5).

The finding of γ-lactones in the bitumen of Aleksinac shale represented a novelty in geolipid chemistry and added a new structural type to the organic compounds found in geological specimens. However, the question was posed whether γ-lactones were indigenous to the organic matter of the shale, and appeared in the acidic fraction from the base hydrolysis and subsequent acidification, or perhaps were produced, also during the isolation procedure, from precursors such as the corresponding 4-hydroxy-acids or Δ-3 or Δ-4 unsaturated carboxylic acids.

Therefore, in an other experiment (22) the neutral fraction was isolated by a careful procedure (extraction of bitumen at room temperature and isolation of acids by weak alkali) to avoid the formation of γ-lactones during the Soxhlet extraction of the bitumen and the possible hydrolysis of γ-lactones. In this experiment
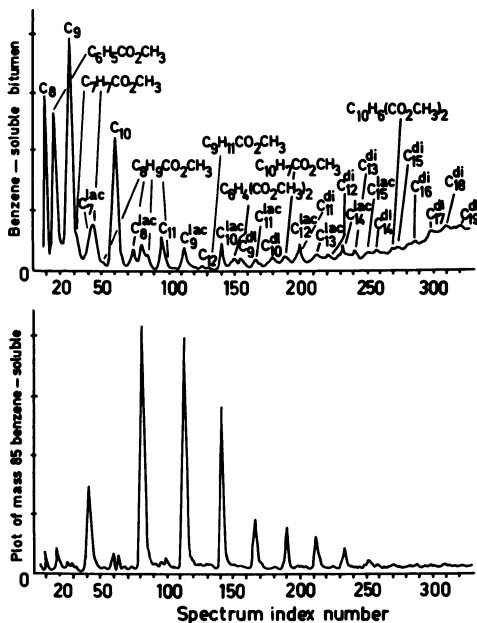
Figure 4. Total ionization plot and plot of mass 85 for the methylated acids from benzene soluble bitumen. (Reproduced with permission from Ref. 15. Copyright 1973, Pergamon Press Ltd.)
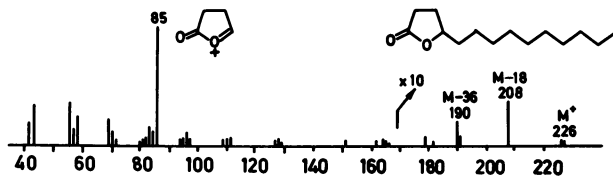

Figure 5. Mass spectrum recorded during the GC/MS analysis of the lactone mixture.

a series of saturated aliphatic γ-lactones was isolated (C_6-C_{16}) in relatively high yields, 0.41% and 0.34% relative to the benzene- and benzene-methanol soluble bitumen, respectively, proving that they were indigenous to the organic matter of the shale.

Gamma-lactones are quite prevalent in biolipids and in microbiological transformation products. Any of these may be the source of γ-lactones. Hydroxy-acids and unsaturated acids may also be the source of γ-lactones in Aleksinac shale. If γ-lactones were found to be typical for certain class of sediments, they might shed more light on the source of the organic matter of these sediments.

In addition to γ-lactones, δ-lactones have also been added to the organic compounds found in geological samples (23). Mass spectrometric identification of δ-lactones in the raw lactone fraction was based on the fragmentation ion m/z 99. However, they were present in very small quantities and their molecular ions in the mass spectra were not particularly pronounced so that it was not possible to establish with certainty which members of the four-member homologous series were present.

Cyclic γ-Lactones. In the preparative chromatographic work, aimed at isolation of aliphatic γ-lactones, it was shown that the Aleksinac shale bitumen, obtained by extraction at room temperature, contained components behaving similarly to γ-lactones, thus making their separation and purification difficult. These components were classified between the nonpolar hydrocarbons and the polar acids according to their polarity. In the raw lactone fraction, after a preparative thin-layer chromatography purification, two cyclic γ-lactones were identified, i.e., γ-lactones of 6-hydroxy-2,2,6-trimethyl-cyclohexylidene acetic acid (dihydroactinidiolide) and 6-hydroxy-2,2,6-trimethyl-cyclohexyl acetic acid (tetrahydroactinidiolide)(23). Figures 6 and 7 show the mass spectra obtained and the reference spectra of authentic compounds from the literature (24). To our knowledge, cyclic γ-lactones have not been reported as constituents of shale bitumens.

It may be supposed that cyclic γ-lactones were formed by lactonization of acids which might represent intermediates in a bacterial or abiogenic oxidation of carotenoids into naphthenic acids. Corresponding acids were isolated from a Californian petroleum and it was assumed that they were formed by oxidation of the β-ionone portion of β-carotene (25).

Since dihydro- and tetrahydroactinidiolides were isolated from bitumen obtained by extraction at room temperature, it is believed that they were indigenous to the shale organic matter, i.e. they were not produced during the isolation procedure from the corresponding acids.

Ketones. Several other compound types were identified in the polar fraction of Aleksinac shale bitumen. In addition to isoprenoid ketones C_{13} (6,10-dimethyl-undecan-2-one), and C_{18} (6,10,14-trimethyl-pentadecan-2-one)(14), which are not a novelty in the chem-
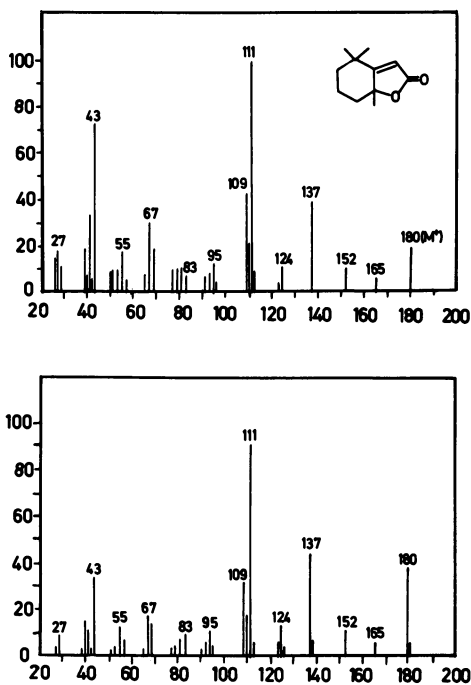
Figure 6. Mass spectrum of authentic dihydroactinidiolide (top) and mass spectrum recorded during the GC/MS analysis of the lactone mixture (bottom).
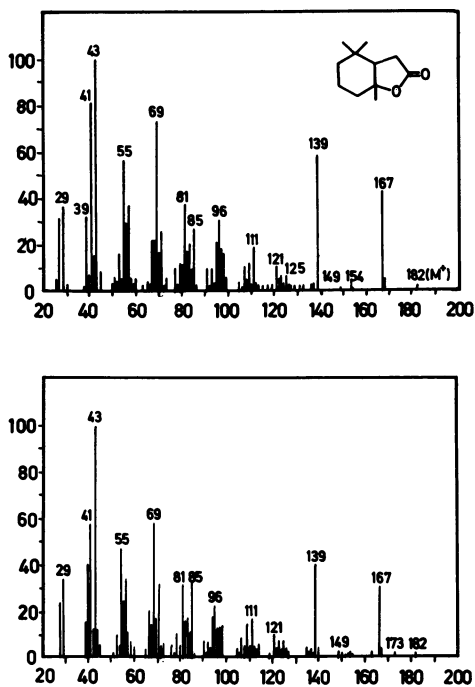
Figure 7. Mass spectrum of authentic tetrahydroactinidiolide (top) and mass spectrum recorded during the GC/MS analysis of the lactone mixture (bottom).

istry of geolipids, C_{13}-C_{24} aliphatic methyl ketones and the tri-
terpenoid ketone adiantone were also identified (14).

The finding of isoprenoid ketones and recently of a range of
isoprenoid acids in the Aleksinac shale bitumen was of interest
because isoprenoid acids had never been identified in the oxida-
tion products of the corresponding kerogen (26,27).

Aliphatic methyl ketones were detected in another of the elu-
ates of the benzene soluble bitumen, obtained with 10% ether in
petroleum ether. Figure 8 shows the total ionization plot of this
eluate (a) together with the mass chromatograms of m/z 43 and 58
(b and c, respectively). The fragmentation ion, m/z 58, is charac-
teristic of aliphatic methyl ketones, while the ion, m/z 43, may
have been derived from both $(COCH_3)^+$ and $(C_3H_7)^+$. Mass spectra
of the GC peaks x, y, and z are shown in Figure 9. Comparison of
the spectra x and y with literature data showed them to be iden-
tical to those of C_{13} and C_{18} isoprenoid ketones, respectively.
The mass spectrum z corresponded to that of n-octadecan-2-one.

As far as we know, aliphatic methyl ketones as such are un-
known as biolipid constituents. It may therefore be assumed that
the aliphatic methyl ketones found in the Aleksinac shale bitumen
are a product of microbiological oxidation of higher fatty acids
or alkanes. This assumption is supported by the fact that methyl
ketones have been found in soil and peat as well as in tobacco
leaves dried in air and sun for two years. The bitumen of Boux-
willer shale was found to contain higher members (C_{27}-C_{36}) of this
homologous series (18), indicating a different composition to that
of the Aleksinac shale fraction investigated.

Adiantone was identified in the same fraction with aliphatic
methyl ketones (Figure 8a). Figure 10 shows mass chromatograms of
the m/z 191 and 412 ions, and Figure 11 the mass spectrum of the
peak w, together with the mass spectrum of authentic adiantone
(18), for comparison. The intensity of fragmentation ion M-43 was
somewhat lower and that of m/z 205 somewhat higher for the compo-
nent found in Aleksinac shale bitumen than for the authentic ke-
tone. Since adiantone, a hopane derivative, may be expected in the
form of three isomers (17βH,21βH; 17αH,21βH; 17βH,21αH), the above
mentioned differences in the mass spectra may be a result of con-
figurational differences at carbon atoms 17 and 21. Figures 10 and
11 indicated that in addition to the most abundant isomer the mix-
ture contained two more isomers.

The triterpenoid ketone adiantone represents an intact bio-
logical indicator, which at the same time confirms that one part
of the organic matter of Aleksinac shale originates from ferns.
Adiantone is also a known constituent of Bouxwiller shale (18).

Physiological Activity of Aleksinac Shale Constituents. Quite re-
cently, physiological activity of the polar constituents of Alek-
sinac shale bitumen, extracted with an azeotropic mixture of chlo-
roform, acetone and methanol, was investigated (28). This prelimi-
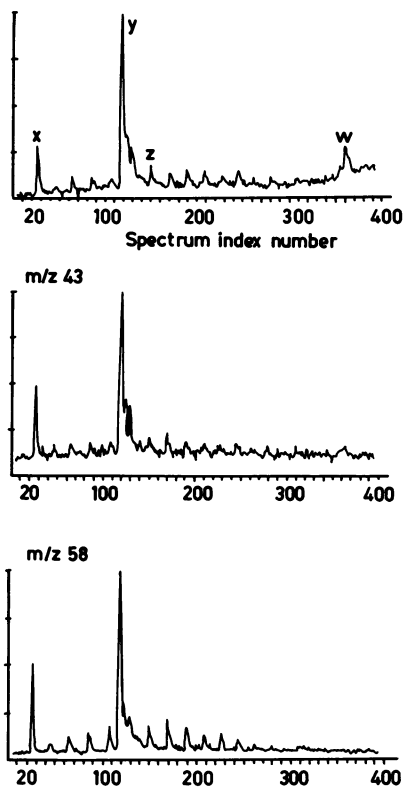nary study was based on an assumption that some of the biological

Figure 8.   Total ionization plot of a polar fraction (top) and plot of mass m/z *43 (middle) and* m/z *58 (bottom). (Reproduced with permission from Ref. 14. Copyright 1979, Pergamon Press Ltd.)*
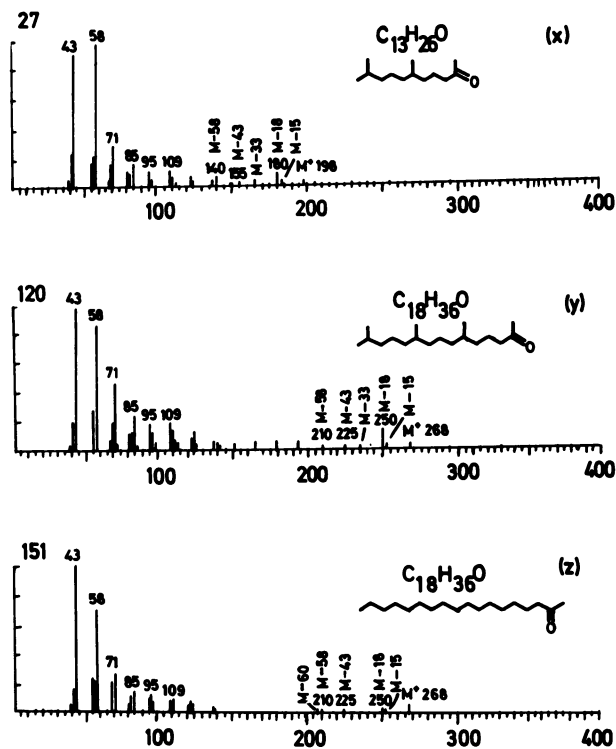
Figure 9. Mass spectra of peaks x, y, and z, obtained by GC/MS analysis of the polar fraction (see Figure 8). (Reproduced with permission from Ref. 14. Copyright 1979, Pergamon Press Ltd.)
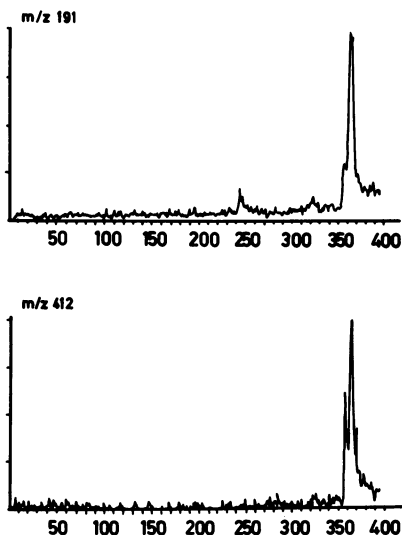
m/z 191

m/z 412

Figure 10. Plot of mass m/z *191 (top) and mass* m/z *412 (bottom), obtained by GC/MS analysis of the polar fraction (see Figure 8). (Reproduced with permission from Ref. 14. Copyright 1980, Pergamon Press Ltd.)*
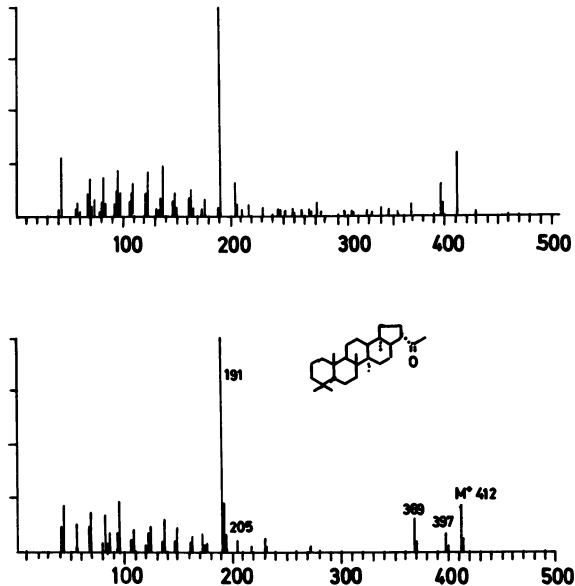
191

205

389   397   M° 412

Figure 11. Mass spectrum of peak w, obtained by GC/MS analysis of the polar fraction (top) (see Figure 8); and mass spectrum of adiantone (bottom) (18). (Reproduced with permission from Ref. 14. Copyright 1980, Pergamon Press Ltd.)

indicators, which were identified in the bitumen of Aleksinac
shale, might have retained their physiological activity in the
same way as they kept chemical structural features. Moreover, the
fact is known that distillation products of some ancient sediments
do have therapeutic effect and hence are used in medicine and vet-
erinary practice.

Preliminary experiments involved tests with a selection of
the main classes of microorganisms. The polar fraction of Aleksi-
nac shale bitumen was fractionated into a number of subfractions,
using column chromatography, controlled with IR analysis of the
eluates. By recombination of the 215 eluates according to struc-
tural similarity, 22 fractions were obtained for testing of phys-
iological activity.

Most of these fractions showed antibiotic effect on bacteria
E. coli and *S. aureus*, as well as on actinomyces *S. griseus*. The
exception was one fraction which gave a negative antibiogram test
with all three microorganisms. Several fractions showed antibiotic
effect on only one of the three microorganisms (four fractions on
S. aureus; three fractions on *S. griseus*). None of the tested
fractions showed antibiotic effect on the following species: *Acti-
nomyces* sp. 468, the yeasts *S. cerevisiae* and *Candida albicans* as
well as the mold *Penicillium notatum*.

The tested fractions did not show bacteriostatic effect.

Fractions which contained predominantly phenols did not have
a more pronounced antibiotic effect, particularly towards *E. coli*
and *S. griseus*, than the rest of the fractions composed of mix-
tures of aliphatic and aromatic compounds.

Conclusions

Most of the geolipids so far identified in the oil shale from
Aleksinac represent well known and ubiquitous constituents of sed-
iments: n-alkanes, iso- and anteiso-alkanes, aliphatic and cyclic
isoprenoid alkanes including steranes, triterpanes and tetrater-
panes, aromatic hydrocarbons, and aliphatic, hopanoic and aromatic
acids. Moreover, several classes of compounds were identified
which were also known as constituents of some ancient sediments
but were not found to be ubiquitous, such as aliphatic isoprenoid
ketones, aliphatic methyl ketones and the triterpenoid ketone adi-
antone.

However, in the Aleksinac shale bitumen geolipid constituents
were identified which had not been found earlier in ancient sedi-
ments: a homologous C_6-C_{16} series of aliphatic γ-lactones, a ho-
mologous series of four members of δ-lactones, two cyclic γ-lac-
tones (dihydro- and tetrahydroactinidiolide), as well as a homol-
ogous series of methyl esters of fatty acids (C_4-C_{25}).

The composition and distribution of identified geolipids sug-
gest: (a) that the Aleksinac oil shale is a relatively immature
sediment (high content of oxygen compounds with unchanged biolipid
molecules, n-alkane CPI values between 1.5 and 2.0, predominance

of phytane over pristane, relatively high amount of unstable ste-
reoisomers in the fraction of steranes and triterpanes), although
indications were observed of maturational changes (the presence of
thermodynamically stable stereoisomers of steranes and triterpanes
and hopanoic acid, nonspecific for biological molecules, and aro-
matic hydrocarbons); and (b) that the organic matter of Aleksinac
shale is of mixed origin; the following precursors of the organic
substance were incorporated in this lacustrine sediment: residues
of terrestrial plants, ferns and algae, as well as residues of
microorganisms, most probably of those which took part in early
diagenetic changes of sedimented organic matter.

Acknowledgments

Literature Cited

1. Jovanovic, S. Lj.; Vitorovic, D. Bull. Soc. chim. Beograd
   1952, 17, 347-60.
2. Saban, M. Ph.D. Thesis, University of Beograd, Beograd, 1975.
3. Vitorovic, D.; Saban, M. J. Chromatogr. 1972, 65, 147-54.
4. Saban, M.; Tesic, Z.; Vitorovic, D. Bull. Soc. chim. Beograd
   1983, in press.
5. Gallegos, E.J. Anal. Chem. 1971, 43, 1151-60.
6. Mulheirn, L.J.; Ryback, G. in ADVANCES IN ORGANIC GEOCHEMISTRY
   1975, Campos, R.; Goni, J., Eds.; ENADISMA: Madrid, 1977;
   p. 173.
7. Petrov, A.A.; Pustil'nikova, S.D.; Abryutina, N.N.; Kagramano-
   va, G.R. Neftekhimiya 1976, 16, 411-27.
8. Ensminger, A.; Van Dorsselaer, A.; Spyckerelle, C.;Albrecht,
   P.; Ourisson, G. in ADVANCES IN ORGANIC GEOCHEMISTRY 1973,
   Tissot, B.; Bienner, F., Eds.; Technip:Paris, 1974; p. 245.
9. Mulheirn, L.J.; Ryback, G. J. Chem. Soc. Chem. Commun. 1974,
   No. 21, 886-7.
10. Kimble, B.J.; Maxwell, J.R.; Philp, R.P.; Eglinton, G.; Al-
    brecht, P.; Ensminger, A.; Arpino, P.;Ourisson, G. Geochim.
    Cosmochim. Acta 1974, 38, 1165-81.
11. Ensminger, A.; Albrecht, P.; Ourisson, G.;Tissot, B. in AD-
    VANCES IN ORGANIC GEOCHEMISTRY 1975, Campos, R.; Goni, J.,
    Eds.; ENADISMA: Madrid, 1977; p. 45.
12. Van Dorsselaer, A.; Ensminger, A.; Spyckerelle, C.;Dastillung
    M.; Sieskind, O.; Arpino, P.; Albrecht, P.; Ourisson, G.;
    Brooks, P.W.; Gaskell, S.J.; Kimble, B.J.; Philp, R.P.; Max-
    well, J.R.; Eglinton, G. Tetrahedon Letters 1974, No. 14,
    1349-52.
13. Murphy, M.T.J.; McCormick, A.; Eglinton, G. Science 1967, 157,
    1040-2.
14. Saban, M.; Porter, S.; Costello, C.; Djuricic, M.; Vitorovic,

D. in ADVANCES IN ORGANIC GEOCHEMISTRY 1979, Douglas, A.G.; Maxwell, J.R., Eds.; Pergamon: Oxford, 1980; p. 559.

15. Hertz, H.; Andresen, B.D.; Djuricic, M.V.; Biemann, K.; Saban, M.; Vitorovic, D. Geochim. Cosmochim. Acta 1973, 37, 1687-95.
16. Sljivar, S.; Saban, M.; Ambles, A.; Vitorovic, D. unpublished data.
17. Seifert, W.K.; Moldowan, J.M. in ADVANCES IN ORGANIC GEOCHEM-ISTRY 1979, Douglas, A.G.; Maxwell, J.R., Eds.; Pergamon: Oxford, 1980; p. 229.
18. Arpino, P. Ph.D. Thesis, University of Strasbourg, Strasbourg, 1973.
19. Foerster, H.J.; Biemann, K.; Haigh, W.G.; Tattrie, N.H.; Colvin, J.R. Biochem. J. 1973, 135, 133-43.
20. Saban, M.; Vitorovic, D. unpublished data.
21. Jovanovic, L.J.; Djuricic, M.V.; Vitorovic, D.; Andresen, B.D.; Biemann, K. Bull. Soc. chim. Beograd 1979, 44, 605-13.
22. Saban, M.; Vitorovic, D. in ADVANCES IN ORGANIC GEOCHEMISTRY 1975, Campos, R.; Goni, J., Eds.; ENADISMA: Madrid, 1977; p. 209.
23. Saban, M.; Jeremic, D.; Vitorovic, D. Bull. de l'Academie serbe des sciences et des arts 1983, in press.
24. Chen, P.; Kuhn, W.F.; Will, F.; Ikeda, R.M. Org. Mass Spectrom. 1970, 3, 199-209.
25. Seifert, W.K. in PROGRESS IN THE CHEMISTRY OF ORGANIC NATURAL PRODUCTS 32, Hertz, W.; Griesebach, H.; Kirby, G.W., Eds.; Springer: Vienna, 1975; p. 1.
26. Djuricic, M.V.; Vitorovic, D.; Andresen, B.D.; Hertz, H.S.; Murphy, R.C.; Preti, G.; Biemann, K. in ADVANCES IN ORGANIC GEOCHEMISTRY 1971, v. Gaertner, H.R.; Wehner, H., Eds.; Pergamon: Oxford, 1972; p. 305.
27. Vitorovic, D.; Djuricic, M.V.; Ilic, B. in ADVANCES IN ORGANIC GEOCHEMISTRY 1973, Tissot, B.; Bienner, F., Eds.; Technip: Paris, 1974; p. 179.
28. Saban, M.; Vrvic, M.M.; Vucetic, J.; Vitorovic, D. Microbiology, Beograd 1983, in press.

RECEIVED April 7, 1983

Comparative Organic Geochemistry of Some European Oil Shales

A. G. DOUGLAS and P. B. HALL [1]

The University, Newcastle upon Tyne, Organic Geochemistry Unit, Department of Geology, NE1 7RU England

H. SOLLI

Continental Shelf Institute, Hakon Magnussons gt.1B, 7001 Trondheim, Norway

A number of European oil shales, ranging from Cambrian to Upper Jurassic in age, have been analysed by organic geochemical and petrological methods. Microscopical analyses of the whole rocks provided information on the nature of the organic material present and this was augmented by spore fluorescence data: the rank of the material was deduced from vitrinite reflectance measurements. The oil shales were retorted to give oil yields, and the shale oils were analysed chromatographically to give gas chromatographic fingerprints. Bitumens were also extracted from the unretorted shales and analysed for their content of aliphatic, aromatic and polar compounds: some of these fractions were analysed by gas chromatography and gas chromatography-mass spectrometry. Kerogens were isolated from some of the shales and used for pyrolysis GC and pyrolysis-GC-MS studies which provided comparative data by way of fingerprints, selected ion chromatograms and a type index for the different kerogens.

Scientific and industrial interest in oil shales has had a chequered history since, in 1694, Martin Eale was awarded a patent for the production of "oyle from a kind of stone". The production of shale oil in the 19th century became less economic when cheap crude oil reached a widening market and, with the exception of a few countries worldwide, the oil shale industry was essentially run down early this century. The energy crisis of the early 1970's reawakened a wide interest in the possible economic production of shale oil, but the current downturn in energy consumption, with a concomitant drop in crude oil prices

[1] Current address: Continental Shelf Institute, Hakon Magnussons gt.1B, 7001 Trondheim, Norway.

today approaching 2/3 of their maximum ever cost, will surely
affect at least short term interest in the production of oil
from oil shale. These vagaries have affected shale oil research
in the recent past, as governments viewed funding in the light
of changing needs. Despite this, there is a need for a longer
term view, to which organic geochemical data on European oil
shales could appropriately contribute.

    Although there are overviews on the genesis of bituminous
rock sequences in Western Europe (1, 2), they deal primarily
with lithologies and depositional environments and provide very
little data on the contained organic material. Older reviews
do include some information on the organic content of a number
of European deposits, but take mainly an economic and
technical approach (3, 4). Modern organic geochemical methods
have been used to investigate a number of European deposits in
greater detail: these include the Toarcian deposits of the
Paris Basin (5, 6), Messel Oil Shale (7), Aleksinac Shale (8),
and the Kimmeridge clays (9). However, the need for an
organic geochemical overview of a wider range of European oil
shales seemed to be opportune, and this paper provides some
information abstracted from a larger volume of data (10)
concerned with the analyses of eighty samples of nineteen
West European bituminous shale deposits. In this report, some
basic organic geochemical information is presented for
twenty-four samples that were selected as representing marine,
non-marine and transitional environments: more detailed
information is provided for a few of the samples.

Samples

    The shales investigated ranged in age from Cambrian to
Oligocene, and their locations are shown on the accompanying
map (Figure 1). Brief details of location, lithology,
mineralogy, environment, basin type etc. for the twenty-four
samples under discussion are provided in Table I which
indicates that they encompass marine to non-marine depositional
environments and include small lake basins associated with
coal-forming swamps as noted by Duncan (11).

Microscopy

    All samples were examined petrographically, using reflected
light methods, after being mounted as small, randomly-oriented
fragments in Bakelite blocks, then polished to a high finish.
Vitrinite reflectance measurements (10-50 per sample) were made
for samples younger than Devonian; values are shown in
Table II. The polished blocks were also used for maceral
analyses, reported on a volume percentage basis, by measuring
500-1000 points in white light. As noted in Table III pyrite,
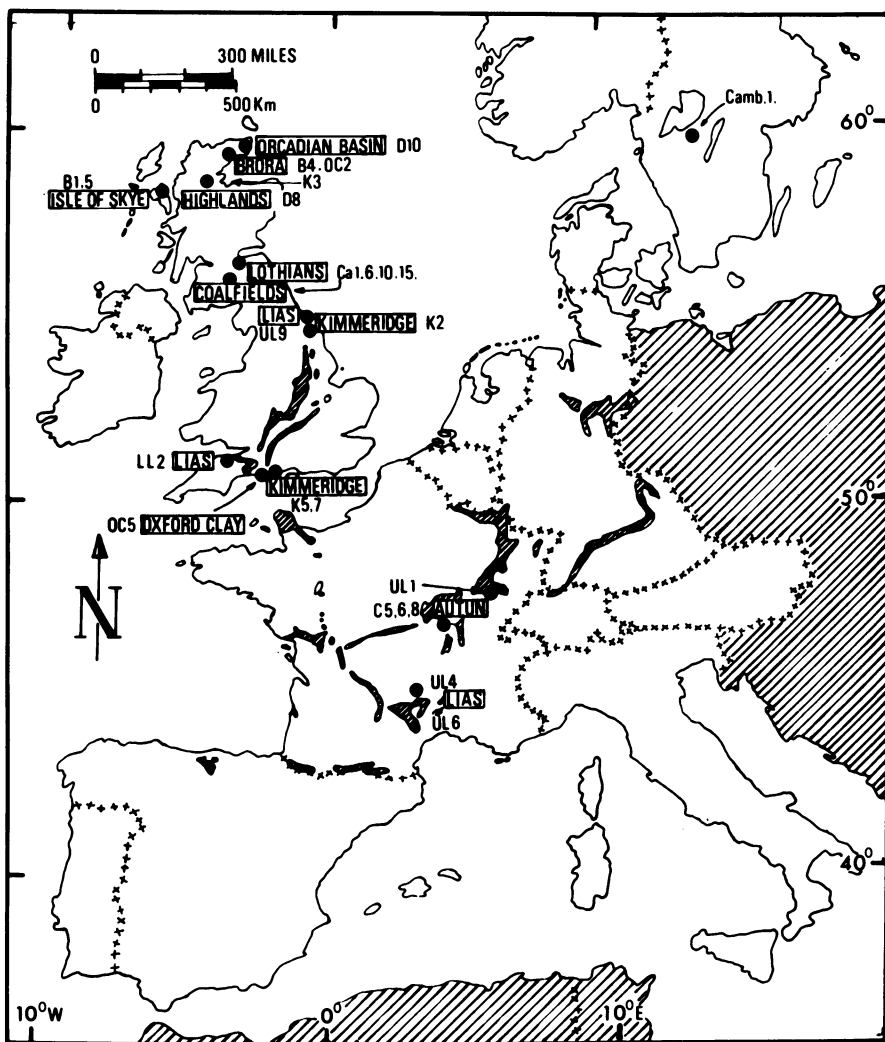which was often present as framboids or small crystals, was

Figure 1. Map of sample locations.

TABLE 1   SAMPLE DETAILS

AGE	CODE	LOCATION	LITHOLOGY	MINERALOGY	ENVIRONMENT	BASIN TYPE	ORGANIC PRECURSOR	MACRO-FOSSILS
Kimmeridge	K2, K5, K7 K3	England Scotland	Calcareous Shales	Pyrite, Clays & Calcite	Marine	Shelf margin Epicontinental	Algae & Higher Plants	Ammonites
Oxfordian Callovian	OC2 OC5	Scotland England	Silty clay Shale	Pyrite, Clays Pyrite	Marine	Epicontinental	Algae & Higher Plants	Ammonites & Reptiles
Bathonian	B1 B4, B5	Scotland	Calc. shale Shale	Pyrite, Calcite, Dolomite Pyrite	Transitional Fresh-Brackish	Deltaic-Lagoonal		Crustaceans
Toarcian	UL1, UL4, UL6 UL9	France England	Calcareous shales	Pyrite, Clays & Calcite	Marine	Epicontinental	Tasmanites & Pollen	Ammonites & Bivalves
Hettangian	LL2	England	Calcareous shales	Pyrite, Clays Calcite	Marine	Epicontinental	Tasmanites Pollen	Ammonites
Permian-Autunian	C5, C6, C8	France	Shales	Pyrite, Clays	Non-marine Freshwater	Continental Lacustrine	Botryococcus Higher Plants	Fish Ostracods
Carboniferous	Ca1, Ca6, Ca15 Ca10	Scotland	Shales	Pyrite & Clays	Non-Marine Brackish Non-Marine Freshwater	Deltaic-Lagoonal Lagoonal	Botryococcus & Higher Plants	Ostracods & Fish
Devonian	D8, D10	Scotland	Calcareous shales	Calcite, Clays Pyrite	Non-marine Fresh-Brackish	Continental Lacustrine	Algae, spores	Fish
Cambrian	Camb 1	Sweden	Shale	Clays, Pyrite	Marine	Epicontinental	Algae	

TABLE II RELFECTANCE AND FLUORESCENCE DATA

R_o	Sample Number	$\%R_{oil}$	Spore Fluoresc.
0.4%	K3 Ethie Haven K7 Ringstead Ca10 Westfield Ca15 Camps	0.4 0.35 0,38 0.39	
0.5%	K5 Kimmeridge OC2 Brora OC5 East Fleet B4 Brora UL1 Crevenay C5,6,8 Autun	0.44,0.48 0.45 0.41 0.46,0.43 0.47 0.36-0.46	Y Y Y Y Y Y
0,6%	K2 Marton B1,5 Skye UL4 Severac LL2 Kilve Ca1 Lothians	0.50,0.54 0.52,0.52 0.51 0.52 0.55-0,59	Y/O Y/O Y/B/G Y/B/G
0.7%	UL6 Ste. Affrique Ca6 Lothians D10 N.E. Scot. UL9 Whitby	0.63 0.57-0.59 - 0.57	L/O L/O Y/B/Y/G Y/B/Y/G
0.7%+	B2 Skye D8 N.E. Scot. Camb 1 Sweden	- - -	No fluoresc.

Y = Yellow; Y/O = Yellow/Orange; L/O = Light Orange;

Y/B/G = Yellow/Brown Groundmass;

Y/B/Y/G = Yellow/Brown/Yellow/Groundmass

TABLE III MINERAL AND MACERAL ANALYSES

Sample No.	Calcite %	Mineral Losses %	Free Sulphur mgs/100g rock	Amorph. OM plus inorg. minerals	Vitrinite %	Inertinite %	Sporinite %	Botryococcus %	Pyrite %
Cambl	-	-	-	-	-	-	-	-	-
D8	11.3	14.5	-	-	-	-	-	-	-
D10	41.5	44.2	-	-	-	-	-	-	-
Ca1	-	43.5	-	82.3	0.3	1.8	0.1	12.9	2.6
Ca6	-	42.7	-	94.0	0.3	1.3	0.4	2.2	1.8
Ca10	5.0	7.2	-	42.5	1.2	0.7	0.8	51.7	3.1
Ca15	-	2.5	-	95.5	0.1	1.5	0.1	1.2	1.6
C5	-	6.0	-	88.9	1.1	2.0	2.7	3.5	1.8
C6	-	7.3	34	87.4	1.3	1.3	1.9	6.2	1.9
C8	-	6.1	-	87.7	1.1	1.6	3.1	2.8	3.8
LL2	20.8	28.5	-	-	-	-	-	-	+
UL1	35.0	43.6	-	91.7	0.1	0.3	6.1	-	1.8
UL4	42.0	52.5	5	-	-	-	-	-	-
UL6	40.5	56.7	-	-	-	-	-	-	-
UL9	3.1	12.4	-	88.8	0.1	0.3	5.0	-	5.8
B1	27.5	32.7	-	-	-	-	-	-	-
B4	-	7.6	6	-	-	-	-	-	-
B5	-	-	-	-	-	-	-	-	-
OC2	-	7.7	57	-	-	-	-	-	-
OC5	-	5.4	12	-	-	-	-	-	-
K2	10.8	11.7	-	-	-	-	-	-	-
K3	13.3	20.9	10	-	-	-	-	-	-
K5	14.0	17.0	-	81.1	0.3	0.9	10.2	-	7.5
K7	10.2	18.4	-	86.1	0.2	0.7	9.6	-	4.4

also included in the point count. Recognisable <u>Botryococcus</u>
remains are tabulated separately from sporinite (taken to include
spores and all other algal material); amorphous organic matter
in a background of inorganic minerals is also shown (Table III).
     These blocks were also examined for fluorescence using
blue light excitation and the fluorescence colours of the
organic material are shown in Table II. Both reflectance values
and spore fluorescence indicate that the rank of most of the
samples was within a window of about R_o 0.4 - 0.63%
(equivalent). Samples Camb 1 and D8 did not fluoresce, and
sample D10 produced a mid/deep orange fluorescence.

Geochemical Analysis

     Wherever possible 100g samples of the powdered rock were
exhaustively extracted with dichloromethane. The extracted
bitumen was stored for further analysis and the dried rock
powder was used to estimate the organic carbon remaining
(Table IV); during this step advantage was taken of measuring
the mineral carbonate content, reported as mineral losses, of
some of the rocks (hot 50% hydrochloric acid). The calcite
content was also measured in a calcimiter using cold, dilute
hydrochloric acid (12). Thus approximate values for calcium
carbonate and other mineral carbonates were obtained (Table III).
During the analyses of the extracted bitumen, an approximate
value was obtained for free sulphur in the bitumen by taking
weight differences before and after silver ion thin layer
chromatography (TLC). These data are reported also in Table III.
     Analyses of the oil shales for the yield and composition
of shale oil they provided on pyrolysis was undertaken. This
series of experiments was not intended to give an economic
assessment of the shale oil potential, which could only have
been achieved by thorough vertical and lateral sampling of the
deposits, instead the values obtained relate to the hand
specimens only. The most frequently used method of determining
oil yield is by Fischer Assay (13) and in this work a
modification of their method using a smaller version of their
retort (5-10g of sample) was attempted. By programming the
furnace from ambient temperature to 500°C in 45 min and soaking
for 15 min at 500°C, a small amount of oil and water was
collected and measured carefully to within 0.01 ml. Yields of
oil and water obtained by this method are reported in
litres/metric tonne (Table V) and represent good estimates of the
potential of the chosen oil shale samples to provide shale oil.
All of the oils were analysed by gas chromatography (GC), and
some again after separation of the aliphatic hydrocarbons
into alkanes and cis- and trans-alkenes using Ag^+ TLC.
     The organic hydrogen richness of the oil shales was
assessed from Rock Eval pyrolysis data (Hydrogen index) which at
high levels of organic richness can be considered to give
reliable data (14, 15).

TABLE IV   ORGANIC CARBON AND EXTRACTABLE BITUMENS

Sample No.	Weight of rock extracted gms	EOM* in mgs	EOM gms/100g	Organic C %
Camb1	100	80.1	0.08	12.5
D8	100	312.0	0.31	5.1
D10	100	293.4	0.30	5.2
Ca1	100	1,224.8	1.23	14.7
Ca6	100	915.0	0.92	8.7
Ca10	100	206.1	0.21	32.5
Ca15	50	245.6	0.49	20.4
C5	72.3	457.3	0.63	10.1
C6	64.5	321.1	0.50	15.7
C8	65	778.3	1.20	13.0
LL2	100	343.0	0.34	4.3
UL1	100	428.6	0.43	6.5
UL4	100	1,453.5	1.45	5.8
UL6	100	907.5	0.91	3.3
UL9	100	316.5	0.32	2.3
B1	100	1,339.9	1.30	5.7
B4	100	456.5	0.46	11.3
B5	100	561.5	0.55	15.13
OC2	100	392.3	0.40	6.6
OC5	100	494.0	0.49	11.7
K2	100	3,019.7	3.10	37.5
K3	100	337.4	0.34	6.7
K5	100	872.1	0.87	18.7
K7	100	397.9	0.40	16.3

*EOM - Extractable organic matter

TABLE V   FISCHER ASSAY

Sample No.	Water Lt/ton	Oil Lt/ton.	Oil gal/ton
D10	6	15	3
Ca1	15	156	34
Ca6	25	65	14
Ca10	23	175	39
Ca15	38	102	22
C5	20	86	19
C6	25	70	15
C8	30	162	36
LL2	47	59	13
UL1	22	39	9
UL4	22	94	21
B1	30	49	11
B4	49	147	32
B5	26	83	18
K2	20	234	51
K5	26	98	22
K7	39	96	21

Bitumens, were separated by chromatography, urea clathration and 5A molecular sieve occlusion before and after analyses of many of the aliphatic sub-fractions by GC and gas chromatography-mass spectrometry (GC-MS). Experimental details are noted in a previous publication (16) in which the distribution of cyclic alkanes in two lacustrine deposits of Devonian (N.E. Scotland) and Permian (Autun, France) age, (the D and C series samples) were discussed. Chromatographic separation into aliphatic, aromatic and polar compounds of the bitumens extracted from the shales gave the results shown in Table VI. Carbon Preference Indices and pristane/phytane ratios were measured in this work: space limitations precluded tabulation of all of the data but the former index, measured from n-alkane chromatograms obtained after separation of the saturated hydrocarbons on 5A molecular sieve, ranged from 0.90 to 2.65: pristane/phytane ratios from 0.6 to 3.9.

Kerogens were isolated by treating the extracted shale sequentially with aqueous hydrochloric and hydrofluoric acids (17). The kerogens were used to obtain carbon, hydrogen and oxygen values, for pyrolysis-gc (Py-GC) and pyrolysis-gc-ms (Py-GC-MS) of selected samples. Py-GC pyrograms provided fingerprints that were compared with those obtained in many similar analyses performed in this and other laboratories (18 and refs therein); classifying the kerogens by a type-index (19) was also attempted. Py-GC-MS analyses helped to identify components in the pyrolysates and, with the use of selected mass chromatograms, illustrate changes in the presence, and relative abundance, of compounds shown in the pyrograms of different kerogens (20, 21). The information obtained by the geochemical analyses outlined here is discussed briefly below.

TABLE VI   CHROMATOGRAPHIC ANALYSES OF EXTRACTABLE BITUMENS

Sample No.	EOM * mgs/100g	Light petrol. eluate mgs/100g	DCM ‡ eluate mgs/100g	Residue ** mgs/100g
Camb1	80.1	17.1	44.9	18.2
D8	312.0	109.8	68.3	133.8
D10	293.4	137.3	108.6	47.5
Ca1	1,224.8	436.0	399.3	389.5
Ca6	915.0	420.0	329.4	165.6
Ca10	206.1	101.4	58.5	46.2
Ca15	491.2	271.1	118.4	101.7
C5	630.8	229.6	170.9	230.2
C6	497.8	169.3	132.4	196.1
C8	1,197.4	487.3	426.3	283.8
LL2	343.0	160.5	103.2	79.2
UL1	428.6	101.1	182.6	144.9
UL4	1,453.5	411.3	578.9	463.7
UL6	907.5	357.4	282.2	267.7
UL9	316.5	96.8	126.6	93.1
B1	1,339.9	271.1	612.3	510.5
B4	456.5	146.5	188.1	121.9
B5	563.1	72.1	218.1	272.8
OC2	392.3	16.1	189.1	183.2
OC5	494.0	93.4	126.5	274.2
K2	3,091.7	785.3	1,221.2	1,085.2
K3	337.4	23.6	129.9	183.9
K5	872.1	164.8	328.8	378.5
K7	397.9	155.0	101.9	280.5

* EOM - Extractable organic matter

‡ DCM - Dichloromethane

** Residue - Polar material not eluted

Discussion

The 24 samples chosen (for which summary data are given) range in age from the Cambrian (Sweden) deposit (Camb 1) to the Upper Jurassic Kimmeridge clays (K series); their sources are shown in Figure 1. From Bitterli (1), and other literature reports, they can generally be classed as marine (Camb, LL, UL, OC and K series), non-marine (D, Ca and C series) and transitional (B series) deposits. Within each series organic matter is often found in quite different facies, for instance acid treatment (Table III) indicates that within the Lothians Upper Oil Shale group samples Ca1 and Ca6 are carbonate rich (> 40%) whereas Ca15 is carbonate poor (2.5%): these differences are obvious within other series as noted in Table III. Microscopical analysis of polished blocks in white and blue light allowed the data in Table II to be compiled. The organic material which is recognisable by these methods can generally be classified within the maceral group exinite (22); inertinite and vitrinite are generally rare in European oil shales (23). In the table shown, sporinite refers to fossil spores and pollen, and to fossil algal cysts (e.g. Tasmanites) while Botryococcus cysts were counted separately. Since much of the mainly algal material cannot be categorised microscopically it is sometimes referred to as amorphous kerogen: it is generally disseminated in the rock matrix and not easy to point count and so cannot be tabulated separately (Table III).

Some of the Carboniferous oil shales are rich in Botryococcus remains, the lagoonal freshwater samples Ca10 (Westfield shale) being almost as rich as the well-known torbanites from Torbanehill: remains of this detrital alga appears in the other Carboniferous (Scotland) and Permain (Autun) samples but, as expected from the known provenance of Botryococcus, they do not appear in the marine deposits.

Nearly all of the samples were immature as evidenced by rank determinations using vitrinite reflectance and spore colouration; they may be considered to have a rank equivalent to that of late diagenesis-early catagenesis (5). Because of lack of spore fluorescence, the Devonian and Cambrian samples have been classified as having a vitrinite reflectance > 0.7%. The microscopical data is shown in Table II where the samples have been subdivided into five groups based on these rank parameters.

Rock Eval analyses (5) of the shales indicates that all but two of the samples have hydrogen indices (mg. hydrocarbon/ g. organic carbon) between 300 and 900: the non-marine samples generally plotted as Type I kerogens and the marine samples as Type II. Shale oils were obtained by modified Fischer Assay, and the yields obtained are plotted against organic carbon in Figure 2: this indicates that there is as good a correlation as might be expected without rank being taken into account. Values for oil yield (Table V) have been compared with
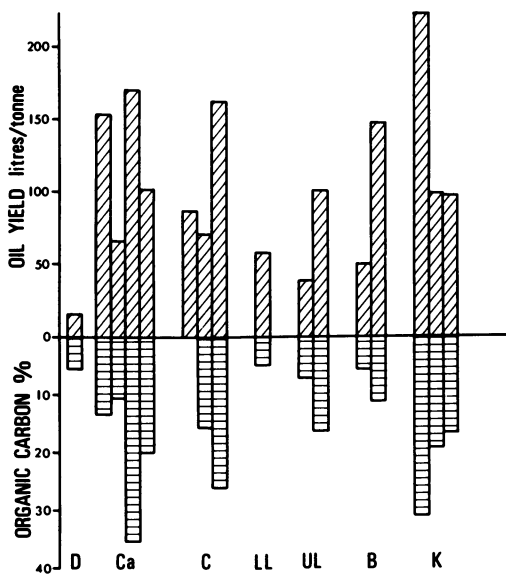
Figure 2. Organic carbon content and yield of shale oil obtained by Fischer Assay. Key: D, D10; Ca, Ca1, Ca6, Ca10, and Ca15; C, C5, C6, and C8; LL, LL2; UL, UL1, and UL4; B, B1, and B4; and K, K2, K5, and K7.

literature values, but yields were only measured on single hand
specimens and a large survey of each deposit was not undertaken.
In the Carboniferous samples of the Lothians the torbanitic
shale (> 50% Botryococcus) yielded 175 l/tonne which compares
with a literature values of 160 l/tonne (24), other samples in
this group provided 65-156 l/tonne which compares with previous
values (24) of 40-200 l/tonne although the highest yield noted
there was rarely achieved. The Permian samples from Autun
provided 70-162 l/tonne which again compares with literature
values of 65-125 l/tonne (25). Middle and Upper Jurassic samples
yielded oils in amounts agreeing reasonably well with literature
values (25, 9). Sample K2 is from the Blackstone band of the
Kimmeridge clay and perhaps represents the only oil shale in
Britain that could now be used to provide commercial quantities
of oil in times of national need. The maximum yield that we
have achieved by standard Fischer assay (370 l/tonne) of this
band was from a sample taken from the basal 5 cm of the
Blackstone band at Clavell's Hard, in Kimmeridge bay (9).

   All of the shale oils were analysed by GC as total
pyrolysates and as separated saturated and unsaturated fractions.
Infra red spectra of the olefinic fraction separated by TLC
indicated that one fraction consisted of alk-1-enes (γ CH
at 910 and 990cm^{-1}) and the other of trans alkenes (γ CH at
965cm^{-1}) of which the former were generally the most abundant;
this accords with literature data on pyrolysis at 600°C (26, 27).
Interestingly, and surprisingly, we have shown previously
(28) that pyrolysis of torbanites at lower temperatures
(225-325°C) provided a small olefinic fraction consisting mainly
of trans-alkenes (IR) present as a complex series of partially
resolved homologies (GC). Many authors have discussed shale oil
composition in terms of retorting temperature, mineral/organic
interactions, original contributing organic matter etc. Urov (29)
proposed a method of classifying oil shale kerogens which
depended on the nature of the GC fingerprint of the n-alkanes in
the retort oil. In this work some of the marine shale oils had
normal aliphatic hydrocarbons ranging to about C_{20} superposed
on a prominent 'hump' of unresolved material while some of the
non-marine shales showed much less of a 'hump' and carbon numbers
extending to about C_{30}: these distributions are illustrated for
samples OC5 and Ca6 in Figure 3. That a distinction based on
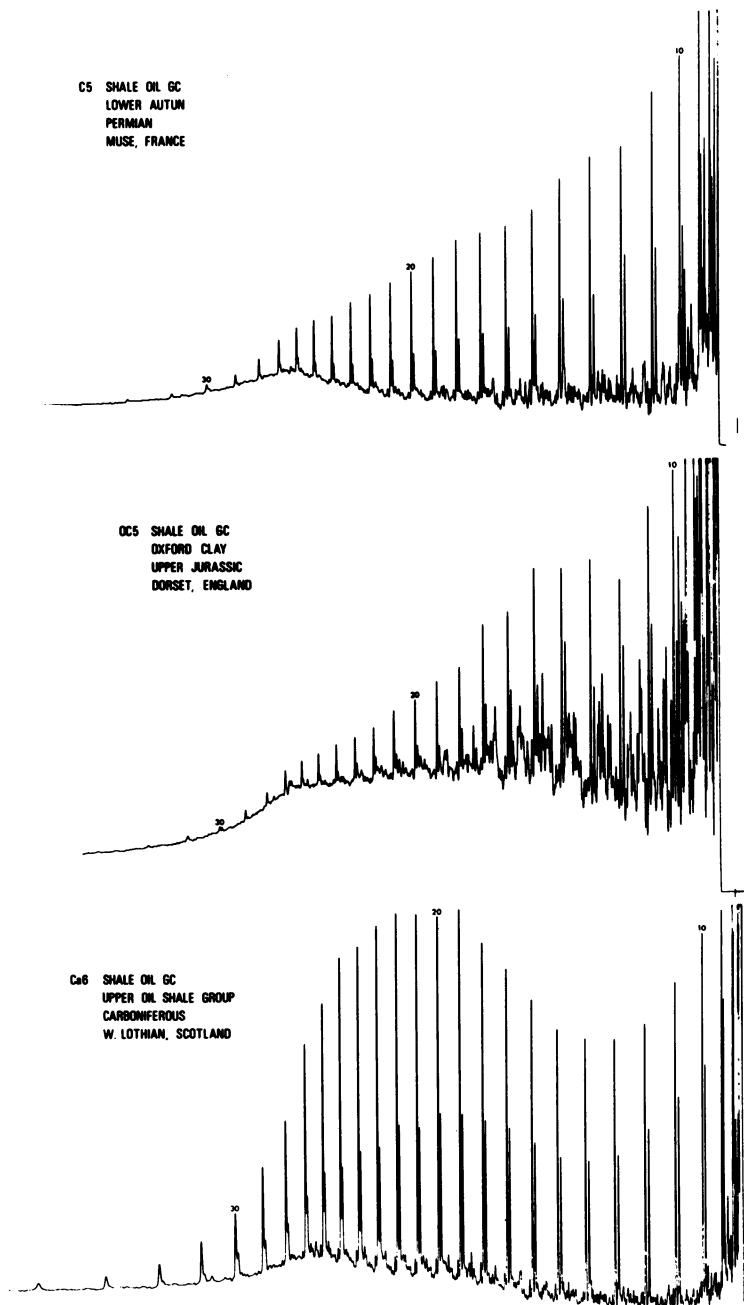such distributions is equivocal is illustrated in the same figure

Figure 3. Gas chromatograms of shale oils obtained from Samples C5, OC5, and Ca6 (numbers on chromatograms denote hydrocarbon chain length). Conditions: column, 25 m × 0.25 mm (inside diameter) glass capillary; OV 101; progression 60–260 °C at 4 °C min^{-1}.

which includes an analysis of the lacustrine sample C5 which,
if anything, has a normal aliphatic hydrocarbon fingerprint
closer to that of the marine shale OC5 than the lacustrine Ca6
sample. We, and others (14, 15, 30), have shown that in clastic
sediments (as opposed to carbonate-rich sediments) the effect of
the mineral matter is to produce a pyrolysate with much more
material at lower molecular weight and with a net reduced yield.
These facts might explain the distribution shown for the non-
calcareous sample C5, but in other lacustrine samples that we
have examined, similar hydrocarbon distributions have been
obtained in highly calcareous shales.

All of the samples were analysed for their hydrocarbon
content and composition, by chromatography of the extracted
bitumens. The proportions of aliphatic and aromatic hydrocarbons
and polar NSO compounds were tabulated. Table VI indicates that
some rocks provide tenfold more soluble bitumen than others
(c.f. K2 and Ca10) and that some of these bitumens were aliphatic
rich (e.g. Ca15) while others were aromatic rich (e.g. OC2).

Most of the alphatic fractions were separated into normal
and branched alkane fractions after the removal of unsaturated
hydrocarbon. Most of these subfractions were analysed by GC
to give fingerprint chromatograms. These analyses were used
to provide data that allowed carbon preference indices,
pristane/phytane ratios etc. to be measured. Also, the relative
amounts of ($17\beta H$, $21\beta H$; $17\beta H$, $21\alpha H$ and $17\alpha H$, $21\beta H$)
hopanes, steranes, 4-methyl steranes, carotenoid and other related
compounds were assessed from gas chromatograms and reconstructed
ion chromatograms. A large number of Kovats Retention Indices
(OV-101) were measured and tabulated for these compounds also (10).

In source rock studies, a number of maturation parameters
are used which depend on relative sterane and triterpane
distributions (6, 31). Since, in this paper, we are concerned
with a broad overview of widely distributed oil shales, use of
these parameters must be considered in that context, and not as
in maturing organic matter within a single sedimentary basin.
Nevertheless, changes seen when the polycycloalkanes are used
as maturation parameters are well-illustrated in many of our
chromatographic analyses when shales of different ranks are
compared. Thus the change from a distribution of hopanes rich
in the $\beta\beta$ -isomers to those rich in $\alpha\beta$ isomers is noted in
progressing from some samples with rank values equivalent to
vitrinite reflectances of 0.4% to 0.6%. Included in the data
that we have plotted (Figure 4) is the change in ratio of the
S and R epimers of the $C_{31}\alpha\beta$ hopanes for shales of increasing
rank. This plot shows a rapid increase in the S/R ratio at
about 0.5% R_0: for the Jurassic samples the ratio changes from
0.1 to 1.0 as the rank changes from 0.3% R_0 to about 0.5% R_0.
Also, for the marine Jurassic samples, a good correlation is
obtained (10) for the maturation parameter of increasing
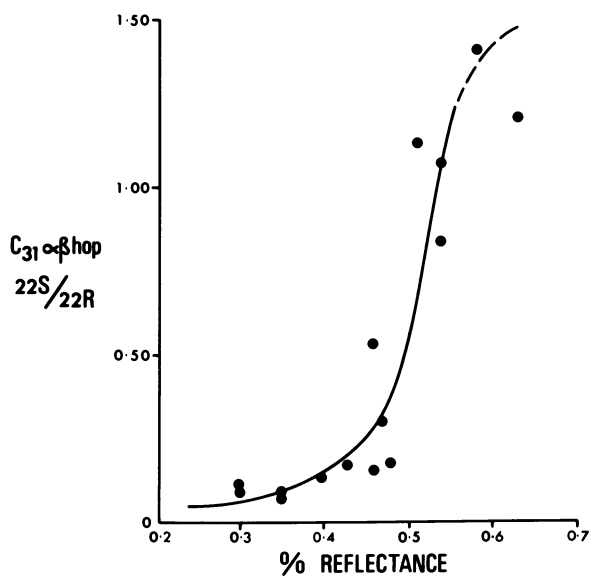C_{27} 13β (H) 17α (H) 20S diasterane $\underline{vs}$ C_{27} 5α (H) 20R regular,

Figure 4. Variation of 22S/22R epimer ratio of 17αH, 21βH homohopane.

immature sterane, to reflectance values; this type of change has
been documented previously by others in, for example, the Paris
Basin sediments (32).

An interesting finding in this survey was that two groups of
shales from lacustrine sedimentary sequences provided a suite of
what appear to be partly degraded carotenoid-derived hydrocarbons.
Their depositional environments are reported to have common
features, namely a semi-arid climate, and a large algal input
into intermontane, fault-bounded basins, in the Devonian of
N.E. Scotland (D samples) and Permian of France (C samples).
Interestingly, Anders and Robinson (33) identified, in Green
River oil shale bitumen, whose depositional environment is
supposedly similar to that described above, twenty-one compounds
whose mass spectra suggested that they were tetralkyl substituted
cyclohexanes such as might be expected as degradation products
of carotanes. The mass spectra of nine of our compounds suggest
they belong to this class of compound. Details of this work
have been published (16).

Py-GC and Py-GC-MS methods have been established as having
value in fossil fuel research (34, 18 and refs therein) and in
consequence both methods were used in this investigation. Using
coal maceral kerogens, and other kerogens obtainable as enriched
monotypes, it had been shown previously that characteristic
fingerprints could be obtained when the kerogens were flash-
heated at 600°C (furnace pyrolyser) and the pyrolysate passed
through a capillary GC column (26, 35). An example of the
fingerprint pyrograms of a torbanite, sporinite and vitrinite,
obtained in the present work using a ribbon pyrolyser, is shown
in Figure 5 and compounds in the pyrolysates, identified by
Py-GC-MS, are shown in Table VII.

Although fingerprints of several hydrogen-rich algal kerogens
could be differentiated from each other (36), all usually
contain abundant extended normal alkanes and alkenes with a very
small contribution from aromatic molecules. In contrast,
vitrinite or humic-rich kerogen pyrograms generally contain
abundant non-homologous peaks representing substituted benzenes,
naphthalenes, phenols etc. as shown. Py-GC of the kerogens
isolated in this work confirmed these findings. For instance
the Carboniferous sample Ca10 which contains 52% of
Botryococcus braunii (by point counting >500 points) provided a
pyrogram typical of that of alginite with aliphatic triplet
alkanes, alkenes and alkadienes extending to about C_{28} (Figure 6).
The contribution of aromatic molecules is small, as expected.
Interestingly, sample Ca15, which gave only 1.2% of
morphologically definable Botryococcus on point counting
provided a fingerprint virtually superposable on that of Ca10
(Figure 6). In ultra-violet light this sample gave a dull
yellow-brown fluorescence, with rare preserved algal bodies,
a few yellow-brown spores and many small flecks of yellow-brown
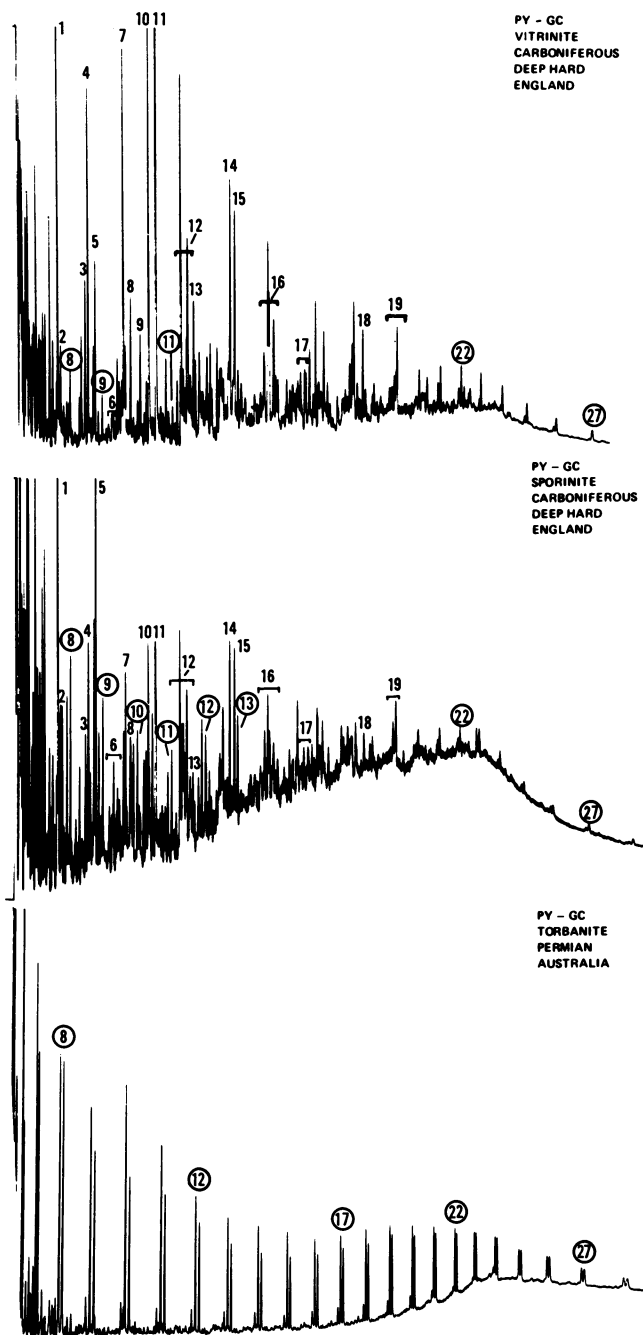fluorescence. We suggest that perhaps the inability to count

Figure 5. Pyrograms of alginite, sporinite, and vitrinite. The numbers circled represent hydrocarbon chain lengths (for other numbers see Table VII). Conditions: CDS Pyroprobe, 600 °C, 5 s; Column, 25 m × 0.3 mm (inside diameter) fused silica; OV-1; progression 40–270 °C at 4 °C min^{-1}.
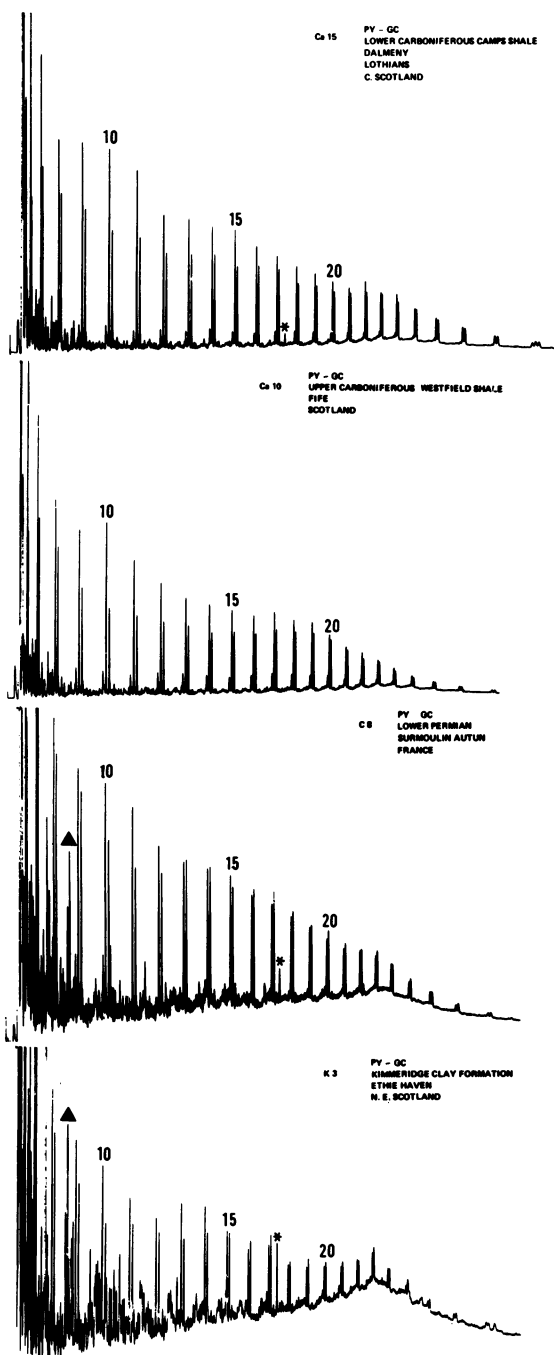
*Figure 6. Pyrograms of kerogens isolated from samples Ca10, Ca6, C8, and K3. Numbers represent hydrocarbon chain lengths. Key: *, prist-1-ene; and ▲, m(p)xylene. Conditions as in Figure 5.*

Botryococcus cysts in this shale belies its content of this alga
which may be preserved only in finely comminuted form. Most of
the other non-marine kerogens provide GC fingerprint pyrograms
generally similar to the above, although where there is a
contribution from spores and/or pollen the pyrogram has a larger
relative content of low molecular weight aromatic molecules
(sample C8, Figure 6): this accords with previous findings for
the pyrolysis of enriched sporinites (26, 35).

TABLE VII   PEAK IDENTIFICATIONS FOR FIGURE 5

1.   Toluene
2.   Methylthiophene
3.   Ethylbenzene + C_2thiophene
4.   m(+p)-Xylene
5.   o-Xylene
6. C_3Benzenes
7.   Phenol
8. C_3Benzene and/or Methylstyrene
9. C_4Benzene + Indane + Indene
10. o-Cresol
11. m(+p)-Cresol
12. C_5Benzene + Methylindane + Methylindene
13. Naphthalene?
14. 2-Methylnaphthalene
15. 1-Methylnaphthalene
16. C_2Naphthalenes
17. C_3Naphthalenes
18. Phenanthrene
19. Methylphenanthrene + Nonadecane

The marine Kimmeridge, Oxfordian and Upper Lias samples
generally provided more complex pyrograms containing more low
molecular weight aromatic hydrocarbons together with homologous
alkanes and alkenes. A typical pyrogram is shown for sample
K3 in Figure 6.
      A measure of the aliphatic/aromatic nature of kerogen, as
indicated by their pyrolysis products, is an approach that has
been made in attempts at classifying them (cf. 18 and refs
therein). We have previously shown that by using the ratio of
m(+p)-xylene/oct-1-ene as an aromatic/aliphatic index it is
possible to augment the fingerprint data for differentiating
kerogens with a numerical "type-index" (19). The "type index"
of kerogens isolated during this work is shown in Figure 7
and illustrates, as before, that algal-rich kerogens have an
index with a value less than 0.6, whereas marine kerogens have
higher values, not unlike those obtained previously (19).
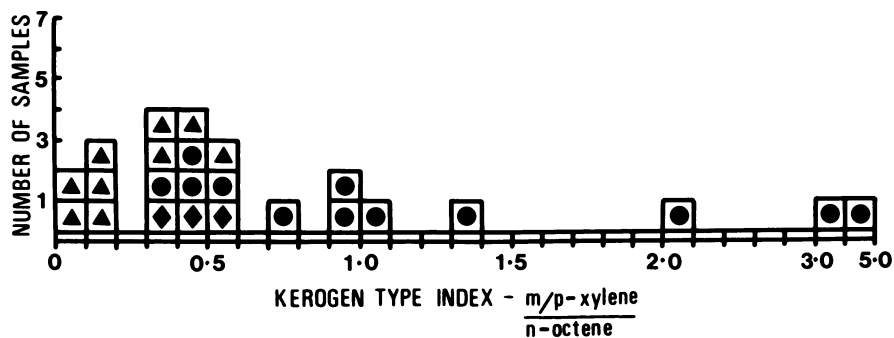Valuable as this index has proved for defining kerogen facies

Figure 7. Type index: m(p)*xylene vs. oct-l-ene. Key:* ▲*, nonmarine kerogens;* ●*, marine kerogens; and* ◆*, transitional kerogens.*

it is probable that refinements to it will prove to be even
more useful: these refinements are currently being
investigated.

Py-GC-MS data were obtained by interfacing the Py-GC system
to a double-focussing mass spectrometer and data system.
Previous analyses (20) of the three principal kerogen types
(I, II, III), obtained by monitoring the fragment ions with
m/z values of 91, 105 and 119 had indicated, in a preliminary
fashion, that the mass chromatograms provided a useable
fingerprint of alkylbenzene moieties for each kerogen type.
For instance reconstructed ion chromatograms of the m/z 105
fragment gave a homologous series of triplets which we ascribe
to the presence of o-, m- and p-isomers of 1-tolylalkanes. In
this work triplets have been shown to occur in a few selected
kerogens representing marine to non-marine deposits: differences
in these fingerprints were again evident, but they did not
differentiate the kerogens so well as when other fragment ions
were used to reconstruct chromatograms. Thus, by reconstructing
the chromatogram for the m/z 97 fragment ion (an abudant
fragment ion in the mass spectra of n-alkenes and
alkylthiophenes) it was shown that there was a clear change in
the fingerprint in the non-marine/marine series (Figure 8). In
the former (e.g. Cal) the chromatogram is dominated by a
homology due to the alk-1-enes, and the presence of thiophene
nuclei were not noted. In the marine samples (e.g. UL1) the
sample alkene homology is interrupted between about C_9 and C_{15}
by the dominance (in the early part of this range) of peaks
whose mass spectra suggest that they are alkylthiophenes. In
sample D8, the thiophene peaks were less abundant, but still
present in the same range.

The fragment ion m/z 141 occurs abundantly in the mass
spectra of alkylnaphthalenes and as a weak ion in those of
n-alkanes, and this fact has been used to monitor aspects of
increasing aromaticity in a variety of kerogens (21, 37). These
changes are well represented in the present work: thus in
Figure 9 the lacustrine, algal rich kerogen Cal provides a
pyrogram dominated, in this reconstructed ion chromatogram, by
homologous n-alkane fragments with small peaks showing 2- and
1-methylnaphthalenes and a group of dimethylnaphthalenes. In
sample C8 these dominances are reversed, and in the marine sample
OC5 the homologous n-alkane series has virtually disappeared. We
emphasise that this indicates relative changes, as the absolute
sensitivities of aromatic and aliphatic species in the mass
spectrometer are quite different (37).

The above discussion, which is part of a more extensive
overview (10), provides some insight into the organic
geochemistry of a selection of European oil shales. It is not
intended as a complete description of the geochemistry of these
shales, which could not easily be accomplished within the
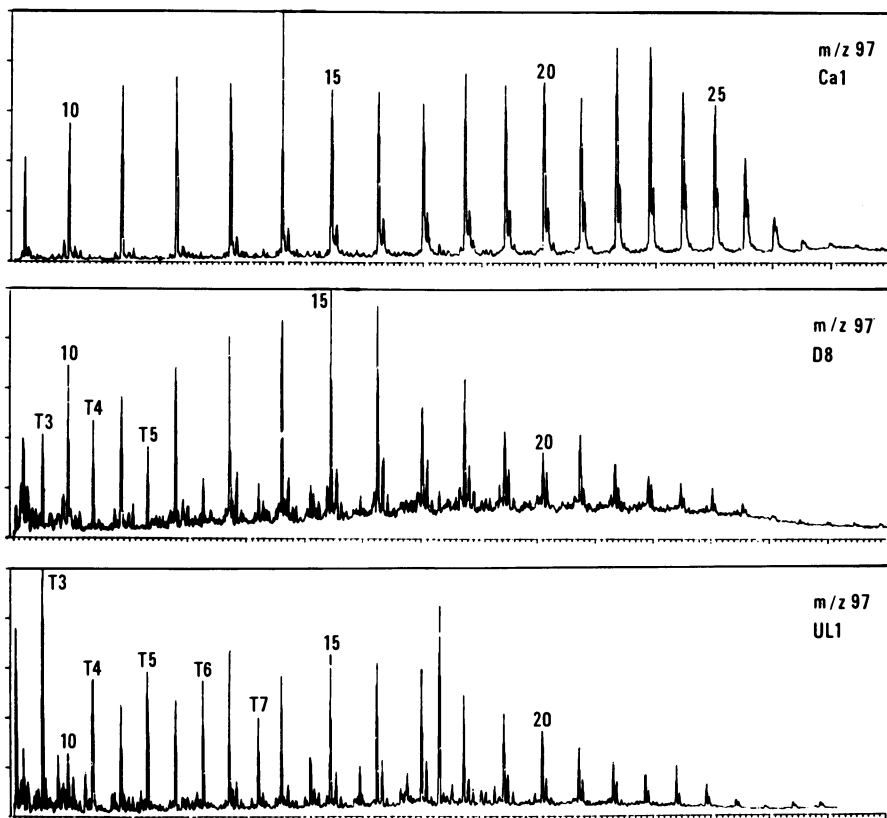general limits of this meeting's proceedings, but it is hoped

Figure 8. Mass chromatogram of fragment ion m/z 97 in pyrograms of kerogens isolated from samples Ca1, D8, and UL1. Pyrolysis and GC conditions as in Figure 5. GC interfaced to VG 70-70H mass spectrometer. Numbers represent hydrocarbon chain lengths, and T3, T4, etc., represent a thiophene substituted with a C_3, C_4, etc., alkyl chain.
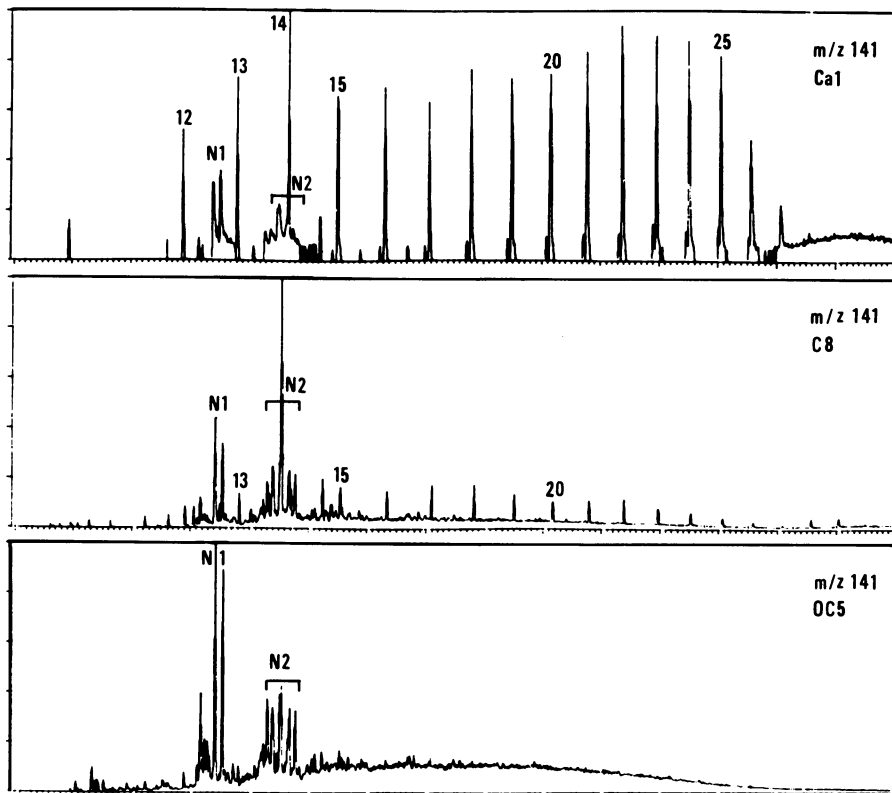
Figure 9. Mass chromatogram of fragment ion m/z 141 in pyrograms of kerogens isolated from samples Cal, C8, and OC5. Conditions as in Figure 8. Numbers represent hydrocarbon chain lengths. Key: N1, 2- and 1-methylnaphthalenes; N2, dimethyl-naphthalenes.

that it will provide data for those interested in aspects of the organic geochemistry of a variety of European bituminous shales.

Acknowledgments

Literature Cited

1. Bitterli, P. Geol. en Mijnb. 1963, 42, 183-201.
2. Schlatter, L.E. "Exploration for Petroleum in Europe and North Africa"; Inst. Petrol. London, 1969, 251-258.
3. Oil Shale and Cannel Coal, I. Inst. Petrol. London, 1938.
4. Oil Shale and Cannel Coal, II. Inst. Petrol. London, 1951.
5. Tissot, B.P.; Welte, D. "Petroleum Formation and Occurrence" Springer-Verlag, 1978.
6. MacKenzie, A.S.; Patience, R.L.; Maxwell, J.R.; Vandenbrouke, M.; Durand, B. Geochim. Cosmochim. Acta, 1980, 44, 1709-21.
7. Kimble, B.J.; Maxwell, R.J.; Philp, R.P.; Eglinton, G.; Albrecht, P.; Ensminger, A.; Arpino, P.; Ourisson, G. Geochim. Cosmochim. Acta, 1974, 38, 1165-81.
8. Vitorovic, D. This meeting.
9. Williams, P.F.V.; Douglas, A.G. "Advances in Organic Geochemistry 1979" Douglas, A.G.; Maxwell, J.R. Eds, Pergamon, Oxford, 1980, p.531.
10. Hall, P.B. Ph.D. Thesis, Newcastle University, England, 1981.
11. Duncan, D.C. "Oil Shale", Yen, T.F. and Chilingarian, G.V. Eds, Elsevier, Amsterdam, 1976, p.13.
12. Bascomb, C.L. Chem. Ind. 1961, 1826-27.
13. Stanfield, K.E.; Frost, I.C. U.S. Bur. Mines Rep. Investig. 4477, 1949.
14. Horsfield, B.; Douglas, A.G. Geochim. Cosmochim. Acta, 1980, 44, 1119-1131.
15. Espitalie, J.; Madec, M.; Tissot, B. Bull. Amer. Assoc. Pet. Geol. 1980, 64, 59-66.
16. Hall, P.B.; Douglas, A.G. "Advances in Organic Geochemistry 1981" Bjoroy, M. Ed. (In press).
17. Durand, B. Kerogen, Editions Technip, Paris, 1980.
18. Larter, S.R.; Douglas, A.G. J. Anal. App. Pyrol. 1982, 4, 1-19.
19. Larter, S.R.; Douglas, A.G. (ref.9, p.579).
20. Solli, H.; Larter, S.R.; Douglas, A.G.; ibid. p.591.

21. Solli, H.; Larter, S.R.; Douglas, A.G. J. Anal. App. Pyrol.
    1980, 1, 231-41.
22. International Handbook of Coal Petrography, 2nd edition,
    Centre National de la Recherche Scientifique, Paris, 1963.
23. Hutton, A.C.; Kantsler, A.J.; Cook, A.J.; McKirdy, D.M.
    A.P.E.A.J. 1980, 20, 44-67.
24. Coanacher, H.J.R. Trans. Geol. Soc. Glasgow, 1917, 16, 164-92.
25. Smith, H.N.; Smith, J.W.; Kommes, W.C.; U.S. Bur. Mines Rep.
    of Investig. 5504, 1959.
26. Larter, S.R.; Douglas, A.G. Environmental Biogeochemistry
    and Microbiology, Krumbein, W.E. Ed. Ann. Arbor.
    Michigan, 1978, p.373.
27. Van de Meent, D.; Brown, S.C.; Philp, R.P.; Simoneit, B.R.T.
    Geochim. Cosmochim. Acta, 1980, 44, 999-1013.
28. Allan, J.; Bjoroy, M.; Douglas, A.G. (ref. 9, p.599).
29. Urov, K.E. J. Anal. Appl. Pyrol. 1980, 1, 323-28.
30. Larter, S.R. In press.
31. Siefert, W.K.; Moldowan, J.M. Geochim. Cosmochim. Acta,
    1978, 42, 77-95.
32. Ensminger, A.; Joly, G.; Albrecht, P. Tetrahedron Lett.
    1978, 1575-78.
33. Anders, D.E.; Robinson, W.E. Geochim. Cosmochim. Acta,
    1971, 35, 661-78.
34. Philp, R.P. Trends in Anal. Chem. 1982, 1, 237-41.
35. Larter, S.R. Ph.D. Thesis, Newcastle University, England,
    1978.
36. Larter, S.R.; Douglas, A.G. In preparation.
37. Larter, S.R.; Solli, H.; Douglas, A.G. J. Gas Chromatog.
    1978, 167, 421-31.

Geochemistry of Israeli Oil Shales

M. SHIRAV (SCHWARTZ) and D. GINZBURG

Geological Survey of Israel, 30 Malkhe Israel St., Jerusalem 95501, Israel

The Maastrichtian (latest Cretaceous) Israeli oil
shales consist of four main groups of components:
organic matter; biogenic calcite and apatite;
detrital clay minerals and quartz, with a little
amount of authigenic pyrite and feldspar. The main
chemical characteristics of the oil shales are
reviewed,with an emphasis on those which may affect
future utilization techniques.

The oil shales in Israel are widely distributed throughout
the country (Figure 1). Outcrops are rare, and the information is
based on borehole data. The oil shales sequence is of Upper-
Campanian - Maastrichtian (latest Cretaceous) age and belongs to
the Ghareb Formation (Figure 2). In places, part of the phospho-
rite layer below the oil shales (Mishash Formation, Figure 2) is
also rich in kerogen. The host rocks are biomicritic limestones
and marls, in which the organic matter is generally homogeneously
and finely dispersed. The occurrence of authigenic feldspar and
the preservation of the organic matter (up to 26% of the total
rock) indicate euxinic hypersaline conditions which prevailed in
the relatively closed basins of deposition during the Maastrich-
tian (1).

Current reserves of oil shales in Israel are about 4,000
million tons (2),(3), located in the following deposits (Figure 1):
Zin, Oron, Ef'e, Hartuv and Nabi-Musa. The 'En Boqeq deposit,
although thoroughly investigated, is of limited reserves and is
not considered for future exploitation. Other potential areas, in
the Northern Negev and along the Coastal Plain are under investi-
gation.

Future successful utilization of the Israeli oil shales,
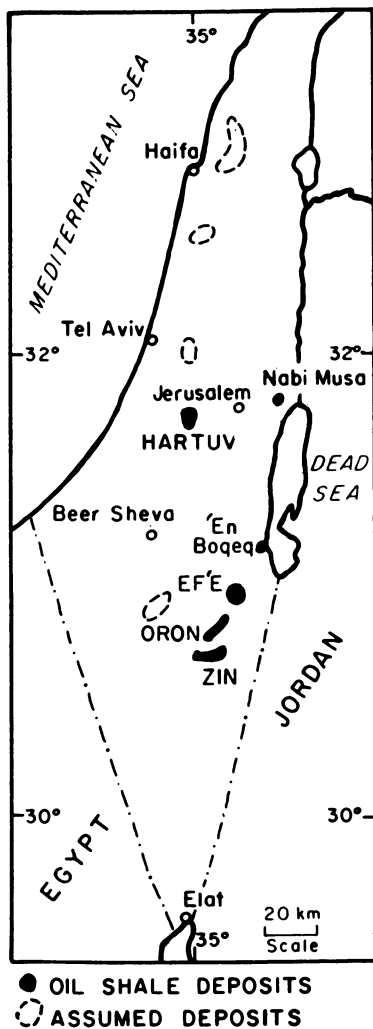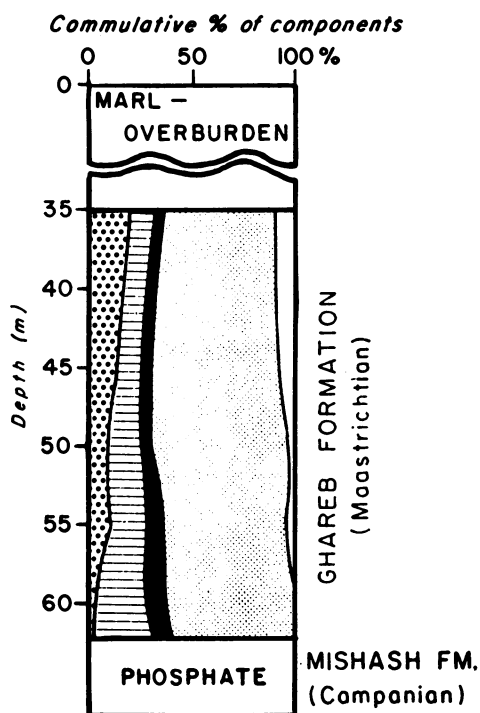either by fluidized-bed combustion or by retorting will contribute
to the State's energy balance.

Figure 1. Map showing location of oil shale deposits in Israel.

Commulative % of components

0   50   100 %

Depth (m)

0 — MARL — OVERBURDEN

35

40

45

50

55

60

GHAREB FORMATION (Maastrichtian)

PHOSPHATE   MISHASH FM. (Companian)

LEGEND

Clay minerals

Organic matter

Apatite

Calcite

Others (Pyrite, gypsum, dolomite)

Figure 2. Mineralogical log (Borehole T-1).

Analytical Methods

Inductively coupled plasma atomic emission spectrometry (ICP-AES) was used for the determination of most major and trace elements. The samples are fused in a Claisse semi-automatic fusion device in Pt-Au crucibles with lithium metaborate (4). The fusion product is dissolved in diluted HNO_3 and brought to volume. For trace elements determination the sample is decomposed by HF, HNO_3 and $HClO_4$. Scandium serves as an internal standard and is added to all samples and solutions. The instrument (product of Jobin Yvon, France) is calibrated using multi-element synthetic standards. The aqueous solutions are nebulized and injected into the heart of a plasma fire ball. A computerized multi-channel vacuum spectrometer has been programmed for multi-element analysis.

Additional methods used were: X-Ray fluorescence spectrometry (for total S determination); flame atomic absorption (Hg and As). Organic C was determined using Leco instrument, after decomposition of the carbonate by HCl. C,H,N,S in the kerogen were analysed using microanalysis techniques.

Major Elements and Mineralogy

Typical analyses of Israeli oil shales are shown in Table I.

Table I. Analyses of Composite Samples (wt.%)

a.*	Ef'e	Ef'e	Hartuv	Hartuv
b.	Bit-1	Bit-1	HRB-1	HRB-1
c.	18-22m	60-70m	62-82m	130-150m
SiO_2	16.9	7.6	7.5	5.0
Al_2O_3	6.8	1.5	1.6	1.3
TiO_2	0.32	0.16	0.1	0.1
Fe_2O_3	2.8	0.7	1.01	0.57
CaO	34.2	36.1	37.7	38.2
MgO	0.57	0.58	1.67	0.39
Na_2O	0.27	0.20	0.14	0.10
K_2O	0.42	0.32	0.15	0.14
P_2O_5	1.6	3.5	3.0	2.3
SO_3	2.3	0.9	0.3	0.26
S (Organ.)	1.4	2.7	1.7	2.4
Organ. Mat.	8.2	24.1	14.8	20.5
Loss on Ign.	33.5	45.7	44.0	49.6

*a.=location b.=borehole No. c.=depth interval of sample

One borehole in the Ef'e deposit, T-1, coord. 1167/0544 (Israel Grid) was analysed meter by meter. The correlation factors between the variables are summed up in Figure 3.
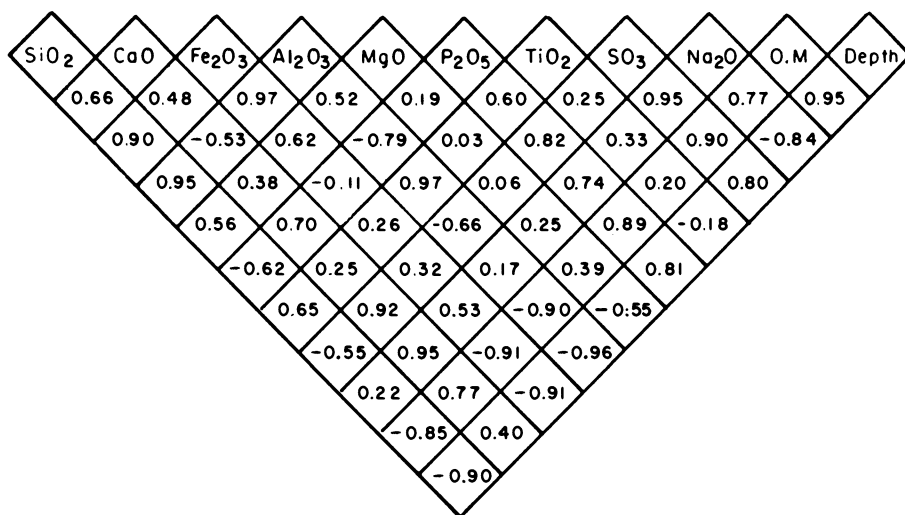
Figure 3. Correlation factors for chemical analyses of samples from Borehole T-1, Ef'e Deposit. (O.M indicates organic matter.)

SiO_2 content is 2-17wt.%. The significant correlation with Al_2O_3 and Fe_2O_3 indicates its residence in clay minerals. Detrital quartz grains are present in a very small amount.

CaO (30-40wt.%) is found largely in calcite (50-70% of the total rock). Small amounts of CaO are located in apatite and gypsum.

Al_2O_3 is a main component in clay minerals. Al_2O_3 is highly correlative with SiO_2, Fe_2O_3 and TiO_2. The content of Al_2O_3 along the oil shale sequence is 1-8wt.%.

Fe_2O_3 content is 0.5-2.8wt.% and it is associated with clay minerals and pyrite.

Sulfur is shown on Figure 3 as SO_3, which includes organic and inorganic sulfur. Direct observations and isotopic composition of sulfur (5) indicate that kerogen-bound sulfur accounts for 60-80% of the total sulfur in the rock while the remainder is pyritic and gypsum sulfur.

P_2O_5 content within the oil shales is 1-5wt.%, while in the phosphorous Mishash Formation it may exceed 30%.

Organic matter (kerogen) composes 5-26wt.% of the rock. The average content of organic matter in Israeli deposits is 14-16wt.%. Only rocks with more than 10% organic matter are considered as "economic" oil shales.

Depth shows significant positive correlation with the following variables: organic matter, sulfur, phosphate; and negative correlation with Al_2O_3, Fe_2O_3 and SiO_2. Since Al, Si and Fe are dependent upon clay content, it is clear that the amount of clay minerals decreases with depth. Organic matter, sulfur and apatite contents increase with depth. The carbonates content along the oil shale sequence does not show any significant change.

Thus, these data represent a mineralogical system of four main variables, changing with geological time (=depth) (Figure 2). The four main mineralogical phases are:

a. organic matter - derived mainly from marine algae and bacteria with some contribution of continental plants. The kerogen is very fine (0.05-0.1 micron), most of it dispersed within the matrix or as a fine film on the grains. Some of the preserved algae show definite structures. Reflectance measurements on vitrinite-type grains indicate a very low maturity grade of the organic matter.

b. clay minerals - mainly very fine detrital kaolinite with a small amount of montmorillonite.

c. calcite - most of it is of biogenic origin. The texture is of sparse biomicrite made of planktonic foraminifera skeletons with cocolithoforides in the matrix.

d. biogenic apatite - located in ovulites, bone fragments and fish scale and teeth.

Other minor constituents are: authigenic pyrite which appears as framboides or separate crystals; secondary gypsum, mainly as vein filling; detrital quartz grains and authigenic feldspar (microcline).

The mineralogical system described above is one clue to the understanding of the paleogeographical set-up during the late Cretaceous in Israel, as well as a main factor for any assessment of oil shale's quality.

Effect of CaCO3 on Combustion

Fluidized bed technology seems to be preferable for oil shale combustion (6). Series of combustion tests which were run in different temperatures resulted in lower effective calorific value with the increase of operating temperatures. Figure 4 shows a DTA curve for a typical Israeli shale. When operating the fluidized bed in the range of 700-800°C, endothermic reactions are only in their begining, but if the operating temperature exceeds 800-850°C, the endothermic reaction of calcite decomposition has a severe influence on the effective calorific value. Fluidized beds burning coal use a certain controlled amount of carbonate for SO_2 trapping, but in this case more than 60% of the material which is feeded into the burner is carbonate.

Thus, the necessity of maintaining delicatly controlled conditions during combustion is a direct outcome of the inorganic composition of the oil shale.

Calorific Value

The High Calorific Value of the oil shales was determined by a "bomb" calorimeter on more than 90 composite samples from different deposits and on one-meter samples along borehole sections. The average value is 1000Kcal/Kg and the highest value measured was 1790Kcal/Kg. The correlation between organic matter content and the calorific value is more than significant (R=0.96). The equation for the Ef'e deposit is:

calorific value (Kcal/Kg) = 77.8+60.2(org. matter wt.%)

and for the Hartuv deposit:

calorific value (Kcal/Kg) = 52.0+71.3(org. matter wt.%)

The line for the Hartuv deposit is steeper than that for the Ef'e deposit (Figure 5) i.e.: in the range of 14wt.% organic matter (average for most deposits) the difference will be 130Kcal/Kg in favour of the Hartuv deposit. As the overall inorganic composition is simillar in the two deposits, we assume that the reason for this difference is due to compositional variations within the organic matter.
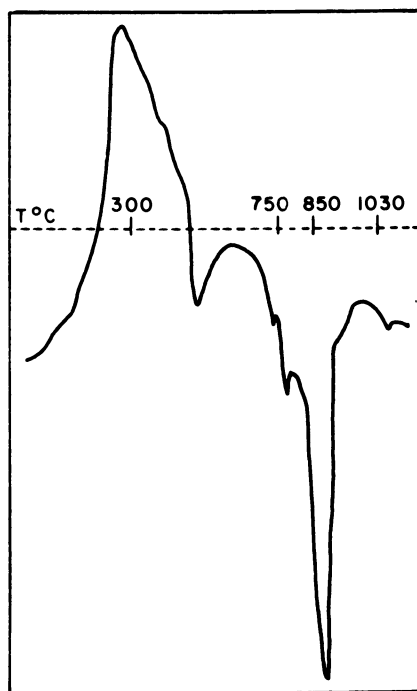
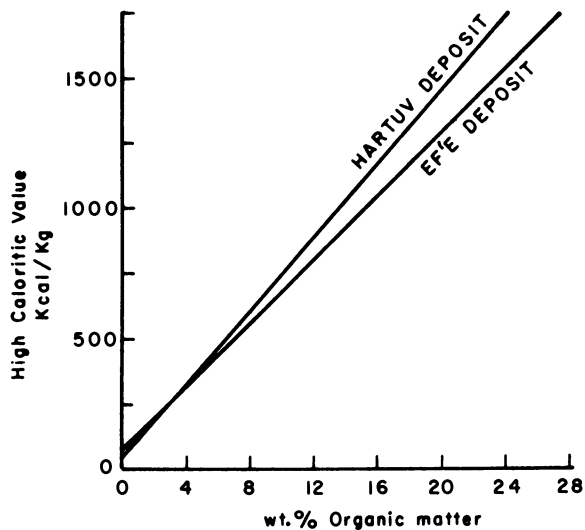*Figure 4. Differential thermal analysis curve for Sample HRB-3a.*

Figure 5. Correlation between organic matter content and high calorific value (Ef'e and Hartuv Deposits).

Fischer Assay

Fischer assay tests were carried out on several boreholes in the Ef'e deposit (7). The average oil yield was 15.6 Gal/ton; sections with high content of organic matter (20-26wt.%) yielded up to 29 Gal/ton. Evidently, there is a positive correlation between Fischer assay results and the content of organic matter; another interesting relation is illustrated in Figure 6: with the increase of depth, more oil is yielded per 1wt.% of organic matter. The data in Table II suggest that this phenomenon may be related to changes in the elemental composition of the oil shale and/or to the content of the bituminous fraction within the organic matter.

Table II. Ultimate Analyses and Oil Yield

Sample No.	SRV 208	SRV 215	SRV 221
Org. C (wt.%)	7.8	10.1	13.6
H (wt.%)	1.28	1.56	1.76
N (wt.%)	0.29	0.35	0.54
S (wt.%)	2.4	3.0	3.1
Oil (Gal/Ton)	11.9	16.5	24.2
%Bitumen out of total org. mat.	6.8	7.1	7.8

The average composition of kerogen from the Ef'e deposit is:

C-64.9%   H-8.0%   N-2.8%   S-9.1%

The average composition of retorted oil from the Ef'e deposit is:

C-79.8%   H-10.1%   N-1.1%   S-7.6%

Infra-Red Spectra of The Kerogen

Infra-red spectra were used as "fingerprints" of different kerogens, as they allow a direct study of functional groups within the kerogen's structure. The main characteristic absorptions were as follows:

2825-2960 cm^{-1}	C-H		aliphatic
1460 cm^{-1}	C-CH$_2$	C-CH$_3$	linear and cyclic
1380 cm^{-1}	C-CH$_3$		linear and cyclic
720 cm^{-1}	C-H		aliphatic
1650 cm^{-1}	C=C		aromatic; water
1710 cm^{-1}	C=O		acid; ketones

Two typical spectra are shown in Figure 7. The spectra are generally similar and indicate the kerogen to be mainly aliphatic. Comparison of the two spectra suggests that alifatic structures
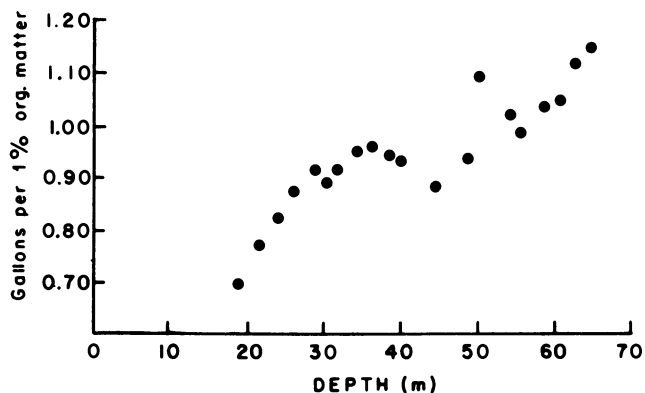
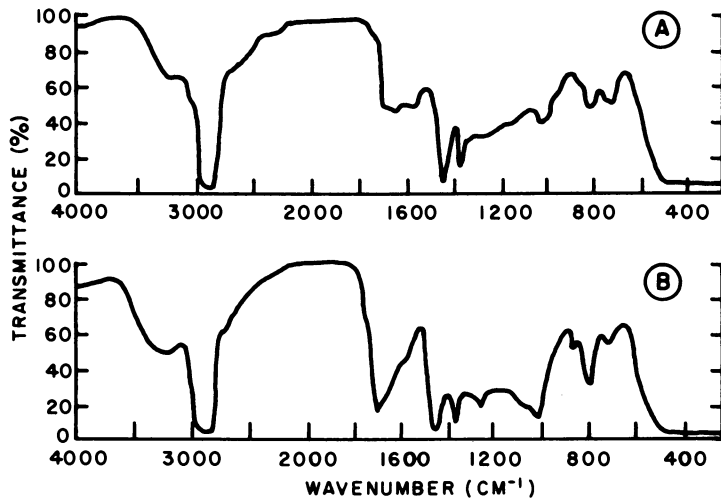*Figure 6. Oil yield per 1 wt % of organic matter content as a function of depth (Borehole Bit-1, Ef'e Deposit).*

Figure 7. IR spectra of Nabi-Musa (A) and Ef'e oil shale (B).

are more common in the Ef'e kerogen. The spectra of Israeli oil
shales are quite similar to those of the Estonian shales (8) and
to the kerogen of the Green River Formation (9).

Trace Elements

Table III summarizes trace elements concentration data in
the oil shales sequence of the Ef'e deposit, the phosphorite
layer from the same area (10) and the Green River oil shale (11).

Table III. Trace Elements Data (wt. ppm)

	Ef'e oil shale Borehole T-1	Ef'e phosphorite	Green River oil shale
Ag	1	n.d	<0.01
As	34	n.d	7.2
Ba	250	500	n.d
Cr	280	200	49
Co	5	n.d	39
Cu	112	25	15
Hg	0.2	n.d	<0.1
Li	17	n.d	850
Mo	26	n.d	4.9
Mn	41	40	34
Ni	138	70	11
V	110	170	29
Pb	10	n.d	10
Y	39	83	1.2
Zn	310	430	13
Zr	38	n.d	9.3
U	27	150	0.99

n.d=not determined

The Ef'e oil shale has higher concentrations of trace eleme-
nts than the Green River oil shale (except for Li and Co).
Concentration of those elements which occur in apatite (10)- V, Y,
U, Zn - are much higher in the phosphorite layers. Ni and V are
associated with functional groups within the kerogen, hence, the
Ni shows definite correlation with the organic matter content and
V shows relative correlation with both organic matter and apatite.
Cu and Zn are associated with pyrite. Since there is a positive
correlation between Zn and organic matter content, it may be con-
cluded   that the content of Zn is divided into three components
of the rock: apatite, pyrite and organic matter. The content of
arsenic is notably high. Generally, there is not any evidence for
an accumulation of trace elements due to organic matter content.

Summary

    The Israeli oil shales may be considered as a multi-
variabled system, in which the main components influencing their
quality are: organic matter, carbonate, clay minerals and apatite.
As the percentage of these components varies over the vertical
section, depth also plays a significant role whenever a quality
assessment of the shale is made. Compositional variations within
the organic matter are responsible for changes in the relative
calorific value and retorted oil yield, while fluidized bed
combustion is affected by the inorganic composition.

Literature Cited

1. Shirav (Schwartz),M.; Ginzburg, D. Proc. 10th Int. Cong. on
   Sedimentology. 1978, p.601-2.
2. Shirav (Schwartz), M.; Ginzburg, D. Special Publication, Int.
   Symp. on Oil Shale Chem. and Tech. 1978.
3. Shirav (Schwartz), M.; Ginzburg, D. Geological Survey of
   Israel, Rep. No. MP 597/80. 1980.
4. Brenner, I.B.; Eldad, H., personal communication.
5. Dinur, D.; Spiro, B.; Aizenshtat, Z. Chem. Geol. 1980, 31,
   37-51.
6. Wohlfarth, A.; Dibner, I.; Keren, Y.; Berkovitz, Y. Proc. Int.
   Symp. on Oil Shale Chem. and Tech. 1980.
7. "Ef'e Oil Shale Deposit", TOSCO Report, 1975.
8. Grassely, G.; Hetenyi, M.; Agois, M. Acta. Mineral. Petrog.
   (Szeged). 1973, 21, p. 55-71.
9. Robinson, W.E. in "Organic Geochemistry", Eglington, G.;
   Murphy, M.T.J., Eds.; Longman, 1969.
10. Nathan, Y.; Shiloni, Y.; Roded, R.; Gal, I.; Deutsch, Y.
    Geol. Surv. of Isr. Bull. 73. 1979.
11. Cook, E.W. Chem. Geol. 1973, 11, p.321-324.

Geology and Geochemistry of Some Queensland Tertiary Oil Shales

A. W. LINDNER

Southern Pacific Petroleum N.L., 143 Macquarie Street, Sydney 2000, Australia

There are at least 13 Tertiary oil shale deposits scattered along 900 km of coastal Queensland with an *in situ* shale oil resource totalling in excess of 25 billion barrels of shale oil. The paper compares aspects of the geochemistry for five of these deposits, which contain about two thirds of the demonstrated resource.

The oil shales are moist, with a dominance of clay and silica minerals, a range of accessory minerals including siderite, feldspar and lesser amounts of gypsum, calcite, dolomite, pyrite and a number of phosphate minerals.

Organic petrography and organic element analysis reveal that the source of the kerogen is algal (lamosites dominating) while other maceral forms dominate locally to form carbonaceous shale and humic coals.

Oil shale was first discovered in Queensland almost a century ago when dredging The Narrows, a 30 km long, shallow passage of the sea separating Curtis Island from the mainland north of Gladstone (Figure 1). The flammable rock aroused some prospecting interest for a number of years but the first serious attempt to assess the resource within The Narrows Graben did not take place until half a century later, during World War II. By this time, several other occurrences of oil shale along the coastal strip of Queensland had been reported. Typically, the Queensland Tertiary oil shales are sparsely exposed and deeply weathered. Because of this the extent of the deposits has only been determined by drilling. At the end of 1980, 38 exploration groups were involved in the search for oil shale deposits in Queensland (1). Much of this effort has been directed towards Tertiary oil shale, now known to occur in at least 13 separate basinal areas (Figure 2).
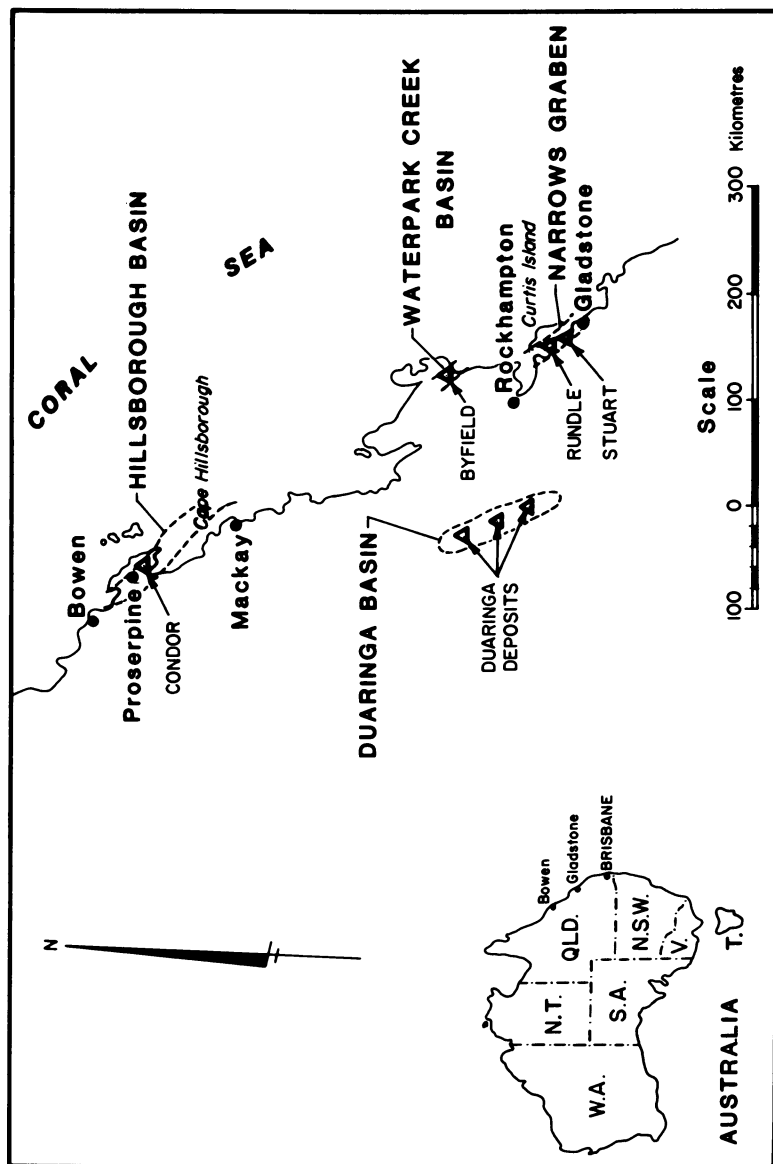
Figure 1. Location of four Tertiary basins in eastern Queensland.
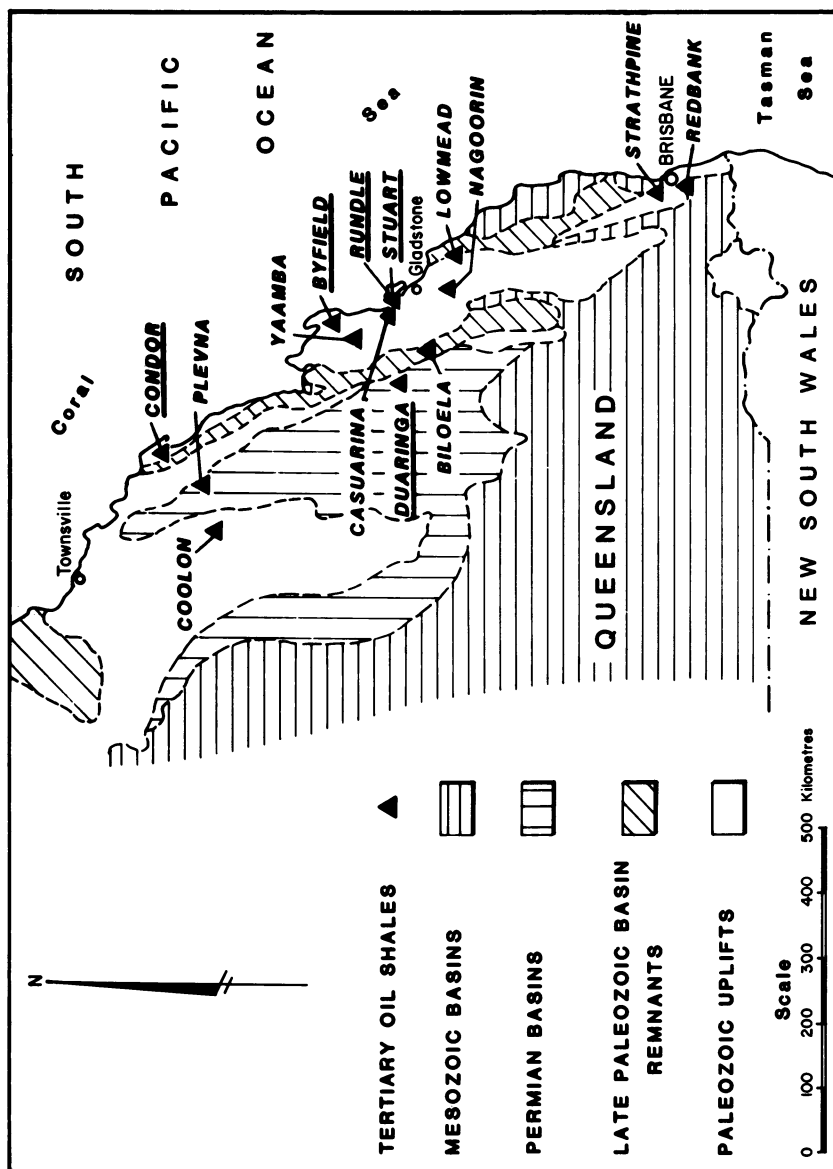
Figure 2. Location of Tertiary oil shale deposits in eastern Queensland.

This paper compares aspects of geology and geochemistry of the oil shales contained in 4 basins : The Narrows Graben containing Rundle and Stuart deposits; Hillsborough Basin containing the Condor deposit; the Duaringa deposits of the Duaringa Basin and the Byfield deposit in the Water Park Creek Basin.

Southern Pacific Petroleum N.L. and Central Pacific Minerals N.L. (SPP/CPM) commenced exploration for oil shale near The Narrows in 1974, concentrating on what was subsequently defined as the Rundle deposit. From 1977, the Stuart deposit was outlined. During 1978, SPP/CPM began prospecting in several of the other basins which held the attraction of favourable location, proximity to population centres and infrastructure facilities. Very little information was available on the thickness and distribution of oil shales in these basins, although Duaringa and Hillsborough were known to be large in areal extent and to have a total section-thickness comparable to that at The Narrows Graben. The Duaringa and Hillsborough Basins had previously been investigated cursorily for their petroleum potential without success.

In the five deposits under review the demonstrated *in situ* shale oil resource exceeds 17 billion barrels (at a cut-off grade of 50 litres/tonne at 0% retort water (LTOW) over a 4 metre minimum mining thickness. This cut-off grade is used herein when resource dimensions are specified).

All exploration drilling by SPP/CPM has had the objective of complete core recovery. The drill core is logged for lithology and bulk density, then split and assayed on 2m intervals, with one half being assayed and the other half retained in trays in the Companies' core storage facilities. Except at Condor, the bulk density has a direct proportional relationship to oil yield.

The modified Fischer Assay (USBM RI 6676 and more recently ASTM D.4904) has been used for determining grade of oil shale. From experience with the Queensland shales, an 80 g charge is used in the Fischer retort. The half core 2 metre interval provides from 3 to 5 kg of sample and the assay rejects are retained and provide a sample bank for characterisation tests carried out on the oil shale seams.

Geology of the Deposits

During the Paleozoic and early Mesozoic, the region now represented by eastern coastal Queensland developed by continental accretion to the Australian Shield. Sedimentary basins with marine and deltaic sequence and containing volcanic deposits have undergone periods of compressive deformation accompanied by igneous intrusions. The tectonic grain superimposed on the basins of this region strikes northwest (Figure 2).

Towards the end of the Mesozoic, a new continental margin developed and oceanic crust initially appeared in the Tasman Sea region, extending later (in early Tertiary) to the Coral Sea region (2). Associated with this new continental margin, a number of grabens developed within the continent along the older tectonic grain, during the Eocene. This appears to be the framework in which the thick, essentially lacustrine sequences containing oil shales accumulated in narrow, linear, fault-bounded basins (3), in some cases with accompanying igneous activity.

The Narrows Graben. From bore data the Rundle and Stuart deposits comprise a composite thickness in excess of 990 metres, as the basement floor of the graben was not reached (Figure 3). The sequence and extent of the resource in the Rundle and Stuart deposits is discussed fully by Henstridge and Missen (4). The basal unit (Worthington beds) includes agglomerate sourced from adjacent Paleozoic basement passing upwards into a sequence of colour-laminated red and green incompetent, soft, moist claystones and sandy claystones.

The oil shale resource is confined to the conformably overlying Rundle Formation (580m) and comprises six seams (Teningie Creek, Ramsay Crossing, Brick Kiln, Humpy Creek, Munduran Creek, Kerosene Creek). As the organic content increases, the claystones become lustrous and develop a waxy streak. Brown to grey- brown colours predominate. The high moisture content of the rock persists. Kerogen adds to the toughness or cohesiveness of the rock; the parting or bedding planes add to the appearance of a shale. Oxidation colours are absent in the Rundle Formation except in some basin margin areas. With experience and attention to the colour variations, the site geologist becomes adept at assessing the grade or oil yield of the oil shale beds. Barren green claystones, ranging in thickness from a few millimetres to several metres in the oil shale seams, reach a notable thickness in the Telegraph Creek unit located towards the top of the Rundle Formation. Nevertheless the formation consists predominantly of oil shale and the highest grade seams are contained in the upper 320m of the formation.

The shale oil average yield for the Rundle oil shales is 99 LTOW and 94 LTOW for those in the Stuart deposit. Average moisture in this formation is 20% by weight and *in situ* bulk density 1.75 g/cc. The measured *in situ* resource in the graben is 5.16×10^9 barrels of shale oil.

Fossil remains are widespread in the formation; most common are ostracods which add a distinctly calcareous content to some beds. A thin-shelled, low-helical gastropod is also common, occurring both in oil shales and barren beds. In
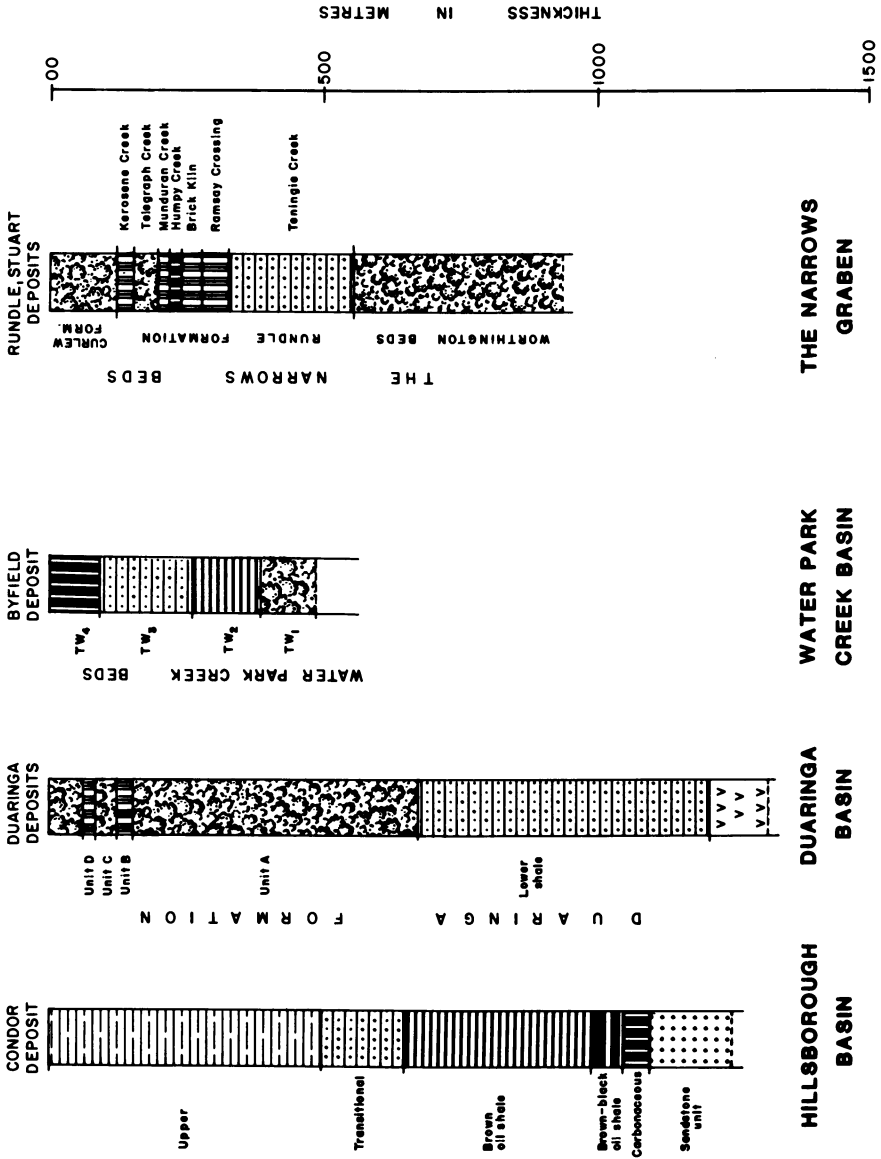
Figure 3. Diagrammatic columnar sections showing oil shales in four basins.

addition, fragments of vertebrate forms (reptilian and piscean) and crustacea, have been logged in drill core. From the faunal and floral assemblage the Rundle Formation is early Tertiary (mid to late Eocene) in age.

Dark brown to black carbonaceous layers occur in the Brick Kiln and Kerosene Creek seams and persist over considerable distances. One such unit is so persistent throughout the graben (and in a portion containing several metres of lignite) as to merit a separate unit classification (Humpy Creek seam). Sedimentary structures (breccias, colour grading, slumping) are prevalent and repeated macro-scale; recent detailed mapping in a cut opened in the Ramsay Crossing seam to provide bulk samples has revealed cyclic sedimentation over a frequency of a few metres (5). Thin, discontinuous, dense dolomitic limestone beds and lenses are present throughout the sequence.

Immediately overlying the Kerosene Creek seam at the top of the Rundle Formation, is another thicker carbonaceous shale with associated lignite, having a low oil yield. This passes upwards into claystones and sandy claystones with oxidation colours; the whole is named the Curlew Formation.

The Narrows Graben has structural asymmetry with a regional dip of the sequence from 4 to 10 degrees to the west. The youngest units are only present along the western margin of the basin and progressively older beds subcrop beneath the soil cover and colluvial outwash towards the east. While both margins of the graben are fault defined, the greater movement has occurred along the western boundary fault. Drag and subsidiary faulting into the main western boundary fault has affected the shale sequence for tens and hundreds of metres along this flank. Some faulting transverse across the grabens has occurred; such faulting associated with a possible basement high, brings the older, lower grade units to the surface, and separates the Rundle and Stuart deposits into two distinct lobes.

An alkaline dolerite has intruded the lower portion of the Rundle Formation at different stratigraphic levels in the Stuart Deposit, thermally metamorphosing the invaded sequence for an average of 46m over an area of 2.25 sq. km. The age of the dolerite is set at 26.8m.y. using the K/Ar method (4). A sill of about 4m thickness also occurs in the Rundle deposit. The thermal effect has been to form and relocate volatile hydrocarbons and leave a non-reactive aromatic residue on the oil shale adjacent to the intrusive (6).

Hillsborough Basin. The basin, defined geophysically during a phase of oil exploration during the 1960's, lies largely offshore from Mackay. It trends northwest towards Proserpine, inshore from Repulse Bay, and covers an area of about 75 x

15km. It is estimated to contain up to 3000m of section
offshore, whereas onshore a stratigraphic test located axially
in the basin, found middle Paleozoic basement at 1280m below a
sequence of Tertiary shales, mudstones, silty sandstones and
basal volcanic agglomerate.

Prospecting for oil shale has been confined to the
western flank of the onshore portion of the basin where
volcanolithic quartz arenites and pelites underlie the oil shale
sequence (7). The main oil shale unit of the Condor deposit is
a remarkably monotonous, massive (to slightly laminated) brown,
kerogenous mudstone (*brown oil shale unit*). The unit ranges
from 300-400m in thickness, persisting for at least 15 km. along
strike. About half of the unit has an average yield of 63 LTOW
and constitutes the main potential economic zone of the deposit.
Towards its base, the *brown oil shale* gradually becomes darker
in colour (*brown-black oil.shale unit*). This unit ranges from
10 - 50m in thickness and its base is marked by a sharp
contrast with a high ash lignite - carbonaceous shale
(*carbonaceous unit*), which in turn grades down into the basal
sandstone. The *carbonaceous unit* has a high volatiles content
and assays up to 135 LTOW have been recorded.

Overlying the *brown oil shale unit* are thinly interbedded
and laminated oil shales and siltstones, the *transitional unit*.
Above it is the youngest horizon (*upper unit*) occurring along
the western flank. This unit consists of cyclic sequences of
volcanolithic sandstones and siltstones with interbedded
laminae of oil shale and mudstone. With the uniform and
regular dip to the northeast, ranging from 10 to 14 degrees,
the *upper unit* of the succession exceeds 500m in thickness at
the downdip limit to which prospecting has been carried (5 km
downdip for 15 km along strike).

The structure of the deposit, with homoclinal northeast
dip, is uncomplicated, although faulting occurs. This appears
to be limited to a set of strike-normal faults, dipping to the
northwest. The western margin of the basin is faulted; the
displacement is probably of considerable magnitude. The
Tertiary beds are masked by up to 30m of alluvial gravels and
sands.

The oil shale of the Condor deposit is a tough, more
competent rock than the other Tertiary oil shales of Queensland
and also possesses a lower moisture content (9% moisture by weight).
The *brown oil shale unit* contains scattered collophane nodules,
commonly enclosed by marcasite and an outer paler carbonate-rich
halo. Buddingtonite occurs persistently in the *brown oil shale*
and younger units, comprising up to 10% of the rock (8).
Fossils are extremely rare in the Condor deposit. The measured
in situ resource is 8.45 x 10^9 barrels of shale oil.

Duaringa Basin. In contrast to the other deposits, the
Tertiary sequence in the Duaringa Basin has positive relief,

standing as three remnant, steep-sided tablelands separated
by water gaps. The tablelands are up to 100m above surrounding
low-lying country which is underlain by Permian sedimentary
rocks of the Bowen Basin. Although some indications of oil shale
had been reported many years ago, nothing was known of its
extent across the expanse of the basin, 180 km x 25 km.
Geophysical surveys in the 1960's indicated the possibility of
1200 metres of Tertiary rocks.
    "Fence line" drill holes across the basin in 1978-79
revealed that oil shale occurs above the base of the tablelands
and although structurally uncomplicated and continuous, is
relatively thin. There are two seams, an upper about 15m thick,
unit D, separated from the lower 25m seam, *unit B,* by a 20m
barren zone. Beds of oil shale also occur deeper (at about
250m below the surface) in the basin. Subsequent stratigraphic
core holes drilled by the Geological Survey of Queensland
(Duaringa 1-2R and 3/3A), proved presence of more than 1200m
of sedimentary rocks. Most of this is bioturbated silty and
sandy oxidised claystones with some oil shale below 600m
underlain by more than 80m of basalt (Noon, pers. comm.).
Basaltic lavas also occur interbedded with the shallow oil
shale layers in the southern end of the basin. A distinctive
and ubiquitous marker bed of centimetres thickness
characterised by abundant grains of sanidine has been found at
the base of *unit B* oil shale. Diatomite and barite are
associated with the oil shale at the northern end of the basin.
Phosphate minerals, including blue vivianite in small amounts are
present in *unit B.*
    The Duaringa tablelands have a deep soil and weathering
profile ranging from 40 to 60m, which has affected much of
unit D as well as *unit B* where topographic relief is not so
pronounced. *Units B* and *D* are estimated to contain 3.72×10^9
barrels of shale oil.

Byfield. At Byfield oil shale is contained in a small graben
2km wide for about 5km along the western flank of the Water
Park Creek Basin. Two oil shale units (*TW2, TW4*) overlie
carbonaceous and pale coloured claystones and sandstones
(*unit TW1*). *Units TW2, TW4* are separated by about 120m of
kerogen-bearing mudstone (*unit TW3*). *Unit TW2* is 120m thick
of which 50m has an average grade of 58 LTOW with a low (9.5%)
moisture and has superficial similarities to the *brown oil
shale* at Condor. At the top of sequence *unit TW4* (up to 110m)
consists of dark brown to black carbonaceous shale - lignitic
coal, with interbedded sandstone and siltstone. The shale oil
yield is relatively high (up to 100 LTOW) but averages 77 LTOW
for a net 50m. Some of the assay-produced oils contain a
tarry fraction, with a relative density >1.0 at $15.6/15.6°C$.
    There is insufficient drill hole control to calculate the
oilshale resource at Byfield; it is probably small, with not more
than 250×10^6 barrels of shale oil.

Composition of the Oil Shales

Maceral terminology for oil shales was modified by Hutton *et al.*
(9) when their study of these rocks pointed out a distinction
between high grade oil shales (such as torbanite and
kukersite both of which are typified by accumulations of
discrete rounded algal bodies) and Queensland Tertiary oil
shales (typified by finely banded lamellar alginite in
intimate association with mineral matter). They termed the
discrete rounded alginite 'Alginite A' and the lamellar
alginite 'Alginite B'. Green algae were believed to be
precursors of alginite A and both green and blue-green algae to
be precursors of alginite B, with both forms producing Type I
kerogen (10).
     For oil shales in which lamellar alginite is the dominant
organic entity, Hutton *et al.* proposed the term lamosite. Using
the form of organic matter as a basis for categorising types of
oil shale, Cook *et al.* (11) concluded that lamosites are of
lacustrine origin.
     The Queensland Tertiary lamosites are high in moisture with
an organic carbon content rarely exceeding 20% by weight.
Pyrite is usually present in trace quantities. An association
of silt-and clay-sized silica and silicate-rich minerals
dominates the inorganic constituents. However, generalisations
have to be kept in perspective. For example, assaying of the
oil shales has been consistently carried out over two metre
intervals. Over this interval, the organic carbon content
rarely exceeds 20%, but over centimetres within this interval,
the range may vary enormously. (A. Hutton, pers. comm., has
recorded a 20 cm interval from a core through the Kerosene
Creek seam at Stuart with 85% alginite content). Thus,
distinctive grade patterns over multiples of the two metre
assay interval commonly persist throughout the preserved areal
dimension of a deposit, coincident with other lithologic
characters of the rock. The seam classification at Rundle
applies also at Stuart, throughout the 28 km length of The
Narrows Graben (Figure 4). Likewise the 10 and 20m thick
seams (*units D* and *B)* at Duaringa persist over a distance of
130 km in the erosional remnants in that basin; and vertical
grade changes through the 300m thick *brown oil shale unit* at
Condor persist for at least 15 km along strike.

Mineralogy. The distribution of the major elements
(expressed as oxides) in the main oil shale seams in three
basins (The Narrows Graben, Duaringa and Hillsborough Basins)
are listed in Table I. The most apparent variations are in the
inorganic components of the carbonaceous units (*Humpy Creek
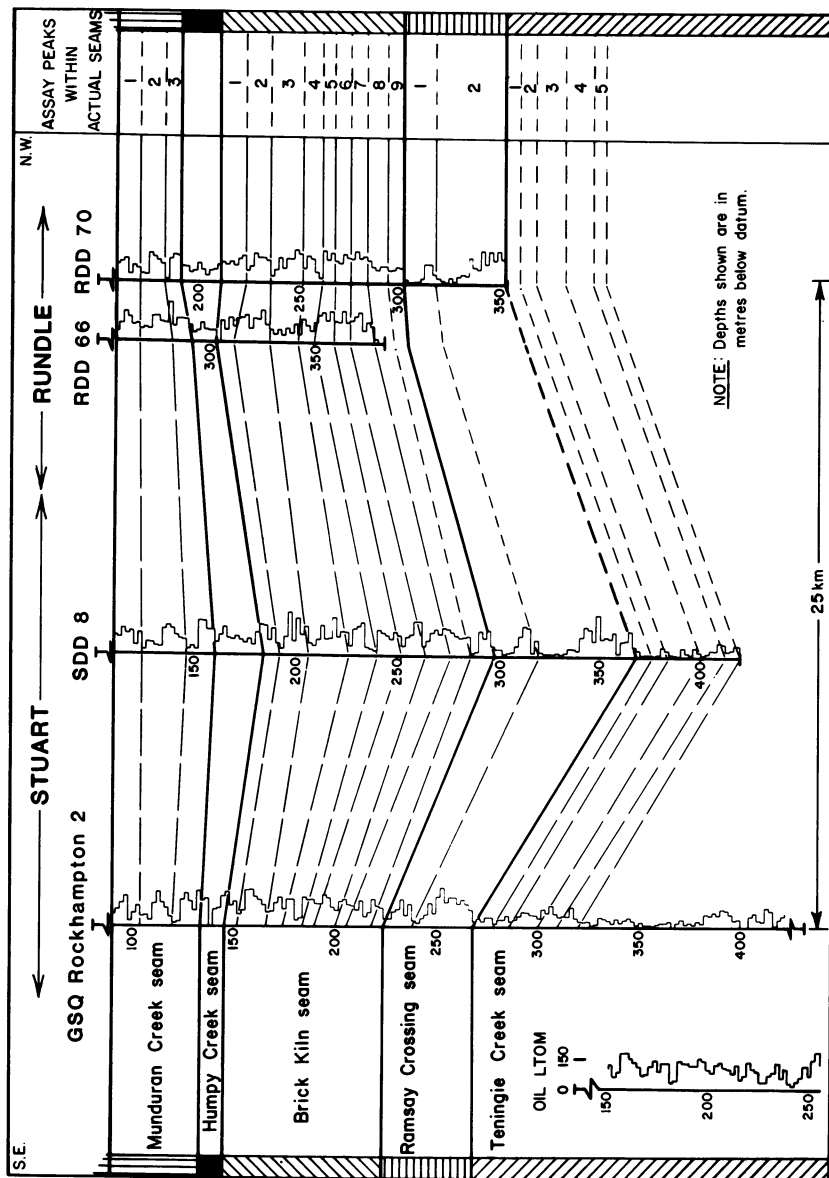seam* in the Narrows Graben; *brown-black oil shale* and

Figure 4. Oil yield histogram correlation of The Narrows Graben. (Reproduced with permission from Ref. 4. Copyright 1982, American Association of Petroleum Geologists.)

Table I. Major Elements as Oxides

Deposit	Seam	Rock Type*	No. of Analyses	SiO_2	TiO_2	Al_2O_3	Total Fe as Fe_2O_3	MnO	MgO	CaO	Na_2O	K_2O	P_2O_5	Range of Yields by mFA** (LTOW)	Av. Moisture*** wt%
STUART	Kerosene Ck.	O.S	4	62.4	0.6	16.1	9.1	0.2	2.4	5.8	0.8	2.2	0.4	45-230	22
	Munduran Ck.	O.S	3	61.5	0.7	16.6	8.7	0.2	2.3	6.3	1.2	2.2	0.3	109-202	18
	Humpy Ck.	C/C.S	3	71.5	0.6	12.7	7.6	0.1	1.6	2.7	2.1	1.0	0.1	81-112	24
	Brick Kiln	O.S.	14	61.2	0.8	16.3	9.7	0.2	2.6	6.1	1.2	1.6	0.3	44-193	18
	Ramsay Crossing	O.S.	9	62.4	1.0	16.0	9.3	0.2	2.9	5.3	1.0	1.9	0.2	25-179	17
	Teningie Ck.	L.O.S.	3	65.2	1.0	18.3	7.0	0.1	2.0	3.5	0.9	1.7	0.3	33-43	N.A.
DUARINGA	Unit B	L,M,H,O.S	18	66.2	0.8	19.0	8.6	0.3	1.3	0.6	0.6	2.3	0.3	27,57,119	24-33
CONDOR	Brown oil shale	O.S	3	68.8	0.9	17.3	8.9	0.1	1.4	0.8	0.5	1.0	0.3	25-104	8
	Brown-black oil shale	L.O.S	3	57.5	1.3	24.6	11.5	0.2	1.6	1.1	0.5	1.4	0.3	22-46	8
	Carbonaceous unit	C/C.S	4	59.0	1.4	30.7	5.0	<0.1	1.0	0.7	0.5	1.4	0.2	48-106	16

*O.S.   Oil shale
C/C.S   Coal, carbonaceous shale
L,M,H,O.S Low, medium, highgrade oil shale

N.A. not available

All analyses are by Australian Mineral Development Labs. (AMDEL), and are normalised to 100%. **Range of oil yields and ***average moisture are included for an appreciation of the organic and volatile components of the various oil shales. **Range of oil yields and ***average moisture are oil yield is expressed as litres per tonne of oil shale on a retort water free basis (LTOW). Average moisture is surface moisture removed by drying for 4 hours at 105°C. Retort water includes surface moisture and mFA combined water.

carbonaceous unit at Condor) when compared to the lamosites. At Condor, the increase in Al_2O_3 at the expense of SiO_2 is very pronounced; whereas in the *Humpy Creek seam* the distribution is reversed. The other aspect to the *Humpy Creek* is the relatively higher incidence of Na_2O and lower level of CaO and MgO compared to the rest of the seams in The Narrows Graben. The values of CaO and MgO for the lamosites are lower in the Duaringa and Condor deposits than in Stuart.

Mineral composition, as determined by X-ray diffraction, shows a dominance of clay minerals, although quartz and opaline silica are persistent as sub-dominant and locally dominant or co-dominant (Table II). Of the clays, expandable lattice clay minerals, predominantly montmorillonite, occur in all the deposits with kaolinite or illite appearing as accessory or subdominant components. A marked contrast in the dominant clay species occurs between the *brown oil shale unit* and the two units below it at Condor. In these lower units, kaolinite is in greater abundance than other clays as well as quartz, an aspect already alluded to in the variations in Table I. (Loughnan (8) also noted that the structure of the kaolinite changes from ordered in the lower units to disordered in the *brown oil shale unit*).

Feldspar occurs as an accessory or trace mineral in all deposits. At Rundle, Stuart and Duaringa it is a K-feldspar and more rarely, plagioclase, while at Condor it is the unusual ammonium feldspar, buddingtonite (8). The presence of buddingtonite in the Condor sequence coincides with the change from kaolinite to montmorillonite dominance. There is minor substitution of ammonium by potassium in the buddingtonite and Loughnan believes the mineral has pseudomorphed from an as yet unidentified progenitor. The feldspars in the deposits may be authigenic. The sanidine in the marker horizon at the base of *unit B* oil shale at Duaringa is considered to be of allogenic origin; probably from volcanic ash.

Apart from recurrent thin dolomitic limestone beds in The Narrows sequence, carbonates are present in all deposits in only trace or accessory amounts. Siderite occurs in all deposits, and is persistent through the sequence at Byfield and Condor, except for the carbonaceous units where its incidence is variable. At Condor, a second, possibly calcian siderite, occurs but only with an identical distribution through the sequence to the buddingtonite. Other evaporites, gypsum, halite and jarosite occur only in trace amount in the deposits. The sulphates may be a secondary development. Phosphate mineralisation occurs in the *transitional* and *brown oil shale* units at Condor; both as a mineral related to jahnsite (8) and as ovoidal collophane nodules up to 5 cm diameter (7). Vivianite is associated with *unit B* shale at Duaringa.

Qualitative emission spectrographic analyses for macro- and trace element distribution have been undertaken routinely

TABLE II. MINERAL COMPOSITION OF OIL SHALE SEAMS IN

DEPOSIT	SEAM	ROCK TYPE	m.FA (LTOM)	AMORPHOUS MATERIAL	QUARTZ	OPALINE SILICA	EXPAND. LATTICE CLAY MINERALS PREDOMINANTLY MONTMORILLONITE
STUART	KEROSENE CK.	O.S.	45-230		xx/xxxx	xx/xxxx	xxxxx
	MUNDURAN CK.	O.S.	109-204		xx/xxx	xxx/xxxx	xxxxx
		CL/O.S.	33- 47		xx	xx/xxx	xxxxx
	HUMPY CREEK	C.O.S.	81-112	xxx	xx/xxxxx		xxx/ xxxxx
	BRICK KILN	O.S.	50-193		xx	xx	xxxxx
	RAMSAY CROSSING	O.S.	25-179		xx/xxx		xxxxx
DUARINGA	UNIT D	O.S.	29- 62		xx/xxx	xxxxx	xxx
	UNIT B	CL/O.S.	5- 20		xxx/ xxxxx	xx/xxx	xx/ xxxx
		O.S.	22-148		xx/xxx	xxx/ xxxxx	xxxx/ xxxxx
	UNIT A	O.S.	∼ 90		xxxxx		xxxx
BYFIELD	UNIT TW4	C.O.S.	∼ 80		xxxxx		xxxx
	UNIT TW2	O.S.	∼ 80		xxxxx		xxx
CONDOR	B.O.S.	O.S.	25-104		xxxxx		xxx
	B/B.O.S.	O.S.	29- 46		xx/xxx		xxx
		C.O.S.			xx		xx/xxx

REFERENCE : - O.S. - Oil shale   C.O.S. - Carbonaceous oil shale   CL - Claystone

xxxxx Dominant, xxxx Co-dominant,   xxx Sub-dominant (>20%),

THE STUART, DUARINGA, BYFIELD AND CONDOR DEPOSITS

MICA/ILLITE	KAOLINITE	FELDSPAR	BUDDINGTONITE	SIDERITE	CALCIAN SIDERITE	CALCITE	CALCITE (SUBSTITUTED Mg)	PYRITE	GYPSUM	JAROSITE	ALUNITE	HALITE	ANATASE
xx	xx	x/xx		x		xx		x/xx	x	x/xx		x	
xx	xx	x/xx		xx		xx	xx	x/xx	x				
x/xx	xx	x		xx			xx/xxx	x	x				
	xx	x						x	x/xx			x/xx	
x/xx	xx	x/xx		xx		xx/xxx		x			x		
x/xx	xx/xxx	x/xx		x/xx		xx/xxx	x	x			x		x
	xxx	x		x				x	x				x
xx	xxx/ xxxx	x		xx									x
xx	xx/xxx	x		x/xx				x	x				x
xxx								x					
xxx													
xx				xxxx				x					
	xx		xx	xx	xx			x					
	xxxxx		x	xx									
	xxxxx			xx		x?		x?					

xx   Accessory (5-20%),   x   Trace (< 5%).
Bulk mineralogy determined by Amdel; except for Byfield, Duaringa A determined by
Commonwealth and Industrial Research Organisation (CSIRO) Division of Fossil Fuels.

since 1974 on composite samples of Fischer assay spent shale
through the oil shale sequence in the Queensland deposits.
Over selected intervals, similar analyses have been made on
fresh shale. These have not revealed any concentration of
metals in anomalous amounts, even though the provenance for
the different basins ranges from sedimentary through igneous
and metamorphic sequences. Limited quantitative analyses
on fresh shale from Condor (*brown oil shale*), and Stuart
(Brick Kiln and Ramsay Crossing seams) confirm the earlier
qualitative assessment of distribution.

Kerogens. In the course of characterisation work, a number of
kerogen samples have been isolated from different seams in the
various deposits. Their elemental composition (on a mineral
free basis) is listed in Table III and atomic ratios plotted
in a Van Krevelen diagram (Figure 5). The diagram demonstrates
the persistence of Type I kerogen in the lamosites from the
Queensland Tertiary deposits with the suggestion that Condor
kerogens may differ from this generalisation. Two of the five
kerogens from the Condor *brown oil shale* show an unusually
high O/C atomic ratio. The other kerogens from this unit
appear to be intermediate between the Type I and II.
     The carbonaceous units (at Condor, Byfield; Humpy Creek
seam at Rundle and Stuart) characteristically fall into Type III
kerogens implying both a lower algal content and the presence
of higher plant material. Thermogravimetric analysis confirms
this distinction in kerogen composition. Type I material
releases most of its volatile matter below 500°; Type III
carbonaceous kerogens give proportionally more above 500°C
(Saxby pers. comm). Higher maturation for the Condor Type III
sample is apparent, from reflectance values obtained on
vitrinite from this unit (Hutton, pers. comm.). Maturation
due to greater burial might also be assumed from the position
in the diagram of Type I Condor and some older kerogens
(Ramsay Crossing and Brick Kiln) in The Narrows Graben.
     Table III includes analyses of kerogen isolates and
derived shale oil. For the oils, the H/C atomic ratios are
higher than for the parent kerogens. This is consistent with
the oils being derived primarily from the algal component
of the oil shales. The oils derived from the carbonaceous
units differ from those derived from lamosites. The
carbonaceous units yield oil with a higher heteroatom content,
indicating presence of vitrinite or kerogen sourced from
higher forms of plant life. A lower oil yield per unit
kerogen content as observed by Eckstrom *et al*. (<u>12</u>) supports a
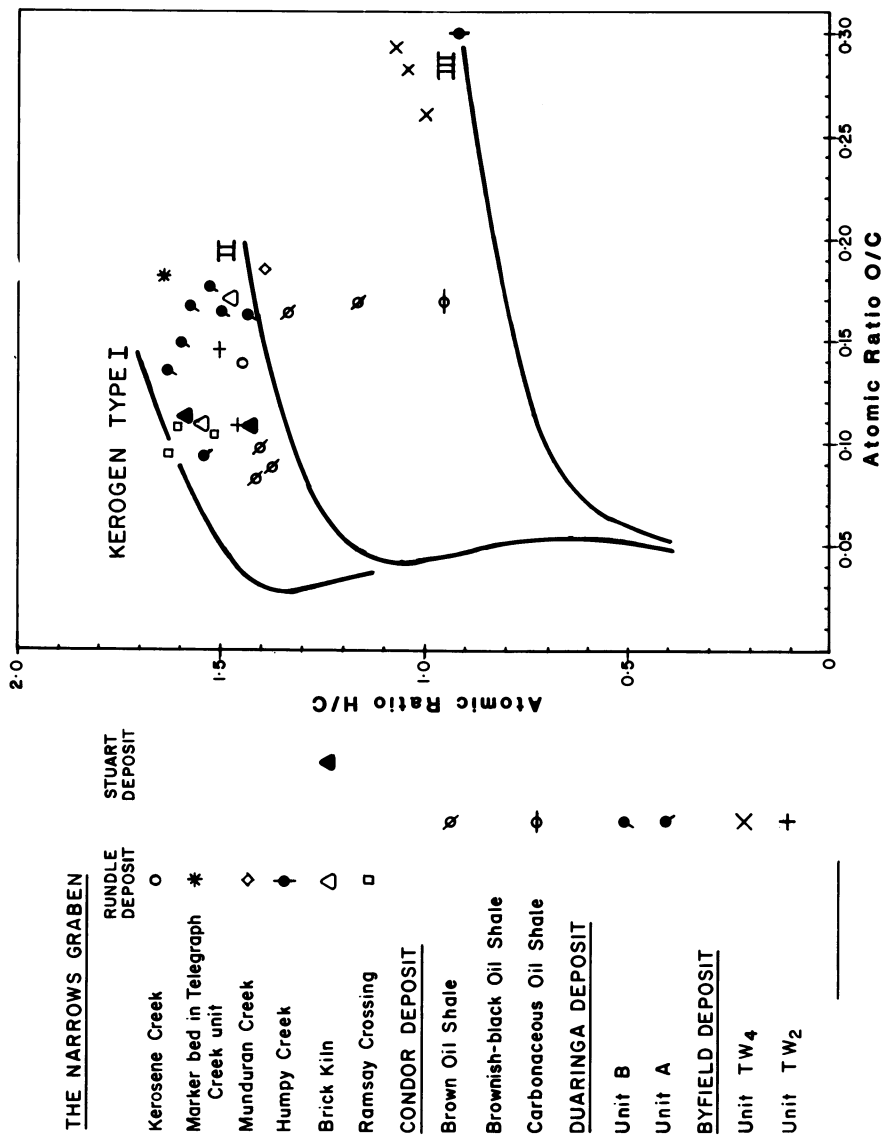highly condensed organic ring structure for the carbonaceous
unit kerogen.

Figure 5. Van Krevelen diagram of some Queensland Tertiary kerogens.

TABLE III. ELEMENTAL ANALYSES, KEROGENS

Deposit	Unit	Location		Fischer Assay Yield (LTOW)
RUNDLE	Kerosene Ck.	Auger sample		High grade
	O.S. Marker in Telegraph Ck.	RDD31	25m	Low grade (<40)
	Munduran Ck.	RDD31	110.5m	High grade
	Humpy Ck.	RDD43	80.5m	Medium grade
	Brick Kiln	RDD31	161.0m	High grade
	Brick Kiln	RDD25	111.0m	High grade
	Ramsay Crossing	RDD41	67.5m	High grade
		RDD41	85.0m	High grade
		RDD41	99.2m	High grade
STUART	Brick Kiln	SDD51	50- 52m	193
		SDD51	62- 64m	76
BYFIELD	TW$_4$	BYD1	68- 70m	98
		BYD1	84- 86m	83
		BYD1	84- 86m	83
			224-226m	Average grade
	TW$_2$	BYD1	290-292m	73
DUARINGA	B	DD10	66- 68m	64
		DD10	74- 76m	130
		DD52	92- 94m	26
	A	DD6	247.4m	Medium grade
CONDOR	Brown Oil Shale	Auger sample		65-77
		CDD1	380.1m	Average grade
		CDD6	352-354m	66
		CDD11	106-108m	82
		CDD11	68- 70m	62
	Carbonaceous	CDD26	308-310m	75
STUART	Brick Kiln	SDD51	36- 38m	172
			92- 94m	75
			134-136m	38
DUARINGA	B	27 Oils		Range 20-130
CONDOR	Brown Oil Shale	18 samples from CDD 6, 8, 11		Range 25-104
	Brown black Shale	3 samples from CDD10A, 11,26		Range 22- 46
	Carbonaceous	3 samples from CDD11,26		Range 48-106

* Analyses by Amdel unless notated B (Bureau Mineral Resources, Geology and Geophysics), C (CSIRO Division of Fossil Fuels)

AND SHALE OILS; ATOMIC RATIOS H/C, O/C

	Elemental Analysis (K=kerogen; O=Oil)						Atomic ratio	
	C	H	N	O	S		H/C	O/C
K	74.4	9.0	2.0	13.7	0.9	C*	1.45	0.138
K	71.8	9.9	1.3	14.9	2.1	B	1.64	0.156
K	70.9	8.3	1.9	17.4	1.5	B	1.40	0.184
K	64.9	4.9	3.1	25.9	1.1	C	0.91	0.300
K	73.4	9.1	1.1	15.1	1.3	B	1.48	0.154
K	75.5	9.7	2.0	11.0	1.8	C	1.54	0.109
K	76.6	10.3	0.7	10.9	1.5	B	1.61	0.107
K	77.6	10.6	1.0	9.6	1.2	B	1.63	0.093
K	77.0	9.8	1.5	10.5	1.2	B	1.52	0.102
K	74.7	9.9	1.7	11.6	0.2		1.59	0.116
O	85.4	12.8	0.9	0.7	0.2		1.80	0.006
K	72.3	8.6	1.2	17.8	0.3		1.43	0.118
O	84.7	13.0	1.0	0.9	0.4		1.84	0.008
K	66.8	5.8	2.2	25.2	0.5		1.05	0.283
K	67.9	5.7	2.1	23.5	0.8	C	1.00	0.260
K	65.6	5.8	2.3	25.6	0.5		1.07	0.292
O	82.0	10.8	1.0	5.6	0.6		1.58	0.051
K	75.3	9.1	2.2	11.9	1.5	C	1.44	0.119
K	72.5	9.2	2.2	14.0	?		1.52	0.144
O	84.7	11.8	1.2	1.7	0.6		1.67	0.015
K	71.6	9.5	1.4	14.2	1.4		1.60	0.149
K	60.6	7.7	1.0	14.2	4.8		1.53	0.176
O	85.9	11.6	1.3	1.4	0.5		1.62	0.012
K	71.3	9.4	1.0	15.5	1.4		1.58	0.166
K	69.1	9.4	1.2	12.3	3.8		1.63	0.133
O	85.1	12.1	1.1	1.3	0.4		1.71	0.011
K	68.8	8.6	1.3	14.9	1.2		1.50	0.163
K	50.4	6.1	1.3	11.1	5.9		1.44	0.165
O	86.1	11.3	0.9	1.5	0.6		1.57	0.013
K	78.3	10.0	1.7	9.5	0.5	C	1.54	0.091
K	77.5	9.1	2.3	8.3	2.5		1.41	0.081
K	78.9	9.0	2.8	9.1	0.4	C	1.38	0.087
K	70.0	8.2	1.9	9.4	4.2		1.41	0.101
K	70.2	7.9	1.9	15.1	5.1		1.34	0.161
K	68.9	6.7	2.7	15.4	6.6		1.17	0.168
K	72.4	5.7	2.9	16.1	1.4		0.95	0.169
O	85.8	12.3	0.8	0.7	0.4		1.72	0.006
O	85.3	12.6	1.1	0.5	0.5		1.77	0.004
O	85.6	12.3	1.2	0.3	0.5		1.73	0.003
O	83.8	11.8	1.1	3.2	0.5		1.69	0.028
O	85.3	12.1	1.5	1.0	0.5		1.70	0.009
O	83.7	11.2	1.4	2.6	0.6		1.61	0.023
O	84.0	10.5	1.4	5.2	0.6		1.50	0.047

Age and Depositional Environment of the Oil Shales

In a review of the Tertiary geology of North Queensland, Grimes (13) has developed a concept of three major cycles during the Cainozoic, each involving initially epeirogenesis with accompanying erosion and deposition, followed by a period of stability and weathering. The first of these commenced as a result of spreading of the Tasman Sea floor towards the end of the Cretaceous and continued through the Paleocene and Eocene when the Coral Sea floor opened, as an extension of the Tasman opening and incidentally when the Australian Plate commenced its northward movement away from the Antarctic Plate. By the end of the Eocene, this first active phase ended in Queensland and a period of stability extended into the Oligocene.

Evidence is accumulating that the oil shale deposits considered in this paper at least, are co-eval, now that the microfloral assemblages in Australia have been tied into the marine succession preserved around the southern margins of the continent. Foster (14 and pers. comm.), in studying additional material supplied from the current exploration activity, has been able to review earlier interpretations and it appears that most, if not all, of the Condor, Duaringa, Byfield, Rundle and Stuart oil shale sequences are confined to the middle and late Eocene. The unique conditions favouring formation of the oil shale deposits may have ended at this time.

Possibly a contributing, if not a constraining, factor to the age and distribution of the Queensland Tertiary oil shales is the climate change from moist, warm and equable to drier and cooler conditions at about the Eocene-Oligocene boundary (15) which in turn may have resulted from modifications to the oceanic currents induced by plate movements in the Pacific region. Third order global cycles of sea level lowering near and at the end of the Eocene (16) coincide with the end of the first of Grimes' cycles.

All the Tertiary sedimentary basins considered contain a substantial proportion by volume of clastic rocks devoid of organic content. Such units typically contain bioturbated, sandy and silty claystones with reddish and brownish colouring. At Duaringa these units are interbedded with oil shales. In the other deposits, low grade or barren interbeds in the oil shales do not display oxidation colours. It seems that once the conditions supporting growth of plant organisms was established, an anaerobic regime persisted, although variation took place in the amount and type of vegetal matter contributed and preserved in the accumulating deposits. Such variations occur with greater frequency in The Narrows Graben (as shown by numerous carbonaceous horizons interbedded in the lamosite sequence) and cyclicity in this sequence has already been mentioned. At Condor, once the lignin-like

material was supplanted by the lamellar alginite dominant
in the *brown oil shale,* conditions remained relatively
unchanged until several hundred metres of sediment had
accumulated.

    While the evidence (fossils, sediment type, stratification)
supports a lacustrine environment for all the deposits, the
monotonous sequence at Condor is unique. At Condor, a
stratified lake system similar to that proposed by Smith and
Lee (17) for density stratification in the Piceance Creek
Basin may have developed.

    There may be a combination of circumstances in the
Queensland Tertiary lakes (sedimentation rate, supply and
range of organic matter, water depth etc.) from which a
regional model can be deduced. The relationship of time,
climate, provenance and preservation of this energy resource
is a topic for much further study and research.

Acknowledgments

    Preparation of this paper has only been possible with the
co-operation of a large number of colleagues representing a
range of disciplines and skills, and all of whom have been
involved in aspects of documenting the properties of
Queensland Tertiary oil shales for the past few years. I am
particularly indebted to Messrs. J. Best, J. Gannon,
D. Henstridge, A. Hutton, J. Ivanac, T. O'Dea, Dr. J. Saxby
and Professor F.C. Loughnan for their suggestions and support
and to Messrs. J. Allcock and R. Gibb for the illustrations.
I gratefully acknowledge permission of the boards of
SPP and CPM to produce this paper.

Literature Cited

1. Day, R.W., Qld. Gov. Mining J., 1981, (82), 214
2. Mutter, J.C., and Garner, G.D., in "The geology and
   geophysics of northeastern Australia" R.A. Henderson and
   P.J. Stephenson, (eds.,) Geol. Soc. Australia (GSA), Qld.
   Division, 1980, 47
3. Lindner, A.W. and Dixon, D.A., J. Australian Petroleum
   Exploration Association (APEA), 1976, 16, 165
4. Henstridge, D.A. and Missen, D.D., Bull. American Assoc.
   of Petroleum Geologists, (Bull AAPG), 1982, 66, 719
5. Neale, R.C., and Coshell, L., Search, J. of Aust. and N.Z.
   Assoc. for Advancement Sci., 1982, 13, 126
6. Saxby, J.D., and Stephenson, L.C., In situ pyrolysis of
   oil shale at Rundle (Australia) by igneous intrusion, to
   be published in "Organic thermogeochemistry" R. Ikan and
   and Z. Aizenshtat (eds.,) Springer-Verlag
7. Green, P.W. and Bateman, R., J. APEA, 1981, 21, 24

8. Loughnan, F.C., Roberts, F.I. and Lindner, A.W., "Buddingtonite in the Condor oil shale deposit, Queensland, Australia" (Min. Mag. in press)
9. Hutton, A.C., Kanstler, A.J. Cook, A.C. and McKirdy, D.M., J. APEA 1980, 20, 44
10. Tissot, B.P. and Welte, D.H., "Petroleum formation and occurrence" Springer-Verlag, Berlin, 1978
11. Cook, A.C., Hutton, A.C., and Sherwood, N.R., "Classification of oil shales", Bull. Centres Rech. Explor. - Prod. Elf-Aquitaine, 1981, 353
12. Eckstrom, H., Hurst, H.J. and Randall, C.J., "The chemical and retorting properties of selected Australian oil shales" (this volume)
13. Grimes, K.F., in "The geology and geophysics of northeastern Australia" R.A. Henderson and P.J. Stephenson, (eds.,) GSA Qld. Division, 1980, 329
14. Foster, C.B., Geol. Surv. Qld. Pub. 381, 1981
15. Truswell, E.M., "Australia's past climates", B.M.R. Year Book for 1979 (1980), 39
16. Vail, P.R., Mitchum, R.M. and Thompson, "Seismic stratigraphy and global changes of sea level, Part 4: Global cycles of relative changes of sea level", in "Seismic stratigraphy-applications to hydrocarbon exploration", AAPG Mem. 26, 1977, 83
17. Smith, J.W. and Lee, K.K. Proc. 15th Oil Shale Symp. Col. School of Mines, 1982, 111 (in press)

Paleozoic Black Shales of Ontario— Possible Oil Shales

J. F. BARKER and R. D. DICKHOUT—University of Waterloo, Department of Earth Sciences, Waterloo, Ontario, Canada

D. J. RUSSELL and M. D. JOHNSON—Ontario Geological Survey, Engineering and Terrain Geology Section, Toronto, Ontario, Canada

P. GUNTHER—Petro Canada, Geological Research and Services, Calgary, Alberta, Canada

Three black, organic-rich, Paleozoic-age shales
occur in southern Ontario - the Ordovician Whitby
(Billings) Formation and the Devonian Kettle Point
and Marcellus Formations. In the Whitby Formation,
the most organic-rich zone is the Lower or Collingwood
member. It is 1.5 to 7 m thick, carbonate-rich with
organic carbon content up to 13%. Organic richness
is quite variable but the richest areas along the
Whitby subcrop occur from Manitoulin Island to Colling-
wood. Fischer Assay oil yields range up to about 60
litres/tonne (14 U.S. gal/ton). The Whitby Formation
appears to have reached a marginally mature thermal
maturation level and so bitumen is a significant com-
ponent of the organic matter. The bulk of the organic
matter is kerogen, dominantly type I and type II, and
of marine origin.
        The Kettle Point Formation subcrops in southwestern
Ontario. It is up to 60 m thick, with organic carbon
values usually in the range 5%-16% and Fischer Assay
oil yields up to 70 l/t (17 gal/ton). The organic
matter is dominantly kerogen of marine origin and has
attained only an immature thermal maturation stage. A
particularly rich upper zone is present over much of
the subcrop area and its thickness seems to be con-
trolled by post-Kettle Point erosion. Although studies
are still preliminary, especially for the Devonian
shales, the Kettle Point Formation appears to have the
most potential for shale oil production in southern
Ontario.

Historically, shale oil was produced in Ontario from a plant
near Craigleigh, on Lake Huron. In 1859, rock of the Ordovician
Whitby Formation was retorted to produce fuel and lubricants. In

1863, this operation became uneconomic in the face of the con-
ventional crude oil newly discovered near Oil Springs, Ontario.

    In 1981, the Ontario Geological Survey began a program to
assess the resource potential of the Whitby Formation and the
other black shales of Ontario. Prior to this study, information
on Ontario's black shales has been very sparse due to poor or
non-existent exposure and limited subsurface information. Exist-
ing data suggested three units were sufficiently organic-rich to
warrant further study--the Ordovician Whitby and the Devonian
Kettle Point and Marcellus Formation (1).

    The initial phase of the project involved shallow sampling
of the Whitby Formation by diamond drilling at 20 locations.
These stretched from Manitoulin Island to Toronto (see Figure 1)
and to Ottawa, where the stratigraphic equivalent Billings For-
mation is present. In 1982, 20 boreholes were located on the
Kettle Point subcrop and 4 boreholes were located on the Mar-
cellus subcrop. Lithological and geophysical logs for these
boreholes are in preparation. A preliminary organic geochemical
study of the Whitby Formation (2)is in press. Studies of the
paleontology, stratigraphy and sedimentology, mineralogy and
inorganic geochemistry of the Whitby Formation are underway.
This paper emphasizes the organic geochemistry of these black
shales.

Geology of the Black Shales

    The Upper Devonian Kettle Point Formation is a continuation
of an extensive series of black shales which are known across
eastern North America; the unit is approximately correlative with
the Antrim shale of Michigan, the Chattanooga shale of Alabama
and Kentucky, the New Albany of Indiana, and the Ohio shales of
Ohio. The Kettle Point strata underlie a broad band of southern
Ontario between Lake Erie and Lake Huron and are flat lying or
gently dipping to the north-west into the Michigan Basin (see
Figure 1). Rocks of the Kettle Point unconformably overlie the
shales and carbonates of the Hamilton group and are overlain
(in the extreme north-west of the subcrop belt only) by the
Bedford shales of the Port Lambton Formation. The upper contact
is sharp. Lithologically, the Kettle Point consists of a dark
grey, brown-grey to black silty argillaceous shale. The southern
and central areas of the Formation are also characterized by an
abundance of green shale interbeds. Large spherical concentra-
tions are also known within the Formation; they are locally
termed "kettles" from which the Formation is named. The unit
has a maximum thickness of 60 metres in Ontario, but average
about 28 m across the subcrop area.

    The Middle Devonian Marcellus Formation consists of black
bituminous shale and minor argillaceous limestone lying con-
formably on the Dundee Formation limestones. Its depositional
setting resembles that of the Whitby Formation and the Marcellus
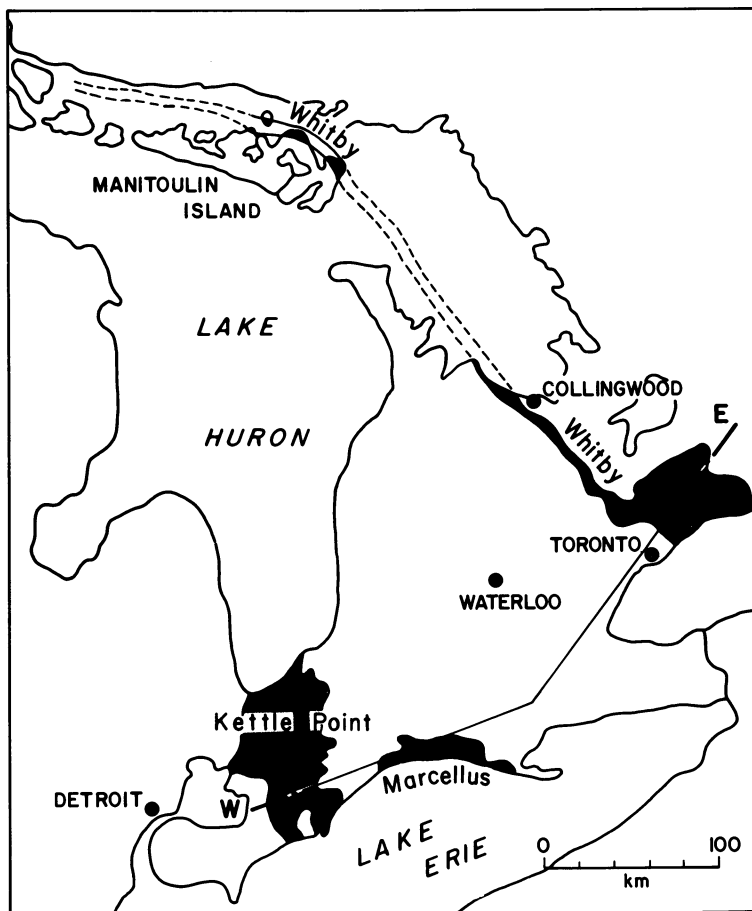
Figure 1. Outcrop or subcrop locations of Paleozoic black shales in southern Ontario.

is also carbonate-rich. Thicknesses of up to 50 m are reported
under Lake Erie, but the Marcellus thins and is less than 20 m
thick where it subcrops on the north shore of Lake Erie. The
presumably more widespread Marcellus shales were stripped off
during subsequent uplift and erosion. The Marcellus is uncon-
formably overlain by Hamilton Group shales and limestones be-
neath Lake Erie, and by unconsolidated Quaternary glacial de-
posits up to 60 m thick where it subcrops under land.

The Upper Ordovician Whitby Formation overlies the Lindsay
Formation of the Middle Ordovician Simcoe Group. The Lindsay
Formation is a limestone with interbedded shaley units. The
character of the contact with the overlying Whitby Formation is
variable and may be an important control over the organic con-
tent of the lower part of the Whitby Formation. The Whitby
Formation is overlain by interbedded limestone and shale of the
Upper Ordovician Georgian Bay Formation.

The Whitby Formation has been subdivided into Upper, Middle,
and Lower (Collingwood) members (3). The Upper member is gener-
ally a greenish-grey fissil shale between 36 and 52 m thick in
the study area. The Middle member is a brownish-grey fissile
shale between 5 and 26 m thick. The Lower member or Collingwood
is a dark brownish-grey marl with black shale interbeds and is
1.5 to 7 m thick. It is sometimes highly fossiliferous.

Considerable lithological variation is observed along the
subcrop, but it is evident that the most organic-rich zone of
the Whitby is the Lower (Collingwood) member which occurs in a
transition from carbonates of the Lindsay Formation to shales of
the Whitby Formation. In fact, lithologic considerations alone
would require that the Collingwood member be included in the
Lindsay Formation rather than in the Whitby Formation. The
Upper and Middle members appear to be much more clay-rich, al-
though considerably different geophysical responses are noted
for the Manitoulin-Collingwood and Toronto areas. Mineralogical
data is very limited (4), but where clay minerals are a major
fraction, illite dominates over chlorite with only minor amounts
of smectite clays reported.

Analytical Methods

Analytical methods are described in (2). Standard methods
were employed for total organic carbon (TOC) and Fischer Assay
(FA) analyses. Kerogen was isolated by solvent extraction to
remove bitumen and acid dissolution to remove mineral matter.
Elemental analysis was performed only on kerogen with low ash
content (<25% by weight).

The yield of hydrocarbons upon pyrolysis of shale (YP) –
gas plus liquid – was determined by heating a known quantity of
raw shale (approximately 5-10 mg) in a helium stream to a temp-
erature in excess of 600°C using a Chemical Data Systems (CDS)
quartz tube pyroprobe. The hydrocarbons were measured with a

flame ionization detector. Methane injections were used for
calibration. The results are expressed as weight percent carbon
(methane equivalents). This unit [%C(CH4 eq.)] has sense only
in the analytical determination and is not equivalent to the car-
bon yield on pyrolysis.

The evolution of hydrocarbon products from shale as the
pyrolysis temperature increased was monitored with a flame ioni-
zation detector and a yield versus temperature profile produced.
Initially, pyrolysis was done with the CDS pyroprobe, but major
limitations were observed, mainly with ensuring prompt removal
of products. Subsequently, an automated concentrator and high-
temperature pyrolysis furnace produced by Envirochem, Inc. was
employed. This system permitted use of larger (50-100 mg) sam-
ples and the helium sweep gas effectively removed pyrolysis pro-
ducts (pyrolysates). However, the pyroprobe system is still
used to measure YP as it provides a rapid, consistent determina-
tion.

Kerogen pyrolysate components were analyzed by gas chromato-
graphy coupled with mass spectrometry (GC/MS). Approximately
10 mg of kerogen were deposited in a quartz tube and pyrolyzed
in a helium stream, while the pyrolysis temperature was raised
to 650°C at 200°C/s and held at the final temperature for 16s.
The pyrolysate was cold trapped with methanol and dry ice, then
rinsed with three 1-µl aliquots of methylene chloride into a clean
sample vial. An aliquot of each pyrolysate solution was injected
onto a 30 m SE30 fused silica capillary column (WCOT) and the
eluting compounds were analyzed via electron impact mass spec-
trometry. The resulting mass fragmentograms were computer
matched with a standard library of organic compounds. Recon-
structed total ion chromatograms were also produced for compar-
ison with the corresponding FID chromatograms.

To obtain FID chromatograms of the kerogen pyrolysates for
kerogen typing, approximately 1 mg of kerogen was deposited in
a quartz tube and pyrolyzed as above with the pyrolysate swept
onto the capillary column used above via a splitless injection
port in a HP5840 gas chromatograph. Kerogen typing as devised
by Larter and Douglas (5) was done by dividing the peak area for
m(+p)-xylene by the peak area for n-octene.

Infrared (I.R.) spectra of kerogens were obtained using
thin (1 mm) discs of kerogen dispersed in KBr. The resulting
spectra were checked for the presence of absorbance bands due to
various functional groups.

Distribution of Organic Matter and Potential Oil Yields

Total Organic Carbon (TOC) analyses of core of the Whitby
Formation indicate that the Upper and Middle members rarely con-
tain more than 2.5% TOC. In contrast, the Collingwood member
often includes considerable intervals with more than 3% TOC
although the maximum thickness where TOC exceeds 5% is always

less than 3 m. Clearly, the major economic potential lies in the Collingwood member.

Only a few TOC analyses of the Marcellus Formation are available. Generally, the Marcellus contains less than 5% TOC, but a few scattered samples contain 9-11% TOC.

Most of the Kettle Point Formation exceeds 5% TOC. Two or three, thin (<2 m) intervals in the lower section contain more than 10% TOC and a rich interval at the top has more than 10% TOC for up to 3.5 m. This upper interval is not encountered in all boreholes and appears to have been removed by post-Devonian erosion except where the Kettle Point Formation is capped by outliers of Port Lampton Group.

The economic potential of these black shales is being assessed partially by measurement of the total hydrocarbon yield upon pyrolysis (YP) and by Fischer Assay (FA). These parameters are then being related to TOC content, so that the economic potential can be assessed on a regional scale from the abundant TOC data being gathered from borehole cores.

In the Whitby Formation, the available FA oil yields (59 samples) are less than 60 litres/tonne (14 U.S. gallons/ton). This oil has a specific gravity in the range 0.893 to 0.942. Twenty FA determinations on Kettle Point samples revealed oil yields up to 72 1/t (17 gal/ton) with specific gravity in the range 0.896 to 0.956. Few FA analyses of Marcellus shales are available; the highest oil yield to date is 64 1/t (15.4 gal/ton).

The relationships between TOC (%C) and Fischer Assay oil yield (1/t) are shown in Figure 2 and the correlation equations are:

$$FA = 5.6 \ TOC - 3.9 \qquad \text{(Whitby)}$$

$$FA = 4.6 \ TOC - 0.73 \qquad \text{(Kettle Point)}$$

The correlation coefficients are 0.868 and 0.969 respectively, indicating a good correlation between TOC and FA. The positive intercept on the TOC axis for the Whitby samples suggests some residual carbon remains after pyrolysis. This was confirmed by TOC determinations on spent shales from FA retorting. This is consistent with the common observation that the oil yield from oil shales is not limited by organic carbon but rather by hydrogen because there is insufficient hydrogen to combine with the available carbon to form hydrocarbons. This probably reflects both the nature of the organic matter and its thermal maturation as discussed later.

The pyrolysis method (YP) was developed as a convenient, rapid alternative to the Fischer Assay. Major disadvantages include the small sample size (5-20 mg) which may not be representative, the poor control of absolute temperature, and the fact that all hydrocarbons--gases and liquids at room temperature--are detected. Thus, the YP provides a relative yield of hydrocarbons which cannot be directly translated into FA oil yield.
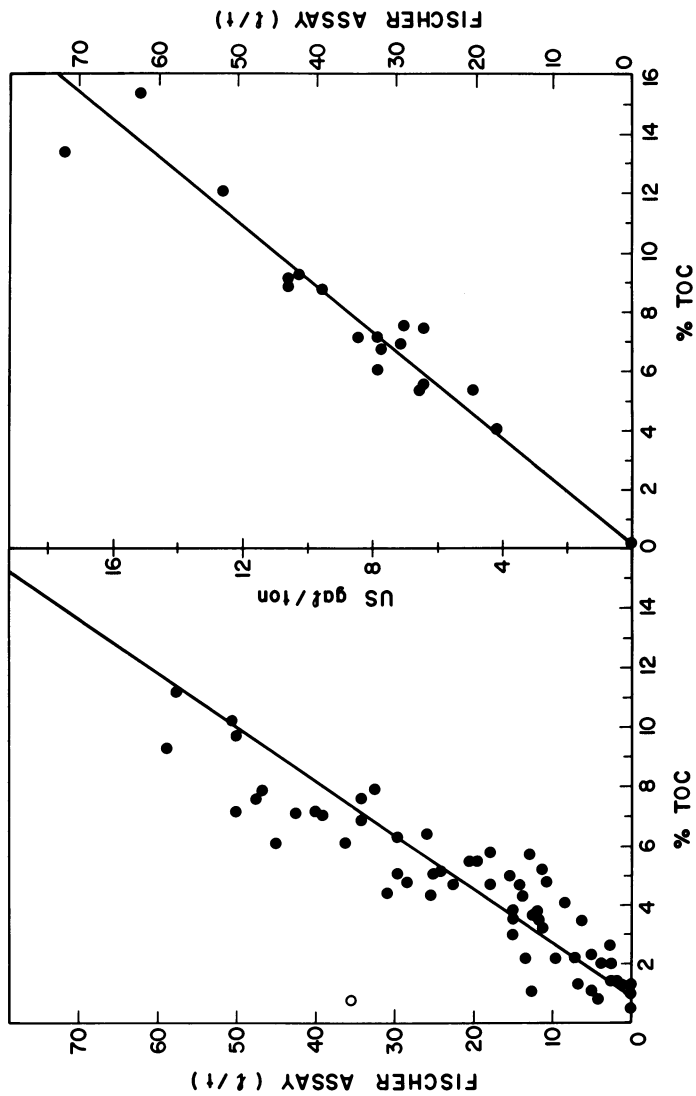
Figure 2. *The relationship between Fischer Assay oil yield and total organic carbon (TOC) content for shale samples from the Whitby (left) and Kettle Point (right) Formations.*

The relationship of YP and FA results are shown in Figure 3. A good correlation (R = 0.934 and 0.961 respectively) between YP (%C) and FA (1/t) exists where:

$$FA = 15.0 \ YP + 0.680 \quad \text{(Whitby Formation)}$$

$$FA = 17.2 \ YP - 1.56 \quad \text{(Kettle Point Formation)}$$

Prediction of FA oil yields from YP analyses seem justified for these formations at least.

Nature of the Organic Matter

Besides evaluating the amount of organic matter present and the yield of hydrocarbons upon pyrolysis, this study examines the nature of the organic matter in these black shales. Basically, two questions are being addressed. What is the maturation state of the organic matter and what is the chemical nature and origin of the organic matter?

Thermal Maturation

The thermal history of kerogen is usually discussed relative to the optimum time-temperature conditions for hydrocarbon (oil) generation. The relationships are presented schematically in Figure 4. Immature kerogen has not been heated sufficiently to produce oil, but the sediment may contain associated hydrocarbon gases, mainly biogenic methane. At perhaps 40-80°C maximum paleotemperature, the kerogen should have been sufficiently matured to begin producing oil as well as natural gas. At higher paleotemperatures, 120-160°C, only hydrocarbon gases should be present as liquid hydrocarbons are no longer stable; the associated kerogen is considered overmature. Only kerogen which is immature to perhaps marginally mature can be expected to produce commercial quantities of oil upon pyrolysis. In fact, commercial retorting or pyrolysis can be viewed as a much more rapid version of natural oil generation in which the mature and overmature levels are reached in the retort. As Figure 5 indicates, a number of thermal maturation indicators are commonly employed. Vitrinite Reflectance, Thermal Alteration Index (T.A.I.) and Conodont Alteration Index (C.A.I.) utilize the temperature-dependent change in colour or light reflectance of various kerogen components (6). The hydrocarbon proportion of bitumen from mature sediments generally exceeds 40% (7) and this maturation indicator is also utilized in southern Ontario.

Table I summarizes the indicated maturation levels of organic matter from the Kettle Point, Marcellus and Whitby Formations and equivalents in various areas. Using Figure 4, these may be related to thermal maturation. Only a few samples have been ex-
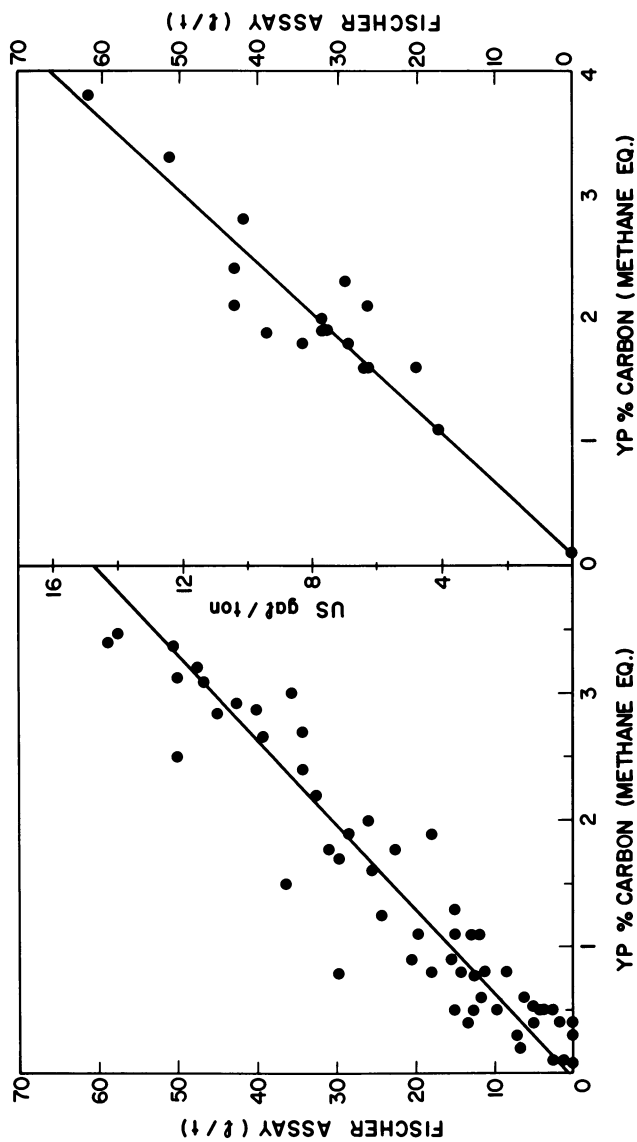
Figure 3. The relationship between Fischer Assay oil yield and yield upon pyrolysis (YP) for shale samples from the Whitby (left) and Kettle Point (right) Formations.
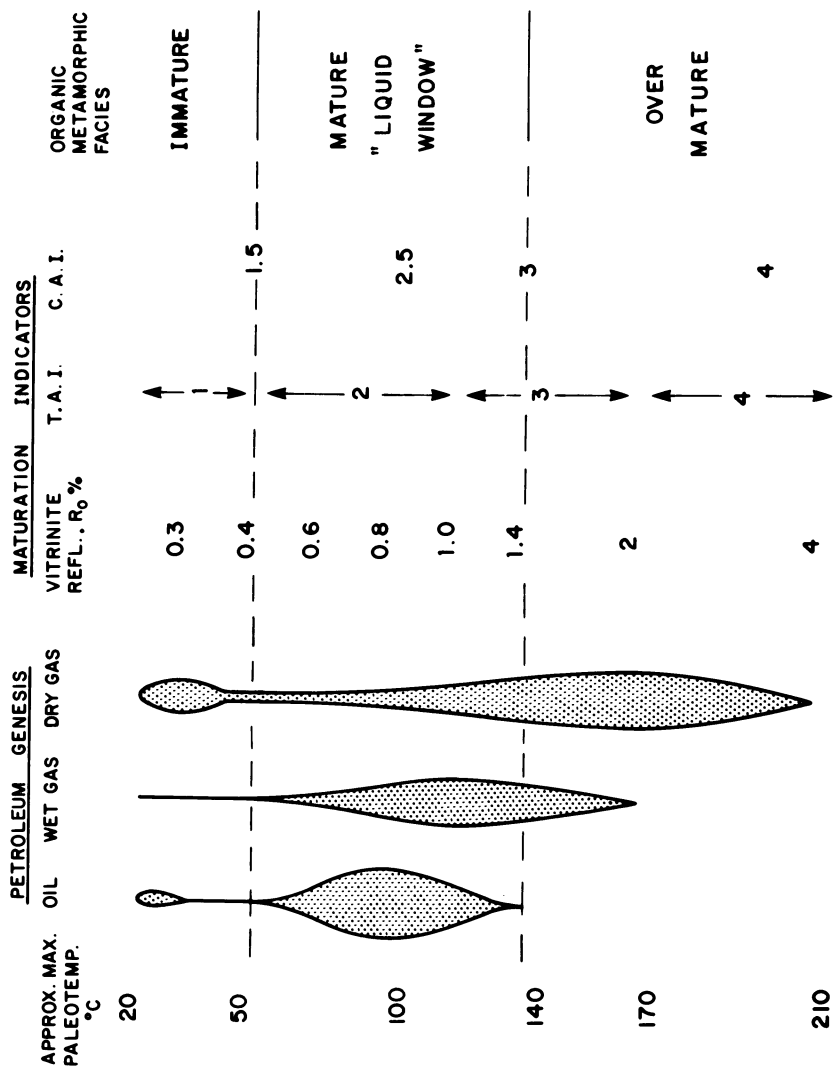
Figure 4. Thermal maturation levels and hydrocarbon generation from organic matter.
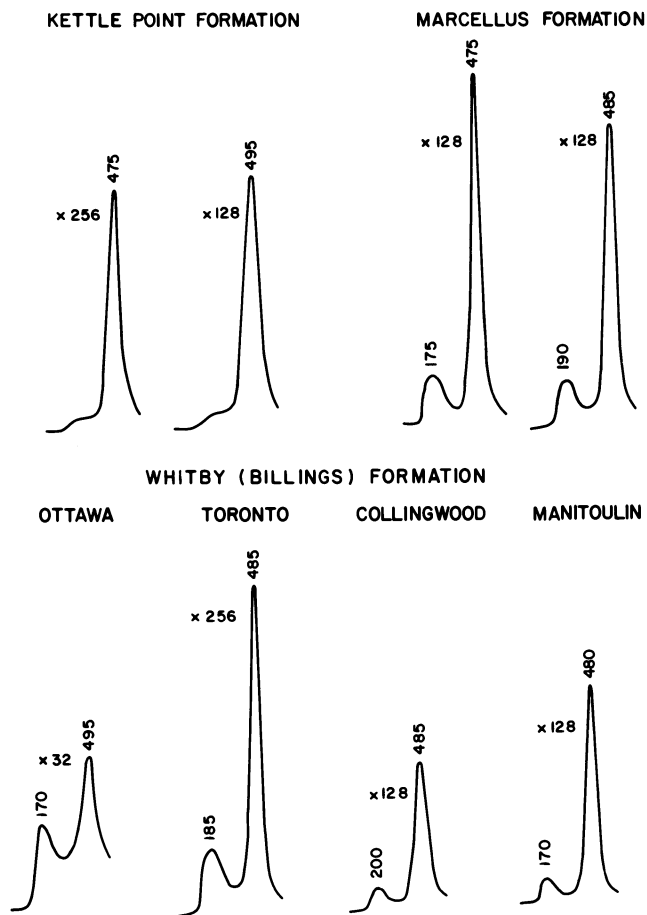
Figure 5. Temperature-programmed pyrolysis for Ontario shales.

Table I.   Selected Thermal Maturation Indicators

Indicator	Kettle Point	Marcellus	Whitby (Billings) Subcrop	Whitby (Billings) Ottawa
		Formation and Area		
Vitrinite Reflectance R_o %	0.39	0.32 to 0.53	0.44 to 0.57	1.38
Thermal Alteration Index (T.A.I.)	2-	1+ to 2-	2 to 3-	3-
Conodont Alteration Index (C.A.I.)	1.5	1.5	1.5 to 2.5	3.0
Hydrocarbons, % in Bitumen	20		40 to 54	
Tentative Conclusion	Immature to Marginally Mature	Marginally Mature	Marginally Mature to Mature	Mature to Overmature

amined to date, but the conclusions are consistent with the more extensive studies in southern Ontario by Legall, et al. (8). None of the indicators alone provide a definitive indication of thermal maturation, but, when considered together, they provide a reasonably consistent picture. It seems that the Billings equivalent of the Whitby Formation in the Ottawa area is mature to overmature, while the Whitby Formation along its subcrop is marginally mature to mature. The Marcellus is marginally mature and the Kettle Point is immature to perhaps marginally mature.

The generation of hydrocarbons during temperature-programmed pyrolysis provides another indicator of thermal maturation and organic matter type (9, 10). Of particular interest is the ratio of hydrocarbons generated at temperatures of less than about 300° to the total hydrocarbons generated up to a temperature of 550° to 600°C termed the transformation ratio (11). The lower-temperature hydrocarbons generally correspond to thermally-desorbed bitumen while the higher-temperature hydrocarbons are generally considered to represent the pyrolysis of kerogen. This ratio has been observed to increase as thermal maturation level increases, at least to the mature-overmature boundary (9) and so this ratio provides another indication of thermal maturation level.

This temperature-programmed pyrolysis of southern Ontario black shales is illustrated by the pyrograms obtained with the Envirochem system (Figure 5). The samples from the Kettle Point Formation show no real bitumen peak, have a transformation ratio <0.3 and are immature. Marcellus samples commonly show a small bitumen peak and the transformation ratio is generally <0.4, which corresponds to an immature sediment. The Billings Formation samples from Ottawa appear mature with a ratio >0.5, while the samples from the Toronto, Collingwood and Manitoulin Island areas are less mature with a ratio generally between 0.2 and 0.3. More quantitative Rock-Eval analyses being conducted by MacCauley and Powell at the Institute for Sedimentary and Petroleum Geology in Calgary indicate an immature to mature state for the Whitby subcrop samples. Relative to the Whitby samples, the Marcellus appears immature to marginally mature while the Kettle Point appears immature. These conclusions are consistent with the other thermal maturation indicators.

Although maturation studies are continuing, it would appear that the Billings shale in the Ottawa area is not a potential oil shale because of its overmature nature. On the other hand, the immature to marginally mature nature of the Kettle Point, Marcellus and Whitby Formation in Ontario is encouraging. It may be advantageous to explore for less mature areas of the Whitby, especially in order to obtain higher pyrolysis yields per unit of organic matter. The Manitoulin Island-Collingwood area of the Whitby subcrop should be emphasized in further assessment. These areas are somewhat less mature than the Toronto area and also have higher TOC values. The immature, organic-rich Kettle Point Formation may be the best oil shale resource in southern Ontario.

Geochemistry of the Organic Matter

Oil generation potential is not only dependent upon the amount and thermal history of organic matter, but also upon its chemical nature. This is controlled by the nature of the source material and by biological and/or chemical transformations following deposition. Both solvent extraction and temperature-programmed pyrolysis indicate that a significant portion (10-50% perhaps) of the organic matter present in Whitby shales is bitumen, with a much lower proportion of bitumen in Kettle Point and Marcellus shales. Initial studies of the organic matter has concentrated on defining the nature of the kerogen in these shales, but studies of the bitumen are underway to evaluate its origin and its influence on the pyrolysis oil yields.

There are many ways to classify kerogen (see 11). A very useful system recognizes essentially three "types" of kerogen --types I, II, and III. These types can be distinguished on the basis of atomic H/C and O/C ratios. Figure 6 also indicates the general chemical evolution of these kerogen types with increasing thermal maturation. Type I kerogen is composed of marine or lacustrine organic material. It has the highest H/C of the kerogen types and is rich in naphthenes so it has a high capacity to generate liquid hydrocarbons. Structurally, kerogen particles are dominantly algal (alginite) or amorphous. Type II kerogen may have a significant component of terrestrial as well as marine material. Its H/C is lower than type I kerogen and its O/C is slightly higher. Dominant hydrocarbons are naphthenes and aromatics. Exinous (cutinite, resinite), vitrinous and fusinous materials are more common relative to amorphous material. Type III kerogen is dominantly terrestrial in origin with higher O/C and lower H/C values than the other types, reflecting the increased proportions of polycyclic aromatics and oxygen-containing functional groups. Vitrinous and fusinous materials dominate over exinous and amorphous materials.

All known oil shales contain type I or II kerogen. Type III kerogen tends to produce mainly gas upon pyrolysis. In this study, kerogen type is being assessed by visual examination under the transmitted light microscope and by geochemical means including atomic H/C determinations, pyrolysate typing and infrared spectrophotometry.

Figure 6 indicates the position of the Ontario shales on the van Krevelen diagram. Atomic O/C ratios are considered to be overstated because of the presence of minor amounts of silicate mineral matter in the kerogen isolates. Therefore, the kerogens may have lower atomic O/C ratios than shown and so could be type I or type II.

The relative proportions of amorphous, exinous and vitrinous plus fusinous kerogen material in the few samples examined to date are shown in Figure 7. Whitby Formation kerogens from the Collingwood area are highest in amorphous material and so one
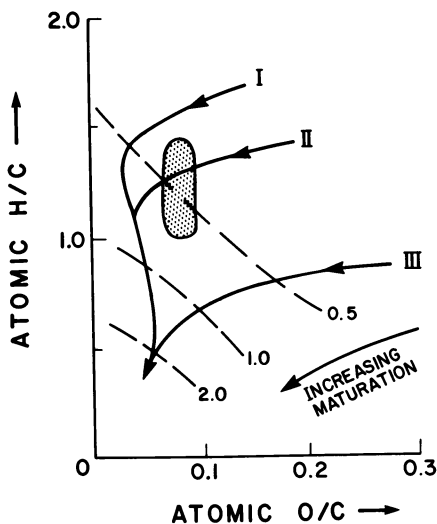
Figure 6. The variation of the elemental composition of kerogens as thermal maturation increases. Iso-vitrinite reflectance (% R₀) lines are dashed. Kerogen from Ontario shales falls within the shaded area.
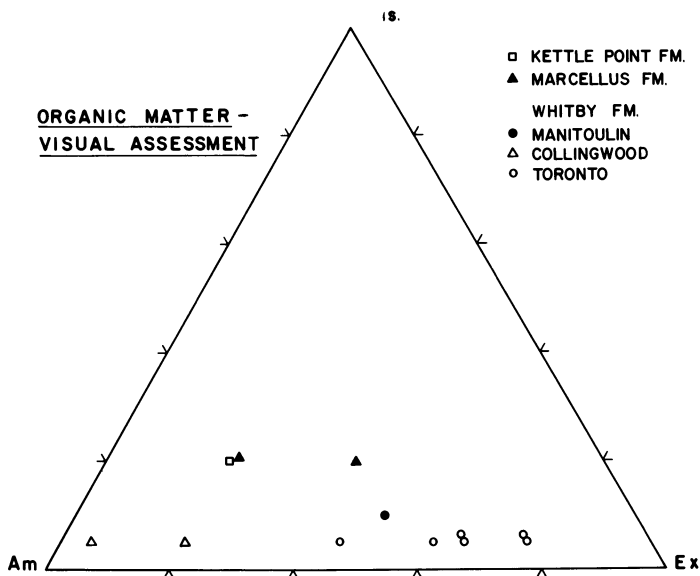
Figure 7. The relative proportions of amorphous (am), exinous (ex), and vitrinous plus fusinous (vit. + fus.) kerogen macerals. Key to formations: □, Kettle Point; ▲, Marcellus; ●, Manitoulin, Whitby; △, Collingwood, Whitby; and ○, Toronto, Whitby.

might predict that oil yields per unit weight organic carbon from Collingwood samples should be higher than for other samples reflecting this difference in type of organic matter. As predicted, for the five samples with appropriate analyses, a general decrease in FA/TOC is observed as the ratio of amorphous to exinous kerogen decreases, that is, Collingwood-area samples produce more oil upon pyrolysis (FA) per unit weight organic carbon than do either Manitoulin or Toronto samples of the Whitby shale.

Generally, there is an increase in the ratio of aromatic to aliphatic hydrocarbon types in the sequence from type I, through type II to type III kerogen. The products of kerogen pyrolysis also show this trend. Larter and Douglas (5), made use of this fact to establish a kerogen type index (R), which is the ratio of a selected aromatic (m- plus p-xylene) to a selected aliphatic (n-octene) pyrolysis product. Type I kerogen has R < 0.4, type II has 0.4 < R < 1.3, and type III has R > 1.3. Only Whitby shales have been "typed" to date. Generally, it was found that shale pyrolysates are more aromatic than kerogen pyrolysates from the same sample, especially for samples with TOC less than about 2%. This is likely the results of secondary reactions among the pyrolysis products catalyzed by mineral matter present in the shale but absent from the kerogen. Horsfield and Douglas (12) showed that such reactions increased the aromatic to aliphatic ratio of pyrolysates. However, for samples with TOC exceeding 3%, R values for raw shale and extracted kerogen from the same sample were in agreement (2), suggesting that secondary pyrolysis reactions were not significant for high TOC samples. The R values for kerogen from the Whitby Formation ranged from 0.28 to 0.66 and are interpreted as Type I and Type II kerogen. This is in agreement with the other kerogen-typing methods.

Infrared absorption (I.R.) spectra provide a qualitative indication of the organic structures present in the kerogen and their variation between samples. In general, the I.R. spectra of Whitby and Kettle Point kerogens are dominated by aromatic and aliphatic absorption bands with a minor OH band. Many samples from the Whitby Formation of the Toronto area show stronger OH absorption, and perhaps a more aromatic than aliphatic nature compared to samples from other locales.

Pyrolysis has been used to thermally degrade the large, complex kerogen molecules. The smaller and less-complex products (pyrolysates) are considered to represent structural units present in the kerogen macromolecules and these pyrolysates are more amenable to identification by gas chromatography and mass spectrometry. Most of the gas chromatograms of Whitby kerogen pyrolysates are very similar to the example shown in Figure 8. Alkene-alkane pairs dominate up to at least C_{15}. These are imposed on a background of polysubstituted benzenes. Above C_{15}, alkylbenzenes, probably including diterpenoids, dominate. Similar long chain alkylbenzenes have also been tentatively identified in the pyrolysate of coal macerals (13), of alginites (14), and of typical kerogen types (15).
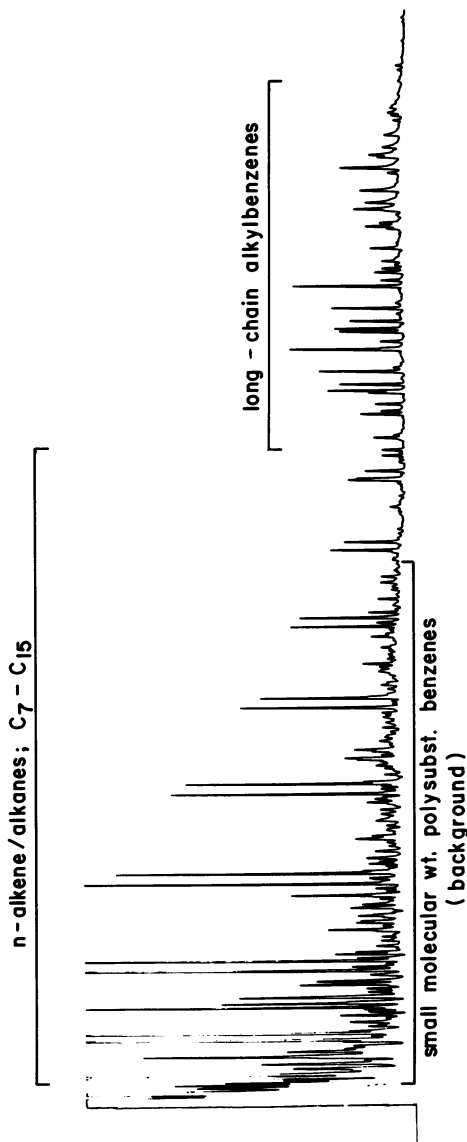
Figure 8. A typical gas chromatogram of pyrolysate of Whitby Formation kerogen. Identifications are from mass spectrometric analysis.

The general view of kerogen structure presented by Tissot and Welte (11) is nuclei of stacked polyaromatic rings with some heterocycles containing O, N and S. Attached to these nuclei are alkyl chains, naphthenic rings and some oxygen-containing functional groups (hydroxyl, carboxyl, etc.). Bridges between nuclei include aliphatic chains and oxygen- and sulphur-containing groups such as ketones, esters, quinone, etc. Almost all of these structural groups are indicated in the I.R. spectra of kerogen isolated from Ontario black shales. The pyrolysates show alkane-alkene chains, some of which may be breakdown products of the nuclei. The nuclei remnants are evident as higher molecular weight alkyl-substituted aromatics and as the lower molecular weight polysubstituted benzenes. No evidence of oxygen- or sulphur-containing heterocycles or bridges is found; however, CO_2 and H_2S are significant products of kerogen pyrolysis and could represent these components.

Significant variation in organic geochemistry has been observed within the Whitby Formation and between the Whitby and Kettle Point Formations. Research is in progress to define the geological controls and to relate the resource potential as measured by TOC analyses and FA oil yields to observed variations in organic matter type and maturation level.

Conclusions

The Upper Devonian Kettle Point Formation represents an episode of deposition of fine-grained, organic-rich material on a broad shallow shelf. In its subcrop area in southwestern Ontario, TOC values are generally in the 5% to 16% range and Fischer Assay oil yields up to 70 l/t (17 gal/ton) are reported. The organic matter is essentially all kerogen, dominantly of marine origin (type I-type II) and has reached only an immature thermal maturation level. The presence of an upper, organic-rich member seems to be critical for potential exploration of this oil shale. This upper member is 3-4 m thick where the Kettle Point Fromation has suffered minimal post-Devonian erosion.

The Middle Devonian Marcellus Formation is much thinner and less extensive where it subcrops on the north shore of Lake Erie, although thicknesses of 50 m have been inferred beneath the lake. TOC values up to 11% and Fischer Assay oil yields of 64 l/t have been found. The organic matter is slightly more mature than that in the Kettle Point, and so some bitumen is present. The kerogen is dominantly of marine origin.

The Upper Ordovician Whitby Formation represents a transition from carbonate to shale deposition on a broad, shallow shelf. The Lower member--the Collingwood member--has the most potential for shale oil production. This member is an organic-rich marl or carbonate with considerable lateral variation along its subcrop trend from Manitoulin Island to the Toronto area. TOC values up

to 10.7% and Fischer Assay oil yields of almost 50 1/t (14 gal/ton) are reported. The Whitby shale is more mature than its Devonian counterparts (perhaps marginally mature to mature) and bitumen makes up a significant (5% to 40%) proportion of the organic matter. The kerogen is dominantly type I-type II and is of marine origin.

Although the Whitby Formation was a viable oil shale in 1860, it does not appear to constitute a major, world-scale oil shale resource today. However, additional research has been undertaken to identify the richest and thickest shales which may be suitable for smaller-scale production as was practiced near Collingwood around 1860. The studies of the Marcellus Formation are very preliminary, but they point towards a resource of similarly limited value.

The Kettle Point has the most encouraging combination of organic richness and thickness of organic-rich zones. Post-Kettle Point erosion seems to control the thickness of an upper, organic-rich zone. Geological and geochemical studies of all three black shale units are continuing in order to provide the geological basis for future engineering and economic assessment of this oil shale resource.

Acknowledgments

Literature Cited

1. Macauley, G. Geological Survey of Canada Open File Report OFR-754, 1981.
2. Dickhout, R. D.; Barker, J. F.; Churcher, P. L. Ont. Geol. Surv. Open File Rept., in press.
3. Liberty, B. S. Geol. Surv. of Can., Memoir 355, 1969.
4. Russell, D. J.; Gale, J. E. Geosci. Canada 1982, 9, 20-7.
5. Larter, S. R.; Douglas, A. G. in "Advances in Organic Geochemistry, 1979," Douglas, A. G.; Maxwell, J. R., Eds. 1980, p. 579-83.
6. Heroux, Y.; Chagnon, A.; Bertrand, R. Am. Assoc. Pet. Geol. Bull., 1979, 63, 2128-44.
7. Powell, T. G. Can. Geol. Surv. Paper 78-12, 1978.
8. Legall, F. D.; Barnes, C. R.; Macqueen, R. W. Bull. Can. Petrol. Geol. 1981, 29, 492-439.

 9. Espitalie, J.; LaPlat, J. L.; Madec, M.; Marquis, S.; Leplat,
    L.; Paulet, J.; Boutefeu, A. Rev. l'Inst. Francais Petrol.
    1977, 32, 23-42.
10. Barker, C. Am. Assoc. Pet. Geol. Bull. 1974, 58, 2349-61.
11. Tissot, B. P.; Welte, D. H. "Petroleum Formation and Occur-
    rence, A New Approach to Oil and Gas Exploration"; Springer-
    Verlag, New York, 1978.
12. Horsfield, H.; Douglas, A.G. Geochim. Cosmochim. Acta 1980,
    44, 1119-31.
13. Larter, S. R.; Solli, H.; Douglas, A. G. J. Chrom. 1978, 167,
    431-31.
14. Allan, J.; Bjoroy, M.; Douglas, A. G. in "Advances in Organic
    Geochemistry, 1979," Douglas, A. G.; Maxwell, J. R., Eds; 1980
    p. 599-618.
15. Solli, H.; Larter, S. R.; Douglas, A. G. in "Advances in
    Organic Geochemistry, 1979, " Douglas, A. G.; Maxwell, J. J.,
    Eds.; 1981, p. 591-7.

Devonian Oil Shales in the Eastern United States

Distribution and Regional Correlation

R. DAVID MATTHEWS and HARLAN FELDKIRCHNER

Institute of Gas Technology, IIT Center, Chicago, IL 60616

Resource studies of oil shale deposits require geologic prediction which is based on the correlation of rock units from surface exposures into the subsurface. Although most of the nation's eastern oil shales are essentially flat-lying and average 30 to 60 feet thick along nearly 1000 miles of outcrop, the shales are widespread. The usefulness of characterization studies in each of the three geologic basins (Michigan, Illinois, and Appalachian) has been hampered by problems of regional correlation. The Institute of Gas Technology has sampled some 150 locations, and the integration of these studies with published data has resulted in new geochemical and geological patterns clarifying some regional correlations. New stratigraphic interpretations are presented as evidence of source-area changes for organic matter and clastics brought into the various basins.

Resource Studies

The Devonian-Mississippian black shales of the eastern United States contain varying amounts of organic carbon that can range up to nearly 25 percent by weight or as much as 40 percent by volume (1), and when they are retorted they will yield shale oil. The Fischer assay yield is typically less than 10 gallons of oil per ton of rock. Such a yield by conventional retorting methods has been low enough when compared to western oil shales to have limited interest in eastern shale until new retorting technology enabled the eastern shales to assume a competitive position. Eastern oil shales having levels of organic carbon similar to those of western shales react comparably when a hydrogen retorting method is used (Table I).

The eastern shales occur over a wide expanse from New York to Oklahoma and from Iowa to Alabama (2), yet as rocks that must be

Table I. U.S. Oil Shales

	Eastern	Western
Ultimate Analysis, (dry basis) wt %		
Organic Carbon	13.7	13.6
Hydrogen	1.6	2.1
Sulfur	4.7	0.5
Carbon Dioxide	0.5	15.9
Ash	78.3	66.8
Fischer Assay Analysis		
Oil Yield, wt %	4.6	11.4
Assay, gal/ton	10.3	29.8
HYTORT Yields		
Oil Yield, wt %	9.1	--
Assay, gal/ton	23.2	--

surface mined to be retorted, the shales of greatest potential are those at or near the surface. A study of the Devonian-Mississippian shales by the Institute of Gas Technology (IGT) to test them as feedstocks for the HYTORT ✱ process (3) included an intensive sampling of the shales. IGT has sampled 180 locations from 15 eastern and western states and has analyzed more than 635 shale samples. Included in these were large-tonnage samples (10 to 50 tons) of shale from seven eastern shales and from four western geologic basins: Green River, Washakie, Uinta, and Piceance Creek. These provided the quantity necessary for a process development unit (PDU) having a 1 ton/h shale capacity which has been operating in Chicago since 1976 (4). Four criteria for resource assessment were imposed by IGT (5) in calculating resource estimates:

● Organic carbon at least 10 percent by weight

● Shale at least 10 feet thick

● Stripping ratio less than 2.5 to 1, and

● Maximum overburden thickness less than 200 feet

The most important eastern oil shale areas are in Kentucky, Tennessee, Indiana, and Ohio, where nearly flat-lying beds, averaging 30 to 40 feet thick, are exposed at the surface in an outcrop belt nearly a thousand miles long. The results of the sampling and testing program suggest a resource base in excess of 420 billion barrels of shale oil (Table II) from shale near the surface. Figure 1 shows the area in square miles considered accessible in each of the several states studied, including thickness and richness data.

The shales have been studied by many people for several reasons. They are the source of natural gas, a resource that has seen the development of over 9000 gas wells and is the subject of active research interest (6). The shales are potential ores for uranium, some as high as 0.033 percent of that metal (7), and they are relatively high in other metals: lead, copper, and zinc (8). They are likely source rocks for conventional crude oil and natural gas where they have been buried deeply enough to have matured. The variety and widespread nature of the black shales has led (9) to a complex local nomenclature (Figure 2). The units named in the geological literature have been identified and used by stratigraphers because they are mappable, visibly recognizable in outcrops or from drill-hole data, and not because of any uniform geochemical characteristics that relate to ore grade or "richness." The stratigraphic framework, based on color and

Table II. Estimated Resources of Shale Oil
Recoverable by the HYTORT Process in the Appa-
lachian, Illinois and Michigan Basin Areas

State	Total Area Suitable for Surface Mining, sq mi	Resources Recoverable by Aboveground Hydroretorting	
		billion bbl	bbl/acre
Ohio	980	140	222,000
Kentucky	2650	190	112,000
Tennessee	1540	44	44,000
Indiana	600	40	104,000
Michigan	160	5	49,000
Alabama	300	4	21,000
Total	6230	423	

(Reproduced with permission from Ref. 5. Copyright 1980,
Institute of Gas Technology.)
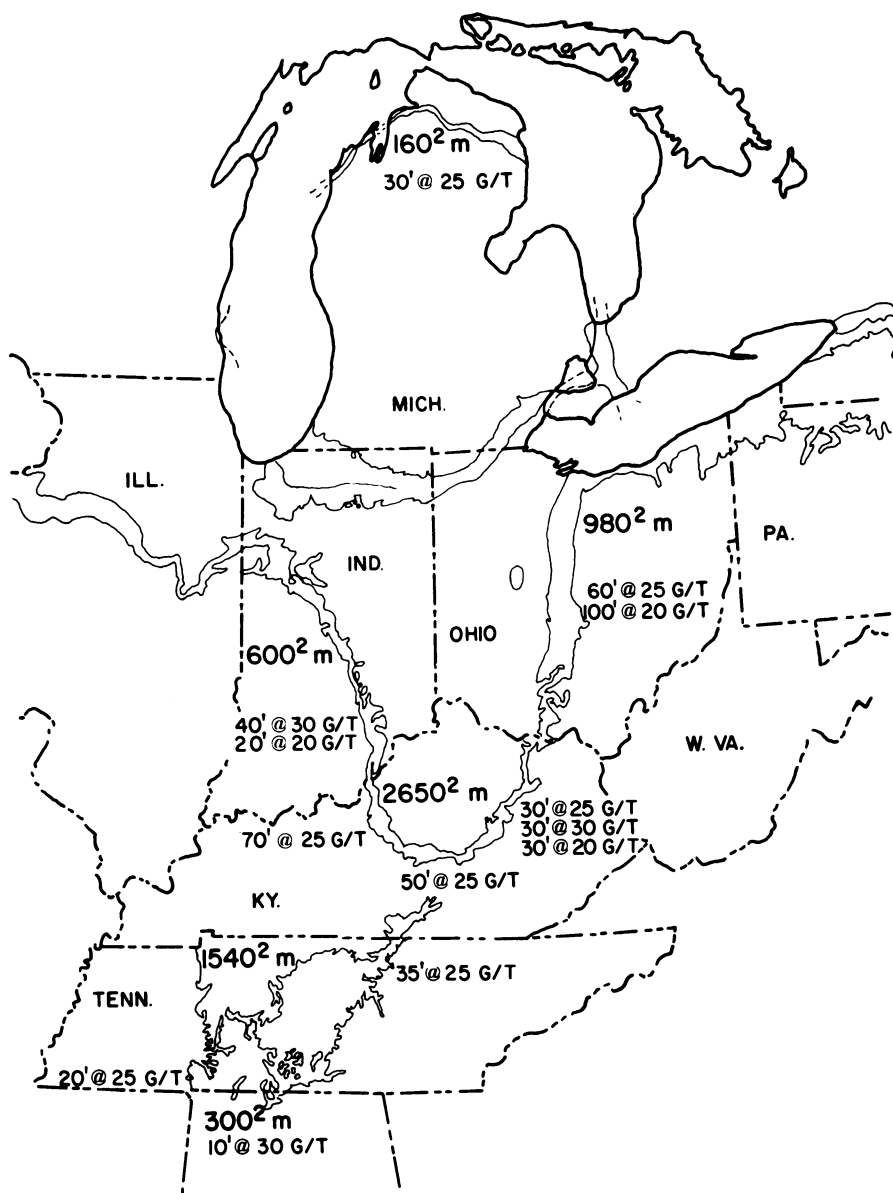
Figure 1. Map showing outcrop areas and resource data for the Devonian-Mississippian oil shales of the eastern United States. (Outcrop is shown by narrow line.) (Reproduced with permission from Ref. 9. Copyright 1981, Institute of Gas Technology.)
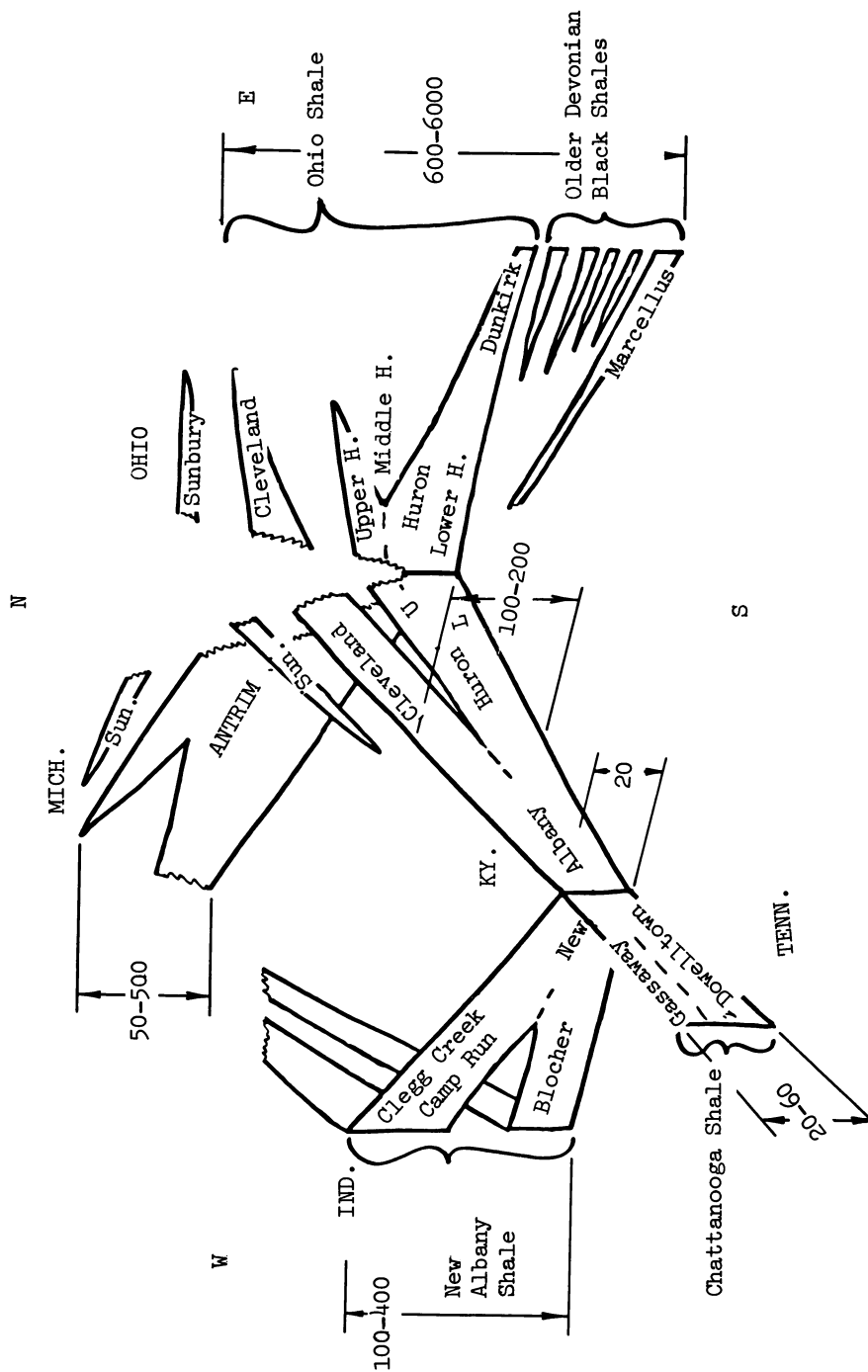
Figure 2. Fence diagram showing black shale nomenclature and thickness in feet. (Reproduced with permission from Ref. 9. Copyright 1981, Institute of Gas Technology.)

natural radiation level, that was available when eastern shales became of recent interest proved inadequate to the understanding and prediction of retorting behavior and resource grade. The vertical and lateral variations within the rocks (10) were found to be great enough to require more detailed testing and correlation of shales from state to state as well as from basin to basin.

The depositional history of Devonian black shales in the Appalachian, Illinois, and Michigan Basins is still a subject of academic argument; it is complicated by the fact that organic matter in marine sediments can be preserved in a number of depositional environments which share a common and necessary requirement of little or no oxygen (11).

One problem in developing a regional shale stratigraphy has been the lack of fossils in the shale that can serve as time markers. A notable exception (Figure 3) is the fossil alga Foerstia, widely scattered across the Appalachian Basin but only found in a very narrow vertical range. Foerstia lived for a brief span of geological time and thus serves as a "time line" wherever found. As astronomical observations can be used to give precision and correlation to ancient history, so a fossil like Foerstia provides an accurate correlation of geologic events. The recent discovery by Kepferle (12) of the fossil alga in the Illinois Basin has clarified the age relationship of rocks between that basin and the Appalachian Basin. Kepperle's work has been confirmed and extended into southern Indiana by Hasenmueller et al. (13). Recognition of Foerstia in the Michigan Basin by Matthews (14) has aided the correlation of depositional events in that basin with those in the Appalachian Basin.

Stratigraphic Interpretations

The Devonian rocks do not present as complete a record as many of the older, more deeply buried rocks, because there has been a loss by erosion of unknown thicknesses of Devonian rocks over the positive areas that separate the geologic basins. These positive areas, or arches, developed and were active at various times during the geologic past (Figure 4). The Algonquin Arch in southwestern Ontario existed as an early Upper Cambrian and Lower Ordovician feature (15), but was not sufficiently active during the Late Devonian Period to prevent a continuous deposition of the Antrim/Kettle Point/Ohio Shales across Ontario. The Findlay Arch now separating northern Ohio from southeastern Michigan did not come into existence until after Devonian time (16) and thus presented no impediment to a complete deposition of black shales from Michigan through northwestern Ohio. These assumed rocks were lost by erosion as the arch lifted following the Pennsylvanian Period. Likewise, the Kankakee Arch now separating the modern Michigan and Illinois Basins in northwestern Indiana did not develop until after the Pennsylvanian and could not have been an obstacle to continuous black shale deposition of Antrim/New Albany material from
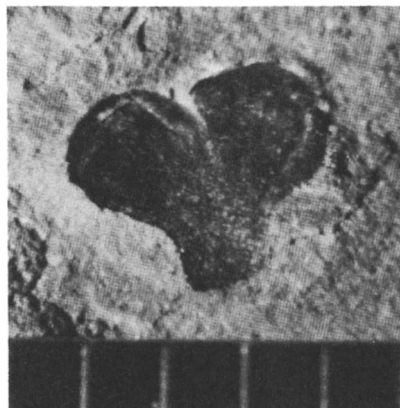
Figure 3. Photomicrograph of Foerstia *from the Huron member of the Ohio shale near Vanceburg, Kentucky. (Millimeter scale in figure.) (Reproduced with permission from Ref. 14. Copyright 1982, Institute of Gas Technology.)*
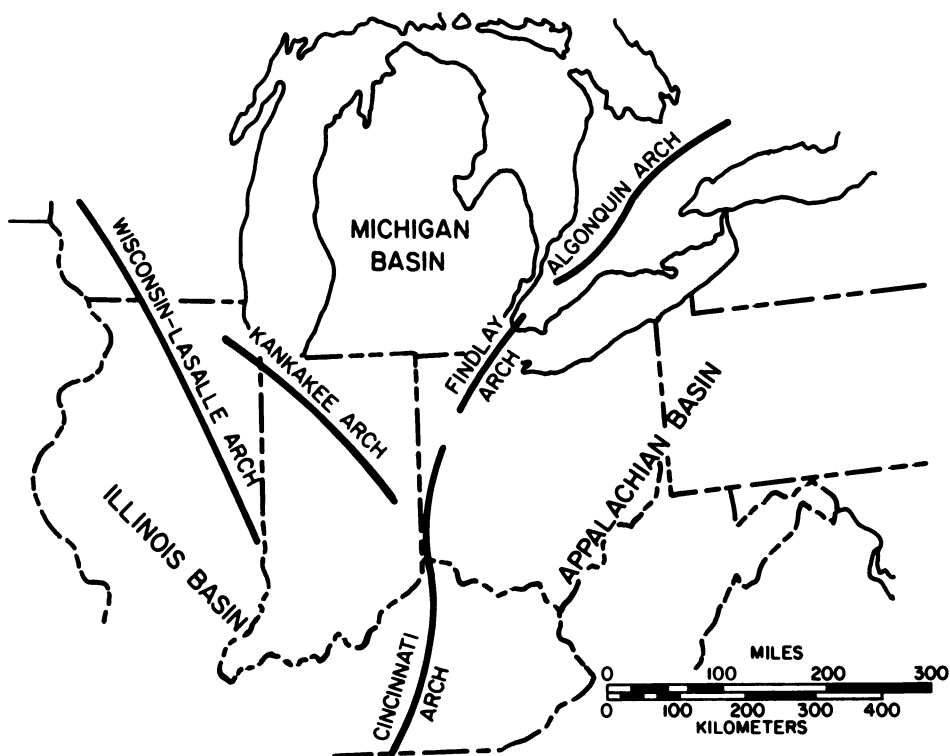
Figure 4. Major structural features mentioned in the text.

Michigan to Illinois; however, these shales no longer exist. The effect of an older Wisconsin-Illinois Arch on the deposition and survival of the Late Devonian shales can be seen in the composited Devonian shale thickness map (Figure 5). In east central Illinois, the shale thins to less than 100 feet over the arch, and the map trace of the outcrop is displaced to the south.

The inference that continuous and related deposition of shales did occur can be supported by the evidence of surviving lithofacies patterns and unit thicknesses. It is axiomatic that space must be available if sediments are to accumulate; thus, the preserved thickness of a sedimentary unit is one measure of crustal subsidence. Downwarped "negative" areas will receive measurable thicknesses of sedimentary rock; however, when there is erosion of rock caused by subsequent crustal up-lift in "positive" areas, the volume and thickness of rock lost cannot be determined easily. Where rocks are eroded, a gap in time occurs; that is to say, a part of the rock record is missing. Richter-Bernberg (17) holds as a general principle that no sediments remain to represent by far the greatest part of geologic time; this would seem to be the case with the Devonian shales of central Kentucky and Tennessee that were deposited (and are preserved) over the positive areas southward along the Cincinnati Arch, because they are very thin (only a few tens of feet thick) or they may be absent. These few feet of shale resting on Silurian or older rock and overlain by Mississippian sediments are all that exists in that area to represent some 50 million years of the Devonian; however, in the Appalachian Basin, more than 11,000 feet of Devonian sediments are preserved.

The thickness of Devonian shale (18) in northwestern Michigan (Figure 5) establishes a depocenter some distance northwest of the center of the modern structural Michigan Basin. A similar area in west central Illinois received an unknown volume of Devonian sediments and has been called the Western Depocenter by Illinois stratigraphers (19). These two depocenters may have been related and joined as one across the line of the older Wisconsin-Illinois Arch. The Ellsworth shale equivalents in Illinois are not preserved in their original thickness because they were eroded by uplift before being covered by the Burlington Limestone of Mississippian age (19). These shales thicken from about 100 feet to 160 feet in about 15 miles (4 feet/mile) as one approaches the depocenter from the southeast, but the increase in thickness beyond 160 feet, whatever that may have been, was removed by erosional truncation. The Ellsworth of Michigan reached a thickness of about 800 feet (20) and probably was not eroded.

A striking feature of the upper Antrim shale in Michigan is the abrupt change in rock type from black, organic-rich shales in the east to greenish-gray, organic-poor shales in the west. The different shales were deposited contemporaneously and exist in a facies relationship to each other. The zone of lithofacies change has been mapped by Fisher (20), and a similar facies change in
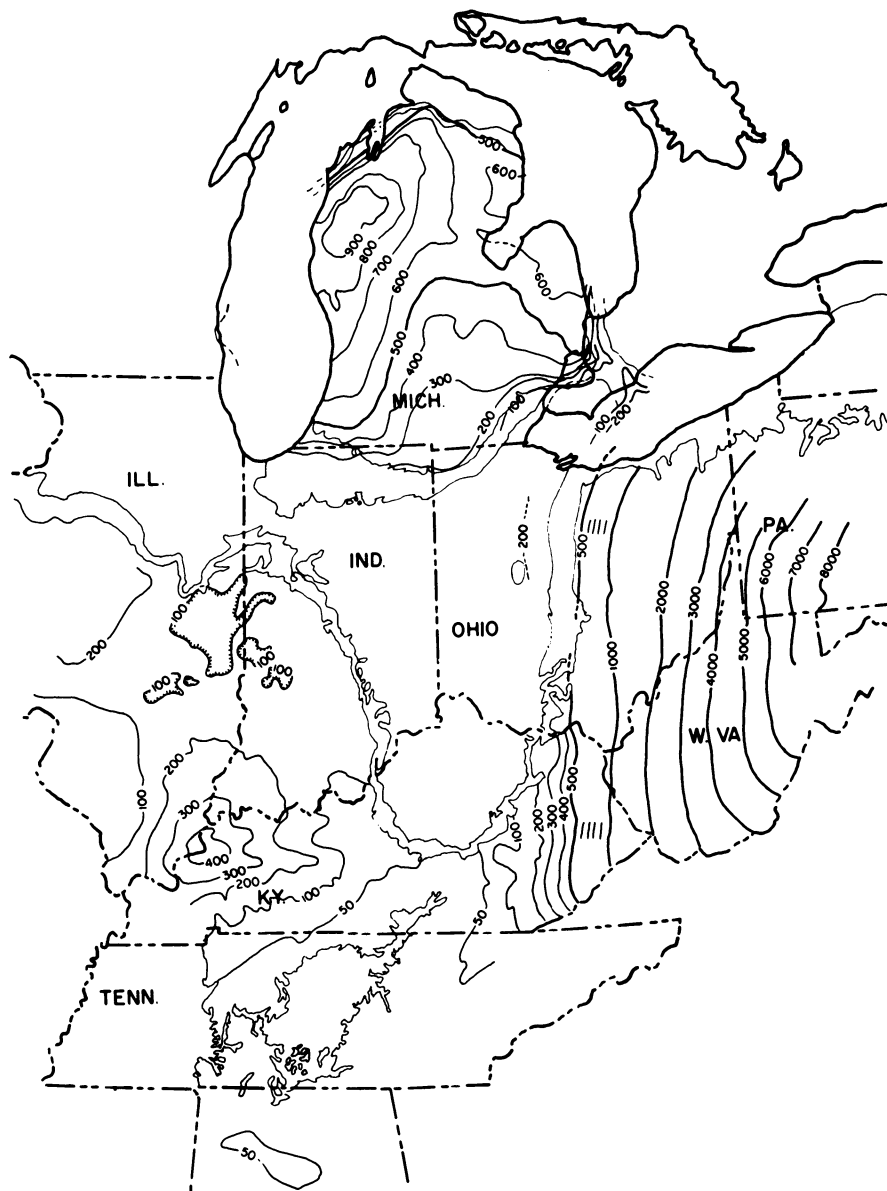
Figure 5. Isopach map of total Devonian shale composited from numerous literature sources. (Reproduced with permission from Ref. 14. Copyright 1982, Institute of Gas Technology.)

Indiana has been described by Lineback (21) and mapped by Hasen-
mueller (22). These two maps have been combined (Figure 6) into a
regional composite as evidence of a northwestern source for sedi-
ment and similar, concurrent environments of deposition throughout
a wide area of western Michigan and northern Illinois. A common
feature of the Ellsworth/Antrim in Michigan and the Ellsworth/upper
New Albany in the Illinois Basin is a similar overall geometry.
The configuration in cross section can be illustrated by a sche-
matic drawing (Figure 7) depicting two episodes of deposition.
The first, called the "lower black" shale here, is widespread,
carries a consistent internal gamma ray signature, and is rela-
tively uniform in thickness. The second, composed of two facies,
is more local and is most apparent as a wedge of sediment having a
black, organic-rich facies (B) forming the thin portion of the
wedge and a green-gray, organic-poor shale (C) comprising the
thick part of the wedge. The black shale (B) is called here the
"upper black" shale, and the gray shale (C) is called here the
"green-gray" facies.
    Applied to the Michigan Basin in east-west cross section, the
"lower black" shale (A) represents the Antrim Shale of western
Michigan and that part of the eastern Antrim Shale identified by
Subunits 1A, 1B, 1C and 2. The "green-gray" facies (C) is the
Ellsworth Shale, and the "upper black" (B) is represented by all
Antrim Shale above Unit 2 and below the base of the Bedford Shale.
The uniformity of the lower beds of the Antrim Shale has been
noted by several others (20, 23), and a westward source for the
Ellsworth has been postulated by several (20, 23-25). Never-
theless, the westward source seems more applicable to those beds
above the western Antrim Shale, i.e., above the beds termed "lower
black" in this paper.
    The schematic black shale sequence also can be applied to the
upper New Albany Shale of the Illinois Basin, where a facies
relationship of the green-gray Hannibal/Saverton Shales with the
Grassy Creek has been described by Lineback (26):

> "The upper part of the Grassy Creek and its Indiana
> equivalents (the combined Morgan Trail, Camp Run, and
> Clegg Creek Members) grades laterally northwestward into
> a thickening wedge of greenish-gray shales and siltstone,
> the Saverton and Hannibal shales in Illinois, the Ells-
> worth Member in Indiana."

Thus the Hannibal/Saverton (C) and the upper part of the Grassy
Creek (B) form the upper wedge in the sequence. The "upper black"
(B) can be postulated to be that part of the Clegg Creek Member of
the New Albany in Indiana above the newly discovered _Foerstia_ zone
(13). If the lithologic and gamma ray correlations developed by
the Illinois Geological Survey stratigraphers establish time
boundaries (19), the _Foerstia_ zone would appear to cut the Grassy
Creek of Illinois into "upper black" (B) and "lower black" (A).
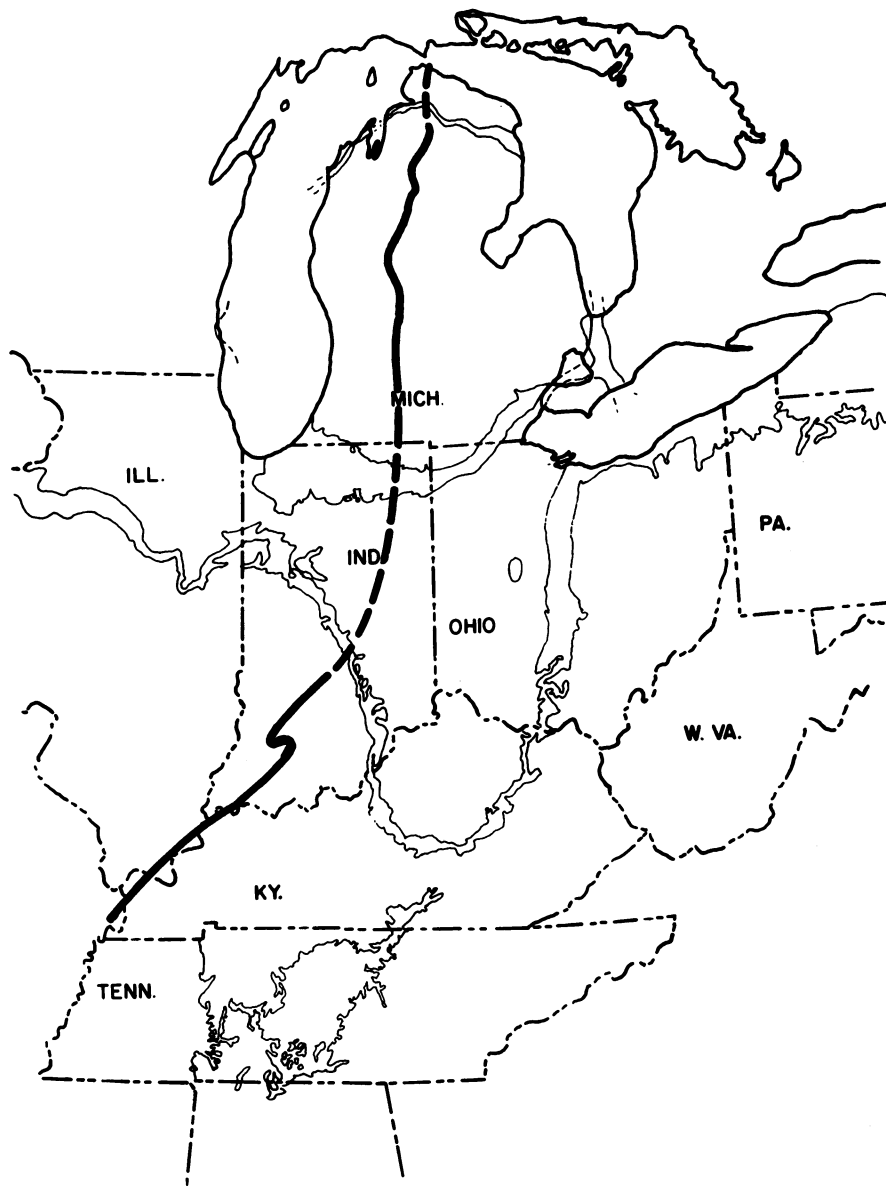
Figure 6. Regional map of the Ellsworth shale zero line, green-gray Ellsworth-type shales to the west and black Antrim-type shales to the east. (Reproduced with permission from Ref. 14. Copyright 1982, Institute of Gas Technology.)

ERODED

C

GREEN-GRAY FACIES

B

ERODED

UPPER BLACK SHALE

A

LOWER BLACK SHALE

A82101823
IGT, 1982
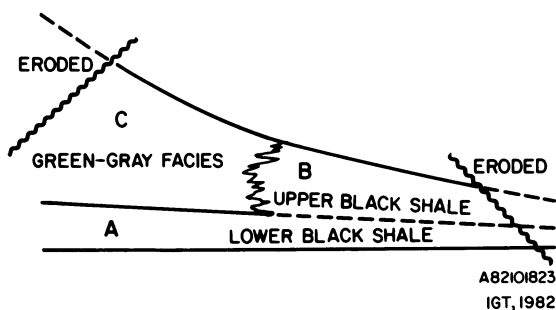
Figure 7.   Hypothetical black shale sequence. (Reproduced with permission from Ref. 14. Copyright 1982, Institute of Gas Technology.)

If _Foerstia_ extends into northwestern Illinois, it should be found just below the base of the Saverton in the top of the western Grassy Creek. The sediment source for this great wedge of Hannibal/Saverton and upper Grassy Creek above _Foerstia_ would have been northwest, but the sediments below the presumed position of _Foerstia_ in the Illinois Basin are not necessarily from that same source. Kepferle's (13) documentation of _Foerstia_ on the eastern edge of the Illinois Basin has established that the great bulk of black shale in the Illinois Basin predates much of the black shale in eastern Kentucky and Ohio (27) and invalidates several recently published correlations.

The hypothetical black shale sequence is also applicable to various parts of the Sunbury Shale (Mississippian) in Michigan and Ohio. In eastern Michigan the Sunbury Shale increases from a typical thickness of 20 to 40 feet across most of the basin to over 140 feet in Sanilac County, where both cores and gamma ray logs document a local increase in thickness (19). The "normal" Michigan Sunbury Shale represents the "lower black" (A); part of the unusual added thickness in the east becomes the "upper black" (B) with some part of the lower Coldwater Shale assumed to be a facies equivalent and representing the "green-gray" facies (C) of the upper wedge. The question whether such a facies relationship exists between a part of the Sunbury and the Coldwater Shale has not been answered, and to date no evidence can be advanced to support a division within the lower Coldwater Shale of central Michigan. Unfortunately the Coldwater Shale, over 800 feet thick, is a unit of no economic interest and has drawn little investigation.

A similar geometry exists in the Sunbury Shale of Ohio and can be illustrated on a section from the 1954 publication (28) by Pepper _et al_. (Figure 8). An abrupt increase in thickness of dark shales, logged as Sunbury by drillers, lies over a "normal" Sunbury Shale spread over most of Ohio. This widespread "normal" unit represents the "lower black" (A), the added local thickness of dark shale becomes the "upper black" (B), and the organic-poor facies (C) is represented by a part of the Orangeville Shale at the base of the Cuyahoga Group. The demonstration of a facies relationship and a division within the lower Cuyahoga is not available at this time; thus, as in Michigan, a two-part Sunbury Shale based on shape must be considered as conjecture.

That two genetic types of Sunbury Shale exist in the Appalachian Basin has been recognized by Van Beuren (29), who attempted to explain the geometric relationships between black shales and laterally adjacent gray/green shales and siltstones by means of a cycle of trangression and regression. His transgressive unit is "characteristically thin and widespread," and his regressive black shale is thicker, more laterally restricted and representative of the distal facies of laterally adjacent non-black clastics. Related to the hypothetical black shale sequence (Figure 8), Van Beuren's transgressive unit is the "lower black" (A), the regres-
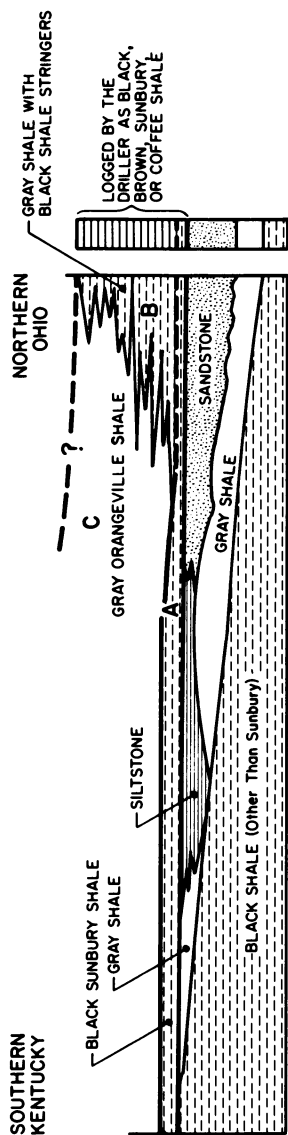
Figure 8. *Generalized cross-section from southern Kentucky to northern Ohio showing the abnormal thickness of Sunbury shale as recorded by drillers—after Pepper (25).*

sive Sunbury unit is the "upper black" (B), and the clastics represent the "green-gray" facies (C). The shape of the wedge composed of "upper black" (B) and its "green-gray" facies (C) indicates that clastics came from the direction of the thick end and that the "upper black" was a deeper water deposit formed a greater distance from the source. The shales of the upper wedges are relatively local as compared with the "lower black" (A) units, which are regional; the Lower Antrim/Kettle Point/Ohio (in part) is continuous and is representative of the black shales to be deposited over the arches between the three basins. The source of the lower unit is not as apparent as that of the upper wedges (B/C). If the "lower black" (A) is cyclic, as Van Beuren advocated for the lower Sunbury Shale, it should have a source similar in direction to the overlying wedge.

A westward or northwestward source for the Ellsworth/upper Antrim, Hannibal-Saverton/upper Grassy Creek, and lower Coldwater/upper Sunbury is appropriate for the overall geometry of those "upper shale" bodies. It is clear that in the Appalachian Basin great volumes of clastic material came from the east and that some of the black shales in that basin are true distal facies of great influxes of clastic material from the east. Nevertheless, because the authors believe that the hypothetical black shale sequence also applies east of the Cincinnati/Algonquin Arches (in mirror image), some of the black shales in the basin may prove to be more regional in nature and of the "lower shale" (A) type.

The pulses of increased clastic influx reflect tectonic activity, as has been suggested by Ettensohn and Barron (30, 31), but with the addition of a northwestern landmass to provide material west of the general line of the Algonquin and Cincinnati Arches. These pulses are represented by the upper wedges (B/C). Between pulses, there was widespread deposition of the "lower black" (A) type of shales which, for the lower Antrim and lower Sunbury equivalents, were little influenced by arches. The southwestern source suggested by Ettensohn and Barron for the Appalachian Basin (30) seems very plausible for the "lower black" shales (A) of the Illinois and Michigan Basins as well.

The 50 million years of the Devonian Period provided sufficient time for over 11,000 feet of sedimentary rocks to accumulate in the Appalachian Basin; this accumulation was controlled by pulses of tectonic uplift to the east. A similar control of a northwestern source area by intermittent tectonic movement is suggested as a source for the upper wedges (B/C) in the Michigan and Illinois Basins. The lower black shales (A) of regional type represent quiescent periods of slow deposition followed by relatively more rapid sedimentation occurring in response to uplift and erosion of source areas and to depositional restrictions caused by rising arches. The total thickness of Devonian shales in either the Michigan or Illinois Basin is less than 1000 feet, so that the sediment volume involved in these two basins is far less than in the Appalachian Basin. Thus there was ample time for

tectonic control of depositional patterns within the Devonian-Mississippian shales of the eastern United States.

Acknowledgments

　　　　Trademark Notice: IGT provides HYTORT research and development, engineering, and technical services related to hydroretorting of oil shale.

Literature Cited

1. Leininger, R. K., "Inorganic Geochemistry," in Hasenmueller, N. R. and Woodard, G. S., Eds., "Studies of the New Albany Shale (Devonian and Mississippian) and Equivalent Strata in Indiana," 53-61, prepared for U.S. Dept. Energy by State of Indiana Dept. Nat. Resources Geol. Survey, Bloomington, September, 1981.
2. Provo, L. J., Kepferle, R. C. and Potter, P. E., Amer. Assoc. Pet. Geol. Bull. 62, 1703-13 (1978).
3. Matthews, R. D., Janka, J. C. and Dennison, J. M., "Devonian Shale — A Major American Energy Resource," presented at Amer. Assoc. Pet. Geol. — Eastern Section Meeting, Evansville, Ind., October 2, 1980. (IGT preprints available.)
4. Feldkirchner, H. L. and Janka, J. C., "The HYTORT Process," in Symposium Papers: Synthetic Fuels from Oil Shale, 489-524, Institute of Gas Technology, Chicago, April, 1980.
5. Janka, J. C. and Dennison, J. M., "Devonian Oil Shale," in Symposium Papers: Synthetic Fuels from Oil Shale, 21-116, Institute of Gas Technology, Chicago, April, 1980.
6. Potter, P. E., Maynard, J. B. and Pryor, W. A., Oil Gas J., 290-318 (1982) January 25.
7. Conant, L. C. and Swanson, V. E., U.S. Geol. Surv. Prof. Pap. 357 (1961).
8. Silverman, M. E. and Spiewak, I., Sep. Sci. Technol. 16 (9), (1981).
9. Matthews, R. D., Janka, J. C. and Dennison, J. M., "New Insights Into the Devonian Oil Shale Resource of the Eastern United States," presented at Amer. Assn. Pet. Geol. Nat. Conv., San Francisco, June 2, 1981. (IGT preprints available.)
10. Leventhal, J. S. and Shaw, V.E.J., Sediment. Petrol., 77-81 (1980).

11. Tourtelot, H. A., Clays Clay Miner. 27 (5), 313-21 (1979).

12. Kepferle, R. C., "Correlation of Devonian Shale Between the Appalachian and Illinois Basins Facilitated by Foerstia (Protosalvinia)," in Roberts, T. G., Ed., Geol. Soc. Amer. Cincinnati '81 Field Trip Guidebooks, Vol. II: Economic Geology Structure Field Trip No. 3, 334-35, Amer. Geol. Inst., Falls Church, Va., 1981.

13. Hasenmueller, N. R., "Resource Assessment of the New Albany Shale (Devonian and Mississippian) in Southeastern Indiana — Preliminary Report," in Proceedings, 1981 Eastern Oil Shale Symposium, 173-80, Univ. of Kentucky, Institute for Mining and Minerals Research, Lexington, 1981.

14. Matthews, R. D., "The Discovery of Foerstia in the Antrim Shale of Michigan," presented at an IGT Seminar, Chicago, December 15, 1982. (IGT preprints available.)

15. Sanford, B. V. and Quillian, R. G., "Subsurface Stratigraphy of Upper Cambrian Rocks in Southwestern Ontario," Paper Geol. Surv. Canada, Canada Dept. of Mines and Techn. Surv., Ottawa, 1959.

16. Levorsen, A. I., Paleogeologic Maps, 174, W.H. Freeman, San Francisco, 1960.

17. Richter-Bernberg, in Brochert, H. and Muir, R. O., Salt Deposits, p. 41, D. Van Nostrand, London, 1964.

18. Sanford, B. V., "Devonian of Ontario and Michigan," in Oswald, D. H., Ed., Int. Symp. Devonian System Proc., Vol. 1, 973-99, Alberta Soc. Pet. Geol., Calgary, 1967.

19. Bergstrom, R. E., Shimp, N. F. and Cluff, R. M., "Geologic and Geochemical Studies of the New Albany Shale Group (Devonian-Mississippian) in Illinois," Final Report for U.S. Dept. Energy, Ill. State Geol. Surv., Urbana, 1980.

20. Fisher, James H., "Stratigraphy of the Upper Devonian-Lower Mississippian of Michigan," U.S. DOE Report No. FE-2346-80, 1980.

21. Lineback, J. A., "Coordinated Study of the Devonian Black Shale in the Illinois Basin: Illinois, Indiana, and Western Kentucky," Final Report for U.S. Dept. Energy, Ill. State Geol. Survey, Urbana, 1981.

22. Hasenmueller, N. R. and Bassett, J. L., "Stratigraphy," in Hasenmueller, N. R. and Woodard, G. S., Eds., "Studies of the New Albany Shale (Devonian and Mississippian) and Equivalent Strata in Indiana," 5-32, prepared for U.S. Dept. Energy by State of Indiana Dept. Nat. Resources Geol. Survey, Bloomington, September, 1981.

23. Ells, G. D., "Stratigraphic Cross Sections Extending From Devonian Antrim Shale to Mississippian Sunbury Shale in the Michigan Basin," U.S. DOE Report No. FE-2346-30, 1978.

24. Cohee, G. V., Macha, C. and Hold, M., "Thickness and Lithology of Upper Devonian and Carboniferous Rocks in Michigan," U.S. Geol. Survey Oil and Gas Inv. Ser., Chart OC-41, 1951.

25. Cross, A. and Bordner, M. A., "Palynology and Environmental Interpretations of the Antrim Shale in Central Michigan," U.S. DOE Report No. FE-2346-81, September, 1980.
26. Lineback, J. A., op. cit., p. 11.
27. de Witt, W., Jr., letter of August 27, 1982.
28. Pepper, J. F., de Witt, W., Jr. and Demarest, D. F., U.S. Geol. Surv. Prof. Pap. 259 (1954).
29. Van Beuren, V. V., "The Sunbury Shale of the Central Appalachian Basin — A Depositional Model for Black Basinal Shales" (Abstract Only), in Prior, W., et al., Eds., Energy Resources of Devonian-Mississippian Shales of Eastern Kentucky, Annual Field Conference April 9-11, 1981, Kentucky Geological Survey, Lexington, 1981.
30. Ettensohn, F. R. and Barron, L. S., "Depositional Model for the Devonian-Mississippian Black Shale Sequence of North America: A Tectonic-Climatic Approach," in Blackburn, W. H., Compiler, "Black Shale Studies in Kentucky," Final Report, Univ. of Kentucky Research Group (Department of Geology and Kentucky Geological Survey), Lexington, 1980.
31. Ettensohn, F. R. and Barron, L. S., "Depositional Model for the Devonian-Mississippian Black Shales of North America: A Paleoclimatic-Paleogeologic Approach," in Roberts, T. G., Ed., Geol. Soc. Amer. Cincinnati '81 Field Trip Guidebooks, Vol. II: Economic Geology Structure Field Trip No. 3, 344-61, Amer. Geol. Inst., Falls Church, Va., 1981.

Geochemistry of Oil Shales in Eastern Kentucky

T. L. ROBL, A. E. BLAND, D. W. KOPPENAAL, and L. S. BARRON

University of Kentucky, Institute for Mining and Minerals Research, Lexington, KY 40512

Recent resource assessment studies of eastern Kentucky oil shales have established that this resource is a potentially economic synthetic fuel feedstock (1). Extensive geochemical characterization of this resource has been carried out by the Institute for Mining and Minerals Research (University of Kentucky) with support from the Commonwealth of Kentucky Energy Cabinet, the U. S. Department of Energy, and private industry. This effort will eventually culminate in the characterization of the entire oil shale resource within the Commonwealth; this particular study addresses the results gained from the first two drilling and sampling phases of the overall effort. The sampling and analysis program was initiated in Lewis and Fleming Counties, Kentucky, resulting in 10 cores being drilled with those core samples being designated as the "K-series" samples in this report. The second phase of the program produced an 11 additional cores in Rowan, Bath, Montgomery, Powell, and Estill Counties; these samples are given the "D-series" designation. The location of these core sites as well as current drilling sites are depicted in Figure 1. This paper summarizes the geochemistry of the Devonian and Mississippian age oil shales of the K- and D-series study areas.

General Geology and Stratigraphy

In Kentucky, black oil shales rich in organic matter (OM) in the Devonian and Mississippian systems crop out in a roughly semi-circular pattern on the flanks of the Lexington Dome. The dome is a structural high on the northern end of the Cincinnati Arch, which stretches between Nashville, Tennessee, and southern Ohio. The black-shale outcrops occur in the Knobs and low hills which border the Bluegrass region from Bullitt County on the west to Lewis and Fleming Counties on the east as shown in Figure 1. From the southern end of the semi-circle south into Tennessee,
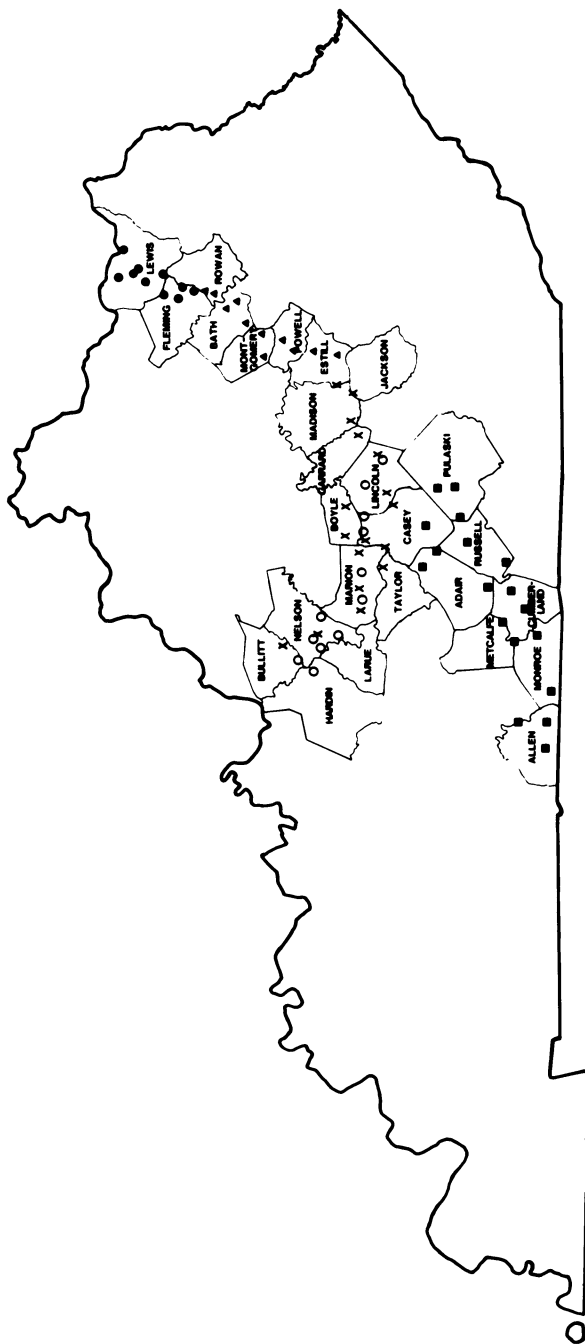
Figure 1. Oil shale resource exploration core sites in Kentucky. Devonian and Mississippian oil shales outcrop in the counties indicated. Drill cores designated as K and D series are the subject of this report. Key to drill cores: ○, A series; ×, T series; ■, L series; ▲, D series; and ●, K series.

the black shale crops out in river valleys where the overburden
is relatively shallow in the Cumberland saddle, a structural low
between the Lexington and Nashville domes on the Cincinnati arch.

West of the Cincinnati arch, the black shale dips into the
subsurface of the Eastern Interior Basin where it becomes over
450 feet thick in Hardin County, Illinois, and Union County, Ken-
tucky (2). On the eastern flank of the Cincinnati arch, the
black shale dips eastward into the Appalachian Basin where it be-
comes over 1700 feet thick. To the south, the overall section
thins to 30 or 40 feet along the crest of the arch.

In each of the three areas described above, the black-shale
sequence differs in overall aspect from each of the other areas
when viewed in outcrops. This difference has led to three sets
of stratigraphic nomenclature having been applied to the black
Devonian-Mississippian shales. The general distribution of the
usages of stratigraphic nomenclature are shown in Figure 2.

In eastern Kentucky the Ohio Shale terminology has been used
where the Mississippian Sunbury Shale and the underlying Bedford
Shale can still be recognized. A typical stratigraphic section
with carbon distribution is shown in Figure 3. Typically the
overburden is a mixture of claystone and siltstone in the Borden
Formation. This unit directly overlies the Sunbury Shale which
is a black, laminated, siliceous shale rich in organic matter
with some pyrite. The Sunbury thins to the south from 20-25 feet
in Lewis County to four feet in Estill County.

The Mississippian Sunbury Shale is separated from the under-
lying OM-rich Devonian Ohio Shale by the Berea Sandstone and Bed-
ford Shale in Lewis County and by the Bedford Shale in the re-
maining counties. This interburden unit thins to the south from
over 100 feet in Lewis County to only a few inches in Estill
County. The Ohio Shale is divided into three units as shown in
Figure 3. The Cleveland Member is the upper unit. Its lower
contact is marked at the upper greenish-gray (OM-deficient) shale
of the Three Lick Bed. The lower greenish-gray shale marks the
top of the Huron Member. Depending on the location with respect
to the Cincinnati arch and the angular unconformity at the base
of the black shale, the underlying unit may be the Middle Devon-
ian Boyle Dolomite, the Silurian Crab Orchard Shale, or the Sil-
urian Bisher Limestone.

The Cleveland Member consists primarily of black to brown-
ish-black laminated siliceous shale. It contains minor amounts
of calcareous laminae and cone-in-cone limestone. Pyrite is pre-
sent as nodules, framboids, and irregular forms. Other primary
minerals include illite clay and clay- and silt-size quartz.

The Three Lick Bed is a regional stratigraphic marker bed
traceable throughout eastern Kentucky, Ohio, West Virginia, and
Tennessee (3). The bed contains three greenish-gray shales defi-
cient in OM interbedded with two brownish-black, OM-rich shales.
The greenish-gray shales contain Lingula, abundant trace fossils,
and pyritized microfossils (4-5).
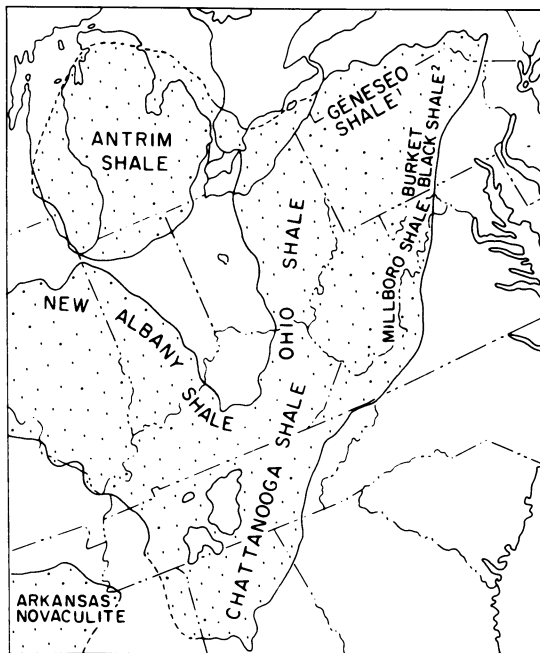
Figure 2. Geographic distribution of Devonian–Mississippian oil shale in the eastern United States (18).

Figure 3 explanation.

BORDEN FORMATION. Most important for study are the Nancy and
Farmers Members and Henley Bed. Nancy Member is a gray to greenish-
gray clay shale. 100-200' thick. Underlying Farmers Member is a
light gray to yellow siltstone with interbeds of silty shale 20-80'
thick. The Henley Bed is a greenish-gray to gray glauconitic shale
7.5-26.8' in thickness in study cores.

SUNBURY SHALE. Finely laminated black shale with small intervals
of brownish-black 13.3-18.4' thick in cores. Common pyrite bands
and nodules, sparsely fossiliferous.

BEREA SANDSTONE. Light gray siltstones and sandy siltstones with
interbedded medium to dark-gray shales, becoming more shaley toward
the base. Contact with underlying Bedford chosen at the point
where shale/siltstone content is equal. 0-75' thick in study
cores. Pyrite blebs and nodules common.

BEDFORD SHALE. Medium to dark-gray shale interbedded with light-
gray siltstones. Unit is generally silty toward the top. Pyrite
bands and nodules, common to abundant. Scattered siderite nodules
also present. Thickness ranged from 25-68' in study cores. De-
creasing in thickness from north to south in Lewis and Fleming
counties. Sparsely fossiliferous.
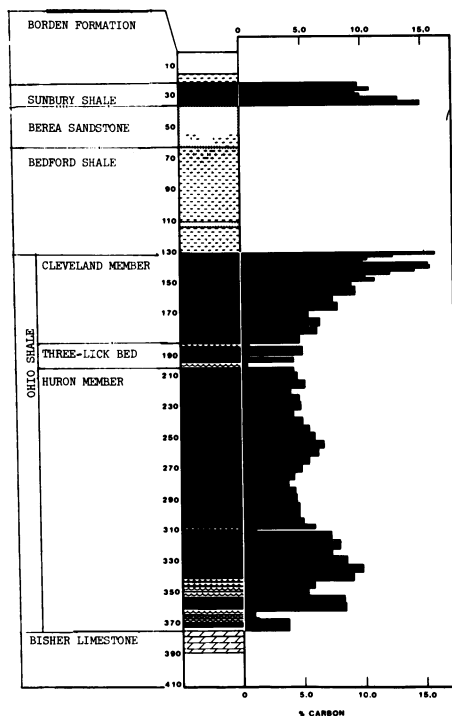
Figure 3. General stratigraphic column for the Devonian-Mississippian black shales in eastern Kentucky.

Explanation continued

OHIO SHALE. Cleveland Member. Black to brownish-black shale in upper part to olive-black to brownish-gray shale in lower part. Pyrite blebs, stringers and bands, phosphate nodules and thin calcisiltite bands are common. Linguloid brachiopods and Tasmanites are common fossils. Thickness from 49.9-65.0' in study cores.

Three-Lick Bed. Unit consists of three greenish-gray bioturbated shales separated by two black shale beds. Pyrite, present as infilling in burrows and calcisiltite bands are found. 19.6-11.6' thick in study cores.

Huron Member. Brownish-black to gray-black to brownish-gray shale, also containing intervals of burrowed and bioturbated greenish-gray shales. These intervals are abundant toward base of the unit. Vitrain bands and all forms of pyrite are present, calcisiltite laminae and bands are abundant. Tasmanites, Foerstia, and linguloid and orbiculoid brachiopods are common fossils in this unit. Thickness in cores ranged from 208.3-127.8', generally decreasing from north to south in study area. A regional unconformity occurs at the base of the Huron.

BISHER LIMESTONE. Sandy styolitic gray to yellowish-gray dolomite. Commonly vuggy with petroleum stained or filled vugs. Highly variable in thickness. Ranging from 0-100', generally thicker to north in study area.

The lower unit of the Ohio Shale which is present in the outcrop area of eastern Kentucky is the Huron Member. Primarily, the Huron consists of black to brownish-black to gray-black, laminated, siliceous, OM-rich shales. Calcareous laminae, cone-in-cone limestone, dolomitic gray shales, dolomite beds and bioturbated greenish-gray shales occur as interbeds and laminae in the lower parts of the member. Pyrite occurs as framboids, nodules, and irregular forms.

Definition of Economic Zones

For the resource assessment studies, it was necessary to define potentially mineable oil shale zones. The resulting nomenclature has subsequently been carried over into the geochemical studies. For the purposes of the resource assessment, only mineable oil shale having an overburden plus interburden to shale ratio of less than 2.5:1 was considered economical. Economic zones were further defined as those resources with greater than 8% carbon (1). In the study area, this included all of the Sunbury Shale and a high grade zone (HGZ) of the upper Cleveland Member of the Ohio Shale. This zone extends from the top of the member to a depth where the carbon content drops below 8%. This 8% level also corresponds to a point at which the carbon concentration is rapidly decreasing with depth (see Figure 3). A zone of +8% carbon also occurs in the lower Huron, but this oil shale is also high in sulfur, mineral carbon, and is separated from the other economic zones by a thick sequence of lean oil shales.

The two defined economic zones (Sunbury Shale and the HGZ of the Cleveland Member) are separated by interburden units of the Bedford Shale throughout the study area and the Berea Sandstone in Lewis County. Thickness histograms of the economic zones and their associated interburden units are presented in Figure 4, which shows that the Sunbury Shale decreases in thickness to the south while the Cleveland HGZ remains fairly constant at 25-30' thick. The Bedford and Berea decrease in thickness rapidly toward the south with less than a foot of interburden separating the two economic zones in Montgomery County.

Organic Geochemistry

General. The organic geochemistry of the study samples is summarized by the elemental analysis data in Table I. Extensive detailed data on these samples on a core-by-core basis are available in previous reports (1-6-7).

Carbon data presented and discussed herein are given as total carbon unless specified otherwise. Mineral carbon contributions from calcite and dolomite are typically insignificant in comparison to total carbon values. Average mineral carbon contents for the K-series stratigraphic units are as follows: Sunbury, 0.01%; Cleveland, 0.06%; and Huron, 0.13%. Comparative
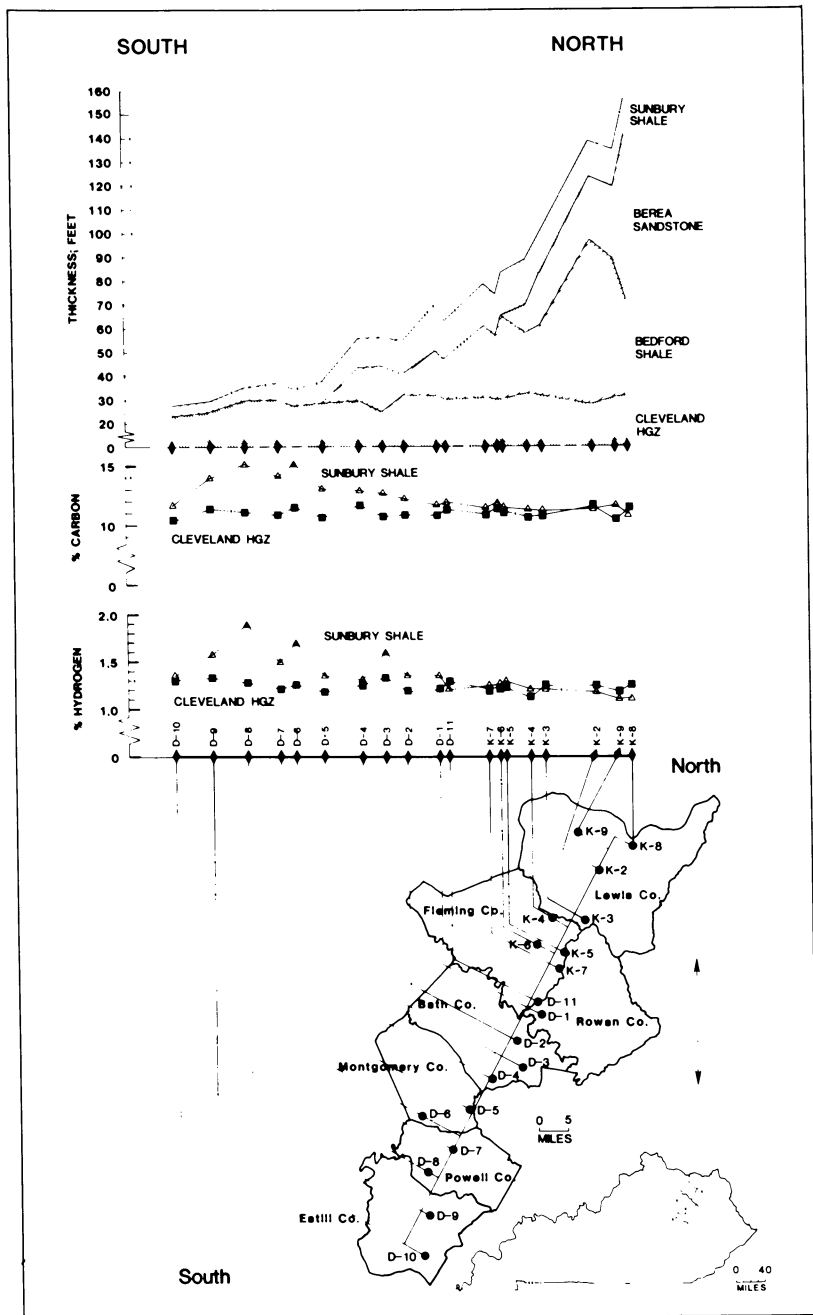
Figure 4.   Cross-section of the thicknesses of the stratigraphic units above the base of the Cleveland HGZ (top), and variation in hydrogen and carbon for the Sunbury shale and Cleveland HGZ in eastern Kentucky (bottom).

TABLE I. ORGANIC ELEMENTAL ANALYSIS DATA FOR K- AND D-SERIES OIL SHALES

| | K-Series | | | | D-Series | | | |
	Sunbury Shale	Cleveland Shale Total	Cleveland Shale HGZ	Huron Shale	Sunbury Shale	Cleveland Shale Total	Cleveland Shale HGZ	Huron Shale
C[1]	11.42(3)[2]	9.04(2)	11.11(3)	5.61(3)	13.12(10)	9.61(4)	11.08(3)	6.57(15)
H	1.20(4)	.99(2)	1.21(7)	.66(6)	1.47(14)	1.09(5)	1.25(5)	.76(12)
N	.41(5)	.39(4)	.39(3)	.22(7)	.44(10)	.32(10)	.36(10)	.23(16)
S	3.54(8)	2.42(6)	2.51(8)	3.15(3)	3.70(12)	2.79(12)	2.93(10)	3.61(7)

[1] wt. % raw shale; H corrected for surface moisture

[2] numbers in parentheses are coefficients of variation x 100

data from the D-series are: Sunbury, 0.14%; Cleveland, 0.10%;
and Huron, 0.44%. A general trend toward increasing mineral car-
bon in the southerly samples of the study area is evident. Dis-
tinct calcitic bands in the cores do occur but were removed and
analyzed separately and thus are not accounted for in the above
data.

Hydrogen is present in these shales as surface moisture,
mineral-bound hydration water, and organically-bound hydrogen.
Surface moisture was determined for each sample; consequently,
this hydrogen contribution is corrected for in the presented
data. Mineral-bound hydrogen, being difficult to determine dir-
ectly, is included in the hydrogen data presented. However, pos-
itive intercepts of H vs. C plots indicate approximately 0.2 wt.%
hydrogen from mineral origins. The consistency of this data for
general assignment to mineral-bound hydrogen contributions is
under current investigation.

Nitrogen occurs almost exclusively as organic nitrogen and
N vs. C plots are linear and possess relatively constant slope
values indicating a uniform geochemical presence of this element
in these shales. Sulfur occurrence in these shales is composed
of organic, sulfide, and sulfate contributions. Our data indi-
cate that >80% of the sulfur occurs in sulfide minerals, predom-
inantly as pyrite (FeS_2). Current research is aimed at refine-
ment of the sulfur-forms data, primarily to assess the organic
sulfur content of these shales.

Based on present data, the overall stoichiometry of the raw
oil shale organic material is given by the empirical formula
$CH_{1.3}N_{.031}$. This can be compared to formulas given for western
oil shales, e.g. $CH_{1.5}N_{0.032}$ ([8]) and $CH_{1.7}N_{.027}$ ([9]). These data
indicate that the eastern oil shales of Kentucky are more aroma-
tic in character than the western oil shales. This characteris-
tic manifests itself in a slight hydrogen deficiency which ulti-
mately limits oil yield. The remarkably similar N/C ratios be-
tween the two oil shales is also notable.

Stratigraphic and Regional Trends. Strong stratigraphic trends
are evident in the distribution of carbon in the study cores, as
Figure 3 illustrates. In general, the carbon content increases
from top to bottom in the Sunbury Shale, with carbon values of
approximately 9-10% at the top to 15% at the base. This pattern
is reversed in the underlying Cleveland Member of the Ohio Shale.
The top of the Cleveland has a carbon content similar to the base
of the Sunbury, with values decreasing to 4-6% toward its base.
The Three Lick Bed of the Ohio Shale shows highly variable dis-
tribution of carbon, which is as expected, as this unit is de-
fined on the basis of 3 OM-deficient, bioturbated green shales.
The pattern of carbon distribution in the Huron Member of the
Ohio Shale is the inverse of the Cleveland; the carbon content
increases toward the base of this unit, reaching values of 9-10%.
This pattern is somewhat broken up by the presence of burrowed

and bioturbated green-shale intervals toward the base of the
Huron.

When the data of Table I are compared, the inter-core organ-
ic geochemistry of the individual shale units is relatively con-
sistent considering the variance among the units. A slight aver-
age decrease toward the lower units is evident, however. Inter-
core H/C ratios for these data are essentially constant, but
slightly higher H/C ratios in the upper Cleveland shales relative
to the Sunbury have been observed. Inter-core N/C ratios are
generally higher for the leaner Huron shales; this correspondence
has also been noted for Western oil shales (8-9).

Regional trends in the study area are illustrated for carbon,
hydrogen, and sulfur in Figure 4. The carbon-hydrogen contents
of the Sunbury Shale are 11 and 1.1% respectively, in the north-
ern (Lewis County) cores and peak at 15 and 1.8% in the Powell
County core sites before decreasing slightly again toward the
south of the study area. The most rapid increase in carbon and
hydrogen occurs as this unit thins and may be reflective of slow-
er depositional rates. Regional C-H trends for the Cleveland HGZ
are also illustrated but are not as distinct as those of Sunbury
Shale. Shale variability as determined by the coefficients of
variation in Table I is generally 2-3 times greater for the D-
series as compared to the K-series samples. This is accounted
for by the greater regional change within the D-series area.
Regional trends for sulfur generally follow carbon for both
units, but levels of the element are noticeably lower in the
Cleveland relative to the Sunbury.

Organic Geochemistry – Fischer Assay Relationships. Conventional
and modified Fischer assay analyses have been performed on many
Sunbury and Cleveland HGZ oil shale samples. The meaning of
Fischer assay results when applied to Eastern U. S. oil shales is
somewhat ambiguous. Such results do provide a basis for compari-
son among the study samples but probably underestimate the amount
of extractable oil from the shale and, consequently, do not pro-
vide an accurate method for assessing the total recoverable ener-
gy from these shales. Comments concerning the applicability of
the Fischer assay test to eastern shales have been made in pre-
vious reports by our colleagues (11-12) and generally indicate
that these oil shales are much more sensitive to heating rate,
product removal, and retort atmosphere variables. The data also
indicate that Fischer assay data for the same samples among dif-
ferent performing laboratories are quite variable and are prob-
ably indicative of both laboratory and oil shale characteristics.

When the body of Fischer assay data on the K-series samples
is evaluated, mean values for the weighted averages of these
cores are 10.3 and 11.9 gal/ton for Sunbury and Cleveland HGZ,
respectively. Coefficients of variation of 8.2% (Sunbury) and
6.9% (Cleveland HGZ) were observed with a total range of assay
values ranging from 5.4 to 18.4 gal/ton. Current data for some

D—series samples are given in Figure 5, which illustrates the
Fischer assay—raw oil shale carbon content relationship for the
two oil shale units. It is evident that the Cleveland oil shale
yields slightly more oil than the Sunbury oil shale, in spite of
the fact that the Sunbury Shale averages more carbon per unit
weight. This same relationship was observed for the two oil
shale units from the K-series (6) and is assumed to be reflective
of kerogen differences between the two oil shales. Correlation
of Fischer assay with hydrogen content yields slightly better
correlations indicating again the criticality of the hydrogen
content of these shales.

     Illustrative Fischer assay yields and associated oil and gas
composition data are presented in Table 2 for both eastern (10)
and western (8) oil shales of nominally similar organic carbon
content. The eastern oil shales yield more gas and water and
less oil than the western oil shale used for comparison. The
major differences in the oil composition include comparatively
lower nitrogen and higher sulfur contents for the Sunbury and
Cleveland shale oils. The lower H/C ratio for the eastern oils
indicate a more aromatic oil, as reported previously (11). Assay
gas composition for the eastern oil shales indicate higher H_2,
CH_4, and H_2S contents with less C_3-C_6 and CO_2 contents. The low-
er C_3-C_6 levels in the case of the eastern oil shales are due to
a more efficient condensation of those gases to the liquid pro-
duct in our assay procedures (12-13). Gas cleanup would ulti-
mately be expected to yield a higher Btu gas for the eastern oil
shale—derived gas than a corresponding western gas due to elimin-
ation of H_2S in the former and high CO_2 levels and condensation
of much of the C_4-C_6 range in the latter. Finally, it should be
emphasized that the compositional information presented is based
on Fischer assay retorting procedures and may not be entirely
representative of products produced under commercial scenarios.

Inorganic Geochemistry

Mineralogic Composition. The subject shales are designated silty
shales due to their high quartz content. The mineralogic compo-
sition of these shales has been studied (14-18) and is summa-
rized in Table III. Illite (2M), muscovite and/or illite/smec-
tite are the predominant clays found in these shales.

Stratigraphic Distribution and Regional Trends. Major and trace
element determinations were performed and are presented as weight
percent or ppm of the 500°C ash fraction of the samples. This
was done to eliminate the effect of variation in organic content
and to facilitate comparisons.

     When the major element chemistry for the various stratigra-
phic units are compared, no large differences are found (Table 4).
The concentration of Al_2O_3 in the shales is less than what would
be expected from a clay shale, which together with the SiO_2 con-
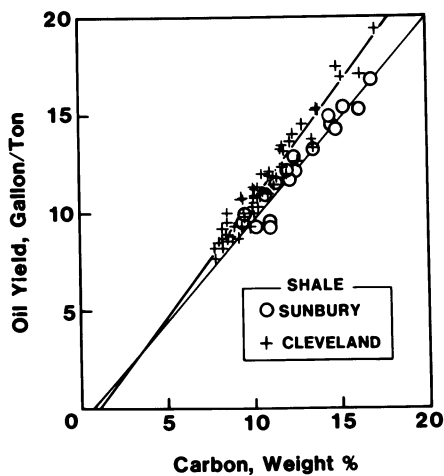
Figure 5. Plot of Fischer assay yields and carbon content for D series oil shales. Regression data are: Sunbury Shale, oil yield = 1.03 (%C) – 0.69 (r = .97); and Cleveland Shale, oil yield = 1.18 (%C) – 1.16 (r = .97).

TABLE II. FISCHER ASSAY YIELDS WITH OIL AND GAS COMPOSITION
DATA FOR EASTERN VS. WESTERN OIL SHALES

Oil Shale Formation	Sunbury[1]	Cleveland[2]	Green River[3]
YIELDS:			
Oil, gal/ton	14.4	13.4	29.8
Gas, ft^3/ton	684.	740.	461.
Water, gal/ton	9.8	16.6	3.8
OIL COMPOSITION:			
C, wt.%	83.25	82.41	84.80
H, wt.%	10.35	10.11	11.60
N, wt.%	0.86	0.77	1.96
S, wt.%	2.38	2.75	0.60
Density	0.9197	0.9199	0.9180
Btu/lb.	17,800	17,800	18,750[4]
GAS COMPOSITION, Vol. %:			
H_2	37.0	30.6	25.7
CH_4	22.2	24.0	16.5
C_2H_4	1.50	1.60	2.30
C_2H_6	5.98	6.09	6.7
C_3-C_6	4.34	3.88	11.7
CO_2	5.53	7.16	31.1
CO	3.33	4.14	0.7
H_2S	20.4	15.2	1.0
Btu/SCF	743	740	776[4]

[1] Data from reference 29, sample SUN-002, Lewis Co., KY,
organic carbon = 13.85%

[2] Data from reference 29, sample CLE-002, Lewis Co., KY,
organic carbon = 14.54%

[3] Data from reference 8, sample 482B 'B', Anvil Points, CO,
organic carbon = 13.61%

[4] Calculated by authors

Table III. Modal Mineralogic Composition of Devonian Oil Shales.

	Cleveland(14)	Chattanooga(15-16-17)
Quartz	30	20-25
Pyrite	5	10-15
Illite	39	
Illite/Muscovite Illite/Smectite Mixed Layered	20	25-30
Kaolinite	Trace	Minor
Chlorite	7	Trace
Carbonates	Minor	Variable
Feldspar	Minor	10
Organics	(on Ash Basis)	15-20

tent, substantiates its significant quartz content. The level of K_2O present (about 4%) indicates that the clays are primarily illite or muscovite-mica which agrees with mineralogic determinations made on the raw shales. The CaO concentration in all of the stratigraphic units is low (generally less than 1.0% (Table IV)), also in agreement with the previous observations made for mineral carbon. Calcium content is generally higher in the Huron, particularly in the D-5 through D-8 cores where the Duffin and Ravenna lithologies are present. There is also a slight geographic trend of increasing CaO concentrations from north to south in the study area.

The coefficients of variation determined among the cores for the major element oxides are generally very low (Table IV) and in many cases almost at the level of analytic uncertainty. Two exceptions to this are CaO and P_2O_5 which are associated with carbonate minerals and phosphate nodules. These are not part of the primary lithologies of the shale and are subject to being either locally abundant or absent.

Unlike the organic elements, the major elemental chemistry does not show large stratigraphic zonation compared to its lateral continuity. Coefficients of variation for the stratigraphic intervals are only slightly greater than those calculated for the average core data. However, the concentration and distribution of the determined trace elements are stratigraphically controlled. Highest concentrations are found in the Sunbury, followed by the Cleveland and the Huron. The elements which show the greatest zonation based on stratigraphic unit include Mo, Ni, V, and Zn. Each of these elements is found to have concentrations in the Sunbury at levels of 2-3 times those of the other units (Table IV). As in the case of the major elements, the coefficients of variation calculated for the trace elements among the cores for the stratigraphic intervals are very low in most cases (Table IV). Unlike the majors, however, the stratigraphic variations of trace

TABLE IV. INORGANIC COMPOSITION FOR K- AND D-SERIES OIL SHALES

	K-Series				D-Series			
	Sunbury Shale	Cleveland Shale Total	HGZ	Huron Shale	Sunbury Shale	Cleveland Shale Total	HGZ	Huron Shale
SiO_2[1]	63.7(3)[2]	66.6(1)	66.5(1)	64.4(1)	64.18(3)	65.78(1)	66.16(2)	61.93(2)
TiO_2	.8(5)	.9(1)	.8(1)	.9(1)	.76(6)	.85(3)	.82(2)	.85(4)
Al_2O_3	16.7(6)	16.4(1)	16.2(1)	16.6(1)	15.58(2)	15.57(3)	15.15(4)	16.12(4)
Fe_2O_3T	8.7(5)	6.8(2)	7.0(3)	7.9(3)	8.12(11)	6.67(4)	6.83(6)	8.20(4)
CaO	.4(28)	.6(21)	.6(20)	.9(29)	.88(114)	.90(36)	.84(43)	1.33(64)
MgO	1.5(6)	1.3(3)	1.4(2)	1.3(5)	1.43(4)	1.37(5)	1.36(5)	1.78(22)
K_2O	4.4(7)	4.3(1)	4.2(2)	4.3(1)	4.11(3)	4.13(3)	4.08(3)	4.26(3)
Na_2O	.4(20)	.5(13)	.5(13)	.5(8)	.38(19)	.50(15)	.47(18)	.54(11)
P_2O_5	ND	ND	ND	ND	.29(77)	.22(44)	.28(48)	.12(23)
Ba[3]	645(4)	619(3)	607(3)	633(3)	622(7)	570(4)	568(4)	564(5)
Co	24(3)	21(2)	20(2)	25(2)	24(6)	19(3)	19(4)	27(3)
Cr	200(3)	159(2)	195(4)	90(1)	175(10)	151(19)	185(4)	93(4)
Cu	113(3)	91(3)	111(4)	57(3)	134(9)	97(6)	114(5)	74(20)
Mo	281(5)	94(3)	89(8)	66(5)	248(15)	104(4)	92(7)	86(6)
Ni	272(3)	125(9)	141(2)	81(3)	288(14)	129(4)	139(3)	96(13)
V	1533(5)	760(5)	1024(5)	209(3)	1155(24)	677(4)	796(6)	216(5)
Zn	1126(6)	444(5)	622(7)	144(8)	1202(15)	412(8)	510(7)	173(9)
U	37(5)	20(7)	20(7)	ND	43(15)	21(4)	19(4)	22(6)

[1] wt. % in 500°C Ash

[2] Coefficients of variation x 100

[3] ppm (wt.) in 500°C Ash

element are high. This concentration reflects the differences
among the stratigraphic units.
     The concentrations of certain trace elements also appear to
show regional trends. As an example of these trends, Figure 6
presents the regional distribution of Mo, Ni, V, and Zn. Each of
these elements shows a slight overall decrease in concentration
between Lewis County (K-9 or 8) in the north and Estill County
(D-10) in the south for both the Sunbury and the Cleveland HGZ.
However, the regional trends for the Sunbury are somewhat ob-
scured by an increase in concentration for Mo, Ni, and Zn, and a
decrease in concentration for V in the region between Montgomery
and Powell Counties. The cause for these regional anomalies is
presently unclear.

Table V. Correlation Coefficients for Metals Affinites of
          Eastern Shales.

		K-Series Data	
Element	Lithologic Unit	Carbon	Sulfur
	Sunbury	−.38	.85
Co	Cleveland	.23	.76
	Huron	.67	.90
	Sunbury	.17	−.34
Cr	Cleveland	.95	.51
	Huron	−.45	−.55
	Sunbury	.81	−.12
Cu	Cleveland	.95	.44
	Huron	.54	.49
	Sunbury	.15	.08
Mo	Cleveland	.11	−.12
	Huron	.90	.78
	Sunbury	.40	.25
Ni	Cleveland	.91	.37
	Huron	.40	.17
	Sunbury	.07	.15
V	Cleveland	.82	.10
	Huron	.01	−.17

Underlined coefficients considered significant

Trace Metal Affinites. Trace-element and major-element associa-
tions in the oil shales have been a subject of two studies (19-
20). In general, the trace elements can be divided into three
groups: those which have an affinity for carbon (Cu, Cr, Ni, V),
those which have an affinity for sulfur (Co, Zn), and those which
have an affinity for the silicates and carbonates (Ba) (not re-
ported here). To some degree the associations are stratigraph-
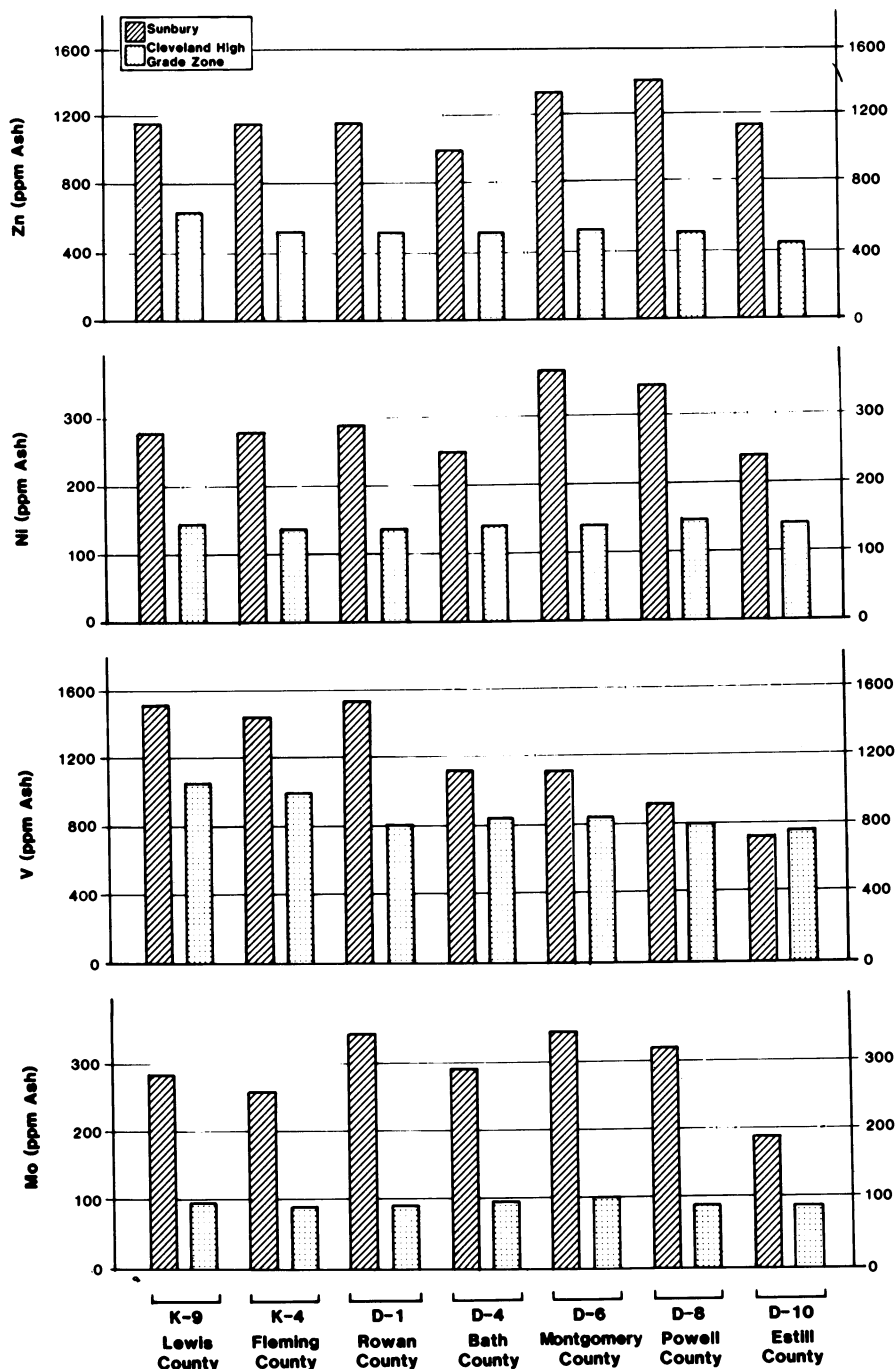
Figure 6. Regional trends for selected trace elements in selected cores of study area.

ically dependent. For example, in Lewis and Fleming Counties, Cr, Ni, and V concentrations were found to be strongly correlated with carbon concentration (correlation coefficients = .95, .91, and .82, respectively) in the shales of the Cleveland Member, but not strongly correlated in the Huron and Sunbury (20). Zn is listed as having an affinity for sulfur, even though it did not have a significant correlation. It is often associated with its own mineral phase (sphalerite, ZnS) and the lack of correlations with total sulfur is not surprising. Correlation coefficients for the trace metal affinities found in the K-series is presented in Table V. The trace element affinities discussed are similar to the observations of Keogh (21) who studied the trace element chemistry of the organic matter separated from the shale.

Economic Implications of Trace Element Geochemistry. The regional trends in the stratigraphy and geochemistry of the defined economic units are relevant to mining, processing, and by-product recovery potential. Trace metal data for the total economic zone are presented in Table VI. These data are weighted for the thickness of the Cleveland HGZ and Sunbury Shale and therefore are representative of potential feedstocks for a retorting system.

The high concentration of metals in the eastern oil shales has led to considerable speculation concerning the potential for by-product metals recovery (23-27). Much of this interest has centered on the recovery of such metals as Mo, V, Ni, Cu, U, Th, and Al. At present, the potential for the recovery of these metals appears to be sub-economic (1).

Several of the metals present in eastern oil shales are of importance from a processing standpoint. Certain elements, particularly those shown to be associated with carbon, (Table V) may tend to concentrate in the oils produced during retorting. Of particular concern in process and oil upgrading are As, V, and Ni. These elements are known to be a problem in upgrading oils due to cracking and reforming catalyst poisoning. During upgrading, these oils require processing to remove these elements. The high trace element concentrations of Ni and V in the eastern oil shales (Tables IV and VI) coupled with their organic affinity imply that they may partition to the oils during retorting. Although the As values for these oil shales are limited, preliminary data for the units are: Sunbury (5-300 ppm), Cleveland (1-80 ppm), and Huron (30-50 ppm). Arsenic also is expected to concentrate in the oils during retorting. These predictions are confirmed by preliminary data presented in Table VII for a single two stage retort produced oil (27). The metals composition of other crude oils are also presented for comparison.

Conclusions

o The principal form of carbon present in the oil shale is as organic matter. Mineral-bound carbon was found to be insigni-

TABLE VI.   TRACE METAL CONTENT OF TOTAL ECONOMIC ZONES

	K-9 Lewis County	K-4 Fleming County	D-1 Rowan County	D-4 Bath County	D-6 Montgomery County	D-8 Powell County	D-10 Estill County	Study Area Mean
Mo	158	151	175	152	145	119	99	148
Ni	191	187	187	172	184	172	153	179
V	1226	1164	1058	911	891	795	738	1025
Zn	819	749	728	663	698	636	545	723

TABLE VII.   TRACE ELEMENT COMPOSITION OF AN EASTERN SHALE OIL (CHATTANOOGA), A WESTERN SHALE OIL, AND TWO PETROLEUM CRUDES

	Chattanooga 1st Stage (25)	Chattanooga 2nd Stage (25)	Paraho (25)	Alberta Canada Devonian Crude (26)	Venezuela Crude (27)	Nigerian Crude (28)	Iranian Crude (28)	California Terhasy Heavy Crude (27)
As (ppm)	50	59	28	.111	.005	1.2	.095	.66
Ni (ppm)	5.0	5.9	1.8	9.4	117	5.9	12	94
V (ppm)	6.3	6.3	.2	13.6	1120	9.5	53	7.5

ficant, with the exception of the Duffin zone, a localized do-
lomitic lithology present near the base of the Huron.

o Carbon and hydrogen are strongly zoned stratigraphically, with
highest levels present in the upper and lower portions of the
oil shale section. The variability of the organic chemistry
among the study cores is low in comparison.

o The Fischer assay yields of the two economic units were simi-
lar, averaging 10.3 gal/ton for the Sunbury Shale and 11.9 gal/
ton for the Cleveland HGZ. The Fischer assay data underesti-
mates the maximum potential oil yield of these shales, however.

o The major element chemistry is found to be both stratigraphi-
cally and laterally consistent for the oil shales.

o Trace element concentrations are found to be highest in the
Sunbury Shale, followed by the Cleveland and Huron members of
the Ohio Shale. Trace element concentrations were found to be
strongly stratigraphically zoned, but relatively consistent,
among the cores.

o The major regional trends which may affect mining, processing,
and by-product recovery (north to south and including Lewis and
Fleming Counties) include:
   1) the thinning and virtual disappearance cf the stratigraphic
       intervals separating the Sunbury Shale and Cleveland HGZ;
   2) the thinning of the Sunbury Shale;
   3) an increase in carbon and hydrogen in the Sunbury Shale
       (concomitant with thinning); and
   4) a decrease in trace element content for the total defined
       economic zone.

o Trace elements exhibited three types of association: those
having an affinity for carbon (Cu, Cr, Ni, V), those having an
affinity for sulfur (Co, Zn), and those having a silicate and/
or carbonate affinity (Ba).

o Trace elements, particularly those associated with the oil
shale kerogen, may be incorporated into the oil product and
present subsequent processing problems.

Literature Cited

(1) Vyas, K. C.; Aho, G.D.; Robl, T.L. Cleveland, Ohio, Jan. 1981, DOE/R4/10185-T1, 2-1 - 2-18.

(2) Schwab, H. R.; Norris, R. L. Morgantown, WV, Feb. 1980, DOE/METC/8215-1, 1-55.

(3) Provo, L. J.; Kepferle, R. C.; Potter, P. E. Amer. Assoc. Petr. Geol. Bull. 1978, 62, 1703.

(4) Barron, L. S.; Ettensohn, F. R. Geol. Soc. Amer. Abstracts with Programs, 1980, 12, 218.

(5) Barron, L. S.; Ettensohn, F. R. Morgantown, WV, April 1981, DOE/ET/12040-151, 1-75.

(6) Barron, L. S.; Bland, A. E.; Robl, T. L.; Koppenaal, D. W.; Thomas, G. A. Synthetic Fuels from Oil Shale II, Nashville, TN, Oct. 1981; Institute of Gas Technology: Chicago, IL; 43-71.

(7) Bland, A. E.; Robl, T. L.; Koppenaal, D. W. "Proceedings", 1981 Eastern Oil Shale Symposium, Lexington, KY, Nov. 1981; Institute for Mining and Minerals Research: Lexington, KY; 183-194.

(8) Singleton, M. F.; Koskinas, G. J.; Burnham, A. K.; Raley, J. H. Livermore, CA, 1982, Lawrence Livermore Laboratory Report UCRL-53273.

(9) Larson, O. A.; Wen, C. S. "Proceedings", 14th Oil Shale Symposium, Golden, CO, April 1981; Colorado School of Mines: Golden, CO.

(10) Rubel, A.; Taulbee, D.; Coburn, T.; Thomas, G.; Yates, L. "Proceedings", 1982 Eastern Oil Shale Symposium, Lexington, KY, Oct. 1982; Institute for Mining and Minerals Research: Lexington, KY.

(11) Fabry, D. A.; Moore, H. F. "Proceedings", 1981 Eastern Oil Shale Symposium, Lexington, KY, Nov. 1981; Institute for Mining and Minerals Research: Lexington, KY, 311-320.

(12) Rubel, A. M.; Coburn, T. T. "Proceedings", 1981 Eastern Oil Shale Symposium, Lexington, KY, Nov. 1981; Institute for Mining and Minerals Research: Lexington, KY, 21-28.

(13) Coburn, T. T.; Rubel, A. M., submitted for publication in Fuel Proc. Tech.

(14) Hosterman, J. W.; Whitlow, S. I. Denver, CO, 1981, U.S.G.S. Open File Report 81-585.

(15) Markowitz, G. M.S. Thesis, University of Kentucky, Lexington KY, 1979.

(16) Bates, T. F. Geol. Soc. Amer. Bull. 1957, 68, 1305.

(17) Miller, M. L. M.S. Thesis, University of Kentucky, Lexington, KY, 1978.

(18) Conant, L. C.; Swanson, V. Denver, CO, 1961, U.S.G.S. Prof. Paper 357.

(19) Bland, A. E.; Robl, T. L.; Koppenaal, D. W. Amer. Assoc. Petr. Geol. Bull. 1981, 65, Abstr., 903.

(20) Bland, A. E.; Barron, L. S.; Robl, T. L. Geol. Soc. Amer.
      Abstracts with Programs, 1981, 13, 411.
(21) Keogh, R. A. In "Geologic and Geochemical Studies of the
      New Albany Shale Group (Devonian-Mississippian) in Illinois"
      Bergstrom, R. E.; Shimp, N. F.; Cluff, R. M.; Morgantown,
      WV, June 1980, DOE/METC/12142-26, 107-114.
(22) Crouse, C. S. Lexington, KY, 1925, Kentucky Geological Sur-
      vey, series VI, 24.
(23) Robeck, B. C.; Conant, L. C. Denver, CO, 1951, USGS Trace
      Element Investigations Report 64.
(24) Chase, C. K. Synthetic Fuels from Oil Shale, Atlanta, Ga.,
      Dec. 1979; Institute of Gas Technology: Chicago, IL; 547-
      578.
(25) Matschler, R. P.; Hill, T. T.; Williams, B. B. Pittsburgh,
      PA, 1976, U. S. Bureau of Mines Report JC 8700.
(26) Gilliam, T. M.; Caron, R. M.; Ryan, A. D.; Watson, J. S.
      "Proceedings", 1981 Eastern Oil Shale Symposium, Lexing-
      ton, KY, Nov. 1981; Institute for Mining and Minerals Re-
      search: Lexington, KY; 323-329.
(27) Sullivan, R. F., Chevron Research Co., personal communica-
      tion, 1982.
(28) Hitchon, B.; Filby, R. H.; Shah, K. R. in "Role of Trace
      Metals in Petroleum", Yen, T. F., Ed.; Ann Arbor Science
      Publishers: Ann Arbor, 1975.
(29) Filby, R. H. in "Role of Trace Metals in Petroleum", Yen,
      T. F., Ed.; Ann Arbor Science Publishers: Ann Arbor, 1975.
(30) Filby, R. H.; Shah, K. R.; Yahgmaie, F. in "Ash Deposits
      and Corrosion Due to Impurities in Combustion Gases",
      Bryers, R. W., Ed., Hemisphere Publishing Corp. and McGraw-
      Hill Co.: New York, 1977.

Upper Devonian Black Shales of the Eastern United States

Organic Geochemical Studies—Past and Present

IRVING A. BREGER ,[1] PATRICK G. HATCHER, and LISA A. ROMANKIW—U.S. Geological Survey, Reston, VA 22092

FRANCIS P. MIKNIS—U.S. Department of Energy, Laramie Energy Technology Center, Laramie, WY 82071

GARY E. MACIEL—Colorado State University, Fort Collins, CO 80523

Upper Devonian black shales of the eastern United States have long been known as major gas producing shales. Our solid-state ^{13}C nuclear magnetic resonance (NMR) studies of the kerogen in shales of the Lower Huron Member of the Ohio Shale have demonstrated a regional gradient in carbon aromaticity that parallels both the known metamorphic gradient and trends normal to inferred paleo-shorelines. The kerogen is essentially coal-like throughout most of the basin with aromaticities of 0.50 or greater. Large changes in carbon aromaticities are observed along an east-west line in our study area, the western half of the basin where maturation levels are low. We believe that the eastward increase in aromaticity is related to increased contributions of vascular plant remains as one approaches paleoshorelines. It is likely that a large proportion of the natural gas in these shales evolves from low-rank maturation of the coaly kerogen.

The Upper Devonian black shales of the eastern United States are part of an eastward-thickening deltaic wedge in the Appalachian basin. The black shales extend from central New York southward and westward to Pennsylvania, Ohio, Kentucky, West Virginia, Tennessee, and Alabama. Similar black shales are present in the Illinois and Michigan basins. Regionally, the more important black shales are known by several different names. In New York, they are the Geneseo, Rhinestreet, and Dunkirk Shale Members of the Genesee, West Falls, and Perrysburg Formations, respectively. The Ohio Shale is present in Ohio, Kentucky, and West Virginia; the Chattanooga Shale is in Kentucky and Tennessee. For many years these shales have

[1]Deceased

elicited much interest because they are a major source of
natural gas. It is of particular interest that these shales have
relatively minor amounts of known associated crude oil compared
with natural gas in spite of the fact that they have some of the
characteristics normally attributed to source beds for crude oil
(e.g. organic carbon content). It has been proposed that the
organic-rich black-shale facies originated from shallow- water
(200m or less) deposition in euxinic environments (1), though
more recently a deep-water depositional model has been suggested
(2). These black shales were deposited in the Chattanooga Sea, a
southwest trending marine basin bounded in the south and east by
Acadian orogenic highlands. The basin extended from Alabama and
Tennessee northward into Kentucky, Virginia, W. Virginia, Ohio,
Pennsylvania, and New York.

     Natural gas in and above these shales is found throughout
the basin. Studies by Claypool and coworkers (3) have shown
that the gas is "dry" in the eastern part of the basin (i.e.,
contains mostly methane) and becomes "wet" towards the north and
west (i.e., other hydrocarbon homologs such as ethane and
propane contribute to the gas). This data combined with data on
the stable carbon isotopic compositions of the gas led Claypool
et al. (4) to conclude that the composition of the organic
matter is essentially uniform throughout the basin and that
thermogenic processes were solely responsible for the production
of natural gas in the shales. Deeper burial in the eastern
parts of the basin apparently led to evolution of "post-mature"
dry gas (4). The model presented by Claypool et al. (3) is in
direct contrast to the model proposed earlier by Breger and
Brown (5,6). Breger and Brown proposed that the source of
organic matter is a primary determinant for the evolution of
gas. Shales containing organic matter that is mainly derived
from terrestrial vascular plants tend to produce gas with
increasing maturation (7) and to occur in parts of the basin
proximal to the paleoshoreline (i.e., to the south and the
east). Distal to the paleoshoreline, in more "open" marine
portions of the basin, a larger contribution of aquatic or algal
type of organic matter is observed (5,6). This type of organic
matter is more likely to produce oil or liquid hydrocarbons
having molecular weights higher than that of methane. These
hydrocarbons, when mixed with methane produced from coaly or
"humic" kerogen, yield "wet" gas.

     The Breger and Brown model does not, however, explain the
stable carbon isotope compositions of either the gas or the
kerogen in the shales. Apparently, the kerogen becomes isotopi-
cally lighter (depleted in ^{13}C) as one progresses away from the
paleoshorelines (8). Maynard (8) proposed that the isotopic
trends reflected the mixing of isotopically heavier vascular
plant components with isotopically lighter algal components.
Unfortunately, the carbon isotopic relationship between vascular
and algal components in modern sediments is the reverse of the

above relationship, but Maynard suggested several possible explanations that might account for the reversed trend. Though this trend is opposite to expected trends based on modern analogs, it is consistent with the trends expected from Claypool's model (3) which suggests that maturation effects were primarily responsible for isotopic gradients. A similar trend is observed in the stable carbon isotopic compositions of the gas (3,4) and is used to support the thermogenic hypothesis. Unfortunately, no simple explanations for the isotopic composition of the gas are apparent, and the question as to whether thermogenic processes or source relationships are responsible for the type and distribution of natural gas is still open to debate.

Many believe that there are regional variations in the composition of the organic matter in the Upper Devonian shales and attempts have been made to quantify and map the distribution of the terrestrial and aquatic components (8,9). As noted above, stable carbon isotopes have not provided a reliable quantitative distinction between terrestrial and aquatic carbon. Neither have elemental compositions, because such measurements are not sensitive to subtle changes in kerogen type and maturation effects often cannot be segregated from source changes. Microscopic examinations have revealed that a major fraction of the organic matter is amorphous (9). However, attempts to classify this material as aquatic should be viewed with skepticism because terrestrial material can also exist in an amorphous state (6). Microscopic examinations by Zielinski (9) revealed the presence of increasing amounts of woody or coaly plant fragments in Upper Devonian shales as one approaches the eastern part of the basin. This suggests that the kerogen becomes more coaly towards the eastern paleoshoreline.

Recently, solid-state ^{13}C NMR (using cross polarization with magic-angle spinning) has been suggested as a method of determining the type of kerogen in shales (10). The degree of aromaticity of Holocene humic substances has been proposed as a method to determine the distal/proximal relationships to modern shorelines (11). In this instance the amount of aromatic carbon was directly related to the contribution of vascular plants which supply lignin to the sediments. Humic substances in marine sediments having no contributions from vascular plants show very low aromaticities (10%) in their NMR spectra (11). Although coalification or maturation processes alter humic substances, the basic chemical framework is expected to survive. Thus, woody debris is coalified to a substance whose NMR spectrum is mostly aromatic, whereas algal kerogen yields a substance whose NMR spectrum is mostly aliphatic (12). Consequently, one should be able to quantify the vascular and nonvascular plant contributions to kerogen simply on the basis of aromaticity.

This relationship, however, is not as straightforward as one might envision. Maturation or metamorphic alteration induced

by time and temperature during burial can lead to changes in
kerogen structure. These structural changes could effectively
involve cracking of aliphatic carbon-carbon bonds, producing
mostly liquid or gaseous hydrocarbons and leaving the residual
kerogen relatively depleted of aliphatic carbon. Thus in the
course of maturation, the kerogen could become progressively
more aromatic. Differentiation of whether aromaticity is intro-
duced by mixing of algal and vascular plant "end members" or by
maturation could be difficult without additional supporting
data. At the present time we are uncertain about the magnitude
of the effect maturation has on kerogen aromaticity although a
generally increasing trend in aromaticity is observed for coal
as a function of rank (13).

The purpose of this paper is to report the preliminary
results of a study of Upper Devonian shales by ^{13}C NMR in an
attempt to understand regional variations in kerogen composition
as related to the evolution of oil and gas.

Laboratory and Field Methods

Sample selection. Samples to be analyzed were chosen from among
a suite of samples taken from the Huron Member of the Ohio Shale
and the Rhinestreet Shale Member of the West Falls Formation.
These stratigraphic units were sampled from cores collected by
the Department of Energy's Morgantown Energy Technology Center
under the auspices of the Eastern Gas Shale Project. They were
selected for study because they are areally extensive throughout
the Appalachian basin (14,15). The cores were sampled at 2-8 m
intervals, depending on formation thicknesses. One sample from
each drill hole (Table I and Figure 1) was selected for
processing.

Sample preparation. Core samples were washed with cold tap
water and a stiff wire brush, then air-dried. Coalified wood
fragments were scraped from bedding-plane surfaces. Elemental
analyses and ^{13}C NMR spectra for these coal samples were
obtained without further preparation.

Approximately 100-200 grams of the shale samples were
crushed in a steel jaw crusher and then ground to -200 mesh in
an agate shatter box. Several grams of the ground shale were
retained for carbon and ash determinations. After grinding, the
pulverized shale samples were extracted for 4-7 days in a large
Soxhlet apparatus, using cellulose extraction thimbles and a
mixture of benzene and methanol (v:v/1:1) as the extraction
solvent. Shale residues were air-dried and a series of acid
extractions was then used to isolate and concentrate the organic
matter (kerogen) from the mineral matrix. The bitumen-extracted
shales were first treated with 0.1 N HCl to remove carbonates.
After a digestion period of 3-5 days, the HCl was decanted and
the shales were washed with deionized water. The shales were

Table I. Location descriptions, mean losses on ignition, and
mean total carbon contents of the zones sampled in this study

Core designation	County	Depth of sample(m)	Mean loss on ignition*	Mean total carbon content
Ohio
OH-3	Knox	329	13.8	6.8
OH-4	Ashtabula	366	18.4	8.1
OH-5	Lorain	331	13.8	6.7
OH-6-1	Gallia	762	12.3	5.2
OH-6-2	Gallia	697	15.1	6.7
OH-7	Trumbull	656	19.4	11
OH-8	Noble	1059	15.6	8.1
OH-9	Meigs	916	11.5	4.8
West Virginia
WV-1	Jackson	1042	9.86	3.8
WV-3	Lincoln	1040	-	7.1
WV-5	Mason	925	23.2	16
Kentucky
KY-1	Perry	931	-	5.1
KY-4	Johnson	432	15.5	8.4
KY-5	Rowan	191	16.6	7.9
Pennsylvania
PA-5	Lawrence	1147	6.49	0.91

* loss on ignition at 750°C

then treated with a mixture of 48% HF and 36% HCl (v:v/1:1) to
remove silicates. Following digestion on a steam bath, the acid
was decanted, and replaced by fresh acid mixture. This proce-
dure was repeated approximately 10 times, after which the
kerogen was rinsed with 6N HCl, thoroughly washed with deionized
water, freeze-dried, and weighed.

Elemental analyses. Elemental (C,H,N, and O) analyses of the
kerogen isolates, and analyses of the total carbon content of
the whole shale were obtained, directly, using a Carlo Erba
Model 1106 Elemental Analyzer(any use of trade names in this
publication are for descriptive purposes only and does not
constitute indorsement by the U. S. Geological Survey. Elemen-
tal analyses (C,H, and N) of the coal samples were accomplished
using a Perkin-Elmer Model 240 Elemental Analyzer, with oxygen
contents calculated by difference. The ash content of the whole
shale was determined by combustion of 10-20 mg aliquots in a
muffle furnace at 750°C. All samples (coal and kerogen) were

●   Huron Member of Ohio Shale

▲   Rhinestreet Shale Member of West Falls Formation

− − − approximate boundary of the Appalachian basin
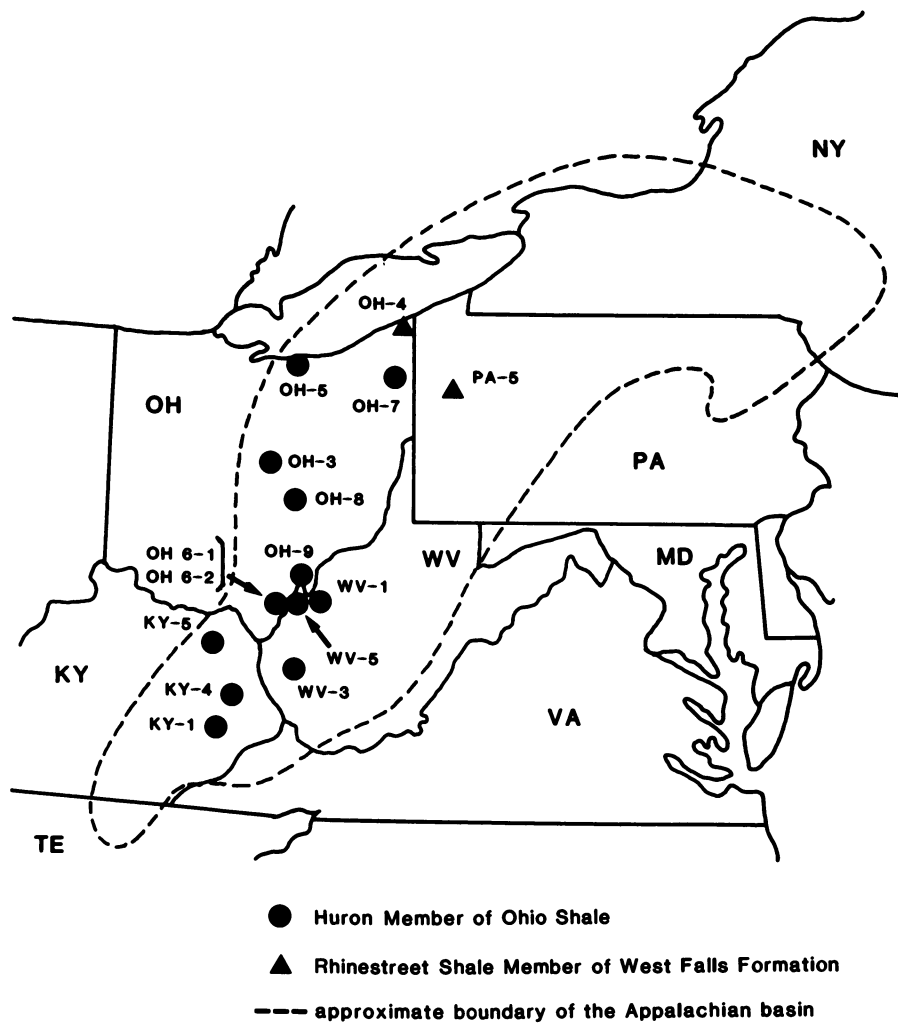
Figure 1. Locations of drill cores sampled in this study.

corrected for moisture content by heating in an oven at 60°C for 2-3 hours prior to analysis.

NMR analyses. ^{13}C NMR spectra of the coal and kerogen samples were obtained on a spectrometer at Colorado State University using the cross polarization magic-angle spinning (CPMAS) technique described by Bartuska et al. (16).   All spectra were acquired at a field strength of 2.5 Tesla.   Solid, powdered samples, packed into a bullet-type rotor, were spun at frequencies of 3.9-4.1 kHz.   The pulse repetition time was 1 second and the contact time was 1 millisecond.   The number of pulses required to obtain spectra having good signal-to-noise ratios ranged from 3000 to 40,000, with an average of 4000-5000 pulses being sufficient for most samples. Carbon aromaticities were calculated by integrating peaks for aromatic carbons (100-170ppm) and dividing the resulting areas by those of the combined aromatic and aliphatic (0-70ppm) peaks. Errors in the measurement of aromaticities are estimated to be $\pm$0.01 (δ) at an aromaticity value of 0.50.

Results and Discussion

Locations, descriptions, and mean total carbon contents of the zones sampled in this study are given in Table I.   The mean total carbon contents of the whole shale samples generally range from approximately 4-16 percent.   These values are similar to the total organic carbon content of most organic-rich Devonian black shales in the Appalachian basin (17). Drill core locations are shown in Figure 1.   We attempted to obtain an adequate sampling of the entire Appalachian basin, but our coverage was limited to samples from drill cores collected mostly in the western part of the basin.

Elemental compositions.   Coalified wood fragments, which indisputably represent terrestrial material, have the following moisture-and-ash-free average elemental compositions:

Carbon	83.6 $\pm$ 2.3 percent
Hydrogen	6.6 $\pm$ 0.5 percent
Nitrogen	2.3 $\pm$ 0.2 percent
Oxygen	8.2 $\pm$ 2.7 percent

These values are typical of high volatile bituminous coals, although the nitrogen content is slightly elevated.   The data, when plotted on a Van Krevelen diagram (atomic H/C vs. atomic O/C ratios, Figure 2), cluster in a region that is slightly above the development trend for vitrain in most humic coals. Generally, the points lie in the range expected for high-
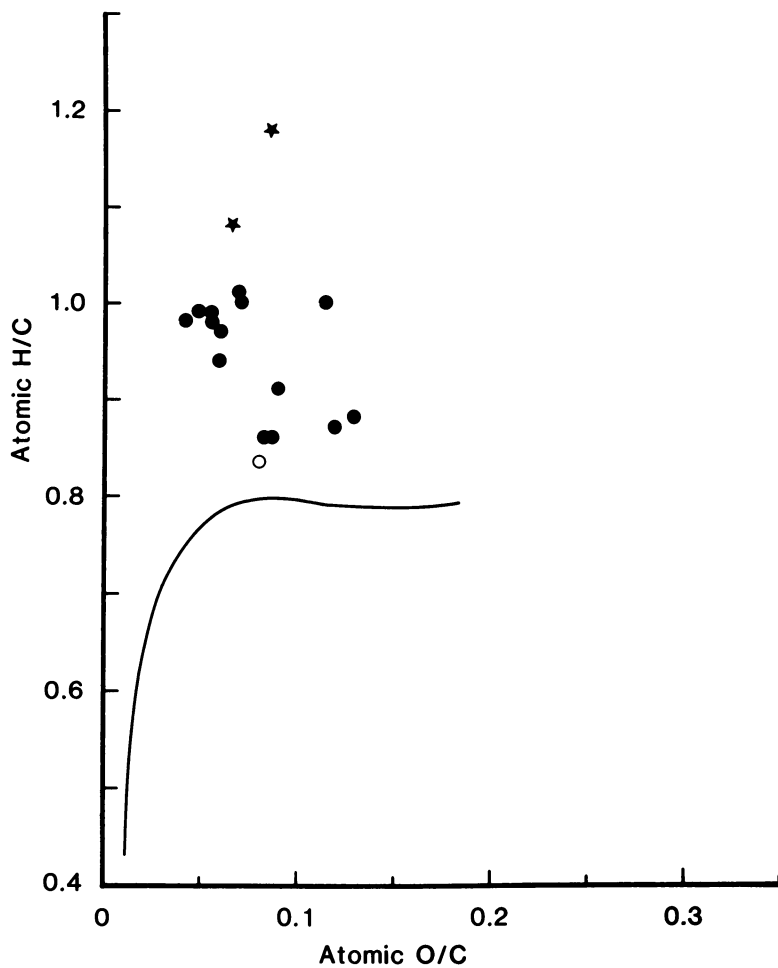
Figure 2. The Van Krevelen plot of atomic H/C vs. atomic O/C ratios for kerogen and coal samples. The two kerogen samples are from cores OH-3 and OH-4. The development line is that of vitrain in coal (18). Key: ★, kerogen; ●, coalified wood fragments; and ○, callixylon from Chattanooga shale.

volatile bituminous coal (18). A number of factors could be responsible for the elevated H/C ratios, including the presence of resinous substances or lipid-rich organic matter adsorbed to the coal. Hatcher et al.(19) observed the atomic H/C ratio of a coalified log buried in a marine shale to be higher than expected, and attributed the discrepancy to fluorescing substances, probably resins. The elemental analysis of a sample of wood (Callixylon) from the Upper Devonian Chattanooga Shale in Tennessee (20) is also plotted in Figure 2. This datum point plots in the same region as the wood fragments mentioned above, but is closer to the region expected for vitrains in coal.

Only two complete elemental analyses (C, H, N, and O) are presently available for the kerogen samples isolated in this study (OH-3 and OH-4). The elemental compositions of these two kerogens are similar to those of the coal samples; however, higher values for hydrogen and nitrogen are observed. The data plot on the Van Krevelen diagram (Figure 2) at higher H/C ratios but similar O/C ratios. Atomic H/C ratios for algal or marine kerogens are typically high (21), about 1.3 to 1.5. The higher H/C ratios and N contents of the two kerogens (compared to the coal) may reflect contributions of algal-derived materials. Unfortunately, the elemental compositions are generally insensitive to quantitative measurements of provenance and caution must be exercised when making the above statements.

NMR data. Representative solid-state ^{13}C NMR spectra for coalified wood and kerogen samples from this study are shown in Figure 3. NMR spectra of (1) an algal oil shale (Australian Torbanite), (2) a Cretaceous black shale from the eastern Atlantic (22-24), and (3) a coalified log of high volatile bituminous A rank from the Connellsville Sandstone Member of the Conemaugh Formation (Waynesburg log,19) are also shown. This latter suite of spectra are presented to show the compositions of vascular and nonvascular plant "end members", and that of a kerogen having a mixed composition. Clearly, the main distinction between algal and coaly kerogen is the degree of aromaticity, f_a, shown in Figure 3. Thus, aromaticity, if it can be quantified, should provide a measurement of terrestrial and aquatic contributions to the kerogen. We hesitate to positively state that quantification is possible at this time, given the fact that NMR signals may not be representative (i.e.,the same signal intensities for all types of carbons). No satisfactory evidence has been presented to show non-quantitative behavior and all indications are that the NMR signals accurately represent true carbon distributions.

The spectrum for the coalified wood from sample WV-5 (Figure 3) shows less aromatic carbon than that of the wood fragment from the Connellsville Sandstone Member. If higher aromaticity is an indication of higher rank in coal (25), then this wood is of lower rank than the Waynesburg log, which is a
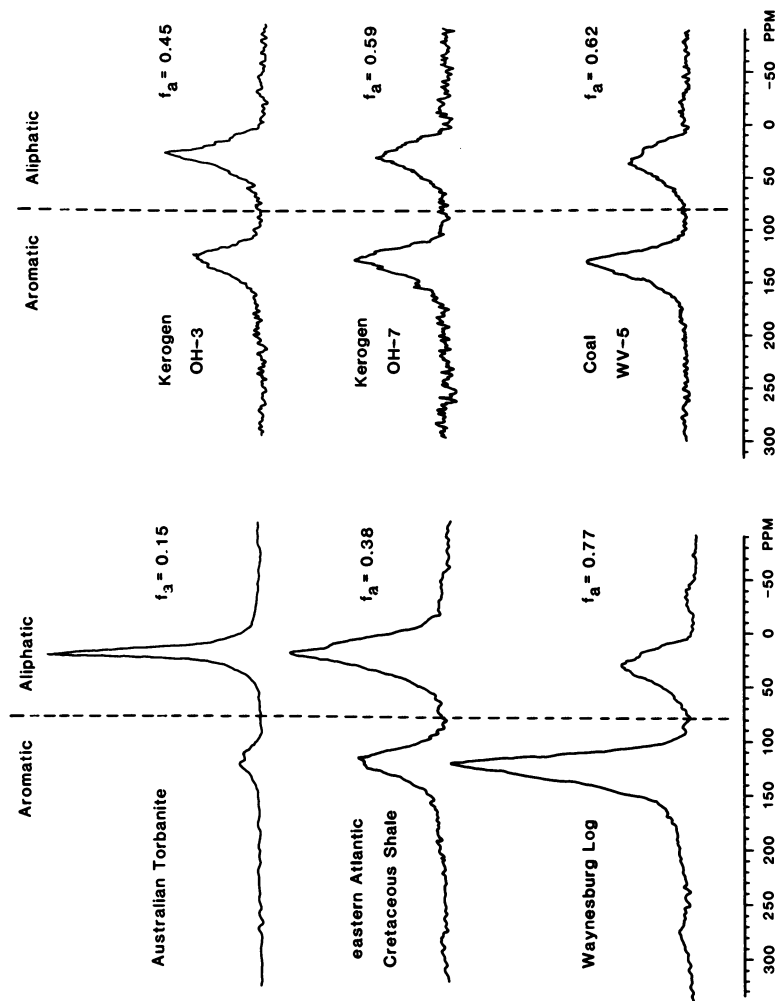
Figure 3. Solid-state ^{13}C-NMR spectra of kerogen and coal samples from Upper Devonian black shales (right) and from other locations as indicated (left).

The Australian Torbanite is an algal shale discussed by Hatcher et al. (12), the Cretaceous black shale is discussed in Dennis et al. (24), and the Waynesburg log is a coalified log from the Connellsville Sandstone Member of the Conemaugh Formation, which has a rank of high-volatile A bituminous coal (R. Stanton, personal communication). (f_a denotes carbon aromaticity.)

high-volatile A bituminous coal. However, we noted earlier that the atomic H/C ratios of wood fragments from the Huron Member of the Ohio Shale were unusually high, suggesting the presence of more aliphatic materials. Thus, the lower aromaticity of wood fragments from the Huron may be related to the presence of these more aliphatic substances. Nevertheless, the aromaticity for these wood fragments should represent the upper limit of aromaticity for terrestrial kerogen in the study area, being that they represent "pure" terrestrial contributions. The aromaticities of coalified woods obtained from samples of the Huron Member analyzed in this study are shown in Figure 4. The mean aromaticity is 0.65 with a standard deviation of 0.03 which is similar to the error expected in the measurement. Thus, there is essentially little variation in aromaticity for the limited area and number of samples examined. This suggests that the rank of coal is approximately constant over the area in question, and the value of 0.65 $\pm$ 0.03 is a maximum aromaticity to be expected for the terrestrial kerogen.

The NMR spectra shown in Figure 3 are characteristic of our kerogen samples from the Huron. With aromaticities of 0.45 and 0.59, these kerogens are clearly more like coal than like unmetamorphosed algal remains. This conclusion is consistent with much of the previous work suggesting that the kerogen in Upper Devonian black shales is of a coaly nature (5,6). This may explain why natural gas rather than petroleum is the dominant form of maturation product in the shales. Although the aromaticities of these kerogens are high, they are lower than those of the coalified woods which have a mean aromaticity of 0.65 $\pm$ 0.03.

The mean aromaticity for the kerogen samples in this study is 0.54 with a standard deviation of 0.08, which is well outside the variation due to measurement errors ($\delta = \pm 0.01$). The larger variation among aromaticities is an indication that regional differences in kerogen composition are significant. The lower mean aromaticity indicates that the kerogens have an additional aliphatic component, most likely derived from algal contributions.

The regional variation in aromaticity for the kerogen of Upper Devonian black shales is shown in Figure 5. Though the data are admittedly sparse at this time, some general trends can be observed. The lowest aromaticities are found in the western and northern portions of the basin - regions distal to inferred paleoshorelines in the southeast and east. There is also a measurably significant difference between the aromaticities of kerogen in eastern and western portions of our study area. Towards the east, aromaticities approach those of coalified wood, whereas towards the western part of the study area, aromaticities drop to values of approximately 0.45.

Two major factors could be responsible for observed trends in aromaticity of the kerogen. One is the mixing of aromatic

--- approximate boundary of the Appalachian basin
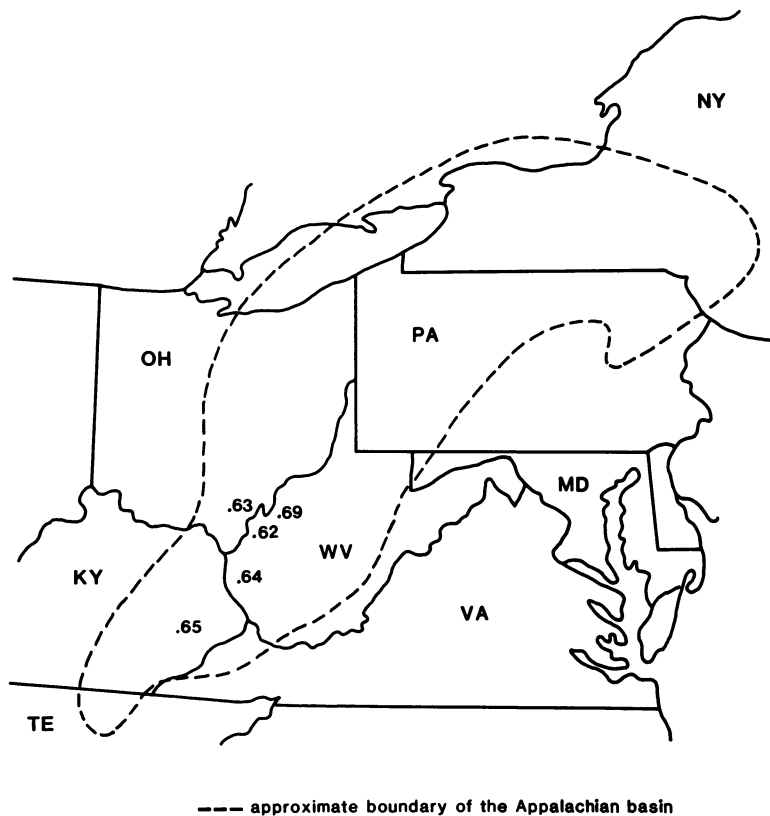
Figure 4. Carbon aromaticities, f_a, for coalified wood fragments in Upper Devonian shales of the Appalachian basin.

—— approximate boundary of the Appalachian basin
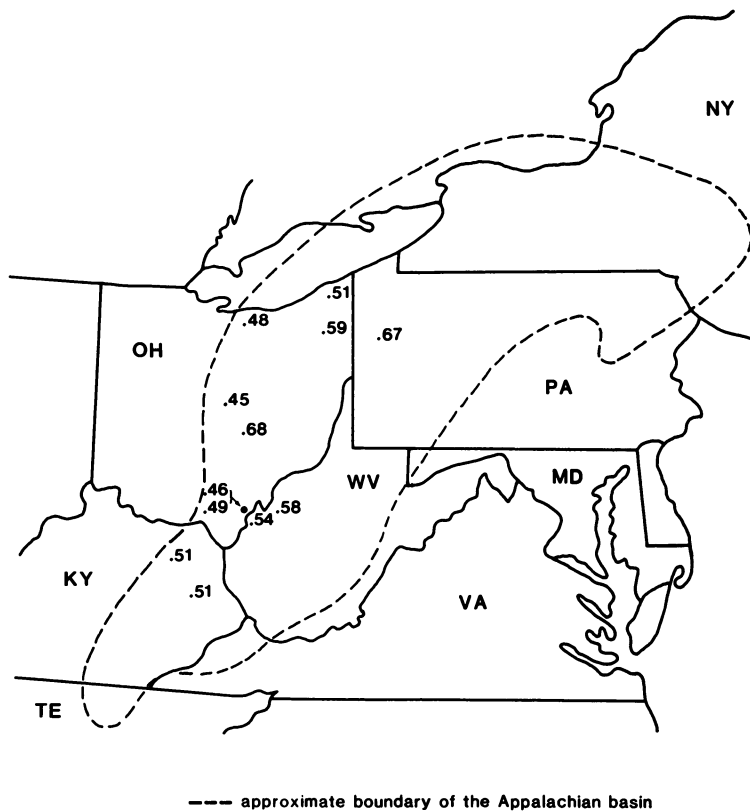
Figure 5. Carbon aromaticities, f_a, for kerogen in Upper Devonian shales of the Appalachian basin.

terrestrial plant-derived kerogen with that derived from the
more aliphatic algal matter. The other, kerogen maturation, also
leads to increased aromaticity (26). The regional metamorphic
gradient in the Appalachian basin follows a trend normal to
paleoshorelines (see 3 and references therein). It is difficult
to determine the relative influence of either factor on the
composition of the kerogen, because both factors are likely to
increase kerogen aromaticity along an east-west line.

Fortunately, the isolation and analysis of phytoclasts
representing the terrestrial component of the kerogen (coalified
plant fragments) has allowed us to estimate an upper limit on
the effect of maturation (i.e., the rank associated with kerogen
in the shale) in our study area. Elemental and NMR analyses show
that the coalified plant fragments are essentially high-volatile
bituminous coal. Conodont color-alteration data (27) have shown
that the rank of kerogen in Upper Devonian through Mississippian
rocks in our study area is essentially that of high-volatile
bituminous coal and that a very gradually increasing metamorphic
gradient exists in the region covered by our data. This rank
corresponds to the maturation level referred to as the zone of
maximum oil generation (21).

Inasmuch as little gas, relative to oil, is thought to be
produced from kerogen at this early stage of maturation, the
presence of significant amounts of natural gas, relative to oil,
in this part of the basin cannot be satisfactorily explained by
maturation processes alone. A possible explanation for gas
occurrence centers on the fact that coal is capable of producing
relatively larger amounts of gas than oil at an early stage of
maturation (21). It is likely that the kerogen in the study area
is mostly composed of coaly material, as inferred from the NMR
data, and thus is capable of producing mostly gas.

It is important to mention that our reported data is res-
tricted to only the western half of the basin where regional
metamorphism has been minimal. This area is remote from the
eastern part of the basin where significant amounts of burial
and tectonic folding have led to accelerated maturation over
relatively short distances (27). Thus, this increased maturation
could have been, in part, responsible for the evolution of
"post-mature" dry gas as suggested by Claypool and co-workers
(3). Whether increased incorporation of woody plant matter, as
suggested by the data of Zielinski (9), is a more important
factor than maturation in this region remains to be determined.

To demonstrate that regional source variations influence
kerogen composition more than maturation effects in the western
half of the basin, we collected samples from three cores along
an east-west line between West Virginia and Ohio. The cores were
separated by only 50km and sample depths increased by about 270m
dipping eastward. The NMR spectra of coalified wood and kerogen
from equivalent horizons are shown in Figure 6. The kerogens
become more aliphatic towards the western part of the basin, a
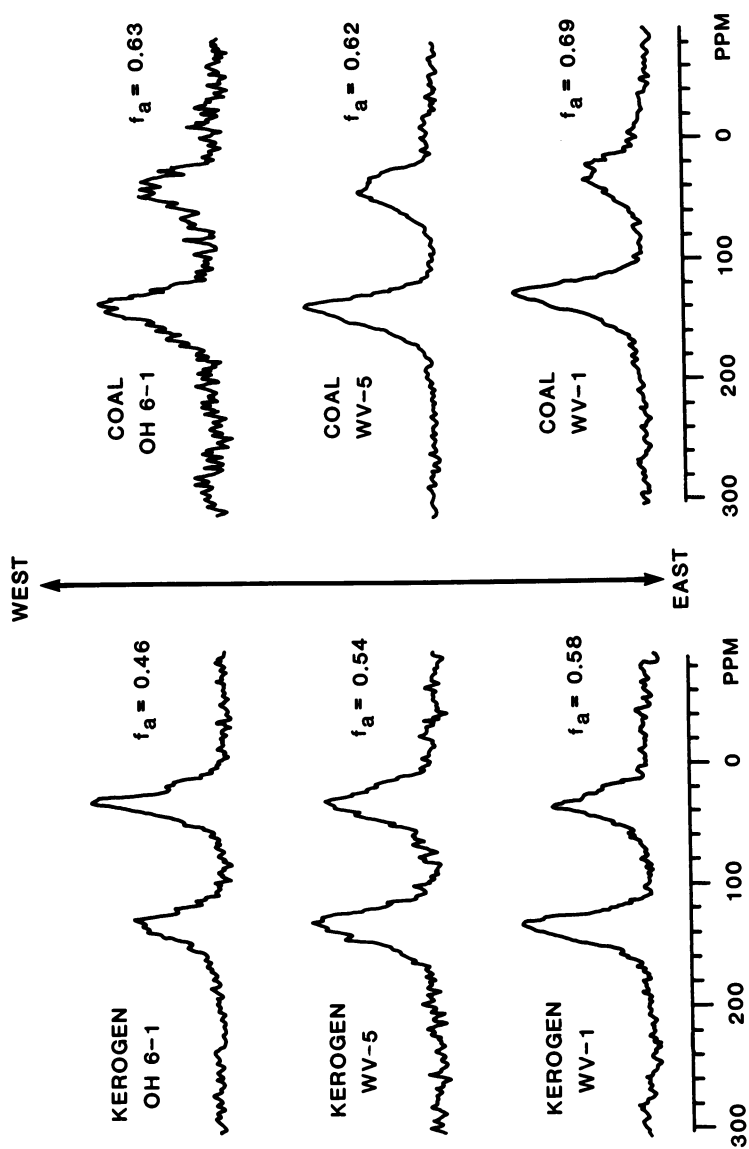
Figure 6. Solid-state ^{13}C-NMR spectra and carbon aromaticities, f_a, of kerogen samples (left) and associated coalified wood fragments (right) in the Huron Member of the Ohio Shale. The three cores trend in an east–west direction in the Appalachian basin.

trend that is not observed for the coalified woods. In addi-
tion, a significant difference in aromaticity is observed
between the coal and kerogen. One could argue that the observed
east-west trend in aromaticity of the kerogen is fortuitous
based on such a limited data set; however, two separate cores
were obtained from the western-most sample in this transect (OH
6-1 and OH 6-2). Aromaticities for these two samples are essen-
tially the same, 0.46 and 0.49, respectively. The difference
between these two samples is certainly less than the variation
in aromaticity across the east-west transect, suggesting the
existence of a bonafide trend.

        Several reasons lead us to believe that the trend in
kerogen aromaticity observed in this transect is unlikely to
have evolved from maturation but is instead the result of
variable source contributions. First, we find it difficult to
envision a large gradient in maturation over such a short area,
especially when conodont color alteration indices do not show
such a gradient in this region (27). Second, the coalified wood
fragments do not show a regular change in aromaticity or elemen-
tal composition that would betray a significant increase in
maturation or coalification. Third, the observed trend of
decreasing aromaticity in a "seaward" direction is logical and
expected, based on basin evolution models.

Conclusions

        Solid-state ^{13}C NMR appears to be a promising tool for
characterizing kerogen in Upper Devonian shales in the
Appalachian basin. Preliminary data indicate that the aromati-
city of kerogen in shales from the eastern part of our study
area is similar to that of coalified wood fragments from the
shales, suggesting that this kerogen is primarily of vascular
plant origin. Towards the west and north, the kerogen becomes
significantly more aliphatic (less aromatic), most likely due to
the incorporation of aliphatic-rich algal kerogen. This trend
agrees with paleocurrent data (2,28) and inferred paleogeography
which suggest that a more open marine environment existed
towards the north and west.

        The data presented here delineate variations in kerogen
composition over the basin and represent new information that
bears on the origin and composition of gas in these Devonian
shales. The assumption that the type of kerogen is generally the
same throughout the basin (3) does not appear to be consistent
with this data. Rather, the data tend to support the model
proposed by Breger and Brown (5,6) which suggests that signifi-
cant variations in kerogen type are to be expected in the basin.
It is important to also note that the coalified wood fragments
in the shale place an upper limit on rank of the kerogen in the
western half of the basin, namely a rank equivalent to high-
volatile bituminous coal. The models for oil and gas formation

(see 21) indicate that this rank corresponds to that of the principal zone of oil formation and not to the so-called "post-mature" zone. Thus, the gas in these portions of the basin is likely to have been formed, in part, by processes other than "post mature" processes. We believe that a primary determinant for gas composition (dry or wet gas) is kerogen type in Devonian shales of the Appalachian basin. Kerogen of an essentially coaly composition, such as that found toward the eastern part of the Appalachian basin, is more likely to yield "dry" gas during maturation. Kerogen that has a more aliphatic composition, such as that in the northwestern part of the basin, is more likely to yield "wet" gas during maturation. It is also possible that kerogen of a more aliphatic nature will produce oil, given that the proper geologic constraints for oil production are met.

Acknowledgments

Literature Cited

1. Conant, L.C.; Swanson, V.E. Geol. Surv. Prof. Paper (U.S.), No. 357, 1961.
2. Broadhead, R.F.; Kepferle, R.C.; Potter, P.E. Am. Assoc. Petrol. Geol. Bull. 1982, 66, 10.
3. Claypool, G.E.; Threlkeld, C.N.; Bostick, N.H. Proc. Second Eastern Gas Shales Symposium, Vol. I, METC/SP-78/6, 1978, p. 54.
4. Claypool, G.E.; Threlkeld, C.N. Proc. First Eastern Gas Shales Symposium, MERC/SP-77/5, 1977, p. 438.
5. Breger, I.A.; Brown, A. Science 1962, 137, 221.
6. Breger, I.A.; Brown, A. Trans. New York Academy of Sciences 1963, 25, 741.
7. Dow, W.G. J. Geochem. Exploration 1977, 7, 79.
8. Maynard, J.B. Geology 1981, 9, 262.
9. Zielinski, R.E. Proc. First Eastern Gas Shales Symposium, MERC/SP-77/5, 1977, p. 546.
10. Vitorovic, D.; Vucelic, D.; Gasic, M.J.; Juranic, N.; Macura, S. Org. Geochem. 1978, 1, 89.
11. Hatcher, P.G.; Breger, I.A.; Dennis, L.W.; Maciel, G.E. in "Aquatic and Terrestrial Humic Materials," Christman, R.F. and Gjessing, E.T.,Eds.; Ann Arbor Science Publishers: Ann Arbor, 1983, Chap. 3.
12. Hatcher, P.G.; Breger, I.A.; Dennis, L.W.; Maciel, G.E. Preprints,Div. Fuel Chem., Am. Chem. Soc. Meeting, Kansas City, Sept., 1982, p. 172.

13. Gerstein, B.C.; Murphy, P.D.; Ryan, L.M. in "Coal Structure,"
    Meyers, R.A., Ed.; Academic Press: New York, 1982, p. 87.
14. Roen, J.B. U. S. Department of Energy, METC/10866-21, 1980.
15. Kepferle, R.C.; Roen, J.B. in "GSA Cincinnati '81 Field
    Trip Guidebooks,II," Roberts, T.G., Ed.; Am. Geol. Inst.:
    Washington, D.C., 1981, p. 259.
16. Bartuska, V.J.; Maciel, G.E.; Schaefer, J.; Stejskal, E.O.
    Fuel 1977, 56, 354.
17. Schmoker, J.W. Am. Assoc. Petrol. Geol. Bull. 1980, 64,
    2156.
18. Van Krevelen, D.W. in "Organic Geochemistry", Breger,
    I.A.,Ed.;Pergamon Press: Oxford, 1963, p.183.
19. Hatcher, P.G.; Breger, I.A.; Szeverenyi, N.M.; Maciel, G.E.
    Org. Geochem. 1982, 4, 9.
20. Breger, I.A.; Schopf, J.M. Geochim. Cosmochim. Acta 1955,
    7, 287.
21. Tissot, B.; Welte, D. Petroleum Formation and Occurrence.
    Springer Verlag, New York, 1978.
22. Simoneit, B.R.T.; Brenner, S.; Peters, K.E.; Kaplan, I.R.
    Nature 1978, 273, 501.
23. Simoneit, B.R.T.; Brenner, S.; Peters, K.E.; Kaplan, I.R.
    Geochim. Cosmochim. Acta 1981, 45, 1581.
24. Dennis, L.W.; Maciel, G.E.; Hatcher, P.G.; Simoneit, B.R.
    Geochim. Cosmochim. Acta, 1982, 46, 901.
25. Miknis, F.P.; Sullivan, M.; Bartuska, V.J.; Maciel, G.E.
    Org. Geochem. 1981, 3, 19.
26. Miknis, F.P.; Smith, J.W. Proc. 15th Oil Shale Symposium,
    Gary, J.H., Ed.;Colorado School of Mines Press, Golden, CO,
    1982, p. 50.
27. Epstein, A.G.; Epstein, J.B.; Harris, L.D. Geol. Surv.
    Prof. Paper (U.S.), No. 995, 1977.
28. Potter, P.E.; Pryor, W.A.; Lundegard, P.; Samuels, N.;
    Maynard, J.B. U. S. Department of Energy, METC/CR-79-22,
    1979.

Geological Setting and Geochemistry of Oil Shales in the Permian Phosphoria Formation

EDWIN K. MAUGHAN

U.S. Geological Survey, Denver Federal Center, Denver, CO 80225

The Permian Phosphoria Formation in the northwestern Interior United States contains two phosphatic and organic-carbon-rich shale members, the Meade Peak Phosphatic Shale Member and the Retort Phosphatic Shale Member. These rocks were formed at the periphery of a foreland basin between the Paleozoic continental margin and the North American cratonic shelf. The concentration, distribution, and coincidence of phosphorite, organic carbon, and many trace elements within these shale members probably were coincident with areas of optimum trophism and biologic productivity related to areas of upwelling. In the Phosphoria sea upwelling is indicated to have occurred by sapropel that was deposited adjacent to shoals near the east flank of the depositional basin.

Maximum organic-carbon concentration is as much as 30 weight percent in the organically richest beds in the shale members and the maximum average in each member is about 10 weight percent. A close association occurs in the distribution of the organic carbon, silver, chromium, molybdenum, nickel, titanium, vanadium, and zinc. Phosphorous differs slightly from the distribution of organic carbon and by contrast seems typically associated with copper, lanthanum, neodymium, strontium, yttrium, and ytterbium.

Subsequent burial of the sapropelic muds by Triassic and younger sediments and the consequent rise in ambient temperature has led to catagenesis of hydrocarbons from the kerogen in these rocks. In some areas of southwestern Montana, however, burial has been minimal, temperatures have remained low, hydrocarbons have not been generated, and these rocks remain oil shales that have the potential for producing synthetic oil and gas.

Studies of the Meade Peak and the Retort Phosphatic Shale Members of the Phosphoria Formation initiated in 1973, have investigated the organic-carbon content and some aspects of hydrocarbon generation from these rocks. The Phosphoria Formation has been previously studied chiefly because of its phosphorite resources. Phosphorite has been mined from the Retort and Meade Peak Members in southeastern Idaho, northern Utah, western Wyoming, and southwestern Montana. Principal studies regarding the phosphorite deposits have been produced by Mansfield (1) and by McKelvey and others (2). The organic-carbon-rich (sapropelic) mudstone beds associated with the phosphorite in these two members also have been the natural sources of petroleum that occurs in the region. Determination of the content and distribution of organic carbon has been reported by Maughan (3), and an evaluation of the hydrocarbon production has been given by Claypool and others (4). In southwestern Montana, however, burial was less than 2 km, ambient temperatures remained low, and the kerogen has not formed hydrocarbons. In this area in Montana, the kerogen in the carbonaceous mudstones has retained the potential for hydrocarbon generation and the Retort Member is an oil shale from which hydrocarbons can be synthetically extracted. A brief evaluation of the oil-shale potential to produce hydrocarbons was reported by Condit (5).

Paleogeographic interpretations by Sheldon and others (6) and by Maughan (7-8) are important to the understanding of the depositional setting of these rocks. Analytical trace-element data have been presented by Gulbrandsen (9-10) and by Maughan (11), and a comprehensive bibliography to published geological and chemical data for these rocks (9) provides sources of much of the ancillary information about the Phosphoria. The present report summarizes the results of recent hydrocarbon-source-rock studies of the Phosphoria Formation. Most of the data and interpretations in this report concerning the relations between the phosphorite and the petroleum source beds have been previously published by Maughan (12), but are included here because of the limited availability of that publication in the United States.

Paleogeographic Setting

The Phosphoria Formation was deposited in a foreland basin between the Continental margin and the North American cratonic shelf. This foreland basin, which is here defined by the area of deposition of the two organic-carbon-rich mudstone members of the Phosphoria (fig. 1), has been named the Sublett basin (8); and it covers an extensive area of approximately 400,000 km^2 (about 700 km by 600 km). The basin has a northwest-southeast-trending axis and seems to have been deepest in central Idaho where deep-water sedimentary rocks equivalent to the Phosphoria Formation are exceptionally thick. The depth decreased toward the shelves and land areas indicated in figure 1. The deepest part of the Sublett
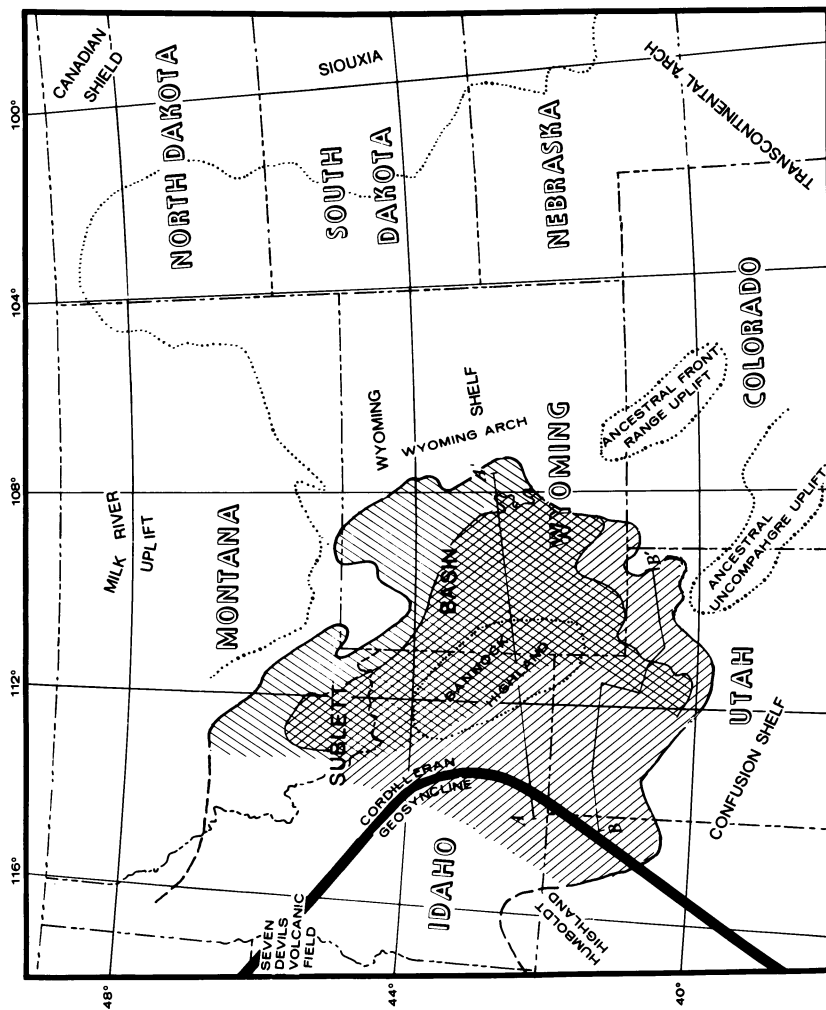
Figure 1. Sublett basin (solid line, dashed where uncertain) in relation to major Permian structural and paleogeographic elements. Areal extent of Meade Peak indicated by left diagonal rules; Retort, by right diagonal rules; limit of middle Permian epicontinental shelf deposits indicated by dotted line. Cross-section A–A' shown in Figure 3, B–B' in Figure 2.

basin lies approximately in the axial bend of the Cordilleran
miogeosynclinal trough shown by Roberts and Thomasson (13). The
southern leg of the miogeosyncline trends approximately N. 30° E.
in Nevada, and the northern leg trends approximately N. 40° W. in
northern Idaho. Shelves that flanked these legs of the
miogeosyncline lay adjacent to the Transcontinental arch and to
the Canadian shield. In central Idaho, Permian rocks believed to
be equivalent to the Phosphoria Formation comprise about 2,000 m
of probable deep-water, thin, planar-bedded, siliceous mudstone
and limestone; but on the shelves, equivalent strata comprise
about 100 m of shallow-water deposits of mostly limestone,
dolomite, and sandstone. The northwestern limit of the Sublett
basin may have been the open ocean, or the basin may have been
semi-restricted by an offshore volcanic island-arc complex that
separated the sea in the foreland basin from the open ocean. The
Lower Permian, probably Wordian, Hunsaker Creek Formation of the
Seven Devils Group along the Oregon-Idaho border (14) represents a
volcanic island-arc complex that could have been an oceanward
barrier to the Sublett basin (12). However, the Seven Devils
Group has been identified as a part of Wrangellia, an exotic
terrane accreted to the North American plate after Paleozoic time
(15). It is conceivable that a more northern sector of the same
archipelago, or another of the volcanic-arc terranes indicated by
Davis and others (16), had been located adjacent to the Sublett
basin but is now posited elsewhere, possibly as a part of the
Wrangellia accreted terrane now located along the British
Columbian to Alaskan coastal margin.

The southwest limit of the Sublett basin in Nevada was along
the Humboldt highland (17). The Humboldt highland was the
principal source of terrigenous sediments incorporated in the
Murdock Mountain Formation (18), which is equivalent to the lower
part of the Phosphoria Formation (fig. 2).

Shelves on the periphery of the Sublett basin were mostly
areas of carbonate bank sedimentation. The Plympton and the
Gerster Formations compose the dominantly carbonate rock deposits
of the Confusion shelf at the south edge of the Sublett basin.
The Park City Formation comprises the carbonate bank deposits on
the Wyoming shelf at the east edge. Some parts of the shelves
adjacent to Permian land areas were areas of littoral sand
deposition that contrast with the area of carbonate and
terrigenous mud deposition. A land area in Montana, the Milk
River uplift, was provenance for littoral sand deposits of the
Shedhorn Sandstone along the northeast edge of the basin.

Tectonic subsidence of the Sublett basin in part of the
region seems to have provided water deep enough for upwelling
circulation, and to have created a change in deposition from
regional carbonates and local sandstone into a more complex
depositional pattern that included the accumulation of the
mudstone-chert-phosphorite facies that constitute the Phosphoria
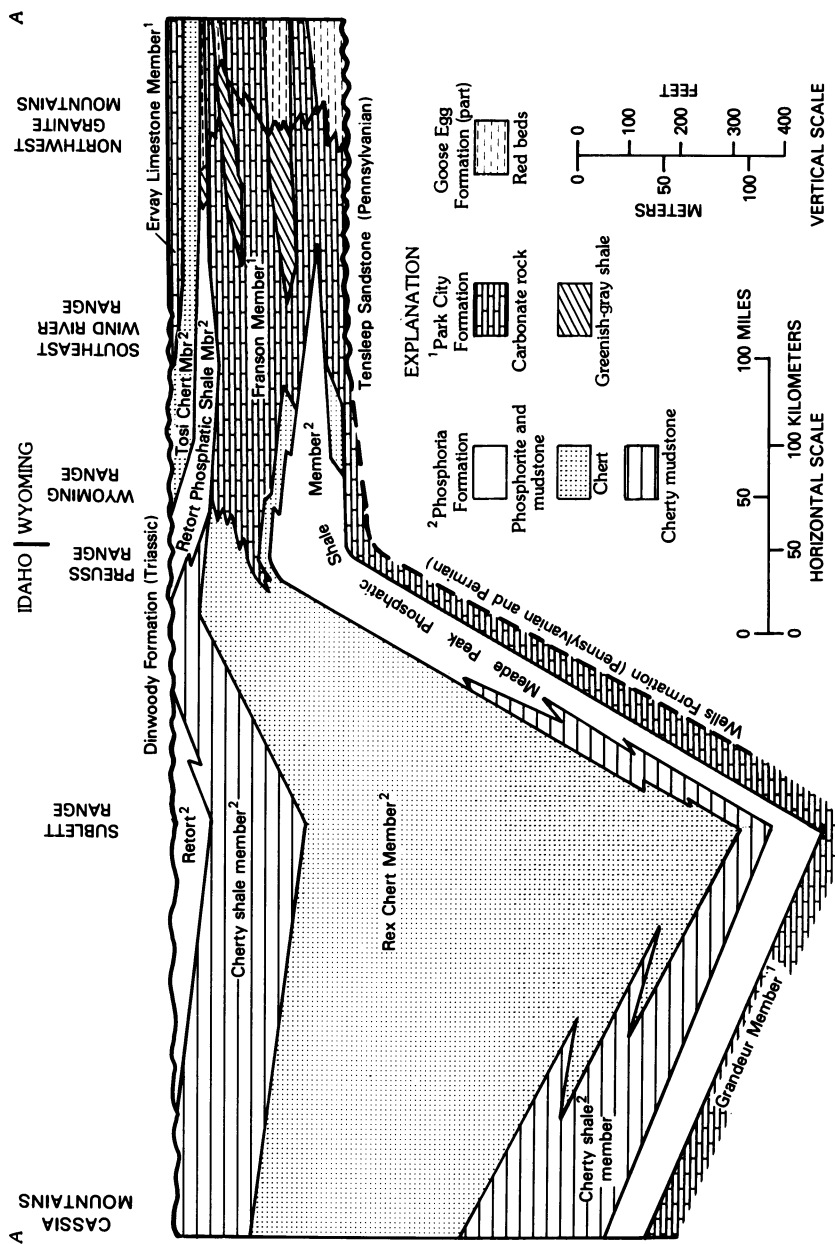Formation. High biological productivity and the accumulation of
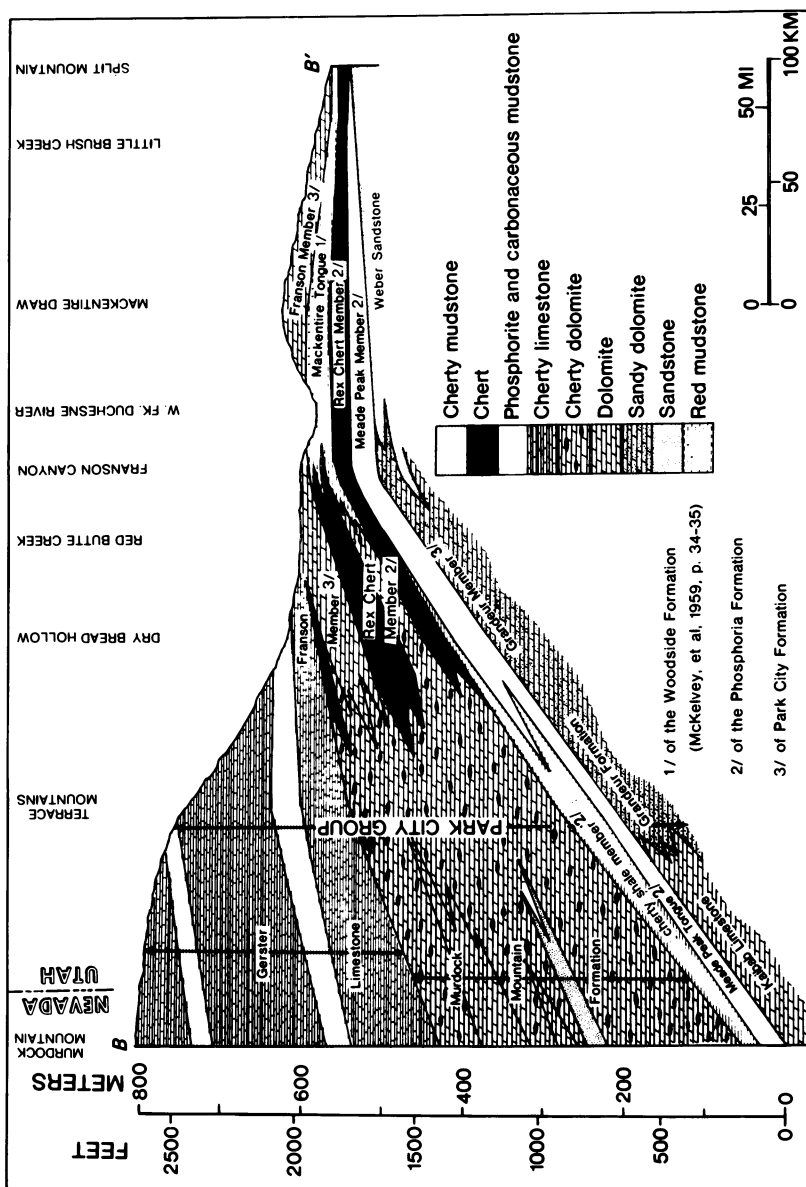
Figure 2. Cross-section B–B' showing generalized facies relations and nomenclature of middle Permian strata across Sublett basin from northeastern Nevada to northeastern Utah. (Section location shown in Figure 1.)

sapropel on the sea floor are associated with contemporary coastal upwelling (19), and similar environmental and depositional conditions in Permian time are attributed to the rich accumulations of organic matter in the Phosphoria Formation.

The Phosphoria Formation was deposited on the foreslope between the carbonate and littoral sand deposits of the shelf and the dominantly cherty mudstone sediments of the axial part of the basin. Winds blowing tangentially offshore across the Phosphoria sea from the Milk River uplift, augmented by the Coriolis force, carried surface water away from the shore and generated upwelling in the sea in eastern Idaho and adjacent areas in Montana, Wyoming, and Utah. The prevailing wind direction, determined from transport directions measured on mid-Permian sand dunes in northern Colorado and adjacent areas in Utah and Wyoming (7), is consistent with placement of the region within the northern hemispheric trade-wind belt. The Sublett basin and adjacent land areas were at approximately latitude 10° to 25° N as determined from the North American plot of the mid-Permian position of the paleomagnetic pole (20). Because of the northerly drift and counter clockwise rotation of the North American continent to its present position, the original northeasterly paleowinds now coincide with the observed northerly origin of these winds seen in the Permian rocks. Surface-water flow of Idaho was toward the southwest according to the study of Brittenham (26) and is consistent with the postulated offshore flow generated by the northeasterly offshore winds. The distribution of organic carbon and phosphorus deposition indicates that the principal locus of upwelling during deposition of the Meade Peak was in the vicinity of the Idaho-Wyoming border, and during deposition of the Retort the principal locus of deposition was in southwestern Montana (3).

Stratigraphic Relations

The intertonguing relations and nomenclature applied to the middle Permian rocks (Roadian and Wordian Stages of Furnish, 21) in the Sublett basin are shown in figures 2 and 3. In the southwestern part of the basin the Phosphoria Formation tongues into the deeper basin Murdock Mountain Formation, and in the eastern part of the basin the Phosphoria tongues into the shelf carbonate deposits of the Park City Formation. Prior to deposition of the Phosphoria, most of the Sublett basin and adjacent areas were the site of extensive deposition of Lower Permian shallow-water carbonate sediments. In the southeastern part of the basin, the carbonate rocks underlying the Phosphoria are the Kaibab Limestone; and in the northeastern part of the basin, where these carbonates are generally sandy and intertongue with sandstone strata, they are called the Grandeur Member of the Park City Formation. Rocks equivalent to the Grandeur in the northern part of the basin in southwestern Montana are dominantly sandstone that are included in the Quadrant Sandstone and those in

Figure 3. *Cross-section A–A' showing generalized facies relations and nomenclature of middle Permian strata across Sublett basin from Cassia Mountains, Idaho to central Wyoming. (Section location shown in Figure 1.)*

the southeastern sector are part of the Weber Sandstone in northeastern Utah.

The Phosphoria and Park City Formations were deposited upon carbonate and sandstone strata of the Kaibab, Grandeur, Quadrant, and Weber in two cyclic sequences. The lower sequence comprises, in ascending order, the Meade Peak Phosphatic Shale Member and the Rex Chert Member of the Phosphoria Formation, and the Franson Member of the Park City Formation. The upper sequence comprises the Retort Phosphatic Shale Member and the Tosi Chert Member of the Phosphoria and the Ervay Limestone Member of the Park City. The members in the upper sequence are not as thick as those in the lower sequence, and the depocenter of the carbonaceous mudstone of the Retort is located about 110 km north-northwest of the depocenter of similar rocks of the Meade Peak in the lower sequence. The northerly shift of the depocenter was accompanied by a shift of both the southern and northern shorelines, the distribution of the lithofacies, and a corresponding shift of the center of maximum average organic carbon and phosphorite deposition of the Meade Peak and Retort Members. This shift probably resulted from regional tilting away from the Transcontinental arch.

The depositional sequence within the two phosphatic shale members comprise sapropelic sediments that include peloidal phosphorite and subordinate phosphatic mudstone near the base, organic-carbon-rich mudstone within the central part, and peloidal phosphorite and phosphatic mudstone in the upper part. Shelfward, the bases of the shale members are in sharp contact with the underlying rocks, but the contacts seem to be sharply transitional in basinal areas. The upper contacts are transitional upward into the cherty beds of the overlying member in all areas.

Thicknesses

Isopachs of the Meade Peak and the Retort are shown in figure 4. Maximum thicknesses of sapropelic mudstone and phosphorite composing the Meade Peak Member is about 60 m in a belt that approximately coincides with the Wasatch and Bear River Ranges from the vicinity of Ogden, Utah to near Pocatello, Idaho (fig. 4). The thickest sections of Meade Peak lie within the Willard-Bannock thrust plate so that spatial relations are complicated by thrust displacement subsequent to Permian deposition. Nevertheless, it is evident that sapropel accumulation was greater near the geographical center of the Sublett basin, rather than coinciding with the center(s) of subsidence where the Park City Group is thickest in the western part of the basin adjacent to the Humboldt positive belt in north-central Nevada. The isopach map of the Meade Peak (fig. 4) shows approximately uniform thinning of the member centrifugally from the central part of the basin along the Ogden to Pocatello line; this is especially evident if palinspastic adjustments are considered. Sapropel accumulation
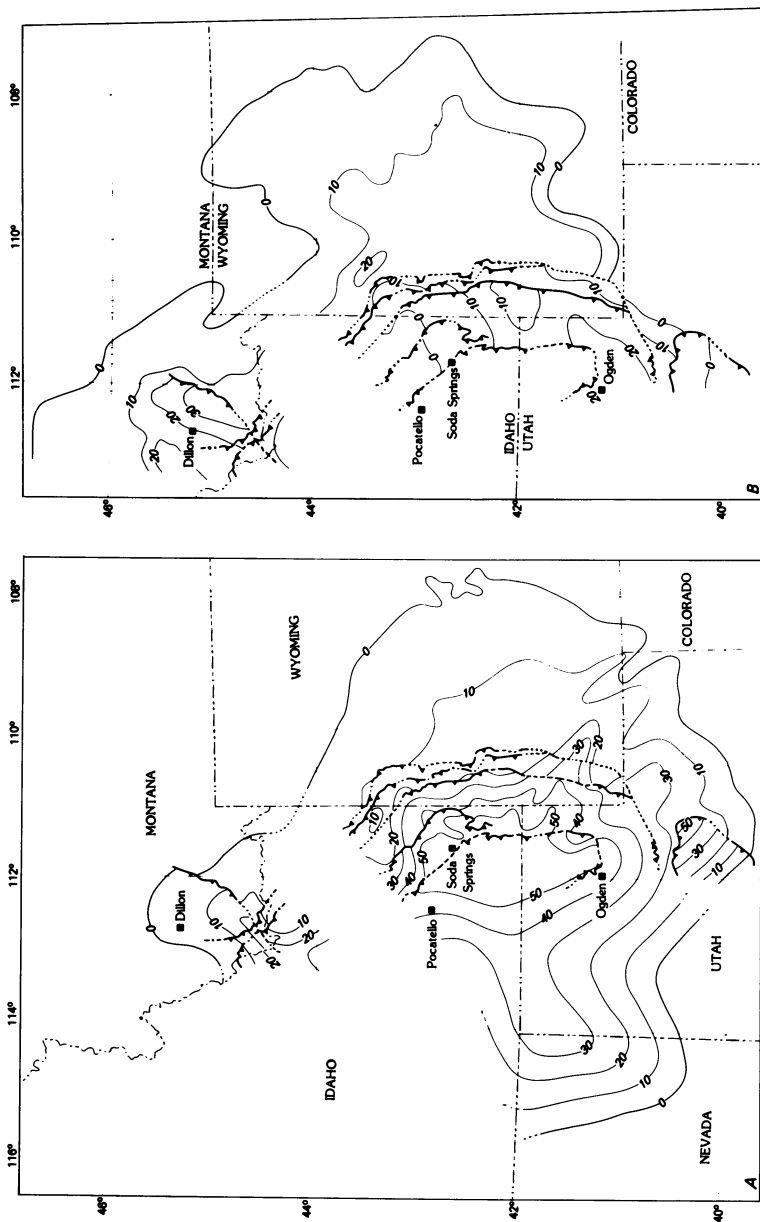
Figure 4. Isopach map of Meade Peak (left) and Retort (right) Members of the Phosphoria Formation; contour interval is 10 m. Principal overthrust faults of the Sevier thrust belt indicated by barbed line; isopachs and faults are dashed where uncertain.

seems to have been syndepositionally displaced eastward from the depocenter of the Sublett basin in northeastern Nevada by the influx of terrigenous detritus from the Humboldt highland to the west. The Meade Peak thins to the north, east, and south away from the area of maximum sapropel accumulation and towards areas of shoaling, which were unfavorable environments for preservation of organic matter in the oxygenated water near the shore of the Phosphoria sea.

The Retort Member is thickest in southwestern Montana. The Retort closely resembles the Meade Peak except that its thickness is about one-half that of the Meade Peak and its shorelines and apparent depocenter are displaced northward. The Retort, like the Meade Peak, is believed to have been deposited along a belt that extended southward into eastern Idaho from the apparent depocenter in southwestern Montana. However, the Upper Permian sequence has been eroded in most of eastern Idaho prior to deposition of Triassic strata (22) and has left the original extent of the Retort unknown.

Organic Carbon

Organic-carbon content in the Meade Peak (fig. 5) is greatest, averaging about 9 weight percent, near the Wyoming border east of Pocatello, Idaho (3), and is offset northeastward from the central axis of the basin onto the flank of the area of thickest accumulation of organic-carbon-rich mudstone. This offset position of the maximum organic-carbon concentration is believed to approximately coincide with an area of upwelling marine currents from out of the deeper parts of the Sublett basin onto the submarine slope of fringing barrier island and carbonate bank deposits. The locus of maximum organic-carbon deposition in the Meade Peak (fig. 5) approximately coincides with that of maximum phosphorus concentration (fig. 6). However, phosphorite and sapropelite were deposited over the entire Sublett basin, possibly because of the production of an exceptionally abundant, probably dominantly phytoplanktonic, biomass and its widespread dispersion throughout the Phosphoria sea.

The average organic-carbon content of the Meade Peak in the Sublett basin, the average of 285 samples from 40 localities, is calculated to be about 2.4 percent, and some beds contain as much as 30 percent organic carbon by weight. These are values substantially higher than the 1.02 percent average determined for marine littoral mudstone by Ronov (23 p. 11). Most of the strata within the Meade Peak contain in excess of the 0.5 percent organic carbon considered necessary for an adequate petroleum source rock.

Organic-carbon content in the Retort is greatest, averaging about 10 weight percent, near Dillon, Mont. (fig. 4). The center of maximum organic carbon deposition in the Retort (fig. 5) approximately coincides with that of maximum phosphorus
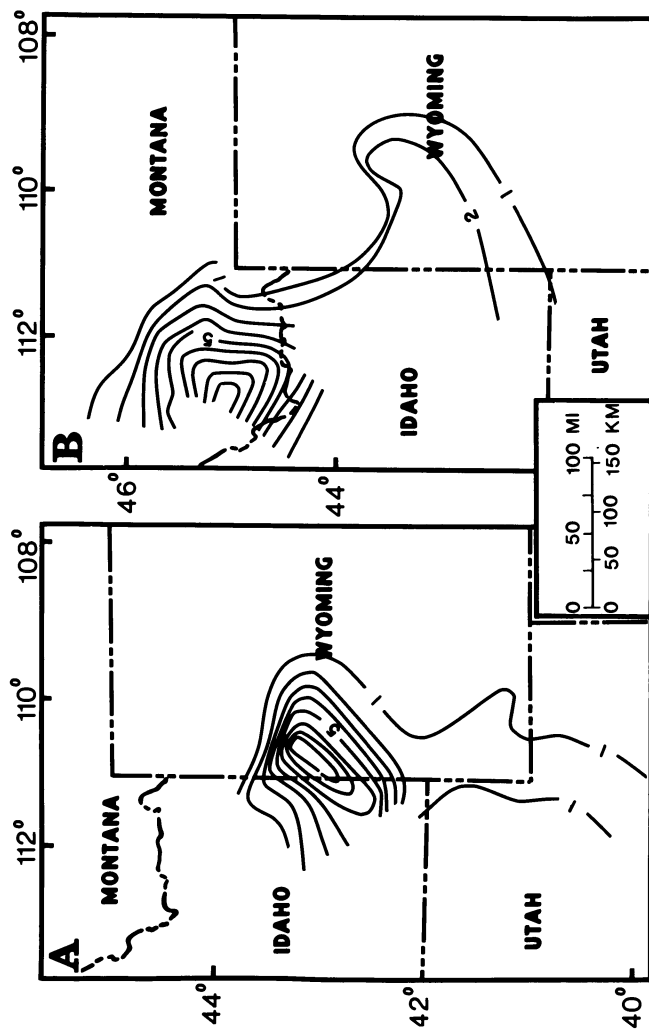
Figure 5. Organic-carbon distribution in Meade Peak (left) and Retort (right) Members of the Phosphoria Formation shown by isograms of average weight percent.
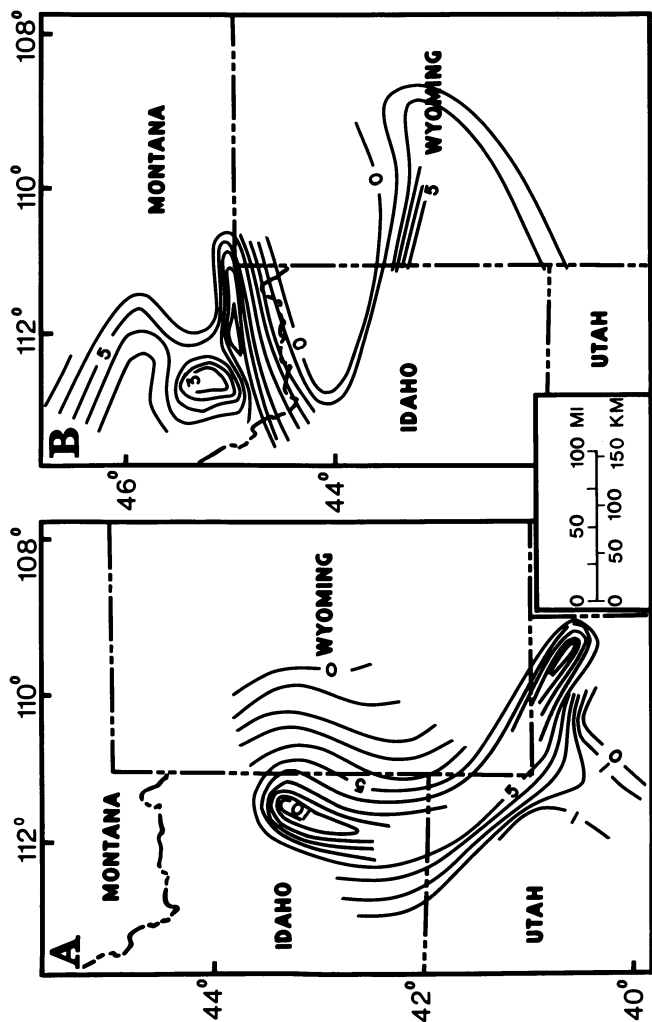
Figure 6. Phosphorus distribution in Meade Peak (left) and Retort (right) Members of the Phosphoria Formation shown by isograms of average weight percent.

concentration (fig. 6). The average organic-carbon content of the Retort, the average of 82 samples from 22 localities, is about 4.9 percent, double the average for the Meade Peak. The difference seems attributable to a statistical bias created by the absence by erosion of leaner sapropelic mudstones of the Retort from large areas to the south of the depocenter in southwestern Montana, rather than to any significant geochemical difference between the Retort and the Meade Peak.

The abundant and ubiquitous organic matter in the Phosphoria sea may have been produced in a way similar to that in Walvis Bay on the southwest African coast, which Brongersma-Sanders (19) explained by the relationship of upwelling, large biomass production, and the accumulation of biological remains on the sea floor as sapropelic ooze.

Phosphorite

Deposits of phosphorite in the Meade Peak Member are most abundant in eastern Idaho and adjacent areas in Wyoming and Utah where they are mined. A belt of phosphorus (fig. 6) projects southeastward from eastern Idaho into the eastern Uinta Mountains. The average phosphorus values shown in figure 6 are an index to the abundance of phosphorite along this belt. Similarly, phosphorus in the Retort (fig. 6) is an index to the phosphorite, which is most abundant in southwestern Montana in this member. Discrepancy between the centers of distribution of the maximum organic carbon and that for the maximum phosphorus are believed to be owing to mechanical sorting. According to Burnett (24), recent phosphorite deposits off the coast of Peru and Chile probably form diagenetically within anoxic, highly organic sediments, and the apatite subsequently is concentrated by winnowing and reworking in response to changes in water currents caused by eustatic sea-level changes or by tectonism. The origin of these Permian phosphorites and the approximate, but not precise, coincidence of depocenters for organic carbon and phosphorus seems best explained by similar winnowing and reworking.

Economically mined beds of phosphorite in the Meade Peak Member in eastern Idaho and adjacent areas in Utah and Wyoming approximately coincide with the location of the Bannock highland (fig. 1). Uplift of this highland early in the Pennsylvanian Period occurred in the area (25). Slight uplift may have recurred in about the same area during the time of deposition of the Meade Peak to form a broad ridge submerged beneath the Phosphoria sea where winnowing could have been active. A detectable irregularity in the level of the sea floor coincident with the Bannock highland is not evident in thickness variations of the Meade Peak Member shown in figure 3A; but possibly the 10-m isopach interval is too coarse to reflect minor shoaling in that area. However, recurrent uplift in approximately the same area as the Pennsylvanian uplift is indicated by shoaling of the Phosphoria sea in southeastern

Idaho as evidenced by bioherms in the Rex Chert Member of the
Phosphoria Formation directly above the Meade Peak (26).
Recurrent uplift and erosion of Permian strata coincident with the
area of the Bannock highland also took place prior to Triassic
deposition (3, 22) as indicated by the absence of Retort (fig. 4B)
and younger Permian rocks in parts of eastern Idaho and some
adjacent areas.

Most phosphorite in eastern Idaho has a peloidal fabric and
is composed of a packstone of spherical to slightly oblate grains
that range mostly from about 0.2 to 2 mm in diameter. Many
peloids are nucleated around a silt-size quartz particle, although
rod-shaped to round phosphatized fecal pellets are common and bone
fragments form the nuclei in some peloids. The texture in the
body of many peloids is non-structured and appears to comprise
phosphatized amorphous, dark-brown organic matter surrounded by a
thin shell of micro-crystalline apatite. Many other peloids
comprise concentrically banded laminae of alternately dark- and
light-brown micro-crystalline apatite and some include amorphous
organic matter. Phosphatized skeletal remains that include
spicules, shell fragments, and bones occur in some thin strata,
but are not common. Intergranular spaces are filled chiefly by
sparry apatite, sparry calcite, dolomite, or additional
phosphatized and amorphous organic matter. Clay minerals are
common, but not abundant in many of these peloidal phosphorites.

The fabric of the phosphorites deposited in northeastern Utah
differs from the fabric of equivalent phosphorite in central
Idaho. Chief differences are believed to be due to the effect of
different water depths and current energies in the two areas. The
northeastern Utah phosphorites were deposited near the margin of
the Sublett basin where there presumably would have been shallower
water and higher energy currents in contrast to the apparent
deposition in a low-energy environment farther from the basin
margin in eastern Idaho. A greater variety of grain sizes,
lithologic components, and textures occur in northeastern Utah.
Fragmented peloids and other angular to sub-rounded clasts are
abundant components of the phosphorite beds, as is phosphatized
skeletal debris. Oolitic phosphorite grains comprised of
concentric layers of micro-crystalline apatite are dominant
constituents, and amorphous organic matter seems less
conspicuous. Peloids commonly are as much as 5 mm in diameter and
apatite nodules are as much as 2 cm in diameter. Silt- and sand-
size quartz grains occur in many beds and are the dominant
components in some of the beds that are interstratified with the
phosphorites. Chert fragments are locally abundant, also, and
phosphorite nodules, which are rare in eastern Idaho, are common
in some beds in the presumed shallower water deposits in
northeastern Utah.

Trace Metals

Traces of many metals, some of unusually high concentration, occur in the carbonaceous shale and phosphorite beds of the Phosphoria.   These   trace   elements   have   been   determined semiquantitatively by emission spectrographic analyses.   The analytical data for the metals have been presented principally by Gulbrandsen (9) and by Maughan (11).

The loci of the average concentration of several metals in the carbonaceous shale members also approximate the loci of organic carbon and phosphorus. The values for these metals are significantly higher than the average for marine shales as reported by Rankama and Sahama (27 p. 226). The distribution of silver in the Meade Peak and the Retort is shown in figure 6, vanadium in figure 7, and lanthanum in figure 8.   It seems probable that some of the trace metals were concentrated from the sea water by the organisms living in the Phosphoria sea. Other metals were adsorbed onto the residual organic matter either during its excursion to the sea floor, or during the residence of the organic matter at or near the depositional interface.   Yet other metallic concentrations resulted from chemical substitutions within the carbonate fluorapatite or within other minerals, especially the clays, during the early diagenesis of the sapropelic mud on the sea floor. The coincidence of the metallic concentrations and the organic carbon in the Retort and the Meade Peak are believed to confirm the indicated location of centers of upwelling in southwestern Montana and in the vicinity of the Idaho-Wyoming border.

Hite (28) has described a mechanism for concentrating phosphorus and other elements and introducing them into the Phosphoria sea by reflux circulation from the adjacent hypersaline lagoon in eastern Wyoming.   This mechanism may have been an important factor in providing the trophic requirements to sustain the large biomass that contributed the organic matter to the floor of the Sublett basin.   On the other hand, volcanism in the probable island arc at the northwestern margin of the basin may have been the primary source of many of the chemical elements that enriched the Phosphoria sea, a concept that hearkens back to earlier speculations that the abundant silica in the adjacent cherty members, which intertongue with the phosphatic shale members, may have originated from Permian volcanism in western Idaho (1 p. 371-372; 2 p. 27). The influx of volcanic ash into the Phosphoria sea is indicated by the data of Gulbrandsen (29), who identified Buddingtonite, an ammonium feldspar mineral formed by the interaction of volcanic glass and organic matter, in samples from the Meade Peak and the Retort Members.

The concentration of trace metals by volcanic input, by the reflux of hypersaline waters, or by other extraordinary metallic ion enrichment of the Phosphoria sea are not required according to data and interpretations given by Calvert (30 p. 201-212).
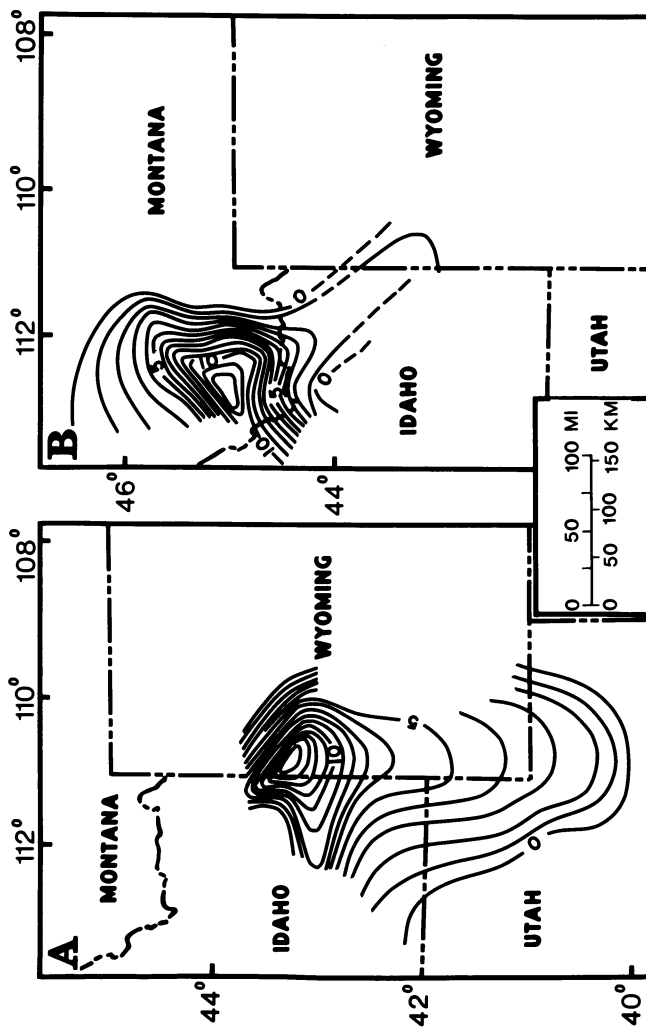
Figure 7. Silver distribution in Meade Peak (left) and Retort (right) Members of the Phosphoria Formation shown by isograms, in parts per million. (Isogram dashed where uncertain.)
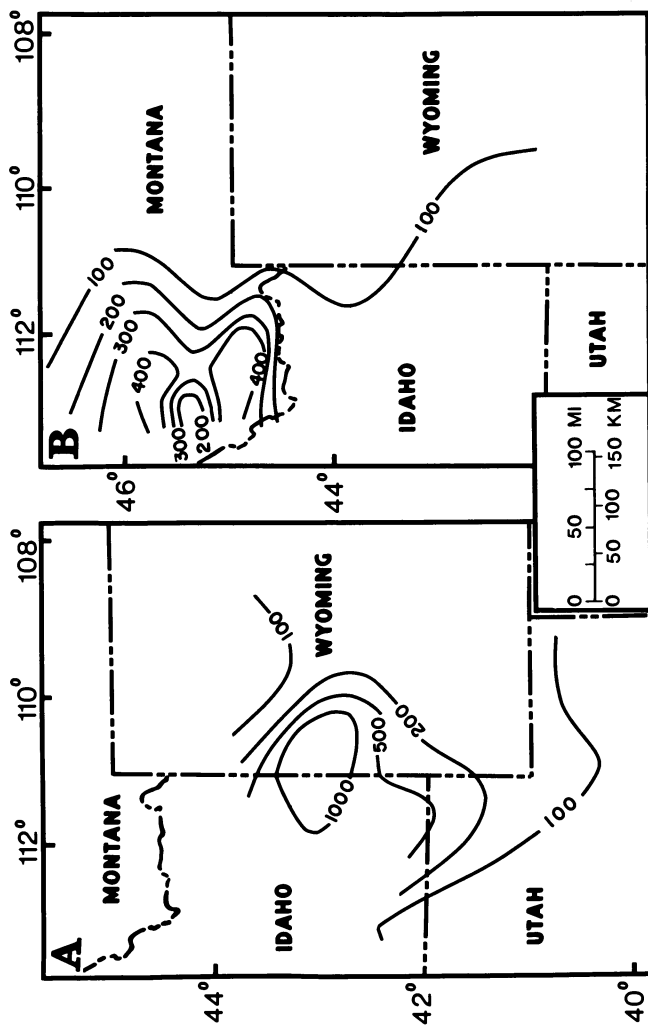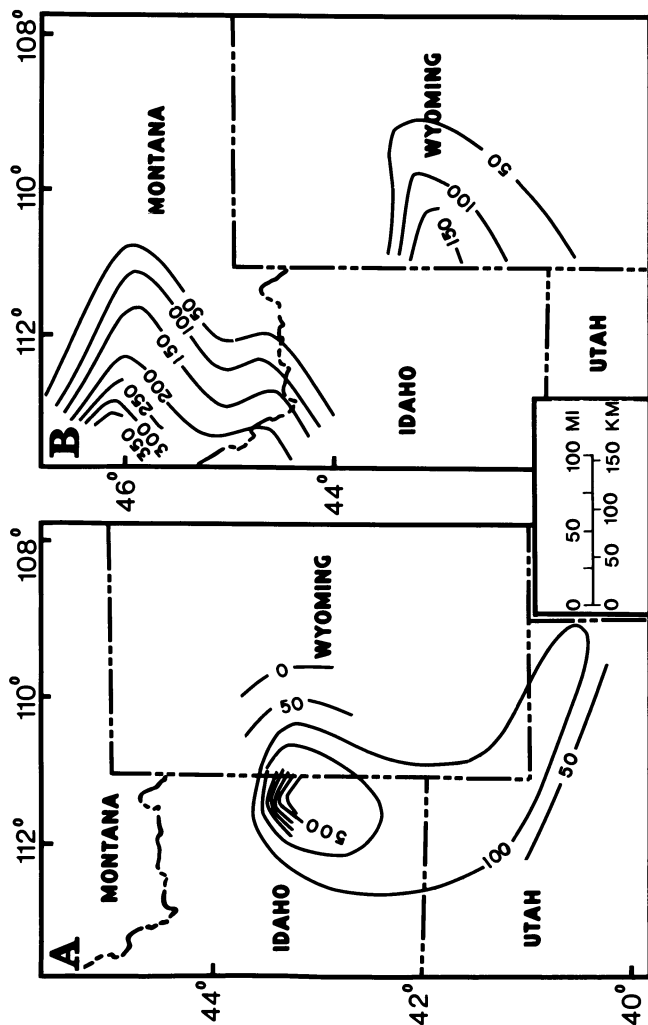
Figure 8. Vanadium distribution in Meade Peak (left) and Retort (right) Members of the Phosphoria Formation shown by isograms, in parts per million.

Phosphorites occur in organic-rich muds deposited on the shelf off southwest Africa, which are also enriched in certain minor metals that are not of terrigenous origin (30 p. 209-210). The metals in these sediments are within the ranges of the metal content of marine plankton (30 p. 212), and the organic material in the bottom sediments probably are enriched in these metals by adsorption. Brongersma-Sanders (31 p. 233) indicated that trace metals generally are not concentrated in the sediments except "...in places of highest organic productivity, where the number of concentrating organisms is high, e.g. in areas of upwelling water." For preservation of this organic matter and its trace metals, anoxic bottom conditions are necessary; but the accumulation and decay of dead plankton settling from the fertile surface waters can quickly lead to de-oxygenation of the bottom waters and the underlying sediment (31 p. 235). Thus, the concentration and distribution of the elements in the Meade Peak and Retort shown in figures 5 to 9 indicate areas of high accumulation of organic matter in the Sublett basin that probably were areas of upwelling and large biological productivity in the Phosphoria sea.

The emission spectrographic data (11) suggest that a close association of organic carbon to silver exists (compare figs. 5 and 7), as well as to chromium, molybdenum, nickel, titanium, vanadium (fig. 8), and zinc. The spectrographic analyses for phosphorus show that a close association of the maximum for this element to maximum organic carbon exists; but that near-maximum values of phosphorus extend from eastern Idaho into northeastern Utah, which is an area of comparatively low organic carbon (compare figs. 5 and 6). Phosphorus seems closely associated with copper, lanthanum (fig. 9), neodymium, strontium, yttrium, and ytterbium. Correlation analyses and other proposed studies, especially into the clay mineralogy, may enable us to better understand these relationships and to determine the origins of these associations.

Petroleum Generation

Petroleum generation from the Phosphoria Formation has been investigated and a total yield of 30.7×10^9 metric tons is estimated by Claypool and others (4 p. 118). The bulk of the Phosphoria oil seems to have been generated from the mudstone strata rather than from the phosphorite beds as suggested by Powell and others (32). Graphic comparisons (fig. 10) of organic carbon, phosphorite, bitumen, and hydrocarbon from the data of Claypool and others (4 p. 105) and from Maughan (3) show an expectable relation between organic carbon and bitumen, but little relationship between the other chemical factors in these rocks, including phosphorus. The graph shows that organic carbon, hydrocarbon, and bitumen are common to abundant in mudstones having a low phosphorous (<7% P) content, but that these

Figure 9. Lanthanum distribution in Meade Peak (left) and Retort (right) Members of the Phosphoria Formation shown by isograms, in parts per million.
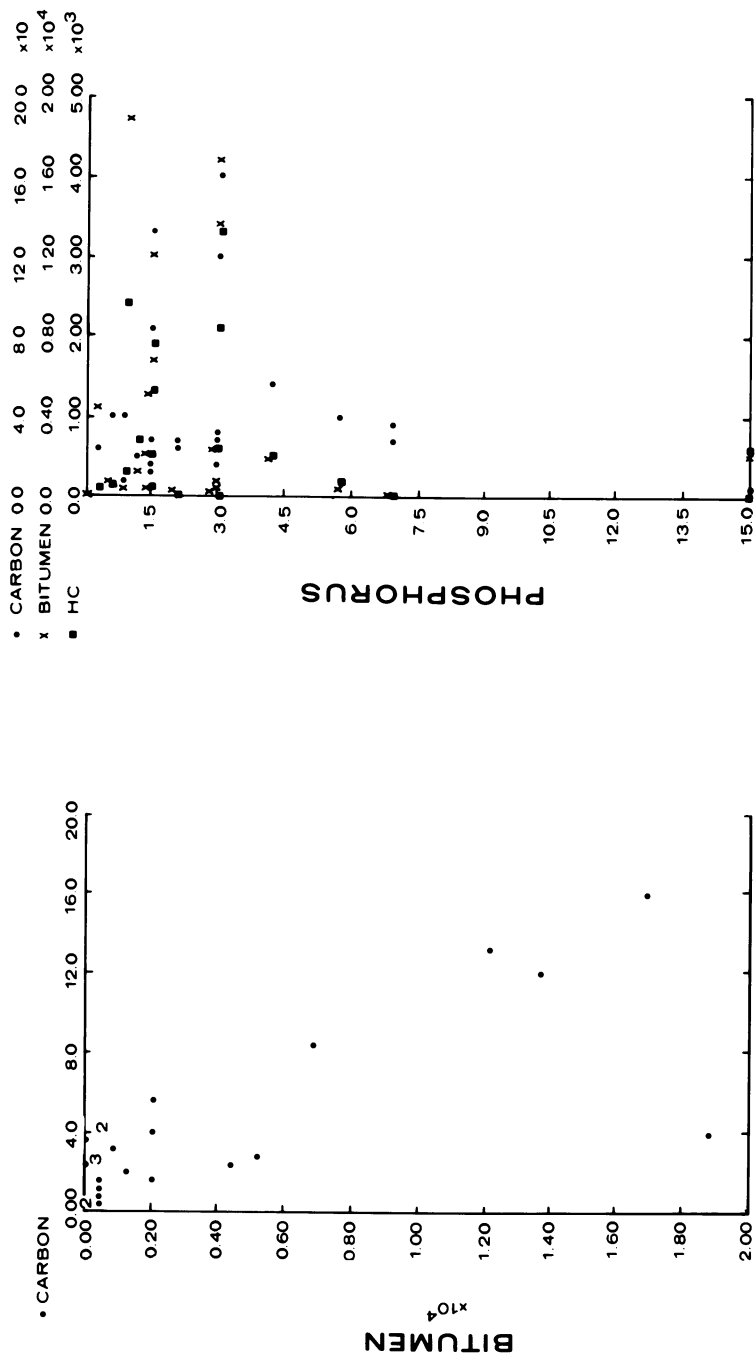
Figure 10. Plot comparing organic carbon and bitumen (left), and phosphorus to organic carbon, bitumen, and hydrocarbons (right) in samples from Meade Peak and Retort Members of the Phosphoria Formation. Values in percent for organic carbon and phosphorus are from Maughan (11); bitumen and hydrocarbons from Claypool et al. (4).

components are comparatively low in the phosphorites (>7% P). Hydrocarbons and phosphorite have a common origin in the sapropel. The anoxic marine depositional environment favorable for the accumulation of organic-carbon-rich mudstone was favorable for the formation of phosphorites and for nitrogen-rich oils. However, the hydrocarbons are chiefly the product of catagenesis that is dependent mostly on burial and the consequent increase of the ambient temperature, whereas phosphorite seems to be the product of penecontemporaneous diagenesis that is chiefly dependent on anaerobic decomposition of the organic matter, mineralogic reconstitution, and mechanical sorting.

Oil that has been discovered and produced from the Pennsylvanian Tensleep Sandstone (fig. 11), the probable Lower Permian part of the Weber Sandstone in northwestern Colorado, and the middle Permian Park City Formation in central Wyoming probably has been derived from the Phosphoria Formation. Oil in the Lower Permian upper member of the Minnelusa Formation in northeastern Wyoming may have migrated into these reservoirs from the Phosphoria source beds, but carbonaceous beds in the middle member of the Minnelusa are a more likely source. Cheney and Sheldon (33) speculated that petroleum originated in the organic-carbon-rich shale beds of the Phosphoria Formation and that the oil migrated eastward and was trapped in reservoirs in the equivalent carbonate rocks of the Park City Formation. Sheldon (34) also related oil accumulation in upper Paleozoic rocks to its probable origin in shales of the Phosphoria and suggested that migration from eastern Idaho and western Wyoming occurred in response to accumulating overburden and progressively eastward-shifting tectonic forces. He indicated that oil generated in the Phosphoria in eastern Idaho began eastward migration early in Jurassic time. Oil generation and migration developed increasingly farther eastward as the Triassic, Jurassic, and Cretaceous sedimentary loading of the Permian strata increased progressively eastward in western Wyoming; but tectonic barriers that developed with the Laramide orogeny prevented further long-distance migration in Maestrichtian and later times.

Data presented by Stone (35) substantiated the hypothesis that most of the hydrocarbons in Paleozoic and Triassic rocks of the Bighorn Basin in north-central Wyoming came from the carbonaceous shale beds of the Phosphoria. The relation of petroleum produced from reservoirs in the Pennsylvanian Tensleep Sandstone to the black shales in the Phosphoria Formation and to the inferred maximum depth of burial of these rocks is shown in figure 11. In eastern Idaho, the critical depth of burial occurred as early as Late Triassic, and regionally the maximum depth of burial of the Permian rocks is inferred to have been at the end of the Cretaceous Period, although sediments continued to accumulate in local, intermontane basins through the Paleocene and into early Eocene time (4 p. 101-104).
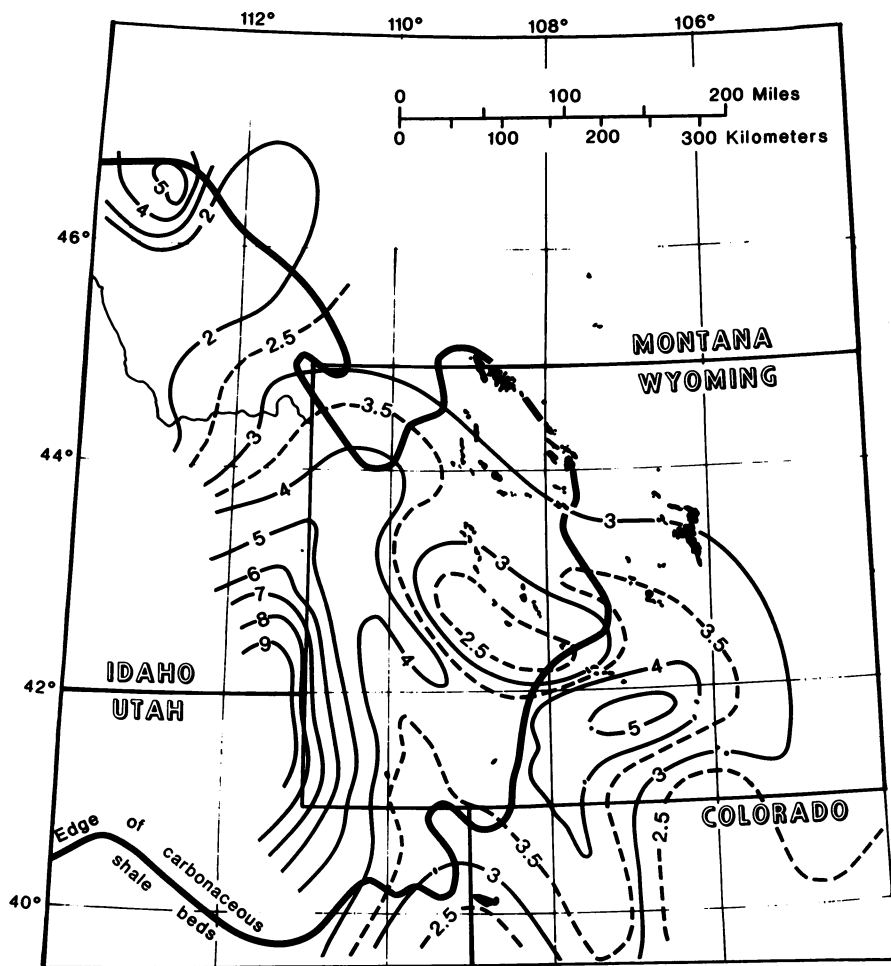
Figure 11. Relation of oil reservoirs (solid patterns) in Pennsylvanian Tensleep Sandstone to carbonaceous shale beds of the Permian Phosphoria Formation and to inferred maximum depth of burial (thickness of Mesozoic rocks, in kilometers) shown by solid lines and supplementary 2.5- and 3.5-km thickness shown by dashed line.

Catagenetic conversion of kerogen to hydrocarbons has taken place throughout most of the Sublett basin. Hydrocarbon generation has taken place in most of the region where burial has been in excess of about 2 km. Burial between about 2 km and 5 km as shown by Claypool and others (4 fig. 7) and the temperature at these depths has brought these rocks into the "oil generation window." At burial depths greater than about 5 km, ambient temperatures have led to the degradation of the hydrocarbons and has exhausted the potential for further catagenetic reaction and hydrocarbon generation from the kerogen. At less than about 3 km of burial, the potential for hydrocarbon generation from the kerogen remains, and where the organic carbon content is high, these thermally immature rocks are classified as oil shales.

Oil Shales

The Retort Member in some parts of southwestern Montana is an oil shale rich in organic carbon, it is thermally immature, and the shale has the potential for the synthetic generation of hydrocarbons. The recognition of oil shale in the Phosphoria was first noted in a report by Bowen (36) and in a more complete report the following year by Condit (5). Attempts to pyrolitically produce oil from the Retort Member near Dillon, Mont., between about 1915 and 1925 were moderately successful, but the expense of mining and processing was not competetive with more cheaply produced crude oil from wells. A 1.7-m-thick bed is reported (5 p. 23) to have yielded 87.5 L/metric ton of oil, and a yield of 100 L/ton had been obtained in the earlier study by Bowen (36 p. 318). In contrast to these moderately high yields from southwestern Montana, samples from genetically and lithologically similar but previously deeply buried and presently thermally overmature phosphatic shale beds of the Meade Peak Member in Idaho and Wyoming, were reported (5 p. 31-32) to yield only traces of oil.

Solid-state nuclear magnetic resonance spectra of Phosphoria shales (37) indicate the residence of higher amounts of aliphatic carbon in the thermally immature samples from southwestern Montana compared to thermally mature samples from Idaho. Similarly, gas chromatographic analyses and the ratio of hydrocarbon to carbon (4) indicate thermal immaturity and the potential for hydrocarbon generation in the southwestern Montana oil shales in contrast to the depleted hydrocarbon-producing potential of kerogenic shales in other areas.

The oil shale in southwestern Montana occurs in structurally complex folded and faulted mountains. Mining and processing of large quantities of these shales would require difficult subsurface methods. Economical exploitation will depend upon the development of extraction technology that may require the recovery of the multiple resources of hydrocarbons, phosphorous, and the other metals.

Literature Cited

1. Mansfield, G. R. U.S. Geol. Surv. Prof. Paper 152 1927.
2. McKelvey, V. E.; and others. U.S. Geol. Surv. Prof. Paper 313-A 1959.
3. Maughan, E. K., in "27th Ann. Field Conf. Guidebook"; Wyo. Geol. Assoc.: Casper, Wyo., 1975; p. 107-115.
4. Claypool, G. E.; Love, A. H.; Maughan, E. K. Am. Assoc. Petrol. Geol. Bull. 1978, 62, 98-120.
5. Condit, D. D. U.S. Geol. Surv. Bull. 711-B 1919, p. 15-40.
6. Sheldon, R. P.; Maughan, E. K.; Cressman, E. R. in "Paleotectonic maps of the Permian System" U.S. Geol. Surv. Misc. Geol. Inv. Map I-450, 1967, text p. 48-54; also in "Anatomy of the western phosphate field"; 15th Annual Field Conference 1968, Intermtn. Assoc. Geol., p. 1-13.
7. Maughan, E. K. in "2nd Symposium on salt, v. 1, Geology, geochemistry, and mining"; North. Ohio Geol. Soc.: 1966; p. 35-47.
8. Maughan, E. K. in "Great Basin Guidebook"; Rocky Mtn. Assoc. Geol., Utah Geol. Assoc.: 1979; p. 523-530.
9. Gulbrandsen, R. A. U.S. Geol. Surv. Open-File Report 75-554 1975.
10. Gulbrandsen, R. A. U.S. Geol. Surv. Open-File Report 79-369 1979.
11. Maughan, E. K. U.S. Geol. Surv. Open-File Report 76-577 1976.
12. Maughan, E. K. in "Géologie comparée des gisements de phosphates et de pétrole, colloque international, 1979"; Bureau de Recherches Géologiques et Minières Document 24: Orleans, France, 1980, p. 63-91.

13. Roberts, R. J.; Thomasson, M. R. in "Short papers in geology and hydrology"; U.S. Geol. Surv. Prof. Paper 475-D 1964, p. D1-D6.
14. Vallier, T. L. U.S. Geol. Surv. Bull. 1437 1977.
15. Jones, D. L.; Silberling, N. J.; Hillhouse, J. W. in "Mesozoic paleogeography of the Western United States"; Pacific Coast Paleogeography symposium 2, Howell, D. G.; McDougall, K. A., eds.; Pacific Section Soc. Expl. Paleontol. Mineral.: Los Angeles, Calif., 1978; p. 71-74.
16. Davis, G. A.; Monger, J. W. H.; Burchfiel, B. C. in "Mesozoic paleogeography of the Western United States"; Pacific Coast Paleogeography symposium 2, Howell, D. G.; McDougall, K. A., eds.; Pacific Section Soc. Expl. Paleontol. Mineral.: Los Angeles, Calif., 1978, p. 1-32.
17. Ketner, K. B. in "Paleozoic paleogeography of the Western United States"; Pacific Section Soc. Econ. Paleontol. and Mineral., Companion to Pacific Coast Paleogeography Field Guide 1 1977, p. 363-369.
18. Wardlaw, B. R.; Collinson, J. W.; Maughan, E. K. U.S. Geol. Surv. Prof. Paper 1163-C 1979, p. 9-16.
19. Brongersma-Sanders, M. K. Nederlandsche Akad. van Wetensch, Afd. Natuurk. 1948, Tweede Sect., Deel XLV, no. 4., p. 1-112.
20. Sheldon, R. P. U.S. Geol. Sur. Prof. Paper 501-C 1964, p. C106-C113.
21. Furnish, W. M. Canadian Soc. Petrol. Geol. Memoir 2 1973, p. 511-548.
22. Schock, W. W.; Maughan, E. K.; Wardlaw, B. R. in "Field conference and symposium guidebook to southwest Montana"; Tucker, T. E., ed.; Montana Geol. Soc.: Billings, Mont., 1981, p. 59-69.
23. Ronov, A. B. Geokhimiya (English translation) 1958, no. 5, 409-423.
24. Burnett, W. C. Geol. Soc. Am. Bull. 1977, 88, 813-823.
25. Williams, J. S. "Pennsylvanian System in central and northern Rocky Mountains", in Pennsylvanian System in the United States--a symposium; Branson, C. C., ed.; Am. Assoc. Petrol. Geol.: Tulsa, Okla., 1962, p. 159-187.
26. Brittenham, M. D. in "Geology of the Cordilleran hingeline"; Hill, J. G., ed.: Rocky Mtn. Assoc. Geol., Denver, 1976; p. 173-191.
27. Rankama, K.; Sahama, Th. G. "Geochemistry"; Univ. Chicago Press: Chicago, 1950, 912 p.
28. Hite, R. J. Mountain Geologist 1978, 15, 97-107.
29. Gulbrandsen, R. A. U.S. Geol. Sur. J. Res., 1974, 62, 693-697.
30. Calvert, S. E. "Chemical Oceanography", v. 6, Riley, J. P.; Chester, R., eds.; Academic: London; p. 187-280.
31. Brongersma-Sanders, M. Proc. 3d Internat. Congress Adv. Org. Geochem. 1970, p. 231-236.

32. Powell, T. G.; Cook, P. J.; McKirdy, D. M. Am. Assoc.
    Petrol. Geol. Bull. 1975, 59, p. 618-632.
33. Cheney, T. M.; Sheldon, R. P. Intermtn. Assoc. Petrol. Geol.
    10th Ann. Field Conf. Guidebook 1959, p. 90-100.
34. Sheldon, R. P. Mtn. Geol. 1967, 4, 53-65.
35. Stone, D. S. Am. Assoc. Petrol. Geol. Bull. 1967, 51, 2056-
    2114.
36. Bowen, C.F. U.S. Geol. Surv. Bull. 661-I 1918, p. 315-328.
37. Miknis, F. P.; Smith, J. W.; Maughan, E. K.; Maciel, G. E.
    Am. Assoc. Petrol. Geol. Bull. 1982, 66, 1396-1401.

The Chemistry That Formed Green River Formation Oil Shale

JOHN WARD SMITH

Consultant, 1472 North Fifth Street, Laramie, WY 82070

The Green River Formation with its energy-rich
oil shales and its remarkable collection of huge
amounts of novel minerals is the product of a
gigantic chemical process system which established
itself in ancient lakes surrounding Utah's Uinta
Mountains. Once established the chemical process
system stabilized and maintained itself, repeating
the same chemical processes continuously for millions
of years on the raw materials entering the lake.
This chemistry produced uniform hydrogen-rich organic
matter, a simple authigenic mineral suite, and massive
deposits of sodium carbonate minerals like nahcolite
($NaHCO_3$), dawsonite [$NaAl(OH)_2CO_2$], shortite
($Na_2CO_3 \cdot 2CaCO_3$), and trona ($Na_2CO_3 \cdot NaHCO_3 \cdot 2H_2O$).
The probable character of these chemical processes
and their origin are reviewed.

The Green River Formation oil shales have produced only a
limited amount of effort aimed at describing how they came to be.
Much that has appeared looks at only one facet of a complex,
integrated system. In 1925 Bradley (1) postulated a stratified
lake to account for development of Green River Formation oil
shale. The stratified lake concept has much strength although
Bradley ultimately was moved away from this postulate. Smith and
Robb (2), Smith (3), and Smith and Lee (4) have extended Bradley's
postulate to develop a comprehensive picture of the chemistry and
mechanics of genesis of the Green River Formation deposits.
These concepts are summarized here.

Green River Formation Characteristics

The oil shales of the Green River Formation in Colorado,
Utah, and Wyoming formed from sediments deposited in Eocene lakes

around the Uinta Mountains. What remains of these deposits is
outlined in Figure 1. These oil shales have been estimated to
offer an oil resource of 1.8 x 10^{12} barrels (260 x 10^9 t) of
shale oil in place (5). They dwarf most other oil shale deposits
of the world in both richness and resource. During their life
spans the Green River lakes, named Gosuite in Wyoming and Uinta
in Colorado and Utah, fluctuated extensively in size. Conse-
quently the oil shale deposits are variable pods of specialized
lacustrine sediments resting on and enclosed in the Wasatch
Formation. The long lived Green River lakes created sedimentary
columns which differ between the Utah-Colorado deposits and the
Wyoming Deposits. Colorado's Green River Formation in Piceance
Creek Basin is the thickest and most continuous deposit and
probably the longest-lived. Figure 2 is a north-south cross
section of the Piceance Creek Basin (6) showing both stratigraphy
and structure of the Green River Formation. Most but not all of
the Colorado oil shale occurs in the Parachute Creek Member of
the Green River Formation. Additional oil shale up to about
400 feet thick underlies the Parachute Creek Member in the north-
central part of the basin. As indicated in Figure 2 this oil
shale is classed as occurring in the Garden Gulch and Douglas
Creek Members. Although U.S.G.S. has attempted to preserve the
two member names, their type sections overlap (7). In the basin's
depositional center these members can't be realistically divided.
They represent a progression from normal lacustrine to saline
lake deposition. A change in mineral composition from clay-rich
to dolomite-rich oil shale marks the bottom of Colorado's Para-
chute Creek Member. A long sequence of saline mineral deposition
which formed nahcolite, dawsonite, and some halite begins at the
bottom of the Parachute Creek Member. Ground water has removed
nahcolite and perhaps halite from the upper part of the section
where the saline minerals initially formed. This section is
referred to as the leached zone. The Mahogany zone (Figure 2)
near the top of the Parachute Creek Member is a stratigraphic
action of very rich oil shale marking the maximum expansion of
ancient Lake Uinta. Utah's Green River Formation oil shales
consist almost entirely of deposits at or above the Mahogany zone
(8).
     The Wyoming deposits of Green River Formation oil shale
received different stratigraphic names, but they show some
striking similarities to the distribution in Colorado (9). The
bottom section called the Tipton Shale Member is predominately
clay-rich oil shale similar to that in Colorado. The next
section, called the Wilkins Peak Member, contains dolomite-rich
oil shale layers interspersed with layers of saline minerals,
particularly trona, or with clastic deposits away from the
depositional centers. The uppermost section, called the Laney
Member, consists of dolomite-rich deposits formed during a re-
expansion of ancient Gosuite Lake.
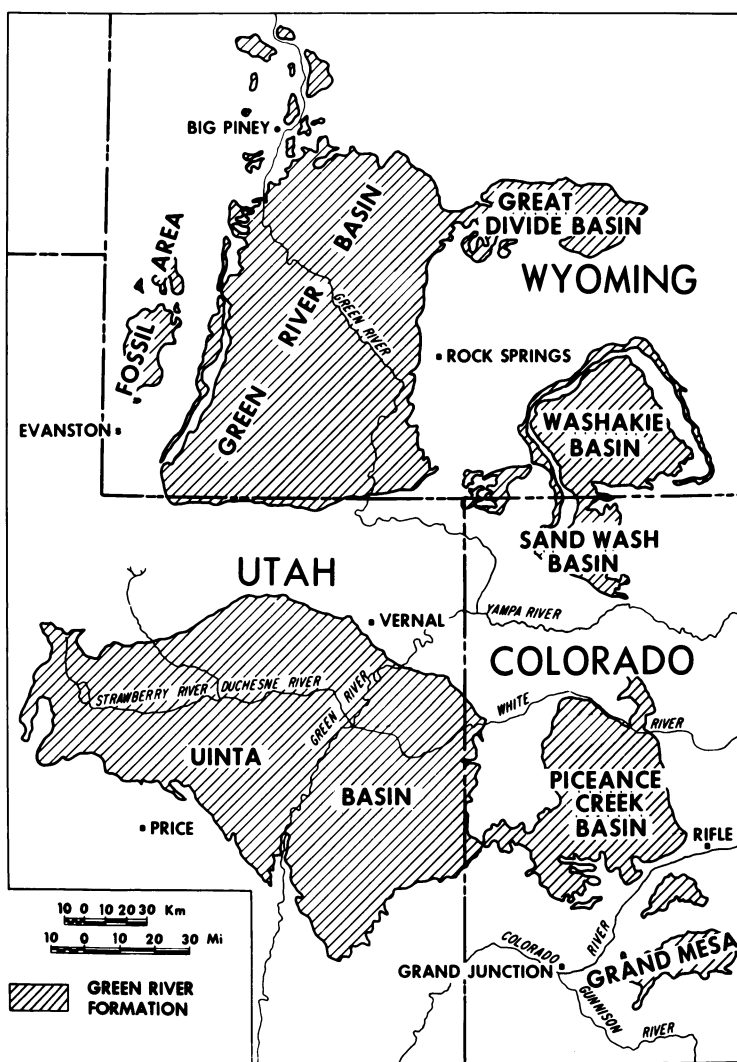
Figure 1. The Green River Formation. (Reproduced with permission from Ref. 5. Copyright 1980, Colorado School of Mines.)
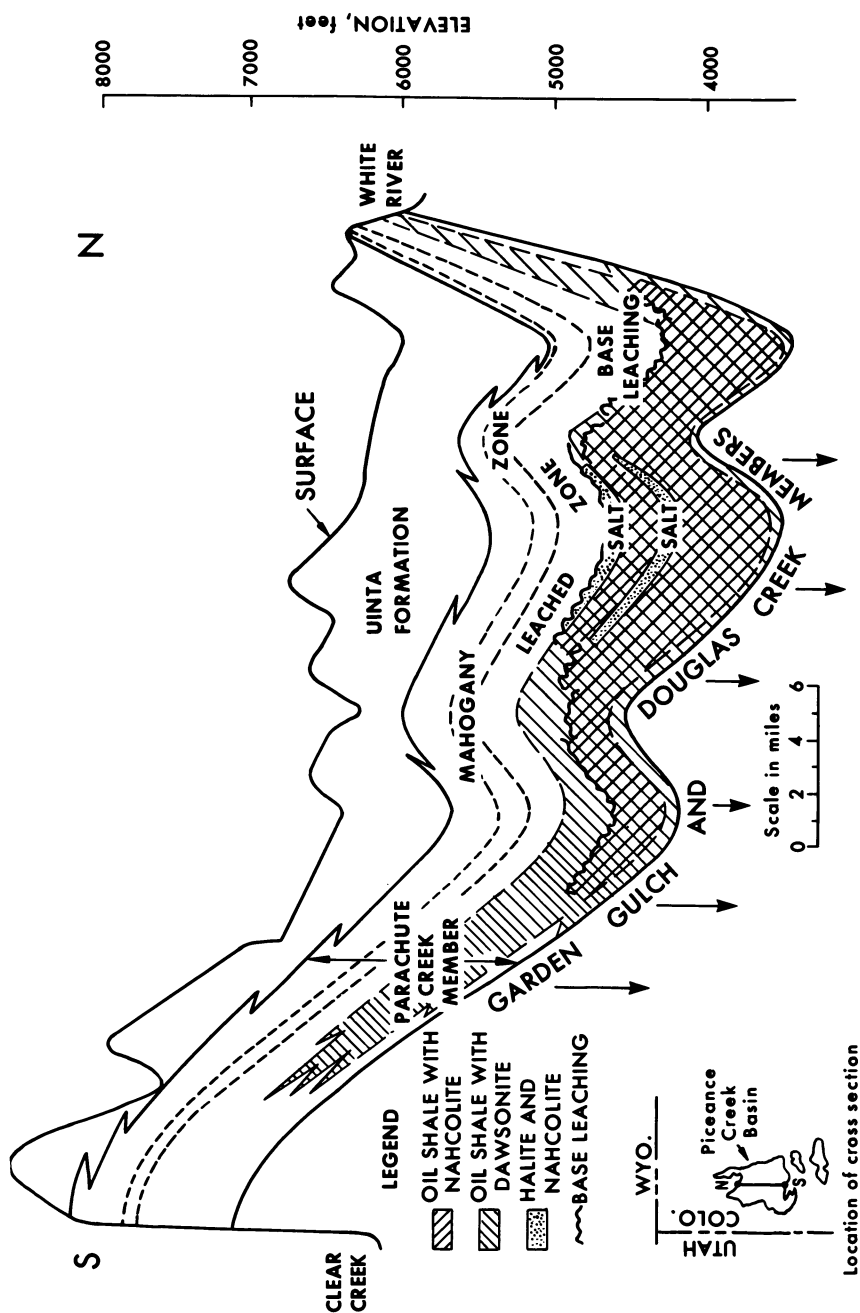
Figure 2. South–north cross-section of Colorado's Piceance Creek Basin. (Reproduced with permission from Ref. 5. Copyright 1980, Colorado School of Mines.)

This paper will concentrate its discussion on Colorado's Piceance Creek Basin. Here, oil shale deposition appears to have lasted longer and matured to a greater degree. Nevertheless, with minor modifications the geochemical conditions that formed Colorado's oil shales extrapolate nicely into the depositional conditions that made Green River oil shale in Utah and Wyoming.

There were possibly three oil shale lakes initially--Lake Gosuite in Wyoming, Lake Uinta in Colorado, and an unnamed lake which deposited what Picard et al (10) describe as the "black shale facies" of the Green River Formation. This black shale facies seems to be dolomitic oil shale which has matured (been heated) to produce oil form its organic matter. Maturation accompanied increased depth of burial resulting from clastic influx from the rising Uinta Mountains. Picard et al (10) point to the black facies as source rocks for the huge (possibly 1 billion barrel) oil resource in the Altamont Trend stretching about 40 miles from the Cedar Rim field to the Blue Bell field. The sediments deposited in this possible oil shale lake began being deposited about the same time as the earliest deposition in Wyoming and in Colorado. Clastics from Uinta Mountain activity apparently destroyed the Utah lake, but oil shale deposition returned to Utah when Colorado's Lake Uinta expanded during the time of deposition of the Mahogany zone (8).

The two (or three) lakes appear to have developed the same characteristics at about the same time. The one major factor they have in common is proximity to the Uinta Mountains. Perhaps the materials exposed by the mountain activity at that particular time led to the development of the unusual chemistry of the Green River lakes.

The Eocene Green River Formation is unique in organic-rich sedimentary deposits. Nothing like it exists elsewhere. While many collections of sedimentary rocks containing organic matter exist, the Green River Formation contains large amounts of organic matter making up unusually large volume fractions of the total sediment. In addition this deposition persisted through literally millions of years. An excellent example of this is the oil shale sampled by the U.S.B.M.-A.E.C. Colorado Corehole No. 1 which demonstrated existence of about 2100 feet (640 meters) of con- tinuous oil shale (11). Average organic content through this section is nearly 25 volume percent of the total rock. This organic matter is remarkably uniform and relatively rich in hydrogen. The carbon-to-hydrogen weight ratio in organic matter throughout the Formation is about 7.7-7.8, similar to the high end of the petroleum spectrum and much lower than most other oil shales of the world. The only major change in the nature of the organic matter through the 2100-foot section is decarboxylation with depth of burial (12, 13). A study purporting to detect variations in organic matter through the oil shales in Colorado Corehole No. 1 (14) actually demonstrates the remarkable and persistent similarity of the organic matter in the Green River Formation thickness deposited over millions of years.

The lateral consistency of the Green River Formation deposition is also remarkable. Figure 3 compares oil yield histograms for about 500 feet (150 meters) of continuous oil shale at two locations in the Green River Formation (8). Figure 4 shows the locations designated A and B of these two coreholes--about 85 miles (136 km) apart on a straight line. The histograms in Figure 3 are deposition profiles correlated in time. They demonstrate the gross lateral continuity of oil shale deposition. This is also demonstratable on a much smaller scale. Figure 5 shows stratigraphic variations in the color changes of laminations across a 2-inch oil shale (5 cm) block. The lightest band is a bed of altered volcanic ash, but most of the color variation is produced by variations in amount of organic matter. The apparent regularity of the bedding is usual. Trudell et al (15) published a classic photograph demonstrating precise correlation of such markings over a 75-mile (120 km) span. A third level of persistence exists on a microscale. Annual depositional cycles produced varving. The varves are too small (~30μ) to be photographed and reproduced here, but they couldn't even be located if they were not laterally persistent.

The lateral continuity of the formation's bedding is matched by the lateral consistency of the deposit's composition. To illustrate this we'll examine analyses conducted on 10 composite samples prepared to represent the Mahogany zone section with an average oil yield of 25 gallons per ton (104 1/t). Locations of the coreholes furnishing cores for these composites are indicated by the numbers 1 through 10 in Figure 4. The method of composite preparation described by Smith (16) produced a sample equivalent to crushing completely a continuous core through the section represented. Although the composites to a specific oil yield average don't represent precisely the same stratigraphic section (discussed later), they all center around the Mahogany bed, the richest portion of the Mahogany zone. And as demonstrated in Figure 4 they represent the Mahogany zone shales over a substantial area.

Element composition of both the organic matter and the mineral matter in these composites are strikingly similar. Smith (16) determined organic element composition on each of them. The resulting average composition for organic element matter in these comparable samples is given in Table I. The confidence limits indicate that if the entire experiment were repeated, the new averages would have 95 percent probability of lying within the indicated limits. Oxygen determined by difference shows the highest degree of uncertainty. Smith's (16) study of maximum analytical errors in the determination method showed them to be on the order of the confidence limits in Table I. This certainly demonstrates uniform elemental composition of the organic matter in the stratigraphically comparable samples over a broad area.
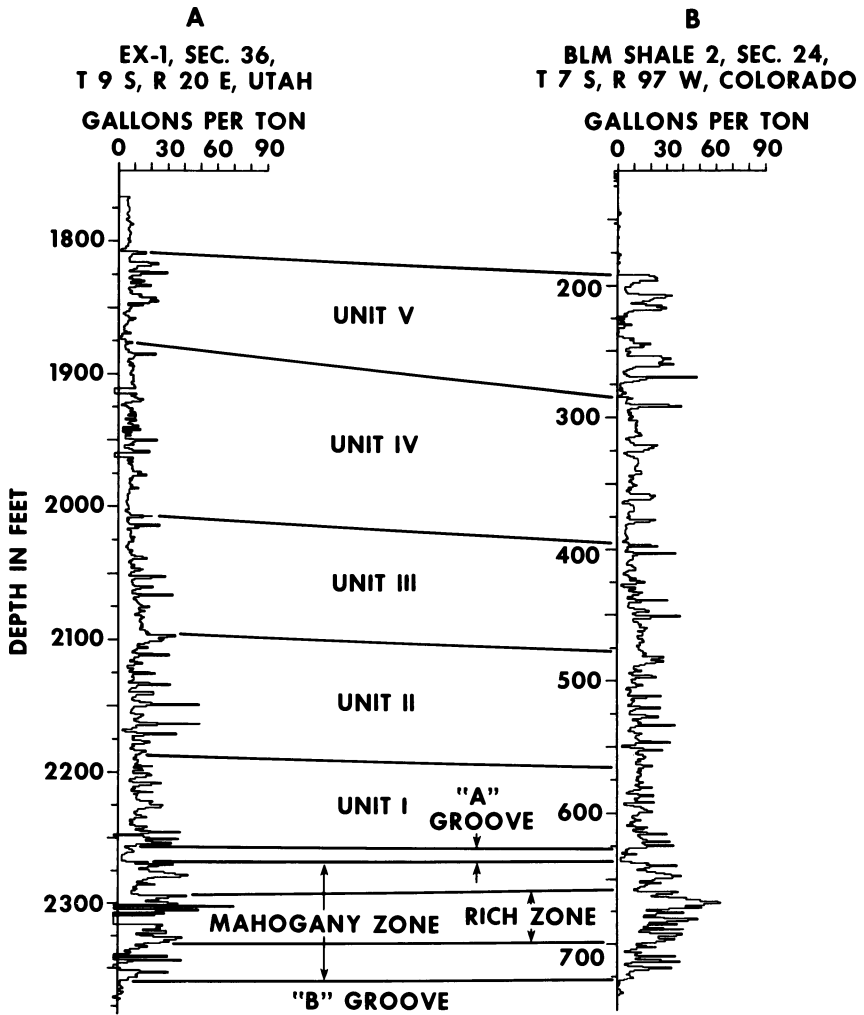
Figure 3. Oil shale correlations between Colorado and Utah deposits (8).
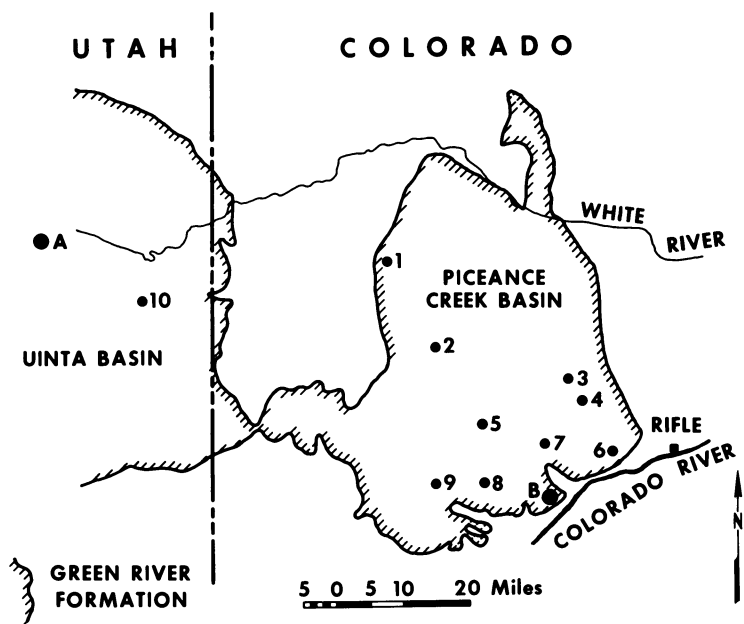
Figure 4. Oil shale locations compared in Figure 3 (A and B) and locations of 10 coreholes from which Mahogany zone composites were prepared.
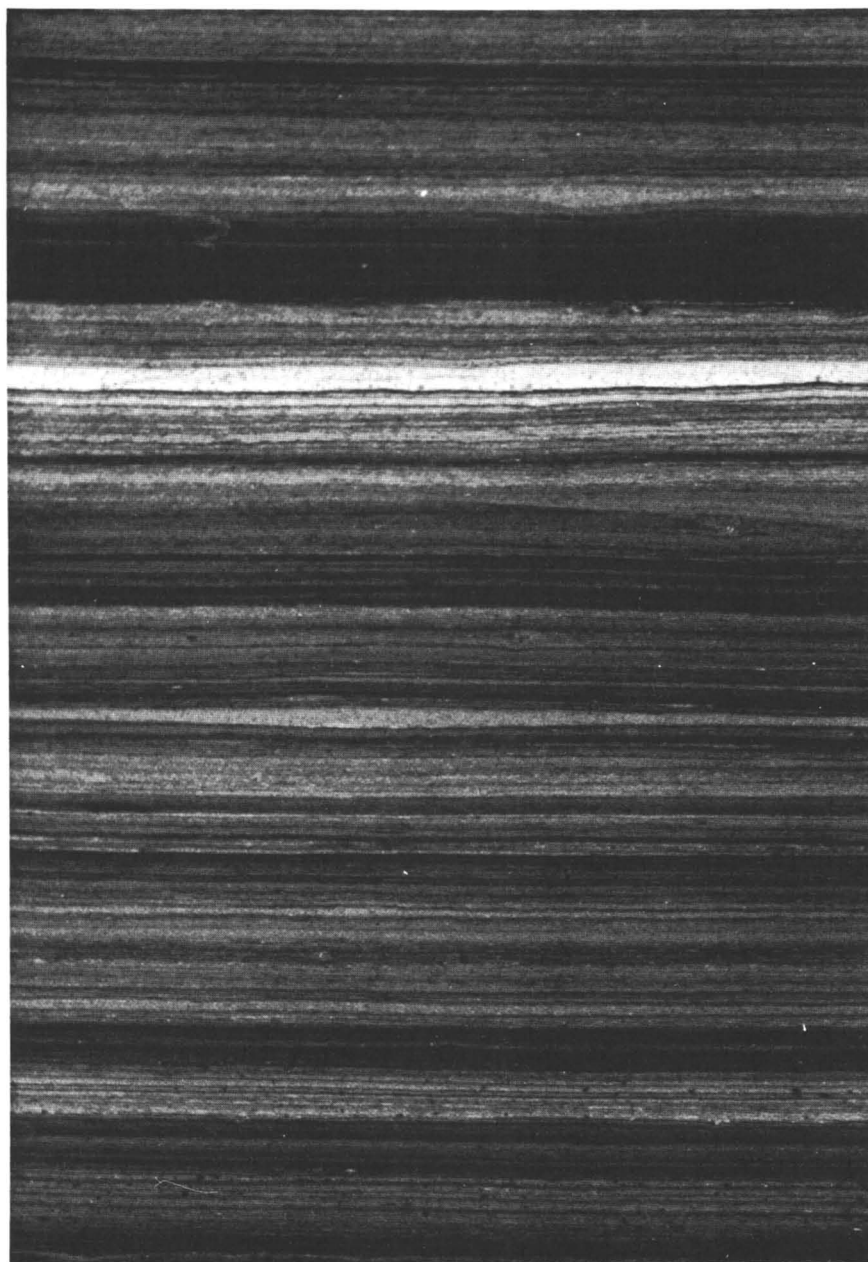
Figure 5. Oil shale laminations in a two-inch block.

Table I. Average Element Composition of Organic Matter in
          Mahogany Zone Composites

Element	Average Composition Weight Percent Organic Matter with 95% Confidence Limits
Carbon	80.52 $\pm$ 0.40
Hydrogen	10.30 $\pm$ .08
Nitrogen	2.39 $\pm$ .10
Sulfur	1.04 $\pm$ .08
Oxygen	5.75 $\pm$ .49

A similar set of results were obtained for the elemental composi-
tion of ash at 1000°C from these 10 Mahogany zone oil shale
composites. The averages of these results is given in Table II
with 95 percent confidence limits of the averages.

Table II. Average Oxide Composition of Ash from Mahogany Zone
           Composites

Component	Average Ash Composition Weight Percent Ash with 95% Confidence Limits
SiO_2	43.33 $\pm$ 0.56
Fe_2O_3	4.43 $\pm$ .16
Al_2O_3	10.64 $\pm$ .52
CaO	23.63 $\pm$ .88
MgO	9.96 $\pm$ .69
Na_2O	2.17 $\pm$ .17
K_2O	2.24 $\pm$ .22
SO_3	2.10 $\pm$ .22
Determined Total	98.50 $\pm$ .39

In spite of the lack of precise stratigraphic matching the oxide
composition of these ashes is strikingly consistent. The SO_3
indicated was generated during the ashing process from reduced
sulfur initially present in the pyrite and the organic matter of
the oil shale. Even this process was consistent.
     Most of the trace elements, which largely account for the
undetermined material in the ash, show similar uniformity. An
excellent example of this comparability is furnished by Giauque
et al.(17) who provided analysis for more than 50 elements on

stratigraphically keyed samples. The stratigraphic sections
sampled by the two analyzed cores include the Mahogany zone and
its overlying oil shale. The cores examined were from Naval Oil
Shale Reserve No. 1 and were drilled about 10 km apart. Their
section on element abundance (17, pg. 34) begins with the follow-
ing sentence "The most notable result of this study was the
demonstration of a remarkable stratigraphic uniformity in mineral
and element composition of both cores". An illustrative example
points out that from the results presented the average Mahogany
bed content of zirconium for the specific core would be 26.2 ppm
Zr with 99 percent probability that the average from a new
determination would lie within +4.6 ppm. Direct comparison of
the results from their (17) two coreholes is difficult because
no correction was made for the diluting effect of organic matter.
One core contains substantially more organic matter than the
other. When this interference is removed the comparability of
the trace elements in the mineral fraction is readily apparent.

Associated with the lateral continuity of the formation's
element composition is the lateral consistency of mineral compo-
sition. This might be startling except for the fact that the
mineral suite in Green River Formation oil shale is uniform
stratigraphically as well as laterally. This mineral suite is
authigenic, formed by the chemistry of the lake. The consistence
of mineral composition through stratigraphy can be illustrated
by the sample sets 1 through 10 described earlier. Figure 6
shows oil yield histograms of the section composited from each
of the 10 cores whose locations are given in Figure 4. For
richer cores the compositing to the same grade elongated the
stratigraphic section included in the composite. Consequently
the 10 composite samples don't represent exactly the same section.
For example, the sections composited in cores 2, 3, and 4
definitely include the low grade section called B-groove, while
cores 9 and 10 definitely do not. Nevertheless the overall
mineralogy of these composites is nearly identical. Figure 7
gives X-ray diffraction plots of the 10 composites. Their
overall similarity is insistent. The only evident variations
appear in cores 3 and 4 where dawsonite formation was competing
with analcite (analcime) for the products of volcanic ash, and
in core 10 where the composite sample did not include any of the
major tuff beds and consequently no analcite is evident.

Consistency and uniformity characterize the Green River
Formation oil shales. However, two major mineral variations
warrant mention because they appear to belie mineral uniformity.
One is the illite concentration deposited early in the formation's
sedimentary history which was rather abruptly replaced by dolomite
although the organic matter remained the same across this change.
The other is the appearance of truly remarkable minerals--
nahcolite ($NaHCO_3$); dawsonite [$NaAl(OH)_2CO_3$]; shortite
($Na_2CO_3 \cdot 2CaCO_3$); and trona ($Na_2CO_3 \cdot NaHCO_3 \cdot 2H_2O$). These minerals
are rare in the rest of the world but appear in billions of tons
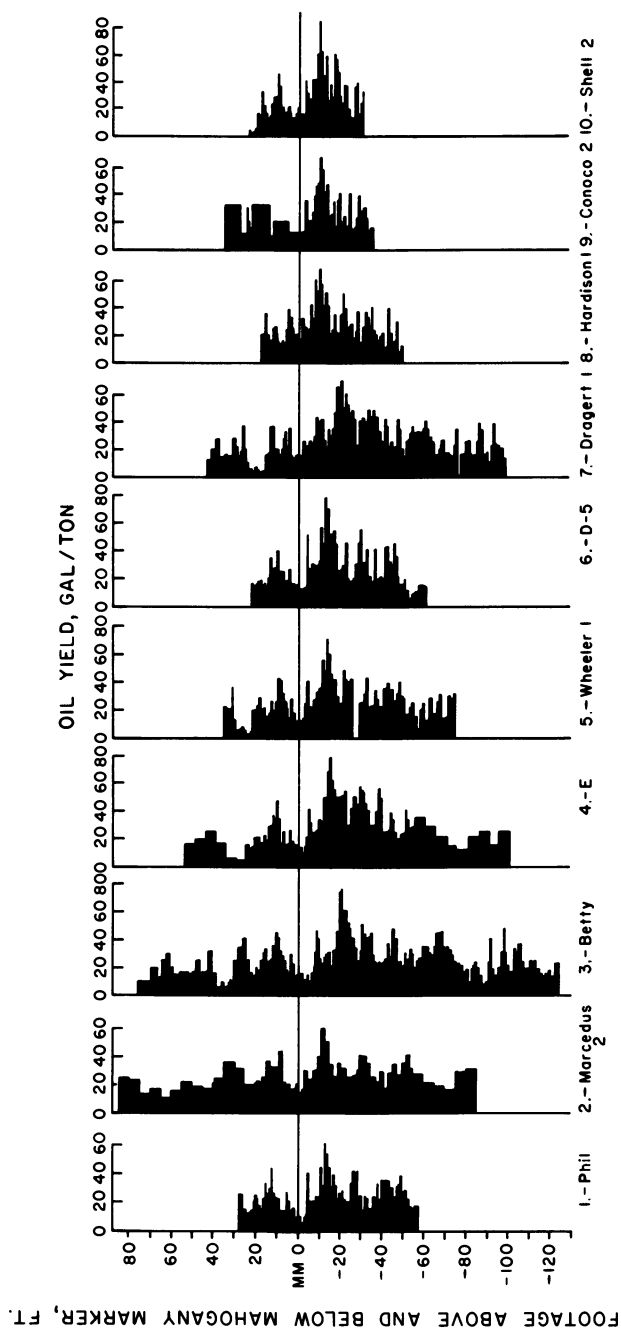
Figure 6. Oil yield histograms for the composited sections of the 10 cores whose locations are shown in Figure 4.
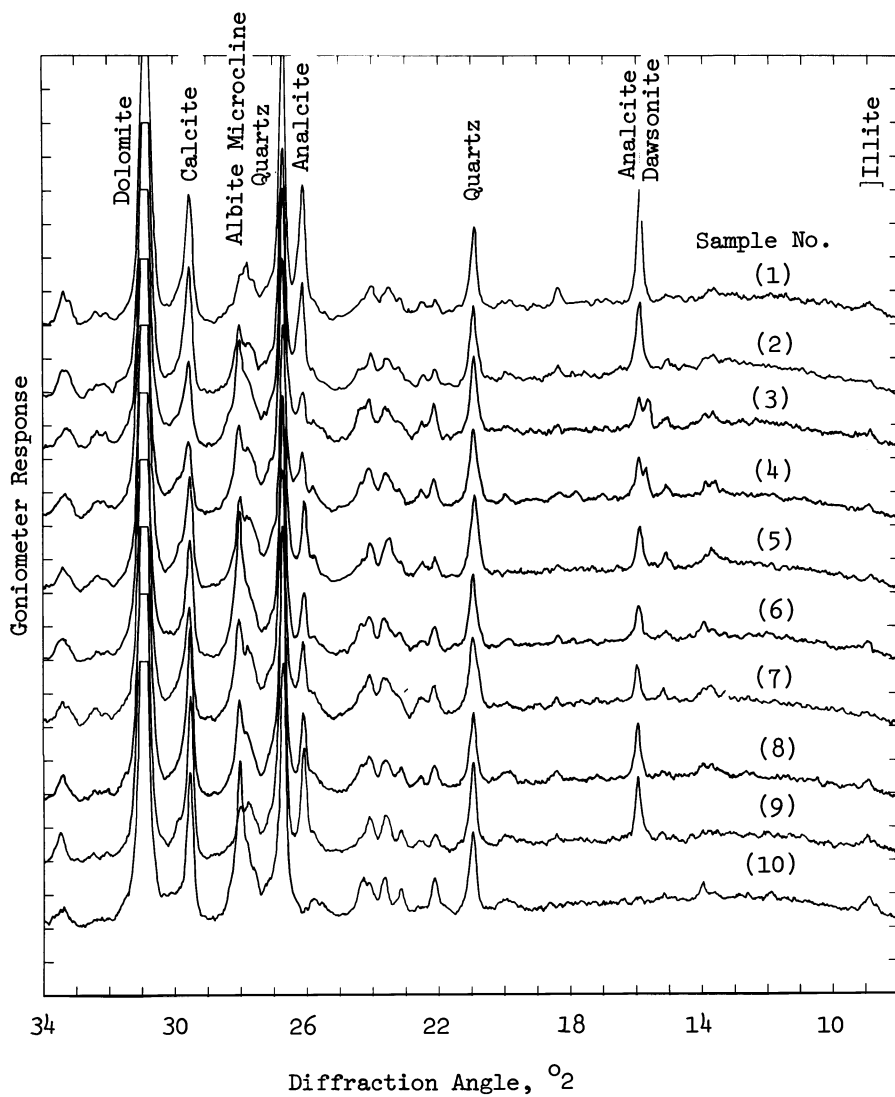
Figure 7. x-Ray diffraction of minerals in 10 Mahogany zone composites.

in the Green River Formation. An additional peculiarity is the
formation of shortite and trona in the Wyoming deposits and the
development of dawsonite and nahcolite in Colorado.

These characteristics pose a set of rather difficult problems
in describing the genesis of the Formation. A geochemical
postulate has been developed (4) to explain this genesis and its
peculiarities. This pattern is outlined.

Lake Uinta's Postulated Chemical History

Depositional conditions postulated for the Green River
Formation must accommodate the major requirements described
above. Generalizations must be made in trying to evaluate
briefly the conditions which formed Green River oil shale through
perhaps six million years. Because the oil shale is so continu-
ously similar, however, that the conditions creating it were
also continuous. Consequently, generalization is appropriate.

The basic postulate for oil-shale genesis is a stratified
lake, separating the lake waters into two nonmixing layers.
Bradley (1) recognized this requirement in his early studies of
the Green River Formation. A number of permanently stratified
lakes, called meromictic lakes, exist currently in the United
States (18) and several sets of conditions leading to stable
stratification have been outlined by Hutchinson (19). Lake
Uinta probably began in the northwestern part of the present
Piceance Creek Basin, where a long sequence of normal lacustrine
sediment occurs (15). Thermal density differences probably
produced the initial stratification. Hydrolysis of local silicates
and aluminosilicates in the stratified lake's lower layer began
to build up a chemical stratification. Garrels and Mackenzie
(20, p. 175) give the following equation as an example of this
hydrolysis, using albite as a simple specimen:

$$2NaAlSi_3O_8 + 2CO_2 + 11H_2O \longrightarrow Al_2Si_2O_5(OH)_4 +$$

Albite   Kaolinite   (1)

$$2Na^+ + 2HCO_3^- + 4H_4SiO_4$$
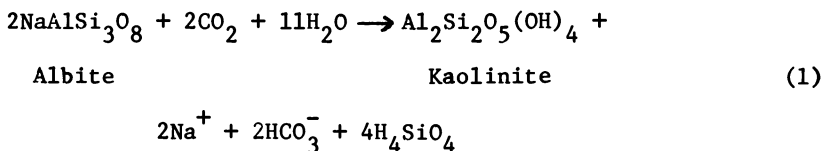
Notice that acid, represented here by CO_2 and water, is consumed
and that sodium and bicarbonate ions are produced as albite
alters to kaolinite. The material entering the lake as the
stratification developed appears to have had two characteristic
properties—easily hydrolyzed sodium and a limited content of
halogens, particularly chlorine. Decomposition of organic
matter furnished carbon dioxide. Concentration of sodium car-
bonates and other dissolved salts in solution in water of the
stratified lake's lower layer built up, raising the water density.
The evolution from normal lacustrine sediments to oil shale in
the northwestern part of the Piceance Creek Basin is continuous

and without evidence of evaporative cycles (15). The acid-consuming hydrolysis indicated in equation 1 probably was the primary mechanism which built up the water density. This created a remarkably stable chemical stratification in ancient Lake Uinta, lasting through the entire period of oil-shale deposition.

Figure 8 illustrates the nature of the chemically stratified lake. The upper (low density) layer, called the mixolimnion, is separated at a level called the chemocline from the high density lower layer called the monimolimnion. The chemocline forms a real barrier. The two layers circulate independently mixing very little. Smith and Lee demonstrated the definite stability of such stratification in ancient Lake Uinta (4).

In ancient Lake Uinta the mixolimnion was exposed to the atmosphere, was oxygenated, and supported life. All fresh water entering the lake (rain, streams, runoff, etc.) joined the mixolimnion. The bottom layer of the lake was isolated from the atmosphere. Notice in Figure 8 that the lower layer (monimolimnion) does not reach the water's edge. Near shore the lake consisted only of the upper layer, forming a normal lake capable of producing shallow water expressions like algal heads, shells, and plant fossils.

Permanent stratification of ancient Lake Uinta was accompanied by a limitation of the supply of materials reaching the lake's lower layer. Currents in the water of the lower layer had to be very slow or the organic matter deposited uniformly in the tiny varves would have accumulated unevenly. Currents in the water of the upper layer could not be strong because of the relatively small flow of water through a huge area. In slow currents larger clastic materials deposit near the lake shore. Only air-borne particles and water-borne particles small enough to remain suspended in slow currents could be distributed over the lake's huge area. Tiny air-borne particles, predominantly silicates, and organic debris plus the small amount of clastic material deposited on the edges of the lake made up the supply of material available to the lake. Both the amount and the composition of this supply was limited and continued to be so through much of the time oil shale was deposited. Composition of mineral particles entering the lake appears to resemble atmospheric dust just now being adequately sampled (21). This consistency of source helps explain the composition uniformity indicated in Table II.

Organic debris from the lake's upper layer fell into the lower layers. This organic matter made up a relatively large portion of the material reaching the lower layer of the stratified lake, not because the lake producing it teemed with life (it didn't) but because the lake strongly limited the available mineral matter. The organic matter chemically consumed the available oxygen. In the stratified lake no oxygen supply could reach the bottom layer which quickly became, and remained, a reducing environment. The reducing environment became powerful
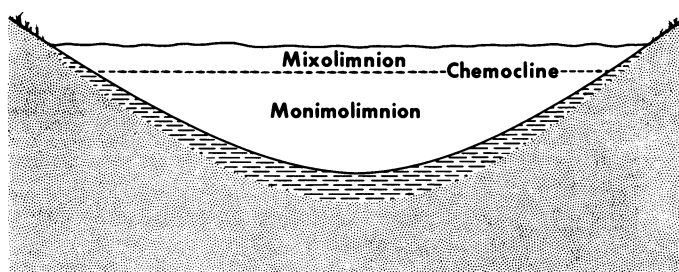
Figure 8. Stratified Lake Uinta. (Reproduced with permission from Ref. 4. Copyright 1983, Colorado School of Mines.)

enough to continually hydrogenate organic matter, making the organic residue rich in hydrogen and poor in oxygen. Oil-shale deposition began.

Water of the lower layer must have been lethal to macrolife and probably also to microscopic life. Bioturbation is not indicated because bioturbation would destroy the well preserved varves and lamina. The upper or surface layer, however, must have been fresh enough for life to exist in it because organic matter was continuously deposited in the sediment. In its travel through the lake's lower layer, the organic matter was exposed to basic reducing solutions which digested it and homogenized it. Only particular chemical structures would survive exposure to the basic environment, automatically selecting similar materials to be deposited. In addition the strongly reducing environment in the lake and the sediment would hydrogenate the organic matter to produce the hydrogen-rich organic matter. This mode of deposition over a wide area explains the lateral uniformity observed in element composition of organic matter in Mahogany zone oil shale (16), and the similarity in properties of the oil-shale organic matter over the entire deposit. The paucity of macrofossils in the oil shale, limited largely to an occasional gar scale and the like, illustrates the power of the lake's lower layer to digest organic matter.

As hydrolysis of the silicates and aluminosilicates continued (equation 1), dissolved sodium ions were continually produced, and acid was consumed. The pH of the water gradually increased. Formation of kaolinite was replaced by formation of montmorillonite and finally by production of illite. Silica was more soluble than alumina and as aluminosilicates were attacked by the water a protective coating of $Al(OH)_3$ formed around the particles. This coating helped transport mineral particulates to the sediment. The reactions indicated by equation 1 were replaced by the family of reactions indicated in equation 2, written using the hydrolysis of albite as an example.

$$3NaAlSi_3O_8 + 2CO_2 + 14H_2O + K^+ \longrightarrow KAl_2(AlSi_3)O_{10}(OH)_2 +$$
$$\text{Albite} \hspace{6cm} \text{Illite}$$
$$3Na^+ + 2HCO_3^- + 6H_4SiO_4 \tag{2}$$
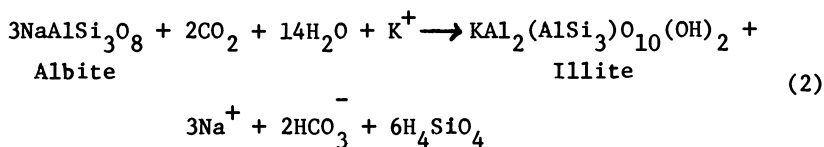
Loughnan (22) gives this chemical composition for illite, pointing out that illite is characterized by substitutions in the silica sheet. Potassium collection and retention by silicate skeletons is a phenomenon recognized in lacustrine environments. As pH of the lake water increased, silica became more mobile than alumina. Formation of the relatively silica-poor illite resulted. Dehydration of the dissolved silica in the sediment's water (equation 3) produced quartz. The large amounts of illite from the reactions

represented by equation 2 and the quartz from equation 3 formed
the major mineral constituents in the oil shales below the

$$H_4SiO_4 \longrightarrow 2H_2O + SiO_2 \qquad\qquad (3)$$
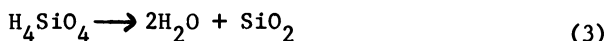
<center>Quartz</center>

horizon where the minerals change from predominately illite to
predominately dolomite.

The illite-producing reaction in equation 2 continued to
consume acid, in amounts greater than could be supplied by CO_2
from the organic matter. This made the water of the lower layer
progressively more basic. When the pH of this water exceeded
10, alumina also became mobile. Solubility of both silica and
alumina increases dramatically as the solution pH increases past
10 (3). The water of the lower layer was now primarily a sodium
carbonate solution, strongly basic and strongly reducing. The
protective layer of $Al(OH)_3$ which had continually formed around
aluminosilicate particles now dissolved because of the amphoteric
behavior of aluminum. Consequently, when the tiny clastic
particles entered the water of the lower layer, they were largely
destroyed. The aluminate ion also began to accumulate in the
lake's lower layer. Illite was no longer produced in quantity
from the protected silicate skeletons. Dolomite, the second
most abundant mineral in the clay shales, now became the dominant
mineral. The mineralogy of the resulting oil shales changed
abruptly.

Mineral particles entering the lake dropped into its lower
layer. Larger particles, particularly those arriving in bulk
like clastic floods or volcanic ash falls, dropped through the
lower layer to the sediment too fast to be altered appreciably.
These appear as individual layers (like the ash fall, Figure 5)
or as oil shale dilutants around the lake edge. The larger
particles sequestered themselves from the lake's influence and
had only limited overall effect on its chemistry. The bulk of
the arriving mineral consisted of tiny air-borne grains, appearing
as atmospheric dust. These particles are so small [<1μ, (21)]
that their travel through the lake's lower layer was slow. They
were attacked chemically by the basic water in the monimolimnion.
Their basic silicate structure was largely destroyed, releasing
the particle's components and elements to the chemical conditions
of the water in the lower layer. Each element's individual
chemical properties came into play in defining what happened to
it. Some components like TiO_2 and ZrO_2 probably went to the
sediment directly upon release. Iron was reduced to the ferrous
state. It then formed an insoluble hydroxide and progressed
toward the sediment with other hydroxides like that formed by
released magnesium. Some like calcium formed carbonate precipi-
tates. Some may have formed sulfides, and some like boron or
fluorine would be managed by their solubility in the lake's
water. Some components of atmospheric dust, like spinels (16),

would proceed to the sediment with the residue from particle digestion. Detailed evaluation of the individual behaviors of all the incoming materials under these chemical conditions is not practical here. However, the chemistry of all the elements in the sediment coordinates with their behavior under the postulated chemical conditions.

The organic matter being deposited changed little across the major change in minerals, but the organic matter now became a major factor in the production of oil-shale minerals. As organic matter (produced seasonally in the lake's upper layer) collected on the lake bottom, it trapped water from the lake's lower layer. This trapped water had a pH above 10, was strongly reducing, and had continued to build up a supply of dissolved materials. Laboratory tests have shown that organic matter from the Green River oil shales has a large capacity for forming a water-retaining suspension (2). In addition the sediment probably acted as an ionic filter, retaining ions as water was forced from the sediment. Reductive conditions in the sediment continued to operate on the organic matter to evolve CO_2 and some H_2S. These gases dissolved in the interstitial water, lowering its pH.

The limits of reduction potential and pH in the sediments which became oil shale of the Parachute Creek Member can now be defined. These are presented as the shaded area in Figure 9. The block's bottom boundary (23) represents the lower stability limit of water. At reductive potentials below this line, water tends to break down to yield hydrogen. This illustrates the strength of the hydrogenating environment in the sediment. The upper boundary, defined by the ratio of sulfate to sulfide ion, is drawn three orders of magnitude below the Eh values represented by equal parts of sulfate and sulfide ions because sulfate has not been observed in unweathered Parachute Creek sediments (24). The lower pH boundary is set because of strong bicarbonate (nahcolite) buffering at about pH 8.4. The upper boundary is set at a pH of 10 because of the sharp increase in silica and alumina solubility above this pH. The pH of the interstitial water in the sediment to become oil shale probably averaged about 9 because the CO_2 and H_2S released by the organic matter lowered the pH of the trapped water.

With the sharp lowering of pH from perhaps 11 to 9 at the organic sediment interface, silicates began to form from the interstitial water trapped in the sediment. The solubility of both silica and alumina decreases sharply as pH changes from 11 down to 9 (3). The resulting chemical conditions in the sediment encouraged development of authigenic feldspars and formation of quartz. If this actually occurred, silicate precipitation should be enhanced by large amounts of organic matter producing larger amounts of CO_2. Silicate mineral content definitely increases with increasing organic matter in Colorado's Green River oil shales (25). Silicates generated in this manner would tend to
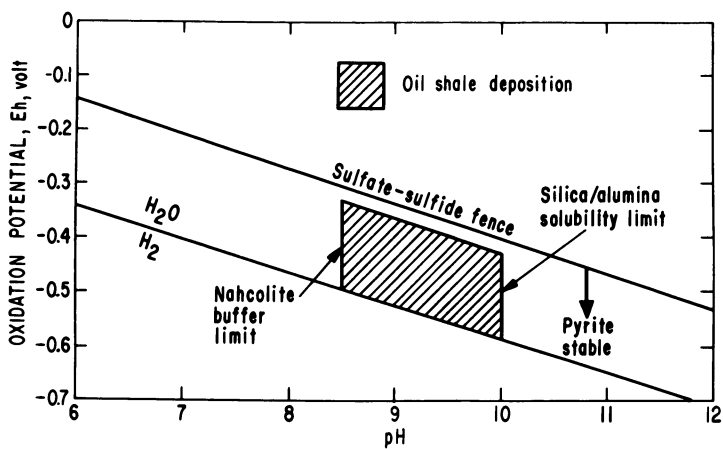
Figure 9. Eh–pH Limits in sediments that became Green River oil shale (2).

concentrate in the organic layers and in the organic-rich (dark) fraction of the light-dark varve cycle.

Smith and Robb ($\underline{2}$) describe the formation of dolomite, calcite, and aragonite in Lake Uinta. Calcite was formed in the lake's lower layer from the calcium released by chemical digestion of silicates and aluminosilicates. Calcium released to a calcite-saturated sodium carbonate solution immediately formed calcite. The calcite crystals settled to the lake bottom as a continuous and very dispersed shower of tiny calcite particles. The Mg^{++} and Fe^{++} released by dissolving particles precipitated as $Mg(OH)_2$ and $Fe(OH)_2$, and also descended to the lake bottom. When these hydroxides were enclosed in the sediment at a lower pH, they dissolved, releasing Mg^{++} and Fe^{++} to form the Green River Formation's iron-bearing dolomite. The calcium carbonates, both calcite and aragonite, were converted to dolomite in the sediment by direct addition of magnesium and ferrous iron carbonates. Dolomite was $\underline{not}$ precipitated directly but formed in steps ($\underline{4}$). Part of the iron was used to form pyrite. During deposition of the Mahogany zone aragonite formed seasonally in the lake's upper layer, fell to the lake bottom, and was partially dolomitized and partially preserved ($\underline{2}$). This generated the dolomite-rich light layers in Mahogany zone varves. Thus the chemical conditions in the stratified lake Uinta explain the generation and lateral persistence of the tiny varves and the large laminations. Widespread uniformity of the lake's chemistry explains why the laminations can be correlated over huge areas. The laminations reflect area-wide changes, particularly in the growing conditions that produced the depositing organic matter.

One event in the life of Lake Uinta remains to be explained, the production of the unique saline mineral suite. The saline mineral suite consists of dawsonite [$NaAl(OH)_2CO_3$] with its accompanying nordstrandite [$Al(OH)_3$], nahcolite ($NaHCO_3$), and halite ($NaCl$) deposited in the Parachute Creek Member around the early depositional center ($\underline{3}$). Two factors combined to produce the saline minerals--(1) The continual buildup of sodium carbonate and aluminate ion in the water of the lake's lower layer, and (2) the gradual loss of water from the lake's lower layer and the accompanying increase in concentration of the materials in solution. The hydrolysis mechanism continuously supplying sodium carbonate and aluminate ion to this water has been described. The loss of water from the lake's lower layer had to be a mechanism at the lake's edges ($\underline{3}$) because the upper layer of Lake Uinta continued to supply organic matter to the lake bottom through the deposition of the saline minerals.

Dawsonite occurs in oil shale as a matrix mineral formed from the lake water as a chemical precipitate in the sediment. Bader and Esch ($\underline{26}$) synthesized dawsonite by bubbling CO_2 into a sodium aluminate solution at a pH of 11. As the pH of their solution dropped, dawsonite precipitated. Dawsonite was obtained only when the sodium carbonate to aluminate ratios were higher

than 15 to 1. This synthesis method is almost an exact description of the natural mechanism which formed dawsonite in the sediment. Carbon dioxide from the deposited organic matter performed on the sodium carbonate and aluminate ion dissolved in the trapped water exactly as in the synthesis method, forming dawsonite. Robb et al (25) observed correlation between amounts of dawsonite and organic matter.

Nahcolite crystallization was also produced by CO_2 from organic matter. Sodium carbonate in the interstitial water was converted to sodium bicarbonate by the reaction shown in equation 4.

$$Na_2CO_3 + CO_2 + H_2O \longrightarrow 2NaHCO_3 \qquad (4)$$
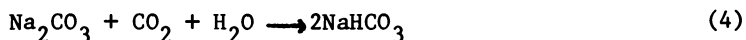
By this reaction 106 grams of sodium carbonate becomes 168 grams of sodium bicarbonate. Sodium bicarbonate is less soluble than sodium carbonate by a factor of 3 or 4. As the concentration of the sodium carbonate salts dissolved in the lower layer gradually increased, a point was reached where nahcolite ($NaHCO_3$) began to crystallize in the sediment. These crystals grew as the sodium bicarbonate in the interstitial water migrated to them. Crystals which grew in sediment make up most of the nahcolite occurrence in the Piceance Creek Basin. As Milton and Eugster (27) point out, nahcolite is the solid phase expected at the relatively high CO_2 pressure in the unconsolidated sediment. None of the other sodium carbonate crystal forms known to occur in nature have been found in core from the Piceance Creek Basin. In Colorado the stratified lake persisted throughout saline mineral deposition. In Wyoming, however, the corresponding lake went nearly or completely to dryness, losing its protective top. When exposed to atmospheric levels of CO_2, sodium carbonate solutions crystallize trona. Wyoming's lake did.

Smith and Lee (4) tested stability of the postulated chemical stratification. These tests indicated that the density stratification would persist largely unmixed through all possible stresses—earthquakes, seiches, tides, temperature variations, and even windstorms stronger than any known.

Summary

The genesis pattern presented for Green River Formation oil shale explains the major observations. Deposition of relatively large quantities of hydrogen-rich organic matter in the oil shales is a natural consequence of the chemical conditions (basic water and reducing atmosphere) and the physical limitation of clastic materials developed in the stratified ancient Lake Uinta. Stability of the stratification produced the continuous deposition of the organic matter and its uniformity over the deposit. Chemical formation of the oil-shale minerals proceeded naturally from the lake stratification, and the varve production

stemmed from the seasonable development of organic matter. The
lake's stratification produced uniform deposition over the
entire area it covered, making the correlatable lateral persis-
tence of the thin laminations a natural consequence. As the
lake developed, the attack on aluminosilicates by sodium carbonate
in the lake's lower layer produced a silicate skeleton protected
by aluminum trihydroxide. On deposition this aluminum-rich
skeleton formed illite in quantity. As the lake became more
basic, the protecting aluminum hydroxide coating dissolved
amphoterically, and illite production dropped. Continual build-
up of sodium carbonate and aluminate ion in the water of the
lake's lower layer reached conditions which precipitated dawsonite
and crystallized nahcolite in the sediment as a result of CO_2
production from organic matter.

Literature Cited

1. Bradley, W. H., *Am. Assoc. Pet. Geol. Bull.*, 1925, p. 247.
2. Smith, J. W.; Robb, W. A., U. S. BuMines Rept. Inv. 7727,
    1973, 21 p.
3. Smith, J. W., in "Twenty-Fifth Field Conference Guidebook",
    D. K. Murray, Rocky Mountain Assn. Geol., Denver, 1974,
    p. 71.
4. Smith, J. W.; Lee, K. K., *Proc. 15th Oil Shale Symposium*,
    J. H. Gary, Ed.; Colorado School of Mines, Golden, 1983,
    p. 101.
5. Smith, J. W., Oil Shale Resources of the United States,
    Mineral and Energy Resources Series, V 23, No. 6, 1980.
6. Beard, T. N.; Tait, D. B.; Smith, J. W., in "Twenty-Fifth
    Field Conference Guidebook", D. K. Murray, Ed.; Rocky
    Mountain Assn. Geol. Denver, 1974, p. 101.
7. Roehler, H. W., in "Twenty-Fifth Field Conference Guidebook",
    D. K. Murray, Ed., Rocky Mountain Assn. Geol., Denver,
    1974, p. 57.
8. Trudell, L. G.; Smith, J. W.; Beard, T. N.; Mason, G.,
    U.S.D.O.E. LETC Rept. Inv.-82/4, 1982, 32 p.
9. Culbertson, W. C.; Smith, J. W.; Trudell, L. G., Laramie
    Energy Technology Center Rept. Inv.-80/6, 1980, 120 p.
10. Picard, M. D.; Thompson, W. D.; Williamson, C. R. Bulletin
    100, Utah Geological and Mineralogical Survey, Salt Lake
    City, 1973, 52 p.
11. Smith, J. W., Trudell, L. G., and Dana, G. E., U. S. BuMines
    Rept. Inv. 7071, 1968, 28 p.
12. Smith, J. W., *Am. Assoc. Pet. Geol. Bull.*, 1963, 47, p. 804.
13. Smith, J. W.; Harbaugh, J. W., U. S. BuMines Rept. Inv.
    6883, 1966, 11 p.
14. Robinson, W. E., Cook, G. L., U. S. BuMines Rept. Inv.
    7492, 1971, 32 p.
15. Trudell, L. G.; Beard, T. N.; Smith, J. W., U. S. BuMines
    Rept. Inv. 7357, 1970, 226 p.

16. Smith, J. W., U. S. BuMines Rept. Inv. 5725, 1961, 16 p.
17. Giauque, R. D.; Fox, J. P.; Smith, J. W., Lawrence Berkeley Laboratory Report LBL-10809, 1980, 176 p.
18. Frey, D. G., "Limnology in North America"; University of Wisconsin Press, Madison, Wis., 1963, 734 p.
19. Hutchinson, G. E., A contribution to the limnology of arid regions: <u>Trans</u>. <u>Connecticut</u> <u>Acad</u>. <u>Arts</u> <u>Sci</u>., 1937, 33, p. 47.
20. Garrels, R. M., Mackenzie, F. T., "Evolution of sedimentary rocks"; W. W. Norton, New York, N.Y., 1971, 397 p.
21. Parrington, J. R., Zoller, W. H., Aras, N. K., <u>Science</u>, 1983, 220, p. 195.
22. Loughnan, F. C., "Chemical weathering of silicate minerals"; American Elsevier, Inc., New York, N.Y., 1969, 154 p.
23. Garrels, R. M., "Mineral equilibria"; Harper and Brothers, New York, N.Y., 1960, 254 p.
24. Smith, J. W.; Young, N. B.; Monster, J., <u>Proc</u>. <u>16th</u> <u>Oil</u> <u>Shale</u> <u>Symposium</u>, J. H. Gary, Ed., Colorado School of Mines, Golden, 1983.
25. Robb, W. A.; Smith, J. W.; Trudell, L. G., U.S.D.O.E. LETC Rept. Inv.-78/6, 1978, 39 p.
26. Bader, E.; Esch, U., <u>Zeitschrift</u> <u>fur</u> <u>Elektrochemie</u>, 1944, 50, p. 266.
27. Milton, C.; Eugster, H. P., in "Researches in Geochemistry"; P. H. Abelson, Ed., John Wiley and Sons, New York, N.Y., 1959, p. 118.

Inorganic Geochemistry of Mahogany Zone Oil Shale in Two Cores from the Green River Formation

MICHELE L. TUTTLE, WALTER E. DEAN, and NANCY L. PARDUHN

U.S. Geological Survey, Denver Federal Center, Denver, CO 80225

The abundance and distribution of 8 major elements (Al, Ca, Fe, K, Mg, Na, Si, and Ti) and 18 trace elements (As, B, Ba, Co, Cr, Cu, La, Li, Mn, Mo, Ni, Pb, Sc, Sr, V, Y, Zn, and Zr) were determined in oil-shale samples from the oil-rich Mahogany zone in two cores of the Green River Formation in the Piceance basin, Colorado. The abundance and distribution of the elements are similar within each core. The Mahogany zone is low in trace elements and high in carbonate-related elements compared to the literature averages for shales and black shales. Q-mode factor modeling was used to group samples into four factors on the basis of compositional similarities. The chemistry, shale-oil yield, and mineralogy of the samples within each group were examined. The factors are: 1) samples containing relatively high concentrations of shale oil and adsorbed or sulfide-associated trace elements, 2) samples containing relatively high concentrations of elements of detrital or volcanic origin, 3) samples containing relatively high concentrations of carbonate-related elements, and 4) samples compositionally similar to those in factor 3, but also containing the trace metals Co, Mo, Ni, and V. Elements having relatively high concentrations within each factor show similar down-hole variations in abundance in each of the two cores.

In northwest Colorado, the Parachute Creek Member of the lacustrine Green River Formation (Eocene) contains thick sequences of rich oil shale that were deposited in ancient lake Uinta. The richest sequence and the richest oil-shale bed within the Parachute Creek Member are called the Mahogany zone

and the Mahogany bed, respectively. The Mahogany zone, containing the Mahogany bed and as much as 40 m of oil shale (1), is stratigraphically between two lean shale-oil zones, the A-groove at the top and the B-groove at the base. The Mahogany oil shale is a kerogen-rich, dolomitic marlstone, commonly containing altered volcanic tuff beds, laminae, and lenses.

Essentially two depositional models have been proposed for ancient lake Uinta, the permanently stratified (meromictic) lake model (2-6) and the playa-lake model (7). Boyer (8) suggested that the two models may be complementary rather than mutually exclusive in that the laminated lacustrine sediments may have been deposited in a meromictic lake within a saline-playa complex. Regardless of which depositional model is correct, the unusual chemical and biological conditions that existed within the lake and its sediments are recorded by the unique mineral assemblage and organic content of the Green River oil shale. During Mahogany times, the lower lake and sediment waters were anoxic and alkaline. These conditions produced sulfides and carbonates (calcite, dolomite, siderite, dawsonite, and nahcolite) and preserved large amounts of organic material. Continuous laminated sediments indicate an absence of burrowing organisms, so bacteria would have been the only organisms.

The distribution of eight major elements within oil-shale minerals was estimated by Desborough and others (10) from major element and bulk mineral data. Saether and others (11) described similar element distributions on the basis of mineral and element contents of different density fractions of Mahogany oil shale. Some minor and accessory minerals have been identified as containing certain trace elements, but most trace-element distributions are based on correlations with major elements and minerals. Therefore, some uncertainty exists as to their residence.

This study provides another approach to the study of major- and trace-element distribution in oil shale. The geochemical abundance and stratigraphic distribution of major and trace elements were determined in samples of oil shale from the Mahogany zone in two cores, U.S. Geological Survey core-hole CR-2 (T. 1 N., R. 97 W., Rio Blanco County) and U.S. Bureau of Mines core-hole 01-A (T. 1 S., R. 97 W., Rio Blanco County). The cores are 12 km from one another (Figure 1) with the oil shale from core-hole CR-2 being deposited nearer the margin of lake Uinta than oil shale from core-hole 01-A. The data for each core are compared using elemental abundances, arithmetic mean (12), and Q-mode factor modeling. The Q-mode factor models for each core are used to interpret the abundances and stratigraphic distributions of the elements in terms of association with oil-shale minerals and organic matter. Possible geochemical processes controlling these distributions are discussed.
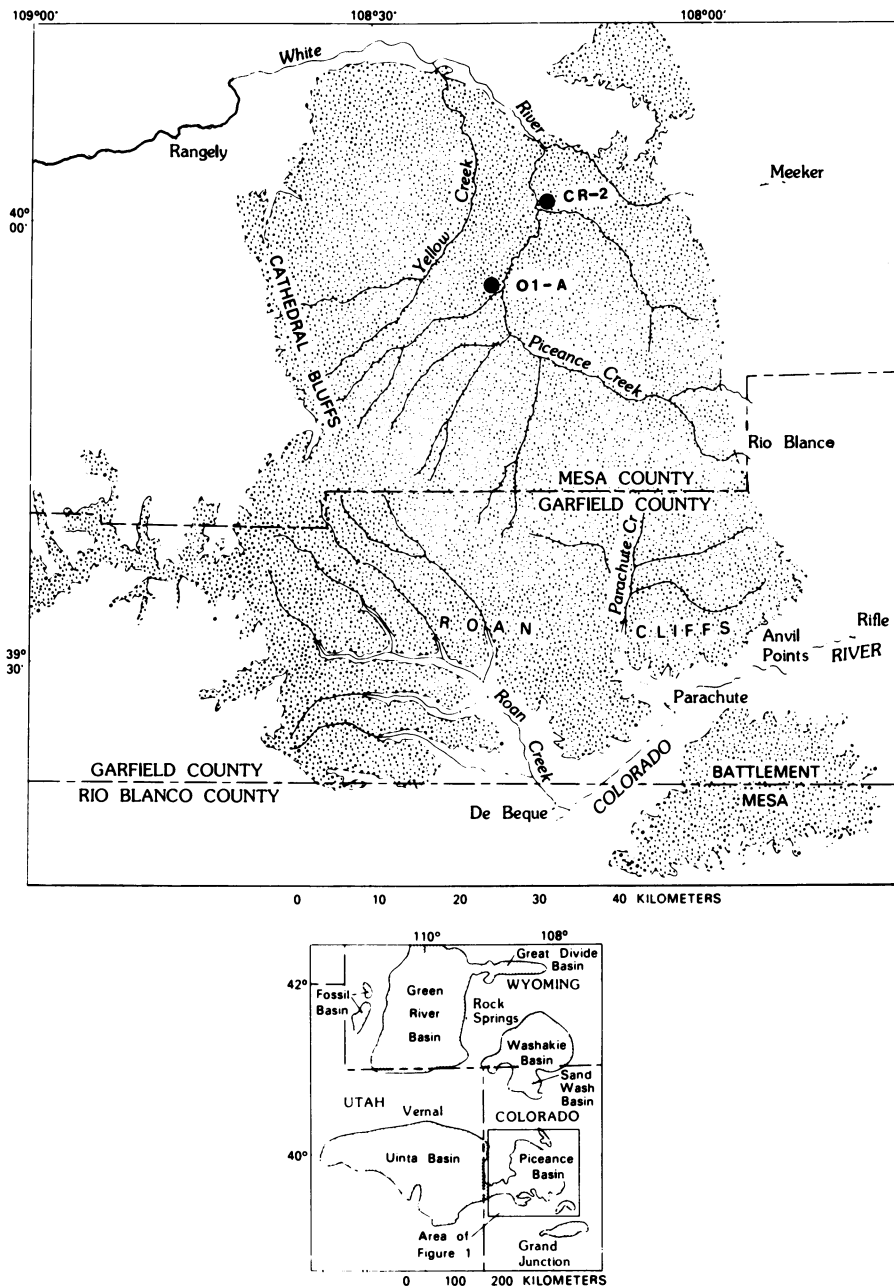
Figure 1. Index map of Piceance basin showing location of core holes CR-2 and 01-A. Stippled area is underlain by the Green River Formation.

Analytical Methods

Forty-four samples of Mahogany oil shale are from core-hole CR-2 between the depths of 237 and 300 m, and 76 from core-hole 01-A between the depths of 273 and 328 m. The samples are splits of larger samples representing 0.3-m lengths of core that were originally collected for Fischer assay analyses. The splits were ground to pass a 100-mesh screen and were analyzed for major elements by wavelength-dispersive X-ray fluorescence analysis (13). Trace elements were semiquanitatively determined in the CR-2 samples by argon-oxygen D-C arc optical-emission spectroscopy (14), and in the 01-A samples by induction-coupled argon-plasma, optical-emission spectroscopy (15). The chemical data for CR-2 samples are part of a larger data set reported by Dean and others (16).

Mineral data (relative concentrations) are available for most samples from the CR-2 core (16) and the 01-A core (17). Bulk mineralogy was determined by X-ray diffraction using nickel-filtered CuKα radiation. The mineral data are reported in X-ray diffraction peak intensities for the following minerals:

Mineral	Peak position (degrees 2θ)	
	CR-2 (16)	01-A (17)
analcime	26.0	26.0
calcite	29.4	29.5
dawsonite	15.9	15.6
dolomite	30.9	30.9
illite	8.9	8.8
potassium feldspar	27.5	27.6
siderite	32.0	32.0
sodium feldspar	28.0	28.0
quartz	26.6	26.6

Because neither of the data sets have been internally standardized, comparison among the minerals of one core, or the mineral content in two cores is not possible.

Results and Discussion

Elemental Analyses. The elemental data are summarized in Table 1 and Figure 2. Significant differences (95-percent probability level) in element concentration between cores are higher concentrations of Ca, Cu, La, Ni, Sc, and Zr in the CR-2 samples, and higher concentrations of As and Sr in 01-A samples. These differences in elemental abundances reflect

Table I. Chemical abundances ($\bar{x}$), standard deviation (s.d.), and observed range of major and trace elements in Mahogany-zone samples from oil-shale cores 01-A and CR-2

Elements	01-A			CR-2		
	$\bar{x}$	s.d.	observed range	$\bar{x}$	s.d	observed range
Major elements (pct)						
Al	3.6	0.82	2.1–6.2	3.3	0.75	1.6–5.6
Ca	11	3.17	4.6–19	13	4.20	6.5–32
Fe	1.9	.50	1.0–3.3	2.0	.43	1.1–3.3
K	1.4	.61	.65–4.1	1.3	.39	.25–2.2
Mg	3.2	.79	1.2–5.2	3.0	.64	.32–4.1
Na	1.5	.45	.44–2.8	1.5	.43	.10–2.5
Si	13	2.40	8.6–22	13	2.43	6.7–22
Ti	.16	.04	.09–.27	.16	.03	.06–.24
Trace elements (ppm)						
As	40	33.8	14–190	16	5.96	4.3–29
B	82	68.1	14–300	107	82	13–400
Ba	450	77.7	270–630	400	106	220–690
Co	8.6	3.51	3.0–18	10	1.79	6.3–14
Cr	34	11.9	18–110	32	9.76	16–71
Cu	32	15.2	9.0–79	52	20.9	19–120
La	19	8.34	6.0–40	33	10.9	13–60
Li	58	31.5	20–210	51	28.8	13–140
Mn	310	77.9	200–730	290	67.5	190–520
Mo	22	10.9	3.0–53	18	7.98	7.4–44
Ni	16	9.47	3.0–44	26	5.20	18–46
Pb	28	12.5	20–80	23	11.5	3.5–68
Sc	4.3	2.72	3.0–18	6.0	1.75	2.8–11
Sr	790	261	130–1300	590	161	200–990
V	83	29.1	43–190	78	24.5	37–145
Y	10	3.94	6.0–29	13	5.33	7.5–40
Zn	77	24.4	39–180	78	17.3	47–136
Zr	48	13.7	30–120	70	15.7	30–100
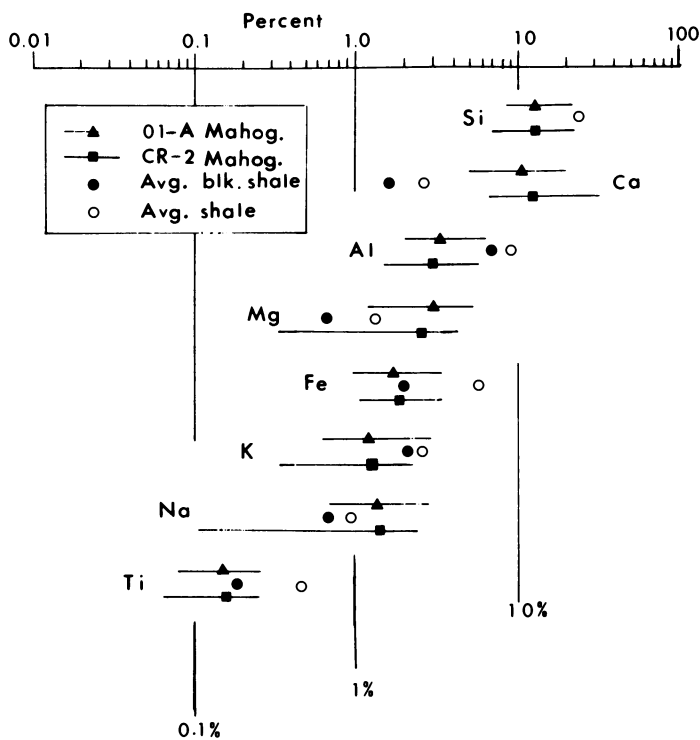
Figure 2.   Observed ranges and geometric means of elemental abundances in 01-A and CR-2 Mahogany zone core samples. Average shale (16) and average black shale (17) are also represented.
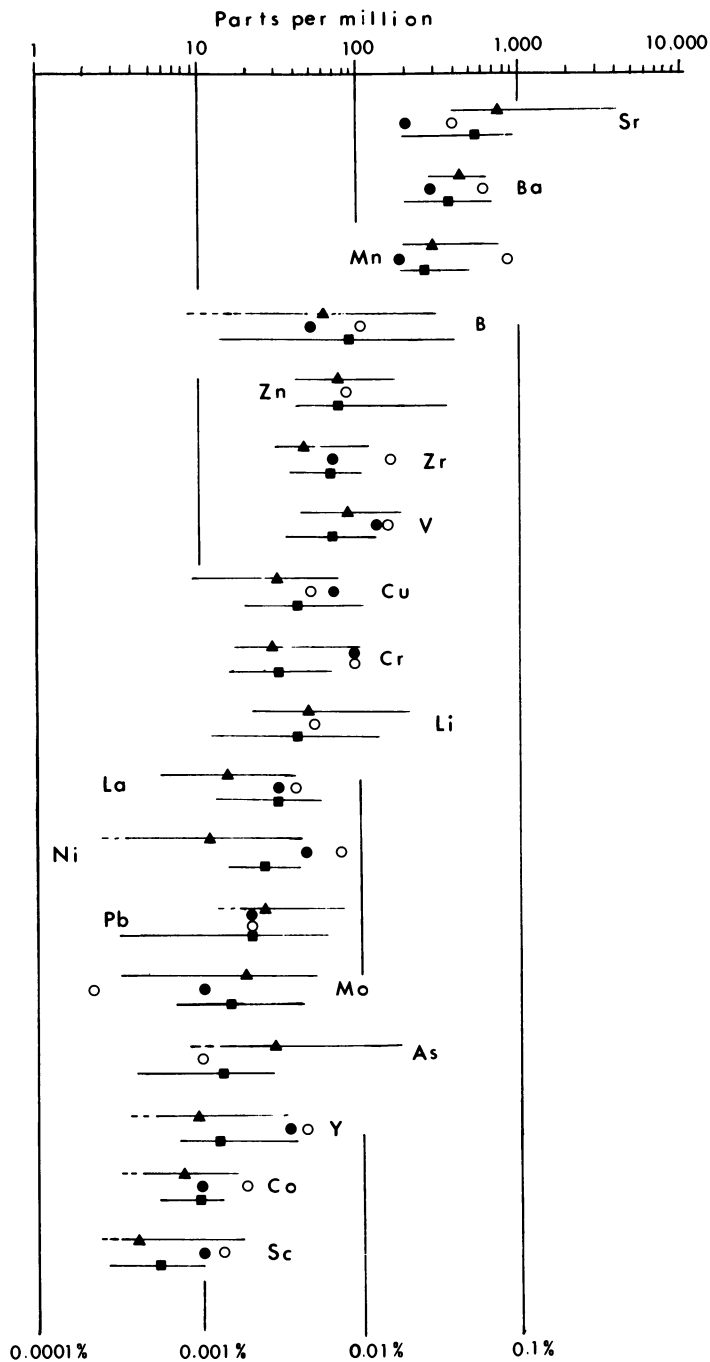
Figure 2. Continued.

slightly different depositional conditions, sediment source material, or diagenesis at the two sites.

Abundances of elements in average shale (18) were plotted in Figure 2 for comparison with the Mahogany data. Vine and Tourtelot (19) compiled a report on elemental abundances in black-shale deposits, including Mahogany oil shale. Their average abundances of elements in black shale also are plotted in Figure 2. These two averages provide two reference points for evaluating how the abundances of elements in Mahogany oil shale compare to other lithologies. Oil shale from the Green River Formation contains several carbonate minerals that vary considerably in abundance and composition (5, 20). As a result, oil shale from the Mahogany zone in the two cores contains higher concentrations of carbonate-related elements (Ca, Mg, Sr, and Na) than average shale or black shale. The abundance of organic carbon is 7.3 percent in the CR-2 core and is 3.2 percent in the average black shale (19). The carbonate minerals and, in some cases, the organic matter act as dilutants so that Mahogany oil shale contains lower concentrations of most trace elements than average shale and black shale (Figure 2).

Q-mode Factor Modeling. A Q-mode factor analysis was performed to determine if any grouping of oil-shale samples occurred on the basis of chemical compositional similarities. The computer program used for the analysis is the extended CABFAC program described by Klovan and Miesch (21). Prior to the analyses, all compositional measurements (percent or parts per million) were normalized to a proportion of their range of concentrations so that all data were on a scale of 0.0 to 1.0. Q-mode factor analysis is a mathematical procedure applicable to analysis of data matrices containing a large number of samples and a large number of variables (in our case, chemical data). The factor analysis determines if a small number of element groups exist that describe the samples almost as well as the large number of the individual elements. The original data matrix is simplified by determining the number of element groups present (the number of factors), the composition of each group in terms of the original elements (determined by ranking each element's importance in the factor and assigning factor scores to each element on the basis of their rank), and a description of each sample in terms of the relative proportion of each group in that sample (factor loading).

Our 26 observed chemical variables are reduced to four groups (factors) by the analysis, explaining 70 percent of the variance in the normalized CR-2 data and 64 percent of the variance in the normalized O1-A data. Increasing the number of factors did not significantly increase the variance explained. The elements that were most important (high factor scores) in grouping samples from each of the two cores into each of the four factors are listed in Table II in decreasing order of

Table II. Elements in 01-A and CR-2 Mahogany oil shale that had
the greatest influence in grouping samples into each of
the four Q-mode factors listed in descending order
of factor scores (n, number of samples
within each factor group)

Factor 1		Factor 2		Factor 3		Factor 4	
01-A n=21	CR-2 n=21	01-A n=5	CR-2 n=13	01-A n=30	CR-2 n=8	01-A n=19	CR-2 n=1
Cu	V	Sc	Sc	Ba	Ca	Ni	Sr
V	Mo	Y	Ba	Sr	Sr	Ca	V
Co	Cu	Mn	Al	La	Mg	Sr	Ca
Mo	Ni	Al	Fe	Ca	Na	Mg	La
B	Pb	Ti	Ti	Na	Ba	Mo	Ni
Pb	B	La	Zr	Mg	Li		Co
Zn	Cr	Fe	Y				
	Li	Cr	La				
	Co	Zr	K				

factor scores. The average concentrations of these elements and the minerals in samples from each core grouped into each factor are listed in Table III.   Smoothed   profiles   of   element concentration for these elements in each factor for samples from the 01-A core and for the CR-2 core are shown in Figures 3-6. The smoothed curve is based on a 5-point weighted moving average for 01-A data (76 samples) and a 3-point weighted moving average for CR-2 data (44 samples).

Factor-1 samples contain high concentrations of many trace elements, particularly boron and the transition elements Co, Cu, Mo, Ni, Pb, Zn, and V (Table III).   These samples also contain illite (CR-2 core) and relatively high concentrations of analcime and oil (both cores) which suggests that adsorption of trace elements onto clay, altered tuffaceous material, and (or) organic matter may be important in controlling the distribution of these trace elements. The sulfide phase also may control the occurrence of these metals (10-11).   Factor 1 samples also contain relatively high concentrations of sodium feldspar in both the CR-2 and 01-A cores.   Moore (22) also observed a correlation between authigenic sodium feldspar and organic matter of Green River oil shale.   The presence of boron in factor-1 samples is consistent with high concentrations of feldspars.   Milton and others (23) reported reedmergnerite (an authigenic boron-rich albite) occurring in Green River oil shale. Desborough and others (10) concluded that boron resides mainly in potassium feldspar, and Sheppard and Gude (24) found boron in authigenic potassium feldspar from closed basins. Concentrations of potassium feldspar, however, are high in factor-2 samples (see discussion following) in both cores. This suggests either that boron is present only in the sodium feldspars or, more likely, that boron is in both authigenic potassium and sodium feldspars in factor-1 samples but that the more abundant potassium feldspars in factor-2 samples are more detrital or volcanic in origin and have lower concentrations of boron.

Factor-2 samples contain relatively high concentrations of elements commonly associated with minerals of detrital or volcanic origin.   In general, the clastic (1, 4) and, more specifically, tuffaceous (25) material increases to the northeast in the Piceance basin so that the CR-2 core should contain more tuffaceous material. Because the CR-2 core is closer to the basin margin, (Figure 1), it should also contain more detrital material. Table III shows that factor-2 samples in the CR-2 core contain considerably more analcime, which is a common alteration mineral within the tuff beds of the Green River Formation closest to the basin margins (25).   Factor-2 samples from the 01-A core do not contain detectable analcime (Table III) but do contain dawsonite which may have formed by reaction of analcime with CO_2 (26). Griggs (25) reported that analcitized tuffs dominate around the edge of the basin and
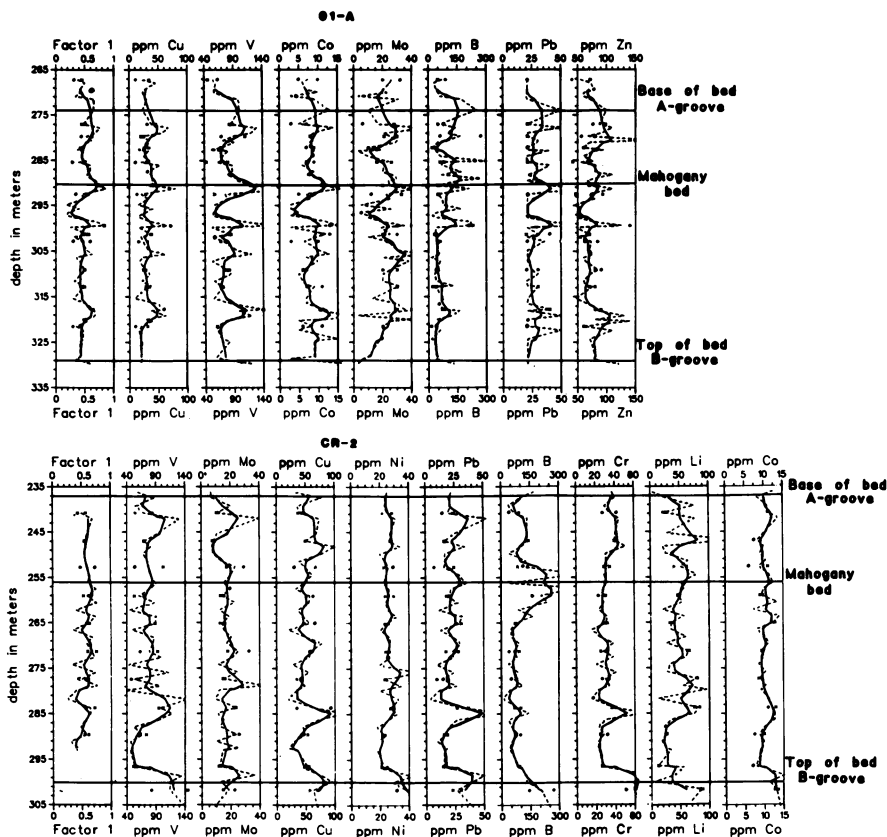
Figure 3. Distribution of Factor 1 elements and factor loadings in core 01-A and CR-2 as a function of depth. Key: ----, raw data; and ——, smoothed data.
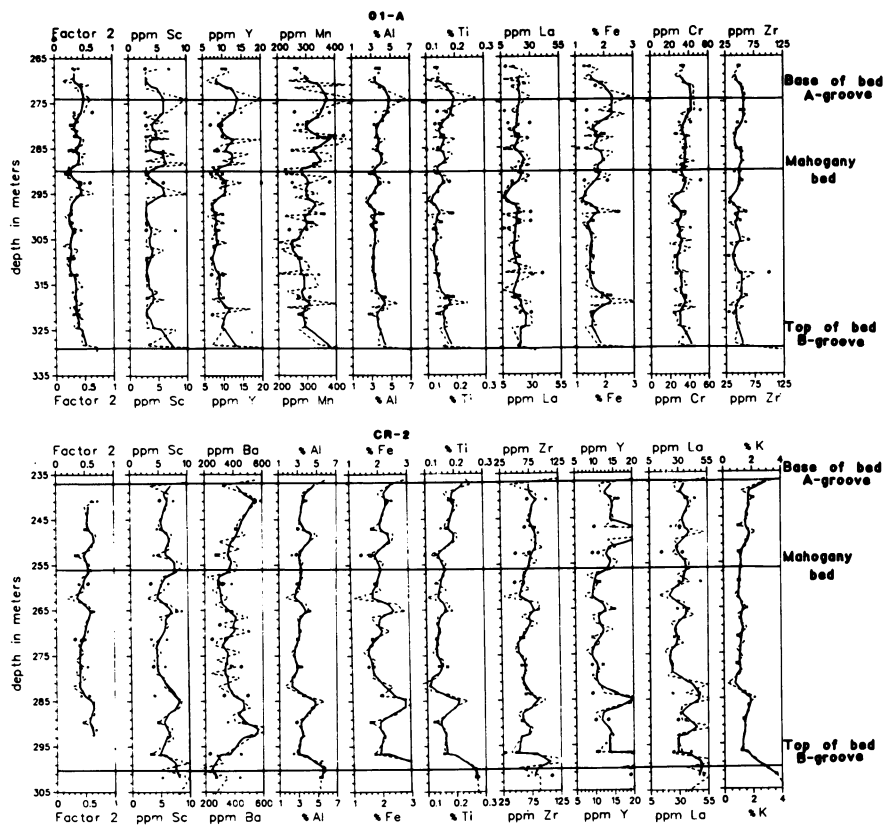
Figure 4. Distribution of Factor 2 elements and factor loadings in core 01-A and CR-2 as a function of depth. Key: ----, raw data; and ——, smoothed data.
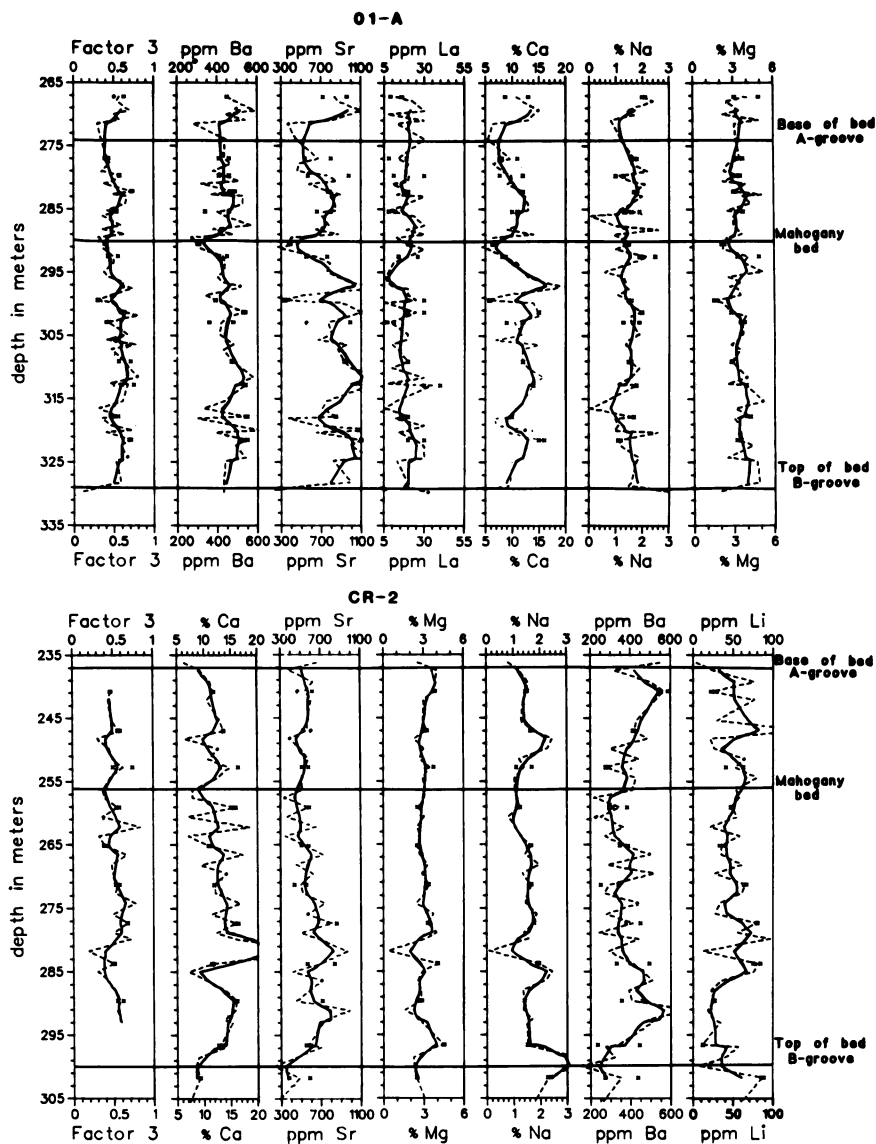
Figure 5.   Distribution of Factor 3 elements and factor loadings in core 01-A and CR-2 as a function of depth. Key: ----, raw data; and ——, smoothed data.
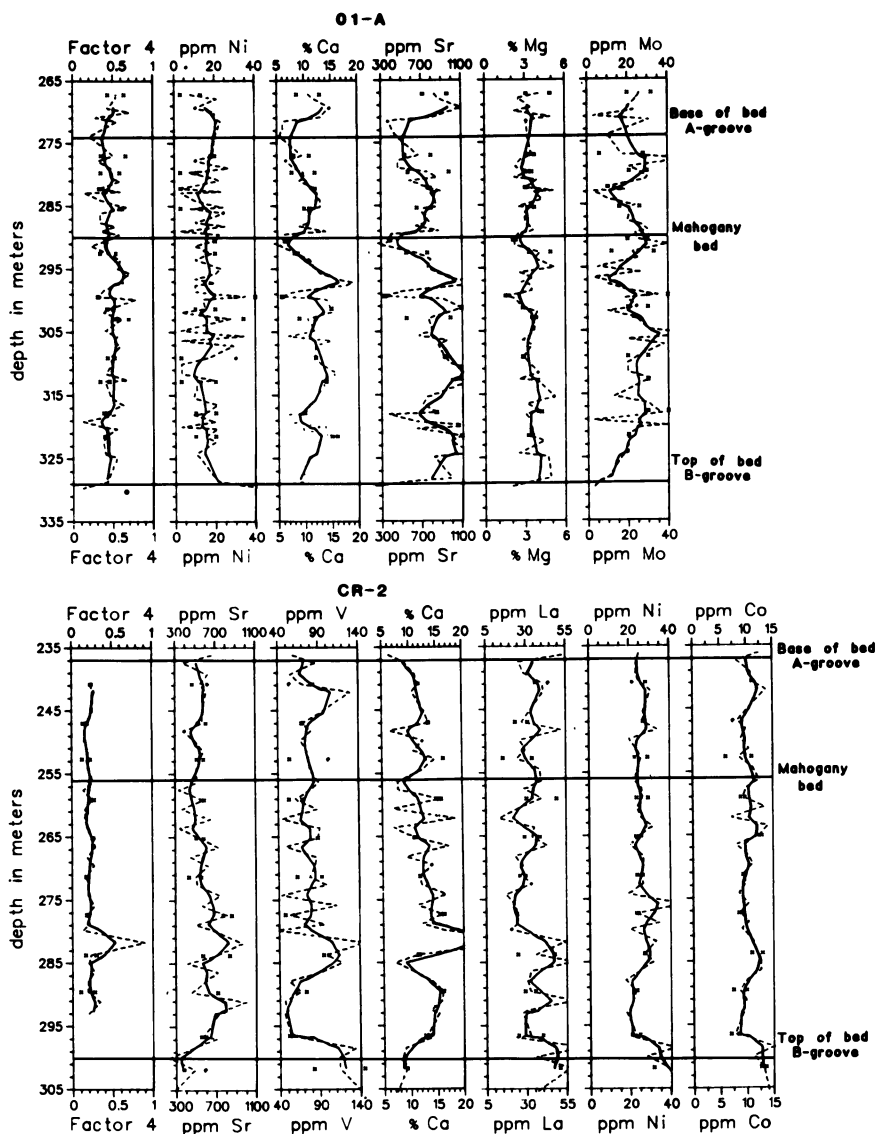
Figure 6. Distribution of Factor 4 elements and factor loadings in core 01-A and CR-2 as a function of depth. Key: ----, raw data; and ———, smoothed data.

Table III.--Abundances for the major and trace elements listed in Table II, relative mineral abundances, and average oil yield for CR-2 and 01-A core samples within the four Q-mode factor group (F1-F4); (-, detected in less than 50 % of the samples; n.d., mineral not determined; XRD, X-ray diffraction)

Element or mineral	01-A				CR-2			
	F1	F2	F3	F4	F1	F2	F3	F4
Major elements (%)								
Al	3.7	4.2	3.6	3.4	3.3	3.8	2.6	1.6
Ca	10	9.5	11	12	11	12	16	32
Fe	2.0	2.1	1.9	1.8	2.0	2.3	1.5	2.4
K	1.4	1.6	1.3	1.3	1.3	1.6	1.0	.25
Mg	3.0	3.8	3.3	3.1	3.2	2.9	3.0	.32
Na	1.4	1.7	1.5	1.4	1.5	1.7	1.4	.10
Ti	.16	.19	.15	.15	.16	.18	.13	.06
Trace elements (ppm)								
B	120	100	51	79	140	75	87	13
Ba	390	420	510	430	350	480	410	290
Co	11	9.6	8.3	6.3	11	11	8.3	11
Cr	36	59	27	34	35	30	27	16
Cu	49	24	26	26	60	49	35	19
La	20	25	23	9.4	33	39	23	55
Li	53	51	59	62	61	36	57	13
Mn	300	470	325	260	280	290	280	360
Mo	30	7.4	19	23	22	14	15	9.7
Ni	21	25	10	18	28	23	23	33
Pb	38	27	25	21	29	21	13	3.5
Sc	4.0	11	3.1	4.9	5.8	7.2	4.6	5.7
Sr	540	450	990	850	510	640	680	970
V	120	94	69	66	91	68	54	150
Y	10	21	8.9	9.0	13	16	9.5	11
Zn	98	98	68	64	84	79	59	85
Zr	54	69	43	43	71	77	54	62
Minerals (XRD peak height) and oil (%)								
Analcime	6	-	5	-	9	15	8	n.d.
Calcite	15	11	27	24	10	15	16	n.d.
Dawsonite	7	13	-	10	-	-	-	n.d.
Dolomite	71	79	82	77	49	47	46	n.d.
Illite	-	-	-	-	2	2	-	n.d.
K-feldspar	15	19	13	15	7	7	6	n.d.
Mg-siderite	8	11	6	-	n.d.	n.d.	n.d.	n.d.
Na-feldspar	28	21	24	30	18	13	14	n.d.
Quartz	71	89	67	75	37	33	28	n.d.
Oil yield	15	7.8	9.4	9.9	11	7.5	8.5	.08

grade into feldspathized tuffs containing authigenic potassium feldspars towards the center of the basin. The low analcime and the high potassium feldspar content in the 01-A core factor-2 samples may be reflecting such feldspathization. Factor-2 samples also contain the lowest concentrations of oil (Table III) which may be due to the diluting effect of more abundant detrital and (or) tuffaceous material. Iron concentrations are relatively high in factor-2 samples from both cores. Iron is reported as occurring as sulfides or iron carbonates (10-11). The only data on sulfur that we have are for ashed samples. These minimum sulfur data should, however, give an approximate indication of the amount of sulfide sulfur present. Little difference exists in ashed-sample sulfur among samples from the four factors, suggesting that the iron differences among the factors are not due to differences in concentrations of iron sulfides. The higher iron content in factor-2 samples may simply be due to the higher amount of tuffaceous material. Another possible source of iron differences may be differences in amount of siderite (iron carbonate) and ferroan or ankeritic dolomite. X-ray diffraction results from the 01-A core show that magnesium-rich siderite is more abundant in factor-2 samples than in samples from any of the other three factors from the 01-A core. Substitution of manganese for iron in carbonate minerals could also explain the relatively high concentrations of manganese in factor-2 samples from the 01-A core (Table III); manganese does not appear to influence the groupings in any of the other factors.

Factors 3 and 4 are essentially carbonate factors. Concentrations of calcium and strontium are high in both factor 3 and factor 4; calcium is in both calcite and dolomite, and strontium substitutes for calcium in both minerals (27). Dolomite appears to be evenly distributed among the factors for both cores, but factor-3 and -4 samples from the 01-A core have higher concentrations of calcite. Concentrations of lanthanum and barium in one or both of the factors are also relatively high; lanthanum substitutes for calcium, and barium can precipitate as a carbonate along with the other alkaline-earth carbonate minerals (28). The concentration of lithium is relatively high in factor-3 and factor-1 samples from the CR-2 core. Desborough and others (10) reported a correlation between Li and Mg, Ca, and F; they suggested that lithium occurs as a carbonate. Cook (29) reported lithium occurring as a carbonate mineral. We did not have fluorine analyses on samples from the 01-A core, but a significant correlation exists between fluorine and lithium in samples from the CR-2 core. Saether (11) concluded that fluorine occurs mainly in illite in Mahogany-zone oil shale. The association between lithium and fluorine in CR-2 samples, and the association between lithium and fluorine in ground waters in the Piceance basin (30) suggest that lithium

may, like fluorine, occur in clay minerals.   The importance of
sodium in defining factor-3 for both cores suggests that at
least some of the sodium may be present in carbonate minerals.
Nahcolite (sodium bicarbonate) is ubiquitous in zones below the
Mahogany zone where leaching by ground water has not taken
place.   The importance of sodium in factor-3 samples from both
cores, however, may indicate that some nahcolite in the Mahogany
zone, below the detection limit of X-ray diffraction, may have
escaped dissolution by the ground waters.
       The importance of nickel in both cores, molybdenum in the
01-A core, and cobalt and vanadium in the CR-2 core in defining
factor-4 is not obvious.   The absence of other trace metals in
this factor suggests that sulfide precipitation or adsorption
processes may not control the occurrence of these four metals
within factor-4 samples.   Abelsonite, a nickel porphyrin, has
been described from the Mahogany zone of the Green River
Formation in Utah (31).   Milton and others (31) stated that the
mineral probably is present in an extensive area of the Green
River Formation.   Cobalt, molybdenum, and vanadium also form
metal-organic complexes (28).   Lewan and Maynard (32) have
identified metal enrichment in bitumens associated with Type I
and Type II kerogen due to metallation of tetrapyrroles
(metallo-organic complexes).   They reported metallation
enrichment of nickel in Green River oil shales (Type I kerogen)
from Utah and Wyoming. Some vanadium concentrations in bitumen
extracted from these samples were close to the theoretical
boundary between endemic and enriched concentrations.

Conclusions

       The Mahogany zone of the Green River Formation is rich in
carbonate-related elements and poor in most trace elements
compared to an average shale or average black shale.   The two
cores have similar chemistry, although CR-2 samples have more
Ca, Cu, La, Ni, Sc, and Zr and 01-A samples have more As and
Sr.   These differences probably reflect slight differences in
depositional conditions, sediment source areas, or diagenesis.
       The sample suite from each core can be divided into four
factors on the basis of similarities in chemical compositions as
defined by Q-mode factor modeling.   Factor-1 samples are rich in
trace metals due to adsorption onto clay, altered tuffaceous
material, and (or) organic matter; and   precipitation as
sulfides. The relatively high concentration of boron is probably
related to its inclusion in authigenic feldspars.   Factor-2
samples are rich in elements commonly associated with minerals
of detrital or volcanic origin.   These samples contain
relatively high concentrations of analcime, dawsonite, and (or)
potassium feldspar, all of which are associated with alteration
of tuffaceous material.   Siderite and ferroan or ankeritic

dolomite probably are the main minerals containing iron and manganese in factor-2 samples. Factors 3 and 4 are carbonate factors. These samples contain higher concentrations of carbonate-related elements and, in core 01-A, calcite and dolomite. The elements Ba, La, Li, and (or) Sr are important in defining factors 3 and 4; this reflects substitution of these elements for calcium in calcite and dolomite, or their precipitation as carbonates along with the other alkaline-earth carbonates. The metals Co, Mo, Ni, and V also define factor 4. Metal-organic complexes may be important in controlling the occurrence of these metals in Factor 4 samples. These Q-mode results are consistent with other studies on element residence (4, 5, 10, 11, 19, 20, 23, 29 31, 32), however, the models indicate that some elements (particularly the trace elements) may have more than one mineral residence.

Acknowledgments

Literature Cited

1. Trudell, L. G.; Beard, T. N.; Smith, J. W. U.S. Bur. Mines Rept. Inv. 7357 1970, 1-10.
2. Bradley, W. H. U.S. Geol. Surv. Prof. Paper 158 1929, 86-110.
3. Bradley, W. H. "Limnology in North America"; Frey, D. G., Ed.; University of Wisconsin Press: Madison, 1963, 621 p.
4. Smith, J. W. "Rocky Mountain Association of Geologists Guidebook to the Energy Resources of the Piceance Creek Bain, Colorado, 25th. Field Conference"; Murray, D. K., Ed.; Rocky Mountain Association of Geologists: Denver, 1974, 71-80.
5. Desborough, G. A. Geol. Soc. America Bull. 1978, 89, 961-971.
6. Johnson, R. C. Geology 1981, 9, 55-62.
7. Lundell, L. L.; Surdam, R. C. Geology 1975, 3, 493-497.
8. Boyer, B. W. Geology 1982, 10, 321-324.
9. Eugster, H. P.; Surdam, R. C. Geol. Soc. American Bull. 1973, 84, 1115-1120.
10. Desborough, G. A.; Pitman, J. K.; Huffman, C., Jr. Chem. Geology 1976, 17, 13-26.
11. Saether, O. M., Runnells, D. D., and Meglen, R. R., "Trace Elements in Oil Shale Progress Report C00-10298-1"; Chappel, W. R.; Runnells, D. D., Eds.; U.S. Department of Energy, 1980, p. 237-255.
12. Miesch, A. T. U.S. Geol. Surv. Prof. Paper 574-5 1967, 1-15.

13. Taggart, J. E.; Lichte, F.E.; Wahlberg, J. S. U.S. Geol. Surv. Prof. Paper 1250 1981, 683-687.

14. Dorrzaph, A. F., Jr U.S. Geol. Surv. Jour. Res. 1973, 5, 559-562.

15. Floyd, M. A.; Fasel, V. A., D'Silva, A. P. Anal. Chem. 1980, 52, 2166-2173.

16. Dean, W. E.; Pitman, J. K.; Harrach, G. H. U.S. Geol. Surv. Open-file Rpt. 81-59 1981, 1-25.

17. Robb, W. E., Department of Energy, unpublished data.

18. Krauskopf, K. B. "Introduction to Geochemistry"; McGraw-Hill Book Company: New York, 1979, 617 p.

19. Vine, J. D.; Tourtelot, E. B. Econ. Geology 1970, 65, 253-272.

20. Desborough, G. A.; Pitman, J. K. "Rocky Mountain Association of Geologists Guidebook to the Energy Resources of the Piceance Creek Basin, Colorado, 25th. Field Conference"; Murray, D. K., Ed.; Rocky Mountain Association of Geologists: Denver, 1974, 81-90.

21. Klovan, J. E.; Imbrie, J. Jour. Internat. Assoc. Math. Geol. 1971, 3, 61-77.

22. Moore, F. E. Jour. Sed. Pet. 1950, 20, 227-231.

23. Milton, C.; Chao, E. C. T.; Axelrod, J. M.; Grimaldi, F. S. Am. Mineralogist 1960, 45, 188-199.

24. Sheppard R. A.; Gude, A. J. U.S. Geol. Surv. Jour. Res. 1973, 1, 377-382.

25. Griggs, R. L. U.S. Geol. Surv. Open-file Rpt. 1968, 1-38

26. Brobst, D. A.; Tucker, J. D. U.S. Geol. Surv. Prof. Paper 803 1973, 1-53.

27. Bathurst. R. G. C. "Carbonate Sediments and Their Diagenesis"; Elsevier Scientific Publishing Company; New York, 1971, 658 p.

28. Rankama K.;Sahama T. G. "Geochemistry"; The University of Chicago Press: Chicago, 1950, 912 p.

29. Cook, E. W.; Chem. Geology 1973, 11, 321-324.

30. Ficke,J. F.; Weeks, J. B.; Welder, F. A. Colo. Water Resour. Basic Data Release 31 1974, 246 p.

31. Milton C.; Dwornik, E.J.; Estep-Barne, P. A.; Finkelman, R. B.; Pabst, A.; Palmer, S. Am. Mineralogist 1978, 68, 930-937.

32. Lewan, M. D.; Maynard, J. B. Geochim. et Cosmochim. Acta 1982, 46, 2547-2560.

Pyrolysis Kinetics of Several Key World Oil Shales

H. E. NUTTALL, TIAN-MIN GUO,[1] SCOTT SCHRADER, and D. S. THAKUR[2]

The University of New Mexico, Department of Chemical and Nuclear Engineering, Albuquerque, NM 87131

World oil shales vary widely in geological age and genesis; thus, it is not surprising that there are substantial differences in their thermal processing behavior. To understand and quantify how these differences affect processing charactersitics, a comparative study of several key international oil shales was performed. Information is presented on the geology, organic composition, minerology, and pyrolysis kinetics. Thermal decomposition was studied through a series of nonisothermal gravimetric analyses. The TGA data were analyzed and compared using kinetic models by Coats and Redfern, Chen and Nuttall, and Anthony and Howard. Oil shales from Australia (Rundle), Brazil (Irati), China (Fushun and Maoming), USA (Green River Formation), Israel (Zefa-Ef'e), Morocco (Timhadit), Sweden (Naerke), and Yugoslavia (Aleksinac) were investigated.

Anticipating a future shortage of petroleum and acknowledging the uncertainty of continuing to obtain this vital resource from some of the major petroleum producing countries have caused an increased world interest in the extraction of liquid fuels from oil shale. This interest is evidenced by the exploration for new deposits, reevaluation of known deposits, new research studies of oil shale conversion, and the development of new retorts and retorting technology. However, there has been little, if any,

[1]Current address: Purdue University, Chemical Engineering Department, Lafayette, IN 47907

[2]Current address: Texas A&M University, Department of Chemistry, College Station, TX 77843

work to date which attempts to integrate an understanding of oil shale geology, chemistry, and processing technology for the many different world oil shales. If oil shale processing is to proceed on an international scale, a better understanding of the major differences among key world oil shales must be achieved; this study investigates some of these differences. Factors considered in this study include the geology and the location of deposits (geological age, origin, extent of deposit), shale grade, composition of the shale, and the kinetic behavior of the shale upon thermal decomposition.

Initially an extensive literature search was conducted to identify key world oil shales, i.e., deposits of large size and/or of current interest to potential developers. The resulting information was used to select a few key world oil shales. Thirteen oil shale samples from eight different countries were studied. Samples were acquired from each of the following countries: Australia, Brazil, Israel, Sweden, the United States, and Yugoslavia. Two samples were acquired from Morocco and five samples were acquired from the People's Republic of China. Fischer, Ultimate, Rock-Eval, ^{13}C Nuclear Magnetic Resonance Spectroscopy (NMR), and X-ray Diffraction Mineral analyses were performed on the samples to identify their compositional characteristics.

An important effort in this investigation was the thermal decomposition study of the shales. Considerable effort has been made to find a simple kinetic model which will accurately describe the weight loss curves for non-isothermal pyrolysis at various heating rates. In the past, many researchers have proposed and tested theoretical kinetic models for this reaction (1-4), however, most attempts at finding a suitable model have been focused on finding a very accurate fit to experimental data. Successive studies have increasingly emphasized microscopic details (i.e., diffusion models, exact chemical composition, etc.) in an attempt to find a precise model to fit the weight loss curves. In this study, we have stressed that the kinetic model should be both simple to use and accurate, thus allowing easy, reliable application of kinetic information to process design.

Two proposed mechanisms were tested: a single-step mechanism: kerogen → products and a two-step mechanism: kerogen → bitumen → products.

Three kinetic models were tested: the Chen-Nuttall model (5) and the Coats-Redfern model (6); both assume a single first order rate equation to describe the decomposition reaction; and the Anthony-Howard model (7) (as developed for coal decomposition studies), which assumes multiple parallel first order reactions to describe the decomposition reaction.

The following material briefly describes the geological and chemical characteristics of each oil shale sample and presents the results of the non-isothermal kinetic studies.

Summary of Deposits

AUSTRALIA: Swarbrick (8) discusses many of the oil shale deposits of Queensland.   The sample used in this study was obtained from the Rundle or Narrows Bed deposit near Gladstone on the Pacific coast of Queensland.   This deposit, discovered in the early 20th century during dredging operations in the Narrows between Curtis Island and the mainland of Queensland, is not considered to be economically recoverable at present, although some study of the deposit continues.   The Rundle deposit is one of the most oil rich deposits of Australia.   The main deposit has an average thickness of about 70 m with an overburden averaging less than 20 m.   The deposit covers an area of about 140 km^2 (9).

BRAZIL: The interest in oil shale exploration in Brazil has been stimulated by a lack of suitable coal deposits and poor success in oil exploration.   Although oil shale deposits have been found in many of the states in Brazil, the two deposits of primary commercial interest are those of the Paraiba Valley, between Sao Paulo and Rio de Janeiro, and the Irati formation, extending through several of the southern states of Brazil and into Uraguay.   Exploration of the oil shale deposits in the Paraiba Valley began in the early 1940s while the Irati deposit was first studied in the mid-1950s.   The oil shale sample used in this study was from the Irati formation.   The Irati formation, a very extensive deposit of oil rich shale averaging 30 to 50 m in thickness, is as thick as 100 m in some areas and covers at least 2500 km^2 (10).   A pilot plant has been operating at Sao Mateus do Sul since the mid-1970s.   The oil shale is mined by an open pit method with the overburden averaging approximately 30.5 m.

CHINA: Extraction of shale oil has been investigated in Fushun, Liaoning, since the 1930s.   At this site, a layer of oil shale from 70 to 190 m thick overlies a rich coal deposit (11).   Thus, oil shale is a by-product of efforts to recover coal by strip mining.   Two retorting plants are in operation at the Fushun mine and an additional retorting plant is in operation at Moaming, Kwangtung Province.   The oil shale at this site is also mined by open pit.   These three retorting plants produce about 300,000 tons of shale oil annually.   This study used three samples from the Fushun mine, and two from the Maoming area (Jinton and Yangu mines).

ISRAEL: The Israeli oil shale sample used in this study originated from the Zefa-Ef'e deposit.   Although exploration of this deposit began as early as 1962, a comprehensive study of the deposit was not undertaken until 1973.   This deposit, located in Mishor Rotem, southwest of the Dead Sea, is covered by an average overburden of 40 m and contains approximately 570 million tons of shale with an organic content greater than 10 percent (12).

MOROCCO: There are three major oil shale deposits in Morocco: one near Tanger, one near Tarfaya, and one at Timhadit. The samples used in this study originated from the Timhadit site,

located in the Middle Atlas Mountains of central Morocco. There
have been extensive studies of the deposits at Timhadit (13) and a
commercial retorting plant is expected to be in operation there by
1986. The deposit averages about 90 m thick with an overburden of
basalt, limestone, and marlstone. The shale is currently mined by
an open pit method. A detailed geologic study has been conducted
to plan future mine layout (13).

SWEDEN: Because of the lack of any petroleum resources as
well as very limited coal resources, the government of Sweden has
been interested in the extraction of its oil shale deposits for
quite some time. The Swedish oil shale sample used in this study
was obtained from the Naerke region, near the city of Orebro, in
south central Sweden. The Naerke deposit is one of three major
deposits considered commercially exploitable. The two others are
Ostergotland, near Omberg, and Vastergotland, near Kinnekulle.
The Naerke deposit, considered to be the most oil-rich of the
Swedish deposits, has an average thickness of about 10 m (15).
The overburden is primarily limestone with a maximum thickness of
about 30 m, with some areas covered by only a few meters of over-
burden (16). Here, open pit mining is considered to be the most
economical method of oil shale extraction. The deposits in the
Naerke region cover an area of about 100 km^2 (15).

UNITED STATES: Over the past decade, the United States has
examined alternatives to foreign sources of petroleum. Among the
alternatives available to the United States is extraction of oil
from its vast oil shale reserves. It has been estimated that 20
percent of the United States' land area is underlain by organic
rich deposits which fall under the definition of oil shale (17).
The most important deposits include the extensive Devonian-
Mississippian deposits of the Mid-West and Ohio Valley as well as
the Permian and Tertiary deposits of the Rocky Mountains. To
date, most attention has been focused on the higher grade deposits
of the western United States.

The world's largest oil shale resource is the Green River
Formation located in the tri-state region of Wyoming, Colorado,
and Utah. This deposit contains high grade oil shale over an area
of approximately 41,400 km^2 (17). The samples used in this study
are from the Uinta Basin in Utah. The Uinta Basin deposit covers
an area of about 14,000 km^2 with high grade oil shale to depths of
about 300 m. However, an area in the southeast section of the
basin, covering about 3900 km^2, contains high grade oil shale at
depths of only 0 to 60 m (17).

YUGOSLAVIA: The Yugoslavia sample used in this study was
obtained from the Aleksinac site in the Socialist Republic of
Serbia. Investigation of this deposit began as early as 1955.
The oil shale deposit in this area ranges in depth from 0 to 700 m
below the surface. The oil shale seam in the currently operating
mine averages about 45 m thick (18). Much of the oil shale in
this region lies over coal deposits which have been mined for

several decades.   Since much of the oil shale is underlain by abandoned coal mines, research is now centered around applying a modified in-situ retorting method for recovery of the embedded oil, although a pilot scale surface retort has been operated in the past.

A summary of the principal geologic characteristics of each of the deposits under consideration is presented in Table I.

Chemistry

The chemical compositions of oil shales and oil shale kerogen have been studied extensively (20). However, little work has been done to integrate chemical composition data in order to aid in the selection of suitable extracting processes. In this study, five analysis methods were used to chemically characterize the samples. These methods included Rock-Eval analysis, Fischer analysis, ^{13}C NMR, Ultimate analysis, and X-ray diffraction mineral analysis.

Table II presents the results of the Rock-Eval analysis. In this table, S1 indicates the amount of free hydrocarbons already generated in the shale and S2 indicates the amount of hydrocarbons generated by the decomposition of kerogen at high temperatures. The sum of these values gives a semi-quantitative evaluation of the genetic potential of the shale in terms of both the abundance and type of organic matter present (21). S3 indicates the amount of CO_2 formed by the decomposition of kerogen. S2/S3 is the ratio of the Hydrogen Index to the Oxygen Index. The Hydrogen Index and Oxygen Index are related to the H/C ratio and O/C ratio, respectively, and can be plotted in a manner similar to a van Krevelan plot. This plot is presented in Figure 1. Also included in this plot are the thermal evolution paths of the three classes of kerogen described by Tissot and Welte (21). The first class contains oil producing kerogens that are characteristically rich in aliphatic hydrocarbons. This class yields a higher amount of oil than do the other classes of kerogen. The second class of kerogens yields a higher amount of gaseous products than does the first. The third class of kerogens does not include any oil shale kerogens. Figure 1 shows that the oil shales in this study contain kerogen from the first class (Type I) with the exception of the China Maoming #2 sample, which falls in the second class (Type II). As shown in Table II, S1/(S1 + S2) characterizes the transformation of kerogen hydrocarbons to petroleum (this value will increase with maturation), and Tmax is related to the degree of thermal maturation (21). In the Rock-Eval analysis, Tmax is the temperature corresponding to the maximum generation of hydrocarbons during pyrolysis.

Table III presents the results of the Fischer, ^{13}C NMR, and Ultimate analyses. The fraction of aliphatic carbon has been correlated to the quality or yield of oil from the shale (22). Although this value appears to correspond to the oil yield from the

TABLE I. General Deposit Information

COUNTRY	SITE	AGE	ESTIMATED RESERVES (MILLION BBLS)	DEPOSITIONAL ENVIRONMENT
Australia	Rundle, Queensland	(Tertiary) (9)	600 (9)	Freshwater (20)
Brazil	Irati	(Permian)	800,000	Marine (20)
China	Fushun	(Tertiary)	1700	Lacustrine (20)
	Moaming	NA	NA	NA
Israel	Zefa-Ef'e deposit, Mishor Rotem	(Cretaceous)	30	Marine (20)
Morocco	Timhadit	(Cretaceous) (13)	15000 (13)	NA
Sweden	Naerke	(Cambrian-Silurian)	600	NA
United States	Uinta Basin, Utah	(Tertiary) (20)	120,000	Lacustrine (20)
Yugoslavia	Aleksinac	(Tertiary)	210	Lacustrine (20)

NA = Not Available   All data from Jaffe (19) except as noted.

Table II. Rock-Eval Pyrolysis Data

SAMPLE	SAMPLE NO.	S1 mg/gm	S2 mg/gm	S3 mg/gm	S2/S3	S1/S1+S2	ORGANIC CARBON	Tmax DEG C	HYDROGEN INDEX	OXYGEN INDEX
Australia	1	1.75	79.85	2.93	27.54	.02	10.85	438	736.9	27.1
Brazil	16	7.74	81.71	0.35	233.46	.09	10.89	426	750.3	3.2
China #1 Fushun #1	7	1.61	44.32	0.58	79.67	.03	8.35	440	524.5	6.6
China #2 Fushun #2	3	1.76	105.72	0.57	151.96	.02	16.52	445	627.8	3.5
China #3 Fushun #3	9	2.15	74.94	1.06	70.90	.03	12.93	442	579.6	8.2
China #4 Maoming #1	10	1.53	64.39	1.39	46.31	.02	12.36	435	521.0	11.3
China #5 Maoming #2	11	3.09	75.19	4.59	16.37	.04	14.90	431	504.6	30.8
Israel	5	2.83	49.30	3.72	13.26	.05	7.14	419	690.4	52.1
Morocco M-Zone	3	6.95	99.58	3.52	28.31	.07	15.34	417	649.1	22.9
Morocco Timhadit	4	2.69	40.97	1.29	31.91	.06	5.00	415	819.4	25.3
United States Uinta Basin #4	15	7.44	130.51	1.5	87.38	.05	18.34	446	711.6	8.2
Sweden	6	2.11	56.90	0.75	75.67	.04	10.91	424	521.5	6.9
Yugoslavia	2	4.40	24.80	0.74	33.31	.15	3.64	433	681.3	20.5
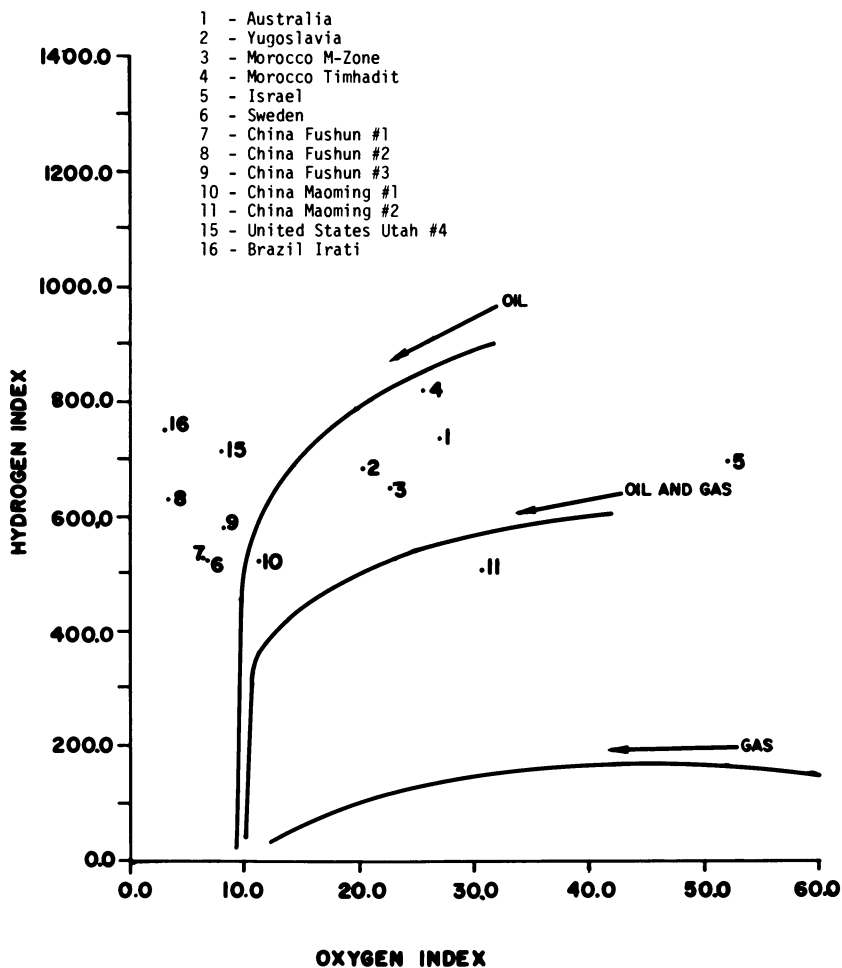
Figure 1. Hydrogen index vs. oxygen index for various oil shales.

TABLE III. Fischer, Ultimate, and C13 NMR Analysis Information

SAMPLE	OIL (GPT/WT%)	WATER (GPT/WT%)	CARBON TOTAL%/%ORGANIC	FRACTION ALIPHATIC CARBON	%HYDROGEN	%OXYGEN	%SULFUR	%NITROGEN
Australia	33.7/12.8	16.6/6.9	16.45/10.83	0.65	2.81	11.67	1.19	0.4
Brazil	25.2/9.6	15.9/6.7	12.85/10.70	NA	1.83	4.58	4.87	0.33
China #1	26.5/10.1	8.3/3.5	10.73/8.83	NA	1.96	10.51	0.48	0.35
#2	30.7/11.7	14.3/6.0	16.61/16.53	0.65	2.71	8.73	0.62	0.54
#3	32.1/12.2	6.9/2.9	11.14/12.93 *	NA	1.93	11.41	0.49	0.43
#4	22.7/8.7	15.3/6.4	14.54/12.36	0.68	2.85	8.33	1.24	0.36
#5	27.4/10.4	14.6/6.1	13.5/14.91 *	NA	2.51	9.86	1.22	0.44
Israel	17.7/6.8	11.7/4.9	14.98/7.14	0.71	1.62	22.75	2.49	0.31
Morocco								
Timhadit	14.6/5.6	3.5/1.5	13.65/5.00	NA	1.02	18.14	1.9	0.26
M-Zone	NA	NA	25.74/15.34	0.68	2.61	17.42	2.73	0.81
Sweden	33.0/12.5	5.2/2.2	17.28/10.91	0.54	1.31	15.81	2.89	0.31
United States								
Uinta Basin								
#4	50.4/19.1	3.1/1.3	18.67/18.34	0.79 **	2.25	10.21	1.3	0.60
Yugoslavia	18.6/7.1	7.0/2.9	9.25/3.64	0.67	1.02	17.25	0.55	0.17

NA = Not Available
* - note that %organic C > total% C -- attributed to experimental error
** - approximated from values for Colorado Green River Oil Shale given by Miknis and Smith (22).

shales in this study, no firm relationship between these values is evident here. Further investigation of the significance of the values in this table is planned.

Table IV presents the results of the X-ray diffraction mineral analysis. The values in this table give relative mineral concentrations. Future investigations of this information should reveal whether or not the mineral concentration has a significant effect on the pyrolysis reaction.

It should be noted that there is a significant range of differing oil shales under consideration in this study. This range of characteristics insures that the scope of our study will be broad enough to be applicable to most international oil shale samples.

Kinetics

The rate of kerogen decomposition into oil and gaseous products can be an important factor in process design, as can the relative amount of oil and gas produced. Nonisothermal gravimetric analysis was used to compare the relative thermal decomposition rates of the kerogens in the shales under investigation. Details of the pyrolysis studies are presented in the following sections.

Experimental Section. The samples used in the TGA study were crushed to minus 200 mesh. Nonisothermal weight loss data were gathered using a DuPont 951 thermogravimetric balance with a DuPont 990 thermal analyzer.

Thirteen samples were analyzed using heating rates ranging from 1.0 to 50.0°C/min. The samples were heated to a maximum of 500°C. This temperature was maintained until the sample weight stabilized.

The fraction of kerogen pyrolyzed, α, was defined by the expression:

$$\alpha = \frac{W_o - W_t}{W_o - W_\infty} \tag{1}$$

where W_o is the initial weight of sample (mg), W_t is the weight of sample at time t minutes (mg), and W_∞ is the weight of sample after complete pyrolysis (mg).

Some typical initial and final experimental weight ratios are listed in Table V for comparison. These values give an indication of the relative quantity of organic matter in each of the shales under investigation, and of the progress of the reaction at 500°C.

Discussion. Over the past several decades, there have been many attempts to characterize the kinetic behavior of oil shales under pyrolyzing conditions. In 1950, Hubbard and Robinson (1)

TABLE IV.   Relative Mineral Concentrations - X-Ray Diffraction Mineralogy

SAMPLE	SMECTITE (6.0 -7.0°)	ILLITE (8.8°)	KAOLITE/CHLORITE (12.3°)		QUARTZ (26.6°)	K-SPAR (27.6°)	NA-SPAR (28.0°)	ANALCIME (26.0°)
Australia	6.0 B	1.0	1.0	ND	60	2.0	3.5	ND
Brazil	1.5 B	2.0	1.7	1.3	100	9.0	10.0	ND
China #1	ND	1.0	5.0	ND	67	2.0	1.0	ND
#2	1.5 B	2.0	3.0	4.0	74	3.5	1.5	ND
#3	2.0 B	1.0	3*		58	2.5	ND	ND
#4	TR	2.0	11*		77	5.5	1.0	ND
#5	2.0 B	2.0	3.0	7.0	63	6.0	ND	ND
Israel	1.0 B	ND	1.0	ND	9	TR	ND	ND
Morocco								
Timhadit	ND	1.0	1.0	ND	51	1.5	2.0	ND
M-Zone	1.0 B	1.0	1.0	ND	29	1.5	1.0	ND
Sweden	ND	2.5	3.5	ND	50	4.0	ND	3.5
United States								
Uinta Basin #4	2.0	3.0	ND	ND	63	ND	27.0	ND
Yugoslavia	ND	2.5	1*		14	3.0	2.5	2.8

Table IV. Continued

SAMPLE	CALCITE (29.5°)	DOLOMITE (30.9°)	SIDERITE (32.0°)	PYRITE (33.0°)	MARCASITE (52.0°)	PYRRHOTITE (43.9°)	GYPSUM (11.7°)	HALITE (31.7°)
Australia	(MG-10)	ND	ND	4.0	ND	ND	ND	ND
Brazil	2	4.0	1.0	18.0	ND	ND	ND	ND
China #1	2	1.0	15.0	2.0	ND	ND	ND	17
#2	2	1.0	2.0	2.0	ND	ND	ND	7
#3	10	ND	22.0	4.5	ND	ND	ND	ND
#4	ND	1.5	10.0	4.0	ND	ND	ND	ND
#5	ND	ND	1.0	3.0	ND	ND	1.5	ND
Israel	166	2.0	3.0	TR	ND	ND	1.5	ND
Morocco								
Timhadit	87	51.0	3.0	3.0	ND	ND	ND	ND
M-Zone	73	46.0	2.0	3.0	ND	ND	ND	ND
Sweden	159	1.0	1.5	11.0	ND	ND	ND	ND
United States								
Uinta Basin								
#4	8	46.0	ND	ND	1.5	1.5	ND	ND
Yugoslavia	ND	67.0	ND	1.0	ND	ND	ND	ND

Values are intensities of primary XRD reflectors using Cu radiation on Philips APD 3500.
Values in parentheses are peak positions used for characterizing each mineral.
* Undifferentiated Kaolinite and/or Chlorite due to masking by other minerals.
ND=Not detected   TR=Trace   B=Broad peak   (Mg-) Indicates Mg rich variety of Calcite.

TABLE V. Comparison of Weight Loss Characteristics
of Various Oil Shale Samples
(Heating Rate: 2.0°C/min)

SAMPLE	$\dfrac{W_{L,500}}{W_o}$	$\dfrac{W_{L,\infty}}{W_o}$	$\dfrac{W_{L,500}}{W_{L,\infty}}$
Australia	0.2309	0.3574	0.6461
Brazil	0.1206	0.1747	0.690
China #1	0.1005	0.1611	0.6237
#2	0.1209	0.1634	0.7399
#3	0.1493	0.2109	0.7079
#4	0.1231	0.2078	0.5924
#5	0.1632	0.2737	0.5963
Israel	0.1452	0.1708	0.8501
Morocco	0.0900	0.0933	0.9646
Sweden	0.1296	0.2920	0.4438
United States Colorado**	--	--	1.0000
Uinta Basin #4	0.1495	0.1937	0.7718
Yugoslavia	0.1157	0.1366	0.8660

* W_o = Original sample weight
  $W_{L,500}$ = Weight loss at 500°C
  $W_{L,\infty}$ = Weight loss at infinite time (temperature held at 500°C)
** Calculated from parameters given by Campbell, et al., (2).

presented the results of a comprehensive study of kerogen decomposition in oil shale pyrolysis. They found that the bitumen concentration had little effect on the decomposition of the kerogen. They assumed that the kerogen decomposition was a first order reaction, based on the earlier work of Maier and Zimmerley (23), and showed that this assumption was suitable. They also noted that the kinetic data could best be modeled by dividing it into two temperature ranges. They attributed the inconsistency of their model to difficulty in measuring the rapid reaction rate of kerogen at higher temperatures, and to the lag period required for the sample to reach the desired temperature. Coats and Redfern (6) developed a mathematical equation which allowed use of nonisothermal thermogravimetric analysis to derive the kinetic parameters of a first order reaction. Braun and Rothman (3) reanalyzed the data of Hubbard and Robinson and made corrections to account for the thermal induction period. They concluded that the pyrolysis of oil shale could best be described by a two-step mechanism, the first step being the degradation of kerogen to bitumen, and the second step being the decomposition of the bitumen to products (including gases, liquids, and solid residues). Campbell, Koskinas, and Stout (3) used isothermal and nonisothermal techniques to study the kinetics of oil generation from oil shale. They presented a comparison of these two techniques and pointed out the advantages of the nonisothermal technique. They compared their results with those of other investigators and found that the nonisothermal technique gave similar results to isothermal techniques. In their report, they also noted that their activation energies seemed somewhat low compared to the strengths of the bonds they assumed were breaking in the organic matter (i.e., C-H, C-O, C-C, and other bonds). They explained this inconsistency by making reference to possible free radical chain mechanisms which would result in much lower activation energies. Chen and Nuttall (5) developed an equation which allowed calculation of kinetic parameters from nonisothermal TGA data. Anthony, et al., (7) presented a model for coal devolatization which assumes multiple parallel first order reactions that can be described by a Gaussian distribution of activation energies. This model gives higher overall activation energies than the single reaction model and thus would seem to better describe the chemical reactions which we expect to be occurring during pyrolysis.

Kinetic Expressions. In this study, we have analyzed nonisothermal TGA data using the Chen-Nuttall equation, the widely accepted Coats-Redfern equation, and the Anthony-Howard equation. These equations are derived from simple rate expressions. The basic single reaction kinetic equation for the decomposition of a solid has been presented by Blazek (24) as

$$\frac{d\alpha}{dt} = kf(\alpha) \tag{2}$$

where α is the fractional conversion at time t, k is the specific rate constant, and $f(\alpha)$ is $(1 - \alpha)$ in first order reactions.

By substituting k in terms of activation energy and frequency factor, Eq. (2) can be rewritten as follows:

$$\frac{d\alpha}{dt} = Z \exp[-\frac{E}{RT}] (1 - \alpha) \tag{3}$$

where Z is the frequency factor (min^{-1}), E is the activation energy (J/gmole), R is the gas constant (J/gmole-K), and T is the temperature (K).

To take into account the nonisothermal conditions, the heating rate must be incorporated as a parameter of the equation as follows:

$$\frac{d\alpha}{dT} \frac{dT}{dt} = Z \exp[-\frac{E}{RT}] (1 - \alpha) \tag{4}$$

or

$$\frac{d\alpha}{dT} = \frac{Z}{\beta} \exp[-\frac{E}{RT}] (1 - \alpha) \tag{5}$$

where $\beta = dT/dt$.

Assuming a constant heating rate, the integrated form becomes:

$$1 - \alpha = \exp \left\{ - \frac{Z}{\beta} \int_{T_o}^{T} \exp[-\frac{E}{RT}] \, dT \right\} \tag{6}$$

Chen and Nuttall's Equation. Chen and Nuttall (5), developed an approximation of Eq. (6) which gives:

$$1 - \alpha = \exp \left\{ - \frac{Z}{\beta} \left[\frac{RT^2}{E + 2RT} \right] \exp[-\frac{E}{RT}] \right\} \tag{7}$$

Equation (7) can be written as

$$\ln \left\{ \left[\frac{E + 2RT}{T^2} \right] \cdot \ln \left[\frac{1}{1 - \alpha} \right] \right\} = \ln[\frac{ZR}{\beta}] - \frac{E}{RT} \tag{8}$$

Equation (8) is of the form

$$y = \alpha + bx \tag{9}$$

where

$$y = \ln\left\{\left[\frac{E + 2RT}{T^2}\right] \cdot \ln[\frac{1}{1 - \alpha}]\right\} \tag{10}$$

$$a = \ln[\frac{ZR}{\beta}] \tag{11}$$

$$b = -\frac{E}{R} \tag{12}$$

and

$$x = \frac{1}{T} \tag{13}$$

An iterative regression analysis will allow calculation of the slope and intercept of Eq. (8). The iteration involves first guessing a value of E, then computing y. Next, the slope and intercept are found using regression analysis. The new value for E, from Eq. (12), is then used to reiterate the regression until suitable tolerance is obtained for values of E and Z. Alternatively, we can use the Simplex optimization technique or the Levenberg-Marquardt least-squares fitting technique to simultaneously find both E and Z. A fourth correlating technique, a weighted regression analysis using the Levenberg-Marquardt algorithm, will allow a better fit to be found for the data points in the higher temperature ranges where most commercial retorting methods are expected to operate.

Coats and Redfern's Equation. A method developed by Coats and Redfern (6) utilizes the following expression as an approximation of the integral in Eq. (6) to determine the energy of activation, E, and the frequency factor, Z, for the thermal decomposition reaction:

$$\ln\left[-\frac{\ln(1 - \alpha)}{T^2}\right] = \ln\frac{ZR}{\beta E}\left[1 - \frac{2RT}{E}\right] - \frac{E}{RT} \tag{14}$$

With this equation, a plot of $\ln[-(\ln(1 - \alpha)/T^2)]$ versus $1/T$ should result in a straight line of slope E/R. (The first term in the right side of Eq. (14) remains essentially constant for most values of E, Coats and Redfern (6).) By extrapolating the curve, a value for Z can be obtained.

Anthony and Howard's Equation. In their work on coal devolatization, Anthony and Howard (7) have proposed a decomposition mechanism based on multiple first order reactions. This model uses a Gaussian distribution function to account for the range of activation energies expected with such a mechanism. The development of this model proceeds from the assumed first order kinetic expression for a single reaction:

$$\frac{dm_i}{dt} = k_i(m_i^* - m_i)$$

(15)

where m is the mass of sample lost at time t, m* is the mass of sample lost at time = ∞, and the subscript i denotes that the parameter is for a single reaction.

Incorporating the heating rate, as is required for nonisothermal analysis, we get:

$$\frac{dm_i}{dT}\frac{dT}{dt} = k_i(m_i^* - m_i)$$

(16)

Letting β = dT/dt, we can rearrange to get:

$$\frac{dm_i}{(m_i^* - m_i)} = \frac{k_i}{\beta} dT$$

(17)

This equation can be integrated, using the initial conditions that m_i = 0 when T = starting temperature, to give

$$m_i^* - m_i = m_i^* \exp\left[-\int_{T_o}^{T} \frac{k_i}{\beta} dT\right]$$

(18)

Theoretically, T_o is absolute zero; however, experimental conditions require that T_o correspond to ambient temperature.

At this point, we turn our attention to the overall reaction in the shale. The assumptions are made that the multiple reactions are occurring simultaneously, that each reaction can be described by a first order rate equation, and that only the activation energies vary. The frequency factors for the many rate equations are assumed to be identical: $Z_1 = Z_2 = Z_3 \cdots$. With these assumptions, the problem is reduced to finding a description of the many reactions in terms of a distribution function of activation energies. With m* representing the mass lost at time = ∞, a distribution function, F, is chosen so that dF describes the fraction of m* which reacts with activation energy E. Mathematically,

$$dF = \frac{dm^*}{m^*}$$

(19)

where dF is the area under the frequency distribution curve, f(E), over the interval dE. Obviously the distribution function should be normalized over the entire range of activation energies:

$$\int_0^{\infty} f(E) \, dE = 1$$

(20)

On the basis of our assumption of a large number of reactions, it can be assumed that the distribution of reactions can be described by a Gaussian distribution curve such that

$$f(E) = \frac{\exp\left\{-\frac{1}{2}\left[\frac{(E - E_o)}{\sigma}\right]^2\right\}}{\sigma(2\pi)^{1/2}} \tag{21}$$

where E_o is the mean activation energy and σ is the standard deviation.

From these assumptions, it can be seen that the mass lost from any single reaction, m_i^*, is simply a differential element of the total mass lost from the sample upon complete pyrolysis, m^*. Thus, an equation can be developed for m_i^* in terms of m^* and $f(E)$:

$$m_i^* = dm^* = m^* \, dF = m^* \, f(E) \, dE \tag{22}$$

We can now return to our single reaction rate equation, Eq. (18), and begin to substitute the distribution expressions, Eqs. (21) and (22), in order to develop a kinetic expression for the totality of reactions occurring in the shale. First, the rate constant is expressed in terms of the frequency factor and activation energy. Then, Eqs. (21) and (22) are used to substitute for m_i^* in terms of the total mass lost, m^*, and the distribution curve, $f(E)$. Upon summation over all the reactions (i.e., over all values of E), we get

$$\frac{m^* - m}{m^*} = \frac{1}{\sigma(2\pi)^{1/2}} \int_0^\infty \exp\left\{-\frac{Z}{\beta}\int_{T_o}^T \exp\left[-\frac{E}{RT}\right] \, dT\right\}$$

$$\cdot \exp\left\{-\frac{1}{2}\left[\frac{(E - E_o)}{\sigma}\right]^2\right\} \, dE \tag{23}$$

where the frequency factor, Z, is assumed to be the same for all reactions. From the definition of α, it can be shown that $m/m^* = \alpha$, so that $(m^* - m)/m^* = 1 - \alpha$. For our purposes, the integration of the activation energy is sufficiently accurate over the range $E_o - 2\sigma$ to $E_o + 2\sigma$. With these changes, the expression becomes:

$$1 - \alpha = \frac{1}{\sigma(2\pi)^{1/2}} \int_{E_o-2\sigma}^{E_o+2\sigma} \exp\left\{-\frac{Z}{\beta} \int_{T_o}^{T} \exp[-\frac{E}{RT}] \ dt\right\}$$

$$\cdot \exp\left\{-\frac{1}{2}\left[\frac{(E - E_o)}{\sigma}\right]^2\right\} dE \qquad (24)$$

This equation can also be altered by substituting an approximation for the integral over the temperature range. This integral is approximated using the Coats-Redfern equation, Eq. (14). Equation (14) can be rearranged to give an expression for $(1 - \alpha)$. Equation (6) shows that $(1 - \alpha)$ is equivalent to the integral over the temperature range. This can be substituted into Eq. (24) to get:

$$1 - \alpha = \frac{1}{\sigma(2\pi)^{1/2}} \int_{E_o-2\sigma}^{E_o+2\sigma} \exp\left\{-\frac{ZRT^2}{\beta E}\left[\exp[-\frac{E}{RT}] \ [1 - \frac{2RT}{E}]\right]\right\}$$

$$\cdot \exp\left\{-\frac{1}{2}\left[\frac{(E - E_o)}{\sigma}\right]^2\right\} dE \qquad (25)$$

Correlation and Analysis

For ease of discussion, the following abbreviations will be used:

CN   denotes the Chen-Nuttall equation, (8),

CR   denotes the Coats-Redfern equation, (14),

AH   denotes the Anthony-Howard equation, (24), where both integrals are evaluated using numerical techniques.

CR-AH   denotes the Anthony-Howard equation, (25), where the first integral is approximated using the Coats-Redfern equation.

LM   denotes that the kinetic parameters were evaluated using the Levenberg-Marquardt nonlinear least-squares method.

To compare the different mechanisms and models, an absolute average deviation (AAD) of predicted weight loss data, with respect to experimental weight loss data, was calculated for each proposed mechanism using the following equation:

$$AAD = \frac{\sum_{I=0}^{NP} \frac{|\alpha(\text{experimental}) - \alpha(\text{calculated})|}{\alpha(\text{experimental})}}{NP}$$

where NP denotes the number of data points gathered in the experiment.

Single Heating Rate Data

Comparison Between Coats-Redfern and Chen-Nuttall Equations. The single heating rate data for the temperature range of 300-500°C have been correlated to the CR equation, Eq. (14), and the CN equation, Eq. (8). Three techniques were used to find the optimum values for E and Z in each of these equations. These techniques include: 1) iterative linear regression, 2) Levenberg-Marquardt nonlinear least-squares regression, and 3) the Simplex optimization method. Similar results were obtained for each method. The computed kinetic parameters and corresponding AAD (absolute average deviation) values, as determined by the iterative linear regression technique, are presented in Table VI. From Table VI, it can be seen that:

1) The kinetic parameters and AAD values are similar for both the CN and CR equations.

2) The numerical values of activation energy, E, and frequency factor, Z, are quite low as compared to those for the AH equation (see Table VIII).

3) The AAD values for some of the sets of data are outside the bounds that we considered reasonable (>10 percent).

Comparison of One-Region and Two-Region Treatments. In order to improve the correlation of the TGA data, the data have been divided into two regions: region one--300-375°C, and region two--375-500°C. These regions were chosen as representative of the two series reactions described in the Introduction. The kinetic parameters were evaluated for each of these regions separately. A comparison of the one region (or one-step) treatment and the two region (or two-step) treatment, using the CN equation, is presented in Table VII. From Table VII, it can be seen that the activation energy and frequency factor values in the high temperature region are significantly higher and that the two-region treatment gives lower values for the AAD and thus could give a significantly better fit. However, it must be noted that the two-region treatment requires the evaluation of two sets of kinetic parameters for each data set.

Comparison of Anthony-Howard and Coats-Redfern Equations. Because the CR equation and the CN equation yielded similar results, the CR equation was chosen as a basis for comparison with the AH equation. The correlated results based on the AH multiple reaction model and the CR model are presented in Table VIII. The kinetic parameters were determined using an equally weighted regression method. From Table VIII, it can be seen that the AH model yields

TABLE VI. Comparison of the Kinetic Parameters and AAD Values Determined from Chen-Nuttall and Coats-Redfern Equations *

One Region: 300-500°C

NUMBER	OIL SHALE SAMPLE	HEATING RATE (°C/MIN)	CHEN-NUTTALL E (KJ/MOL)	Z (MIN^{-1})	AAD	COATS-REDFERN E (KJ/MOL)	Z (MIN^{-1})	AAD
1	Moroccan	1.0	50.175	150.60	0.0497	50.723	176.41	0.0502
2	Moroccan	2.0	47.098	116.68	0.0443	47.721	139.72	0.0444
3	Moroccan	5.0	48.120	267.40	0.0540	48.717	317.71	0.0544
4	Moroccan	10.0	43.579	138.29	0.0454	44.307	170.79	0.0457
5	Moroccan	20.0	38.279	79.86	0.0346	39.222	105.13	0.0343
6	Moroccan	50.0	31.587	37.64	0.0542	32.964	56.38	0.0538
7	Australian	2.0	41.342	15.10	0.0469	42.151	19.10	0.0475
8	Australian	5.0	45.880	66.23	0.1214	46.536	80.10	0.1226
9	Australian	10.0	41.245	42.44	0.1374	42.057	53.76	0.1388
10	Australian	20.0	42.340	91.34	0.1596	43.111	114.25	0.1610
11	Swedish	2.0	44.905	11.78	0.1382	45.589	14.37	0.1393
12	Swedish	10.0	43.517	34.66	0.2515	44.248	42.84	0.2529
13	Chinese #2	1.0	46.863	21.96	0.1526	44.273	12.88	0.1412
14	Chinese #3	1.0	46.724	19.567	0.1177	45.428	15.23	0.1052
15	Chinese #4	1.0	47.421	23.664	0.0945	45.534	16.55	0.0861

* Parameter values were determined by iterative linear regression method.

TABLE VII.   Comparison of One-Region and Two-Region

NUMBER	OIL SHALE SAMPLE	HEATING RATE (°C/MIN)	Two-Region 300-375°C		
			E (KJ/MOL)	Z (MIN^{-1})	AAD
1	Moroccan	1.0	42.612	30.294	0.0327
2	Moroccan	2.0	47.500	242.64	0.0101
3	Moroccan	10.0	43.495	138.93	0.0508
4	Australian	2.0	35.725	4.346	0.0292
5	Australian	5.0	27.440	1.164	0.0389
6	Australian	10.0	22.660	0.0695	0.0445
7	Swedish	2.0	21.296	0.0615	0.0646
8	Swedish	10.0	13.300	0.0395	0.0131
9	Chinese #1	1.0	29.768	0.4626	0.0288
10	Chinese #1	2.0	10.822	0.0133	0.0457
11	Chinese #1	5.0	27.862	0.0034	0.0278
12	Chinese #2	1.0	22.585	0.1042	0.0468
13	Chinese #2	2.0	13.893	0.0342	0.0336
14	Chinese #3	1.0	27.823	0.3094	0.0692
15	Chinese #3	2.0	20.012	0.0893	0.0583
16	Chinese #4	1.0	32.020	0.8304	0.0391
17	Chinese #4	2.0	29.025	0.5938	0.0541
18	Chinese #5	1.0	27.308	0.4761	0.0179
19	Chinese #5	2.0	20.732	0.1790	0.0205
20	Chinese #5	5.0	20.064	0.2518	0.0150

* Parameter values were determined by simplex optimization
  method.

Treatment Based on Chen-Nuttall Equation *

	Two-Region				One-Region		
		375-500°C				300-500°C	
	E (KJ/MOL)	Z (MIN⁻¹)	AAD		E (KJ/MOL)	Z (MIN⁻¹)	AAD
	51.477	170.29	0.0215		44.706	130.43	0.0432
	45.129	140.74	0.0568		44.432	66.14	0.0458
	40.827	81.35	0.0326		42.964	121.03	0.0432
	43.561	1471.19	0.0741		42.368	15.10	0.0417
	59.048	730.40	0.0425		43.984	43.16	0.1157
	54.740	500.99	0.0609		39.476	28.27	0.1218
	58.648	147.82	0.0357		45.930	13.72	0.1356
	71.325	5340.09	0.0869		41.396	19.97	0.2342
	67.348	941.58	0.0518		48.772	28.74	0.1332
	59.586	360.52	0.0577		36.935	4.94	0.1721
	63.179	1105.09	0.1040		33.970	4.58	0.2801
	57.851	155.18	0.0493		43.400	10.13	0.1401
	65.512	1433.90	0.0876		38.857	9.23	0.1782
	56.908	124.69	0.0413		44.799	12.65	0.1042
	55.864	161.37	0.0608		43.502	15.81	0.1537
	57.047	135.23	0.0389		44.859	13.62	0.0855
	55.970	152.29	0.0365		44.714	18.28	0.0948
	49.000	39.99	0.0328		37.726	4.77	0.0766
	37.507	5.918	0.0367		28.658	1.069	0.0686
	51.781	166.41	0.0497		34.638	6.46	0.1219

Table VIII.   Comparison of the Kinetic Parameters and AAD Values
Determined from Anthony-Howard and Coats-Redfern Equations*
(Single Heating Rate)

NUMBER	OIL SHALE SAMPLE	HEATING RATE (°C/MIN)	ANTHONY-HOWARD/LEVENBERG-MARQUARDT				COATS-REDFERN/LEVENBERG-MARQUARDT		
			E (KJ/MOL)	σ (KJ/MOL)	Z (MIN^{-1})	AAD	E (KJ/MOL)	Z (MIN^{-1})	AAD
1	Australian	2.0	125.92	16.120	0.5166×10^{8}	0.0509	42.153	19.00	0.0422
2	Australian	5.0	118.00	12.440	0.1180×10^{8}	0.0685	44.402	50.12	0.1207
3	Moroccan	1.0	90.11	9.205	0.3240×10^{6}	0.0379	44.103	44.09	0.0727
4	Moroccan	5.0	90.40	9.416	0.5799×10^{6}	0.0459	45.344	157.58	0.0431
5	Swedish	2.0	130.57	12.195	0.1511×10^{9}	0.1192	45.680	14.35	0.1307
6	Chinese #1	1.0	114.61	8.098	0.2028×10^{7}	0.1166	55.918	90.19	0.1104
7	Chinese #1	5.0	122.44	9.633	0.1213×10^{8}	0.1472	31.497	2.46	0.2421
8	Chinese #2	1.0	112.83	12.365	0.1636×10^{7}	0.1149	44.273	12.83	0.1412
9	Chinese #2	2.0	115.33	14.255	0.2512×10^{7}	0.1321	59.290	7.84	0.1631
10	Chinese #3	1.0	121.97	13.373	0.7874×10^{7}	0.0772	45.428	15.23	0.1052
11	Chinese #4	1.0	117.85	13.061	0.3367×10^{7}	0.0632	45.535	16.55	0.0461
12	Chinese #5	2.0	122.50	21.397	0.6453×10^{7}	0.0584	30.467	1.79	0.0715

* Parameter values were determined by equally weighted regression.

slightly lower AAD values and therefore provides a better fit of the data. It can also be noted that the values for the activation energy, E, and the frequency factor, Z, as determined from the AH model are much more reasonable than those predicted by the CR equation.

Multiple Heating Rate Data. The major effort of this study has been to correlate the data in a model which will be valid for multiple heating rates. The advantage of the AH model was more evident for this purpose. Three models were used to correlate the multiple heating rate data: 1) CR-LM, 2) AH-LM, and 3) CR-AH-LM. A comparison of the correlated results of these three models is presented in Table IX. From Table IX, it can be seen that:

1) The CR model is not suitable for correlating multiple heating rate data as the AAD values were much higher than those of the other models.

2) The AH-LM method and CR-AH-LM method yield similar results. However, the later method appreciably reduced the computation time of the correlation.

3) For most sets of multiple heating rate data investigated, both the AH-LM and CR-AH-LM models give a reasonably good fit.

4) The general trend is an increase in the deviation between calculated and experimental data in the high temperature range (425-500°C).

To improve the fitting of data in the high temperature region, the following two schemes were tested:

1) Two-region treatment: The TGA data were divided into two temperature regions (300-425°C and 425-500°C). The AH equation was used to determine the kinetic parameters of each region.

2) One-region treatment: An unequally weighted regression technique was used to place greater emphasis on the data in the higher temperature range (400-500°C).

Although the two-region treatment yields satisfactory results in both regions, it is difficult to search for the optimum parameters which will give a continuous change in calculated rate constant, k, at the point of transition between the two regions. Furthermore, the two-region treatment requires two sets of parameters to represent the TGA data and is thus somewhat more complicated. The one-region unequally weighted regression technique can significantly improve the fitting of data in the high temperature region at the expense of higher overall AAD values and a poorer fit in the low temperature region (which is less important in industrial applications).

TABLE IX. Comparison of the Kinetic Parameters and AAD Values
(One-Region: 300-500°C, equally weighted)

NO.	OIL SHALE SAMPLE	HEATING RATES (°C/MIN)	COATS-REDFERN/LEVENBERG-MARQUARDT		
			E (KJ/MOL)	Z (MIN^{-1})	AAD
1	Australian	2,5,10,20	52.058	221.46	0.3857
2	Moroccan	1,2,5,10	59.855	2060.7	0.2418
3	Moroccan	1,2,5,10,20,50	69.834	20144	0.3576
4	Swedish	2,5	52.385	72.07	0.2589
5	Chinese #1	1,2,5	60.821	326.22	0.3435
6	Chinese #2	1,2	45.074	18.142	0.2291
7	Chinese #3	1,2	47.122	25.625	0.2189
8	Chinese #4	1,2	46.562	23.409	0.1525
9	Chinese #5	1,2	37.292	5.565	0.1512
10	Chinese #5	1,2,5	39.676	10.499	0.2634
11	Brazil	1,2	38.286	7.304	0.1802
12	Israel	1,2	38.276	12.93	0.1320
13	U.S. Utah	1,2	48.891	83.080	0.0639
14	Yugoslavia	1,2	38.216	11.667	0.0833

Determined by Three Models for Multi-Heating Rate Data

COATS-REDFERN/ANTHONY-HOWARD/ LEVENBERG-MARQUARDT				ANTHONY-HOWARD/LEVENBERG-MARQUARDT			
E (KJ/MOL)	σ (KJ/MOL)	Z (MIN^{-1})	AAD	E (KJ/MOL)	σ (KJ/MOL)	Z (MIN^{-1})	AAD
147.419	17.834	0.14403×10^{10}	0.0694	147.984	17.884	0.15683×10^{10}	0.0693
118.095	13.569	0.75242×10^{8}	0.0523	118.801	13.649	0.84669×10^{8}	0.0522
122.590	15.589	0.15565×10^{9}	0.0736	129.585	16.501	0.53395×10^{9}	0.0727
121.636	10.779	0.5082×10^{7}	0.2428	116.580	10.045	0.2111×10^{7}	0.2496
113.072	9.245	0.18222×10^{7}	0.1594	127.605	11.438	0.19397×10^{8}	0.1421
104.858	11.643	0.45466×10^{6}	0.1252	115.029	13.397	0.23875×10^{7}	0.1287
110.681	11.520	0.12402×10^{7}	0.0932	122.988	13.368	0.95017×10^{6}	0.0962
112.777	11.739	0.17372×10^{7}	0.0512	101.697	9.929	0.27213×10^{6}	0.0479
102.111	15.610	0.31938×10^{6}	0.0785	101.641	15.573	0.28695×10^{6}	0.0784
109.937	16.493	0.12881×10^{7}	0.0853	106.148	15.924	0.66506×10^{6}	0.0850
106.281	16.214	0.82854×10^{6}	0.0893	107.082	16.196	0.95273×10^{6}	0.0894
111.685	15.948	0.9682×10^{7}	0.0445	106.456	15.103	0.37061×10^{7}	0.0460
105.106	10.839	0.2120×10^{7}	0.0840	107.950	11.283	0.3466×10^{7}	0.0860
96.657	12.948	0.48469×10^{6}	0.0731	107.44	14.601	0.32428×10^{7}	0.0802

For simplicity in correlation and computation, we recommend the use of a one-region unequally weighted nonlinear regression technique to treat the TGA data.

A comparison of the kinetic parameters obtained by this technique for a variety of international oil shales is presented in Table IX.

Comparison of Reaction Rate Constants of Various Oil Shale Samples. Based on Anthony and Howard's assumption of a Gaussian distribution of activation energies and on the Arrhenius equation, the kinetic parameters and the reaction rate constant for a specific temperature were calculated according to the following equation:

$$k = \frac{Z}{\sigma(2\pi)^{1/2}} \int_{E_o - 2\sigma}^{E_o + 2\sigma} \exp\left\{ [-\frac{E}{RT}] \; [-\frac{1}{2}] \; \left[\frac{(E - E_o)}{\sigma} \right]^2 \right\} dE \qquad (27)$$

The calculated rate constants (based on the parameter values given in Table X at 425°C) for the various oil shales are presented in the last column of Table IX. The rate constants of the shales under study vary widely. However, it has not yet been determined whether the variation is due to significant geological and chemical differences or whether it is within the limits which might be expected within a single deposit. The Arrhenius plots (ln k versus 1/T) of the various oil shales are shown in Figure 2. From this plot, it can be seen that the pyrolysis rates vary from lowest to highest by about a factor of ten over the decomposition temperature range. The Moroccan shale gave the highest rate with one of the Chinese samples showing the lowest rate. Curve 13 is for the oil appearance not TGA kinetics and therefore has a greater slope or activation energy.

Summary

This study addresses the measurement, analysis, and comparison of pyrolysis kinetics and other characteristic parameters for several key international oil shales. Geologic and chemical information about each of the oil shale samples is presented to illustrate the widely varying nature of oil shale.

A summary of the kinetic models and data analysis methods is presented below along with the more significant kinetic results.

I.   The weight loss data were first treated using the two parameter models (Coats-Redfern and Chen-Nuttall). The calculated activation energies were generally very low in comparison to the energies of the bonds that are considered to be breaking in the reaction, thus leading to the evaluation of more sophisticated treatment methods and kinetic models.

Table X. Comparison of the Kinetic Parameters of Various Oil Shales*

NUMBER	SAMPLE	HEATING RATES (°C/MIN)	E (KJ/MOL)	E (KCAL/MOL)	σ (KJ/MOL)	σ (KCAL/MOL)	Z (MIN^{-1})	k, MIN^{-1} (at 425°C)
1	Moroccan	1,2,5,10	106.819	25.512	9.240	2.207	0.9654×10^7	0.2304
2	Moroccan	1,2,5,10,20,50	97.750	23.346	11.163	2.666	0.2202×10^7	0.3617
3	Australian	2,5,10,20	164.514	39.292	17.911	4.278	0.3140×10^{11}	0.2508
4	Swedish	2,5	142.903	34.170	18.290	4.368	0.8943×10^8	0.0326
5	Chinese #1	1,2,5	164.537	39.309	18.442	3.210	0.1064×10^{11}	0.0284
6	Chinese #2	1,2	141.769	33.364	10.190	2.434	0.3589×10^9	0.0247
7	Chinese #3	1,2	154.975	37.013	13.016	3.109	0.2928×10^{10}	0.0341
8	Chinese #4	1,2	111.045	26.521	8.290	1.980	0.1604×10^7	0.0157
9	Chinese #5	1,2,5	135.710	32.412	15.328	3.661	0.1393×10^7	0.0836
10	Israel	1,2	104.904	25.055	9.949	2.376	0.2519×10^7	0.0952
11	Brazil	1,2	111.271	26.575	10.581	2.527	0.2679×10^6	0.0382
12	Yugoslavia	1,2	97.952	23.394	8.027	1.917	0.5902×10^7	0.0528
13	U.S. Utah	1,2	107.950	25.782	11.283	2.695	0.3466×10^7	0.1006
14	U.S. Utah	1	107.921	25.775	9.381	2.241	0.5472×10^7	0.1107

* Parameters values were determined by CR-AH-LM program (unequally weighted).
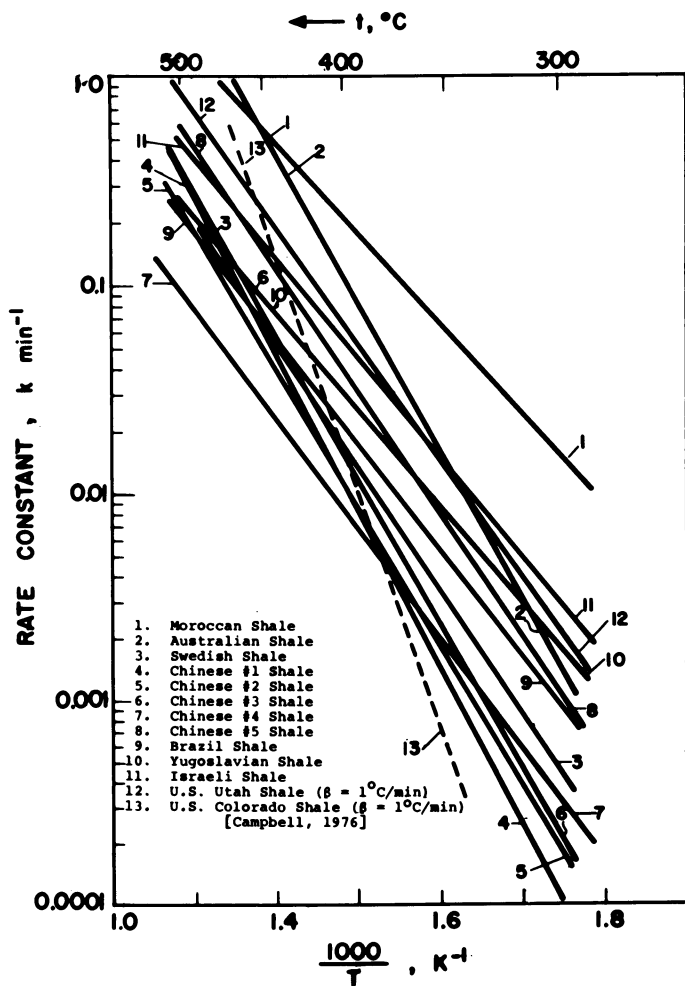
Figure 2. Arrhenius plot of various oil shales (one-region, unequally weighted).

II.   Next, the TGA data were treated using the models men-
tioned in (I), but the temperature range was divided
into two regions (i.e., regions above and below
375°C). This approach gave a better fit to the single
heating rate data, but was not satisfactory for corre-
lating the full multiple heating rate data.

III. The three parameter model, by Anthony and Howard, was
best for correlating the full range of nonisothermal
data. Although other investigators have used the
Anthony-Howard model to describe gas evolution from oil
shale (25-27), this is the first time that the model
has been applied in a TGA study of oil shale pyroly-
sis. The calculated activation energies were deemed
more reasonable with respect to bond energies and the
overall fit to the data was improved as compared to the
two-parameter models. This model gave satisfactory
results for the full range of heating rates tested. Of
course, a different set of model parameters was
required for each sample.

IV.   The Moroccan shale exhibited the highest kinetic rate
constant.

V.   The Moaming Chinese samples gave the lowest pyrolysis
rates.

VI.   The pyrolysis results clearly show that oil shales
differ greatly in their thermal decomposition behavior,
and that for some processes, modifications or new reac-
tor designs may be needed to optimally treat a specific
oil shale. Since oil shales are from widely different
geographical locations and were formed at greatly dif-
ferent geological times, it is not surprising that the
pyrolysis kinetics and other properties vary widely.

Acknowledgment

Literature Cited

1   Hubbard, A. B. and W. E. Robinson, "A Thermal Decomposition
Study of Colorado Oil Shale," USBM Rept. of Invest. 4744,
1950.

2   Campbell, J. H., G. Koskinas, and N. Stout, Fuel 1978, 57, 372.

3   Braun, R. L. and A. J. Rothman, Fuel 1975, 54, 129.

4   Granoff, B. and H. E. Nuttall, Fuel 1977, 56, 234.

5   Chen, W. J. and H. E. Nuttall, "A TGA Study of Colorado Oil Shale with a New Kinetic Model," 86th AICHE National Meeting, Houston, Texas, April 1979 (unpublished).

6   Coats, A. W. and J. P. Redfern, Nature 1964, 201, 68.

7   Anthony, D. B., J. B. Howard, H. C. Hottel, and H. P. Meissner, Fifteenth Symposium (International) on Combustion, The Combustion Institute 1975, p. 1303.

8   Swarbrick, C.F.J., Geological Survey of Queensland, Rept. No. 83 1974, p. 56.

9   Lindner, A. W. and D. A. Dixon, The APEA Journal 1976, 16:1, 165-172.

10 Kraemer, A. J., USBM Rept. of Invest. 4655 1950, p. 36.

11 Qian, J. L., "Oil Shale Industry of China," United Nations Conference on New and Renewable Sources of Energy, August 1981.

12 Shirav, M. and D. Ginzburg, International Symposium on Oil Shale Chemistry and Technology, Jerusalem, Israel, 1978.

13 Bouchata, R. and A. Marcil, 6th IIASA Conference "World Oil Shale Resources and Their Potential Development" 1981.

14 Thakur, D. S., H. E. Nuttall, and C. Y. Cha, American Chemical Society, Division of Fuel Chemistry 1982, 27, 131-142.

15 Guthrie, B. and S. Klosky, USBM Rept. of Invest. 4776 1951, p. 33-43.

16 Hellestane, S., 6th IIASA Conference "World Oil Shale Resources and Their Potential Development" 1981.

17 Smith, J. W., CSM Mineral and Energy Resources--A Review of Developments 1980, 23:6.

18 Mijatovic, I. N. and B. Kapor, 6th IIASA Conference "World Oil Shale Resources and Their Potential Development" 1981.

19 Jaffe, Felix C., Mineral Industries Bulletin 1962, 5:2.

20 Yen, T. F. and G. V. Chilingarian, Ed., "Oil Shale," vol. 5, New York, Elsevier Publishing Co., 1976.

21 Tissot, B. P. and D. H. Welte, "Petroleum Formation and Occurrence," Springer-Verlag, New York, 1978.

22 Miknis, F. R. and J. W. Smith, 15th Oil Shale Symposium Proceedings 1982, p. 50-62.

23 Maier, C. G. and S. R. Zimmerley, University of Utah Bulletin 1924, no. 14, p. 62-81.

24 Blazek, A., "Thermal Analysis," J. F. Tyson (Translation Ed.), Van Nostrand-Reinhold Co., London, U.K., 1973.

25 Huss, E. B. and A. K. Burnham, Fuel 1982, 61, 1188.

26 Campbell, J. H., G. J. Koskinas, G. Gallegos, and M. Gregg, Fuel 1980, 59, 718.

27 Campbell, J. H., G. Gallegos, and M. Gregg, Fuel 1980, 59, 727.

RECEIVED April 7, 1983

Molecular Mechanism of Oil Shale Pyrolysis in Nitrogen and Hydrogen Atmospheres

F. HERSHKOWITZ, W. N. OLMSTEAD, R. P. RHODES, and K. D. ROSE

Exxon Research and Engineering Company, Corporate Research-Science Laboratories, Linden, NJ 07036

This paper describes the changes in carbon functionality that occur during the pyrolysis and hydropyrolysis of Colorado oil shale. This paper is different from earlier work in that characterization of shale and products is combined with highly mass-balanced reactions to allow a mechanistic discussion of the role of functionalities in the generation of oil during shale pyrolysis. We identify some important factors in maximizing the conversion of kerogen to oil. Colorado oil shale was pyrolyzed under conditions of slow heatup ($6°C/min$) and short gas residence times (2-4 sec) in a nitrogen or hydrogen atmosphere at 2600 kPa. Product characterization was by elemental analysis, GC (gas), and NMR (solid & liquid). The aliphatic portion of the shale either cracks to give oil and gas or aromatizes to give aromatics in the oil or spent shale. There is an 80% increase in aromatic carbon during pyrolysis. The aromatic portion of the kerogen either cracks to give oil or ends up in the spent shale. Mineral carbonates, rather than organic functionalities, are the source of most of the CO_2. Hydrogen is effective at inhibiting the reactions which lead to aromatization and formation of residual carbon. Molecular hydrogen in the system also reduces carbonates to methane and water.

Increased knowledge of the molecular transformations which occur during oil shale pyrolysis (retorting) is essential for maximizing the yield and quality of products from this vast source of hydrocarbons. Compared to other sources such as petroleum and coal, there is little known about the molecular structure of the insoluble organic material (kerogen) in oil shale. There is

even less known about the molecular transformations that occur
during pyrolysis of oil shale to give gaseous, liquid and solid
products.   Pyrolysis in a hydrogen atmosphere gives enhanced
liquid yields, but little is known about the chemical origin of
this effect (1,2).   This paper describes a study designed to
fill these gaps in our knowledge of the molecular mechanisms of
oil shale pyrolysis in nitrogen and hydrogen atmospheres.
     There is little literature on the chemical mechanisms of
pyrolysis of oil shale to give gaseous, liquid and solid prod-
ucts.   One reason for this is that workers in that field have
either studied the kinetics of pyrolysis and have not fully
analyzed the products, or they have analyzed the products (es-
pecially the oil) without fully material balancing the starting
material and products.   A second reason is the lack of knowledge
about the molecular structure of the starting material, the
shale organic kerogen.
     One important parameter, the aromaticity of shale kerogen,
has been quantified using recent advances in solid state ^{13}C-NMR
(nuclear magnetic resonance).   This technique has placed the
carbon aromaticity value at about 20% for Colorado oil shale and
has led to some elucidation of the pyrolysis mechanism (3-5).
There is a strong correlation between shale Fischer Assay oil
yield and the quantity of aliphatic carbon in the kerogen.
There is also a nearly quantitative equivalence of aromatic
carbon in the spent shale to aromatic carbon in the original
shale under Fischer assay conditions.   The conclusion is that
the aromatic carbons in the shale are largely inert towards
thermal processing and remain in the spent shale as residual
carbon.   An admitted limitation of the model (4) is the failure
to account for aromaticity of the oil product which is typically
25% (6,7).   It will be seen in this paper that an important
reaction during oil shale pyrolysis is the transformation of
aliphatic carbon in the starting shale to aromatic carbon in the
products.
     The kinetics of shale pyrolysis have been studied exten-
sively.   In the late 1940's, Hubbard and Robinson (8) studied
the conversion of shale kerogen (the insoluble organic matter)
to bitumen (soluble organic matter), oil (volatile organic mat-
ter) and gas.   Their comprehensive data set for conversions
versus temperature and time has been the subject of kinetic
analyses by subsequent theorists (9,10).   These kinetic analyses
present a shale pyrolysis model as follows:

$$\text{Kerogen} \xrightarrow{\quad k_1 \quad} \text{Bitumen} \xrightarrow{\quad k_2 \quad} \text{Oil}$$
$$\qquad\qquad\qquad (+ \text{ gas} + \text{coke}) \qquad (+ \text{ gas} + \text{coke})$$
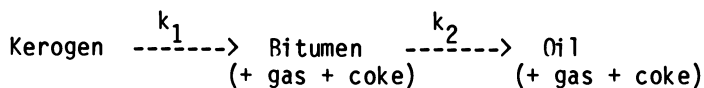
Although considerable experimental refinements have been made
(11), this model has remained as a phenomenologically sound
representation of retorting kinetics.   As discussed above, a

more scientific understanding of retorting kinetics requires an understanding of the chemical changes that occur during pyrolysis. The following studies are of note in this regard.

The study of shale and product aromaticity mentioned above led to the proposal of the mechanism in Figure 1. Although no attempt was made to quantify the reactions in this figure, it presents a significant increase in our understanding of shale pyrolysis. In other studies, a kinetic analysis was combined with detailed characterization of the gaseous products of pyrolysis (12-14). This has resulted in a good understanding of the mechanisms of gas formation: the evolution of H_2 and CH_4 involves processes that were interpreted as a "primary" pyrolysis of the kerogen to generate oil, and a higher temperature (>500°C) "secondary" pyrolysis of the carbonaceous residue.

Recent shale hydropyrolysis research is limited (in the open literature) to a program at the Institute of Gas Technology (1,2). Product characterization and mass balancing were combined to develop some understanding of the reactions of Colorado oil shale hydropyrolysis. Kerogen was converted predominantly in the 425 to 525°C temperature range at pressures up to 3450 kPa. In constant heating rate experiments, organic carbon conversions exceeding 90% were achieved by 550-600°C before the inorganic carbon significantly decomposed. Above 600°C, further increases in organic carbon conversion were achieved only with large simultaneous conversions of carbonate minerals. As the temperature approached 700°C, carbonate mineral conversion approached 100%. The organic carbon and carbon oxide balances indicated that some carbon oxides (from mineral decomposition) were being converted to methane by hydrogen in the reactor.

We have retorted Colorado oil shale under nitrogen and hydrogen atmospheres in one reactor under the same conditions. Characterization of the gaseous, liquid and solid products together with good material and elemental balances has enabled an increased understanding of what reactions occur during retorting. Comparison of results in a hydrogen vs. nitrogen atmosphere has elucidated the important pathways which are affected by hydrogen, leading to enhanced oil yields.

Experimental

Oil shale (33 gal/ton by Fischer assay) from the Piceance Basin (Green River Formation, Colony mine) in Colorado was crushed and sieved to -16/+60 mesh. Retorting was carried out in a fixed bed reactor at a pressure of 2.6 MPa (380 psig) with a slow (6°C/min.) heat up to 600°C followed by 10 min. at 600°C. Short gas residence times were used to minimize secondary oil degradation reactions. Gases were analyzed by GC using a Carle 157A refinery gas analyzer. Liquids were collected in a cyclone, and the water was separated from the oil by distillation.
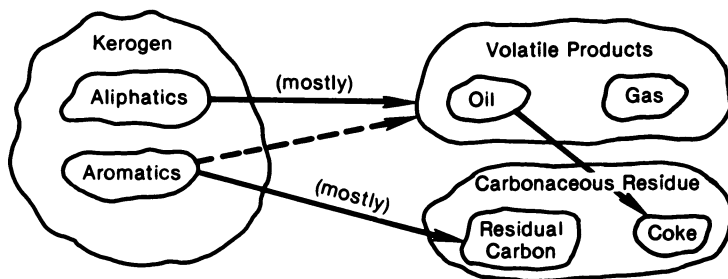
Figure 1. A proposed reaction model for oil shale pyrolysis. (Reproduced with permission from Ref. 4. Copyright 1981, Colorado School of Mines.)

Carbon and hydrogen contents were determined by combustion analysis, nitrogen by the Mettler method, sulfur by the Leco method and carbonate carbon by measuring the CO_2 evolved on acid treatment. Hydrogen and carbon NMR spectra were obtained using Varian EM-360 and Varian XL-100 spectrometers, respectively. For ^{13}C measurements on chloroform-d_1 solutions, sample and instrument conditions were chosen which consistently provide quantitative carbon ratios, including the use of a chromium paramagnetic relaxation reagent and gated proton decoupling for NOE suppression. Solid-state ^{13}C NMR spectra were obtained on a JEOL-FX60OS spectrometer using high-power dipolar deoupling, ^1H-^{13}C cross-polarization and magic-angle sample spinning. A two-millisecond CP contact time and two second repetition delay were used throughout. Kel-F rotors filled with 400 mg of sample were rotated at about 2200 Hz. Carbon aromaticity values on solid samples were determined by measuring the fraction of total inte-grated intensity which appeared between 200 and 90 ppm (relative to externally referenced tetramethylsilane). This chemical shift region also includes carboxyl carbons. The carboxyl con-tent of the shale used in this work is <1% of the organic car-bon, judging from NMR results (5) and the CO_2 yield from the organic kerogen.

Results and Discussion

Analysis of the starting shale, retorting yields and conver-sions, elemental analysis of the oil and spent shale, and NMR analysis of the oil are summarized in Tables I-IV.

The oil yield in an N_2 atmosphere is less than Fischer assay because of the high pressure used here (15,16). The oil yield in an H_2 atmosphere is 117% of Fischer assay and 130% of the yield in N_2 at the same pressure. Comparison of the two oils shows that they have similar carbon and hydrogen contents and aromaticities, but oil produced in an H_2 atmosphere has a higher nitrogen content and lower sulfur content. The elemental and NMR oil analyses are similar to results for Fischer Assay and IGT Hytort (H_2) shale oils (17).

The data in Tables I-III have been used to calculate ele-mental balances. The results are shown in Table V with all of the numbers put on a molar basis and normalized to 100 organic carbons in the starting shale. This treatment makes it easy to follow the movement of the elements and simplifies the discus-sion of molecular transformations occurring during retorting. The recovery of carbon (organic plus inorganic) is 95-96% for each experiment.

Table V has been further refined and combined with the NMR analysis to give diagrams (Figures 2 and 3) showing the relative abundances of each carbon functionality in reactants and prod-ucts. The organic carbon in the spent shale is assumed to be aromatic, as has been found by ^{13}C NMR for spent shales genera-

Table I. Analysis of Shale

	% On Dry Shale
C	20.55
H	2.22
N	0.73
S	0.82
Carbonate C	5.08
Organic C	15.47
^{13}C Aromaticity, % of Org C	24.

Table II. Yields and Conversions

Yield, % of Dry Shale	Atmosphere	
	N_2	H_2
Char	82.03	72.56
Oil (Fischer Assay = 13.3)	11.97	15.61
Water	1.48	6.16
Total Gases	3.92	5.29
C_1-C_4	0.98	2.12
CO	0.09	1.47
CO_2	2.76	1.56
H_2S	0.08	0.07
Total Recovery	99.40	99.62
Conversion[a], %		
Mass	17.97	27.44
Carbon	60.4	79.8
Organic Carbon	73.5	91.6
Carbonate Carbon	20.7[b]	44.0

[a] Derived from analysis of spent shale.

[b] This value is higher than for Fischer Assay because of the higher maximum temperature (600°C).

Table III. Elemental Analysis of Products

		Atmosphere	
Oil		N_2	H_2
C		82.66	83.12
H		11.02	10.91
N		1.72	2.36
S		0.74	0.52
H/C molar ratio		1.59	1.56
Spent Shale			
C		9.91	5.72
H		<0.3	<0.3
N		0.50	0.32
S		0.92	0.70
Carbonate C		4.91	3.92
Organic C		5.00	1.80

Table IV. NMR Analysis of Oils

		Atmosphere	
		N_2	H_2
^1H	% Aromatic	6.6	7.3
	% Olefinic	3.1	2.6
	% Aliphatic	90.3	90.1
^{13}C	% Aromatic[a]	23.2	21.4
	% Aliphatic	76.0	78.0
	% Terminal Olefinic[b]	0.8	0.6
H_{arom}/C_{arom}		0.45	0.53
H_{aliph}/C_{aliph}		1.89	1.80

[a] Includes olefinic carbons other than terminal olefins.
[b] Estimated from carbon spectrum.

Table V. Molar Balances from Retorting Of Colorado Oil Shale

Starting Shale: $Corg_{100}Cin_{33}H_{171}N_{4.0}S_{2.0}$

	N_2	H_2
Spent Shale	$Corg_{27} Cin_{26} H?^a N_{2.3} S_{1.8}$	$Corg_8 Cin_{18} H?^a N_{1.3} S_{1.2}$
Oil	$Corg_{64} H_{101} N_{1.1} S_{0.2}$	$Corg_{84} H_{131} N_{2.0} S_{0.2}$
Water	$H_{13} O_{6.5}$	$H_{53} O_{26.5}$
C_1-C_4 Gases	$Corg_5 H_{17}$	$Corg_{11} H_{39}$
CO	$Cin_{0.3}$	$Cin_{4.1}$
CO_2	$Cin_{4.9}$	$Cin_{2.8}$
Total	$Corg_{96} Cin_{31} H^a_{131} N_{3.4} S_{2.0}$	$Corg_{103} Cin_{25} H^a_{223} N_{3.3} S_{1.4}$

[a] H in spent shale too low for accurate analysis; see text for discussion of hydrogen incorporation during hydropyrolysis.
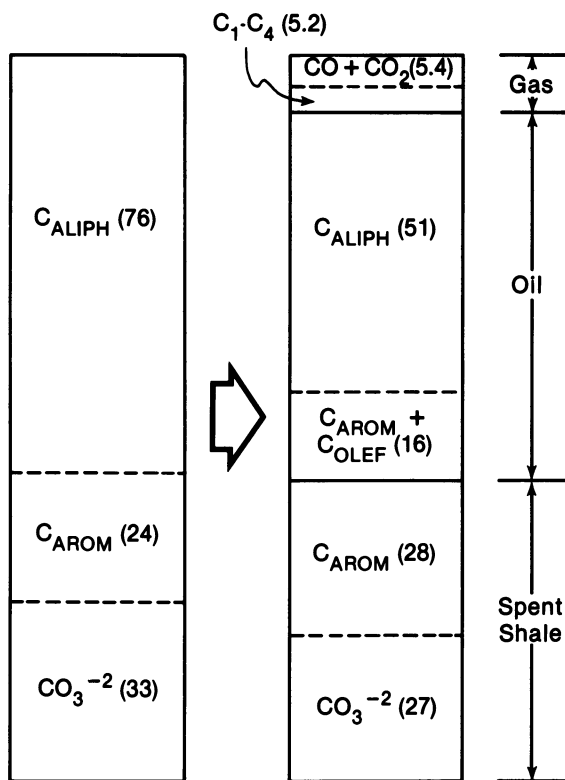
Figure 2. Distribution of carbon functionalities in Colorado shale and products from retorting in an inert atmosphere. Numbers in parentheses are the percentages of starting organic carbon in each fraction.
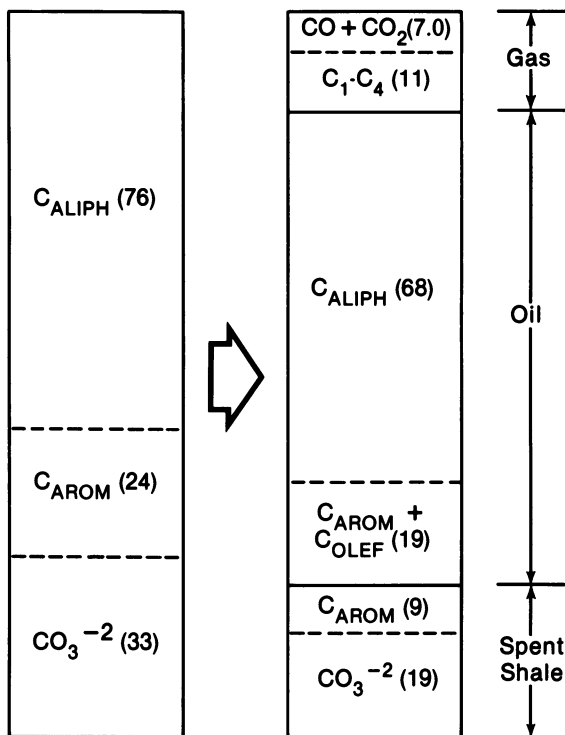
Figure 3. Distribution of carbon functionalities in Colorado shale and products from retorting in a hydrogen atmosphere. Numbers in parentheses are the percentages of starting organic carbon in each fraction.

ted at a maximum temperature 100°C less than the maximum temperature for these runs (5). In these figures, the height of any bar segment is proportional to the amount of carbon that is present as the indicated functionality. In addition, for Figures 2 and 3, but <u>not</u> for Table V, the products have been normalized to 100% carbon balance by assuming a uniform loss of carbon from all products. The product distributions are for the conditions stated in the Experimental section and would vary for different conditions. In particular, the data in a nitrogen atmosphere are at an elevated pressure and therefore are somewhat different from what would be attained under Fischer assay conditions(16).

Previous discussions of the role of aromaticity in shale pyrolysis have led to the proposal that aliphatic carbon evolves as oil and aromatic carbon remains in the spent shale (3-5). Although it describes the major reactions, this oversimplified mechanism cannot quantitatively account for all of the products shown in Figure 2. The reactions responsible for these changes can be summarized as follows:

C_{ALIPH}: Most of the aliphatic carbon in the oil shale evolves and is collected in the shale oil as aliphatic carbon. One-third (25 out of 76) of the aliphatic carbon takes part in disproportionation reactions, yielding hydrogen-rich gases and hydrogen-poor aromatic carbon. The aliphatic carbon-carbon bond cleavage (cracking) reactions which lead to C_1-C_4 gas formation are also partially responsible for the depolymerization of kerogen to form oil. The free radicals which are formed during the cracking reactions are capped by hydrogen atoms from aliphatic portions of the kerogen. This removal of hydrogen converts a fraction of the aliphatic carbon to aromatic carbon. Some of this aromatic carbon evolves with the oil, and some remains in the spent shale. It is impossible to tell the proportions of each from the data because the aromatic carbon in the products can come from either aliphatic or aromatic carbon in the starting shale.

C_{AROM}: Aromatic carbon tends to remain in the spent shale as a refractory carbonaceous material we call residual carbon. An unknown proportion evolves as part of the oil.

CO_3^{-2}: The inorganic carbonates are mostly stable and end up in the spent shale. Those which decompose are quantitatively recovered in the gas as CO_x (principally CO_2). Most of this CO_x is evolved at temperatures over 500°C. Very little CO_x (<1/100 C_{org}) comes from the organic kerogen in this oil shale.

Because of the tendency for aromatic carbon to form residual carbon, the reaction of aliphatic carbon to form aromatic carbon during retorting is deleterious to the goal of obtaining high yields of oil from shale. In fact, there is more aromatic carbon in the spent shale than in the original shale, (28 vs. 24 in Figure 2) proving that some aliphatic carbon becomes residual carbon during retorting.

One way to inhibit the aromatization and residual carbon formation is to carry out the retorting in the presence of molecular hydrogen. The distribution of carbon functionalities in the products from hydropyrolysis is shown in Figure 3. There is very little aromatization during retorting in hydrogen, resulting in almost complete recovery of the shale aliphatic carbon as oil aliphatic carbon. Hydrogen also inhibits the condensation reactions which lead to residual carbon in the spent shale, resulting in more aromatic carbon in the oil than in the spent shale. This proves that the aromatic fraction of the kerogen is reactive and can be converted to oil. It is not a refractory, highly crosslinked carbonaceous material which is destined to remain in the spent shale. A hydrogen induced pathway is the hydrogenolysis of carbon-carbon bonds to give hydrocarbon gases. The higher values of H_{arom}/C_{arom} (Table IV) may be an indication that hydrogen cleaves some aromatic-aliphatic bonds. This reaction has been observed under coal liquefaction conditions (450°C, 11 MPa H_2) (18).

Solid state NMR spectra group together different types of aliphatic carbons such as hydroaromatic (e.g. tetralin), naphthenic (e.g. decalin), or paraffinic (e.g. decane or 1-phenyldecane). Any or all of these could be dehydrogenated by hydrogen abstraction by free radicals to form aromatic carbon during pyrolysis. The two most likely roles of molecular hydrogen in inhibiting this conversion are: (1) hydrogenation of aromatic rings to regenerate hydroaromatics and naphthenes and (2) an alternative source of H atoms (rather than the aliphatic portion of the kerogen) for capping free radicals by equation 1. Without further characterization of the aliphatic carbon in the

$$R\cdot + H_2 \rightarrow RH + H \qquad\qquad (1)$$

starting shale it is impossible to quantify either the source of the aromatic carbon which is formed during pyrolysis or the exact role(s) of hydrogen in inhibiting this aromatization.

Molecular hydrogen also induces the decomposition and reduction of carbonate minerals, as observed by others (1). This can best be seen from our data by comparing the larger yield of total C_{org} and lower yield of total C_{in} under H_2 in Table IV. This reduction leads to more H_2O, CH_4, and CO in an H_2 atmosphere. The reactions involved are summarized in Scheme 1. The larger amount of carbonates decomposed in H_2 vs. N_2 and the comparative yields of H_2O, CO_2, CO, and CH_4 (5.2 out of the

extra 5.8 C$_{org}$ in the gases in a hydrogen atmosphere appear as CH$_4$) all fit this scheme quantitatively. Although the first reaction in Scheme 1 is endothermic (12) and thermodynamically unfavored under our conditions, the second and third reactions are favored; by removing CO$_2$ from the system, they drive the first reaction forward.

<u>Scheme 1 (M = Ca or Mg)</u>

$$MCO_3 \rightleftharpoons MO + CO_2$$

$$CO_2 + H_2 \rightleftharpoons CO + H_2O$$

$$CO + 3H_2 \rightleftharpoons CH_4 + H_2O$$
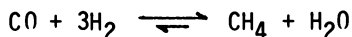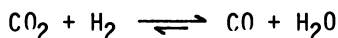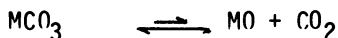
A diagram for the fate of native hydrogen (organic and inorganic) in retorting products is shown in Figure 4. This diagram is drawn to scale using the data in Tables IV and V. The H/C$_{org}$ ratio (organic and inorganic hydrogen) of the spent shales is estimated as 0.7. For the N$_2$ run, the hydrogen balance is 92%; an additional amount of H$_2$ (3%, as found elsewhere (12)) has been added since the gases were not analyzed for this product. The larger amount of the hydrogen atmosphere products reflects incorporation of molecular hydrogen into the products. A large part of the hydrogen incorporated is as a result of the reactions in Scheme 1. There is very little known about hydrogen types in shale, so the other reactions cannot be discussed in detail.

As shown in Table V, there is a great propensity for nitrogen to end up in the spent shale. An important factor behind this is the association of nitrogen with aromatic carbon in heterocyclic ring structures coupled with the tendency for aromatic carbon to form residual carbon as discussed above. Another important factor behind the propensity for nitrogen to end up in the spent shale is the existence of nitrogen in thermally unreactive mineral matter in the starting shale(19, 20). Also shown in Table V is the propensity for sulfur to end up in the spent shale. The reason for this is that most of the sulfur is present as iron pyrite, which is not very reactive thermally (21).

Conclusions

Through well controlled retorting and careful collection and characterization of the gaseous, liquid and solid products, many of the molecular transformations which occur during retorting have been elucidated. In an inert gas, at high pressure and slow heating rates, the aliphatic carbon portion of the kerogen predominately cracks to give oil and a small amount of hydrocarbon gases. A significant fraction aromatizes and ends up in
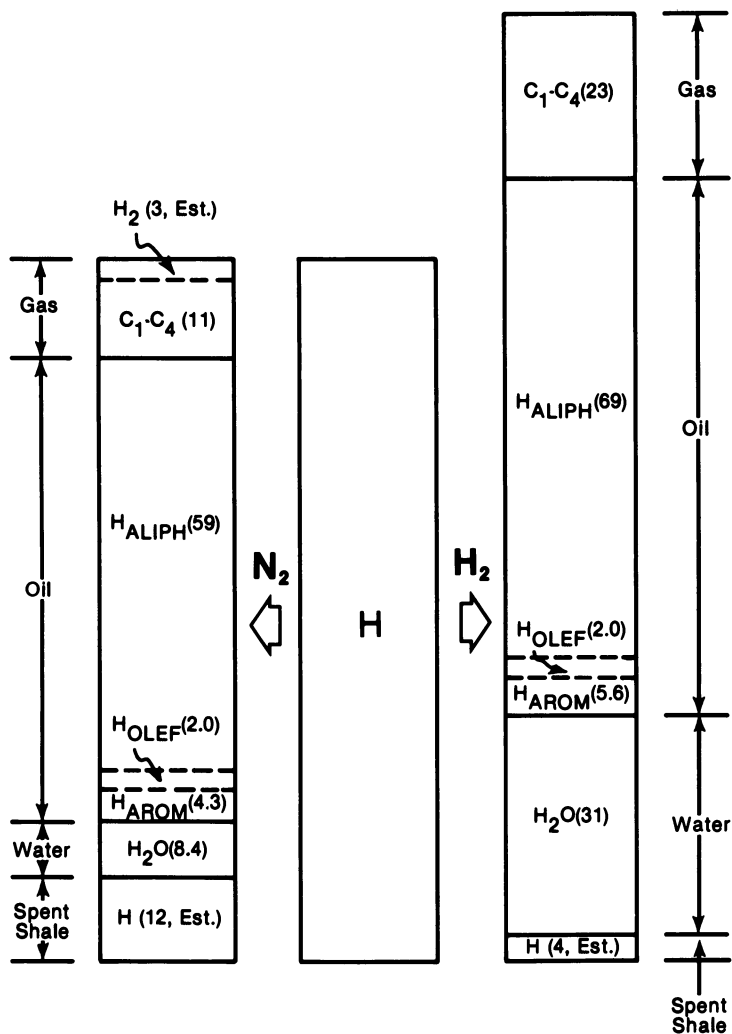
Figure 4. Distribution of hydrogen functionalities in products from retorting Colorado shale in nitrogen and hydrogen atmospheres. Numbers in parentheses are the percentages of starting hydrogen in each fraction.

either the oil or spent shale. Both aromatic carbon and nitrogen have high tendencies to coke and end up in the spent shale.
    Retorting in a hydrogen atmosphere is an effective method of increasing the conversion of the organic kerogen in oil shale to oil. A total of 87% of the organic carbon in Colorado oil shale is recovered as oil in a hydrogen atmosphere, compared to 67% in an inert atmosphere. The principal reason for this is that hydrogen inhibits the conversion of aliphatic carbon to aromatic carbon and inhibits the conversion of aromatic carbon to residual carbon. Hydrogen also increases the conversion of inorganic carbonate minerals by reducing them to methane and water.

Acknowledgments

Literature Cited

1. Neil, S. A.; Feldkirchner, H. L.; Tarman, P. B. in "Shale Oil, Tar Sands, and Related Fuel Sources," Yen, T. F., Ed.; ADVANCES IN CHEMISTRY SERIES No. 151. ACS: Washington, D.C., 1974; p. 55.
2. Feldkirchner, H. L.; Janka, J. C. Proc. IGT Synthetic Fuels from Oil Shale Symp. 1979; p. 489.
3. Miknis, F. P.; Maciel, G. E. Proc. 14th Oil Shale Symp., Gary, J. H., Ed.; Colorado School of Mines Press: Golden, CO, 1981; p. 270.
4. Fausett, D. W.; Miknis, F. P. ibid., p. 154.
5. Miknis, F. D.; Szeverenyi, N. M.; Maciel, G. E. Fuel 1982, 61, 341-345.
6. Resing, H.; Garroway, A. N.; Hazlett, R. N. ibid. 1978, 57, 450-454.
7. Netzel, D. A.; McKay, D. R.; Heppner, R. A.; Guffey, F. D.; Cooke, S. D.; Varie, D. L.; Linn, D. E. ibid. 1981, 60, 307-320.
8. Hubbard, A. B.; Robinson, W. E. "A Thermal Decomposition Study of Colorado Oil Shale," Report of Investigation 4744, Bureau of Mines, Washington, D.C., 1950.
9. Allred, V. D. Chem. Eng. Prog. 1966, 62, 55-60.
10. Braun, R. L.; Rothman, A. J. Fuel 1975, 54, 129-131.
11. Wallman, P. H.; Tamm, P. W.; Spars, B. G. in "Oil Shale, Tar Sands, and Related Materials," Stauffer, H. C., Ed.; ACS SYMPOSIUM SERIES No. 163, ACS: Washington, D.C., 1981; p. 92.
12. Campbell, J. H.; Koskinas, G. J.; Gallegos, G.; Gregg, M. Fuel 1980, 59, 718-726.
13. Campbell, J. H.; Gallegos, G.; Gregg, M. ibid. 1980, 59, 727-732.

14.   Huss, E. B.; Burnham, A. K. ibid. 1982, 61, 1188-1196.
15.   Noble, R. 0.; Tucker, W. F.; Harris, H. G., ibid. 1982, 61, 482-484.
16.   Burnham, A. K.; Singleton, M. F. This Symposium.
17.   Netzel, D. A.; Miknis, F. P. Fuel 1982, 61, 1101-1109.
18.   Vernon, L. ibid. 1980, 59, 101-106.
19.   Cooper, J. E.; Evans, W. S. Science 1983, 219, 492-493.
20.   Vadovic, C. This Symposium.
21.   Burnham, A. K.; Taylor, R. W. Proc. 15th Oil Shale Symp., Gary, J. H., Ed.; Colorado School of Mines Press: Golden, CO, 1982; p. 299.

Chemical and Retorting Properties of Selected Australian Oil Shales

A. EKSTROM, H. J. HURST, and C. H. RANDALL

Lucas Heights Research Laboratories, CSIRO Division of Energy Chemistry, Private Mail Bag 7, Sutherland, NSW, 2232, Australia

The rates of oil, hydrogen, methane, carbon dioxide and carbon monoxide evolution during the retorting of five Australian oil shales at linear heating rates have been determined and analysed in terms of the Anthony-Howard model for non-isothermal kinetics. Significant differences in the retorting properties of these shales were obtained, particularly with respect to the rates of the hydrogen and carbon dioxide evolution.

Much of the present understanding of the chemical processes occurring during the heating and retorting of oil shales is based on work carried out with shales from the American Green River deposit (1-3). However, this shale is not typical of oil shales found in other deposits, and comparative studies of the chemical properties and retorting chemistry of a variety of shales might provide further insights into the undoubtedly very complex chemistry of these materials.

This paper presents results of some laboratory scale studies of the chemical and retorting properties of representative samples from five Australian oil shale deposits. In general terms, the results indicate that these shales differ significantly in their chemical properties both from each other and from the shale of the Green River deposit.

Experimental Procedures

The kinetics of oil and gas formation during the retorting of the shales were determined using an apparatus essentially identical to that described by Campbell et al (2). Heating rates of 3°K/min were used and the argon carrier gas flow rates were 130 cc/min for the determination of oil formation, and 30 cc/min for determination of the rates of gas evolution. The shale samples used in these studies were sized, and dried at 110°C for 12 hours prior to use.

Demineralisation of the shales was carried out using HF/HCl digestion on -90 μm sized samples, followed by extensive washing with demineralised water. The ash content of the kerogens so obtained was determined by heating samples to 800°C in air. Solvent extraction studies of the demineralised shale were carried out using conventional soxhlet extractors. TGA studies were carried out using a computer-controlled Cahn thermobalance (Model No. RG2000) of conventional design. Elemental analyses were performed on samples dried at 110°C and were carried out by the Australian Microanalytical Service of the Australian Mineral Development Laboratories.

Results and Discussion

The samples of shale used in this work all originated in various shale deposits located near the coastal areas of central Queensland. These deposits are believed to be of Tertiary age and of lacustrine origin, and in contrast to the Green River deposit contain only small amounts of mineral carbonates. As summarised in Table 1, the chemical composition of these shales differ widely, ranging from the Nagoorin carbonaceous shale with an organic carbon content of 65%, to the Duaringa shale with an organic carbon content of 11%. The precise origin and nature of the black or carbonaceous shales found in the Nagoorin and Condor deposits are not completely understood at present but, from a chemical viewpoint, significant differences between the black and normal shales are readily apparent. Thus the black shales are generally characterised by a high kerogen content of lower H/C ratio and a markedly lower oil yield per gram of organic carbon in the shale. As will be shown below, the kinetics of the gas evolution from the black shales also differ from those of the normal shales.

The results of extraction of the kerogens isolated from the Stuart and Nagoorin shales with solvents of increasing polarity (Table 2) indicate that these kerogens contain significant proportions of relatively low molecular weight, and presumably polar compounds. The fraction of kerogen extractable with a given solvent appears to be comparable with the results of similar studies on the Green River kerogen (4) and indeed with those obtained for bitumenous coals (5,6). The appearance of the extract ranged from pale waxes for the less polar solvents to black, lustrous solids for pyridine, dimethyl formamide and dimethyl sulphoxide. The nature of extracts are not known at present, but elemental analysis on the dimethyl sulphoxide extracts showed these to have a lower H/C and higher O/C, S/C and N/C ratios than the original kerogen. This result suggests that these extracts are composed of heteroatom containing aromatic compounds. This very tentative conclusion is supported by TGA results which showed that pyrolysis of the extracts resulted in a significantly higher proportion of involatile residues when compared to the original kerogen.

TABLE I.   SUMMARY OF THE PROPERTIES OF OIL SHALES USED

Sample	Fischer Assay(a) (Litres/Tonne)	% Organic Carbon(b)	Kerogen Content (wt.%)(c)	Ash Content of Kerogen (wt.%)	H/C Ratio of Kerogen(d)	Oil Yield as cc of oil/g organic carbon
Nagoorin Carbonaceous	232	65.2	72	0.2	0.93	0.36
Condor Carbonaceous	69	28.3	33	0.4	1.11	0.24
Condor	93	12.3	12	3.9	1.42	0.76
Stuart	178	19.3	25	0.3	1.48	0.92
Duaringa	86	11.0	14	4.7	1.48	0.78

(a) Data supplied by Southern Pacific Petroleum (NL).
(b) Determined on shale dried at 110°C for 12 hours.
(c) These figures are approximate only.
(d) Determined on kerogen dried at 110°C for 12 hours.

TABLE II. EFFECT OF SOLVENT POLARITY ON THE EXTRACTION OF KEROGEN

Solvent	% Kerogen Extracted	
	Stuart	Nagoorin
Hexane	2.4	2.0
Acetone	4.4	5.8
Chloroform	6.0	6.2
Methanol	7.9	3.2
Pyridine	9.9	16.4
Dimethylformamide	19.5	25.6
Dimethylsulphoxide	27.2	30.2

The retorting properties of the various oil shales heated at a linear rate of 3°K/min in an inert gas atmosphere are summarised in Table 3. The most notable features of these data is the relatively high water yield obtained from the retorting of two carbonaceous shales, the poor oil yield (relative to the Fischer assay) obtained by this technique and the very high concentrations of organic carbon remaining in the char for the two carbonaceous shales. The low oil yields appear to be at least in part a consequence of the low heating rates used and recent work (7) showed that at a heating rate of 15°K/min, an oil yield equivalent to the Fischer assay can be obtained for the Condor shale. In this respect, the Condor shale studied in the present work appears to differ significantly from the Green River shale, for which it has been shown (8,9) that the oil yields decrease significantly only at heating rates below 1°K/min. It is possible that the much greater effect observed for the present shales is a reflection of the greater tendency of the oil produced to undergo coking reactions.

Typical results of kinetic studies on the rates of oil formation from various shales (Figure 1, Table 4) show some differences in kinetic behaviour amongst the various shales, although the general appearance of the curves and the temperatures at which the oil yields are maximum are similar to those reported for the Green River Shale (2). Least squares analyses of these data in terms of the Anthony-Howard model (3,10) for non-isothermal kinetics (Table 4) showed that the results of the Nagoorin, Condor, Stuart and Duaringa shales could be reproduced quite well by a single process with activation energies in the range 200-232 kJ mol^{-1} and relatively small ($\sim$0-5 kJ mol-1) distribution parameters. By comparison, the activation energy for the evolution of oil from the Green River shale heated at 2°K/min has been determined (3) as 219 kJ mol^{-1}. Only in the case of the Condor Carbonaceous shale was it necessary to consider two distinct processes for the oil formation, in which the first process was responsible for 54% of the total oil yield.

The effects of temperature on the rates of hydrogen, methane, carbon monoxide and carbon dioxide evolution from the five oil shales are shown in Figures 2-5, the integrated gas yields summarised in Table 5, and the activation parameters for various representative contributing processes determined by analysis of the data in terms of the Anthony-Howard equation compiled in Table 6. The accuracy with which the gas evolution curves could be described by this procedure is illustrated in figure 6, which compares the calculated and observed rates of methane evolution from the Condor carbonaceous shale. However, other cases, e.g., the H_2 evolution profile from Duaringa shale, were much more complex, and fits of the Anthony-Howard equation to only the major contributing processes were attempted.

Table III.   Summary of Retorting Characteristics(a)

| Sample | Fischer Assay Litres/Tonne | Weight Loss on Drying(b) % | Product Yields (c) | | | | Organic Carbon in Char % | Oil Yield (% of Fischer Assay) |
			Oil %	Water %	Char %	Gas + Losses %		
Nagoorin Carbonaceous	232	20.1	12.8	9.7	62.4	15.1	75.8	62
Condor Carbonaceous	69	14.3	5.1	3.0	79.9	6.0	50.1	99
Condor	93	3.4	6.0	3.8	82.3	7.9	5.2	75
Stuart	179	6.2	12.7	4.7	75.9	6.7	14.8	85
Duaringa	86	10.3	5.5	2.9	83.6	8.0	6.8	73

(a) Heating rate of 3°C/minute in helium flowing at 130 cc/minute. Particle size:- −3.3 mm +1.4 mm
(b) Samples dried at 120°C for 12 hours
(c) Expressed as % of weight of dried shale
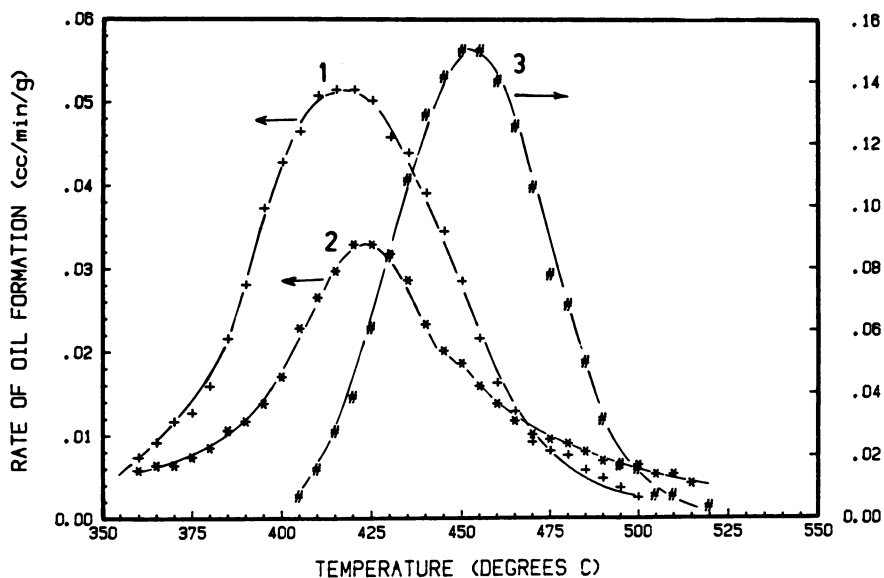
Figure 1. Effect of temperature on the rate of oil evolution expressed per gram of organic carbon. Key: Curve 1, Nagoorin shale; Curve 2, Condor carbonaceous shale; Curve 3, Stuart shale.

TABLE IV. SUMMARY OF ACTIVATION PARAMETERS FOR OIL FORMATION[a]

Sample	Log (A) [b]	Activation Energy kJ mol -1	σ kJ mol -1 [c]	Temperature at which rate of oil formation is maximum (°C)
Nagoorin Carbonaceous	12.4	201	5	420
Condor Carbonaceous Process (1)	12.0	195	1	420
Process (2)	12.0	206	8	480
Condor	14.0	232	0.05	455
Stuart	13.0	215	5	445
Duaringa	14.0	225	5	430

(a) Heating rate of 3°C/minute, carrier gas flow rate of 130 cc/minute. Values determined by least squares fit of data to Anthony-Howard equation.
(b) Log_{10} (Preexponential factor)
(c) Distribution parameter of activation energies.
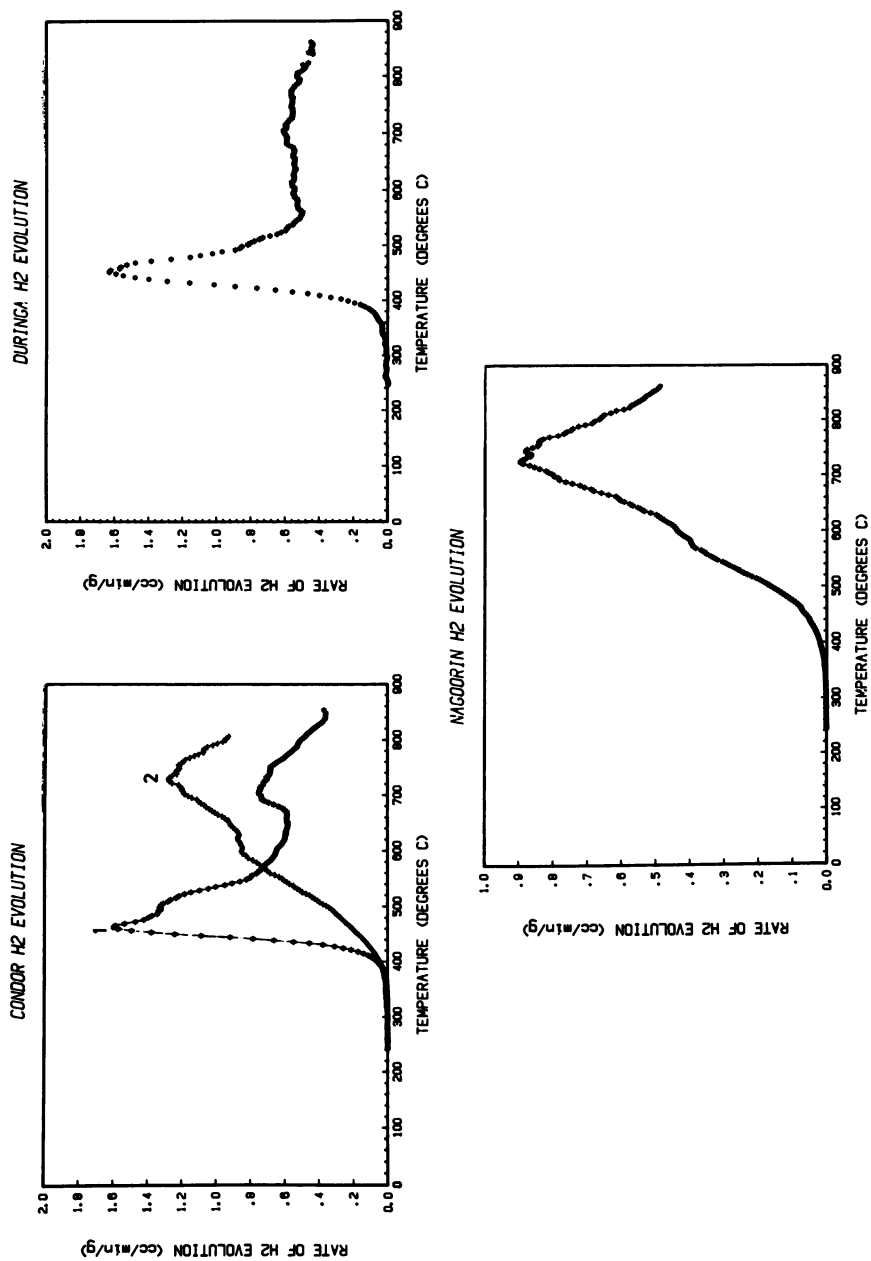
Figure 2. Effect of temperature on the rate of hydrogen evolution expressed per gram of organic carbon. For the Condor shale, Curve 1 represents the normal shale; Curve 2 represents the carbonaceous shale.
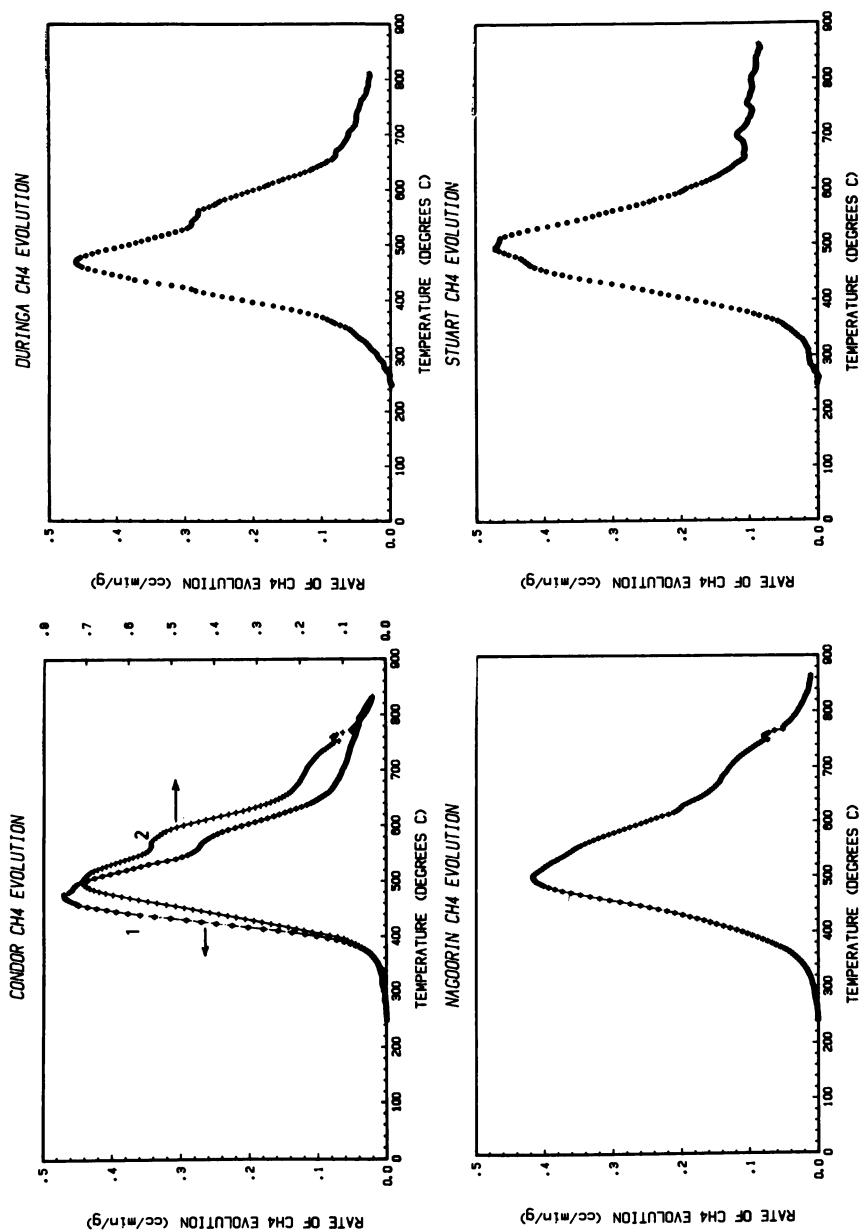
Figure 3. Effect of temperature on the rate of methane evolution expressed per gram of organic carbon. For the Condor shale, Curve 1 represents the normal shale; Curve 2 represents the carbonaceous shale.
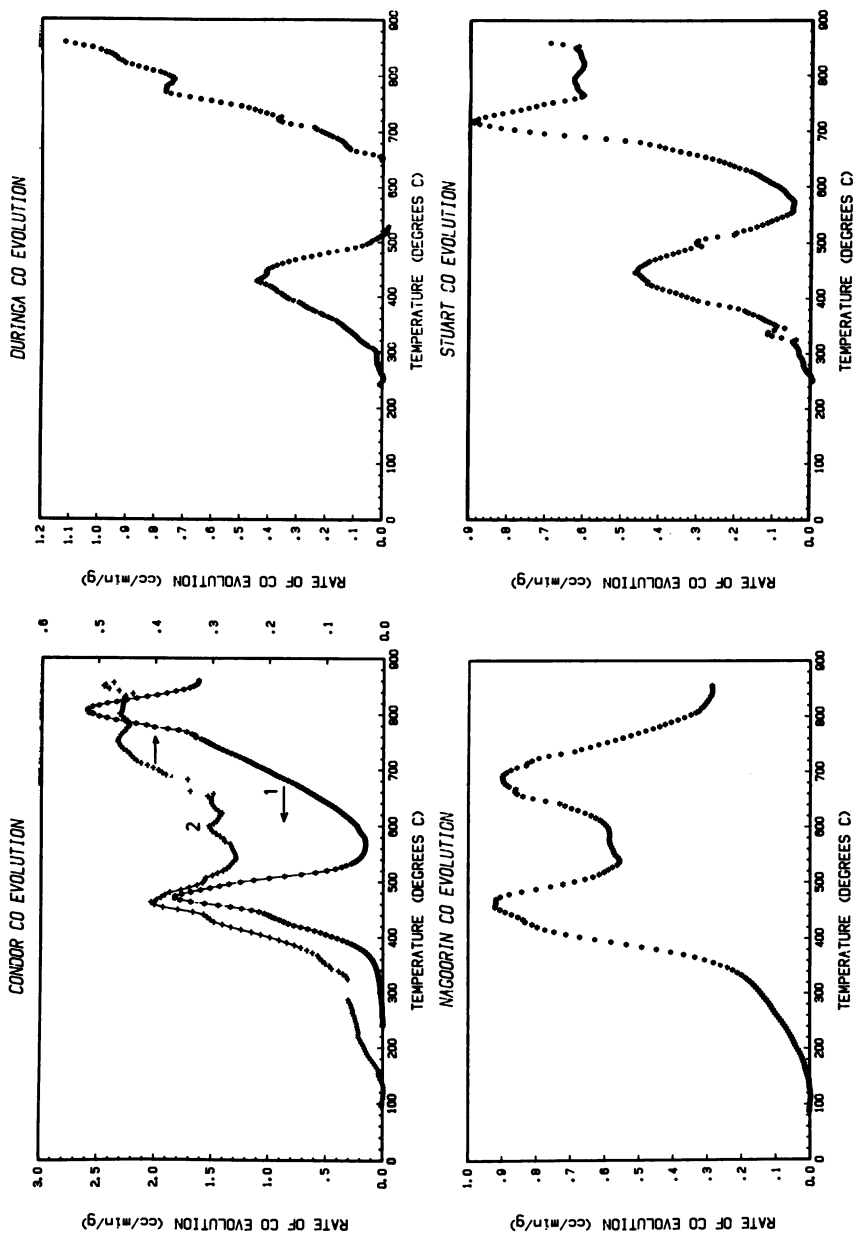
Figure 4. Effect of temperature on the rate of carbon monoxide evolution expressed per gram of organic carbon. For the Condor shale, Curve 1 represents the normal shale; Curve 2 represents the carbonaceous shale.
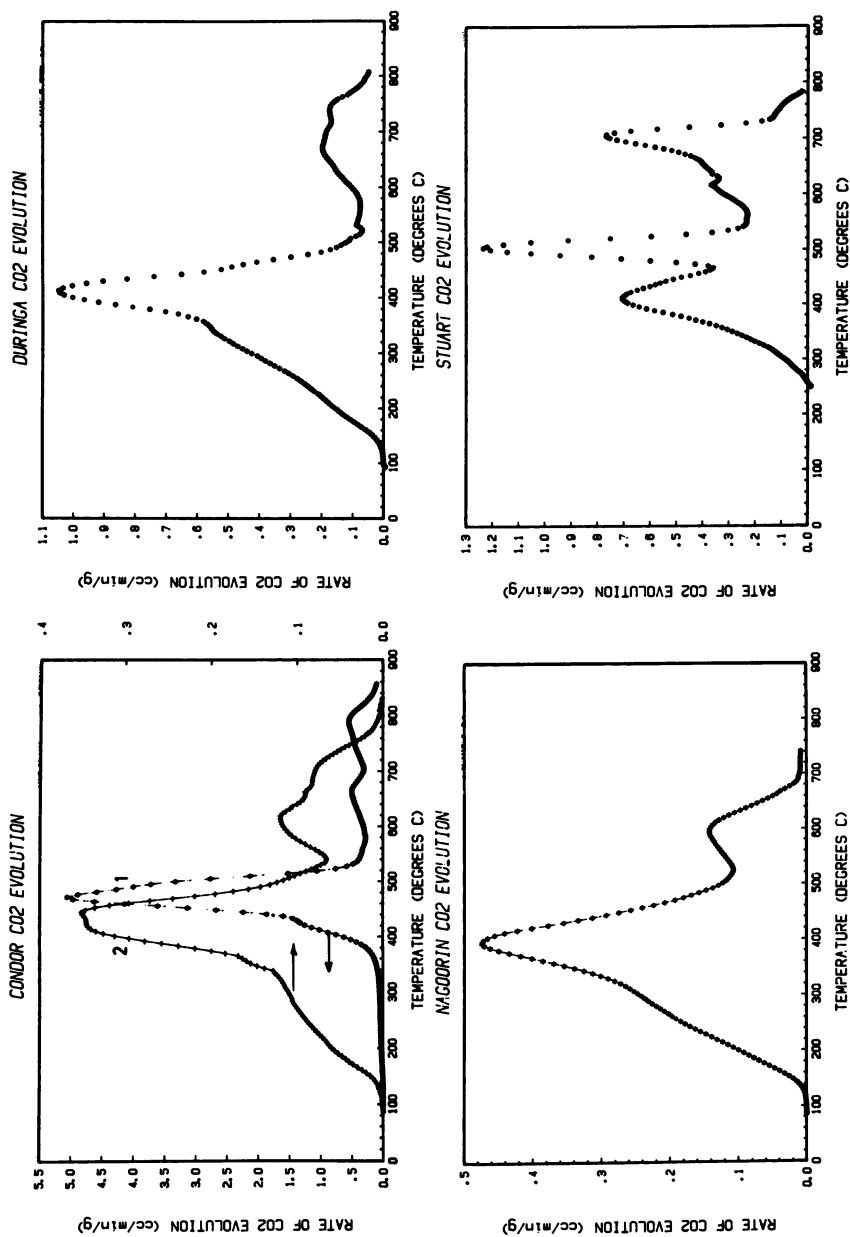
Figure 5. Effect of temperature on the rate of carbon dioxide evolution expressed per gram of organic carbon. For the Condor shale, Curve 1 represents the normal shale; Curve 2 represents the carbonaceous shale.

TABLE V. TOTAL GAS YIELDS TO 850°C(a)

Sample	Gas Yields (cc/g) (b)			
	H_2	CH_4	CO	CO_2
Nagoorin Carbonaceous	47 (72)	20 (31)	73 (113)	23 (35)
Condor Carbonaceous	28 (100)	14 (50)	17 (60)	7 (58)
Condor	13 (110)	4 (33)	21 (171)	20 (162)
Stuart	-	7 (36)	17 (86)	13 (67)
Duaringa	11 (100)	3 (29)	6 (52)	7 (63)

(a) Heating rate:- 3.0°C/minute
(b) At 0°C and 0.1 MPa pressure. Figures in brackets are the gas yields expressed as cc/g of organic carbon.
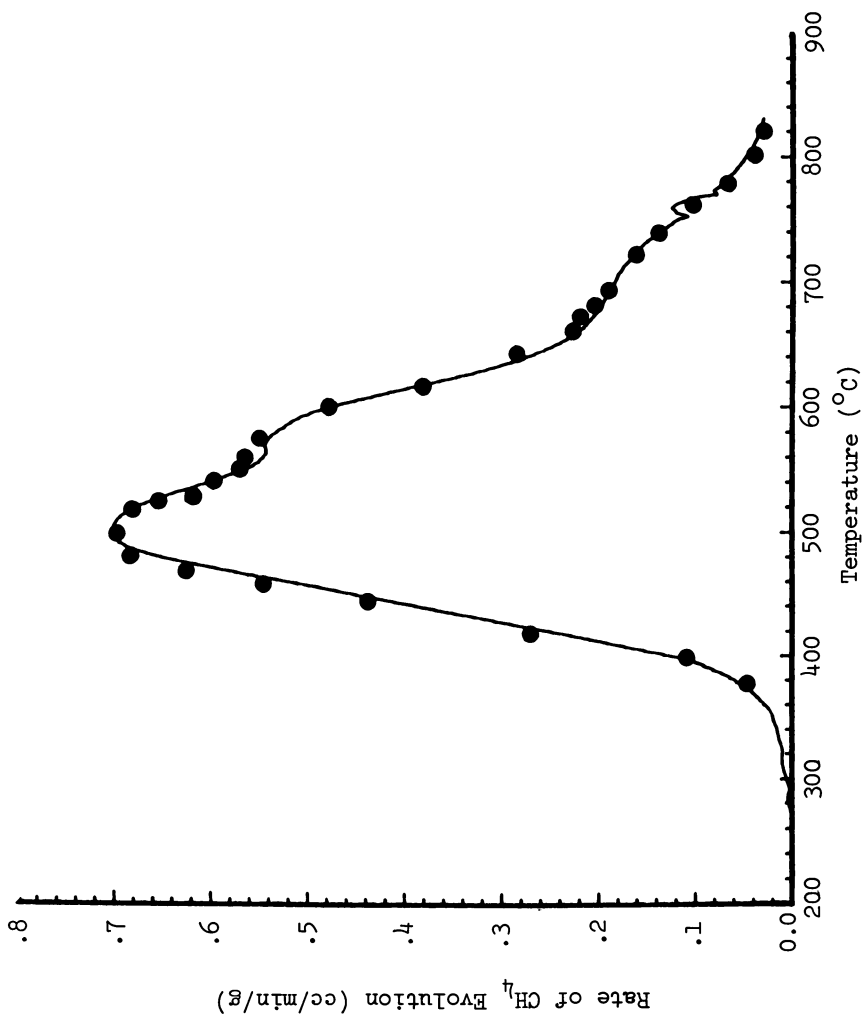
Figure 6. Comparison of the observed and calculated rate of methane evolution expressed per gram of organic carbon from Condor carbonaceous shale. Key: ——, calculated from the Anthony–Howard equation using the parameters summarized in Table VI; ●, experimental data.

Hydrogen.   Examination of the hydrogen evolution profiles shows a striking difference between those observed for the carbonaceous shales and those of the normal shales.   For the two carbonaceous shales, hydrogen evolution reaches a maximum in the temperature range 700-720°C with a minor contribution from a process having a maximum at 600°C.   As summarised in Table 6, the activation energies are in the range 300-320 kJ mol^{-1} for the 600°C process, and 360-380 kJ mol^{-1} for the 700°C process. The hydrogen evolution from these samples thus occurs in a temperature range in which the secondary pyrolysis reactions of the residues which remain after the primary bitumen decomposition is complete are thought to take place (2).   In contrast, the hydrogen evolution rates from the Condor and Duaringa deposits resemble those observed for the Green River Shale (2) and show a sharp peak at 460°C, close to the temperature at which the oil formation is maximum.   For the Duaringa shale this process is associated with an activation energy of $\sim$ 165 kJ mol^{-1} and is followed by further hydrogen evolution obviously comprising many processes occurring in the secondary pyrolysis region.

Methane.   The methane evolution profiles for all five shale samples are surprisingly similar, but occur at significantly higher temperatures than has been observed (2) for the Green River shale.   Although some methane evolution accompanies the oil formation, the major part is formed in the secondary pyrolysis region.   At least three major processes with maxima in the vicinity of 500, 580 and 700°C appear to contribute to the total methane formation.   Activation energies for these processes were determined for Condor carbonaceous shale and are summarised in Table 6.

Carbon Dioxide.   The carbon dioxide evolution profiles for the Nagoorin, Duaringa and Condor carbonaceous shales are characterised by significant contributions commencing at temperatures as low as 150°C.   It is unlikely that these processes are the result of mineral decomposition reactions, and their presence must reflect a contribution from thermally unstable components of the kerogen.   A further major contribution to the CO_2 yield from these shales was found at temperatures corresponding to the maximum rate of oil formation, but little CO_2 was formed in the secondary pyrolysis temperature range.   In this respect, the behaviour of these shales differs significantly from the Green River shale which were reported (2) to show only a negligible CO_2 evolution rate accompanying the oil release, but a very large rate at temperatures above 550°C resulting from the decomposition of the carbonate minerals.
    The CO_2 evolution from the Condor and Stuart shales shows sharp peaks at 500°C superimposed on a peak corresponding to the temperature at which the oil evolution occurs.   These sharp

TABLE VI. SUMMARY OF REPRESENTATIVE PARAMETERS DETERMINED BY FITTING THE ANTHONY-HOWARD EQUATION TO THE RATES OF GAS EVOLUTION

Sample	Gas	Process	Temperature at which rate of process is maximum, °C	Log (A) (a) s-1	E kJ mol-1	σ (b) kJ mol-1	Fraction (c)
Nagoorin Carbonaceous	H_2	1	570	17.0	318	20	0.14
	H_2	2	700	17.0	384	31	0.86
	CO_2	1	280	8.0	110	8	0.23
	CO_2	2	400	8.0	140	8	0.57
	CO_2	3	600	8.0	182	8	0.20
Condor Carbonaceous	CO_2	1	300	8.0	120	18	0.40
	CO_2	2	430	8.0	148	6	0.60
	CH_4	1	500	15.0	256	12	0.36
	CH_4	2	570	8.0	287	14	0.42
	CH_4	3	700	8.0	330	20	0.22
	H_2	1	600	15.8	297	23	0.26
	H_2	2	730	15.8	361	29	0.74
Condor	CO_2	1	460	9.7	178	0.05	1.00
	CH_4	1	500	12.9	223	10	0.40
	CH_4	2	580	12.9	249	21	0.60
Stuart	CO	1	450	9.7	174	11	1.00
Duaringa (d)	H_2	1	460	9.0	165	0.05	1.00

(a) Log10 (Preexponential factor)
(b) Distribution parameter of activation energy.
(c) Fractional Contribution of the process considered to the total gas yield.
(d) Only the process with a maximum rate at the indicated temperature was considered in the analysis of the data.

peaks are probably associated with the decomposition of mineral constituents of the shale, but further work with acid washed shales would be required to confirm this proposition.

Carbon Monoxide. All shale samples showed a significant peak in the CO evolution rates in the temperature range over which oil evolution occurs. At these relatively low temperatures, it is unlikely that the reaction between CO_2 and residual char could be a significant source of carbon monoxide (2), and it appears that for these shales and in contrast to the Green River shale (2), the decomposition of the kerogen results in the formation of CO. In the case of the Stuart shale, the processes leading to the formation of the CO in the low temperature range are characterised by a mean activation of $\sim$ 174 kJ mol-1 and a distribution of 11 kJ mol-1 (Table 6).

In conclusion, the results of this study have shown that the retorting properties, and particularly the gas evolution profiles observed for these five selected Australian shales differ significantly from similar results obtained for Green River shales. However, of particular interest are the results obtained for the two carbonaceous shales. The retorting of these materials was found to be characterised by the evolution of hydrogen in a temperature range normally associated with secondary pyrolysis reactions, by an oil yield low in comparison to the high organic carbon content of these shales, and by the consequent very high residual organic carbon in the spent shale. Preliminary NMR studies (11) of the oil produced from the Condor shales have also shown the presence of high concentrations of phenolic materials only in the oil from the carbonaceous material. These properties are more characteristic of brown and even bituminous coals, and it is appears that the kerogen of the carbonaceous shales contains a substantial proportion of material of lignin origin (12). A petrographic comparison of these shales and a more detailed comparison of the composition of the oil produced from the carbonaceous and normal shales may provide further confirmation of this hypothesis.

Acknowledgments

Literature Cited

1.   Campbell, J.H., Koskinas, G.J. and Stout, N.D. Fuel (1978), 57, 376.
2.   Campbell, J.H., Koskinas, G.J. Galligos, G. and Gregg, M. Fuel (1980) 59, 718.

3. Campbell, J.H., Galligos, G. and Gregg, M. Fuel (1980) <u>59</u>, 727

4. Robinson, W.E. 'Kerogen of the Green River Formation' Chpt. 26 in 'Organic Geochemistry, Methods and Results' G. Eglinton and M.J.J. Murphy ed. Springer-Verlag Belin, 1969.

5. Marzec, A., Juzwa, M., Betley, K. and Sobkowiak, M. Fuel Process. Technol. (1979), <u>2</u>, 35.

6. Marzec, A., Juzwa, M. and Sobkowiak, M. in 'Gasification and liquefaction of coal'. Symposium on the gasification and liquefaction of coal, Katowice, Poland, April 1979. Coal/Sem. 6/R. 62 United Nations, Economic Commission for Europe, (1979).

7. Ekstrom, A. and Randall, C.H. unpublished observation.

8. Campbell, J.H., Koskinas, G.J., Stout, N.D. and Coburn, T.T. In-Situ (1978) <u>2</u>, 1.

9. Evans, R.A. and Campbell, J.H. In-Situ, (1979) <u>3</u>, 33.

10. Anthony, D.B. and Howard, J.B. AIChEJ. (1976) <u>22</u>, 625.

11. Ekstrom, A. and Fookes, C., unpublished observation.

12. The authors thank Dr. J. Saxby for drawing their attention to this interpretation.

High-Pressure Pyrolysis of Green River Oil Shale

ALAN K. BURNHAM and MARY F. SINGLETON

Lawrence Livermore National Laboratory, Livermore, CA 94550

Oil yields, compositions and rates of evolution
are reported for heating rates from 1 to 100°C/h
and pressures of 1.5 and 27 atm. Pyrolysis
occurred in an autogenous atmosphere and volatile
products were allowed to escape the pyrolysis
region continuously. Higher pressures and lower
heating rates during pyrolysis cause a decrease in
oil yield, although the effects are not additive.
The lowest oil yield was approximately 72 wt% or
79 vol% of Fischer assay. Lower oil yield is
generally accompanied by lower boiling point
distribution, nitrogen content and density and
higher H/C ratios. Oils produced at high pressure
and slow heating rates are a clear amber color
instead of the usual opaque brown. The effect of
pyrolysis conditions on biological markers and
other diagnostic hydrocarbons is also discussed.
Existing kinetic expressions for oil evolution
slightly overestimate the shift in the oil
evolution rate vs temperature with a decrease in
heating rate. Finally, the rate of oil evolution
is retarded by pressure, a factor not taken into
account by current kinetic expressions.

Pyrolysis of kerogen-rich rocks under pressure provides
information that is useful for evaluating oil-shale-processing
schemes (1-5) and understanding the formation of petroleum
(6,7). Reliable extrapolation from laboratory experiments to
commercial situations generally requires a kinetic model that
can properly describe the effects of temperature (or heating
rate), pressure, residence time and gas atmosphere on oil yield
and composition. None of the existing studies have been designed
to separate and quantify these dependencies, so such a model has
not yet been derived.

In this work, we pyrolyzed Green River oil shale in a reactor with an initial total porosity of 29% where the products are allowed to escape as they are produced. This self-purging design results in the pyrolysis occurring in a nearly autogenous atmosphere, unlike most other studies where the gas atmosphere is dominated by an added pressurizing fluid. We discuss the effect of initial porosity, hence product residence time at high temperatures, on the pyrolysis results. The experiments were designed to simulate the temperature-pressure histories anticipated in radio-frequency in-situ oil-shale processing (8) so that oil yields could be estimated more reliably. The results presented here may also be useful for understanding petroleum formation in the Uinta basin (Utah) and from other type I source rocks. We do not consider the present report to be definitive; future experimental work and analysis will be directed at developing a tractable kinetic model of high-pressure pyrolysis.

Experimental Procedures

The sample in this study was a 94-L/Mg (22.4-gal/ton) Green River oil shale (marl) from the Anvil Points mine near Rifle, CO. The particle size was 0.42 to 0.84 mm (-20 +40 mesh). It contained by weight 10.88% organic C, 4.76% mineral C, 1.64% H, 0.42% N, and 0.59% S. The sample is approximately representative of mine-run shale, which covers most of the Mahogany zone.

The apparatus is shown schematically in Figure 1. To reduce the porosity in the reactor, hence residence time of the volatile products, the following procedures were used. The sample was compressed into 3.2-cm-diam. by 4-cm-long pellets using a pressure of 165 MPa. Two of these pellets, weighing a total of about 110 g, were placed into the sample can (3.3 cm diam.) along with quartz sand above and around the pellets, and a top was welded on. We determined the total porosity of the pellets to be about 24% from the helium-buoyancy density of the raw shale and the weight and dimensions of the pellets. Total porosity in the reactor averaged 29%, or equivalently, the total void volume was about 20 cm^3.

The sample was heated from room temperature to 500°C at heating rates ranging from 1 to 110°C/h. Previous experience indicates that the difference in temperature across the sample is less than 5°C for this size sample and heating rates less than 120°C/h. For the near-atmospheric pressure experiments, a thermocouple was used to measure the temperature near the center of the oil shale sample. For the high-pressure experiments, this sample thermocouple was omitted, and the sample temperature was estimated from the furnace temperature. The difference between the sample and furnace temperatures was determined in the near-atmospheric pressure experiments.

The sample and oil collection system was evacuated and then pressurized with argon to prevent oxidation. The pressure was
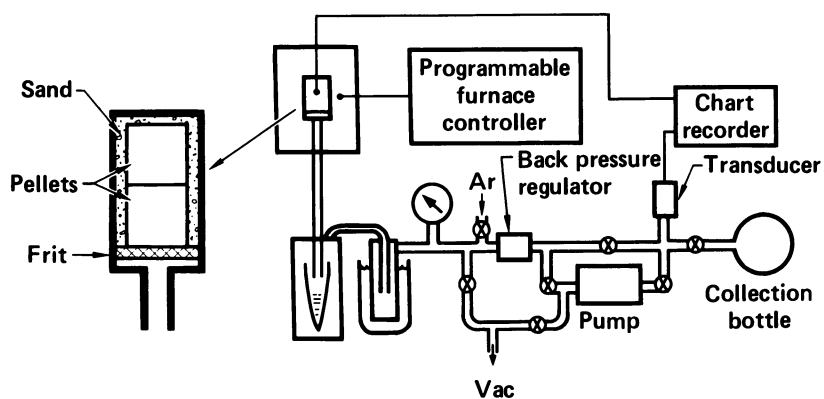
Figure 1. Apparatus for pyrolysis under an autogenous atmosphere.

maintained approximately constant during the experiment by a
back-pressure regulator releasing gas at approximately the same
rate as it is produced. The pressure in the reactor increased
somewhat (<1 atm) during the experiment as the gas collection
system filled. Sufficient steam and pyrolysis gas were produced
at temperatures below 200°C at 1.5 atm (0.15 MPa) and below 300°C
at 27 atm (2.7 MPa) to purge the argon from the reactor. We
believe that the diffusion of argon back into the reactor was
sufficiently slow that the pyrolysis occurred in an atmosphere
consisting almost completely of the pyrolysis products. At the
end of the experiment, all the gas in the system was pumped into
the gas collection bottle by a bellows pump. A trap between the
oil receiver and back-pressure regulator was cooled to -77°C
during pumping to prevent oil from being transferred to the
gas-collection bottle. Other analytical procedures have been
described previously (9).

Results and Discussion

     The material balance, oil yields and distribution of organic
carbon are shown in Table I. Oil properties are given in Table
II. Oils were all less dense than that from Fischer assay (FA)
so the yield depends significantly on whether it is calculated on
a weight or volume basis, by 6 to 7% for the high pressure
experiments.
     At near-atmospheric pressure, the oil yield decreases with a
decrease in heating rate. Of the carbon no longer evolved as oil
at the slow heating rates, nearly four times as much is converted
to coke as to gas, and the principal gaseous products are H_2 and
CH_4 (see Table III). The yields of oil, gas and coke at different
heating rates are in excellent agreement with those previously
reported by Campbell (10,11). Also evident in Table II is that
the slow-heating-rate oil has lower density and nitrogen content,
in agreement with Stout et al. (12), and a lower boiling-point
distribution, in agreement with Jackson et al. (13).
     In pursuing an explanation of the decrease in oil yield with
heating rate, we have previously proposed (10,14) the mechanism
shown in Figure 2. Oil generated below its boiling point under-
goes two competing reactions: evaporation and oil coking. Oil
coking is defined as a liquid-phase process that leads primarily
to coke. It is related to the liquid-phase residence time at
high temperatures and is enhanced by slow heating rates. Coking
has been related to condensation and polymerization reactions of
hydrogen-deficient heterocycles because it causes a decrease in
the nitrogen content and an increase in the H/C ratio of the
remaining oil (10,12).
     A second mechanism causing decreased oil yield is cracking,
which is the thermal decomposition, probably by a free-radical
mechanism, of long alkyl chains (14). It causes a downward shift
in the boiling-point distribution and an increase in hydrocarbon

Table I. Product distribution

Heating rate (°C/h)	Pressure (atm)	Mass balance (%)[a]	Condensed oil yield		Organic carbon distribution[b]				
			wt% FA	vol% FA	Condensed oil[c]	Total oil[c]	Gas[d]	Shale[e]	Total[f]
720	1.0	99.56	100	100	65.0	66.4	5.9	22.7	95.0
110	1.5	99.73	97	98	63.5	64.6	6.1	25.2	95.9
11	1.5	99.29	86	89	56.1	57.5	7.6	29.0	94.2
1	1.5	99.18	77	81	49.6	51.0	7.5	31.9	90.3
108	27	99.34	78	84	50.3	50.5	9.1	31.5	91.1
9	27	99.41	73	80	46.3	46.4	9.7	35.4	91.5
1	27	99.36	72	79	45.7	45.9	7.3	34.1	87.2

a) Oil + water + gas + retorted shale/ raw shale; sample size ~10 g.
b) Percent of the raw shale organic carbon in products.
c) Includes C_5+ compounds in gas.
d) CO, CO_2 and C_1-C_4 hydrocarbons.
e) Includes a very minor contribution from coke deposited in the sand surrounding the cores.
f) Sum of total oil, gas and shale. Totals differ slightly due to rounding.

Table II. Oil properties

Heating rate (°C/h)	Pressure (atm)	Density (g/cm^3)[a]	Elemental analysis (wt%)				Simulated distillation[b]				
			C	H	N	S	10%	25%	50%	75%	90%
720	1.0	0.906	83.3	11.2	2.7	0.66	175	258	361	450	504
110	1.5	0.888	84.0	11.2	2.8	0.69	155	238	340	429	485
11	1.5	0.872	83.9	11.6	2.3	0.70	151	226	319	403	459
1	1.5	0.862	82.6	12.3	1.6	0.56	155	225	303	381	440
108	27	0.842	82.4	11.4	2.6	0.57	104	168	250	332	403
9	27	0.823	81.5	11.7	2.2	0.43	111	169	241	317	385
1	27	0.826	81.6	12.9	1.5	0.36	122	178	256	330	395

a) 23°C
b) Temperature (°C) at which the given percentage has distilled – ASTM-D-2887.

Table III. Gas production (mmoles of product/g of raw shale organic carbon)

Heating rate (°C/h)	Pressure (atm)	H_2	CH_4	$\dfrac{H_2}{CH_4}$	C_2H_x	$\dfrac{C_2H_4}{C_2H_6}$	C_3H_y	$\dfrac{C_3H_6}{C_3H_8}$	C_4H_z
720	1.0	1.47	0.98	1.50	0.47	0.30	0.34	0.88	0.21
110	1.5	2.02	1.17	1.73	0.46	0.20	0.32	0.68	0.19
11	1.5	2.98	1.69	1.76	0.60	0.12	0.40	0.45	0.23
1	1.5	3.36	1.88	1.79	0.90	0.08	0.35	0.28	0.21
108	27	1.14	2.26	0.50	0.85	0.05	0.38	0.23	0.20
9	27	0.82	3.36	0.24	1.00	0.01	0.38	--	0.05
1	27	0.39	2.87	0.14	0.61	0.003	0.21	--	0.03

- **Oil generation**

  (Kerogen· Bitumen) $\xrightarrow{k_d}$ Oil (ℓ, v, g) + Gas + Char

- **Oil coking**

  $\overbrace{\text{Oil}(\ell) \rightleftharpoons \text{Oil (v)}}^{k_\ell} \longrightarrow$ Oil evolved

  $\downarrow k_c$ $\longrightarrow$ mostly coke

- **Oil cracking**

  Oil (v, g) $\xrightarrow{k_f}$ mostly gas
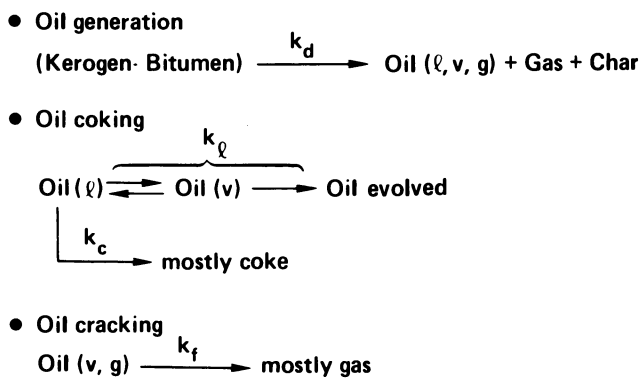
Figure 2. Previously proposed (10, 14) kinetic scheme for shale oil generation and degradation.

gases, but relatively little coke is formed. At atmospheric pressure, oil cracking occurs mainly to oil vapors which have a long transit through the pyrolysis region or pass through a region hotter than the pyrolysis region. Oil cracking is less important than oil coking in affecting oil yield as a function of heating rate for pyrolysis in an autogenous environment at atmospheric pressure.

The oil yields from all the pyrolysis experiments at 27 atm are lower than the lowest oil yield from the atmospheric pressure experiments. The oil yields at 27 atm also decrease with a decrease in heating rate, but the effect is much smaller than at atmospheric pressure. As shown in Figure 3, the difference between the yields at 1.5 and 27 atm becomes small for heating rates below 1°C/h. As in the case of yield loss caused by slow heating, most of the yield loss caused by high pressure is accounted for by coke production. This conclusion must be qualified with the caution that the organic carbon balances on the high pressure experiments (Table I) are significantly lower than desirable. The most likely source of loss is in gas, especially light hydrocarbons. Besides the possibility of leakage, which we did not detect, gas collection is complicated by high gas solubility in the oil at 27 atm. About 1.5 cm^3 of "liquid" boils away when the pressure is released at the end of an experiment. It is likely that C_3 and C_4 hydrocarbons were transferred from the oil receiver to the dry-ice trap when the liquid-collection system was evacuated to 200 torr during final gas transfer. These hydrocarbons then evaporated during warmup of the trap before weighing.

That oil yield should decrease with increasing pressure for a self-purging reactor is easily explained. Pressure causes an increase in both liquid- and gas-phase residence times, thereby increasing coking and cracking. The more difficult task is developing a quantitative kinetic model that can account for coking and cracking in the correct proportions. The model should also be qualitatively consistant with changes in the oil composition. Work is currently in progress on developing such a model.

The chemical mechanisms affecting oil yield and composition are somewhat different at high pressure. The nitrogen content of the oil from the high-pressure experiments is only slightly less than that of the oil produced at the same heating rate at atmospheric pressure, despite the increased coke production. This suggests that the principal mechanism of coke deposition at high pressure is probably different from that at atmospheric pressure, although our oil characterization is too incomplete to be more definitive. In contrast, the sulfur content appears to be independent of heating rate at atmospheric pressure, but is significantly reduced at high pressure, especially at slow heating rates. The effect of pressure on nitrogen and and sulfur contents agrees with that observed by Wise et al. (2) The high pressure oil is also lighter than the low-pressure oil as
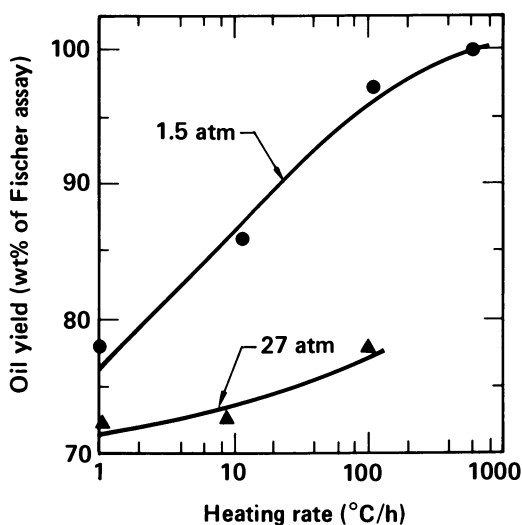
Figure 3. Plot of oil yield expressed as wt% of Fischer assay (FA). Placement of the lines is subjective. The convergence of oil yield at slow heating rates for the two pressures is even closer when vol% of FA is plotted.

measured by density, boiling-point distribution and color. For example, the product from the 27-atm pyrolysis experiments at 1 and 9°C/h is a clear amber rather than the usual opaque brown. A similar observation was made by McKee (15). Apparently the highly light-absorbing chromophores, presumably aromatic heterocycles, are not formed or are partially hydrogenated by the pyrolysis gas. In this regard, we note that the H_2 production is decreased at high pressures although the total hydrogen contained in H_2 plus CH_4 is greater.

　　We performed only a limited characterization of the liquid product. Examples of analysis by capillary-column chromatography are shown in Figure 4 and Table IV. Alkene/alkane ratios, as exemplified by 1-dodecene/n-dodecane, decrease with both decreased heating rate and increased pressure. We have noted previously that ratios involving sums of alkenes and alkanes are nearly independent of heating rate (oil coking) (16), so they are more characteristic of the source rock than ratios of alkanes alone when comparing oils prepared at different heating rates. The ratio of phytane to n-octadecane plus 1-octadecene (C_{18}s) is nearly constant in the atmospheric pressure experiments. Likewise, the pristane+enes/phytane ratio is approximately constant although the prist-1-ene/pristane and prist-2-ene/phytane ratios vary dramatically with conditions. This indicates that there is little thermal cracking of the generated oil because thermal cracking of long-chain hydrocarbons causes the phytane/ C_{18}s ratio to decrease. Figure 5 shows additional analysis of old data on shale oil cracking (16). The phytane/C_{18}s ratio decreases because longer chain normal alkanes can crack to

Table IV. Indicator ratios determined by capillary-column gas chromatography.

Heating rate (°C/h)	Pressure (atm)	1-dodecene / n-dodecane	phytane / C_{18}s	pristane+enes / phytane	sterane content
720	1.0	0.84	0.53	2.2	high
110	1.5	0.60	0.47	2.1	medium
11	1.5	0.34	0.45	1.9	medium
1	1.5	0.22	0.43	1.8	medium
108	27	0.21	0.38	1.9	low
9	27	0.09	0.34	1.7	low
1	27	0.03	0.31	1.9	low
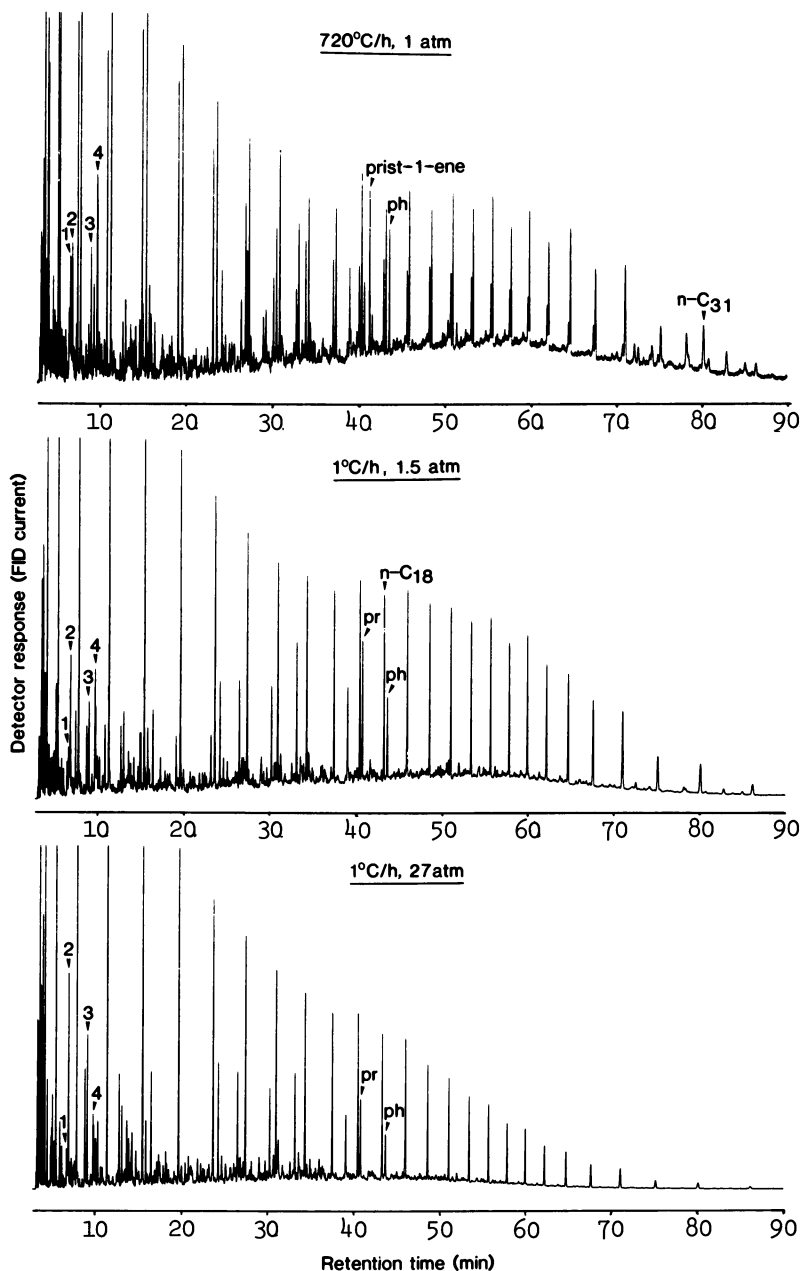
Figure 4. Capillary-column gas chromatograms of three oil samples produced by pyrolysis.

Labeled compounds include toluene (1), branched C_8H_{18} (2), trimethyl cyclohexane (3), m,p-xylene (4), pristane (pr) and phytane (ph). Examples of trends evident are the reduction by slow heating and high pressure of alkene, polycycloalkane, and unresolved background content, and changes in the odd/even predominance of n-alkanes.
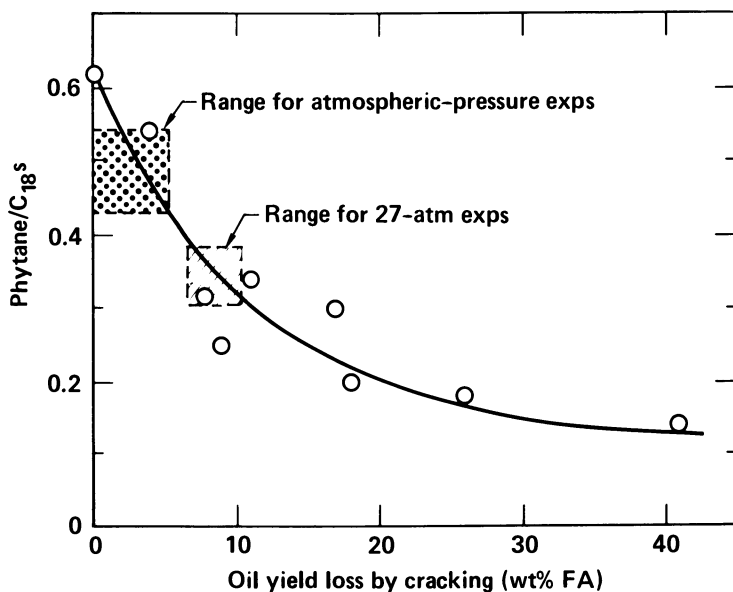
Figure 5. Relationship between phytane content and oil cracking determined from previously reported results (14).

n-octadecane and 1-octadecene, but there are essentially no
longer-chain isoprenoids to produce phytane.

The phytane/C_{18}s ratio does decrease somewhat in the
27-atm experiments. A comparison of the results in Table IV and
Figure 2 indicates that oil yield loss at 27 atm by cracking long-
chain hydrocarbons to (primarily) hydrocarbon gases ranges from
about 5% at 108°C/h to about 10% at 1°C/h. This is also reflected
in the lower boiling-point distribution given in Table II.

We also note that the high-pressure pyrolysis almost completely
eliminates the sterane and pentacyclic-triterpane content of the
oil. Gas chromatography/mass spectrometry analysis of the oil
indicates that these large cyclic compounds are forming smaller
branched and cyclic hydrocarbons. Little or no additional alkyl
benzenes are formed. Apparently, enough hydrogen is available
from coke formation to saturate the products formed by cracking
of the large normal and cyclic hydrocarbons.

The destruction of steranes and triterpenes caused by the
oil cracking may be less in experiments using a solid core of
material having essentially no initial porosity than with our
compressed pellets. The residence time is determined by the
ratio of the porosity (initial plus generated) to the production
rate of gases and oil vapors. If the initial porosity were
reduced tenfold to 3%, the residence time of the biomarker
compounds in the reactor would be nearly 10 times lower because
they are the first compounds to be evolved (15) and little
additional porosity would yet be generated. The later-evolving
products would be affected less if the initial porosity were
decreased. This is because 94 L/mg shale generates about 25%
additional porosity during oil evolution (17), which would only
result in a two-fold change in residence time. The overall yield
for a lower-porosity reactor might be about 5% higher at our
slowest heating rate and highest pressure.

Finally, high pressure delays evolution of oil out of the
reactor (but not necessarily oil generation within the reactor).
This effect has been previously noted by Noble et al. (3). The
temperature for ∿99% completion of oil evolution is compared in
Table V with that predicted by the kinetic expressions of Campbell
et al. (18) and Shih and Sohn (19), both of which were derived at
atmospheric pressure. In all cases, a higher temperature is
required than calculated. The disagreements are greatest at slow
heating rates and at high pressures, although the effect of
pressure itself appears to be lowest at the slowest heating
rates. A more complete comparison of time-dependent oil yield is
given in Figure 6. The calculation numerically integrated the
kinetic expressions of Campbell (10) for oil generation, oil
coking and oil evaporation. The normalized oil evolution rates
from this calculation are nearly identical to those using oil-
generation kinetics alone, but the complete kinetic scheme is
able to accurately calculate the atmospheric yields reported in
Table I. Pressure would be expected to affect the oil evolution
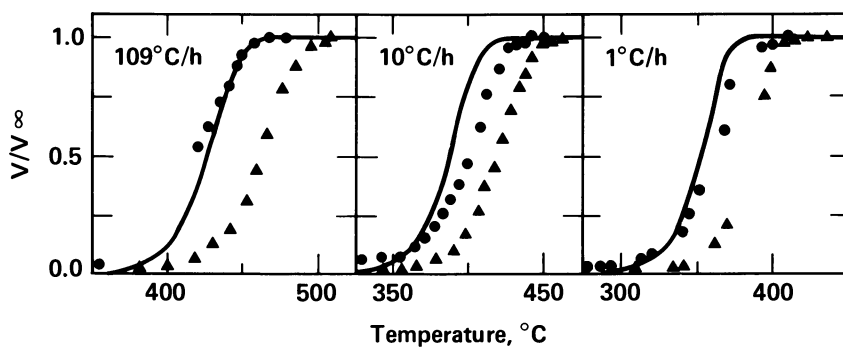
Figure 6. Experimental (points) and calculated (lines) volumes of oil evolved as a function of temperature as the sample is heated at the indicated heating rate. Key: ●, 1.5 atm; and ▲, 27 atm.

Table V. Experimental (+5°C) and calculated temperatures for 99% of oil evolution.

Heating rate (°C/h)	Pressure (atm)		Calculated	
	1.5	27	Campbell et al. (18)	Shih and Sohn (19)
110	465	495	460	465
10	435	455	415	415
1	400	410	380	375

rate if the rate of evaporation is comparable to or slower than the rate of generation. Campbell's treatment of oil evaporation is too empirical to account for pressure effects. An accurate description of oil evaporation is needed to untangle the various contributions to changes in oil yield and composition. It is especially important when applying the results of this work to situations where the transport mechanisms are different than in our experiments, e.g., petroleum formation.

Conclusions

Pressure causes a decrease in oil yield in an autogenous atmosphere, but the effect of pressure is smaller at slow heating rates. The changes in oil composition related to decreased oil yield at elevated pressure are somewhat different than the corresponding changes with heating rate at atmospheric pressure. Heating rate principally determines nitrogen content while pressure determines sulfur content. Pressure significantly retards the oil-evolution rate even though a lower-boiling product is formed. In fact, the longer residence times caused by increased pressure may cause the decrease in boiling point by increasing oil cracking. A kinetic model that can accurately calculate yields, compositions and rates of evolution will have to treat the effect of pressure on oil evaporation and its relationship to cracking and coking of oil. Further experiments with variable porosity, hence residence time, would be helpful in developing such a kinetic model.

Acknowledgments

analytical support, and R. Taylor for numerous helpful discussions.

Work performed under the Auspices of the U. S. Department of Energy at Lawrence Livermore National Laboratory under contract #W-7405-Eng-48.

Literature Cited

1. Bae, J. H. Soc. Petrol. Eng. J., 1969, 278-292.
2. Wise, R. L.; Miller, R. C.; George, J. H. ACS Div. Fuel Chem. Preprints 1979, 21(6), 87.
3. Noble, R. D.; Wang, C.-C. "Kerogen Decomposition Under Elevated Pressures" Rept. DOE/LC/01761-T2, 1981 (Aval. NTIS).
4. Weil, S. A. Symposium Papers: Synthetic Fuels from Oil Shale 1980, p. 353.
5. Sresty, G. C.; Dev H.; Snow, R. H.; Bridges, J. E. 15th Oil Shale Symposium Proceedings 1982, p. 411.
6. Lewan, M. D.; Winters, J. C.; McDonald, J. H. Science 1979, 203, 897-899.
7. Bandurski, E. Energy Sources 1982, 6, 47-66.
8. Mallon, R. G. "Economics of Shale Oil Production by Radio Frequency Heating," Lawrence Livermore National Laboratory Rept. UCRL-52942, 1980.
9. Singleton, M. F.; Koskinas, G. J.; Burnham, A. K.; Raley, J. H. "Assay Products from Green River Oil Shale," Lawrence Livermore National Laboratory Rept. UCRL-53273, 1982.
10. Campbell, J. H.; Koskinas, G. J.; Stout, N. D.; Coburn, T. T. In Situ 1978, 2, 1.
11. Evans, R. A.; Campbell, J. H. In Situ 1979, 3, 33.
12. Stout, N. D.; Koskinas, G. J.; Raley, J. H.; Santor, S. D.; Opila, R. J.; Rothman, A. J. Colorado School of Mines Quart. 1976, 71, 153.
13. Jackson, L. P.; Allbright, C. S.; Poulson, R. E. Anal. Chem. Liq. Fuel Sources, P. C. Uden, Ed., ADVANCES IN CHEMISTRY SERIES No.170, ACS: Washington, D. C., 1978, p. 232.
14. Burnham, A. K. Oil Shale, Tar Sands and Related Materials, W. C. Stauffer, Ed., ACS SYMPOSIUM SERIES No. 163, ACS: Washington, D. C., 1981, p. 39.
15. McKee, R. H. "Shale Oil," Chemical Catalog Co., 1925, p. 82.
16. Burnham, A. K.; Clarkson, J. E.; Singleton, M. F.; Wong, C. M.; Crawford, R. W. Geochim. Cosmochim. Acta 1982, 46, 1243.
17. Slettevold, C. A.; Biermann, A. H.; Burnham, A. K. "A Surface-Area and Pore-Volume Study of Retorted Oil Shale," Lawrence Livermore National Laboratory Rept. UCRL-52619, 1978.
18. Campbell, J. H.; Koskinas, G. J.; Stout, N. D. Fuel 1978, 57, 372.
19. Shih, S. M.; Sohn, H. Y. I&EC, Process Design and Devel. 1980, 19, 420-426.

¹H-NMR Thermal Scanning Methods for Studying Oil Shale Pyrolysis

L. J. LYNCH and D. S. WEBSTER

CSIRO Physical Technology Unit, 338 Blaxland Road, Ryde, NSW, 2112, Australia

This paper reports on the use of ¹H NMR thermal
scanning for studying the pyrolysis of oil shales.
The strength and sensitivity of the ¹H NMR signals
of oil shales are sufficient such that pulsed NMR
techniques afford a means of dynamically observing
thermal transformation processes. Parameters can
be extracted from the NMR data that relate to the
hydrogen content, phase structure, molecular
mobility and free radical content of the specimen.
The temperature dependencies of these parameters
reveal chemical and physical transformations that
occur in the nature of the kerogen materials and
the pyrolysis products. Examples of ¹H NMR thermal
scanning of Australian oil shales are presented
which illustrate this method of ¹H NMR thermal
analysis.

Dynamic experimental techniques by which non-equilibrium
states of a system can be observed during thermally induced
transformations allow the kinetics of pyrolysis mechanisms to be
directly studied. This paper reports on the novel use of simple
low resolution proton nuclear magnetic resonance (¹H NMR) measure-
ments as a reaction time probe to monitor the state of oil shales
during heating from room temperature to ∿870K. The method
involves the observation of the ¹H NMR transverse relaxation
transient at regular intervals during heating. Similar studies of
coal pyrolysis (1-6) and a description of the apparatus (7) used
have been previously reported. In these reports the ability to
obtain non-equilibrium data during fossil fuel pyrolysis despite
the limited scope for signal averaging and the deterioration of
signal-to-noise of the ¹H NMR signal with rise in temperature was
demonstrated. This method of thermal analysis has a particular
advantage over conventional thermal analysis methods such as thermo-
gravimetry and differential thermal analysis in that it is highly
selective of the organic kerogen to the exclusion of the inorganic
parts of the shale.

The experiments reported here involve measurements of the ^{1}H NMR during pyrolysis of shale specimens contained in open tubes and flushed with dry nitrogen gas so that volatile pyrolysis products are quickly removed. A number of different parameters extracted from the data are investigated for their usefulness in monitoring changes that occur in the properties of the specimen. These parameters relate to the loss of hydrogen from the specimen and changes that occur in the molecular structure and mobility as a consequence of chemical and physical transformations.

The results presented are not part of a systematic study of oil shale pyrolysis but rather those of various experiments selected to demonstrate the utility and potential of the method.

Experimental

The specimens for measurement consisted of 300–500 mg of finely ground material predried under nitrogen at 378K and contained in open glass tubes. The ^{1}H NMR measurements were made at 60 MHz using high temperature specimen probes and temperature control apparatus described previously (7). Specimens were positioned within the inner 2/3 of the measurement radio-frequency coil of the NMR probe and were continuously flushed with a stream of dry nitrogen gas throughout the heating cycles which rapidly removed volatile products formed from the measurement zone. Thus at all stages during an experiment the ^{1}H NMR signal of all the residual material was recorded.

Results are reported here for experiments made on a Sydney basin oil shale from Glen Davis and on a Julia Creek shale and its demineralized organic residue. These specimens were obtained from CSIRO Division of Fossil Fuels and CSIRO Division of Energy Chemistry respectively. We do not have analyses of these specimens but they are considered typical of the particular deposits. H/C ratios of 1.52 and 1.4 and O/C ratios of 0.04 and 0.8 for Glen Davis and Julia Creek kerogens respectively have been published (8).

The $90-\tau-90_{90}$ NMR pulse sequence (9) was used to stimulate the ^{1}H NMR transverse relaxation signal as shown in figure 1. This method of observing the signal is preferred to the simpler single $90°$ pulse method in an attempt to overcome the receiver dead-time problem which is significant for many of the rapidly relaxing ^{1}H NMR transient signals observed. Receiver dead-time was ∼4µs and a pulse spacing, τ, of 15µs was used.

Measurements were recorded dynamically at regular intervals while the specimens were heated at a uniform rate of 4K/minute from room temperature to temperatures greater than 850K. Temperatures were recorded with an accuracy of ±1K and care was taken to maintain tuning of the NMR probe during the changing conditions of the experiment. A Bruker BC-104 transient digitizer carefully compensated for spurious signals was used to record the ^{1}H NMR signals. A typical ^{1}H NMR 'solid-echo' signal recorded during heating is shown in figure 1.
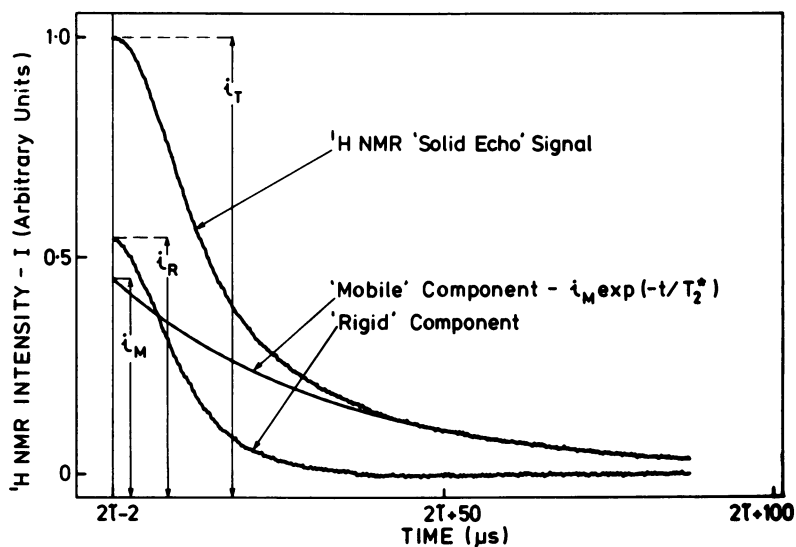
Figure 1. A ¹H-NMR solid-echo signal recorded during heating of a Glen Davis oil shale. The method of its separation into rigid and mobile components is indicated.

Results and Analysis

For a rigid-lattice pair-wise dipolar coupled population of proton spins, the $90-\tau-90_{90}$ pulse sequence stimulates the so called solid-echo signal which is a full representation of the transverse relaxation and the peak of the echo, i_T, a measure of the total hydrogen content of the specimen (9). The extent to which the proton populations of the heated oil shales deviate from such a model will vary in a complex way during pyrolysis and we expect a corresponding variation in the nature of the recorded ^{1}H NMR signals which therefore cannot be considered only in terms of the theory for a pair-wise dipolar coupled solid. It is expected that deviations from such a model will occur because of the variable degree of molecular mobility that occurs, the occurrence of unlike-spin dipolar interactions of the proton with paramagnetic species, and because of multiple proton dipolar interactions. Details of how these factors affect the solid-echo experiment have been considered to some extent by others (9,10).

The experimental echo peaks that are clearly visible for pulse spacings of $\tau = 15\mu s$ (figure 1) however occur 2-3μs earlier than the 31μs predicted for a true solid echo. This discrepancy is consistent with the facts that when the specimens exhibit only 'rigid-lattice' like behaviour the condition $\tau \ll T_2$ does not hold, where T_2 is the transverse relaxation time, and that under other conditions where there is significant molecular mobility the signals are not purely the solid-echoes of dipolar coupled solids.

In this analysis we treat the signals as full representations of the ^{1}H NMR transverse relaxation and the echo peak-height, i_T, is chosen as a measure of the total hydrogen remaining in the residue at any given time during pyrolysis. Because the sensitivity of the ^{1}H NMR signal of a population of spins is inversely related to some power of the temperature (11), it is necessary to apply an amplitude correction to the measured values of i_T. An empirical temperature calibration of the experimental probe was made using a coal char specimen sealed in a glass ampoule. This material had been previously pyrolysed at a temperature of greater than 950K and besides having a constant hydrogen content, appears relatively constant in its ^{1}H NMR properties over the temperatures of the calibration (i.e. 300-770K). The ^{1}H NMR signals for a Glen Davis and a Julia Creek oil shale observed dynamically at four temperatures during heating are shown in figures 2a and 2b respectively. The ^{1}H NMR data have been compensated for temperature dependence using the coal char calibration so that the echo peak amplitudes therefore represent the apparent hydrogen contents. This calibration has been found qualitatively successful when applied to the data of a number of coal pyrolysis experiments (5,6) but when used for most oil shale experiments an anomaly occurs in that there is an initial increase in the apparent hydrogen content on heating above room temperature. This anomaly can be seen in the plots of the temperature
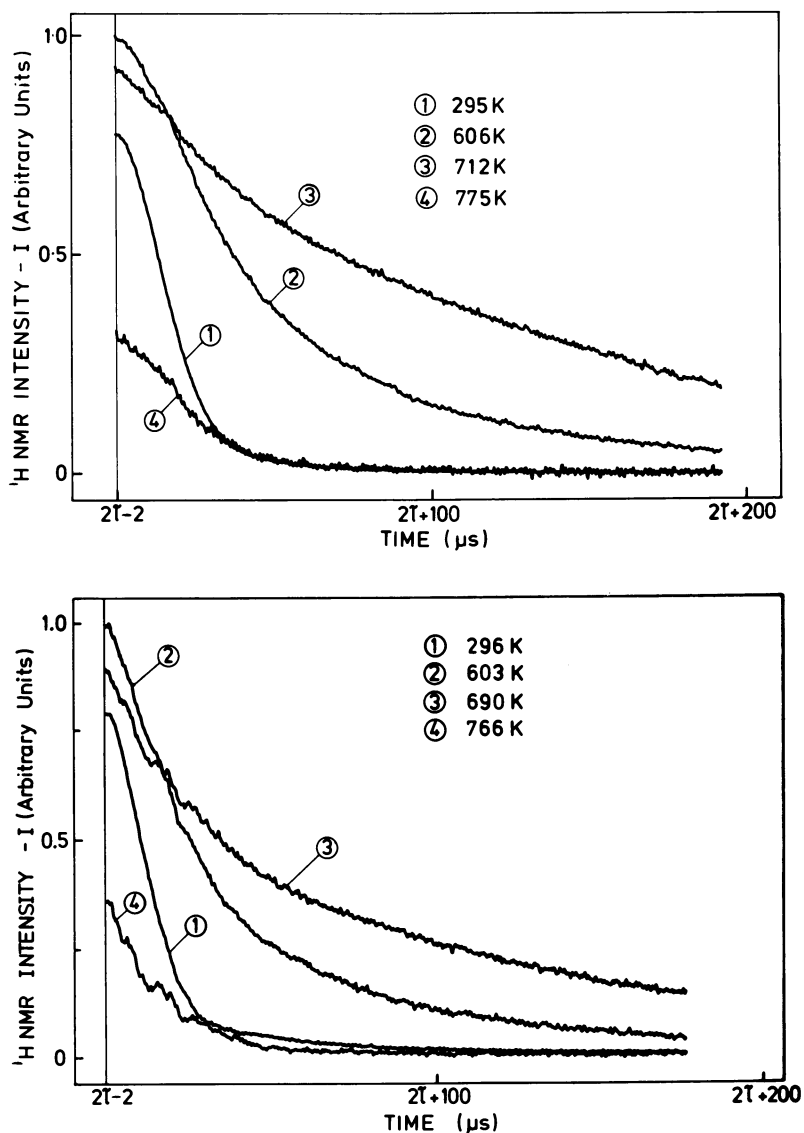
Figure 2. The ¹H-NMR signals of a Glen Davis (top) and a Julia Creek (bottom) oil shale are shown at four instances during heating at 4 K/min. The signals for the original shale (1), that near maximum molecular mobility (3), and that of the char residue at high temperature (4) are included.

dependencies of the apparent hydrogen content for both a whole and
a demineralized Julia Creek oil shale (figures 3b and 3c) and for a
Glen Davis oil shale (figure 3a). We consider this effect to be
related to the presence of paramagnetic species in the specimens
(12) and the fact that it occurs greatly reduces the quantitative
usefulness of this method of hydrogen content determination.   It
nonetheless is very useful for at least qualitatively defining the
main pyrolysis regions at higher temperatures, where there is a
rapid loss of volatile material.   Numerical differentiations of
these data (figures 3a,3b,3c) show the temperature region of
maximum rate of '% hydrogen loss'.   These 'hydrogen loss' scans
are analogous to thermogravimetric analyses and in the several
instances where parallel measurements have been performed, similar
temperature regions have been observed for the maximum rates of
'hydrogen loss' and weight loss respectively.

In addition to detecting thermal decomposition of the specimen
these ^{1}H NMR signals contain other information about changes that
occur in the state of the specimen during pyrolysis.   It is useful
to postulate that, at all stages of pyrolysis, the organic material
contains both 'rigid' hydrogen with a rapidly relaxing ^{1}H NMR
transient and 'mobile' hydrogen with a relatively slower relaxing
transient.   We have attempted to make such a distinction by
resolving the observed transients into two components.   The
procedure for doing this is to a large extent arbitrary and the
accuracy to which a particular method can be applied varies greatly
with the condition of the specimen.   The method we have used is to
fit an exponential – $i_m \exp(-t/T_2^*)$ – to the tail of the transients
where it is assumed only the 'mobile' slowly relaxing protons are
represented.   This method of analysis is outlined in figure 1.   From
this analysis two parameters are obtained: (i) the percentage of
the residual hydrogen in the 'rigid' state – i.e.

$$i_R\% = 100(i_T - i_M)/i_T$$

and, (ii) the time constant T_2^* of the 'mobile' hydrogen component
of the ^{1}H NMR transient.   The results of such analyses of pyrolysis
data for Glen Davis, Julia Creek and Julia Creek demineralized shale
specimens are shown in figures 5a,5b and 5c respectively.

A parameter that has been widely used in the study of the
structure and thermal properties of solid organic materials (13-16)
and particularly coals (14-16) is the ^{1}H NMR second moment.   To
compute such a parameter from our solid echo data requires its
Fourier transformation from the time domain to obtain a complex
frequency domain ^{1}H NMR spectrum, i.e. $g'(\nu) = u'(\nu) + iv'(\nu)$.   The
quadrature components of this spectrum represent linear combinations
of the pure absorptive ($u(\nu)$) and dispersive ($v(\nu)$) modes of the
true spectrum, i.e,

$$u'(\nu) = v(\nu)\cos\theta + u(\nu)\sin\theta$$
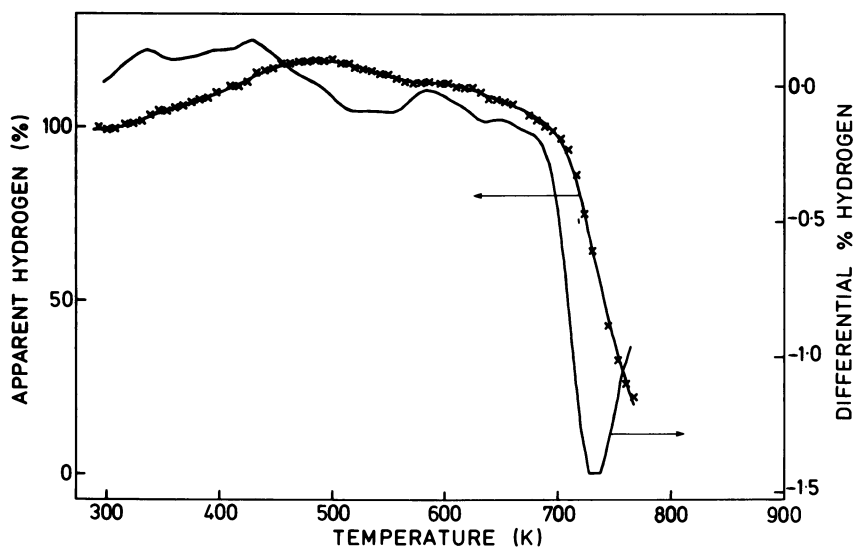
Figure 3a. The apparent hydrogen content and differential hydrogen content parameters of Glen Davis oil shales from ¹H-NMR thermal analyses. Heating rate, 4 K/min in a nitrogen atmosphere.
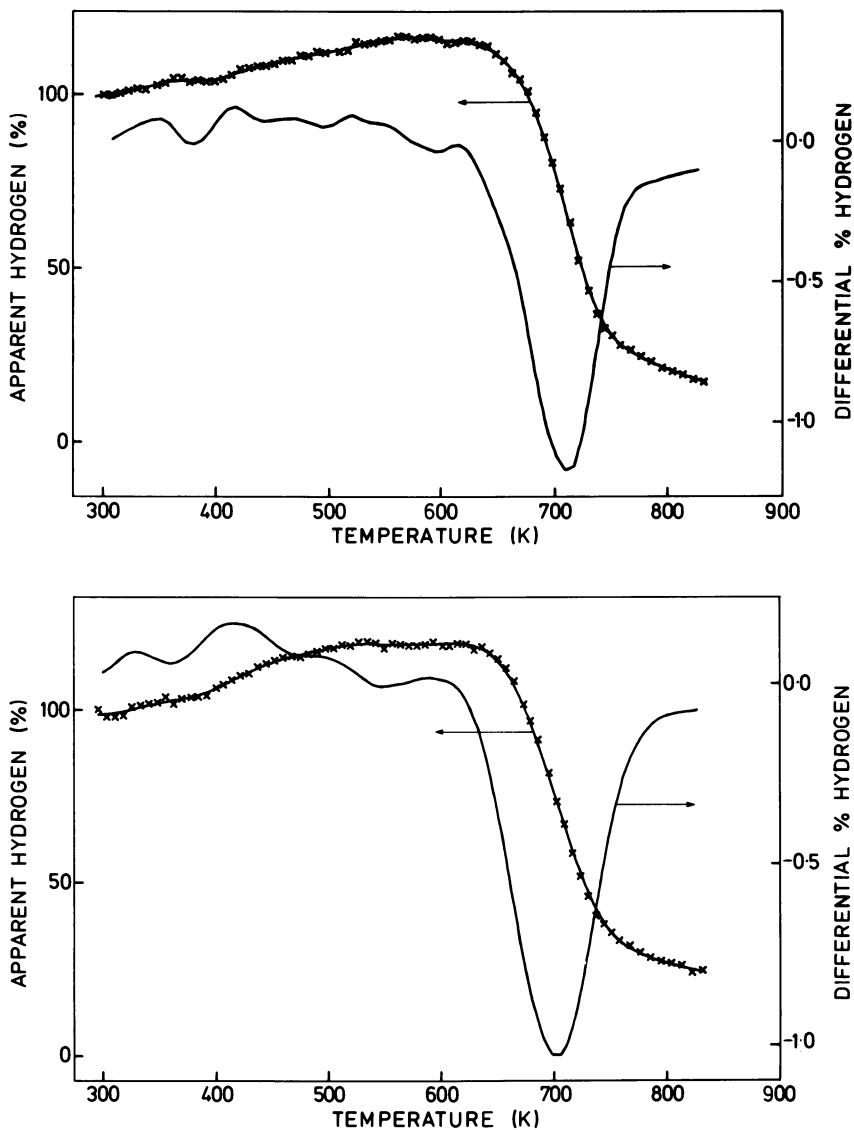
Figure 3b.   The apparent hydrogen content and differential hydrogen content parameters of Julia Creek (top) and demineralized Julia Creek (bottom) from ¹H-NMR thermal analyses of oil shales. Heating rate, 4 K/min in a nitrogen atmosphere.

$$v'(\nu) = v(\nu)\sin\theta - u(\nu)\cos\theta$$

where θ is a frequency dependent phase shift nominally resulting from an error in the zero of time in the time domain data. For our data its value is determined by the time selected for the 'solid-echo' peak which is uncertain to varying degrees. It is usual to empirically adjust the phase relationship to separate the absorptive and dispersive modes. However the computed second moment parameter of the frequency spectrum is critically dependent on this phase adjustment with the result that there is considerable scatter in the values obtained for a thermal scanning experiment. To bypass this problem we have instead computed the power spectrum given by

$$a(\nu) = u'^2(\nu) + v'^2(\nu) = u^2(\nu) + v^2(\nu)$$

which is independent of the phase error. Such power spectra computed for the Glen Davis ¹H NMR transient signals shown in figure 2 are shown in figure 4. Ejchart and Wroblewski (17) have demonstrated the validity of using this power spectrum rather than the absorption spectrum for line shape analysis in high resolution spectroscopy. We have therefore computed a 'second moment' parameter, M_2^*, of the power spectrum defined as

$$M_2^* = \int_{\nu_o}^{\nu_x} a(\nu)\Delta\nu^2 d\nu \Big/ \int_{\nu_o}^{\nu_x} a(\nu) d\nu$$

where ν_o is the central resonance frequency, $\Delta\nu = (\nu - \nu_o)$, and the limit of integration, ν_x, is chosen to be a frequency where $a(\nu_x) = a(\nu_o)/10$. Truncation at this value of ν_x has been chosen by trial as a compromise between increased random errors that accrue for truncation at higher values of ν_x and the increase in systematic errors that result from truncation at lower values. We have found that the temperature dependence of M_2^* computed for this truncation is qualitatively the same as for truncations at higher values and most of the quantitiative features are relatively the same.

Examples of the temperature dependence of M_2^* are shown in Figure 5a and Figures 5b and 5c for Glen Davis shale and for Julia Creek and Julia Creek demineralized shales, respectively.

Discussion

The results presented here are unique in that they are from ¹H NMR measurements made under the non-equilibrium conditions pertaining to temperature controlled pyrolitic decomposition of the shales. We have established experimental techniques that ensure good reproducibility of the changes manifest in these dynamically recorded ¹H NMR 'solid echo' signals. By this technique of ¹H NMR thermal analysis it is possible to obtain a set of data characterizing the pyrolysis properties of the shale.
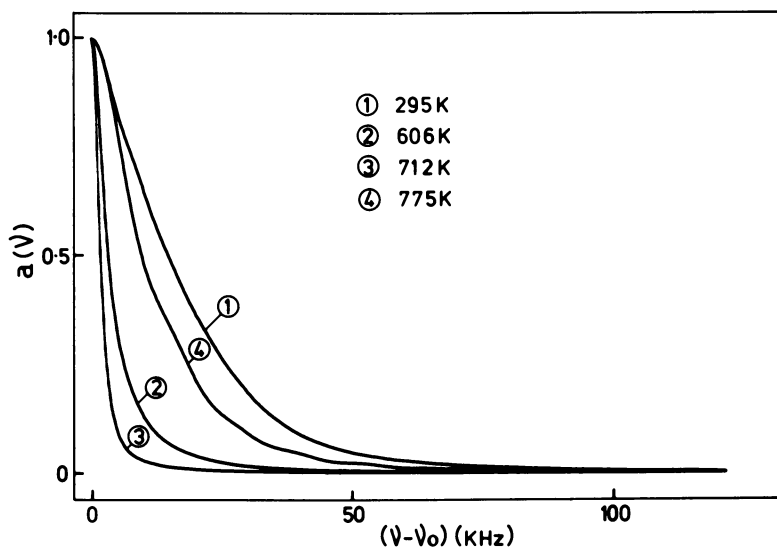
Figure 4. The ¹H-NMR power spectra obtained by Fourier transformation of the ¹H-NMR signals recorded during heating of a Glen Davis oil shale as shown in Figure 2 (top).
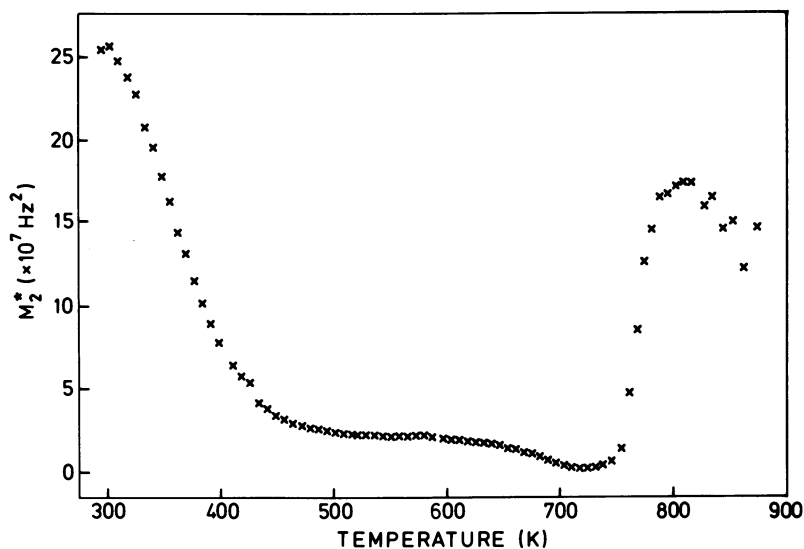
Figure 5a. The variations of the power spectrum second moment parameter (M_2^*) of Glen Davis from ¹H-NMR thermal analyses. Heating rate, 4 K/min in a nitrogen atmosphere.
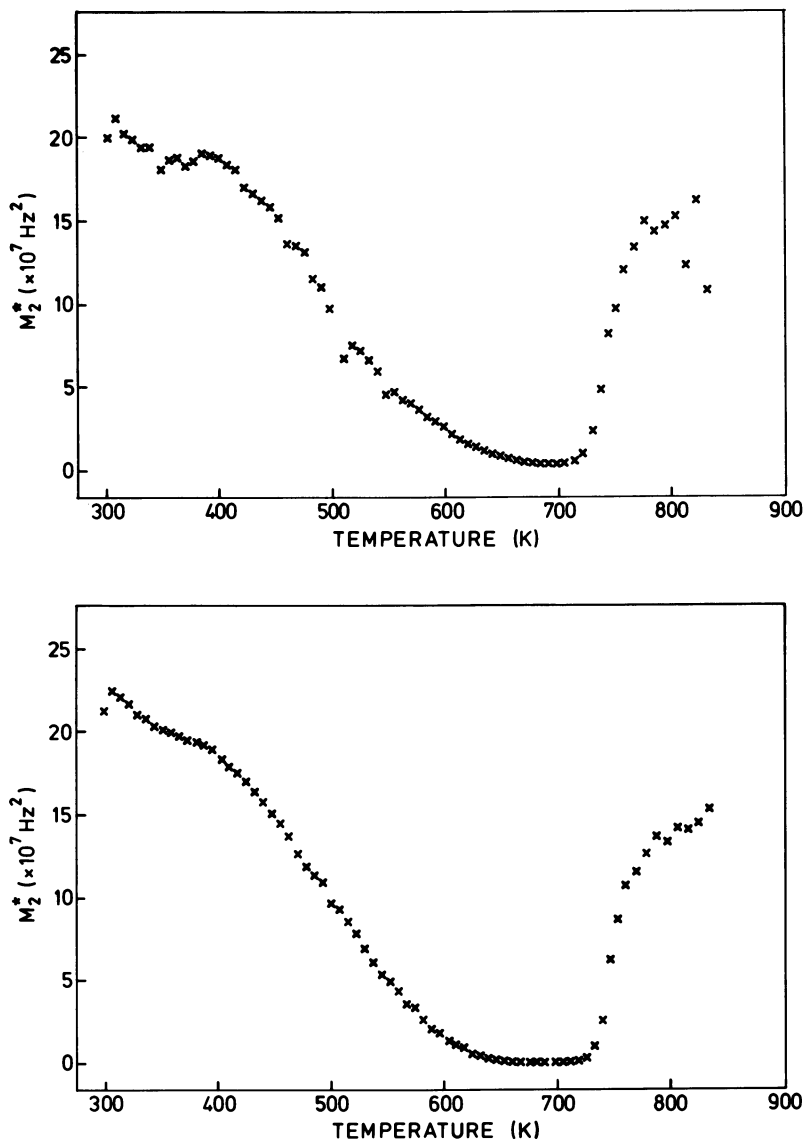
Figure 5b. The variations of the power spectrum second moment parameter (M₂*) of Julia Creek (top) and demineralized (bottom) from ¹H-NMR thermal analyses. Heating rate as in Figure 5a.

The analysis of the ^{1}H NMR thermal scan data has been in three parts:

(i) An intensity parameter, i_T, directly related to the hydrogen content of the residual, has been used to monitor the loss of volatile products and thereby detect the main region of pyrolitic decomposition.

(ii) The ^{1}H NMR signals have been resolved into two components implying the existence of two phases that differ in molecular mobility. It should be emphasized that this division is to a large extent arbitrary, and, that although these analytical components are referred to as 'rigid' and 'mobile' respectively, the distinction is only relative and in fact the so called 'rigid' component need not be that of a truly rigid-lattice structure in the NMR sense. Also obtained by this method of analysis is a parameter, T_2^*, which is the time constant of the 'mobile' component of the ^{1}H NMR transient. This is a measure of the average molecular mobility of the 'mobile' material – the greater the average mobility, the greater the value of T_2^*. It is expected that as the temperature is raised a number of different factors would therefore influence the value of T_2^* – (a) the rate of transformation of material from the 'rigid' to the 'mobile' state, (b) thermal activation and/or breakdown of the 'mobile' molecules, (c) the rate of loss by volatilization of presumably the smaller and more mobile of the molecules, and, (d) at higher temperatures, the formation of the rigid residue from the 'mobile' material.

(iii) A 'second moment' parameter of the power spectrum, M_2^*, has been derived as a parameter which monitors the changes in the structural composition and mobility of the material that are manifest in the total line shape function of the ^{1}H NMR signals. Low temperature ($\sim$90K) ^{1}H NMR second moments, calculated for the frequency spectrum rather than for the power spectrum, have been used by others (16) to estimate the gross chemical composition of coals. The basis of this estimation is that the second moment of the coal can be defined as the weighted average of the second moments of all the constitutent groups. For a rigid-lattice solid each chemical group can be assigned a characteristic second moment which is a measure of the dipolar interactions and therefore critically dependent on the interproton distances. The higher hydrogen concentration ensures that the second moment values for rigid lattice aliphatic structures are about three times those typical of aromatic structure (13-16). The static dipolar interactions of even slowly reorienting molecular groups are greatly reduced by the motion so that these groups no longer significantly contribute to the overall second moment of the specimen. Thus by monitoring the normally used second moment of the frequency spectrum or the closely related parameter, M_2^*, used by us, effects due to thermally induced changes both in the chemical composition of the shale and in the net molecular mobility of the constitutent groups can be observed.

Although each of the three methods of analysis is subject to uncertainty in interpretation and precision of measurement they separately and in combination provide much information on the processes involved in shale pyrolysis.

The apparent hydrogen content and differential hydrogen content data for the Glen Davis shale (figure 3a) delineate a period between 700K and 800K where rapid thermal decomposition and loss of volatile material occurs. In the course of heating it is seen that there is a steady conversion of hydrogen from the rigid to the mobile state (Figure 6a) and that this process seems to occur in two stages. The first stage occurs between room temperature and 660 K and the second and more rapid conversion between 660 K and 720 K by which time all of the material is in the mobile state. This is reflected in the temperature dependence of M_2^* (Figure 5a). At 720K M_2^* attains a very small value consistent with the absence of any significant amount of rigid-lattice hydrogen. Between 720K and 800K and accompanying the rapid loss of hydrogen in volatile products from the specimen a rigid residue is formed which contains more than 10% of the initial total hydrogen and has a M_2^* value consistent with it being a rigid-lattice-like aromatic material. Beyond 800K the decrease in M_2^* could be evidence of molecular mobility in this residue. We have observed this same phenomenon for bituminous coals and more particularly in an inertinite concentrate but not for a vitrinite concentrate (12).

The behaviour of the T_2^* parameter reflects its sensitivity to a range of thermally induced changes in the 'mobile' component of the residue. The definitive maximum in T_2^* that occurs during heating near the temperature of maximum rate of 'hydrogen' loss (Figures 3a and 6a) can be explained as the resultant of a trend for the average molecular mobility of the 'mobile' phase to increase because of molecular breakdown and thermal activation on the one hand, and, the tendency for it to decrease due to the loss of mobile material by volatilization and perhaps conversion to rigid residue on the other.

The ^{1}H NMR thermal scanning data for the Julia Creek shale and demineralized shale are similar to each other but are quite different from those of the Glen Davis shale. Compared to the data for the Glen Davis shale we note the following general differences for the Julia Creek materials. (a) The onset of thermal decomposition is not as rapid (figures 3b and 3c) and the major zones of thermal decomposition as indicated by the apparent hydrogen loss and differential hydrogen loss occur at significantly lower temperatures. Also the temperatures of maximum rate of percentage hydrogen loss are at lower temperatures and these rates are lower. (b) There is little change in the molecular mobility of the Julia Creek specimens below 450K as indicated by changes in either M_2^* (Figures 5b and 5c) or the proportion of rigid hydrogen (Figures 6b and 6c) but beyond 450 K the rate of molecular mobilization as revealed by these parameters proceeds more rapidly. Whereas M_2^* reaches a very small minimum value
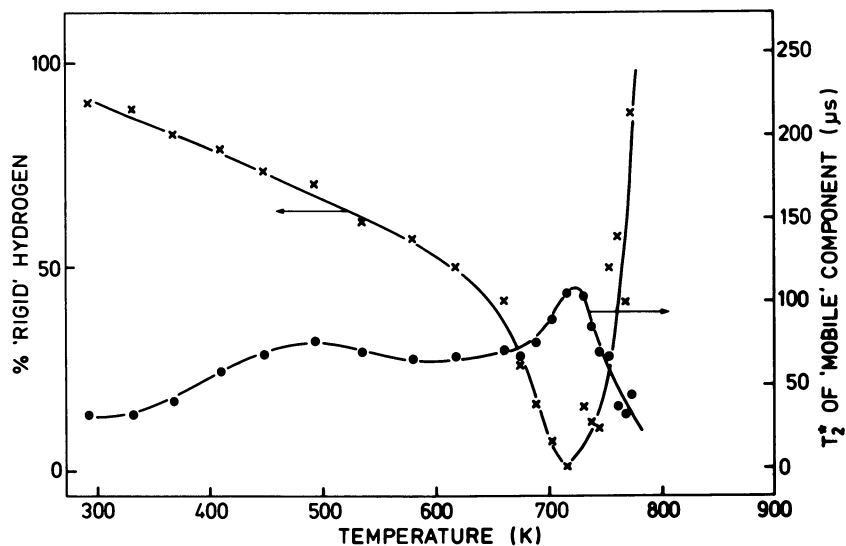
Figure 6a. The variations of the proportion of rigid hydrogen and of the mobile hydrogen time-constant parameter (T₂) of Glen Davis from the ¹H-NMR thermal analyses of oil shales. These parameters result from the deconvolution of the ¹H-NMR signal as outlined in Figure 1. Heating rate, 4 K/min in a nitrogen atmosphere.*
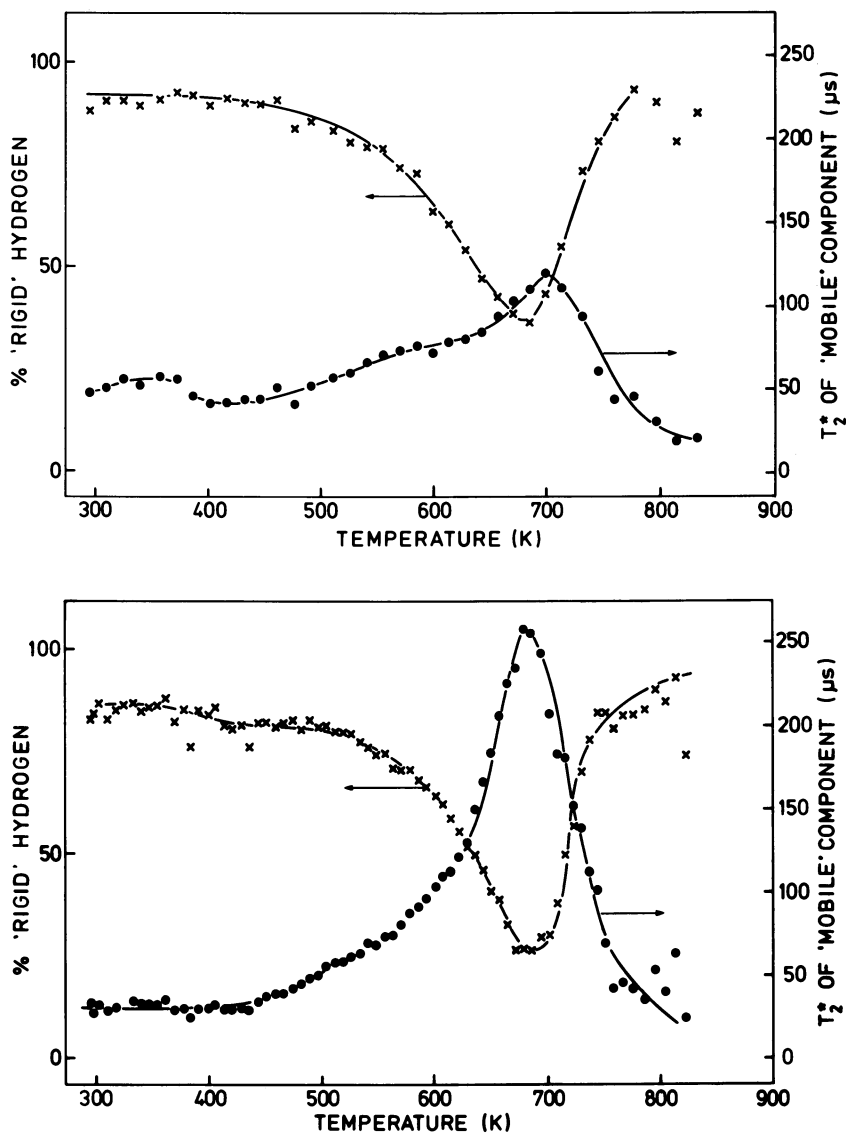
Figure 6b. The variations of the proportion of rigid hydrogen and of the mobile hydrogen time-constant parameter (T₂*) of Julia Creek (top) and demineralized Julia Creek (bottom) from the ¹H-NMR thermal analyses of oil shales. See Figure 6a for further discussion.

indicating the absence of any significant rigid lattice component
in the Julia Creek materials at a lower temperature than for the
Glen Davis shale, the minimum in the 'rigid' hydrogen content
(Figures 6b and 6c) only reaches 30-40% as compared to 0% for the
Glen Davis shale. This apparent contradiction stems from the
method used for separation of the ^{1}H NMR signals into components.
The low M_2^* value is a reliable guide to the absence of any
significant rigid-lattice type material whereas the method of
phase separation is rather arbitrary. Thus although the so-called
'rigid' hydrogen fraction of the Julia Creek shales near 690K
(figure 2b) is considerably less mobile than the corresponding
'mobile' fraction it is not in fact representative of a rigid-
lattice structure. (c) The formation of the rigid residues occur
earlier and again in conjunction with the loss of volatile material
but a much greater fraction of the hydrogen remains in the residue
(figures 6b and 6c and figures 3b and 3c).

In comparing the ^{1}H NMR thermal scanning data of the whole and
demineralized Julia Creek materials we note the following. (a) A
general similarity in the apparent hydrogen loss behaviour, but
that the maximum rate of percentage hydrogen loss occurs sooner for
the demineralized shale although the maximum rates are similar
(figure 3b and 3c). (b) There is little difference in the
behaviour of M_2^* except that the demineralized shale acquires
'mobility' at a slightly lower temperature. The same small
minimum values of M_2^* are attained indicating the absence of rigid
components in either structure over a temperature range (figures
5b and 5c). (c) The proportion of rigid hydrogen falls to a
lower value for the demineralized shale and there is a major
difference in the variation of the T_2^* parameter. This parameter
shows that a greater molecular mobility is acquired by the mobile
fraction of the demineralized shale (Figures 6b and 6c).

This comparison of the whole and demineralized Julia Creek
shales shows that although the degree of molecular mobility of the
material 'softened' during the heating is inhibited by the presence
of the inorganic material it does not have much effect on the
eventual thermal decomposition of the organic material.

The observations of Miknis et al (18) that the aromatic
component of some oil shales remains inert during pyrolysis does
not appear to be the case for the shales studied here. This is
apparent from the transient behaviour of the molecular mobilities
as indicated by the parameter M_2^*. The very low values of M_2^*
achieved prior to the main pyrolysis zone clearly show that all
significant components of the organic hydrogen in both the Julia
Creek and Glen Davis shales pass through a mobile stage before a
residual rigid lattice component is formed during the main
pyrolysis periods. It is unlikely that the original aromatic
materials in these shales could undergo the transient 'softening'
observed here without the occurrence of at least some chemical
change as well as the obvious physical changes.

Literature Cited

1. Lynch, L.J.; Webster, D.S. Fuel 1979, 58, 235.
2. Webster, D.W.; Lynch, L.J. Fuel 1981, 60, 549.
3. Lynch, L.J.; Webster, D.S. 4th Australian Workshop on Coal Hydrogenation, Richmond, Victoria, Nov. 1979, Abstracts and Papers, Paper 15.
4. Lynch, L.J.; Webster, D.S. Proc. Intern. Conf. on Coal Science, Dusseldorf, 7–9 Sept. 1981, D14, p.675.
5. Lynch, L.J.; Webster, D.S. 6th Australian Workshop on Coal Hydrogenation, Clayton, Victoria, Dec. 1981, Abstracts and Papers, 5a–6.
6. Lynch, L.J.; Webster, D.S.; Bacon, N. Symposium on Characteristics of Australian Coals and their Consequences for Utilization, North Ryde, N.S.W., Australia, May 1982, Abstracts and Papers, 33–1.
7. Webster, D.S.; Cross, L.F.; Lynch, L.J. Rev. Sci. Instrum. 1979, 50, 390.
8. Saxby, J.D. in "Oil Shale", Yen, T.F.; Chilingarian, G.V.; Eds.; Elsevier: New York, 1976; Chap. 6, p.103.
9. Powles, J.G.; Strange, J.H. Proc. Phys. Soc. (London)1963, 82, 6.
10. Cosgrove, T.; Barnett, K.G. J. Magn. Reson. 1981, 43, 15.
11. Abragram, A. "The Principles of Nuclear Magnetism"; Oxford Univ. Press (Clarendon), London 1961, p.39.
12. Lynch, L.J.; D.S. Webster, Proc. Int. Coal Science Conference, Pittsburg, August 1983, paper 175, to be published.
13. Andrew, E.R.; Eades, R.G. Proc. Roy. Soc. (London) Series A, 1953, 216, 398.
14. Ladner, W.R.; Stacey, A.E. Fuel 1963, 42, 75.
15. Sircar, R.; Gupta, R.C. Indian J. Phys. 1982, 56A, 55.
16. Sharkey, A.G.; McCartney, J.T. in "Chemistry of Coal Utilization", 2nd Suppl. Vol., Elliot, M.A., Ed.; John Wiley & Sons: New York, 1981, p.159.
17. Ejchart, A.; Wroblewski, K. J. Magn. Reson. 1980, 40, 469.
18. Miknis, F.P.; Szeverenyi, N.M.; Maciel, G.E. Fuel 1982, 61, 341.

Pyrolysis of Shale Oil Crude and Vacuum Distillate Fractions

ROBERT N. HAZLETT and ERNA J. BEAL

Naval Research Laboratory, Washington, DC 20375

The vacuum distillate from Paraho shale oil crude was separated on silica gel into three fractions – saturate, aromatic, and polar. The carbon-13 NMR spectra indicated that these fractions contained 58, 15 and 36 percent, respectively, of unbranched alkyl groups. These fractions were subjected to pyrolysis at 450°C for various times. The yield of JP-5 jet fuel was good for the saturate fraction, varying between 24 and 27 percent for pyrolysis times of 15 to 120 minutes. The JP-5 yield for the polar fraction was lower, 18 to 22%. The n-alkanes and 1-alkenes were determined by capillary gas chromatography. The sum of these two classes comprised over 30 percent of the JP-5 cut in the saturate pyrolysis product but less than 15 percent for the polar and aromatic pyrolysis products.

The freezing point of U.S. Navy jet fuel (JP-5) has been related to the amounts of large n-alkanes present in the fuel (1,2). This behavior applies to jet fuels derived from alternate fossil fuel resources, such as shale oil, coal, and tar sands, as well as those derived from petroleum. In general, jet fuels from shale oil have the highest and those from coal the lowest n-alkane content. The origin of these n-alkanes in the amounts observed, especially in shale-derived fuels, is not readily explained on the basis of literature information. Studies of the processes, particularly the ones involving thermal stress, used to produce these fuels are needed to define how the n-alkanes form from larger molecules. The information developed will significantly contribute to the selection of processes and refining techniques for future fuel production from shale oil.

Carbon-13 nmr studies indicate that oil shale from the Green River Formation contains much aliphatic meterial (3). Further, the shale oil derived from the rock also gives indication of considerable straight chain material with large peaks at 14, 23, 30 and 32 ppm in the C-13 nmr spectrum.

Previous pyrolysis studies at NRL stressed fractions of crude shale oil residua, measured the yields of JP-5, and determined the content of potential n-alkanes in the JP-5 distillation range (4). Additional studies have pyrolyzed model compounds with long unbranched alkyl groups (5). These types of compounds are thought to be present in shale crude oil.

This work presents the results of two studies: (a) the pyrolysis of Paraho crude shale oil and (b) the separation, analysis and pyrolysis of the shale oil vacuum distillate. In part (b), a shale crude oil vacuum distillate (Paraho) was separated into three chemical fractions. The fractions were then subjected to nmr analysis to estimate the potential for n-alkane production and to pyrolysis studies to determine an experimental n-alkane yield.

Experimental Details

Pyrolysis Procedure. The shale oil samples were stressed at conditions similar to the petroleum refining process known as delayed coking (6). These conditions are 450°C and about 90 psi pressure. Each thermal stress was conducted in a 1/4 inch o.d. 316 stainless steel tube fitted with a stainless steel valve via a Swagelok connection. The tube, with a weighed amount of sample (approximately 0.1 g), was attached to a vacuum system, cooled to -78°C, and pumped to remove air. The tube was then thawed and the cooling/pumping process repeated. The tubes were heated by inserting them into 9/32-inch holes in a six-inch diameter aluminum block fitted with a temperature controller.

Complete details of sample workup and analysis can be found in reference (4). One gas chromatographic (GC) technique determined the JP-5 yield from the pyrolysis by summing the total FID area for carbon numbers 9 through 16. A second GC analysis determined the individual n-alkanes and 1-alkenes with a fused silica capillary column.

Separation of Vacuum Distillate. Paraho shale oil was distilled at atmospheric pressure to an end point of 300°C. A second cut was obtained by continuing the distillation at reduced pressure, 40 mm Hg. This vacuum distillate, with an end point of 300°C, was used in the studies described below.

The vacuum distillate was separated on silica gel into saturate, aromatic, and polar fractions by the procedure described earlier (4). The vacuum distillate comprised 33% of the crude shale oil and contained 1.82% (W/W) of nitrogen. The

three chemical classes represented 36%-saturates, 22%-aromatics, and 42%-polars of the vacuum distillate and contained <0.01, 0.23 and 3.0% nitrogen, respectively. The olefins elute with the saturate fraction in this separation scheme. The mass recovery from the silica gel separation was 94%, but the nitrogen recovery was only 67%. The vacuum distillate contained 7.8% n-alkanes and 1.3% 1-olefins (21.5% and 3.5% of saturate fraction), respectively.

The concentrations of n-alkanes and 1-alkenes in the saturate fraction are listed in Table I. In keeping with the distillation characteristics of this fraction, the bulk (82%) of these compounds contained 17 or more carbons. However, this saturate material did contain significant amounts of the C_{14}, C_{15} and C_{16} n-alkanes and 1-alkenes, compounds which fall within the JP-5 distillation range.

Carbon-13 nmr Analysis. Samples of the three compound classes were analyzed by C-13 nmr. The C-13 spectrum affords a distinct separation of the aromatic and aliphatic absorption regions plus a good resolution of many peaks due to specific molecular structure. Thus, a good amount of useful information can be obtained even for a complex mixture such as a fuel fraction. With respect to the present study, the aliphatic region of the spectrum is of particular importance. A spectrum for the aliphatic region of the polar fraction is shown in Figure 1. The distinctive peaks at 14, 23, 32, and 30 ppm demonstrate the presence of significant amounts of long (greater than 12 carbons) unbranched groups in this fuel fraction. Quantitation of the spectral information using the methanol internal standard gives the data listed in Table II. As expected, the content of long unbranched alkyl groups is greatest for the saturate fraction. Further, the straight chain alkyl groups in the saturate fraction are longer on the average than those in the aromatic and polar fractions. We conclude that there is a definite potential for making n-alkanes and 1-olefins in the jet fuel distillation range by cracking compounds found in the shale oil vacuum distillate.

Pyrolysis Yields

Crude Shale Oil. The whole crude prior to thermal stress contained about 18 percent material in the JP-5 boiling range. This range was set for purposes of this experiment as the mid-point between the GC retention times for n-octane and n-nonane through the midpoint between the retention times for n-hexadecane and n-heptadecane. Pyrolysis increased the JP-5 content irrespective of pyrolysis time. Table III shows that the yields of JP-5 were about the same for all stress times and that at least 24% was attained for all stress times. Thus, pyrolysis of Paraho shale oil at 450°C affords good yields of JP-5.

Table I. n-Alkanes and 1-Alkenes in Unstressed and Stressed Saturated Fraction

			Percent Concentration			
	Unstressed			Stressed (30 min., 450°C)		
Carbon Number	n-Alkane	1-Alkene	n-Alkane + 1-Alkene	n-Alkane	1-Alkene	n-Alkane + 1-Alkene
8	--	--	--	0.41	0.49	0.90
9	--	--	--	0.25	0.40	0.65
10	--	--	--	0.32	0.42	0.74
11	0.17	--	0.17	0.43	0.43	0.86
12	0.16	0.04	0.20	0.41	0.39	0.80
13	0.28	0.08	0.36	0.51	0.36	0.87
14	0.65	0.19	0.84	0.85	0.41	1.26
15	0.94	0.38	1.32	0.97	0.41	1.38
16	1.24	0.38	1.62	1.15	0.41	1.56
17	1.90	0.53	2.43	1.52	0.39	1.91
18	1.67	0.52	2.19	1.31	0.34	1.65
19	2.08	0.39	2.47	1.49	0.32	1.81
20	1.70	0.41	2.11	1.18	0.22	1.40
21	1.87	0.19	2.06	ND	ND	ND
22	1.52	0.19	1.71	ND	ND	ND
23	1.59	0.12	1.71	ND	ND	ND
24	1.17	0.05	1.21	ND	ND	ND
25	1.31	0.05	1.36	ND	ND	ND
26	0.86	0.02	0.88	ND	ND	ND
27	0.94	0.03	0.97	ND	ND	ND
28	0.75	--	0.75	ND	ND	ND
29	0.75	--	0.75	ND	ND	ND
TOTALS (11-29)	21.55	3.57	25.12	4.89	3.23	8.12
TOTALS (9-16)	3.44	1.07	4.51	--	--	--
JP-5 range						
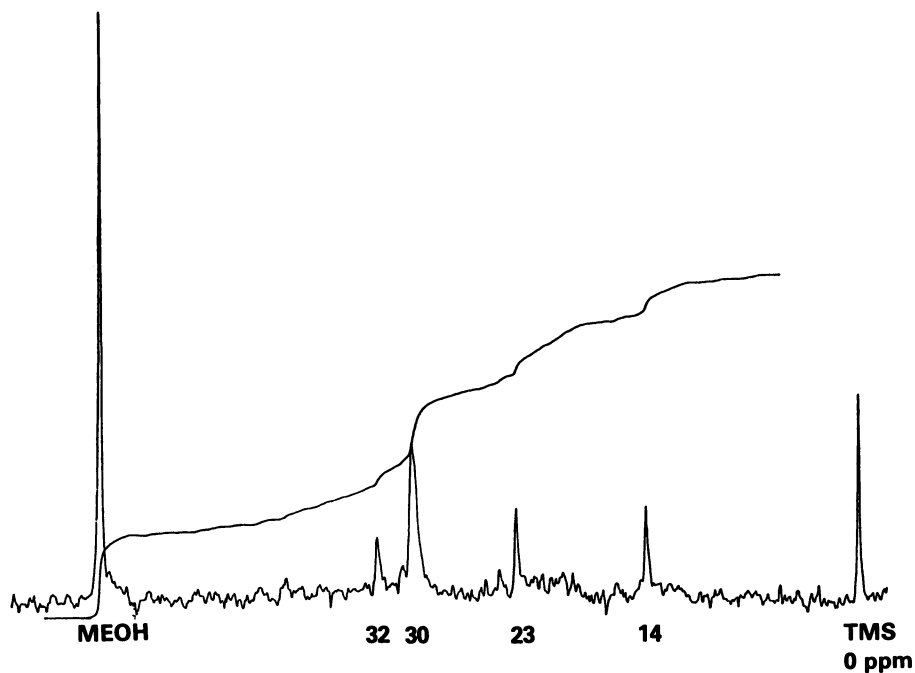
Figure 1. ^{13}C-NMR spectrum of shale oil vacuum distillate polar fraction; aliphatic region, TMS reference, methanol internal standard; and integration trace (upper curve).

Table II. Carbon-13 NMR Examination of Shale Oil Vacuum
Distillate Fractions

Fraction	Wt.% Carbon in Aliphatic Region	Wt.% Unbranched Alkyl Groups*	Average Carbon Chain Length**
Saturate	100	58	19
Aromatic	48	15	13
Polar	55	36	13

* Sum of areas of absorption peaks at 14, 23, 30 and
  32 ppm.
** For unbranched alkyl groups: based on ratio of 30 ppm
   peak area to average of 14, 23 and 32 peak areas.
Precision: ±10%

Table III. JP-5 Yield—Whole Crude Shale Oil

Pyrolysis* Time (min.)	Yield Percent
0	17.9
15	26.0
30	29.1
60	24.5
120	27.2
180	23.7

* Pyrolysis Temperature – 450°C

The potential n-alkane yield is listed in Table IV. This yield is the sum of the n-alkanes plus 1-alkenes for C_9 through C_{16} hydrocarbons divided by the JP-5 yields from Table III. The potential n-alkane yield exhibited an increasing trend up to 120 min. and then fell sharply at 180 min. Thus, the reactions involved in production and fragmentation of the n-alkanes and 1-alkenes have rates similar to reactions involving other compounds present in the crude. The highest yield, 25% at 120 min. stress, is significantly less than that found for JP-5 made in a U.S. Navy shale oil refining program (1). A tentative conclusion is that the pyrolysis conditions used in the current laboratory study were somewhat different from the delayed coking process used in the early refining project.

The distribution of n-alkane + 1-alkene by carbon number shifts with pyrolysis time. Figure 2 illustrates the trends. Compared to the crude, all carbon numbers exhibit increases in 15 min. of stress with C_{11} showing the maximum concentration. This trend continues at longer times and reaches its maximum at 120 min. A sharp reversal occurs at 180 min. For this latter time period, the concentration of large hydrocarbons is significantly reduced and the highest concentration occurs at C_8. The concentration of a particular compound is a balance between its formation by fragmentation of larger molecules and its decomposition to smaller secondary products. The 1-alkene concentration was always less than that of the n-alkane with the same carbon number. This differential became more pronounced as stress time increased, particularly for large carbon numbers. In fact, 1-alkenes with 15 or more carbons were not present after a 180 minute stress.

Vacuum Distillate Fractions. Pyrolysis of the saturate fraction for 30 minutes at 450°C gave the n-alkane and 1-alkene product distribution shown in Figure 3. This same data in tabulated form is compared in Table I with the starting material. The comparison indicates a net loss in concentration for the n-alkanes C_{16} and larger and a net gain for those with 14 or less carbons. The 1-alkenes exhibit a similar relationship with carbon number. For this pyrolysis time, the yield of small olefins equals or exceeds the yield of small n-alkanes.

The effect of stress time on yield for the saturate fraction is illustrated in Figure 4. The n-alkane plus 1-alkene sum for each carbon number is plotted. The combined alkane/alkene yields for carbon numbers above 16 decrease with increasing stress time and are almost depleted at 180 minutes. The yields for carbon numbers below 13 increase with stress time through 120 minutes but exhibit a drastic reversal at 180 minutes. Thus, the larger n-alkanes and 1-alkenes are undergoing Fabuss-Smith-Satterfield pyrolysis (7) to smaller hydrocarbons. The smaller alkanes and alkenes are initially products but, at the longer stress time,

Table IV. n-Alkane Yield from Whole Crude Shale Oil

Pyrolysis Time (min.)	Potential n-Alkane Yield* (Percent)
0	17.0
15	20.4
30	21.1
60	22.3
120	24.8
180	18.3

* Pyrolysis Temperature – 450°C; yield in percent is sum of n-alkanes + 1-alkenes for C_9 to C_{16} hydrocarbons divided by JP-5 yield from Table III.
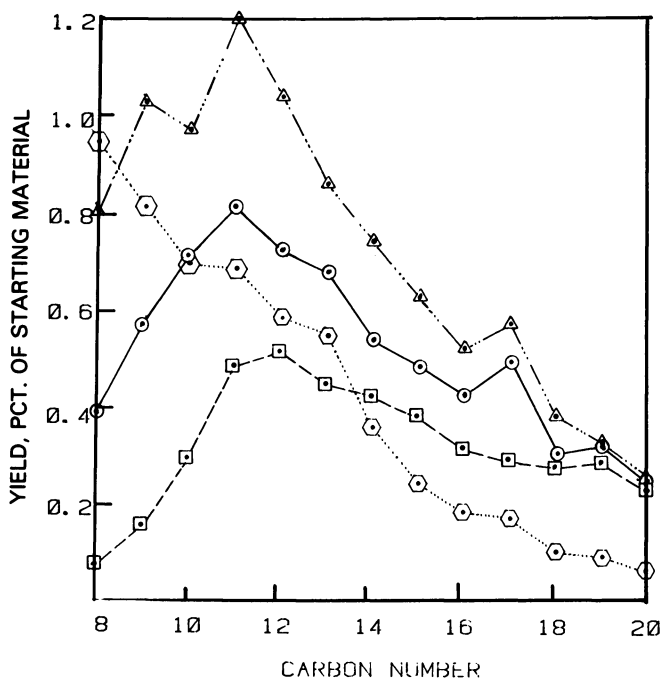
Figure 2. Pyrolysis of Paraho crude shale oil at 450 °C. The yield is the sum of n-alkane plus 1-alkene for the indicated chain length. Key: △, 120 min; ⊙, 15 min; ▯, 0 min; and ⊙, 180 min.
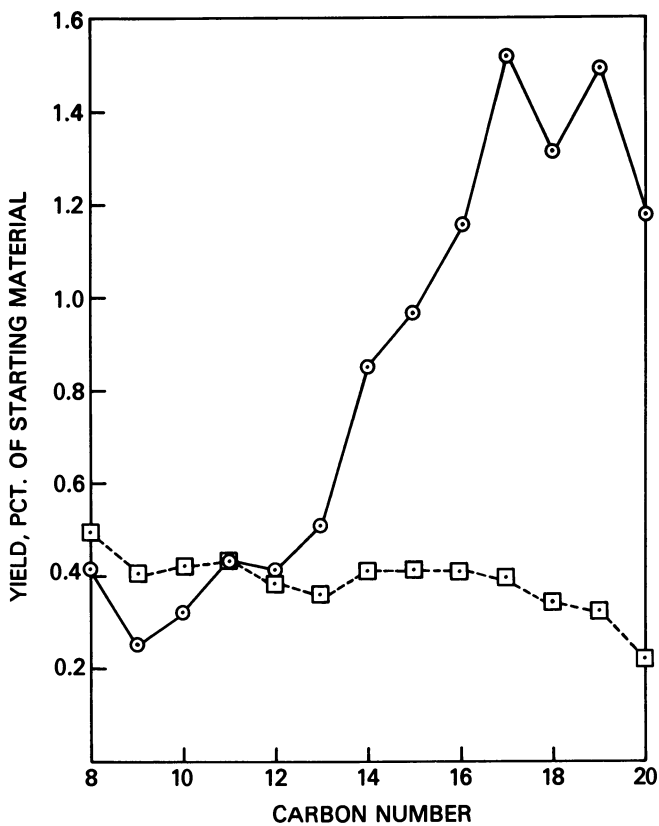
Figure 3. Pyrolysis of shale oil vacuum distillate saturate fraction at 450 °C for 30 min. Key: ⊙, n-alkanes; and ⊡, 1-alkenes.
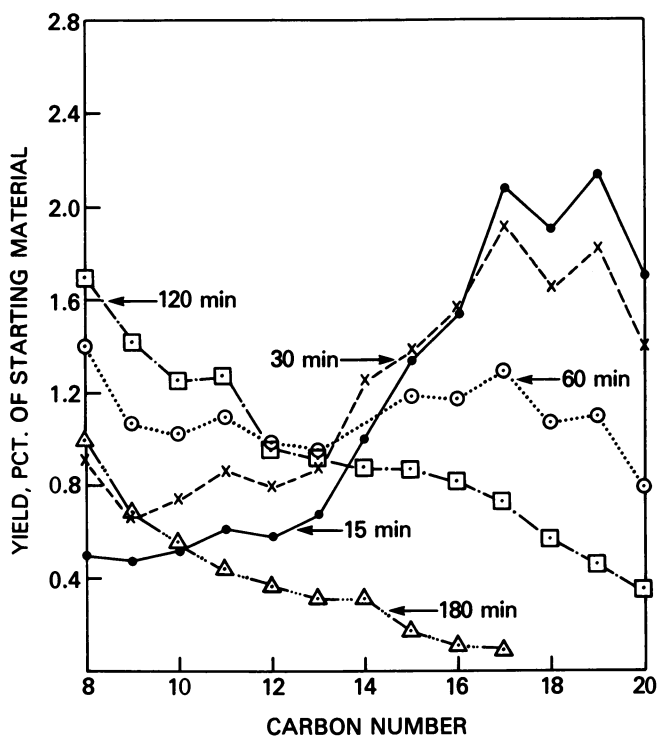
Figure 4. Pyrolysis of shale oil vacuum distillate saturate fraction at 450 °C. The yield is the sum of n-alkane plus 1-alkene for the indicated chain length.

these compounds fragment also. The 1-alkenes are less stable than the n-alkanes; consequently, the latter predominate at the longer stress times.

Yields for the polar fraction pyrolyses are depicted in Figure 5. The combined n-alkane/1-alkene yields for carbon numbers less than 15 were reasonably good for a 15-minute pyrolysis but secondary fragmentation sharply reduced the yields for longer stress periods. The olefins were more reactive in the polar environment than the saturate environment and were generally minor products at all stress times. The low yield of alkanes and alkenes for carbon numbers above 14 corroborates the average chain length of 13 found by carbon-13 nmr analysis.

Limited experiments with the aromatic fraction from the vacuum distillate indicated this material resembled the polar fraction much more than the saturate in pyrolysis behavior. This would be consistent with the carbon-13 nmr results.

A summary of the JP-5 yield data for all fractions stressed for various times at 450°C is presented in Table V. The saturate fraction affords the highest yield of JP-5 but the polar fraction also gives good yields. The maximum yields for these two fractions came at 60 minutes stress but the overall effect of time on yield was moderate. The results for the aromatic fraction were inconclusive because of limited amount of starting material. The general pattern of JP-5 yield for the vacuum distillate fractions was similar to that found for shale oil residual fractions (4).

The potential n-alkane yields in the JP-5 cut are listed in Table VI. These values were obtained by summing the capillary GC yields of n-alkanes and 1-alkenes for carbon numbers 9 through 16. This total was divided by the corresponding JP-5 yield in Table V to give the potential n-alkane yield.

The saturate fraction gave substantial yields of potential n-alkanes in the JP-5 range at all stress times. The highest yields were for shorter stress times, however, and the maximum of 33% was found at 60 minutes.

The potential n-alkane yield for the aromatic and polar fractions fell much below that of the saturates. This is consistent with the much lower wt.% unbranched alkyl group and average chain length data found by nmr.

Discussion and Conclusions

Over 50% of unbranched alkyl groups in the saturate fraction from the vacuum distillate can be converted to potential n-alkanes in the JP-5 distillation range. This indicates that the alkyl fragments, with an average chain length of 19, are fragmenting during the pyrolysis to give substantial amounts of n-alkanes and 1-alkenes with carbon numbers in the 9 to 16 range. Single step Fabuss-Smith-Satterfield breakdown would explain this
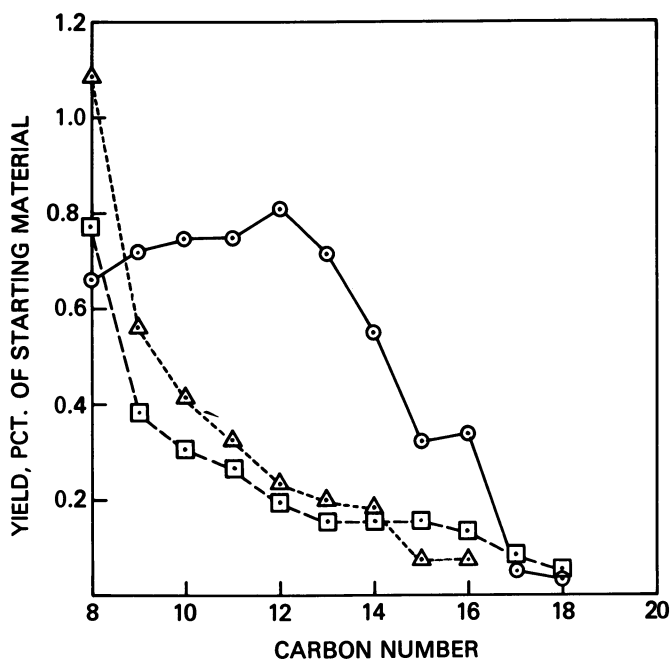
Figure 5. Pyrolysis of shale oil vacuum distillate polar fraction at 450 °C. The yield is the sum of n-*alkane plus 1-alkene for the indicated chain length. Key: ⊙, 15 min; ▵, 180 min; and ⊡, 60 min.*

Table V. JP-5 Yield-Vacuum Distillate Fractions

Pyrolysis* Time (min.)	JP-5 Yield (Percent)		
	Saturate	Aromatic	Polar
15	24.0	--	17.8
30	25.6	11.8	17.9
60	27.0	25.8	21.7
120	24.8	--	20.4
180	15.7	--	20.2

* Pyrolysis Temperature - 450°C

Table VI. Potential n-Alkane Yield from Vacuum Distillate Fractions

Pyrolysis Time (min.)	Potential n-Alkane Yield* (Percent)		
	Saturate	Aromatic	Polar
15	31.0	--	12.7
30	31.0	4.2	11.4
60	33.0	15.5	10.3
120	24.8	--	11.5
180	18.5	--	9.4

* Pyrolysis Temperature - 450°C; yield in percent is sum of n-alkanes + 1-alkenes for C_9 to C_{16} hydrocarbons divided by JP-5 yield from Table V.

behavior. The potential n-alkane yields in excess of 30% approach those of 37% found for JP-5 made from shale oil by a delayed coking operation (1). Thus, the saturate molecules in the vacuum distillate portion of Paraho shale oil seem to be significant contributors to JP-5 and n-alkane production in the delayed coking process.

The aromatic and polar fractions in the shale oil vacuum distillate contribute much less than the saturate fraction to n-alkane production. This is consistent with studies on model compounds (5). Substituted benzenes and pyridines preferentially fragment to give n-alkanes and 1-alkenes with one and two fewer carbons than the length of the side chain. For the average side chain of 13 for the polar fraction, which contains large amounts of pyridines, the alkane/alkene fragment would be primarily 11 or 12 carbons. Figure 5 illustrates a high yield near these carbon numbers at the 15 min. stress time for the polar fraction.

Highest yields of JP-5 come at 60 minutes for the various fractions. Unfortunately, this time also gives the highest yield of potential n-alkanes for the saturate fraction. Thus, differentiation between a good yield of JP-5 and a low yield of n-alkanes cannot be made on the basis of pyrolysis time.

Acknowledgment

Literature Cited

(1) Solash, J.; Hazlett, R. N.; Hall, J. M.; Nowack, C. J. Fuel 1978, 57, 521.
(2) Affens, W. A.; Hall, J. M.; Holt, S.; Hazlett, R. N. Am. Chem. Soc. Div. of Fuel Chem., Preprints 1981, 26, 178.
(3) Resing, H. A.; Garroway, A. N.; Hazlett, R. N. Fuel 1978, 57, 450.
(4) Hazlett, R. N.; Beal, E.; Vetter, T.; Sonntag, R.; Moniz, W. in 'Oil Shale, Tar Sands and Related Materials,' Stauffer, H. C., Ed.; ACS SYMPOSIUM SERIES No. 163, ACS: Washington, D. C., 1981, p. 285.
(5) Hazlett, R. N.; Mushrush, G. W.; Am. Chem. Soc. Div. of Fuel Chem., Preprints 1982, 27, 214.
(6) Gary, J. H.; Hardwerk, G. E. 'Petroleum Refining,' Marcel Dekker: New York, 1975, Chap. 5.
(7) Fabuss, B. M.; Smith, J. O.; Satterfield, C. N. Adv. Pet. Chem. and Refin. 1964, 9, 157.

Sink Float Procedures for Shale Characterization

CHARLES J. VADOVIC

Exxon Research and Engineering Company, Baytown, TX 77520

A new characterization procedure has been developed
which directly calculates the organic H/C and N/C
ratios in raw shale from elemental analyses. The
procedure eliminates the need for the acid extrac-
tion of kerogen for organic analyses and resultant
uncertainty caused by the extraction of basic
organic compounds. The procedure involves the
accurate analyses of fractions obtained via sink
float techniques and has been compared with kerogen
analyses for Brazil, Rundle, and Colony shale
samples from Colorado. Good agreement with both the
H/C and N/C ratios has been achieved. Also,
estimates of the hydrogen and nitrogen contents of
the mineral matter in raw shales have been
obtained. The method appears to be valid for raw
shale and eliminates the need to extract rock with
acid to obtain kerogen for H/C and N/C analyses.

The analysis of the organic fraction in shale leads to
important processing insights. However, the analysis is com-
plicated by the presence of a substantial fraction of rock. The
rock often contains carbon, as carbonates, and hydrogen, as water
of hydration, which make it difficult to obtain a true organic
analysis. The route used most often to obtain organic analyses is
to isolate the kerogen by acid removal of the inorganics. This
poses numerous problems in that the acids used, HCl and HF, can
interact with and be incorporated into the organic matrix. Also
basic nitrogen compounds are easily extracted from the shale as
well as inorganic nitrogen compounds. The presence of inorganic
nitrogen from Green River shale has been demonstrated and quanti-
fied in the literature (1, 2). To obviate these difficulties a

procedure has been developed which utilizes the analyses of raw sink float shale samples to calculate the ratios of organic hydrogen and nitrogen to organic carbon. In addition an estimate of the hydrogen and nitrogen content of the mineral matter is obtained.

Sink Float

The starting point for the procedure outlined here is the floating of material containing rock and mineral matter at a predetermined specific gravity. The principles involved are depicted in Figure 1. At a low media specific gravity essentially all of the material will sink. As the specific gravity increases more of the material floats. At a sufficiently high specific gravity all of the material will float. Details of the beneficiation aspects of the sink float procedure are found in references 3 to 7.

In the procedure described here a method analogous to the collection of distillation cuts was employed. The shale was subjected to a low specific gravity and the float fraction collected. The sink fraction was subjected to an incrementally higher specific gravity and the float fraction collected. The procedure was repeated until very little material remained. In this manner a series of samples, differing primarily by organic to rock ratio, was collected.

The nature of the shale plays a role in the selection of the media. Heavy hydrocarbon media may be used on dry, impervious shales such as from Colorado. For shales of high moisture content, such as from the Rundle deposit, it is more practical to use an aqueous based heavy media system. The judicious selection of media prevents contamination of the shale and allows accurate analysis.

Analytical Procedures

The techniques used for analyzing shales are summarized below. Most are modified ASTM coal methods.

Carbon-Hydrogen. The carbon-hydrogen analysis was performed in a Hallikainen combustion furnace at 1000°C. The .2 gram sample was combusted in air for 3 minutes and then combusted for 3 minutes in oxygen. The resultant CO_2 and H_2O were collected using traps specified by ASTM D3178 and determined gravimetrically.

Ash. The ash was determined by ASTM D3174 using the coke procedure (950°C).

CO_2. Mineral CO_2 was determined by ASTM D1756 with a residence time of 45 minutes.

NOTE: EACH PARTICLE CONTAINS SOME ROCK OR MINERAL MATTER

ORGANIC - S.G. 0.9 TO 1.3

INORGANIC - S.G. 2.5 TO 3.0

1.5 SP. GR.   1.8 SP. GR.   2.1 SP. GR.   2.4 SP. GR.

LABORATORY FLOAT / SINK TESTS

FLOAT

FLOAT				
SINK	SINK	SINK	SINK	SINK
2.0 SG	2.1 SG	2.2 SG	2.3 SG	2.4 SG

FLOAT
SINK
2.5 SG
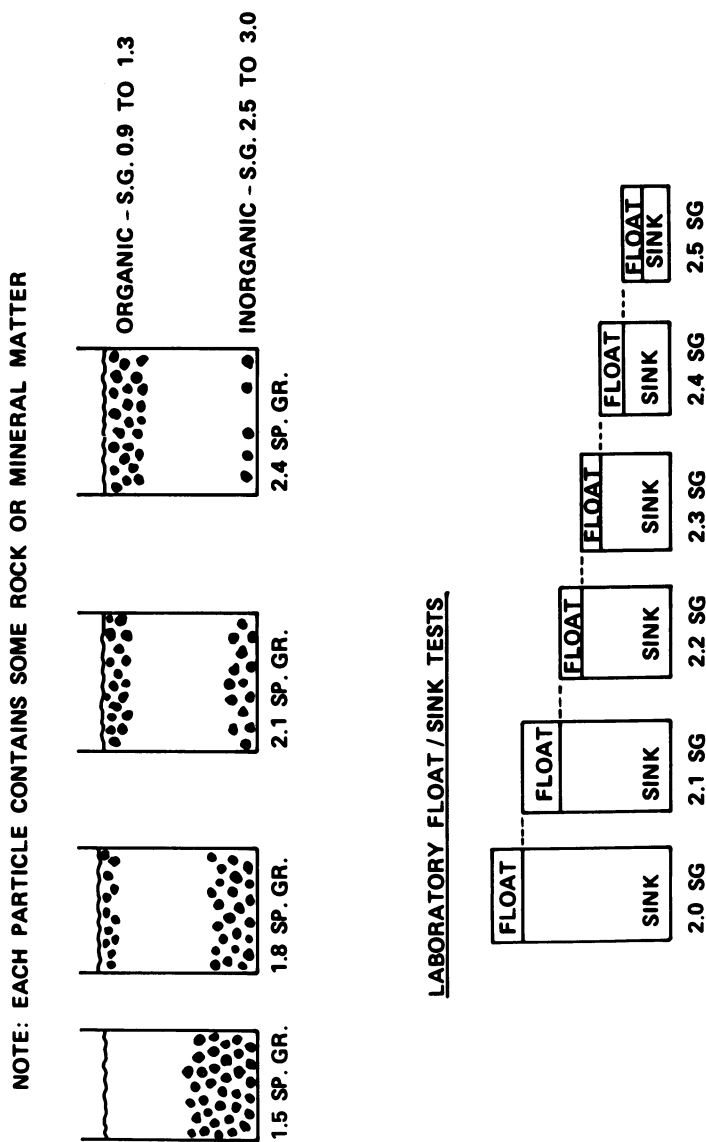
Figure 1. The mechanism of physical shale beneficiation.

Nitrogen. Nitrogen was determined using a LECO CHN analyzer at a combustion temperature of 1425°C.

Procedural Details and Results

The basis for the procedure presented here is an element balance of the form

$$X_i^{total} = X_i^{organic} + Y_i \cdot X_{mineral}/100$$

where X_i^{total} and $X_i^{organic}$ are the total and organic weight percent of component i in the sink float sample, respectively, $X_{mineral}$ is the weight percent of minerals in the sample Y_i is the weight percent of component i in the minerals and i is hydrogen or nitrogen.

By assuming that the weight percent of minerals is equal to the sum of the ash and mineral CO_2 content the equation

$$X_i^{total} = X_i^{organic} + Y_i^{minerals} \times (Ash + CO_2)/100$$

is derived. In describing a series of sink float samples $X_i^{organic}$ varies with the organic content of the sample. However as the organic is fairly uniform from one sink float sample to another the ratio $X_i^{organic}/C_{organic}$ should be a constant. The above equation can be rewritten as

$$X_i^{total} = (X_i^{organic}/C_{organic}) \, C_{organic} + Y_i^{minerals} (Ash + CO_2)/100$$

To convert to an atomic ratio the molecular weights are included and the equation rearranged to

$$\frac{100 \, X_i^{total}}{Ash + CO_2} = \frac{12 \, X_i^{organic}}{MW_i C_{org}} \frac{100 \, C_{org} \, MW_i}{(Ash + CO_2) \, 12} + Y_i$$

The total component X_i and the organic carbon are determined by elemental analyses. To effectively use the above equation, a series of samples containing varying amounts of organic and inorganic constituents must be obtained.

The sink float procedure yields a series of samples which contain various levels of organic and inorganic material. It is assumed that in these samples variations in both organic and inorganic composition are minimal. The variation in ash elements for Brazil and Rundle shale are shown in Figure 2. The approximate mineralogy corresponding to the ash elements contained in the Brazil shale samples is 40% illite, 30% quartz, 10% albite, 10% pyrite and 10% other. The approximate Rundle mineralogy is 50% montmorillinite, 25% illite, 5% kaolinite, 15% quartz and 5% other. The variations observed in sink float samples from these
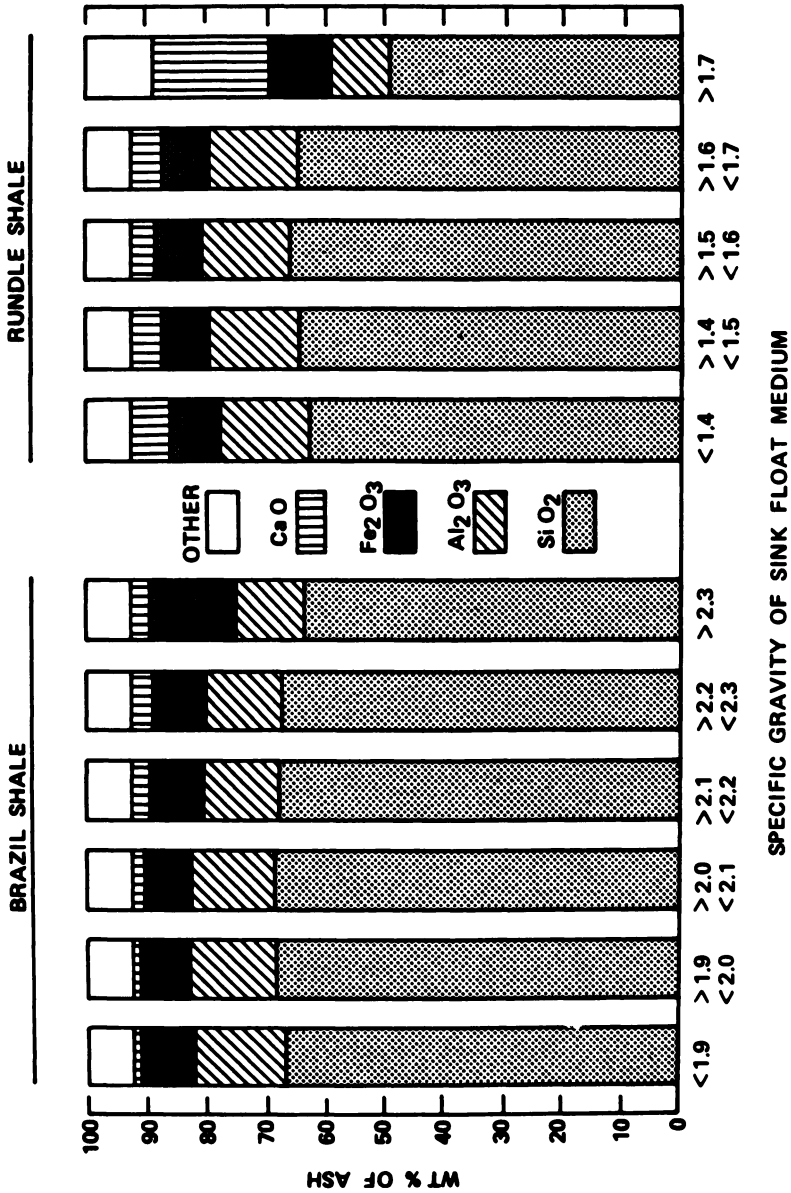
Figure 2. Ash elements are uniform in sink float fractions.

clay-containing shales are slight. By plotting $100 X_i^{total}$/ Ash + CO_2 vs/ $100\ C_{org}MW_i/12$ (Ash + CO_2) two results are achieved. The slope is the atomic X_i/C_{org} ratio and the intercept is an estimate of the inorganic content of the element i. The results of such a plot for Brazil and Rundle shales are shown in Figure 3.

The mineralogy of the Colony sink float samples is illustrated in Figure 4. Colorado shale is made up of primarily non hydrated minerals: calcite, dolomite and quartz. There are, however, measurable quantities of clays and analcime which do contain water of hydration. Also there is more variation in mineralogy with specific gravity than has been observed for the Rundle and Brazil samples. However for the sink float samples analyzed here the mineral fraction containing hydrated species is almost constant. The plot of $100\ H_{total}$/(Ash + CO_2) vs. $100\ C_{organic}/12$ (Ash + CO_2) for Colony shale is shown in Figure 5. Again a straight line results.

The method, as outlined here, is also applicable to nitrogen. The approach was applied to Rundle, Brazil and Colony shale samples and the results are plotted in Figure 6. The resultant plots are linear for these three shales. At zero organic content all shales exhibit some nitrogen content. The calculated nitrogen content of the mineral matrix of both Rundle and Colony shale is similar. It has been postulated (1, 2) that compounds composed of ammonia (NH_3) are present. Buddingtonite, a naturally occuring ammonia mineral has been identified in both Rundle and Colony shale (8).

The calculated atomic ratio of H/C and N/C are compared with values calculated from analytical results on acid extracted kerogens in Table I. The results calculated from the procedure suggested here compare quite favorably with the values calculated from extracted kerogen analyses. The results show that the H/C ratio for the Rundle shale tested (1.68) is greater than that calculated for Colony, 1.55, which in turn is higher than that of Brazil. The N/C ratio for Colony is significantly higher than that of Rundle, 0.029 vs. 0.019. The slight differences between the sink float and the kerogen values suggest that the kerogen extraction prodedure gives reasonable results despite the potential loss of both organic carbon and nitrogen during acid extraction.

Table I. H/C & N/C Ratios Compare Favorably With Extracted Kerogen Values

	H/C, Atom/Atom		N/C, Atom/Atom	
	Sink-Float	Kerogen	Sink-Float	Kerogen
Rundle	1.68	1.63	0.017	0.016
Brazil	1.32	1.30	0.024	0.023
Colony	1.55	1.56	0.029	0.027
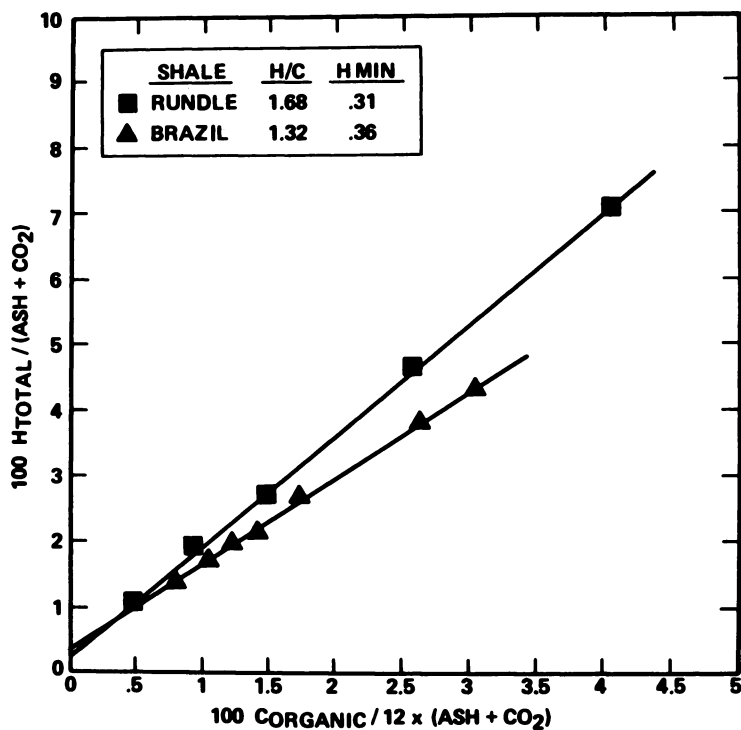
● ORGANIC H/C RATIO IS FAIRLY UNIFORM IN SINK FLOAT SAMPLES

Figure 3. Hydrogen analysis for clay containing shales.
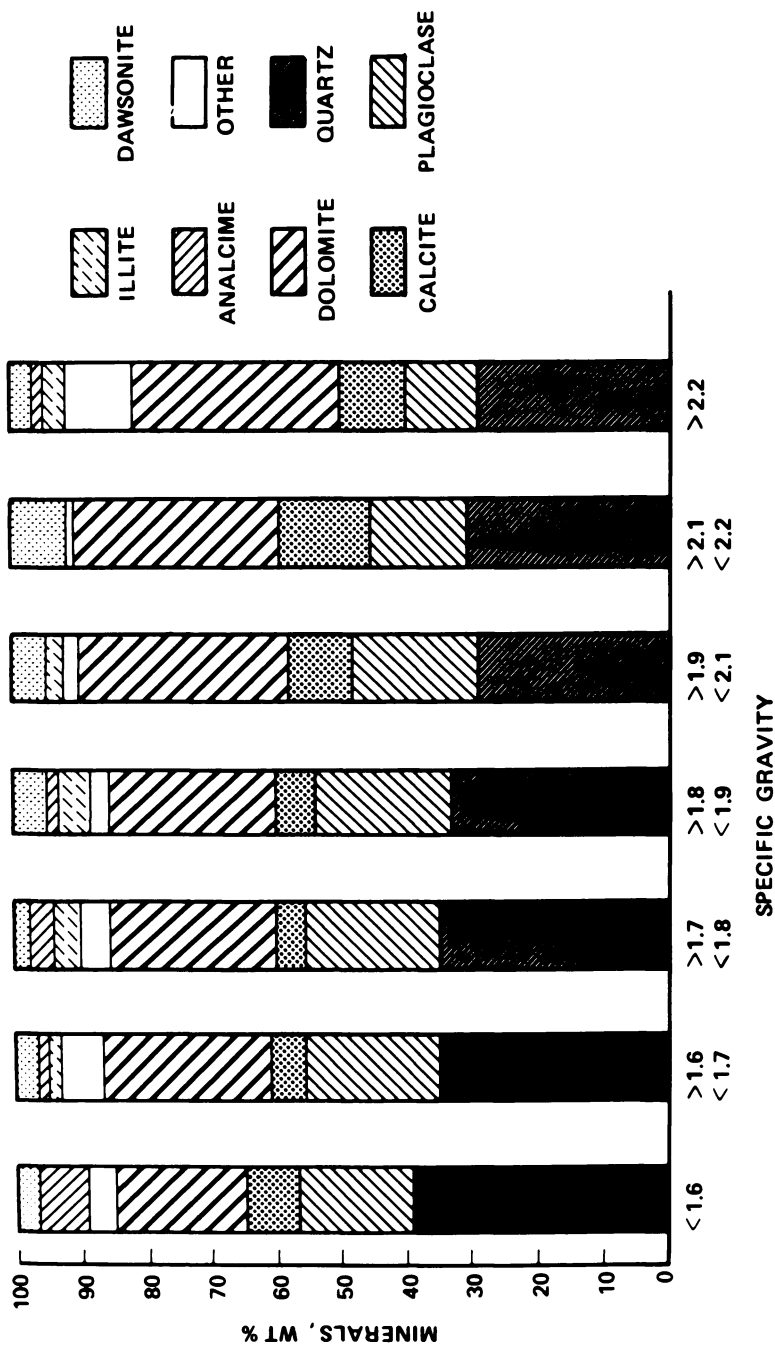
Figure 4. Minerals in Colony sink float samples.
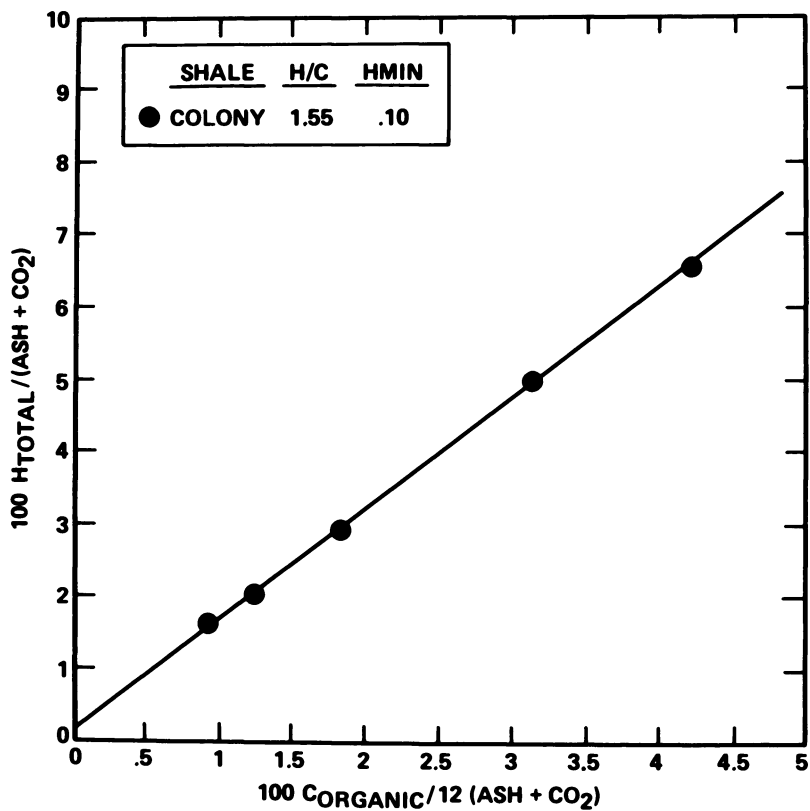
Figure 5. Hydrogen analysis for Colony shale.
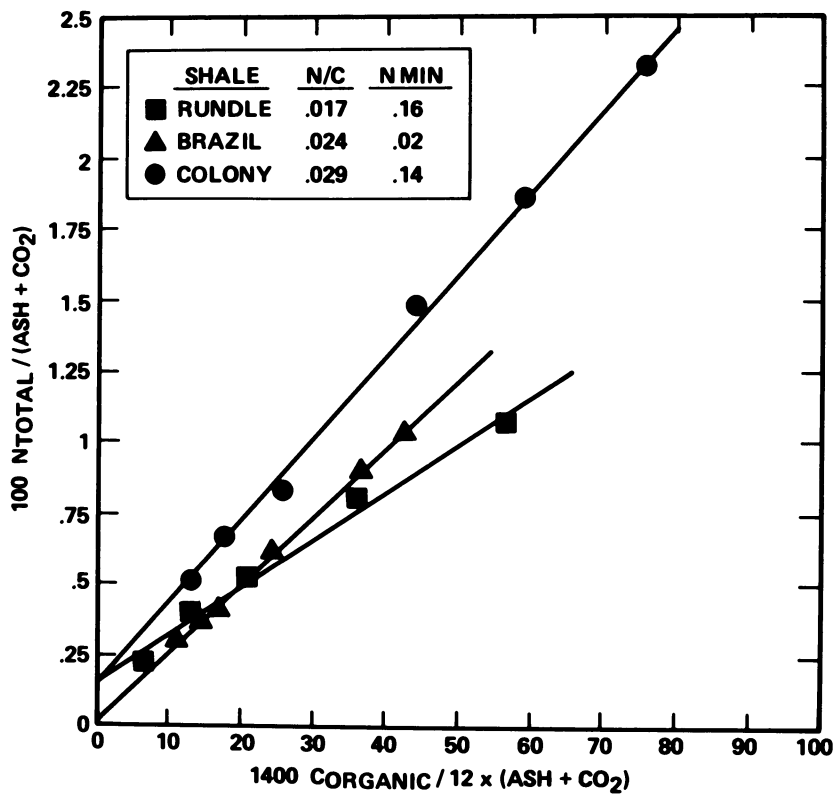
Figure 6.   Approach applicable to nitrogen.

The amount of mineral hydrogen and nitrogen relative to the total amount of hydrogen and nitrogen present is shown in Table II. The total levels are representative of the average yield of the shales analyzed. The average yields for the Rundle, Brazil and Colony oil shales tested are 25, 20 and 35 gallons per ton respectively. The estimated mineral hydrogen content ranges from 3 to 15% of the total hydrogen, and the estimated mineral nitrogen content ranges from 4 to 31% of the total.

Table II. H&N Content Of Minerals Are Small But Significant

● Levels Representative of Average of Deposit

	Hydrogen			Nitrogen		
Shale	Min, Wt%	Total, Wt%	Min/ Total	Min, Wt%	Total Wt%	Min/ Total
Rundle	0.25	2.16	0.11	0.13	0.42	0.31
Brazil	0.28	1.86	0.15	0.02	0.41	0.04
Colony	0.08	2.83	0.03	0.10	0.83	0.12

Conclusions

A method has been developed, utilizing sink float procedures, which calculates the H/C and N/C ratios in raw shales. In addition the technique eliminates the need for acid extraction to obtain kerogen and also estimates the H and N content of the mineral matrix.

The procedure has been tested on Brazil, Rundle and Colorado shales and agreement with extracted kerogen analyses has been achieved.

Acknowledgments

Literature Cited

1. Forsman, J. P.; Hund, J. M. in "Habitat of Oil"; L. G. weeks, Ed. American Association of Petroleum Geologists, 1958; p. 223.
2. Cooper, J. E.; Evans, W. S. SCIENCE 1983, 219, 492-3.
3. Dismant, J. H. The Mines Magazine 1961, 15-22.
4. Frost, I. C.; Stanfield, K. E. Anal. Chem. 1950, 22, 491-2.
5. Fahlstrom, P. H. in "Proceedings of 12th Oil Shale Symposium" Colorado School of Mines, 1979.

6. Larson, O. A., Schultz, C. W. and Michaels, E. L. in "Oil
    Shale Tar Sands and Related Materials"; ACS SYMPOSIUM SERIES
    No. 163, ACS:Washington D.C. 1981; 139-154.
7. Reisberg, J. ibid; 155-166.
8. Pevear, D., personal communication.

Reduction and Phenol Acid Depolymerization of Colorado Oil Shale Kerogen

J. SOLASH, D. C. CRONAUER, and T. P. KOBYLINSKI

Gulf Research & Development Company, Pittsburgh, PA 15230

Colorado oil shale kerogen has been chemically altered to promote its solubility. Reductive alkylation using Na-HMPA was attempted. While some kerogen alkylation occurred, little increase in toluene solubility was noted. Ether and ester cleavage reagents also failed to promote an increase in kerogen solubility. Phenol-tosyl acid treatment of kerogen resulted in large product weight gains. The toluene soluble product fractions were analyzed by IR, NMR, and MS techniques. The results indicate that aryl-alkyl bonds are important crosslinks for these kerogens.

The chemical structure of U.S. Western oil shale kerogen is not known with certainty. Many structure studies employed strong le- oxidants to degrade kerogen (1-4). Acidic products were isolated and analyzed. In most cases, relatively small amounts of material were analyzed. Structural inferences from analysis of small quantities (generally less than 20% of kerogen) of degraded material are apt to be misleading.

The literature is in conflict regarding even basic structural features of kerogen. Yen and co-workers have used X-ray analysis to deduce that kerogens contain very little aromatic material (5). However, ^{13}C CP/MAS NMR measurements show that Western kerogens are 20-30% aromatic carbon (6,7). The structure of nitrogen-containing moieties is also in doubt. It has been suggested (8) that tetrapyrroles in kerogen pyrolyze to yield pyridines, quinolines, and other classes of nitrogeneous compounds found in shale oil. No quantitative data were given. Pyrolysis of simple pyrroles was found to give low yields of pyridines (9). Pyridines and quinolines are the major nitrogen-containing species in distillate shale oils.

A better approach would be to degrade Western U.S. oil shale kerogen under mild conditions. There has been a report of reducing kerogen using dissolving metals (10). Jones and Dickert reported that treating Colorado oil shale kerogen with lithium aluminum hydride, HI, or lithium in ethylene diamine were all ineffective in increasing kerogen solubility (10). Interestingly, HI has been reported to convert kukersite (Estonian oil shale) to 100% ether and benzene solubles (11). No data were reported on the possible extent of reduction with lithium in ethylene diamine.

We would like to report our results of treating kerogen with two known reagent systems: sodium-hexamethylphosphoric triamide (Na-HMPA) and phenol-p-toluenesulfonic acid (phenol-tosyl acid). Reductively alkylating kerogen using Na-HMPA should result in a more extensively reduced product. Na-HMPA has been reported to be a superior medium to produce solvated electrons (12). Na/HMPA is capable of reducing isolated double bonds or highly hindered aromatics (13). Using a "solvated electron" system to reductively alkylate avoids the complications of adding elements of the solvent or electron transfer agent to the substrate (14). There is a rich literature dealing with similar reductions of coal and model compounds (15-18).

Products resulting from phenol-tosyl acid reacting with coal have been studied (19). Solubilizing of coal is thought to result from an attack of phenol on aryl-alkyl bonds (19). The reaction is Lewis or Bronsted acid catalyzed. An important feature of this chemistry is the apparent facile attack of phenol at benzylic sites.

Experimental

General Methods. The kerogens used in this study were derived from Colorado oil shale. The oil shales used were: A, a 95.0 L/t shale; B, a 84 L/t shale; and C, a 198 L/t pretreated shale. These oil shales were all mined from the Gulf C-a tract. A is a Mahogany Zone oil shale of unknown geographic origin. The B and C samples were mined from the Parachute Creek member of the Green River formation. Shale B is a composite of Mahogany through R-4 zones. (20). Shale C is a composite from the R-4 zone. The C sample was beneficiated by gravity methods (1.60 sp. gr. float) prior to our treatment. Minerals were removed from the oil shales by sequential HCl then HF treatment. Bitumen was removed from the kerogens by extracting with benzene-methanol (7:3) prior to the initial HCl treatment. The shale was further extracted with benzene:methanol before and after HF treatment. Elemental analyses of the three kerogens used are presented in Table I. Others at our laboratories are investigating the nature of residual mineral matter in kerogen after various beneficiation treatments.

Table I

ELEMENTAL ANALYSES OF KEROGEN CONCENTRATES

Sample	Elemental Analysis, wt%							
	C	H	N	S	O	F	Cl	Ash
A	69.35	8.75	1.61	4.84	5.90	1.16	---	6.44
B	65.12	8.15	2.10	4.59	10.21	0.77	1.03	11.03
C	65.40	8.79	2.05	3.24	5.37	1.49	0.22	13.57

Elemental analyses were determined by Microanalysis Inc., Wilmington, Delaware; oxygen was directly determined by a modified Unterzaucher technique. IR spectra were recorded on a Digilab Model 15C interferometer using KBr pellets. NMR spectra were recorded on a Varian XL-200.

Dissolving Metal Reduction. A typical experiment is as follows: a 100 mL round-bottom flask, equipped with pressure equalizing addition funnel, efficient condenser, and gas addition tube was used. The apparatus was oven-dried, assembled hot, and allowed to cool under dry N_2. The flask was charged with 15 mL of freshly distilled HMPA. Sodium (about 1.5 g) was freshly cut into small pieces. Several pieces of sodium were added to the HMPA with stirring. After several minutes, the solution turned blue. About 1 g of kerogen was added; 5 mL of HMPA were used to rinse any kerogen adhering to the sides of the flask. The blue color disappeared upon adding kerogen. After solvated electrons reappeared, the addition funnel was charged with the calculated quantity of quencher (methanol or alkyl iodides). The quencher was added dropwise until the blue color was removed; when solvated electrons reappeared more quencher was added. Sodium was added as required. Typically, 24 h was allowed for the addition of the quencher. The quantity of quencher was calculated on the basis of the aromatic content (assume fa = .25) and the oxygen content. After all quenching agent was added, the mixture was poured into 50 mL of water and filtered. The solids were washed with large volumes of water, dried in vacuo (85°C, 24-48 h, 300-400 torr), and weighed. The solids were then Soxhlet-extracted with toluene and submitted for elemental analysis. Incorporated [13]C (from ethyl iodide-1-^{13}C) was determined by Global Geochemistry, Inc., Canoga Park, California, using a combustion method.

Phenol-p-Toluene Sulfonic Acid Depolymerization. The kerogens were treated with phenol-tosyl acid according to literature methods (24). After reacting, excess phenol was removed by steam distilling. The products were filtered, washed with water, and dried in vacuo. The products were then Soxhlet-extracted with toluene, methanol, and finally pyridine. Extracts were isolated,

weighed, and analyzed as outlined in the text. Product recoveries
are outlined in Figure 1. For instance, for the B kerogen, 3.87 g
of solids were recovered from 2.00 g of starting kerogen (193%
yield). From the recovered (phenolated) product, 46% was soluble
in toluene.

The toluene-soluble products from each reacted kerogen were
subjected to SARA analysis (saturates, aromatics, resins, asphal-
tenes) (22). The B toluene solubles gave almost 91% asphaltenes.
The C kerogen toluene solubles were almost 81% asphaltenes. The C
toluene solubles were more difficult to handle; 14.5% of the
material was unrecovered from the chromatographic column.

Results and Discussion

Reductive Alkylation. The kerogens described in the experimental
section were reductively alkylated by continually quenching the
intermediate anions. The method requires that the dark blue
solution (solvated electrons) be stoichiometrically quenched with
alkylating agent. When the dark blue solution reappears, more
alkylating agent is added. The results of reductively alkylating
three kerogens with methanol (protonate) and ethyl-, butyl-, and
octyliodide are presented in Table II.

<div align="center">Table II</div>

<div align="center">ELEMENTAL ANALYSES FOR Na/HMPA TREATED KEROGENS</div>

Sample	Elemental Analysis, wt%					AA^1	$\#Gp/^2$ 100 C	Recovery
	C	H	N	S	O			
A (1)	65.35	8.97	2.94	--	--	M	14^2	97.6%
(2)	71.22	9.4	2.34	2.59	9.61	O	3.3	105
B								
(3)	63.79	8.40	2.15	4.32	11.45	M	8	93.5
(4)	64.95	8.36	2.50	5.88	8.75	M	4	83.5
(5)	64.08	8.37	2.34	2.14	--	E	2.8	88.3
(6)	66.67	8.82	2.34	3.04	7.95	E-^{13}C	3.6	97.4
(7)	65.76	8.75	2.35	3.60	8.94	B	4.4	106
(8)	66.61	8.95	2.45	2.31	8.24	B	4.9	95
C								
(9)	64.96	8.75	2.48	1.51	5.75	M	0.0	91.8
(10)	62.45	7.95	2.30	2.54	9.10	M	−8	88.7
(11)	66.24	9.01	3.40	1.93	--	E	0.8	108
(12)	65.61	8.89	2.12	2.66	5.10	E-^{13}C	0.4	97
(13)	63.54	8.85	3.00	1.79	--	B	2.7	108

[1] AA = alkylating agent; M = methanol, E = ethyl iodide, B =
butyl iodide, O = octyl iodide.

[2] All entries in this column refer to the calculated number of
alkyl groups incorporated per 100 atoms C of substrate (see
text for details).

KEROGEN (BITM FREE; MM FREE)

2.00g

REFLUX, 3 DAYS (183 °C) — OH / TsOH

UNREACTED PHENOL

STEAM DISTILL PRODUCTS

(SOLIDS)

1. WASH WITH H_2O
2. DRY IN VACUUM

SOLIDS

B = 3.87g
C = 3.66g

SEQUENTIAL SOXHLET EXTRACT

a. TOLUENE
B - 1.77g (46%)
C - 1.53g (42%)

b. MeOH
0.77g (20%)
0.45g (12.3%)

c. Py
0.19g (5%)
0.28g (7.6%)

SARA (HEX)

SAT[+]
AROM[+]
RESIN
B - 9.3
C - 4.7

INSOL

90.7
80.5 (14.5% UNRECOVERED)
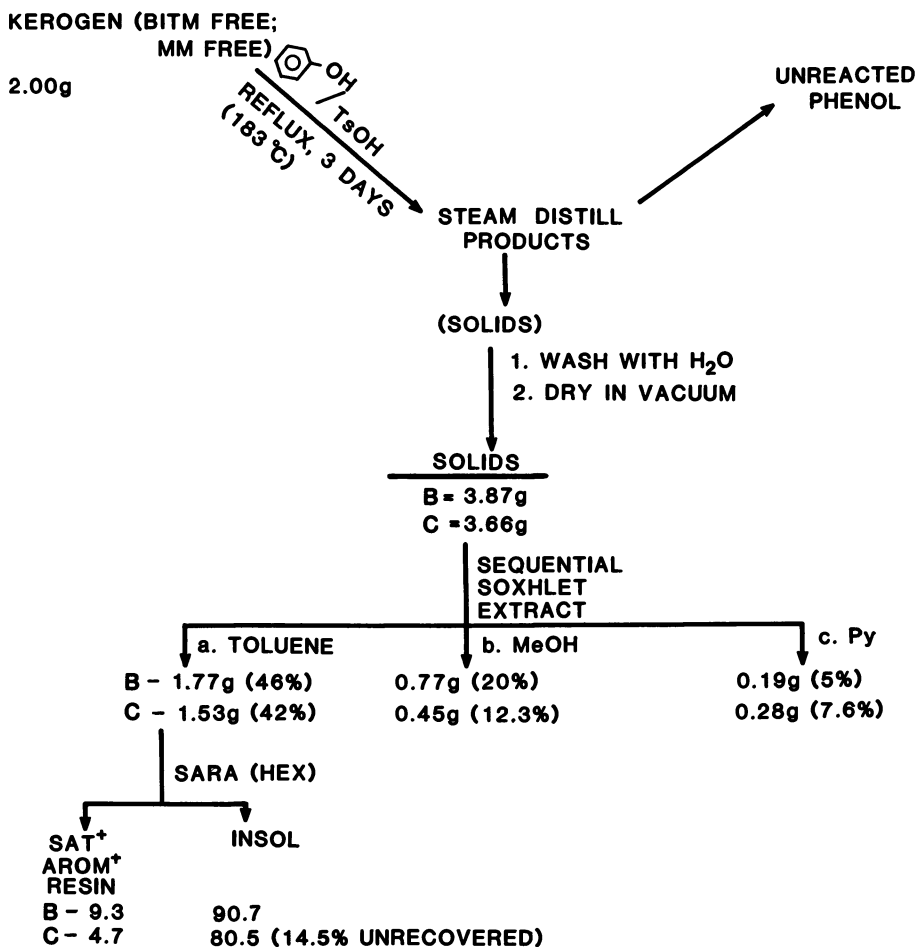
Figure 1. Phenol–TsOH reaction with kerogen.

Table II presents the recovery and elemental analysis data of the solids recovered after reductively alkylating. In a number of cases, the recovery of material was greater than 100% based on starting kerogen. Nitrogen levels in the recovered products are about the same as in starting material in most cases. This indicates that only small quantities of HMPA remained on the kerogen. Using the elemental analysis data in Tables I and II, we calculated the number of alkyl (or proton) groups added to the kerogens. The A and B kerogens incorporated more protons and alkyl groups than the C kerogen. In two experiments (Table II, Runs 6 and 12) we used ^{13}C labelled ethyl iodide as alkylating agent and measured incorporated ^{13}C in the product solids. We found that the B kerogen incorporates almost twice the number of ethyl groups as the C kerogen (2.44 vs 1.25 ethyl groups/100 atoms C) based on ^{13}C labelling data. This compares fairly well with the elemental analysis data in Table II (Runs 6 and 12).

While kerogen can be alkylated, the alkylated products were only slightly (<5%) soluble in toluene. These results must be compared to those found for reductive alkylates of coal (15,16). Reductively alkylating coal generally results in very large increases in benzene or toluene solubility of the alkylated coal product. Dissolving metals are very effective for reductively cleaving many kinds of ethers and esters. We have observed increases in carboxylate by IR after reductive alkylation (not shown). Some carbon-carbon bonds are also cleaved by reductive alkylation (17). The lack of increased alkylated-kerogen solubility implies that ether linkages are not important in kerogen bonding. To confirm this, kerogen was treated with $FeCl_3$/Ac_2O (23) and $(H_3C)_3SiCl$/NaI (24). These known ether cleavage reagents failed to increase the toluene solubility of our kerogens. Ethers and ester linkages can be ruled out as important crosslinks of kerogen.

Phenol-Tosyl Acid Depolymerization. The use of phenol-p-toluene-sulfonic acid to dissolve coal is well known (19, 21, 25, 26). This method apparently has not been applied to oil shale kerogens (27).

In Figure 1, an outline of the product recovery results from phenol-tosyl acid treatment of kerogen is shown. Product recoveries are high (183-193%). Our kerogens are much more reactive toward phenol than is coal. The recovered products were sequentially extracted with toluene, methanol, and pyridine. The extracts were isolated and weighed. As shown in Figure 1, the depolymerized products are 42-46% soluble in toluene. In Tables III and IV are shown the results of elemental analyses and

Table III

DEPOLYMERIZATION OF B OIL SHALE KEROGEN VIA PHENOL-TsOH

Kerogen	Soxhlet[2] Solvent	Elemental Analysis, wt%					MW[1]
		C	H	N	S	O	
Unreacted		64.5	8.4	2.1	5.6	6.4	
C-a, B	Tol. Sol.	78.4	6.0	0.13	1.7	12.0	272(VPO) 334(GPC)
	MeOH Sol.	73.0	6.1	1.3	5.2	13.3	494(VPO) 343(GPC)
	Pyridine Sol	77.2	6.7	2.3	2.9	10.0	

[1]   Wt. Aver. MW by GPC for Tol. Extr. and MeOH Extr. are less than 1000.

[2]   Solvent soluble fraction of crude, isolated phenol kerogen product.

some molecular weight measurements on the toluene soluble material from depolymerized B and C kerogen.

The results shown in Tables III and IV reveal some interesting features of these kerogens. The elemental analyses of the extracts from both kerogens are remarkably similar. There is a partitioning of nitrogen and sulfur heteroatoms among the solvents according to solvent polarity. The oxygen content of the extracts remains approximately constant. The H/C atomic ratio of the various solvent extracts also does not vary much (H/C = 1.00 ±

Table IV

DEPOLYMERIZATION OF C OIL SHALE KEROGEN VIA PHENOL-TsOH

Kerogen	Soxhlet[2] Solvent	Elemental Analysis, wt%					MW[1]
		C	H	N	S	O	
Unreacted		65.4	8.8	2.1	3.2	5.4	
C-a, C	Tol. Sol.	80.6	5.8	0.25	1.5	11.6	276(VPO) 370(GPC)
	MeOH Sol.	73.4	6.1	1.2	4.1	12.8	
	Pyridine Sol.	61.2	6.4	2.8	8.0	16.3	

[1]   Wt. Aver. MW by GPC for Tol. Extr. and MeOH Extr. are less than 1000.

[2]   Solvent soluble fraction of crude, isolated phenol kerogen product.

.08) for the B kerogen extracts (Table III). The H/C average value of 1.00 shows that much less hydrogen is present in the products. This is consistent with large amounts of incorporated phenol. The H/C atomic ratio varies more for the solvent extracts of phenol-reacted C kerogen; H/C is 0.86 for toluene solubles, 1.0 for methanol solubles, and 1.26 for pyridine solubles. If we assume that the toluene soluble fraction of the C kerogen should have an oxygen content of about 5.4% (assume uniform elemental distribution among solvent extracts), then 11.6% oxygen found represents oxygen from incorporated phenol. The amount of phenol incorporated in the toluene solubles on this basis is 33% for the

B kerogen $\left(\left(12\text{-}6.4\right) \times \left(\frac{94}{16}\right)\right)$ and 36% for the C kerogen $\left(\left(11.6 - 5.4\right) \times \left(\frac{94}{16}\right)\right)$. Good mass balances, however, must await the results of a ^{13}C-labelled phenol experiment (in progress).

Large quantities of incorporated phenol are also evident from the ^{1}H and ^{13}C spectra of the toluene solubles (Figure 2). The sharp bands in the aromatic regions of the ^{1}H and ^{13}C spectra are due to substituted phenol moieties. The ^{13}C spectrum integral can be used to calculate how much phenol was incorporated in the B toluene solubles. Using the data shown in Figure 2 (first correcting for small amounts of residual toluene), we calculate that the toluene solubles from the B depolymerized kerogen is about 46 wt% (incorporated) phenol.

The data in Tables III and IV also reveal that individual 'fragments' of oil shale kerogen are of very low molecular weight. For instance, the major toluene soluble fraction of each depolymerized kerogen has an average molecular weight of about 300–400. If almost half the carbons of toluene soluble depolymerized B kerogen are from reagent phenol, then the molecular weights of 'fragments' kerogen units shown in Table III should be decreased by one or two incorporated phenol molecules (94–188 units).

The molecular weight data for the toluene soluble fractions of both depolymerized kerogen products were confirmed by field ionization mass spectroscopy (FIMS). A FIMS spectrum for the depolymerized B kerogen toluene solubles is shown in Figure 3. The number average molecular weight calculated from Figure 3 is 401. Figure 3 shows that much of the ion intensity is concentrated in a relatively small number of peaks. The FIMS data cannot be compound-class analyzed using hydrocarbon classes only since the toluene solubles for this fraction contain about 12% oxygen. We do not want to assume that all oxygen in the toluene solubles is from incorporated phenol (the data do not support this assumption). Thus, assigning our FIMS data to specific hydrocarbon classes is not possible. We are applying low voltage-high resolution mass spectroscopy methods to these samples. We are also further fractionating our depolymerized samples to allow for simpler structure analysis.
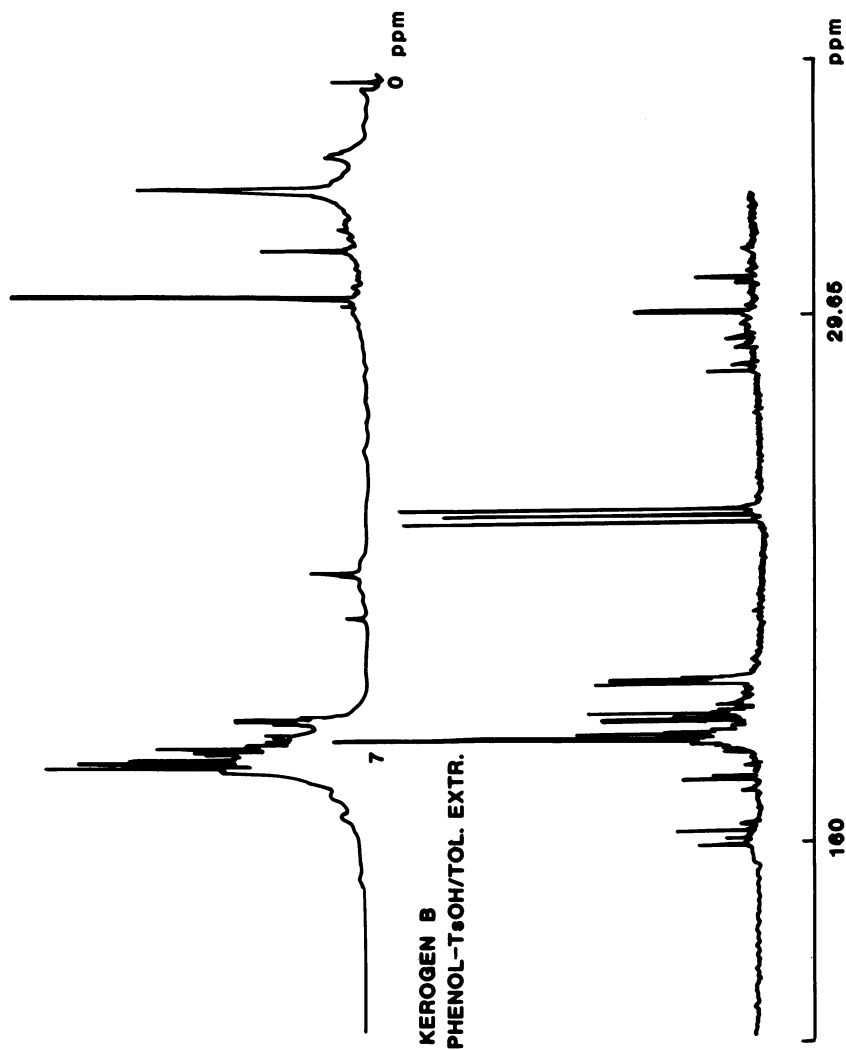
Figure 2. *NMR spectra of depolymerized B kerogen, toluene solubles. Key: top, ^1H-NMR spectrum; and bottom, ^{13}C-NMR spectrum.*
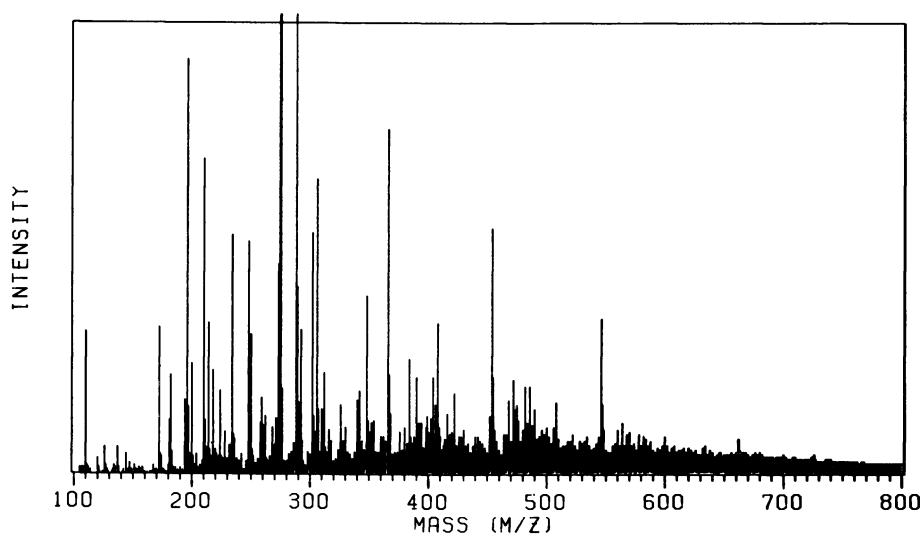
Figure 3. FIMS spectrum of depolymerized B kerogen, toluene solubles.

The elemental analysis data (Tables III and IV) and the NMR
spectra (Figure 2) of the depolymerized kerogen are surprising.
The alkyl carbon portion of the ^{13}C NMR spectrum is dominated by
long chain saturates (chain length ≈15 carbons). There is some
saturated cycloalkyl carbon present. Recently it was proposed
that kerogens are composed primarily of saturated condensed cyclo-
alkanes (28). The depolymerized products also appear to be "too
aromatic." For instance, on the basis of the ^{13}C NMR spectrum, we
calculated that the depolymerized B kerogen toluene solubles had
46 wt% incorporated phenol. The atomic H/C ratio of the original
B kerogen (Table 1) is 1.49. After correcting for incorporated
phenol (and residual toluene) by NMR, the calculated atomic H/C
for the toluene soluble B products is 0.95. This is much lower
than expected for the least polar fraction from a Western U.S.
kerogen. We are currently engaged in studying the effect of
phenol-tosyl acid on model compounds.

The B kerogen is more reactive toward reductive alkylation
and phenol depolymerization than the C kerogen. It is tempting to
suggest that the reactivity differences are structure related.
However, if this were true, then these differences should be
reflected in the soluble reaction products. We cannot adequately
detect such differences solely with instrumental methods. We are
currently engaged in performing several additional experiments.
First, we are performing a depolymerization using ^{13}C-labelled
phenol. This will permit an accurate mass balance to be made.
Second, we have methylated the toluene soluble products from
unlabelled phenol depolymerization. The methylated fractions
should be more easily fractionated by chromatography. Analysis of
the chromatographic fractions should be simpler.

Major Conclusions. The data presented above are insufficient to
support an average structure for our kerogen. The data, however,
are sufficient to refine the structural proposals for Western U.S.
oil shale kerogen that have been previously suggested (5). In the
hypothetical model suggested by Yen (5), linkages between cyclic
clusters were of the following type: disulfide, ether, ester,
cartonenoid, and isoprenoid. The first three of these 'bridges'
are susceptible to cleavage by reductive alkylation or the ether
(ester) cleavage reagents used. The absence of increased toluene
solubility implies that such structures are not important for
crosslinking kerogen. The very large reactivity of our kerogen
toward phenol-tosyl acid suggests that aryl-alkyl carbon linkages
are important in binding kerogen fragments together. Limited
model compound work has been performed to define the ability of
phenol-tosyl acid to cleave various structures. We hope to be
able to define the qualitative and quantitative aspects of this
chemistry as it relates to kerogen structure. Such experiments
are now in progress.

Literature Cited

1. Burlingame, A. L. and Simoneit, B. R. Nature, 1969, 222,
    741.
2. Robinson, W. E.; Heady, H. H.; Hubbard, A. B. Ind. Eng.
    Chem., 1953, 45, 788-791.
3. Robinson, W. E; Lawlor, D. L. Fuel, 1961, 40, 375-388.
4. Ishiwatari, R.; Machihara, T. Geochim. Cosmochim. Acta,
    1982, 46, 825-831.
5. Yen, T. F. Amer. Chem. Soc., Div. Fuel Chem., Preprints,
    1974, 19, 109-114; Young, D. K.; Yen, T. F. Geochim.
    Cosmochim. Acta, 1977, 41, 1411.
6. Resing, H. A.; Garroway, A. N.; Hazlett, R. N. Fuel, 1978,
    57, 450.
7. Miknis, F. P.; Maciel, G. E.; Bartuska, V. J. Org. Geochem.,
    1979, 1, 169; Miknis, F. P.; Szenerengi, N. M.; Maciel, G.
    E. Fuel, 1982, 61, 341.
8. Jackson, L. P.; Decora, A. W. Amer. Chem. Soc., Div. Fuel
    Chem., Preprints, 1975, 20 (2), 147.
9. Jacobsen, Jr., I. A.; Heady, H. H.; Dineen, G. U. J. Phys.
    Chem., 1958, 62, 1563; Jacobsen, Jr., I. A.; and Jensen, H.
    B. J. Phys. Chem., 1962, 66, 1245; Jacobsen, Jr., I. A.;
    Jensen, H. B. J. Phys. Chem., 1964, 68, 3068.
10. Jones, D. G.; Dickert, Jr., J. J. Amer. Inst. Chem. Eng.,
    Symp. Series, 1965, 61 (54), 33-41.
11. Randsepp., Kh. T. Izvest. Akad. Nauk SSSR, Otdel. Tekh.
    Nauk, 1954, (3), 130-136; in Chem. Abstr., 1955, 49, 4969c.
12. Fraenkel, G.; Ellis, S. H.; Dix, D. T. J. Amer. Chem. Soc.,
    1965, 87, 1406-1407.
13. Whitesides, G. M.; Ehmans, E. J. J. Org. Chem., 1970, 35,
    3565.
14. a. Franz, J. A.; and Skiens, W. E. Fuel, 1978, 57, 502-504;
    b. Garst, J. F. Accts. Chem. Res., 1971, 4, 400-406.
15. a. Ouchi, K.; Hirano, Y.; Makabee, M.; Itoh, H. Fuel, 1980,
    59, 751-756; b. Sternberg, H. W.; Delle Donne, C. L. ACS
    Div. Fuel Chem. Preprints, 1968, 12(4), 13-18.
16. Sternberg, H. W.; Delle Donne, C. L. Fuel 1974, 53, 172-175;
    and previous papers in this series.
17. Collins, C. J.; Homback, H. P.; Maxwell, B.; Woody, M. C.;
    Benjamin, B. M. J. Amer. Chem. Soc., 1980, 102, 851-853.
18. Birch, A. J.; Hinde, A. L.; Radom, L. J. Amer. Chem. Soc.,
    1981, 103, 284-289; also see same authors, Ibid, 1980, 102,
    6430, 4074, 3370 and 1978, 100, 4681.
19. For a review: Larsen, J. W.; Kuemmerle, E. W. Fuel, 1976
    55, 162-169.

20. Cashion, W. B.; Donell, J. R. "Revision of Nomenclature of the Upper Part of the Green River Formation, Piceance Creek Basin, Colorado, and Eastern Uinta Basin, Utah," U.S. Geological Survey Bulletin, 1974, 1394-G.
21. Ouchi, K.; Imuta, K.; and Yamashita, Y. Fuel 1973, 52, 156-157; 1965, 44, 29-38; 1965, 44, 205-209.
22. Suatoni, J. C.; Swab, R. E. J. Chrom. Sci., 1975, 13, 361.
23. Ganem, B.; Small, Jr., V. R. J. Org. Chem., 1974, 39, 3728-2730.
24. Olah, G. A.; Narang, S. C.; Gupta, B. G. B.; and Malhotra, R. J. Org. Chem., 1979, 44, 1247-1251.
25. Heredy, L. A.; and Neuworth, M. B. Fuel, 1962, 41, 221-231; Heredy, L. A.; Kostyo, A. E.; Neuworth, M. B. Fuel, 1963, 42, 182-184; 1964, 43, 414-416; 1965, 44, 125-133.
26. Yurum, Y.; Yiginsu, I. Fuel, 1981, 60, 1027-1030; Yurum, Y. Fuel, 1981, 60, 1031-1038.
27. Transalkylating of fossil fuels substrates, including petroleum resids, has been studied by M. Farcaisu, Presentation at Fuel Science Meeting, Gordon Conferences, 1982. The transalkylating reagent used was xylene in the presence of a strong acid catalyst.
28. Bandurski, E. Energy Sources, 1982, 6, 47-66.

Petroporphyrins Found in Oil Shale from the Julia Creek Deposit of the Toolebuc Formation

A. EKSTROM, H. LOEH, and L. DALE

Lucas Heights Research Laboratories, CSIRO Division of Energy Chemistry, Private Mail Bag 7, Sutherland, NSW, 2232, Australia

The oil shale of the Julia Creek deposit has been shown to contain a very complex mixture of vanadium porphyrin compounds. Several groups of compounds were isolated by column chromatography and high pressure liquid chromatography and examined by ultra-violet-visible spectroscopy, insertion probe, fast atom bombardment and field desorption mass spectrometry. These groups of compounds were found to consist of several homologous series, and included some compounds tentatively identified as phylloerythrin and chlorin derivatives.

The nature of the petroporphyrins found in a variety of crude oils, oil shales, ancient and recent sediments have been a subject of continual interest since these compounds were first isolated from such materials by Treibs (1) some fifty years ago. It is now generally agreed (2) that the petroporphyrins represent the degradation products of chlorophyll and that they consist predominantly of homologous series of deoxophylloerythroetioporphyrin (DPEP) and aetio porphyrins. However, as yet unidentified porphyrin compounds which do not belong to either of these two classes have been observed (3) in some samples and the proposition that all petroporphyrins are derived from chlorophyll has also been questioned (4).

The oil shale of the Toolebuc formation in Queensland, Australia has been shown (5) to contain relatively high concentrations of vanadium and nickel porphyrin compounds. Riley and Saxby (5) have suggested that these porphyrins are largely of the DPEP and aetio type and also observed significant variations in their concentrations in samples taken from various sites in the deposit. In this paper we describe two further aspects of the porphyrin compounds in this deposit. First, the variations in the concentrations of the chloroform extractable metal

porphyrin compounds through well characterised drill cores were determined, and second, the nature of the vanadium porphyrins was examined using absorption spectrophotometry and insertion probe, fast atom bombardment (FAB) and field desorption (FD) mass spectrometry techniques.

Experimental Procedures

Samples from two drill cores from the Julia Creek deposit were ground and sieved, the $-90\,\mu m$ fraction being used. Samples of 15-20 g were exhaustively extracted with chloroform in soxhlet extractors. The extract was filtered through a Millipore filter, and analysed for V, Ni, Fe and Cu. Atomic absorption, inductively-coupled plasma emission and X-ray fluorescence spectrometry were used to analyse both the extracts and the raw shale.

The separation of the extract into polycyclic hydrocarbons, and nickel and vanadium porphyrin fractions was accomplished using $CCl_4/CHCl_3$ chromatography with Kieselgel (Merck). The vanadium porphyrin fraction was then further separated into seven major fractions using a variety of column chromatography procedures. Demetallation of the porphyrin fractions was carried out with methanesulphonic acid (Merck) using published procedures (6).

UV-visible spectra were obtained using a Cary 118C spectrophotometer. Insertion probe mass spectra were obtained with a Dupont 21-491B mass spectrometer, the FAB spectra with a VG MM-ZAB instrument, and the FD spectra with a JEOL DX-300 mass spectrometer. High pressure liquid chromatography measurements were made with a Waters instrument fitted with dual channel (405 and 546 nm) optical detection and using C18 analytical and semi-preparative columns.

Results and Discussion

Table 1 summarises the concentrations of trace elements extracted with chloroform from oil shale samples of the two drill cores. Although vanadium is clearly the major element present in the form of metal-organic complexes, significant concentrations of compounds containing nickel, iron, copper and chromium are similarly extracted. As will be shown below, the nickel and vanadium appear to be present largely as porphyrin complexes, but it has not been possible to demonstrate that elements such as iron and copper are also present as porphyrins or as some other form of metal-organic complex.

Variations in the total (i.e. organic and inorganic) concentrations of vanadium, nickel, iron and copper and of the chloroform extractable forms of these elements through the two drill cores are summarised in Figure 1. These results demonstrate the preferential concentration of the chloroform extract-

TABLE 1. METAL-ORGANIC COMPLEXES EXTRACTABLE WITH CHLOROFORM
FROM JULIA CREEK SHALE

Element	Concentration Extracted μg g-1	
	Sample 1 OIL SHALE, Deep Core 90-92 m	Sample 2 OIL SHALE, Shallow Core 331-33 m
VANADIUM	104.0	27.0
NICKEL	6.0	4.0
IRON	3.0	7.0
COPPER	0.26	0.74
CHROMIUM	1.0	0.13
MOLYBDENUM	0.26	0.43
MANGANESE	0.09	0.09
MAGNESIUM	0.30	0.06
ZINC	0.39	0.20
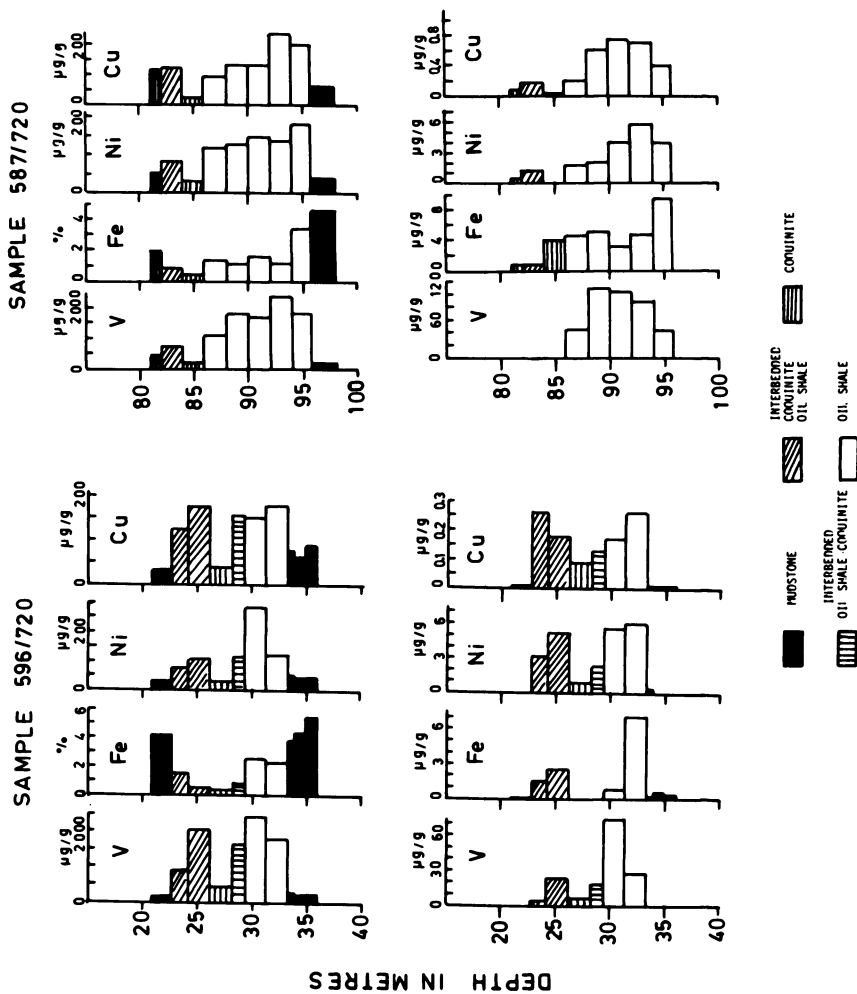
Figure 1. Distribution of the total (upper diagram) and chloroform extractable (lower diagram) concentrations of vanadium, iron, nickel, and copper in two drill cores from the Julia Creek deposit.

able forms of these elements in coquinite and particularly the oil shale segments of the two cores, and the virtually complete absence of these compounds in the mudstone underlying and over-lying the deposit. It is also apparent that there are signifi-cant differences in the concentrations of the organic forms of these elements within the coquinite and oil shale layers. Indeed, the variations in the soluble organic vanadium concen-trations within the individual drill cores are comparable to the variations found in samples from widely different locations of the Toolebuc formation (5). It is also interesting to note that the variation with depth of the concentrations of the chloroform soluble forms of vanadium, nickel, iron and copper are significantly different from each other. This observation may indicate that the various metal ions are complexed by different types of organic ligands, and, as indicated below, some evidence was obtained that the porphyrins complexed to the nickel ion are different from those complexed to the vanadyl ion.

Although there are obvious differences in the concen-trations of the organic vanadium complexes found in the shallow and deep drill cores, the nature of the vanadium complexes present appeared to be virtually identical, as shown by high pressure liquid chromatography (C18 column, methanol solvent at 3 cc/min) of the vanadium porphyrin fractions extracted from core samples taken at depths of 90-92 m and 29-31 m. It would clearly be desirable to extend such studies to samples taken from much greater depths in the Toolebuc formation.

It was possible to separate the vanadium porphyrins extracted from the oil shale into seven distinct fractions using column chromatography. These seven fractions represent only the major groups of compounds present in the shale extract and many other groups of compounds were present in the extracts at lower concentrations and could not be isolated. Analysis of the seven isolated fractions by X-ray fluorescence spectroscopy showed that all were vanadium compounds and none were found to contain any measurable concentrations of iron, nickel or copper.

Comparison of the uv-visible absorption spectra of these fractions (Figure 2) with the spectra of known vanadium chlorin, phylloerythrin and DPEP complexes (7) suggested that two (samples 422 and 4422) with absorption maxima at 600 nm were probably vanadium phylloerythrin complexes. These two fractions do not appear to be identical to the rhodo-type petroporphyrins with an absorption maximum at 590 nm isolated by Millson et. al. (8) and discussed in detail by Baker et. al. (9) because of the significant difference in the absorption spectra. One fraction (sample 630) may be a vanadium chlorin derivative, while the absorption spectra of the remaining four fractions (samples 3, 61, 421 and 441) were typical vanadium porphyrin spectra with maxima at 412, 538 and 575 nm. For these samples the ratios of the intensities of the 575 and 538 nm bands were in the range 1.15-1.20 which are consistent with the ratios
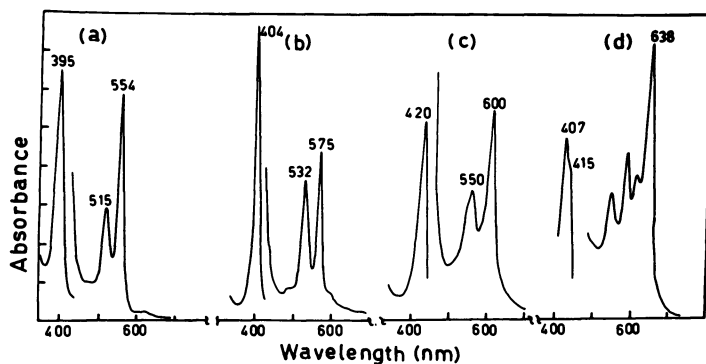
Figure 2. Typical absorption spectra of the various porphyrin fractions determined in chloroform solution.

Key: a, spectrum of nickel porphyrin fraction; b, spectrum typical of Samples 3, 61, 421, and 441 and identified as vanadyl porphyrins; c, spectrum typical of Samples 422 and 4422, tentatively identified as vanadyl phylloerythrin derivatives; and d, spectrum of Sample 630; possibly a vanadyl–chlorin complex. This sample contained some vanadyl porphyrin impurities as shown by the absorption peaks at 407, 575, and 533 nm.

reported for vanadyl-DPEP complexes (2). Sample 3 was the predominant fraction, and comprised approximately 60-70% of the total vanadium porphyrins present.

Insertion probe mass spectra were obtained for these samples using both electron (EI) and chemical ionisation (CI), typical results being shown in Figure 3. The spectra obtained using these two ionisation modes were similar except that the peaks in the CI spectra were located, as expected, one mass unit higher than the corresponding EI peaks. The sequence of peaks at m/e = 513, 527 and 541 observed for sample 3 are typical of vanadyl-DPEP homologues. The insertion probe spectra of samples 422 and 4422 were, surprisingly, virtually identical to that of fraction 3, even though samples 422 and 4422 were clearly not vanadyl DPEP derivatives. The mass spectra of samples 61, 441 and 421, which all have typical vanadyl porphyrin visible spectra, showed prominent even mass number peaks at m/e = 526, 540 and 554. Similar observations have been made by Blumer and Rudrum (11) and are attributed to the effects of the pyrolysis of the sample in the probe.

It was also possible to obtain FAB mass spectra of several of the porphyrin fractions. The most notable difference in the insertion probe and FAB spectra were obtained for sample 441 (Figure 4) for which the FAB spectra showed not only a completely different distribution of peaks in the mass range 500-600 amu, but also yielded a second set of peaks in the range 1022-1078 amu. Particularly prominent in this spectrum was the series 495, 509, 523, 537, 551 and 565 i.e. (541-4) ± 14n; which presumably indicates the presence of unsaturated substituent groups on the porphyrin ring. The high molecular weight peaks appear in a mass range corresponding to 35-40 carbon atoms additional to those of the basic DPEP structure. These compounds are thus superficially similar to the high molecular weight vanadium porphyrins isolated by Blumer and Rudrum.(11)

The FAB spectra of the two phylloerythrin fractions (samples 422 and 4422) also showed significant differences from the insertion probe spectra (Figure 5). FAB spectra of samples 4422, 422 and 61 also showed peaks in the range 1000-1200 amu, but these were not as clear as those observed for sample 441, and further work would be required to confirm their presence. The low molecular weight spectra were again dominated by peaks corresponding to (541-2) ± 14n and (541-4) ± 14n suggesting some degree of unsaturation in the substituent groups. These two sequences appear to be similar to those of an as yet unidentified series reported by Thomas and Blumer (3).

The high pressure liquid chromatogram of sample 3 using a C18 semipreparative column and methanol solvent at a flow rate of 0.5 cc/min, showed seven major peaks. The compounds contained in these peaks were collected as they eluted from the column and examined by FD mass spectrometry. As shown in Figure 5, relatively simple mass spectra were obtained for these
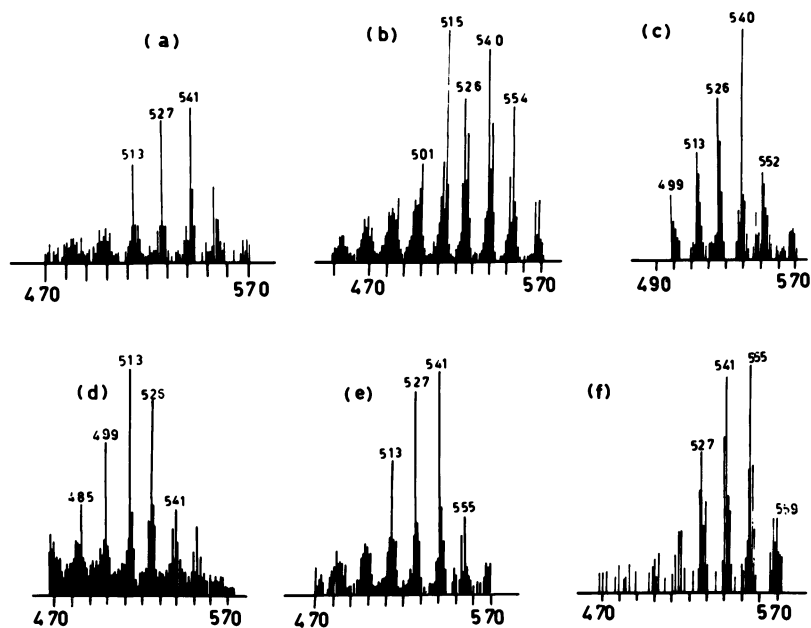
Figure 3. Insertion probe mass spectra (electron ionization) of various porphyrin fractions. Key: a, Sample 3; b, Sample 61; c, Sample 441; d, Sample 421; e, Sample 422; and f, Sample 4422.
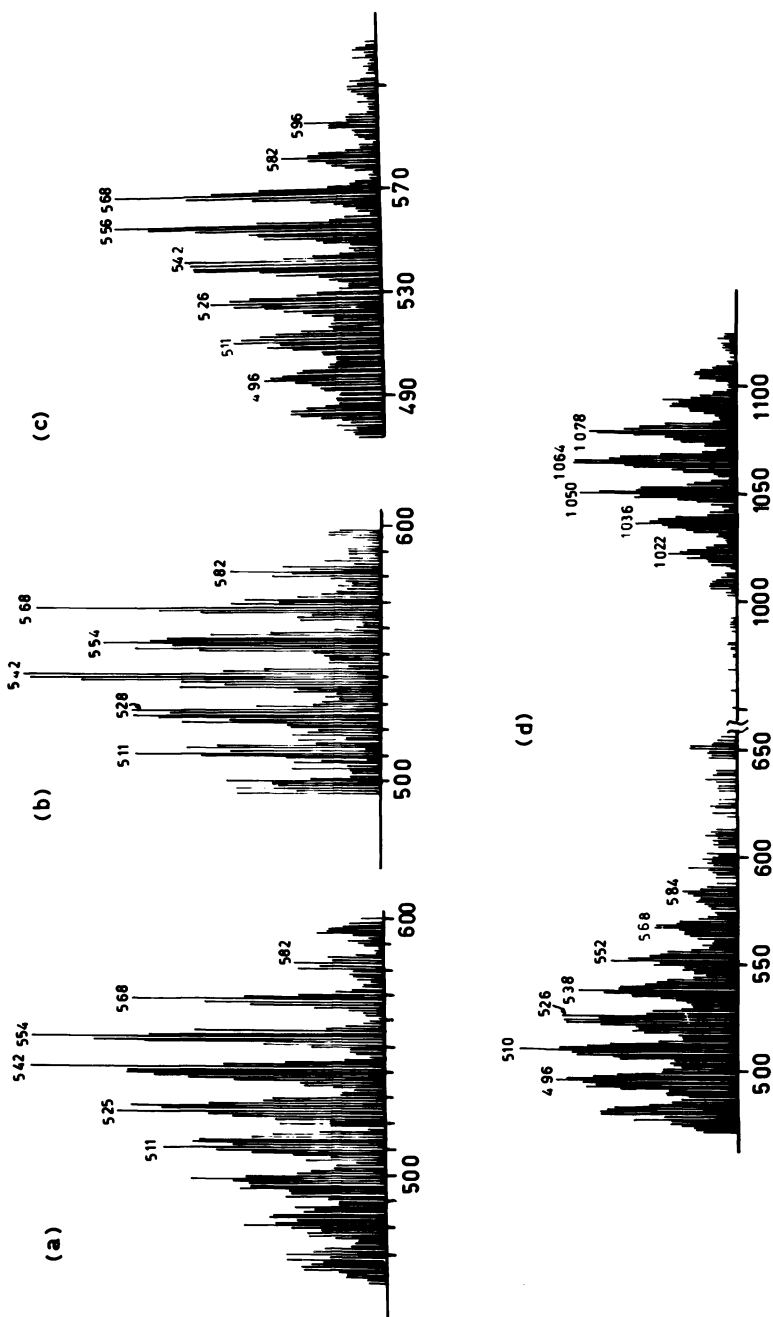
Figure 4. Fast atom bombardment spectra (electron ionization) of various porphyrin fractions. Key: a, Sample 61; b, Sample 4422; c, Sample 422; and d, Sample 441. The parent peaks would appear as $[M + H]^+$ ions.
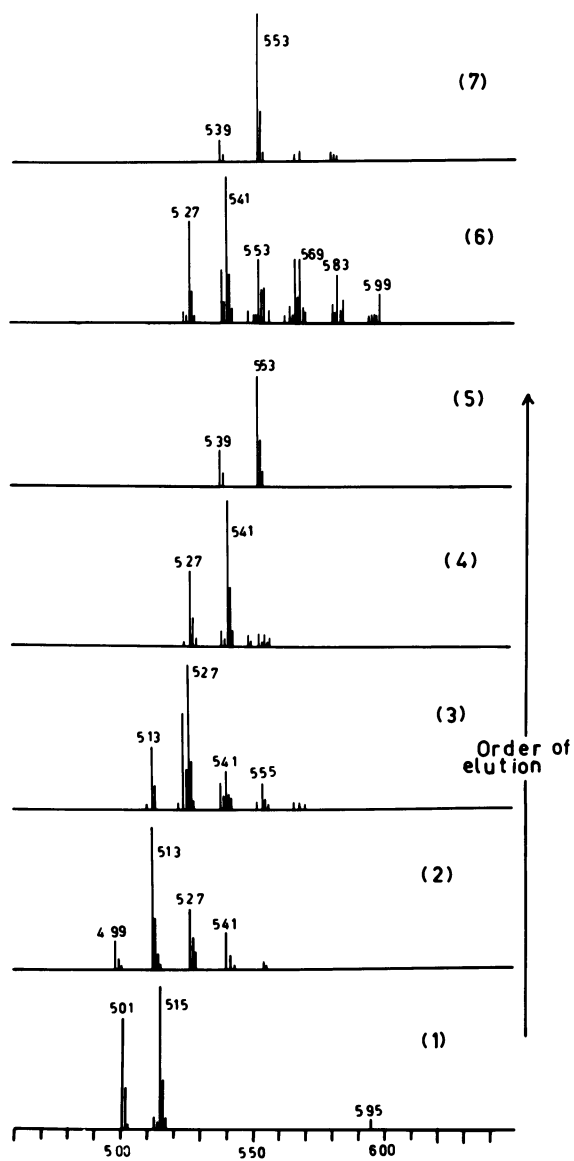
Figure 5.   Field desorption mass spectra of the seven major fractions found by HPLC in Sample 3.

samples.   Peak 1 appears to consist of two aetio homologues at
m/e = 515 and 501, while peaks 2, 3 and 4 are consistent with
compounds of the DPEP series.   Peaks 5 and 7 show identical mass
spectra consistent with a DPEP-2 series but are surprisingly
separated by peak 6 which appears to be a mixture of the DPEP
(527, 541, 555, 569, 583 and 599) series and DPEP-2 (553, 567)
series.   To a first approximation, these compounds would be
expected to be eluted in order of decreasing polarity on this
reverse phase column, and it is difficult to interpret these
results without postulating that several compounds having
molecular weights corresponding to the DPEP series but of
significantly different chemical constitution are present in the
samples.

    Attempts to demetallate the various porphyrin fractions
appeared partly successful only in the case of the nickel
porphyrins and for sample 3, while demetallation of samples 630,
422 and 4422 yielded no porphyrin type compounds at all.   HPLC
runs on the demetallated nickel porphyrins and the vanadium
porphyrins from fraction 3 showed these to be significantly
different.   Similar observations have been made previously (12)
and may explain why the nickel and vanadium porphyrins appear to
have different distributions in the drill cores.   However,
because of the possibility of decomposition of the porphyrins
during demetallation, these observations are far from
conclusive.

    In conclusion, it should be noted that this investigation
describes only preliminary attempts to identify some of the
porphyrinic compounds present in what appears to be an exceed-
ingly complex mixture in the oil shale of the Toolebuc for-
mation.   A more complete identification of the compounds present
should assist in developing a clearer understanding of the
origin and of the reactions of petroporphyrins in a geological
environment.

Acknowledgments

Literature Cited

1.   Treibs, A., Angew.Chem. (1936), 49, 682.
2.   Baker, E.W. and Palmer, S.E., 'Geochemistry of Porphyrins'
    in 'The Porphyrins', D. Dolphin (Ed.), Academic Press, New
    York, N.Y., Vol.1, pp.485.

3.   Thomas, D.W. and Blumer, M., Geochim.Cosmochim.Acta (1964),
      28, 1147.
4.   Hodgson,   G.W.   and   Whiteley,   C.G.,   'The   Universe   of
      Porphyrins' in Proceedings of the Fourth International
      Symposium in Environmental Biogeochemistry.   Springer
      Verlag, (1980), p.35.
5.   Riley, K.W. and Saxby, J.D. Chemical Geol. (1982), 37, 265.
6.   Quirke, J.M.E., Shaw, G.J., Soper, P.D. and Maxwell, J.R.,
      Tetrahedron, (1980), 36, 3261.
7.   Hodgson, G.W. and Baker, B.L., Chemical Geol. (1967), 2,
      187.
8.   Millson,   M.F.   Montgomery,   D.S.   and   Brown,   S.R.,
      Geochim.Cosmochim.Acta, (1966), 30, 207.
9.   Baker, E.W., Yen, T.F., Dickie, J.P. Rhodes, R.E. and
      Clark, L.F., J.Am.Chem.Soc., (1967), 89, 3631.
10.   Blumer, M. and Rudrum, U., Inst.of Petroleum Jnl., (1970),
      56, 99.
11.   Haj Ibrahim, S.K., Presented at 183rd ACS National Meeting,
      Las Vegas, Nevada March 18–April 2, 1982.   Division of
      Geochemistry Abstracts, paper 51.

Organometallic Geochemistry
Isolation and Identification of Organoarsenic and Inorganic Arsenic Compounds from Green River Formation Oil Shale

RICHARD H. FISH

University of California, Lawrence Berkeley Laboratory, Berkeley, CA 94720

The molecular characterization of methylarsonic acid, phenylarsonic acid and the inorganic anion, arsenate, found in a methanol extract of a Green River Formation Oil shale sample was accomplished by HPLC–GFAA analysis. In addition, derivatization of the acids, HPLC purified, by reaction with 3-methylcatechol to form the five coordinate organoarsenic catecholates as well as reaction, via trimethylsilylation, of the ammonium salt of arsenate to form tristrimethylsilylarsenate was followed by GC–EIMS analysis to provide unequivocal evidence for the presence of these organometallic and inorganic compounds of arsenic as natural products in oil shale.

Transformations and bioaccumulation of trace metals and metalloids, especially arsenic, are well known to occur in modern microorganisms, including the bacteria (1,2) molds, (3) and marine plankton or algae. (4,5) Such microflora demonstrate capacities for uptake of both inorganic and organic forms of elements, and in some instances, are shown to involve biomethylation of inorganic substrates which result in cellular incorporation of organometal(loid)s, e.g., methylarsonic acid or dimethylarsonic acid. (5) Arsenic is known to bioaccumulate in higher marine organisms to a substantial degree, (6,7) where it resides in some shellfish tissues as arsenobetaine. (8)

Similar considerations for ancient metal(loid) uptake or transformations appear quite reasonable for primordial microflora, especially the algae which account for the present ubiquitous distribution of kerogen in shale rocks. (9,10) In general, the fossil deposition record suggests that substantial metal(loid) accumulation also occurred in higher plants which underwent diagenesis to form modern petroleum and coal deposits. (11,12) In many instances, various present-day species of plants are known to both selectively and extensively hyperaccumulate various metal(loid)s

to such a degree that geochemical prospection is feasible by correlating metal concentration profiles with local flora. (13) It is not unexpected, therefore, to discern characteristic concentration patterns for trace elements in various fossil deposits – whether we regard these as essential or toxic to life – and to expect that gross differences in the profiles between the three main types: coal, kerogen, and petroleum, as summarized in Table I. (14-18) Similarly expected, though far more subtle, we might anticipate that element distributions for these three main fossil sources also depend upon specific sites, and reflect their terrestrial or marine origins, subsequent geochemical history, and maturation. (19-21)

The molecular forms of trace metal(loid)s in fossil deposits is doubtless complex, probably consisting of varying proportions of inorganic, metallo-organic (no covalent element-carbon bonds), and true organometallic chemical species residing in unspecified

Table 1.

Comparison of Selected Elemental Concentrations[a] in Petroleum, Coal, and Oil Shale

Element	Petroleum	Petroleum	Coal	Oil Shale
As	0.111	0.263	15	44.3
Be	--	--	2.0	--
Cd	--	--	1.3	0.64
Cr	0.093	0.008	15	34.2
Fe	10.8	40.7	1.6%	2.07%
Ge	--	--	0.71	--
Hg	0.051	3.236	0.18	0.089
Ni	9.38	165.8	15	27.5
S	0.83%	1.31%	2.0%	0.573%
Se	0.052	0.530	4.1	2.03
Si	--	--	2.6%	15%
U	--	0.060	1.6	4.5
V	13.6	87.7	20	94.2

[a]Concentrations in ppm except as noted.

sites within the carbonaceous matrix. Over the years a very sub-
stantial solvent differentiation methodology has emerged, (22-24)
which greatly aids the analyst in assessing the broad matrix
categories of fossil materials, and produces reproducible informa-
tion concerning possible ligation, elements present, and approxi-
mate molecular size (weight) of the soluble components.

The determination of the molecular forms of trace
metal(loid)s in fossil materials ideally requires a technique with
extreme selectivity, lack of interferences, sensitivity to the
sub-ppm level, and the ability to deal with heterogeneous samples.
The state-of-the-art analytical methods which are capable of meet-
ing these criteria to varying degrees, without extensive sample
preparation, are quite limited and have only recently been applied
to limited types of fossil samples.

The coupling of chemical separations, which provide selec-
tivity and reduce interferences, with instrumental techniques,
which are capable of providing further selectivity and the neces-
sary sensitivity, has been an active area of analytical research,
being performed in both off-line and on-line modes. The recent
emergence of a number of on-line "hyphenated" techniques, (24)
GC-MS, MS-MS, LC-ESD (including variable- and scanning UV, IR,
NMR, GFAA, FAA and electrochemical detectors) appears to be the
most effective and versatile method to quantitate organic, inor-
ganic, organometallic and metallo-organic compounds in complex
matrices. Among these, automated coupling of high performance
liquid chromatography (HPLC) in normal, reverse phase, ion
exchange, or size exclusion modes with element-selective detectors
appears most promising for the characterization of metal(loid)
containing molecules in complex matrices. (25)

Reports of on-line, element-selective detection of chromato-
graphic effluents of fossil materials have appeared more recently
and offer the advantages of increased resolution and easier
chromatographic optimization because of the real time acquisition
of elemental distributions during the chromatographic run.
Recently, Brinckman et al. (26) have coupled a graphite furnace
atomic absorption (GFAA) spectrometer to a high performance liquid
chromatograph, which has been applied by Fish et al. (27) and
Weiss et al. (28) to the analysis of arsenic compounds in process
waters and oils generated during oil shale retorting.

Results and Discussion

From the above-mentioned results with the oil shale retorting
products, the pertinent question of whether the inorganic arsenic
and organoarsenic compounds were actually natural products that
were formed in the fossilization process of oil shale formation or
were pyrolysis products formed during retorting, needed to be
answered.

Since components of Green River Formation oil shale, namely,

kerogen and bitumen, constitute the organic material regarded as biogeochemical fossil products derived from lipid fractions of ancient algae, we decided to examine this material by HPLC–GFAA analysis after extraction with a polar organic solvent. The Green River Formation oil shale sample (~20 ppm total As) was extracted with methanol and the extract containing about 20% (~4–5 ppm) of the total arsenic available was analyzed on a Dionex anion exchange column (27,28) to provide initial indications that in fact the arsenic compounds identified as being in the shale oils and the retort waters were natural products and not pyrolysis products (Figure 1).

Simultaneously, we were studying the reactions of methyl- and phenylarsonic acids with substituted catechols. In that study, (29) we discovered that the reaction products, five-coordinate, organoarsenic catecholates, could be gas chromatographed on fused silica capillary columns (30 m x 0.3 nm DB-5) and characterized by mass spectrometry (GC-MS). Therefore, we decided to apply this derivatization technique to the unequivocal identification of methyl- and phenylarsonic acids present in the oil shale extract.

We purified the methanol extract by preparative HPLC (the area from 22 to 35 min. was collected, Figure 1) and lyophilized the extract before dissolving in benzene. To this solution was added excess 3-methylcatechol and the reaction mixture was refluxed for 5 h and worked up to remove the excess 3-methylcatechol. A concentrated sample was subjected to GC-EIMS analysis to provide spectra and scan numbers (retention times) that were identical to the known samples of the 3-methylcatecholates of both methyl- and phenylarsonic acids.

Figure 2(A) shows the reconstructed ion chromatogram of the two standards, 3-methylcatecholates of methyl- and phenylarsonic acids, and the single ion chromatograms show pertinent fragments of interest at m/e 197 and 212 for the methylarsonic acid derivative (Figure 2 B,C) and m/e 197 and 274 for the phenylarsonic acid derivative (Figure 2 B,D). Figure 3(C) shows the region we purified by HPLC containing the organoarsonic acids, which were derivatized, and the expanded sections of this chromotogram containing the organoarsenic catecholates with the important ions, m/e 197, 212 and 274, clearly evident for the 3-methylcatecholates of methyl- (Figure 3 A) and phenylarsonic (Figure 3 B) acids. Additionally, the inorganic anion, arsenate (AsO_4^{3-}), was verified in a similar fashion (preparative HPLC of the region from 35.5–41 min) by preparation of the tris(trimethylsilyl-) derivative of the ammonium salt of arsenate and analyzing the purified extract by GC-EIMS for ions at m/e 207, 343, and 358. (30) The organoarsenic compound(s) that elutes with the solvent front (Figure 1) has not been as yet identified and further work is in progress to verify its structure.

We believe these identifications of the organoarsonic acids to be the first such molecular characterizations of trace

Standard

$$\text{Me}\overset{\overset{\displaystyle O}{\|}}{\text{As}}(\text{OH})_2 \qquad \text{⬡}-\overset{\overset{\displaystyle O}{\|}}{\text{As}}(\text{OH})_2 \qquad \text{AsO}_4^{3-}$$
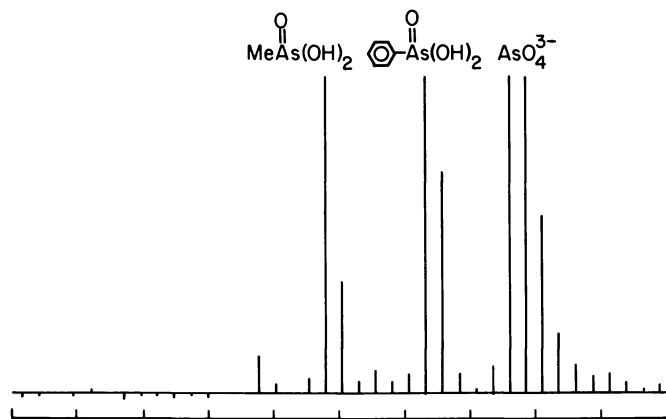
Methanol Extract of Green River Formation Oil Shale

Unknown Organo-arsenic Compounds

Methyl- and Phenylarsonic Acids

Arsenate

0 5 10 15 20 25 30 35 40 45 50

Min
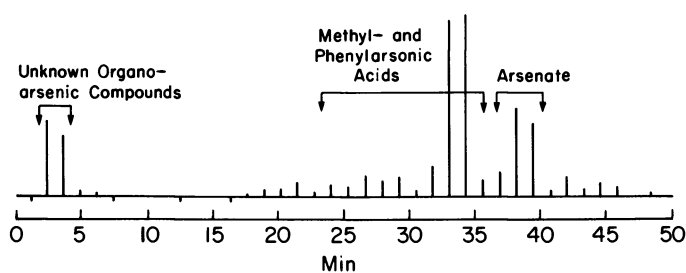
Figure 1. The HPLC-graphite furnace atomic absorption (GFAA) analysis of Green River Formation oil shale extracted with refluxing methanol.

The AA detection of arsenic was at 193.7 nm. The HPLC column was a Dionex anion exchange column with 0.2 M (NH$_4$)$_2$CO$_3$ in aqueous methanol as the eluting solvent. The bracketed areas were isolated by preparative HPLC.
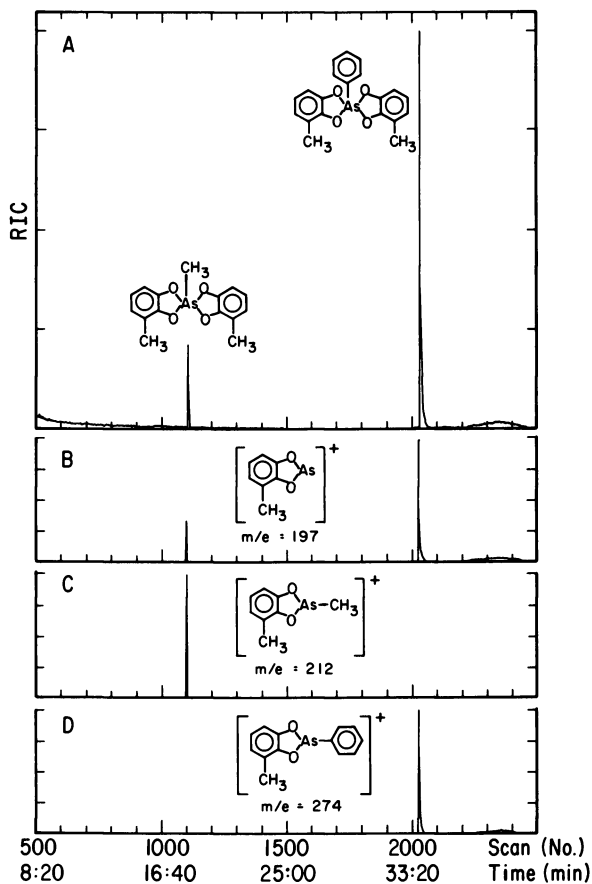
Figure 2. GC-EIMS analysis of the 3-methylcatecholates of methyl- and phenylarsonic acids. Key: A, reconstructed ion chromatogram of known methyl- and phenylarsonic acid derivatives of 3-methylcatechol; B, selected ion chromatogram showing m/e 197 for each derivative; C, selected ion chromatogram for methylarsonic acid-3-methylcatecholate at m/e 212; and D, selected ion chromatogram for phenylarsonic acid-3-methyl-catecholate at m/e 274.
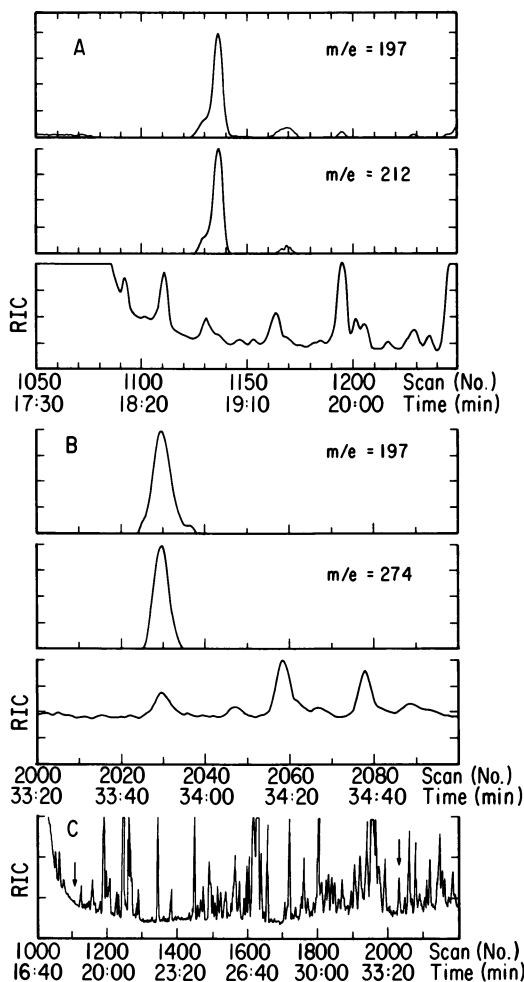
Figure 3. GC-EIMS analysis of the derivatized, HPLC purified, methanol extract. Key: A, selected ion chromatograms near Scan 1137 for m/e 197 and m/e 212 confirming the identification of the 3-methylcatecholate of methylarsonic acid in the expanded reconstructed ion chromatogram; B, selected ion chromatograms near Scan 2030 for m/e 197 and m/e 274 confirming the identification of the 3-methylcatecholate of phenylarsonic acid in the expanded reconstructed ion chromatogram; and C, reconstructed ion chromatogram of HPLC purified methanol extract with arrow on left designating methylarsonic acid-3-methylcatecholate and arrow on right designating phenylarsonic acid-3-methylcatecholate.

organometallic compounds to be reported for any fossil fuel precursors and initiates the area of organometallic geochemistry, a field that has hithertofore been largely unexplored.

The implications are that these organoarsonic acids are natural products and hence have a biogeochemical origin in the oil shale taphonomy (fossilization) process. It is also interesting to note that no examples of biophenylation have been reported, whereas biomethylation of arsenic compounds is a well known reaction. (31) How the phenylarsonic acid forms will have to be answered with the examination of precursors to the oil shale such as freshwater marine algal mats as well as other biogeochemical samples.

Finally, the fact that these organoarsonic acids are released upon oil shale pyrolysis has important implications in the various synthetic fuel processes, where the role of organometallic compounds in poisoning process catalysts and contributing to environmental problems, is paramount. (32,33)

Experimental

The HPLC–GFAA instrumentation and analyses condition have been described previously (see references 25–28). The AA detection of arsenic was at 193.7 nm. The HPLC column was a Dionex anion exchange column with 0.2M $(NH_4)_2CO_3$ in aqueous methanol as the eluting solvent. The GC–MS analyses were accomplished using a Finnigan 4023 mass spectrometer system with a 30 m x 0.3 mm DB–5 (J&W) capillary column, conditions: 55° 3 min.) – 300°/min. Reconstructed ion chromatograms and single ion chromatogram data was accomplished with the INCOS Data System.

Acknowledgments

Literature Cited

1. McBride, R.C.; Wolfe, R.S. Biochem., 1971, 10, 4312–17.
2. Cheng, C.N.; Focht, D.D. Appl. Environ. Microbiol., 1979, 38, 494–8.
3. Cullen, W.R.; McBride, B.C.; Pickett, A.N. Can. J. Microbiol., 1979, 25, 1201–5.
4. Bottino, N.R.; Cos, E.R.; Irgolic, K.J.; Maeda, S.; McShane, W.J.; Stockton, R.A.; Zingaro, R.A. "Organometals and

Organometaloids Occurrence and Fate in the Environment," Brinckman, F.E.; Bellama, J.M., Eds,; AMERICAN CHEMICAL SOCIETY SYMPOSIUM SERIES No. 82, ACS:Washington, D.C., 1978; p. 116.

5. Andrae, M.O.; Klumpp, D. Environ. Sci. Technol., 1979, 13, 738-1.

6. Maher, W.A. Anal. Chem. Acta., 1981, 126, 157-5.

7. Benson, A.A.; Summons, R.E. Science, 1981, 211, 482-3.

8. Edmonds, T.S.; Francesconi, K.A. Chemosphere, 1981, 10, 1041-4.

9. Cane, R.F. in "Oil Shale," Yen, T.F., Ed.; Elsevier: Amsterdam, 1976, p. 27-60.

10. Abelson, P.H. "Researcher in Geochemistry," Abelson, P.H., Ed.; Wiley: New York, Vol. II, 1967, p. 63-86.

11. Manskaya, S.M.; Diozdova, T.V. "Geochemistry of Organic Substrates," Pergamon Press: Oxford, 1968.

12. Yen, T.F. "The Role of Trace Metals in Petroleum," Yen, T.F., Ed.; Ann Arbor Sci.: Michigan, 1975, p. 1-30.

13. Erdman, J.A.; Harrach, G.H. J. Geo. Chem. Explor., 1981, 14, 83.

14. Hitchon, B.; Filby, R.H.; Shah, K.R. "The Role of Trace Metals in Petroleum," Yen, T.F., Ed.; Ann Arbor Science Publishers, Inc.: Ann Arbor, 1975.

15. Shah, K.R.; Filby, R.H.; Haller, W.A. J. Radioanal. Chem., 1970, 6:185:192.

16. Shah, K.R.; Filby, R.H.; Haller, W.A. J. Radioanal. Chem., 1970, 6:413-422.

17. "Trace-element geochemistry of coal resource development related to environmental quality and health", U.S. National Committee for Geochemistry, National Academy Press: Washington, D.C., 1980.

18. Fruchter, J.S.; Wilkerson, C.L.; Evans, J.C.; Sanders, R.W. Environ. Sci. & Tech., 1980, 14:1374-1381.

19. Van Krevelen, D.W.; Schuyer, J. "Coal Science, Aspects of Coal Constitution," Elsevier: Amsterdam, 1957, p. 96-103 and p. 211-220.

20. Yen, T.F.; Chilingarian, G.V., Eds; "Oil Shale," Elsevier Scientific Publishing Co.: New York, 1976.

21. "The Role of Metal-Heteroatom Complexes in Fossil Fuel Production," in National Bureau of Standards Special Publication NBS-DOE SP 618, 1981, p. 9.

22. Saxby, J.D. in "Oil Shale," Yen, T.F.; Chilingarian, G.V., Eds.; Elsevier Scientific Publishing Co.: New York, 1976.

23. Mima, M.J.; Schultz, H.; McKinstry, W.E. "Analytical Methods for Coal and Coal Products," Karr, Jr., Clarence, Ed.; Academic Press, New York, 1978, Vol. 1, Chapter 19.

24. Filby, R.H. "The Role of Trace Metals in Petroleum," Yen, T.F., Ed.; Ann Arbor Science: Michigan, 1975, p. 31.

25. Jewett, K.L.; Brinckman, F.E. "Detectors in Liquid

Chromatography," Vickery, T.M., Ed.; Marcell Dekker: New York, in press.

26. Brinckman, F.E.; Blair, W.R.; Jewett, K.L.; Iverson, W.P. J. Chrom. Sci, 1977, 15:493-503.

27. Fish, R.H.; Brinckman, F.E.; Jewett, K.L. Environ Sci. Technol., 1982, 16, 174.

28. Weiss, C.S.; Jewett, K.L.; Brinckman, F.E.; Fish, R.H. National Bureau of Standard Special Publication 618 197 (1981).

29. Fish, R.H.; Tannous, R.S. Organometallics 1982, 1, 1238.

30. Butts, W.C.; Rainey, Jr., W.T. Anal. Chem.2 1979, 43, 538.

31. McBride, B.C.; Merilees, H.; Cullen W.R.; Pickett, W. Brinckman, F.E.; Bellama, J.M., Eds.; ACS SYMPOSIUM SERIES No. 82, ACS:Washington, DC, 1978, p. 94.

32. A preliminary account of this study has been published. Fish, R.H.; Tannous, R.S.; Walker, W.; Weiss, C.S.; Brinckman, F.E. 1983, J. Chem. Soc. Chem. Commun. 490.

33. For a review of this area of speciation of arsenic compounds in fossil precursors and products see: Brinckman, F.E.; Weiss, C.S.; Fish, R.H. "Chemical and Geochemical Aspects of Fossil Energy Extraction," Yen, T.F., Ed.; Ann Arbor Science: Ann Arbor, MI, 1983, Chapter 13, p. 197.

Occurrence of Biomarkers in Green River Shale Oil

MARY F. SINGLETON, ALAN K. BURNHAM, JEFFERY H. RICHARDSON, and JACK E. CLARKSON

Lawrence Livermore National Laboratory, Livermore, CA 94550

Biological markers, compounds derived essentially
unchanged from living organisms, are found in oil-
bearing rocks, petroleum and most ancient sediments.
We are investigating the variation in ratios of cer-
tain biomarkers in shale oils and their use as tracers
for relating oil to source rock during in-situ retort-
ing. We have produced oil samples at heating rates
of about 10°C/min from 1- and 2-foot shale composites
from three Green River formation cores and have
measured the occurrence of several isoprenoid and
polycycloalkane compounds in the oils using capillary
gas chromatography. To eliminate the effect of
heating rate on alkene/alkane ratios, we used the sum
of ene and ane forms where applicable to calculate
ratios. Variations in biomarker content with depth,
grade, odd/even ratios, normal alkene/alkane ratios
and atomic nitrogen/organic carbon ratios were studied
and cross correlations were determined. Correlations
were particularly high between pairs of isoprenoid
compounds. There is sufficient variation to use
biomarkers as retort diagnostics and to demonstrate a
variation in source material.

Biological markers, compounds with carbon skeletons derived
essentially unchanged from living organisms, have been used by
petroleum geologists to relate oils to their original source rock
material (1,2). These techniques are based on the ubiquitous
nature of biological markers (biomarkers) in ancient sediments
and on the characteristic ways in which ratios of biomarker
skeletons vary from location to location, depending on source and
migration parameters.

We are extending these techniques to the oil shale industry by determining biomarker ratios in oils produced from Green River formation shales and by studying the manner in which these ratios vary with depth and other characteristics of the shale within a given core. Time-dependent application of a technique (3) that determines the amount and nature of shale oil degradation in combustion retorts is hampered by variable and unknown oil drainage times. We have previously proposed (4) that comparison of time-dependent biomarker ratios from a vertical modified in-situ retort with those from a core over the same stratigraphy would be helpful for relating the time-dependent oil yield from the retort to the corresponding conditions. Other techniques might be based on relating isomeric changes in biomarker skeletons to thermal history.

Past work on the biomarkers in oil shale has involved characterization of the the biomarkers in bitumen, the soluble organic portion of oil shale, and determination of the manner in which their quantity varied with depth in relation to other hydrocarbon types (5,6). Biomarker derivatives from kerogen, the insoluble organic portion of oil shale, have been determined by a variety of methods (7) and compared to their bitumen analogs (8-10). Because not all the biomarker compounds from a given shale sample occur in the same proportions in both the bitumen and the oil, and because heat treatment is involved in commercial oil production, we have evaluated biomarker occurrence in the whole oil product prepared at a heating schedule comparable to the standard Fischer assay procedure (12°C/min, maximum 500°C). We previously established (4) that the biomarkers from kerogen occur in the oil as both unsaturated and saturated compounds (ene and ane). Although the ene/ane ratio for a given carbon skeleton varies with heating rate, the ratios involving sums of ene and ane are fairly constant at slow to moderate (4) and very rapid (11) heating rates. This is important in validating the use of biomarker ratios in oils produced at widely varying heating rates (geological, in-situ retorting, assay, very rapid pyrolysis).

In this work, oils were prepared from cores in varying locations in the Green River formation in order to compare biomarker ratio characteristics that correlate across the resource, as well as the factors that distinguish one location from another. Besides being of diagnostic value for oil shale retorts, this information provides possible insights into the geochemistry of oil shale and the structure of kerogen and bitumen.

Shale Samples

Oil shale core samples were available from two widely separated (East, West) locations in the Green River formation (Figure 1). The first core studied was from the Geokinetics site south of Vernal, Utah. In this area the Mahogany zone is close
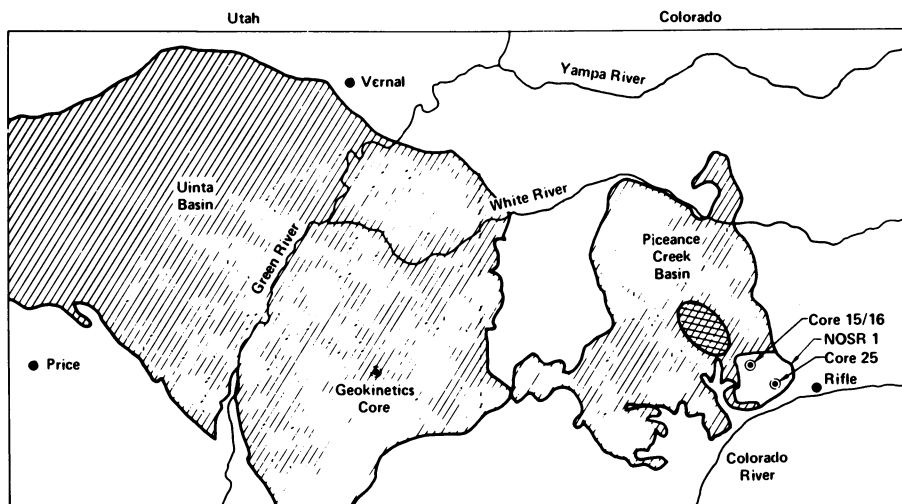
Figure 1. Map of portion of the Green River Formation showing the three core holes studied.

to the surface and less than 50 feet thick. Oils were prepared
as described below from 1-foot composite shale samples spanning
45 to 85 feet in depth. These shale samples had been previously
prepared at our laboratory (-20 mesh) and elemental analyses for
total carbon, mineral carbon, hydrogen, nitrogen and sulfur were
available. Grade was calculated using a correlation established
at our laboratory (12) between organic carbon content and grade
that has a standard error of 0.56 gal/ton. These samples varied
in grade from 4.2 to 52.3 gal/ton. Geokinetics' designation for
this core is "Exp. 22". The Mahogany Marker is located at 47.6
feet (13). The Mahogany Marker, a thin bed of analcime-rich
tuff, lies about 25 feet below the bottom of the A-groove. The
A-groove is an easily identifiable bed of very lean shale that
weathers more rapidly than its surrounding shale and has greatly
reduced electrical resistivity (14).

        The other two cores studied are Naval Oil Shale Reserve
(NOSR) cores 25 and 15/16 from the Anvil Points area near
Parachute Creek, Colorado. These shale samples were prepared for
a comprehensive study by Giauque et al. (15) and were the
consistency of fine talc. Their grade had been determined (at
Laramie Energy Technology Center) by the ASTM standard method
(16) and varied from 2.0 to 56.5 gal/ton in core 25 and from 7.0
to 75.7 gal/ton in core 15/16. NOSR core 25 was located near the
edge of the Piceance Creek Basin and spanned a depth of 623 to
750 feet composited at 1- and 2-foot intervals except for two
5-foot composites at the top and a 5-foot and a 42-foot composite
at the bottom. The Mahogany Marker is estimated from the grade
variation to occur close to 664 feet. The A-groove, which occurs
from approximately 630 to 640 feet, was included in analysis of
this core as was the 42-foot composite sample that extended into
the lean region below the Mahogany zone. NOSR core 15/16 was
located nearer the depositional center of the basin (17) and
spanned a depth of 1190 to 1346 feet composited in 1- and 2-foot
intervals except for four 5-foot composites at the top of the
core. The Mahogany Marker is estimated to occur at about 1236
feet and the A-groove from about 1200 to 1208 feet. This core is
unique in the inclusion of a Lower Mahogany zone that extends
almost 100 feet below the Mahogany Marker with highly variable
shale grade.

Oil Generation Procedure

        Ten untreated oil shale samples were simultaneously
pyrolyzed in a segmented reactor constructed of stainless steel
(Figure 2). Approximately 12 g of shale was weighed into each
6-inch high individual sample vessel with stainless steel frit
bottom. The vessels were placed into the 10 compartments of the
reactor resting on a wire mesh so as to be positioned near the
center of the furnace. The lid with 3 thermocouples and a gas
inlet was bolted into place with a Viton O-ring seal (the top

Top of reactor

4¾ in.

1 in.

Single sample vessel

Shale

6 in.

S.S. frit

Exit line

Argon

Flowmeter

Thermocouple in shale

3 zone furnace

Controller
Microcon 823

Reactor

Heated exit lines
Collection tubes (u-shaped)
packed with glasswool cooled to 0°C

Exhaust

Flowmeter
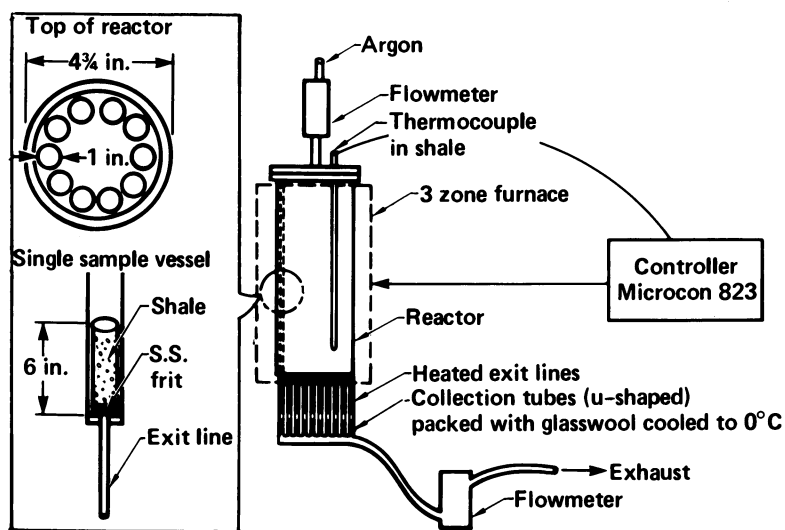
Figure 2.   Apparatus for producing oil from 10 oil shales simultaneously.

flange was positioned just outside the furnace). The charged
reactor was placed in a 3-zone furnace and the samples were
heated at about 10°C/min up to 500°C where the temperature was
held for 30 minutes. An argon flow was maintained through out
the experiment to aid in removing vapors from the reactor and to
minimize their residence time in the hot zone. Oils were
collected in individual U-shaped glass tubes packed with glass-
wool and immersed in an ice bath. Noncondensable gases were
vented through a common manifold and exit line containing a
flowmeter. Comparison of gas chromatographs of oils produced by
this technique gives biomarker ratios very similar to Fischer
assay oils.

Chromatography

In order to avoid problems with sample inhomogeneity, the
entire oil sample from each sample of shale was dissolved in 1.5
to 2.5 mL of CS_2 (about 1 g oil to 1.5 mL solvent). One μL
of this solution was injected into a Hewlett-Packard Model 5880
Gas Chromatograph equipped with capillary inlet and a 50 m x
0.25 mm Quadrex "007" methyl silicone column. Injection on the
column is made with a split ratio of approximately 1 to 100. The
column temperature started at 60°C and increased at 4°C/min to
280°C where it remained for a total run time of 90 min. The
carrier gas was helium at a pressure of 0.27 MPa flowing at a
rate of 1 cm^3/min. The injector temperature was 325°C and the
flame ionization detector (FID) temperature was 350°C. Data
reduction was done using a Hewlett-Packard Model 3354 Laboratory
Automation System with a standard loop interface. Identifica-
tion of various components was based on GC/MS interpretation
described previously (4). For multiple runs on the same shale,
the relative standard deviations of the biomarker ratios were
about 10%.

Data Analysis

A list of some of the ratios calculated from the
chromatograms is given in Table I. By cores, these ratios for
the individual oils were entered into a data file which also
included depth of burial, grade and atomic nitrogen/organic
carbon (N/O.C.) of the raw shale. Using computer codes available
on an LLNL CDC-7600 (CRSCOR and CROSSPLOT2), cross-correlation
coefficients for all pairs of variables were calculated and
various data pairs were plotted.

Results and Discussion

We have investigated the variations in two groups of
biomarker compounds, acyclic isoprenoids and polycycloalkanes
(steranes and triterpanes), in gas chromatograms of oils produced

Table I. Ratios calculated from the GC peaks for each oil sample

---

C_8 through C_{28} normal hydrocarbons: 1-alkene/alkane

C_{11} through C_{29} normal hydrocarbons: odd/even ratios*

Phytane/C_{18}s + C_{19}s   (2,6,10,14-tetramethylhexadecane, C_{20})

Phytane/Pristane

Phytane/Pristane + 1-ene + 2-ene

Phytane/Prist-2-ene

Phytane/Prist-1-ene

Pristane/C_{17}s + C_{18}s   (2,6,10,14-tetramethylpentadecane, C_{19})

Prist-1-ene/C_{17}s + C_{18}s

Prist-2-ene/C_{17}s + C_{18}s

Pristane + 1-ene + 2-ene/C_{17}s + C_{18}s

Norpristane/C_{16}s + C_{17}s   (2,6,10-trimethylpentadecane, C_{18})

2,6,10-trimethyldodec-1-ene/C_{13}s + C_{14}s   (1-ene of farnesane)

Farnesane/C_{13}s + C_{14}s   (2,6,10-trimethyldodecane, C_{15})

2,6-10-trimethyldodec-1-ene/Farnesane

2,6,10-trimethyldodec-1-ene + Farnesane/C_{13}s + C_{14}s

2-6,10-trimethylundec-2-ene/C_{13}s

2,6,10-trimethyltridec-1-ene/C_{13}s + C_{14}s

2,6,10-trimethyltridecane/C_{14}s + C_{15}s

2,6,10-trimethyltridecane + 1-ene/C_{14}s + C_{15}s

ergostane/C_{29}s + C_{30}s   ($C_{28}H_{50}$)

stigmastane/C_{30}s   ($C_{29}H_{52}$)

polycycloalkane 1/C_{29}s + C_{30}s

polycycloalkane 2/C_{29}s + C_{30}s

polycycloalkane 3/C_{29}s + C_{30}s

polycycloalkane 4/C_{31}s

polycycloalkane 5/C_{31}s

Note: C_{17}s implies the sum of the 1-alkene + alkane of the normal C_{17} hydrocarbon, etc.

---

*Odd/even ratios were calculated with the formula:

$$\frac{2 \times (C_{odd} \text{ alkene + alkane})}{(C_{odd-1} \text{ alkene + alkane}) + (C_{odd+1} \text{ alkene + alkane})}$$

from 166 shale samples from three Green River formation cores.
The acyclic isoprenoids ranged from 14 to 20 carbons in size and
included several alkene forms. Seven polycycloalkanes were
studied, two of which were identified as isomers of the steranes
ergostane and stigmastane. The other five are referred to as
polycycloalkanes 1 through 5 in the tables. We also measured the
ratios of normal alkenes to alkanes from C_8 through C_{28} and the
odd/even carbon preferences from C_{11} through C_{29} for comparison
purposes.

For the Geokinetics core, we prepared 38 oils from 1-foot
composites. For NOSR core 25 we prepared 45 oils from 1- and
2-foot composites with the exception of two larger composites at
the bottom. Since this core included the A-groove immediately
above the Mahogany zone and a large composite sample below the
Mahogany zone, we also analyzed the 28 samples from the Mahogany
zone (600 to 702 feet) separately to look for any differences
resulting from these inclusions. Although the C_{17} odd/even
ratio, N/O.C. ratio, and several biomarker ratios were consider-
ably higher in both these regions as compared to the Mahogany
zone, the over-all averages and the final correlations were not
appreciably changed. For NOSR core 15/16 we prepared 83 oils
from 1- and 2-foot composites with the exception of four 5-foot
composites from the top of the core. Since this core was closer
to the depositional center of a basin than the other two cores,
it contains rich oil shale to a greater depth of burial. A
comparison of the grade and span of the three cores is shown in
Figure 3. Note that the composite samples were not weighted
according to the distance spanned in calculating the averages for
the cores. This was intentional, since we were primarily
interested in the Mahogany zone where samples were available over
1- and 2-foot intervals.

There has been considerable speculation about the source
material responsible for biomarker compounds in oil shale and
about the effect of deposition and aging conditions on their
distribution (18-22). The effect of source material is almost
certainly a stronger influence on biomarker ratios than is the
effect of maturation in the samples considered here due to the
relatively short depositional intervals. We are primarily
concerned with the variation in relative amounts of biomarkers in
oils with stratigraphy in the Mahogany zone and with the possible
application of this information to the commercial development of
the resource. At the same time, we have looked at the relation-
ship of biomarkers to other variables in the oil and the shale
and to the geochemistry of the resource.

Biomarker compounds are present in varying proportions in
both the bitumen and kerogen of oil shale, the non-bitumen forms
being chemically bound or physically trapped by the kerogen and
mineral matrix (6,23). For biomarkers occurring mainly in the
bitumen, such as phytane and steranes, the production mechanism
during oil generation is basically distillation, and the amount
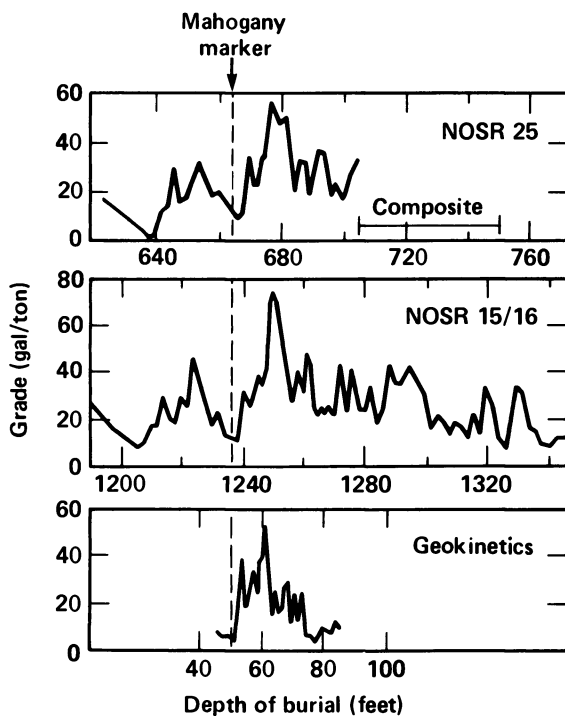
Figure 3.   Plots of grade vs. depth for NOSR cores 25 and 15/16 and Geokinetics core showing stratigraphic relationship.

produced does not depend strongly on heating rate. In contrast, the ene/ane ratios of several acyclic isoprenoid compounds produced mainly from kerogen behave like the n-alkanes, e.g., ratios of ene/ane pairs varied strongly with heating rates, but ratios based on sums of ene plus ane pairs were more nearly constant (4). Therefore, we have reported some of our ratios as the sums of the ene and ane forms, since we have established that these ratios are approximately constant over a wide range of conditions including very rapid pyrolysis in a fluidized bed and very slow pyrolysis at high pressures (11,24).

Although two cores in this study were located about 60 miles from the third, there was very good agreement of the average values for odd/even preferences (Figure 4) and alkene/alkane ratios (Figure 5) vs carbon number among all three cores. This demonstrates a consistency in the average values for these ratios in Mahogany zone oils. Another comparison of the three cores is presented in Table II based on biomarker ratios. The average values and ranges agree fairly well for the three cores with the exception of the pristane+1-ene+2-ene/phytane ratio which goes considerably higher in the NOSR core 15/16.

The ratios of pristane compounds (ane, 1-ene, 2-ene) to phytane are of interest since pristane/phytane ratios in bitumen and/or kerogen are often cited as indicators of terrestrial/ lacustrine source material (1,2,5), although they also depend on the thermal history of the material. Prist-1-ene from kerogens and sediments has been linked to a common precursor of pristane and phytane (25,26). Anders and Robinson (5) report pristane/ phytane ratios averaging 0.44 in Green River formation bitumens. However, these ratios are not indicative of the whole shale oil ratios because most of the phytane comes from the bitumen and most of the pristane compounds are produced from the kerogen. Connan and Cassou (21) discuss pristane/phytane ratios in a variety of crude oils and conclude that ratios lower than 1.5 are indicative of oils derived from "marine shale--carbonate sequences" while ratios greater than 3.0 indicate a significant amount of terrestrial source material. These crude oil ratios are probably more valid for comparison to whole shale oil samples than to the bitumen ratios. Including the three pristane forms in the ratio of pristane+1-ene+2-ene/phytane gives us values indicative of usually small, but significant, and highly variable terrestrial input at differing levels within two of the cores we have studied. The pristane/phytane ratios varied from 0.52 to 1.33 (average 0.78) in the Geokinetics core and from 0.40 to 1.14 (average 0.58) in NOSR core 25, while pristane+1-ene+2-ene/phytane ratios varied from 1.54 to 4.35 (average 2.78) and from 1.61 to 5.26 (average 2.63) respectively. It is interesting to note that although these two cores are located near the opposite boundaries of the resource, the ranges and averages for these ratios are nearly the same. However, NOSR core 15/16, which is closer to the depositional center of the basin, yielded oils from the lower
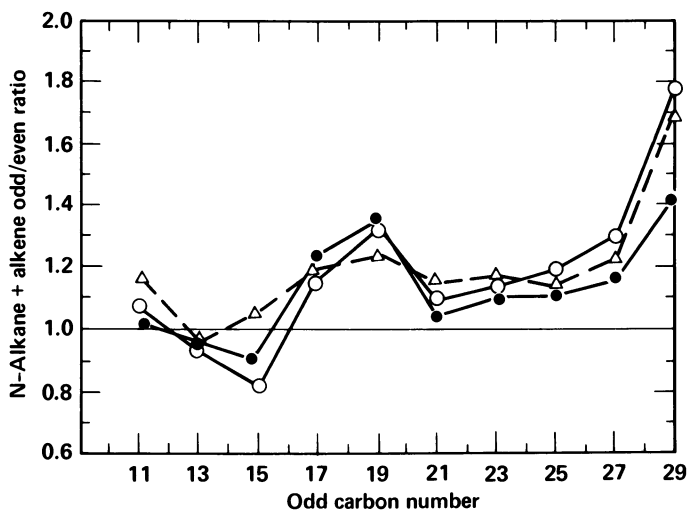
Figure 4. Plot of the average normal alkane + alkene odd/even ratios vs. carbon number in NOSR cores 25 (○) and 15/16 (●) and Geokinetics core (△).
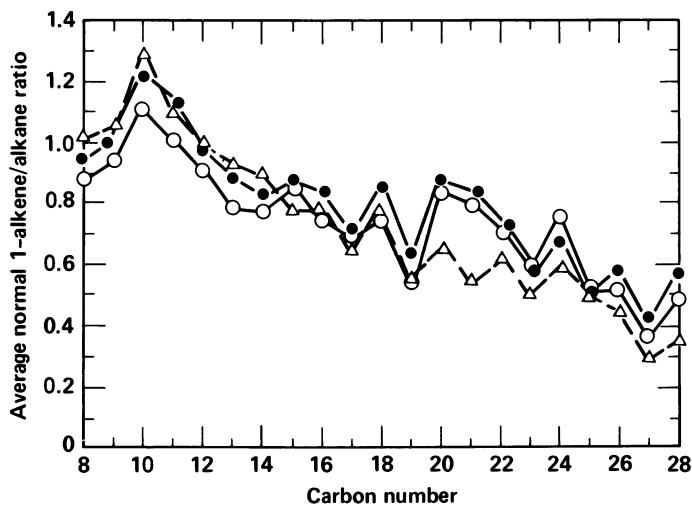
Figure 5. Plot of the average 1-alkene/normal alkane ratios vs. carbon number in NOSR cores 25 (○) and 15/16 (●) and the Geokinetics core (△).

Table II. Comparison of biomarker ratios

Biomarker ratio*	Geokinetics Core		
	Min.	Max.	Avg.
pristane	0.09	0.55	0.21
prist-1-ene	0.15	0.76	0.40
prist-2-ene	0.05	0.31	0.14
pristane+1-ene+2-ene	0.30	1.22	0.75
phytane	0.08	0.90	0.29
prist-1-ene/phytane	0.52	2.63	1.41
prist-2-ene/phytane	0.27	1.00	0.48
pristane+1-ene+2-ene/phytane	1.54	4.31	2.96
pristane/phytane	0.52	1.34	0.82
norpristane	0.70	0.32	0.18
trimethyldodec-1-ene	0.01	0.19	0.10
farnesane	0.06	0.20	0.13
trimethyldodec-1-ene/farnesane	0.55	1.07	0.78
trimethyldodec-1-ene+farnesane	0.11	0.38	0.22
trimethylundec-2-ene	0.15	0.47	0.31
trimethyltridec-1-ene	0.06	0.22	0.14
trimethyltridecane	0.09	0.37	0.20
trimethyltridecane+1-ene	0.16	0.59	0.35
ergostane	0.02	0.39	0.12
stigmastane	0.19	1.68	0.65
polycycloalkane 1	0.02	0.26	0.10
polycycloalkane 2	0.03	0.59	0.16
polycycloalkane 3	0.02	0.70	0.23
polycycloalkane 4	0.08	0.81	0.40
polycycloalkane 5	0.14	2.21	0.78

*For incomplete ratios, values reported are for ratios
 of biomarkers to the respective alkenes
 plus alkanes as expressed in Table I.

in three Green River formation cores.

NOSR cores					
25			15/16		
Min.	Max.	Avg.	Min.	Max.	Avg.
0.03	0.38	0.15	0.05	0.38	0.17
0.13	1.03	0.39	0.15	1.41	0.51
0.04	0.54	0.12	0.02	0.62	0.09
0.21	1.62	0.66	0.24	2.03	0.77
0.06	0.59	0.28	0.07	0.60	0.23
0.83	3.13	1.49	1.05	8.33	2.06
0.20	1.64	0.40	0.15	2.56	0.36
1.61	5.16	2.78	1.67	11.19	3.90
0.40	1.14	0.62	0.41	1.90	0.84
0.07	0.50	0.18	0.09	0.56	0.23
0.04	0.25	0.11	0.03	0.27	0.11
0.05	0.29	0.13	0.07	0.28	0.15
0.47	1.26	0.82	0.44	0.97	0.69
0.10	0.54	0.25	0.11	0.54	0.26
0.19	1.07	0.44	0.17	1.16	0.44
0.06	0.45	0.20	0.06	0.36	0.17
0.08	0.56	0.24	0.10	0.45	0.26
0.14	1.00	0.44	0.17	0.78	0.43
0.01	1.61	0.28	0.03	0.90	0.18
0.02	6.30	1.51	0.17	4.48	0.85
0.05	0.72	0.22	0.05	0.62	0.21
0.01	0.31	0.10	0.03	0.98	0.19
0.01	0.42	0.15	0.01	0.88	0.15
0.01	2.29	0.36	0.08	2.55	0.40
0.02	0.94	0.32	0.12	1.45	0.44

levels which had considerably higher pristane+1-ene+2-ene/phytane
ratios than the other cores at stratigraphic levels below the
bottom of the other two cores. In NOSR core 15/16, pristane/
phytane ratios varied from 0.41 to 1.90 (average 0.84) while
pristane+1-ene+2-ene/phytane varied from 1.67 to 11.19 (average
3.9) as shown in Figure 6. The fact that bitumen can migrate
within the shale bed (i.e., phytane leaving) may distort these
ratios to some extent, but the other biomarker ratios (sterane/
normal) were somewhat elevated in this region of high
pristanes/phytane.

The average prist-1-ene content of the oil is markedly
higher than the pristane or prist-2-ene for all three cores with
a few exceptions, mostly around the A-groove, where prist-2-ene
has the highest concentration. Although the correlations are not
strong in all three cores, it may be significant that the prist-
2-ene/prist-1-ene vs N/O.C. correlation coefficients are 0.52,
0.92 and 0.25 for Geokinetics, NOSR cores 25 and 15/16, respec-
tively. Perhaps this indicates a difference in source material
or production mechanism for these two forms. Larson and Wen (27)
have suggested that nitrogen compounds are very important in
hydrogen transfer reactions during kerogen pyrolysis and thus
elevated nitrogen content may enhance the rearrangement of prist-
1-ene to the more stable prist-2-ene. However, much of the
nitrogen, especially in the lean zones, may be inorganic (28).
Clays may also catalyze the rearrangement (29). We attempted to
test this hypothesis by examining the relationship between water
production and prist-2-ene/prist-1-ene ratios in Core 15/16. The
correlation coefficient was .01, but this may be due to the
production of water by other minerals besides clay, e.g., anal-
cime and nahcolite. The unravelling of the 2-ene/1-ene relation-
ship will require further work. It is also noteworthy that both
van de Meent (20) and Larter (25) found prist-1-ene to be present
in pyrolysis products from a large variety of kerogens.

Both grade and N/O.C. ratio in the raw shale vary character-
istically with depth in the three cores through the Mahogany
zone. This variation, shown for NOSR core 15/16 in Figure 7, is
typical of all three cores. The A-groove in NOSR core 25 has the
maximum N/O.C. ratio (.24) as well as the leanest shale material
(2.0 gal/ton) in the three cases. This inverse relationship
between grade and N/O.C. has been noted previously (12). The
occurrence of maximum C_{17} odd/even ratio is very pronounced in
this region of high N/O.C. for NOSR core 25, as are maxima for
some of the biomarker compounds (Figure 8). In NOSR core 15/16,
a maximum for prist-2-ene occurs at the A-groove, as well as
maxima for some biomarkers (Figures 6 and 9).

The depth profiles of various types of compounds studied are
given in Figures 8-10 and indicate the variation observed in these
ratios throughout the three cores. Their behavior is similar at
some levels and not at others which would be expected, due to
local variations in source materials and diagenic conditions.
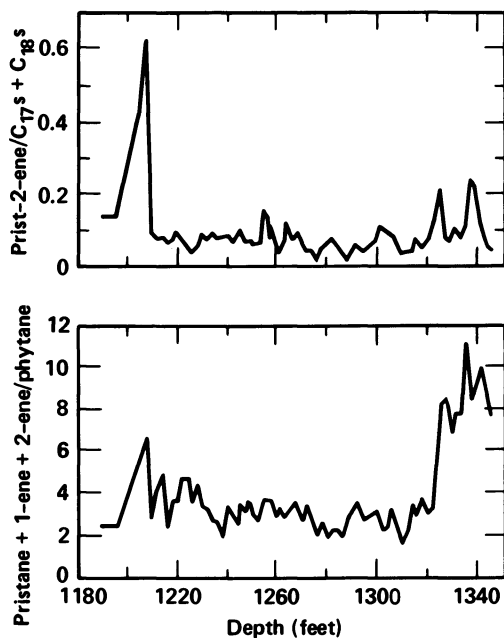
Figure 6. Plot of some ratios involving pristane and pristenes vs. depth in NOSR core 15/16.
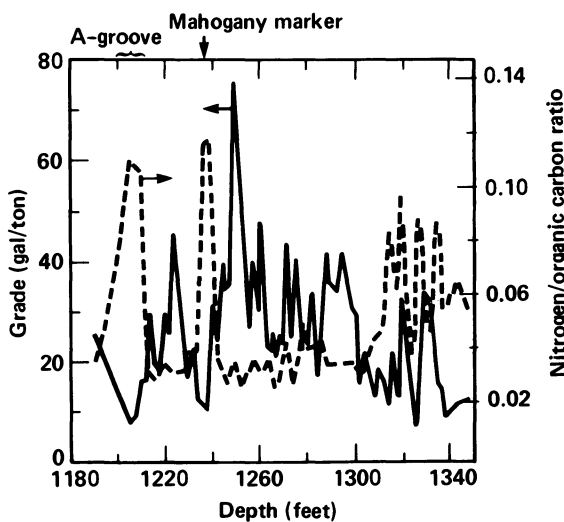
Figure 7. Plot of shale grade and nitrogen/organic carbon ratio vs. depth in NOSR core 15/16.
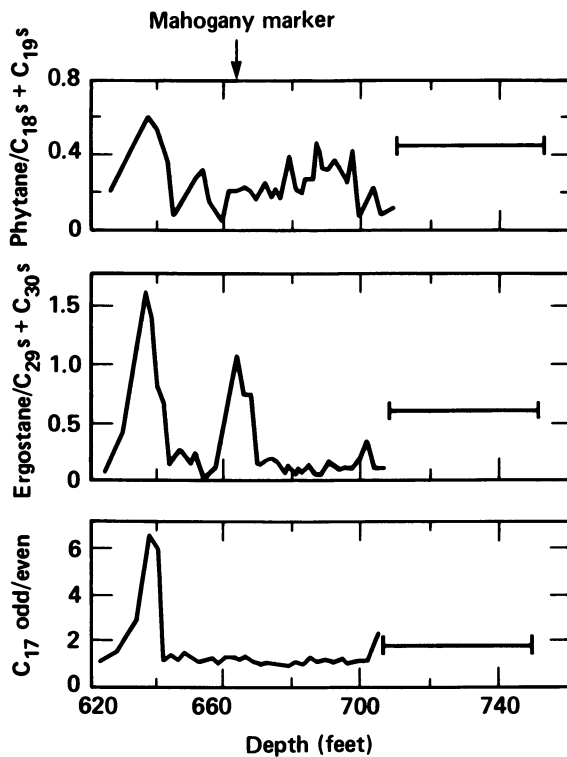
Figure 8. Plot of biomarker compounds vs. depth in NOSR core 25.

Mahogany marker
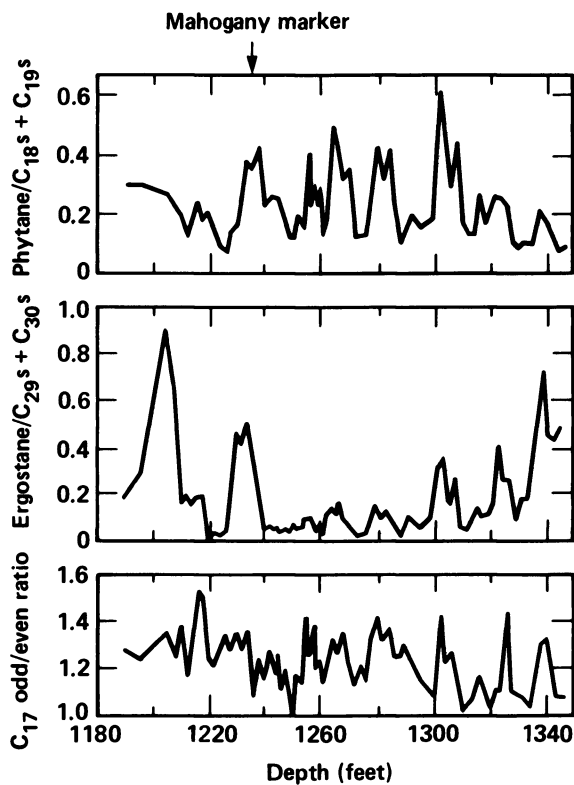
Figure 9. Plot of biomarker compounds vs. depth in NOSR core 15/16.
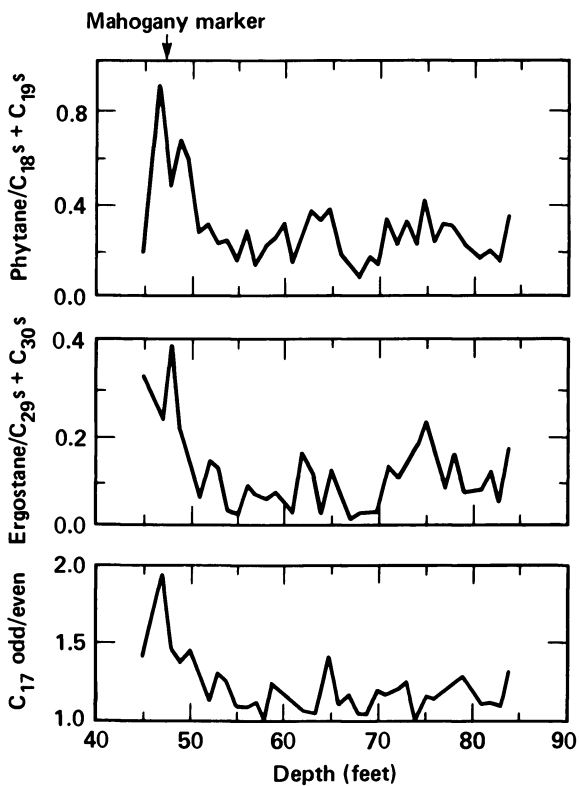
Figure 10. Plot of biomarker compounds vs. depth in Geokinetics core.

   The cross-correlation coefficients for all pairs of biomarker ratios, odd/even ratios, ene/ane ratios, shale grade, N/O.C. and depth were calculated for each core separately. A selected portion of this data is presented in Table III for comparison of the behavior of biomarkers relative to each other and to shale properties. This is a very abbreviated list of the cross-correlation data and represents either the best correlations in some cases or those with special significance. There was no consistent correlation of biomarkers in all three cores with grade or depth over the ranges investigated.

   In general, the correlations were similar for the three cores (Table III). The acyclic biomarkers correlated well with each other in most cases and these correlations were especially high for compounds differing by only one carbon number, i.e., pristanes to norpristane, farnesanes to trimethyltridecanes, phytane to pristane. Phytane to pristane correlated better in all cores than phytane to pristane+1-ene+2-ene. Ergostane correlates better than stigmastane with the acyclic biomarkers, the highest correlations being with the farnesanes and trimethyltridecanes. Stigmastane and ergostane correlate well with each other in all three cores. This consistency of correlation among like groups of biomarkers was also observed by Anders and Robinson (5). It may indicate separate source materials for the chain isoprenoids and the steranes and/or it may indicate a series of degradation products from a different precursor for each group.

   The five polycycloalkanes which were studied, but were not specifically identified, showed varying degrees of correlation from core to core. In NOSR core 15/16 all cross correlations between stigmastane, ergostane and the polycycloalkanes are greater than 0.55 and are as high as 0.92 for polycycloalkanes 1 and 2. This pattern did not hold true in the other two cores although there are a few strong correlations between pairs of polycycloalkanes. All cross correlations for polycycloalkanes not listed in Table III are less than 0.5 in both Geokinetics and NOSR core 25. Part of the lack of correlation may be due to overlapping peaks in this region. While specific-ion chromatograms from GC/MS would remove most of this problem, we had no practical way of using GC/MS on the large number of samples examined in this work.

   Two gas chromatograms showing the region of the steranes and polycycloalkanes for oils from NOSR core 15/16 are presented in Figure 11. One oil was produced from shale at 1208 feet (A-groove) with a grade of 9.1 gal/ton and N/O.C. ratio of 0.106, while the other oil was from shale at 1274 feet (Mahogany zone) with grade of 24.9 gal/ton and N/O.C. ratio of 0.037. There is a marked variation in the chromatograms of these two oils in this region which shows the changes in concentrations of the polycycloalkanes relative to the normal alkanes and each other. Although correlations of biomarker ratios with either shale grade or N/O.C.

Table III.   Correlation coefficients for selected variable pairs.

Variable 1[a]	Variable 2[a]	Coefficient, r Geokinetics core[b]	Coefficient, r NOSR cores 25[c]	Coefficient, r NOSR cores 15/16[d]
phytane	pristane	0.90	0.83	0.72
phytane	trimethylundec-2-ene	0.67	0.80	0.46
phytane	farnesane	0.65	0.80	0.60
phytane	trimethyltridecane	0.79	0.79	0.61
phytane	norpristane	0.77	0.68	0.46
phytane	pristane+1-ene+2-ene	0.67	0.79	0.50
pristane+1-ene+2-ene	trimethylundec-2-ene	0.85	0.84	0.95
pristane+1-ene+2-ene	farnesane	0.87	0.81	0.91
pristane+1-ene+2-ene	trimethyltridecane	0.83	0.81	0.91
pristane+1-ene+2-ene	norpristane	0.93	0.88	0.97
farnesane+1-ene	trimethyltridecane+1-ene	0.85	0.95	0.95
farnesane+1-ene	trimethylundec-2-ene	0.86	0.91	0.95
farnesane+1-ene	ergostane	0.39	0.82	0.70
trimethyltridecane+1-ene	trimethylundec-2-ene	0.80	0.92	0.93
tirmethyltridecane+1-ene	norpristane	0.89	0.88	0.93
trimethyltridecane+1-ene	ergostane	0.45	0.79	0.66
stigmastane	ergostane	0.79	0.84	0.81
stigmastane	polycycloalkane 1	0.39	0.78	0.72
stigmastane	polycycloalkane 2	0.42	0.58	0.75
stigmastane	polycycloalkane 3	0.30	0.18	0.87
stigmastane	polycycloalkane 4	0.04	0.09	0.70
stigmastane	polycycloalkane 5	0.10	0.40	0.58
polycycloalkane 1	polycycloalkane 2	0.85	0.64	0.92
polycycloalkane 1	polycycloalkane 5	0.73	0.56	0.59
polycycloalkane 2	polycycloalkane 5	0.57	0.20	0.66
polycycloalkane 3	polycycloalkane 4	0.35	0.57	0.84
nitrogen/org. carbon	stigmastane	0.36	0.42	0.41
nitrogen/org. carbon	ergostane	0.51	0.59	0.55
nitrogen/org. carbon	prist-2-ene/prist-1-ene	0.52	0.92	0.25
nitrogen/org. carbon	grade	-0.06	-0.65	-0.58
nitrogen/org. carbon	C_{17} odd/even	0.54	0.88	-0.08
grade	stigmastane	-0.44	-0.56	-0.52
grade	ergostane	-0.50	-0.61	-0.61

[a]For incomplete ratios, values reported are for ratios of biomarkers to the respective alkenes plus alkanes as expressed in Table 1.
[b]38 samples.
[c]45 samples.
[d]83 samples.
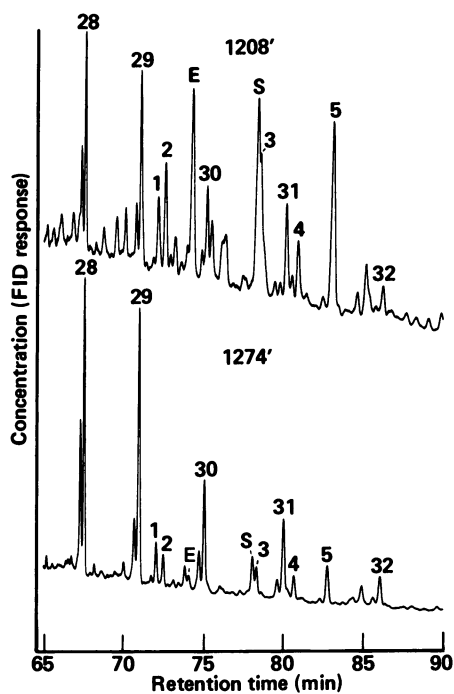
Figure 11. Capillary gas chromatograms of two oils from NOSR core 15/16 (1208 and 1274 ft) showing peaks for ergostane (E), stigmastane (S), n-alkanes (carbon chains 28–32) and cycloalkanes (1–5).

are highly variable from core to core, there may be some relation-
ship between one or both of these properties and the occurrence
of biomarker compounds.

Conclusions

We investigated some biomarkers present in oils produced
from three Green River formation cores using capillary column gas
chromatography and found strong correlations between acyclic
compounds and between the two sterane compounds in all three
cores. The biomarker compounds showed measurable changes in
their ratios to associated alkanes with stratigraphy, thus
supporting the validity of relating shale oils to their source
rocks using biomarker ratios. The possibility of using bio-
markers to relate time-dependent process variables to an oil
product, subject to indefinite migration times through an in-situ
retort, looks promising. Our only reservation in this regard is
that the high biomarker concentrations typically occur in regions
of low grade, the oil from which may be too highly diluted or
burned during processing to retain useful information. Further
research is necessary to resolve this question.

The three Green River formation cores show good agreement in
ranges and average values for the alkene/alkane ratios and odd/
even ratios of normal hydrocarbons across the resource. Of the
two groups of biomarker compounds studied, the chain isoprenoids
showed better agreement in ranges and averages than the steranes
and polycycloalkanes. This may be partially due to overlapping
peaks in the gas chromatograms of the steranes and higher alkanes.
The maximum variations in ratios of all three groups of compounds
occur near the Mahogany marker in many cases and in the NOSR
cores again near the top of the A-groove and near the bottom of
core 15/16. The relationship of variations in these biomarker
ratios in oil to other properties of the oil shale source
material could provide a better understanding of the structure
and geochemistry of kerogen.

Acknowledgments

Literature Cited

1. Tissot, B. P.; Welte, D. H. "Petroleum Formation and Occurrence"; Springer-Verlag: New York, NY, 1978.
2. Seifert, W. K.; Moldowan, J. M. Geochimica et Cosmochimica Acta 1981, 45, 783-794.
3. Burnham, A. K. and Clarkson, J. E. "13th Oil Shale Symposium Proceedings 1980, p. 269.
4. Burnham, A. K.; Clarkson, J. E.; Singleton, M. F.; Wong, C. M.; Crawford, R. W. Geochimica et Cosmochimica Acta 1982, 46, 1243-1251.
5. Anders, D. E.; Robinson, W. E. "Geochemical Aspects of the Saturated Hydrocarbon Constituents of Green Rover Oil Shale--Colorado No. 1 Core" U. S. Bureau of Mines Rept. of Inv. 7737, 1973.
6. Tissot, B. P; Deroo, G.; Hood, A. Geochimica et Cosmochimica Acta 1978, 42, 1469.
7. Gallegos, E. J. "Developments in Petroleum Science 5"; Yen, T. F.; Chilingarian, G. V. Eds.; Elsevier: New York, 1976, p. 149.
8. Cummins, J. J., Doolittle, F. G. and Robinson, W. E. "Thermal Degradation of Green River Kerogen at 150°C to 350°C" U. S. Bureau of Mines Rept. of Inv. RI 7924, 1974.
9. Seifert, W. K. Geochimica et Cosmochimica Acta 1978, 42, 473.
10. Burlingame, A. L.; Simoneit, B. R. Nature 1969, 222, 741.
11. Richardson, J. H.; Huss, E. B.; Ott, L. L.; Clarkson, J. E.; Bishop, M. O.; Taylor, J. R.; Gregory, L. J.; Morris, C. J. "Fluidized-Bed Pyrolysis of Oil Shale: Oil Yield, Composition and Kinetics" Lawrence Livermore National Laboratory Rept. UCID 19548, 1982.
12. Singleton, M. F.; Koskinas, G. J.; Burnham, A. K.; Raley, J. H. "Assay Products from Green River Oil Shale" Lawrence Livermore National Laboratory Rept. UCRL 53273, 1982.
13. Geokinetics, private communication 1982.
14. Smith, J. W. AAPG Bulletin 1963, 47, 804.
15. Giauque, R. D.; Fox, J. P.; Smith, J. W. "Characterization of Two Core Holes from the Naval Oil Shale Reserve Number 1" Lawrence Berkeley Laboratory Rept., LBL-10909, 1980.
16. "Standard Test Method for Oil from Oil Shale," D3908-80 Annual Book of ASTM Standards, 1980.
17. Smith, J. W.; Lee, K. K. 15th Oil Shale Symposium Proceedings 1982, p. 102.
18. Philp, R. P.; Calvin, M. in "Kerogenous Material in Recent Algal Mats at Laguna Mormona, Baja California"; ADVANCES IN ORGANIC GEOCHEMISTRY 1975, Ensidema Publishing Co.: Madrid, Spain, 1977.
19. van Graas, Ger; de Leeuw, J. W.; Schenck, P. A.; Haverkamp, J. Geochimica et Cosmochimica Acta 1981, 45, 2465.
20. van de Meent, Dik; Brown, S. C.; Philp, R. P.; Simoneit, B. R. T. Geochimica et Cosmochimica Acta 1980, 44, 999.

21. Connan, J.; Cassou, A. M. Geochimica et Cosmochimica Acta 1980, 44, 1-23.
22. Cane, R. F. "Developments in Petroleum Science 5"; Yen, T. F. and Chilingarian G. V., Eds.; Elsevier: New York, 1976, Chap. 3.
23. Vandegrift, G. F.; Winans, R. E.; Scott, R. G.; Horwitz, E. P. Fuel 1980, 59, 627.
24. Burnham, A. K.; Singleton, M. F. "Chemistry and Geochemistry of Oil Shale"; Miknis, F.; McKay, J., Eds.; ACS SYMPOSIUM SERIES, ACS:Washington, D. C., 1983.
25. Larter, S. R., Solli, H., Douglas, A. G., DeLange F. and de Leeuw, J. W. Nature 1979, 279, 405-8.
26. van de Meent, D., de Leeuw, J. W. and Schenck, P. A. "Advances in Organic Geochemistry 1979"; Pergamon: London, 1981, p. 469.
27. Larson, O. A., Wen, C. S. 14th Oil Shale Symposium Proceedings 1981, Colorado School of Mines Press, Golden, p. 61.
28. Cooper, J. E.; Evans, W. S. Science 1983, 219, 492.
29. Larter, S. R. Internat. Anal. Pyrolysis Meeting, Vail, CO. 1982.

Ferric Chloride–Clay Complexation Method

Removal of Nitrogen-Containing Components from Shale Oil and Related Fossil Fuels

TEH FU YEN, FENG-FANG SHUE,[1] WEN-HUI WU,[2] and DONGJAW TZENG

University of Southern California, School of Engineering, Los Angeles, CA 90089-0242

Nitrogen-containing compounds in shale oil were con-
centrated by $FeCl_3$-clay complexation chromatography.
Similarly the nitrogen compounds were also inves-
tigated from petroleum as well as coal liquids.
Comparison was made for the separation ability from
different transition metal chloride-clay complexa-
tions. Based on GC/MS peak identification, several
pyridines, quinolines, and their benzologues were
identified.

Nitrogen-containing compounds always pose problems for oil
refinery industry via catalyst poisoning (1). Their combustion
products also cause great concern in air pollution (2). Due to
higher nitrogen content in shale oil and coal liquid (1-2%) than
in crude oil (<0.5%), it is essential to lower the nitrogen
content in shale oil before any refinery processes are performed.
Methods have been developed for the separation of the heavy-
end distillates of crude oil (1-3). Anion-exchange resin, cation-
exchange resin, $FeCl_3$-Clay complexation and silica gel were used
with different acidity and basicity. This separation scheme is
very useful in compound identification. Our interest is to find
a much simpler way to achieve the removal of nitrogen-containing
components from fossil fuels. Previously, we reported that by
using a ferric chloride-clay complexation chromatography column,
the nitrogen content in deasphalted shale oil was concentrated in
certain portions of eluents. The mechanism of the concentrating
process is attributed to the fact that the nitrogen containing
compounds (electron rich) are basic toward ferric ions (electron
deficient) and hence more polar solvents are needed to elute
them out (4). In this paper, we would like to extend our work

[1]Current address: UOP Corporate Research Center, 30 Algonquin Rd., Des Plaines, IL 6101
[2]Current address: Research Institute of Petroleum Processing, P.O. Box 914, Beijing, China

to other fossil fuels, namely crude oil, coal liquid, and shale
oil. All these crudes were used without deasphalting. The
results from deasphalted shale oil are cited frequently for the
purpose of comparison. Other transition metal chlorides, such
as $CoCl_2$, $NiCl_2$, and $MoCl_3$, are also used in the nitrogen
concentrating processes.

       After the nitrogen concentrating process, a nitrogen-rich
portion was further separated into subfractions of intrinsic
basic nitrogen compounds and basic nitrogen compounds after
reaction with lithium aluminum hydride (LAH). The intrinsic
basic compounds are those extractable by HCl solution. Several
nitrogen compounds from these subfractions were identified by
GC/MS analyses and different types of nitrogen compounds in
different subfractions were discussed.

Experimental

Reagents. Shale oil used in this study was obtained by retorting
at $500^\circ C$ the Green River Oil Shale from Anvil Point, Colorado.
Petroleum Crude oil was obtained from Long Beach Field,
California. Coal liquid was obtained from the PAMCO process.
All oil samples were subjected to vacuum distillation at $100^\circ C$/
1 torr to remove volatile material. $FeCl_3$-clay was prepared by
contacting the attapulgus clay (Engelhard Minerals and Chemicals)
for 1 hour with a methanolic ferric chloride solution (Saturated
$FeCl_3 \cdot 6H_2O$ in methanol). The $FeCl_3$-clay was filtered, washed,
and extracted with pentane for 48 hours in a Soxhlet extractor
to remove entrained, non-adsorbed iron salts, then dried under
nitrogen. Amberlite IRA - 904 anion exchange resin (Rohm and
Haas) was washed with a 1 N methanolic HCl solution and then
rinsed with distilled water until the washings were neutral to
litmus paper. Final preparation of the resin was made by 24-
hour Soxhlet extraction successively with each of the following
solvents: methanol, benzene, and cyclohexane. The alumina
(Alcoa F-20, Aluminum Co. of America) was activated at $200^\circ C$ for
24 hours and subsequently deactivated by adding 4ml of water per
gram of adsorbent under nitrogen. The treated alumina was
allowed to stand for 24 hours in a sealed container before use.
Alumina and silica gel cartridges (Waters Associates Inc.) were
used for purification of the base samples.

$FeCl_3$-clay chromatography: All fossil oil samples were frac-
tionated into three fractions, P_0, P_1, and P_2 in the manner
described below: Approximately 8 g of sample was charged on 80g
of $FeCl_3$-clay column under nitrogen pressure. The first fraction
P_0, referred to as the hydrocarbon fraction, was obtained by
eluting the column with cyclohexane. The first polar fraction
P_1, was obtained by eluting with 1,2-dichloroethane followed by
contacting the eluent with the anion exchange resin to remove
the iron salts. The second polar fraction, P_2, was eluted with

50% ethanol – 45% toluene – 5% water. Solvents in each fraction were removed by rotary evaporation. The residue was redissolved in toluene and the solution was filtered to remove most of iron salts. Residual iron was removed by passing through the anion exchange resins.

Isolation of Intrinsic Basic Nitrogeneous Components: P_1 was chosen for base isolation. P_1 was dissolved in toluene and exhaustively extracted with 2N HCl in 67% methanol. The base fraction designated as B_1 was recovered by neutralization and extraction with toluene. B_1 was charged on an alumina column and then percolated with toluene. A silica gel cartridge was used for further purification and fractionation. The fraction eluted from alumina by toluene was rotary evaporated to remove toluene, redissolved in hexane, and then charged to the silica gel cartridge. The following solvents were used in sequence to give the indicated subfractions: 10% $^v/_v$ $CHCl_3$–90% hexane (N_0), 20% $^v/_v$ $CHCl_3$–80% hexane (N_1), and $CHCl_3$ (N_2). The N_0 subfraction, containing mainly hydrocarbons, was discarded. N_1 and N_2 were called intrinsic basic subfractions.

Isolation of Basic Nitrogen Compounds after LAH Reduction: The first polar fraction after removal of bases, B_1, was used for LAH reduction. The reduction was carried out with a 5:1 LAH to sample ratio using freshly distilled THF as the solvent. The reaction was continued for 48 hours at THF refluxing temperature under dry nitrogen. After hydrolysis, neutralization, filtration and extraction, the products were collected and dissolved in toluene and again exhaustively extracted with 2N HCl in 67% methanol. The extracted bases, designed as B_2, were purified by alumina column and silica gel cartridge and then eluted with 10% $^v/_v$ $CHCl_3$–90% hexane (N_0). Basic nitrogen compounds (N_3) were obtained by eluting with $CHCl_3$ from a silica gel cartridge. All fractions and subfractions are listed in the flow chart in Figure 1.

Elemental Analysis: Elemental analyses were performed by Huffman Laboratories, Inc., Wheat Ridge, Colorado. Total nitrogen was determined using the Dumas method. Total organic oxygen content was determined by difference based on ash–free samples.

Gas Chromatography/Mass Spectrometry: The GC column was a 30m, 0.25 mm i.d. fused silica capillary column coated with SE–54 and was coupled directly to the Finnigan Model 4000 mass spectrometer interfaced with a data system containing the NBS computer library. The oven temperature program was from 100°C (hold 2 min) to 260°C (hold 20 min) with a linear heating rate of 10°C/min. Mass spectra were obtained by EI mode at 70eV.
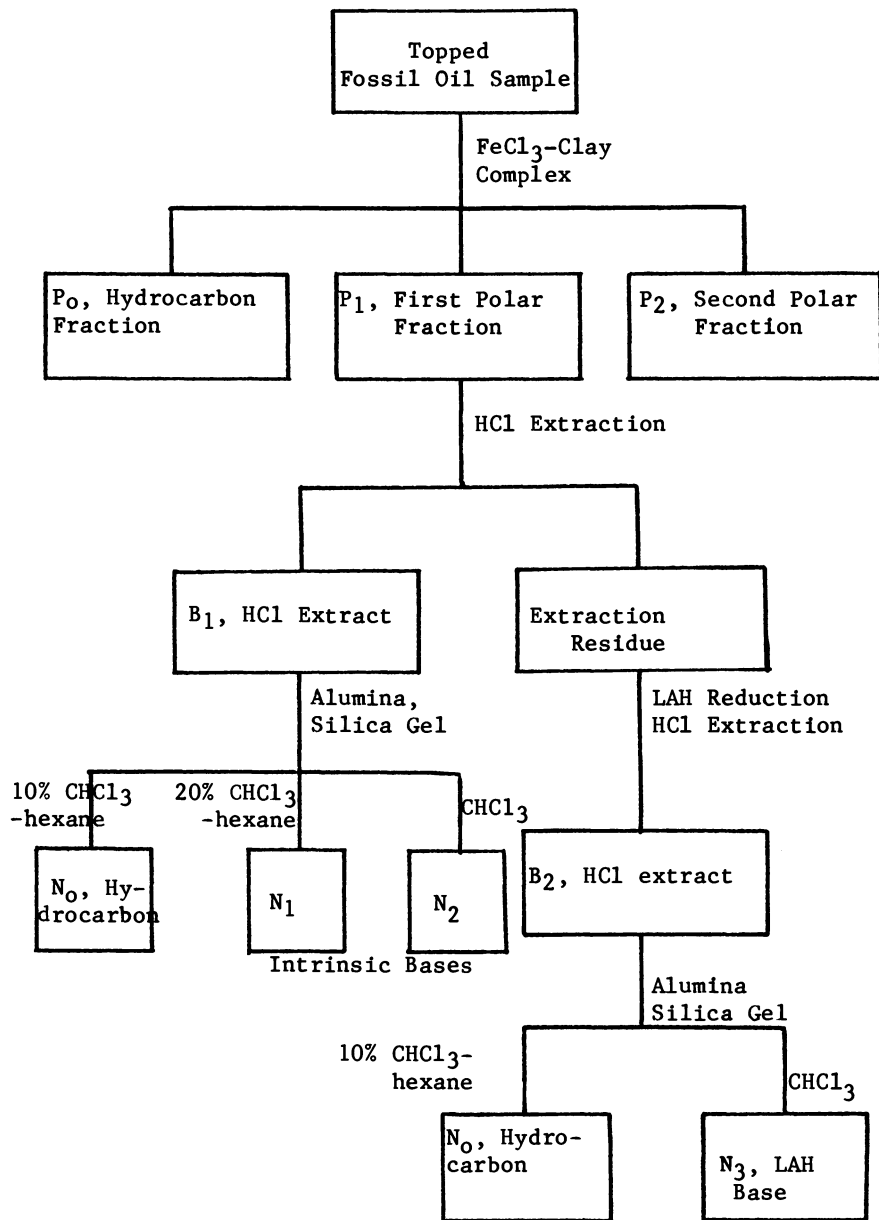
Figure 1. Separation of nitrogen compounds.

Results and Discussion

Results of total nitrogen analysis for fractions from all
fossil oil samples by using FeCl3-clay chromatography are listed
in Table I. Also in Table I, Np_1/Np_0 is a parameter measuring the
ratio of nitrogen content in the first polar fraction and the
hydrocarbon fraction. High P_0 recovered percentage weight (%wt),
low P_0 nitrogen content (%N), and high Np_1/Np_0 value are charac-
teristic of a good separation column. Clearly, the FeCl3-clay
chromatography is excellent for the crude oil sample. For the
two shale oil samples, the nitrogen components are much better
separated in the case of the non-deasphalted sample (in terms of
Np_1/Np_0, 24 to 5.7 in favor of the non-deasphalted sample).
However the deasphalted sample has higher p_0 recovered percentage
weight. With extremely low p_0 nitrogen content (0.15%) from the
shale oil sample, it is believed that with some modification on
the eluting solvent system, a much higher p_0 recovery percentage
weight can be achieved with nitrogen content in the comparable
range. The coal liquid sample yields only 40% p_0 with excellent
nitrogen content (0.11%). A different eluting solvent system is
believed to be the solution to increase yield on p_0. A new study
on eluting solvent system is initiated for achieving higher yield
on p_0 while keeping comparable nitrogen content. We also want to
point out that in all three non-deasphalted cases, the total
nitrogen recovery percentage is less than 80%. We assumed that
a large portion of nitrogen-rich compounds is retained in the
FeCl3-clay column. In the case of shale oil, 8.3% of the total
material was retained in the column, while 36% of the total
nitrogen was retained. That translates into 8.4% nitrogen content
for the material retained in the column. This unexpected result
is only a preliminary one. More work is to follow.

The same separation scheme was followed by three other
transition metal-clay complexation columns. The results are
shown on Table II. Among these complexes, FeCl3 is by far the
best to achieve our goals. Roughly, the nitrogen concentrating
ability by clay columns is decreasing in the following order:
crude oil > shale oil ≃ deasphalted shale oil > coal liquid.

From GC/MS results, shown on Table III, we conclude that the
pyridine ring is the major structure of these intrinsic basic
nitrogen components. Alkyl pyridines having substituents ranging
from C_5 to C_{12} were detected for the N_1 subfractions. Alkyl-
quinolines and/or alkylisoquinolines having substituents ranging
from C_1 to C_3 together with their higher benzologs were identified
in the N_2 subfractions. Two aromatic amines, N-ethyl-tetrahy-
droquinoline and N-ethyl-4-methyltetrahydroquinoline were ten-
tatively identified in the N_3 subfraction. Possible precursors
leading to these compounds are amides as compound A or B in
Fig. 2-a.

Alkylpyridines constituted the major part of N_3 subfractions.
One reasonable precursor is compound C in Figure 2-b. The
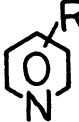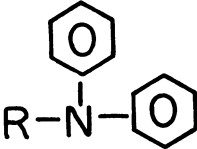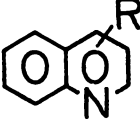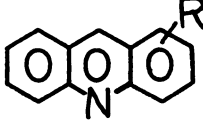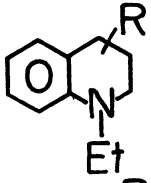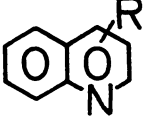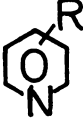
Table I.   Nitrogen Content and Separation Ability of $FeCl_3$-
           Clay Chromatographic Column on Fossil Oil Samples

Sample	%wt	%N	Np_1/Np_0	%N recovery
Crude oil		0.86		
P_0	66.7	0.05	39	78
P_1	33.0	1.94		
Shale oil		1.94		
P_0	59.6	0.15	24	64
P_1	32.2	3.60		
Coal liquid		1.35		
P_0	40.0	0.11	15.5	62
P_1	26.0	1.71		
P_2	26.2	1.32		
Deasphalted Shale oil		1.70		
P_0	78.0	0.76	5.7	95
P_1	15.6	4.35		
P_2	6.4	5.49		

Table II. Fractionation of Fossil Oils by Transition
Metal Chlorides–Clay Chromatography

Sample	FeCl$_3$			CoCl$_2$			NiCl$_2$			MoCl$_3$		
	% Wt.	%N	NP$_1$/NP$_0$	% Wt.	%N	NP$_1$/NP$_0$	% Wt.	%N	NP$_1$/NP$_0$	% Wt.	%N	NP$_1$/NP$_0$
Crude Oil												
P$_0$	66.7	0.05	39	70.1	0.18	9.8	75.4	0.22	7.9	75.8	0.20	15.5
P$_1$	33.0	1.94		25.4	1.77		29.8	1.75		15.1	3.10	
P$_2$										11.4	0.66	
Shale Oil												
P$_0$	59.6	0.15	24	59.3	0.27	11.6	59.0	0.20	15.2	66.2	0.29	11.5
P$_1$	32.2	3.60		43.9	3.12		38.1	3.04		7.9	3.03	
P$_2$										15.7	2.88	
Coal liquid												
P$_0$	40.0	0.11	15.5									
P$_1$	26.0	1.71										
P$_2$	26.2	1.32										

Table III. Nitrogen Compounds Identified from GC/MS

Class	Type	Skeleton	Substituents
Intrinsic Basic Compound	N_1		C_5 to C_{12}
			Methyl
Intrinsic Basic Compound	N_2		2-methyl, 3-methyl, 4-methyl, Dimethyl, trimethyl, or ethyl-methyl
			H, methyl
LAH Basic Compounds	N_3		4-methyl
			trimethyl, ethyl-methyl and C_4-alkyl
			C_8 to C_9 alkyl
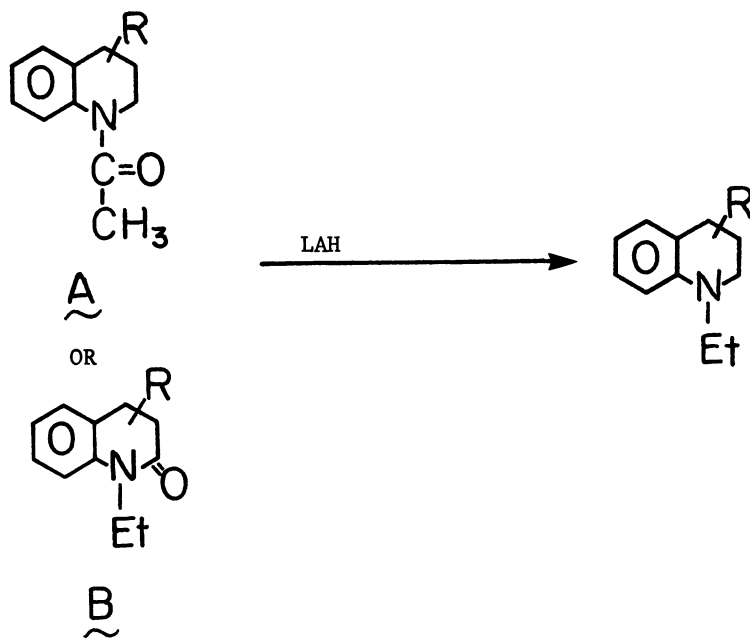
Figure 2-a
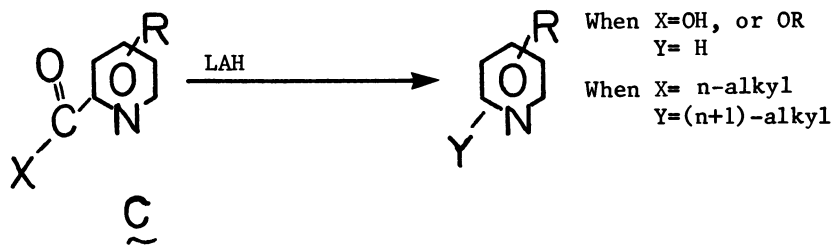
Figure 2-b

Figure 2. Structure of possible precursors for aromatic amides (a) and carbonyl pyridines (b).

carbonyl groups in compounds A,B, and C reduce the basicity on the nitrogen atom and hence prevent those compounds from being extracted into the HCl layer as intrinsic basic components. These results support Poulson's report that pyridines were the major nitrogen compounds in shale oil (5).

Conclusions

Three conclusions are drawn:

1.   The $FeCl_3$-clay chromatography column has been developed for the reduction of nitrogen content and a practical denitrogenation process can be developed.
2.   For the removal of nitrogen containing compounds, the $FeCl_3$-clay column appears to be an alternative to the costly exhaustive catalytic hydrogenation which is currently used.
3.   Lithium aluminum hydride would prompt the removal of nitrogen containing compounds by simple extraction.

Acknowledgments

Literature Cited

1.   Jewell, D.M.; Weber, J.H.; Bunger, J.W.; Plancher, H; Latham, D.R., Anal. Chem., 1972, 44, 1391.
2.   Hirsch, D.E.; Hopkins, R.L; Coleman, H.J.; Cotton, F.P; Thompson, C.J. Anal. Chem. 1972, 44, 915.
3.   Suatoni, J.C.; Swab, R.E. J. Chromatogr. Sci. 1976, 14, 535.
4.   Shue, F.F.; Yen, T.F. Anal. Chem. 1981, 53, 2081.
5.   Poulson, R.E.; Frost, C.M.; Jensen, H.B. in "Shale Oil Tar Sands and Related Fuel Sources"; Yen, T.F., Ed. American Chemical Society: Washington, D.C., 1976; Adv. Chem. Ser. pp 1-10.

Petrology of Spent Shale—A Review

THOMAS R. WILDEMAN and DANIEL C. MELCHIOR

Colorado School of Mines, Department of Chemistry and Geochemistry, Golden, CO 80401

From metamorphic and igneous petrology, an anal-
ysis is made of what minerals should be present
in spent shale. Many of the traditional methods
used in metamorphic petrology are inappropriate
because fluid pressures are so low and spent
shales are highly undersaturated with respect to
SiO_2 However, decarbonation reactions found in
the metamorphism of carbonate rocks allow more
possibilities than are typically suggested for
oil shale. From igneous petrology, the pyrox-
enes and olivines found in spent shale are con-
firmed, but nepheline and leucite should be pre-
sent but are not usually discovered. Melilite,
which is ubiquitous to spent shale, is found in
metamorphic and igneous rocks formed under simi-
lar circumstances.

Recently, studies have been made on the mineralogy of spent
shale for a number of reasons. Some research groups, such as
those at Lawrence Livermore Laboratories, have attempted to better
define the energy balance and kinetics of oil shale retorting ([1-
3]). Other studies have concentrated on how the evolved gases
might react with the minerals or how the minerals might control
what gases are evolved ([4-6]). Another objective has been to
determine how the minerals formed during retorting might affect
the environment by gas evolution or the leaching of spent shale
([7-11]). Control of the minerals that are formed during oil shale
retorting appears to be a key factor to economic and environmental
success of this industry.
     In petrology one takes data from the rock – such as chemical
composition, mineralogy, and grain relationships – and tries to
establish how the rock evolved. Of the tools used in petrology,
thermodynamics and chemical reaction relations are the two most
useful ([12-15]). In the case of spent shale, temperatures of 500°C

and higher are involved and this is in the realm of igneous and
metamorphic petrology. In these areas of petrology, innumerable
laboratory studies of silicate systems have been made and, for
most rocks formed at high temperatures, a good guess can be made
on what the stable minerals should be (12-15).
     This paper begins the attempt to join what is known in ig-
neous and metamorphic petrology with what has been learned about
the composition and mineralogy of spent shale. The purpose of
this joining is to establish what minerals should be stable in
spent shale formed under various conditions. If that can be
established, then studies can be made on whether the stable mine-
rals would require excessive energy to be formed; on whether the
gases released in forming these minerals would be deleterious to
the product oil or to the environment; on whether the stable
minerals would be good hosts for environmental-problem elements
such as fluorine, boron, molybdenum, and arsenic; and on whether
the stable minerals are susceptible to leaching by ground waters.
With this information, assessments can be made on whether it is
advantageous to form the stable minerals in spent shale or whether
retorting should be adjusted to form the intermediate products.
This paper attempts to put the study of spent shales on grounds
that are more familiar to other geochemists.

The Chemical Data

     Among the many analyses of raw and spent shales, the suite of
samples studied by Fox (8) represent a wide range of Colorado
shales which have been accurately analyzed. For this study, three
Colorado shales and one Moroccan shale were chosen from Fox's
suite. The Moroccan shale is CS-65; the three Colorado shales are
CS-62 (low SiO_2), CS-60 (median SiO_2), and CS-64 (high SiO_2).
     For this petrologic analysis, the elemental abundances have
been adjusted from the reported spent shale analyses. First, only
the nonvolatile major elements (Si, Al, Fe, Mg, Ca, Na, K) are
considered. Volatile major elements such as H, C, N, S, and P are
eliminated. The major element break is made at Ti which rarely
exceeds 0.20% in spent shales (8). Next, the percentages of
oxides are calculated and for this iron is considered as FeO.
Then, the percentages are summed and normalized to 100%. The
purpose for these adjustments is to make the normative mineral
calculation for the rocks.
     A normative mineral calculation - or norm - is a casting of a
rock analysis into a hypothetical assemblage of standard minerals
(12-14). The norm should be distinguished from the mineral assem-
blage that is actually present which is termed the mode. Some
simplifications are used to calculate a norm (12). The important
assumptions for this paper are that anhydrous conditions prevail
so no hydrous phases are formed and that ferromagnesium minerals
are free of Al_2O_3 and all the Al_2O_3 goes to feldspars. Although
a norm calculation is hypothetical, it often shows a close

correspondence with the modal mineralogy. Also, normative
calculations serve as a good foundation for considering mineral
reaction possibilities in igneous and metamorphic petrology.

Table I presents the actual elemental abundances for the four
spent shales (8). Then the percentages of oxides normalized to
100% are given. Finally, the normative mineral assemblages are
given using the rules established by Cox and others (12). Table I
serves as the basis for much of the discussion that follows.

Ground Rules for Possible Models

Possibilities for retort conditions and spent shale compo-
sitions can be almost endless. The previous section established
some limits on composition. This section establishes more of the
assumptions that will be made for this petrologic analysis. As
with all studies of this type, some of the ground rules will be
based on obvious retort conditions and other will be gross pre-
sumptions that must be made to have reality fit theory.

Undoubtedly, the worst assumption that is made in this paper
is that the kinetics of mineral reactions are irrelevant and that
all reactions have had sufficient time to proceed. In other
words, the mineral phases are themodynamically and not kinetically
controlled. Although this assumption is in error for an oil-shale
retort, it does allow for two consequences of special merit.
First, this assumption allows one to use all the thermodynamic
data from petrology; and second, it allows one to establish what
the stable minerals should be if reactions proceeded to their
conclusion. This is an assumption often made to determine how
rocks are similar or different from the typical systems (12-15).

Ground rules on temperature and pressure are set by typical
retort conditions. For pressure, this is 1 atmosphere; for tem-
perature, this is 500-800°C (7). The composition of the gas is
more difficult to establish, but for this study, it is assumed
that most of the hydrocarbons have been pyrolyzed from the system
and that reactions with the carbon char are taking place. This
establishes the primary volatiles as CO, CO_2, H_2O, and H_2 in roughly
equimolar amounts. This assumption is based on typical retort gas
analyses (16) and on laboratory studies of oil shale pyrolysis (5,
17). Establishing a more limited range on the temperature is
dictated by that temperature at which decarbonation is definitely
complete. This will be discussed later in the paper. For now,
it's assumed that decarbonation is complete and that the tempera-
ture needed for this is at least 600°C.

In igneous and metamorphic petrology, the oxygen fugacity is
considered to be an important parameter indicating the fate of
iron minerals in a rock system (13, 15). For example in a norma-
tive calculation, if iron exists as Fe(III) it is assigned to the
oxides hematite (Fe_2O_3) and magnetite (Fe_3O_4) whereas Fe(II) is
assigned to magnetite (Fe_3O_4) and silicates. In a recent paper,
the authors pointed out the dichotomy that exists between the

Table I. Chemical Data on Spent Shales Adapted from Fox (8).

	Colorado Shales			Moroccan Shale
	low SiO_2	median SiO_2	high SiO_2	
Element	Original Abundances in Percent			
Si	15.4	17.4	18.1	13.8
Al	3.84	4.58	4.87	4.51
Fe	2.00	2.48	2.99	2.33
Mg	4.45	4.11	3.86	2.64
Ca	14.2	10.8	8.04	14.8
Na	1.91	2.28	3.36	0.14
K	1.38	1.93	1.51	0.86
Oxide	Oxide Abundances Normalized to 100%			
SiO_2	44.3	48.7	51.1	43.8
Al_2O_3	9.77	11.3	12.1	12.6
FeO	3.46	4.18	5.08	4.46
MgO	9.94	8.91	8.45	6.50
CaO	26.8	19.8	14.8	30.8
Na_2O	3.46	4.02	5.98	0.28
K_2O	2.24	3.05	2.40	1.54
Mineral	Normative Mineral Abundances in Percent			
orthoclase	-	-	9.45	-
leucite	10.5	14.0	3.49	6.98
nepheline	15.9	18.5	27.0	1.13
anorthite	4.4	3.89	-	28.9
diopside	26.8	46.5	59.0	24.5
olivine	17.0	5.45	1.25	8.52
monticellite	29.2	12.7	-	28.4

Normative Mineral Formulas

orthoclase	-	$KAlSi_3O_8$	diopside	-	$Ca(Mg,Fe)Si_2O_6$
leucite	-	$KAlSi_2O_6$	olivine	-	$(Mg,Fe)_2SiO_4$
nepheline	-	$NaAlSiO_4$	monticellite	-	Ca_2SiO_4
anorthite	-	$CaAl_2Si_2O_8$			

Other Minerals of Interest

talc	-	$Mg_3Si_4O_{15}(OH)_2$	gehlenite	-	$Ca_2Al_2SiO_7$
wollastonite	-	$CaSiO_3$	akermanite	-	$Ca_2(Mg,Fe)Si_2O_7$
melilite	-	$(Ca,Na)(Mg,Ca,Fe)(Al,Si)SiO_7$			

oxygen fugacities derived from studies of the iron minerals found
in spent shale and oxygen fugacities derived from the composition
of gases in an oil shale retort (4). The minerals show a higher
oxidation where hematite and magnetite are stable whereas the
gases predict that Fe(II) should be the predominant species.
Eugster (18) developed the ideas in Figure 1 which shows the
oxygen fugacity in various iron mineral systems that could act as
oxidation-reduction buffers. Figure 2 shows what the oxygen
fugacity would be by applying the ideas in Figure 1 and what it
would be by considering the gas equilibria. The gap is awesome.
Because of this dilemma the oxygen fugacity cannot be firmly
established. Consequently, in this paper all the iron is made
Fe(II) to see in what possible silicate minerals iron could re-
side.

Petrologic Interpretation of Spent Shales

Ideas from Metamorphic Petrology.

In metamorphic petrology, it is
almost always assumed that there is a finite fluid pressure and
that fluid contains H_2O and, in the case of carbonate rocks,CO_2
(15, 19). In these cases, a finite pressure is typically defined
as 1000 atmospheres (15). In oil-shale retorting, the pressure
rarely exceeds one atmosphere. For spent shales, this makes
analyses of what should happen on the basis of metamorphic petro-
logy quite difficult. Essentially, the spent shale system is a
very shallow anhydrous system and little study is made of such
systems. Of particular importance is the concept of water always
being present to promote crystal reactions and allow the possi-
bility of the formation of hydrous materials. Except for the case
of steam retorting, the amount of water available is less than one
atmosphere (5, 16, 17) and this makes the formation of hydrous
minerals difficult. Also, since the pressure of CO_2 is less than
one atmosphere, decarbonation reactions are accelerated over what
is found in the metamorphism of carbonate rocks. Studies on the
heating of oil shale over different gases have confirmed this
observation (1, 11).

Another popular concept for analyzing metamorphism can also
be eliminated for spent shales. In the majority of cases, the
progression of metamorphism from low temperatures to high is
followed by graphical representations of the abundances of the
oxides in the rocks. The ACF (Al_2O_3, CaO, FeO) and AKF (Al_2O_3,
K_2O, FeO) diagrams are the prime examples of this type of analysis
(15). Howver, graphical analyses such as these depend upon there
being enough SiO_2 in the rock that free quartz can be formed
(15). From an investigation of Table I, it is seen that the
abundance of SiO_2 in spent shale is very low. What this means
will be discussed in the next section. For now, notice none of
the rocks have quartz as a normative mineral. Consequently,
metamorphic analysis through the use of graphical representations
is eliminated.
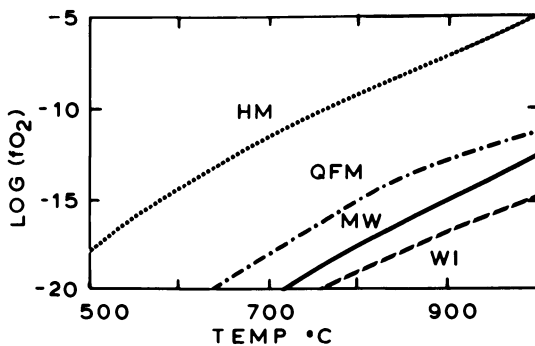
Figure 1. Values of the oxygen fugacity in various Fe–O–Si buffer systems. Key: F, fayalite; H, hematite; I, iron; M, magnetite; Q, quartz; and W, wustite.
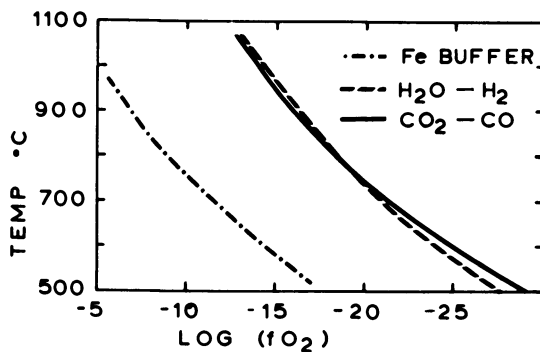
Figure 2. Values of the oxygen fugacity in spent shale determined from mineral equilibria and from gas equilibria.

Where metamorphic petrology is of obvious help is in the area of decarbonation reactions. Although fluid pressures are higher, there are well known reaction sequences. In particular the reaction:

$$CaCO_3(s) + SiO_2(s) \rightarrow CaSiO_3(s) + CO_2(g) \qquad (1)$$
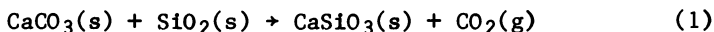
is the preferred method by which calcite loses CO_2 whenever quartz is present ([15], [18]). Indeed, Campbell ([1], [2]) and Park ([11]) have presented evidence that calcite is decarbonating during retorting by this reaction or something similar. With regard to the decarbonation of dolomite, Campbell presents evidence that the following reaction occurs:

$$CaMg(CO_3)_2(s) \rightarrow CaCO_3(s) + MgO(s) + CO_2(g) \qquad (2)$$
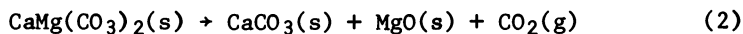
Winkler ([15]) and Mueller and Saxena ([19]) suggest that reaction (1) occurs at a lower temperature than reaction (2). Also if any water is present, the reaction of dolomite to form talc occurs at temperatures of about 300°C:

$$3CaMg(CO_3)_2 + 4SiO_2 + 1H_2O(g) = Mg_3Si_4O_{15}(OH)_2(s) +$$

$$\text{talc}$$

$$3CaCO_3 + 3CO_2(g) \qquad (3)$$
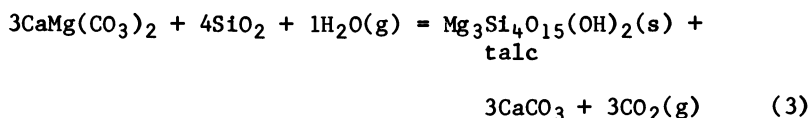
If oil shale is retorted in the presence of steam, dolomite would disappear, calcite would still form, but the other product could be talc instead of MgO. X-ray diffraction evidence ([15], [20]) suggests that reaction (2) is favored over reaction (3) even in the presence of steam.

The above discussion suggests that there may be a number of reaction paths by which dolomite and calcite can decarbonate. Campbell has presented the evidence for reactions (1) and (2) being spontaneous at 600°C and at 1 atm pressure ([1], [20]). Metamorphic studies give arguments for all three of the above reactions having equilibrium constants greater than one at 600°C and 1 atm ([15], [19]). The conclusion is that, from a thermodynamic viewpoint, decarbonation of oil shale should be complete at 600°C.

Ideas from Igneous Petrology. A major concept in determining the course of mineral crystallization is whether the magma is saturated with silica ([12], [13], [19]). Silica-rich rocks contain pyroxenes, feldspars, and free quartz while silica-poor rocks contain olivine and feldspathoids. Although the division depends on the complete composition, it is usually around 50% SiO_2. The spent shales in Table I and all spent shales from economic grade oil shales are undersaturated with respect to SiO_2. The undersaturation is due not only to the low abundance of SiO_2 but also

to the high abundance of calcium in comparison to the other
metals, particularly aluminum. Silica undersaturation has a
primary effect on what minerals are thermodynamically feasible in
spent shale.

At 600°-800°C if reactions are allowed to be controlled only
by thermodynamics, the following should be true. There should be
no free quartz and the complete elimination of quartz has been
observed in spent shale mineral reactions ([10], [11], [20]). Ortho-
silicates such as olivine and monticellite will be present and
this also has been observed in spent shale studies ([9],[10], [11], [20]).
If Na and K concentrations are at typical levels, the feld-
spathoids leucite and nepheline should be present. Although there
may be reasons for nepheline not appearing, K is a large ion and
leucite is the only reasonable host for it in oil shales with
low SiO_2 abundance. Leucite has been observed in one study of
spent shale mineralogy ([10]).

A mineral which consistently appears in spent shales but
which is not commonly studied is melilite - (Ca,Na)(Mg,Ca,Fe)
(Al,Si)SiO_7 ([10], [11], [20]). Melilite is found in certain basalts
with low SiO_2 abundance ([13], [19]) and also in carbonate rocks that
have been metamorphosed at low pressures and high temperatures
([15]). Rittman ([14]) describes the formation of melilite type
minerals by the desilication of pyroxenes:

$$4CaMgSi_2O_6 - 3SiO_2 \rightarrow 2Ca_2MgSi_2O_7 + Mg_2SiO_4 \qquad (4)$$
diopside   quartz   akermanite   forsterite
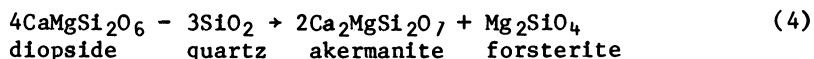
or by the accommodation of lime from calcite by pyroxenes:

$$CaMgSi_2O_6 + CaCO_3 \rightarrow Ca_2MgSi_2O_7 + CO_2 \qquad (5)$$
diopside   calcite   akermanite
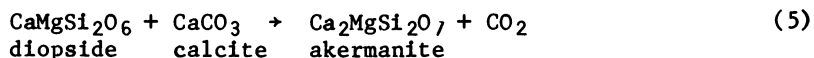
In these examples akermanite is a mineral in the melilite group.
When comparing the conditions for the formation of spent shale
with the above situations, melilite is an obvious possibility.

Even though melilite minerals are not common, Yoder ([21]) has
extensively studied the conditions of their occurrence. Conse-
quently, a great deal is known about the conditions under which
they are stable, especially in magmatic rocks. The information
should be useful for answering questions concerning melilite in
spent shales. Among the questions to be answered are: 1) Is
melilite formed at the expense of nepheline, or can the minerals
coexist? 2) Since it appears that melilite can accommodate a
number of different cations, is it a suitable host for copper,
zinc, cadmium, or boron which are of environmental interest?
3) If reaction (5) is the pathway of melilite formation in spent
shale, does the reaction occur in one step or does CaO form first
and then melilite?

Summary

This analysis of spent shale from a more formal viewpoint has verified many of the reactions and minerals that have been observed. The decarbonation reactions are realistic, the pyroxenes and olivines that are observed should be stable under the conditions of spent shale formation, and free quartz is readily used up to form the minerals found in spent shales. Also, the melilite which is ubiquitously found in spent shales appears to be a reasonable product, however more study should be made in the literature about melilite to see if it is stable under typical retort conditions.

Within the realm of research on linking spent shale composition to oil shale retorting, this exercise uncovered some areas that require more study. Research ideas on melilite were delineated in the previous section. The area of oxygen fugacity in a retort requires considerable research. How the oxidation states of nonvolatile elements can be linked to the retort gases and under what conditions might the oxidation state of mineral iron change are both questions that need to be answered. Concerning decarbonation, there are possible reactions that can occur under steam retorting that would make decarbonation of dolomite proceed at much lower temperatures. The question of whether these reactions are feasible should be investigated. From preliminary calculations, it appears that SiO_2, MgO, and CaO should not be present as final minerals in spent shale. How they are incorporated into silicates needs study. From a petrologic analysis, leucite and nepheline should occur in spent shales. The presence of these minerals should be more definitely confirmed since their structures offer good sites for elements of environmental concern.

It appears that many of the reactions forming the minerals in spent shale have been discovered and are corroborated from a petrologic analysis. However, this success makes the study of other possible reactions a reasonable approach to the study of how the formation of spent shale can help make oil shale retorting a commercial possibility.

Acknowledgments

Literature Cited

1. Campbell, J.H. "The Kinetics of Decomposition of Colorado Oil Shale: II. Carbonate Minerals"; UCRL Report No. 52089, 1978; 53 pp.
2. Campbell, J.H.; Burnham, A.K. Proc. 11th Oil Shale Sym., Colorado School of Mines Press, Golden, CO, 1978, pp. 242-260.

3. Campbell, J.H.; Burnham, A.K. <u>In-situ</u> 1980, 4, 1.
4. Wildeman, T.R.; Melchior, D.C. <u>Preprints, ACS Division of
    Fuel Chemistry</u> 1983, 28, in press.
5. Campbell, J.H.; Koskinas, G.J.; Gallegos, G.; Gregg, M. <u>Fuel</u>
    1980, 59, 718.
6. Burnham, A.K.; Taylor, R.W. <u>Proc. 15th Oil Shale Sym.</u>,
    Colorado School of Mines Press, Golden, CO, 1982, pp. 299-
    319.
7. Melchior, D.C.; Wildeman, T.R.; Williamson, D.L. <u>Fuel</u>, 1982,
    61, 516.
8. Fox, J.P. Ph.D. Thesis, University of California Berkeley,
    1980.
9. Smith, J.W.; Robb, W.A.; Young, N.B. <u>Proc. 11th Oil Shale
    Sym.</u>, Colorado School of Mines Press, Golden, CO, 1978, pp.
    100-113.
10. Krause, J.B.; McLean, W.J.; Veblen, D.R.; Gann, D.E.
    "Mineralogy-Groundwater Quality: A Study of In-situ Retorted
    Oil Shale", EPA report on Grant R-804162, 1980.
11. Park, W.C.; Lindemanis, A.E.; Raab, G.A. <u>In-situ,</u> 1979, 3,
    353.
12. Cox, K.G.; Bell, J.D.; Pankhurst, R.J. "The Interpretation
    of Igneous Rocks"; George Allen & Unwin: London, 1979, 450
    pp.
13. Carmichael, I.S.E.; Turner, F.J.; Verhoogan, J. "Igneous
    Petrology"; McGraw-Hill: New York, 1974, 739 pp.
14. Ritmann, A. "Stable Mineral Assemblages of Igneous Rocks";
    Springer-Verlag: New York, 1973, 262 pp.
15. Winkler, H.J. "Petrogenesis of Metamorphic Rocks" 4th Ed.;
    Springer-Verlag: New York, 1976, 334 pp.
16. Goodfellow, L.; Atwood, M.T. <u>Quarterly of the Colorado
    School of Mines</u> 1974, 69, 205.
17. Campbell, J.H.; Gallegos, G.; Gregg, M. <u>Fuel</u>, 1980, 59, 727.
18. Eugster, H.P. "Researches in Geochemistry"; P.H. Abelson,
    Ed.; John Wiley and Sons Inc.: New York, 1959, pp. 397-427.
19. Mueller, R.F.; Saxena, S.K. "Chemical Petrology"; Springer-
    Verlag: New York, 1977, 394 pp.
20. Burnham, A.K.; Stubblefield, C.T.; Campbell, J.H. <u>Fuel</u>,
    1980, 59, 871.
21. Yoder, H.S. Jr. "The Evolution of Igneous Rocks"; H.S.
    Yoder, Ed.; Princeton Univ. Press: Princeton, 1979, chap.
    13.

Characterization of Oil Shales

Analytical Techniques

R. A. NADKARNI

Exxon Research and Engineering Company, Analytical Research Laboratory, Baytown, TX 77522

Extensive analytical efforts to fully characterize the oil shales are underway at Exxon Research and Engineering Company's Baytown Laboratories. No significant losses of any metals of concern are observed during high temperature ashing. An alternate means of rapid ash determination uses a Parr combustion bomb. The ash can be dissolved by alkaline fusion in a Claisse fluxer or by acid dissolution in a Parr bomb. The solutions thus prepared are analyzed by atomic absorption or by inductively coupled plasma emission spectrometry for major (Al, Ca, Fe, K, Mg, Na, Si, Ti) and trace elements (As, B, Ba, Be, Cd, Co, Cr, Cu, Li, Mn, Mo, Ni, P, Sr, U, V, Zn). Kerogen enriched shales need to be ashed before the dissolution, otherwise low recoveries are obtained. Overall accuracy and precision of metals determination is within $\pm 5 - 10\%$. Other major shale constituents such as C, H, N, and S are determined by thermal decomposition and instrumental detection methods. Oxygen is determined by 14 MeV neutron activation analysis. Parr or Leco BTU bomb combustion and subsequent ion chromatographic determination is used for halogens, sulfate and nitrate. Ion chromatography is also suitable for anionic characterization of shale process waters. Two analytical procedures for oil shales should be used with caution. Kjeldahl nitrogen procedure has been found to give reproducible but considerably low results for certain oil shales. Similarly, ASTM procedure for the determination of sulfur forms in coal, when applied to oil shales, gives reproducible but erroneous results.

Oil shale, a fine grained sedimentary rock containing insoluble organic material that yields oil by destructive distillation, or retorting, occurs in large quantities in many parts of the world and in the United States. The identified resources of shales outside the United States total over 1.1 trillion barrels of oil (1). The richest deposits in the United States are located in the Eocene Green River formation of Colorado, Utah, and Wyoming. In part of this formation, the Piceance Basin, the oil shales are thought to contain energy equivalent of about 1.2 trillion barrels of oil, or about forty times the nation's present proven reserves of petroleum. Environmental issues associated with shale retorting require substantial monitoring and control of waste products, which can be quite large.

At Exxon Research and Engineering Company's Baytown Research and Development Division, analytical methods for coal and coal products have been developed and are being used (2-4). These methods are now being extended to the characterization of oil shales. This extension is not straightforward in all cases because in several respects shale is almost the exact opposite of coal. For example, shale is high in inorganics and low in organics, the opposite of most coals, and shale organics have a high H/C ratio, also the opposite of coal.

The major analytical techniques used for the shale analyses are neutron activation analysis (5), X-ray fluorescence (5), and atomic spectroscopy (6-8). In addition, we describe our approach to the multielement analysis of oil shales and their products utilizing mainly inductively coupled plasma emission spectrometry (ICPES) for metals, and ion chromatography (IC) for some nonmetals. Other major elements such as carbon, hydrogen, nitrogen, sulfur, and oxygen are determined by a variety of combustion techniques.

Experimental

Shale Preparation. The oil shale samples were pulverized to -100 mesh before sampling. Representative portions of the samples were ashed at 750°C for five hours starting with a cold muffle furnace following the ASTM procedure.

Kerogen was isolated from the shale samples by sequential demineralization with HCl and HF, a procedure developed at the U.S. Bureau of Mines (9).

Parr Bombs. Two types of Parr bombs were used. The acid digestion bombs were used for the ash dissolutions. About 0.2 g of shale or ash was dissolved in 3 mL aqua regia and 2 mL HF in the acid digestion bomb and heated at 110°C in an air-oven for two hours. After the dissolution, 1 g of boric acid was added to each sample solution, which was heated on a water-bath

for 15 minutes. If any unburned carbon was visible, the solutions were filtered; otherwise, they were diluted to 100 mL. A blank containing the same amounts of the acids was also prepared.

The Parr oxygen combustion bombs were used for a rapid ash determination and for sample preparation for IC. About 0.5 g of shale or shale oil was mixed with 0.5 g of white oil in a stainless steel cup. Five mL of water was placed in the bottom of the bomb which was then assembled and pressurized to 30 atmospheres of oxygen. After combustion, the bomb was allowed to cool for ten minutes and then opened slowly. The inside walls of the bomb were washed with water, and all the washings were combined, filtered if necessary, and diluted to 50 mL. The residue in the cup was dried at 110°C for 15 minutes and reweighed for ash determination.

<u>Claisse Fusion Device.</u> The detailed procedure is described by Botto (<u>10</u>). This is an automated device which simultaneously fuses six samples. In this procedure, the finely powdered sample was mixed with ten times its weight of lithium metaborate in a platinum crucible and heated at ~950°C for 15 minutes. The melt was dissolved in either dilute HCl or HNO_3 and the elements of interest were then determined by AAS or ICPES. Phosphorus was determined from the same solution by a separate molybdenum blue colorimetric procedure.

<u>Inductively Coupled Plasma Emission Spectrometer.</u> Details of our instrumentation are given by Botto (<u>11</u>). It is a Jarrell-Ash AtomComp Model 750 with 34 elemental channels. A list of these elemental channels, the wavelengths used for the determinations, the detection limits, and the upper dynamic range for each element was given in the preceding paper. Six of the elemental channels are also focussed on weaker lines of lesser sensitivity for determining the higher elemental concentrations. This eliminates the necessity of diluting the samples further to prevent major elements in shale from exceeding the upper dynamic limit. The data from ICPES are processed by an on-line PDP-8M computer interfaced to an HP-1000 off-line computer.

<u>Ion Chromatograph.</u> A Dionex Model 14 was used for the determination of anions. The working parameters are given elsewhere (<u>12</u>). Quantification was done by comparing the peak heights on the strip-chart recorder of the standards with the sample solutions.

<u>Other Instrumentation.</u> - An Orion Model 901 microprocessor ion analyzer was used for pH and for ion selective electrode measurements. A Norelco PW-1212 was used for X-ray fluorescence measurements. Certain of the ICPES results were

checked with an Instrumentation Laboratory 951 atomic absorption spectrophotometer. Carbon, hydrogen, and nitrogen were determined using a Hallikainen CH analyzer or Leco CHN-600 analyzer. Sulfur was determined using a Leco SC-32 analyzer. Oxygen was determined using 14 MeV neutron activation analysis.

Reagents. All of the acids used in this work were of "Ultrex" quality from J. T. Baker Chemical Company. Deionized water was obtained from a Millipore Corporation MilliQ system. An ICPES scan of this water showed a total of 33 elements to be ~1 ppm or less. Oil shale standards were provided by Dr. F. J. Flanagan of the U.S. Geological Survey. These were dried for two hours at 110°C before analysis.

Results and Discussion

Ashing of Oil Shales. Because of potential difficulties due to carbonate content of the shales, the normal ASTM ashing procedure for coals was evaluated to find the optimum ashing temperature with minimum elemental losses for shales. A Colorado oil shale was ashed at 750°C for 15 hours, and then successively ashed for 3 hours each at 850, 950, and 1050°C. From each stage, the percentage ash was determined. All of these ashes and the original shale sample were analyzed for their carbonate content by evolution-gravimetry, and for elemental composition by ICPES. The results are summarized in Table I. Essentially all of the carbonate is decomposed at 750°C; heating further up to 1050°C showed no loss of any element determined. Thus, it seems feasible that a shale sample can be heated overnight to ~800°C and the ash subsequently analyzed for the elements of interest with good precision.

The Parr oxygen bomb can be used if only a rapid ash determination is desired. The residue left in the ignition cup is equivalent to the ash content of a given shale. Having water as an absorbant in the bomb is not necessary; however, if water absorbant is used, it is necessary to dry the residual ash before final weighing to remove the moisture. Pressing the shale sample into a pellet helps in achieving uniform combustion and in reducing the risk of some sample being blown out of the cup during combustion. Typical results on two raw shales and two shale oil samples are given in Table II. The agreement between the values by the ASTM method for coals and the proposed method is very good (accuracy between 0.2 and 5% with an average of 4%). The precision of the method varies from 0.6 to 13% with an average relative standard deviation of 5%. Thus, the Parr oxygen bomb method can be used for a quick ash determination of coal or shale in a pilot plant laboratory situation as an alternative to the time-consuming ASTM D-3174 procedure.

Table I.   Analysis of Inorganic Constituents in
Colorado Oil Shale

Ashing Temperature, °C	Unashed	750	850	950	1050
Ash, wt %	---	63.1	62.8	62.6	61.9
CO_3, %	26.4	*0.81	*0.42	*0.27	*0.19
Al, %	3.30	3.15	3.15	3.18	3.14
Ca, %	12.0	12.5	12.8	12.3	12.7
Fe, %	1.69	1.64	1.63	1.62	1.61
K, %	0.98	1.00	0.97	0.95	0.95
Mg, %	2.85	2.71	2.85	2.78	2.79
Na, %	1.37	1.35	1.35	1.34	1.36
P, %	0.12	0.11	0.11	0.10	0.10
Si, %	10.7	10.5	10.5	10.6	10.8
Ti, %	0.12	0.10	0.11	0.12	0.12
Ba, ppm	502	515	516	512	513
Cr, ppm	31	33	29	24	35
Cu, ppm	134	133	130	136	126
Li, ppm	48	50	49	51	49
Mn, ppm	302	282	283	282	277
Sr, ppm	762	726	738	726	722
V, ppm	55	68	56	50	78
Zn, ppm	79	85	79	85	78

* Remaining in ash

Table II. Ash Determination by Parr Oxygen Combustion Bomb

Sample/Wt % Ash By:	High Temperature Ashing	Parr Oxygen Combustion Bomb [a]
Colorado Shale	62.8	62.7 ± 0.4 (5)
Colorado Shale	72.7	72.2 ± 0.4 (2)
Australian Shale Oil	1.80	1.72 ± 0.11 (3)
Australian Shale Oil	1.87	1.64 ± 0.21 (3)

[a] Number of replicate analysis.

Claisse Fluxer Analysis – Lithium tetraborate or metaborate fusion for the dissolution of rocks has been in use for many years. The Claisse Fluxer fusion device simply makes this fusion automated. We have used the method in the past for the fusion of coal and fly ashes (10,13). Oil shales can be dissolved by this method without pre-ashing. Once the solution is prepared, it may be analyzed for the most part by ICPES or by AAS. Analysis of U.S.G.S. Devonian Ohio shale SDO-1 by fusion followed by AAS or ICPES measurements is illustrated in Table III.

In the predominantly AAS scheme, phosphorus and titanium are colorimetrically determined. The results obtained on five replicates of the solution by each method are given in Table III and are compared with the values obtained for this standard at the Indiana Geological Survey.(7) The ICPES and AAS results are in very good agreement with each other and with the literature values. The precision and the accuracy of the measurements are ±5% for most elements analyzed.

Table III. Analysis of Shale SDO-1 By Fusion and ICPES-AAS

Oxide/Wt % By:	ICPES	AAS	Literature (7)
Al_2O_3	15.6 ± 0.15	15.2 ± 0.12	15.6
CaO	1.37 + 0.02	1.33 ± 0.01	1.42
Fe_2O_3	11.8 ± 0.1	11.7 ± 0.1	12.2
K_2O	4.13 ± 0.12	4.00 ± 0.06	4.23
MgO	1.91 ± 0.02	1.86 ± 0.00	1.87
Na_2O	0.46 ± 0.01	0.44 ± 0.00	0.52
SiO_2	62.4 ± 0.6	63.7 ± 1.1	64.4
TiO_2	0.87 ± 0.01	0.97	0.90
P_2O_5	0.37 ± 0.07	0.18	0.14
BaO	0.05 ± 0.01	--	0.055
MnO	0.06 ± 0.00	--	0.056
Total	99.0	99.4	101.3

Combining the fusion technique with ICPES measurements gives a rapid and accurate method for the ash elemental analysis. The total analysis time needed is 20-25 minutes per sample. However, although the fusion procedure is excellent for the determination of all major elements, it is not suitable for the determination of trace elements, because the final solution (1 L) is too dilute for detection of trace elements. If the solution volume is kept small, extremely high concentrations of lithium and boron in the solution give an undesirable high background spectrum for trace element measurements. Hence, it is necessary to resort to a separate procedure where both trace and major elements can be simultaneously determined.

Parr Bomb Dissolution of Shales. Originally the acid digestion bomb was developed by Bernas (14) for the dissolution of silicate matrices. An adaptation of this bomb is now marketed by Parr Instrument Company of Moline, Illinois. The dissolution procedure has been adapted to shales and was described in the Experimental Section.

Other workers have used different acid combinations for the dissolution of ashes in the acid digestion bomb. Thus, HCl + HF, HNO_3, $HClO_4$ + HF, aqua regia + HF, and HNO_3 + $HClO_4$ have all been used in the acid digestion bombs. We have found the aqua regia + HF mixture to be quite effective in accomplishing the dissolution. It is important to have a boric acid blank subtracted from the sample spectrum in the ICPES analysis to correct for the boron interferences with other elemental lines. It is also necessary to add boric acid to the sample solution immediately after opening the bomb, and then to heat the solution on a waterbath for 15 minutes so that all of the boric acid goes in solution and reacts with insoluble fluorides. When boric acid was added only during the final dilution step, low recoveries were obtained, since Al, Ba, Ca, and Mg, which form insoluble fluorides, were filtered off along with the unburned carbon.

The results of using the acid digestion bomb for shales are included in Table IV. These three shales are distributed by the U.S. Geological Survey as "standard" shales: Green River shale SGR-1, Cody shale SCO-1, and Devonian Ohio shale SDO-1. Not enough information is available in the literature on the composition of these shales. The U.S.G.S. values given in Table IV for shales SGR-1 and SCO-1 are averages of values from five papers given in an U.S.G.S. report (15), while the literature values for the shale SDO-1 are from the Indiana Geological Survey (7). We analyzed each sample in four replicates by the Parr acid digestion bomb procedure. Overall, the agreement between this procedure and the literature results is good. For SGR and SCO shales, chromium and nickel results could not be obtained by this procedure due to contamination

Table IV. Analysis of Oil Shales By Acid Digestion Bomb Dissolution and ICPES

Element, wppm	SGR-1		SCO-1		SDO-1	
	Found	USGS[15]	Found	USGS[15]	Found	IGS[7]
Al, %	3.31±0.27	3.71	7.39±0.17	7.23	6.43±0.25	6.4
As	25-40	75	<13	10.8	-	-
Ba	259±6	337	558±10	594	373±16	-
Be	0.5-1.0	0.91	0.4-2.3	1.58	<0.4	-
Ca, %	6.52±0.12	5.64	2.03±0.07	1.92	0.84±0.04	0.78
Cd	10.3±2.7	-	21.7±2.3	-	-	3
Co	13.5±4.5	11.6	<3	10.3	26;41	-
Cr	-	-	-	64.7	59±9	66
Cu	76±8	65.2	34±3	29.7	58±1	66
Fe, %	1.59±0.05	2.25	3.17±0.07	3.87	6.33±0.68	6.83

K, %	1.26±0.02	1.38	2.00±0.12	2.25	1.92±0.12	2.77
Mg, %	2.28±0.05	2.67	1.56±0.04	1.53	0.93±0.07	0.88
Mn	230±6	295	396±8	444	327±25	325
Mo	36-70	36	<10	2.79	146±5	156
Na, %	2.36±0.08	2.11	0.71±0.04	0.66	0.23±0.03	0.30
Ni	-	34.3	-	29.1	119±18	105
P	562±22	1540	429±33	860-1900	138±36	436
Si, %	11.8±0.3	13.8	25.4±0.8	29.2	19.6±1.1	23.3
Ti, %	0.14±0.002	0.25;0.069	0.36±0.01	0.37	0.44±0.03	0.42
V	114±3	124	119±4	116	156±7	157
Zn	85±3	79	99±5	108	76±9	71

from the metal body of the bomb. Somewhat lower silicon results indicate partial volatilization of SiF_4 during dissolution. Phosphorus results for all three shales are lower than the literature values. If phosphorus is partly present as an organic complex in the shale, it will not be totally decomposed by the dissolution procedure.

The Parr bomb dissolution method seems to give satisfactory results on unashed oil shale samples. However, when the method was used for shales which had an organic content greater than about 20 weight percent, lower recoveries for many elements were observed. Agreement between the data on the ashed samples by fusion and the unashed samples by the Parr acid digestion bomb dissolution was poor, with the latter data always being low. The higher the kerogen content of the shales, the greater the discrepancy.

Preashing of samples with high kerogen content eliminated this problem. The results in Table V for a typical Colorado oil shale kerogen-enriched fractions compare the data between the fusion procedure and the Parr acid digestion bomb methods, the latter with and without preashing. While agreement for the unashed sample is poor, the data from the ashed sample are in good agreement with the fusion procedure.

Table V. Effect of Ashing on Element Determination in Beneficiated Colorado Shale

Element wt %	Lithium Tetraborate Fusion	Parr Acid Digestion Bomb	
		No Ashing	Preashing
Si	11.6	7.04	11.2
Al	3.09	2.28	2.97
Fe	1.76	1.30	1.71
Mg	1.36	1.02	1.18
Ca	4.78	3.75	4.37
Na	1.39	1.05	1.32
K	0.92	0.56	0.88
Ti	0.13	0.03	0.092
P	0.24	0.10	0.15

The kerogen concentrates prepared by acid demineralization are analyzed for metals by ICPES after ashing the sample and dissolving it in aqua regia + HF. Typical analyses of an Australian oil shale and the kerogen isolated from it are given in Table VI. Drastic reduction in the metals content of the shale during the kerogen preparation is indicated. Almost complete demineralization of the major metals such as aluminum, calcium, and silicon is evident. Pyrite, FeS_2, is the only mineral left in the kerogen concentrate, since only HNO_3 will

dissolve it. The elevated levels of fluorine and chlorine in the kerogen compared to the shale, originate from the HCl and HF used for the demineralization. Shale oils are "wet"–ashed with concentrated H_2SO_4 on a hot plate and in a muffle furnace before ICPES determination of metals.

Table VI. Analysis of Australian Shale and Kerogen

Element, ppm	Shale	Kerogen
Al	6.28%	225
As	--	16
Ba	315	14
Ca	1.13%	391
Cl	412	7070
Co	8.6	9
Cr	34	8.9
Cu	34	81
F	604	1800
Fe	4.26%	2.66%
K	9580	25
Li	28	22
Mg	7040	50
Mn	875	19
Na	4860	132
Ni	41	31
Si	17.0%	107
Ti	1880	12
V	98	--
Zn	97	61

Determination of Nonmetals. Ion chromatography (IC) has been used for the determination of fluorine, chlorine, nitrogen and sulfur in oil shales and shale oils. This determination also requires dissolution using the Parr combustion bomb technique to bring the sample into aqueous solution. Determination of these elements in coal analyses has been described previously (3) where the halogens were determined with ion selective electrodes, nitrogen with a chemiluminescent detector, and sulfur by X-ray fluorescence. However, all these elements can be simultaneously determined by IC. With the fast separator columns and 0.0024 M Na_2CO_3 + 0.0030 M $NaHCO_3$ eluant at 2.30 mL/min flow rate, the retention times for F^-, Cl^-, NO_3^-, and SO_4^- were found to be 2.5, 3.5, 9, and 10.5 minutes, respectively. Thus, in less than 15 minutes four anions can be quantitatively determined, significantly less time than required by the other specific techniques. Typical IC results for the shales are given in Table VII. The difficulty of acccurately determining the halogens in the rock matrix is evident from the

disagreement between the various literature results for the
U.S.G.S. standard shales. Previously using this method on coal
samples, good agreement was obtained between certified and IC
results (12). Unfortunately, the shale standards have not been
extensively analyzed and reported in the literature to enable
one to form a true picture of their halogen concentrations.
The sulfur results by Parr combustion bomb-IC are in good
agreement with the published data.

Table VII. Ion Chromatographic Determination of Halogens and
Sulfur in Oil Shales

Sample	U.S.G.S. SGR-1	U.S.G.S. SCO-1	Colorado Kerogen, %
Fluorine, ppm			
Literature	2285 (17)	1500 (19) 779 (17,20)	0.22[b]
Found[a]	307 ± 36	425 ± 37	0.25
Chlorine, ppm			
Literature	92 (17) 45 (18)	1600 (19) 68 (18) 49 (17)	1.64[b]
Found[a]	1400 ± 87	742 ± 26	1.48
Sulfur, %			
Literature	1.90 (18) 1.64 (17)	0.12 (19) 0.06 (17,18)	2.68[b]
Found[a]	1.71 ± 0.05	0.052 ± 0.001	2.42

[a] Shale results mean of triplicate analysis.
[b] Fluorine and chlorine were determined by ion selective
electrodes after Parr bomb combustion, and sulfur was
determined by Leco SC-32.

Determination of Carbon, Hydrogen and Nitrogen. Methods for
the determination of these elements are based on the combustion
of oil shale samples, usually at 1000°C, and measuring the CO_2,
H_2O, and N_2 produced, by different techniques, after scrubbing
from the gases the halogens, SO_2, and excess oxygen. Various
instruments use gravimetry, infrared, or thermal conductivity
for final measurements. Comparative performance of several CH
instruments is illustrated in Table VIII. All appear to give
reasonably satisfactory results for carbon and hydrogen. The

precision of the results appears to be of the order of ±1% of the C, H, N values.

Table VIII. Determination of Carbon Hydrogen in Oil Shales

Instrument	Colorado Shale	Australian Shale
	Carbon, wt %	
Hallikainen	20.4 ± 0.06 (3)	14.4 ± 0.10 (3)
Leco CHN-600	20.1 ± 0.11 (28)	14.04 ± 0.06 (28)
Leco CR-12	19.8 ± 0.5 (3)	13.6 ± 0.17 (3)
Perkin Elmer	20.0 ± 0.10 (3)	13.7 ± 0.17 (3)
ASTM Combustion	20.4 ± 0.12 (3)	14.2 ± 0.17 (3)
	Hydrogen, wt %	
Hallikainen	2.24 ± 0.01 (3)	2.24 ± 0.01 (3)
Leco CHN-600	2.15 ± 0.04 (28)	2.18 ± 0.04 (28)
Perkin Elmer	2.10 ± 0.03 (3)	2.16 ± 0.02 (3)
ASTM Combustion	2.25 ± 0.02 (3)	2.31 ± 0.02 (3)

Numbers in parentheses are the replicate number of analyses.

The classical method for nitrogen determination is the Kjeldahl procedure. The method is very precise and well characterized. However, recently we have found this method to give erroneously low nitrogen results for some oil shale samples. The data in Table IX illustrate this problem. Two samples of Colorado and Australian shales were analyzed by the Kjeldahl procedure in five different laboratories. The same samples were also analyzed by four different instruments in three different laboratories. Good agreement is apparent among all methods for the Australian shale, but for the Colorado shale there are significant differences. The results can be subgrouped as (a) Kjeldahl data and (b) instrumental data. All of the Kjeldahl results are close, but they are low roughly by a factor of 2 compared to the instrumental techniques. The different instruments have also produced remarkably close results. We believe the non-aminoid nitrogen compounds present in the oil shales are not being determined by the Kjeldahl procedure. Attempts to obtain higher Kjeldahl results by more vigorous digestion did not succeed. We believe it is advisable to use the instrumental methods rather than the Kjeldahl procedure for the determination of true nitrogen content of oil shales. The fact that the Australian shale gave equivalent results by chemical and instrumental methods, but the Colorado shale did not, probably indicates the presence of different specific nitrogen compounds in oil shales as a result of their different genesis.

Table IX. Determination of Nitrogen in Oil Shales

	Weight Percent N	
Method	Colorado Shale	Australian Shale
Kjeldahl-Lab A	0.42 ± 0.02 (3)	0.38 ± 0.01 (3)
Kjeldahl-Lab B	0.40 ± 0.01 (3)	0.38 ± 0.01 (3)
Kjeldahl-Lab C	0.42 ± 0.00 (3)	0.39 ± 0.02 (3)
Kjeldahl-Lab D	0.49 ± 0.01 (3)	0.41 ± 0.01 (3)
Kjeldahl-Lab E	0.50 ± 0.05 (2)	0.57 ± 0.01 (2)
Leco NP-28	0.70 ± 0.01 (3)	0.42 ± 0.01 (3)
Leco CHN-600	0.79 ± 0.04 (28)	0.57 ± 0.04 (28)
Perkin Elmer	0.79 ± 0.05 (3)	0.46 ± 0.03 (3)
Mettler	0.65 ± 0.02 (3)	0.43 ± 0.01 (3
Mean-All	--	0.46 ± 0.08
Mean-Kjeldahl (a)	0.45 ± 0.05	0.43 ± 0.08
Mean-Instrumental (b)	0.74 ± 0.06	0.47 ± 0.07
ASTM Kjeldahl Repeatability	0.05	0.05

Numbers in parentheses are the replicate number of analyses.

Determination of Sulfur Forms. A knowledge of the forms and the concentrations of sulfur present in the oil shales is desirable for determining the composition, heating value, thermal degradation properties and eventually relating the sulfur forms found in the shale to those found in the oil. The separation and analysis methods were primarily developed for coal products (ASTM D-2492 procedure). However, when applied to oil shales, this procedure has resulted in reproducible but erroneous results. Smith, et al (16) have pointed out the drawbacks of this procedure and have devised a new procedure based on the $HClO_4$ dissolution of sulfate and $LiAlH_4$ reductive dissolution of pyrite. However, many of the laboratories in the U.S. are still using the ASTM procedure. We found the ASTM method to overestimate the sulfate and pyrite forms, thus resulting in underestimating organic sulfur, even giving negative values in some cases. Our attempts to obtain better results by using a variety of other decomposition aids have not met with success so far. We have been reluctant to apply the U.S.B.M. procedure (16) in our laboratory on a routine basis because of the hazardous nature of $HClO_4$ and particuarly $LiAlH_4$. The best alternative to the ASTM and U.S.B.M. procedures appears to be the demineralization-kerogen isolation procedure for the determination of pyrite. This U.S.B.M. procedure (9) uses HCl-HF to remove the carbonate and the silicate minerals in the shales, leaving the kerogen residue with only pyrite as the mineral component. In the proposed pyrite determination procedure, this isolated kerogen is analyzed for its iron content by dissolution in HNO_3 and

subsequent AAS or ICPES measurement. A single analysis each carried out by this procedure on four shale samples gave results that were definitely lower than the ASTM procedure, but much closer to the $LiAlH_4$ procedure (Table X). Further work needs to be carried out to determine the quantitative validity of the isolated kerogen procedure.

Table X. Determination of Pyrite in Oil Shales

Method	ASTM	$LiAlH_4$	Demineralization
Colorado	0.68±0.09 (11)	0.43±0.02(3)	0.41
Australian	0.79±0.07(11)	0.64±0.01(3)	0.48
Morocco	0.74	0.64	0.43
Green River	0.67	0.27	0.22

Numbers in parenthesis are the replicate number of analysis.

In summary, the methods developed using ICPES and IC, and other thermal decomposition procedures for metals and nonmetals, are now routinely used at Exxon's Baytown Research and Development Division for the characterization of a large number of oil shales and shale products with precision and accuracy of ±1-5 percent. Problems remain with the determinations of nitrogen and sulfur forms in oil shales.

Acknowledgments

Literature Cited

1. Culbertson, W. C., Pitman, J. K. U.S.G.S. Prof. Paper, 1973, 820, 497-503.
2. Nadkarni, R. A., Anal. Chem. 1980, 52, 929-935.
3. idem, Amer. Lab., 1981, 13(8), 22-29.
4. idem, Anal. Chim. Acta, 1982 135, 363-368.
5. Fruchter, J. S., Wilkerson, C. L., Evans, J. C., Sanders, R. W., Environ. Sci. Technol., 1980, 14, 1374-1381.
6. Shendrikar, A. D., Faudel, G. B., ibid, 1978, 12, 332-334.
7. Lechler, P. J., Leininger, R. K., Jarrell-Ash Plasma Newslett., 1979, 2(1), 8-10.

8. Amini, M. K., DeFreese, I. D., Hathaway, L. R.,
    Appl. Spectrosc., 1981, 35, 497-501.
9. Smith, J. W., U.S. Bureau of Mines Rept. Investig. 1961,
    5725.
10. Botto, R. I., Jarrell-Ash Plasma Newslett., 1979, 2(2),
    4-8.
11. idem, Proc. Int. Conf. Dev. At. Plasma Spectrochem. Anal.,
    Barnes, R. M., Ed., Heyden, New York, 1980, 141.
12. Nadkarni, R. A. and Pond, D. M., Anal. Chim. Acta, 1983,
    146, 261-266.
13. Nadkarni, R. A., Botto, R. I., and Smith, S. E.,
    At. Spectroscopy, 1982, 3, 180.
14. Bernas, B. Anal. Chem., 1968, 40, 1682-1686.
15. Flanagan, F. J., U.S.G.S. Prof. Paper, 1976, 840.
16. Smith, J W., Young, N. B., and Lawlor, D. L., Anal. Chem.,
    1964, 36, 618.
17. Evans, K. L., Tarter, J. G., and Moore, C. B.,
    Anal. Chem., 1981, 53, 925-928.
18. Fabbi, B. P. and Espos, L. F., U.S.G.S. Prof. Paper, 1976,
    840, 89-93.
19. Schultz, L. G. Pourtelot, H. A., and Flanagan, F. J.,
    U.S.G.S. Prof. Paper, 1976, 840, 21-23.
20. Malchacek, V. Rubeska, I., Sixta, V., and Sulcek, Z.,
    U.S.G.S. Prof. Paper, 1976, 840, 73-77.

Organic–Mineral Matter Interactions in Green River Oil Shale

K. M. JEONG and T. P. KOBYLINSKI

Gulf Research & Development Company, Pittsburgh, PA 15230

A chemical extraction procedure was used to preferentially disassociate the carbonate and silicate mineral matrices in Colorado Green River (Mahogany Zone) oil shale. The percentages of organic matter isolated in two sets of acid/ether extracts were determined. Approximately four times more bitumen-free organic matter appears to be associated with the silicate mineral matrix than the carbonate minerals. Benzene/methanol Soxhlet extraction results indicate that up to 21 wt% of the bitumen in these samples is trapped by the carbonate mineral matrix. The bitumen-free organic matter extracted in association with the two mineral types can be considered to be a portion of the interfacial layer between kerogen and the inorganic mineral matrix. Spectroscopic identification of the interlayer structures indicated several differences in the composition of the two acid/ether extracted organic fractions which suggest possible types of kerogen-mineral matter bonding effects. One major distinction is a larger concentration of ester functional groups in the ether extracted organic matter associated with the silicate mineral matrix. Relatively more olefins and branched paraffins were identified with the carbonate mineral matrix. These results are discussed in terms of possible chemical bonding and physisorption interactions.

Oil shales contain large quantities of insoluble organic matter, kerogen, which upon pyrolysis at higher temperatures, yields oil products. Kerogen, which usually represents 80-90% of the total organic matter in Green River oil shales, is neither soluble in aqueous alkaline/acidic solvents nor in the common

organic solvents at mild conditions. The remaining 10-20% of the
organic fraction in shale is extractable with organic solvents and
is referred to as bitumen. The mineral constituents of oil shale,
generally far more abundant than kerogen, vary largely according
to types, but usually include carbonate, clay, and silicate
minerals.

     Relatively little information is currently available concern-
ing the association between kerogen or bitumen and the mineral
matter phase. The objective of this study was to further charac-
terize the nature of the bonding between these shale constituents
using a chemical extraction procedure followed by spectroscopic
studies, Fourier Transform Infrared (FTIR) and Nuclear Magnetic
Resonance (NMR), of the various separated fractions. Additional
information on the mineral and organic matter composition is
obtained from particle size distribution data. Although there
have been several studies using analogous analytical procedures to
investigate marine sediments, (1) studies of the association
between organic and mineral matter in oil shale have been very
limited. (2-5) This information may also be useful toward under-
standing the formation of oil shale deposits and perhaps provide
insight into beneficiation and enrichment of the organic
matter. (6)

     The mineral matter phase in samples of Colorado Green River
oil shale (C-a tract, Mahagony Zone) was preferentially disassoci-
ated in a series of acid extractions (HCl, HF) in order to sepa-
rately isolate carbonate and silicate minerals. (Bitumen was
removed using the benzene/methanol Soxhlet extraction method.) It
is well known that at varying concentrations over a range of
temperatures, HCl dissolves most carbonates and that pure HF or
HF/HCl mixtures effectively remove silicates, quartz, and clay
minerals. (7,8) Although the minerals encapsulated by kerogen
cannot be extracted by an acid treatment, particle size distribu-
tion data and ash content measurements indicate this to be a minor
problem. The relative amounts of acid/ether extracted organics
isolated with both carbonates and silicates were determined, as
was the fraction of bitumen trapped by each of these minerals. The
data are discussed in the context of other published results as
well as possible types of bonding between kerogen and mineral
matter.

Experimental

     Samples of Colorado Green River oil shale were obtained from
the C-a tract, Mahagany Zone. The mine-run samples of 7.6 cm x
0.64 cm material were stage-crushed to pass a 5.1 cm screen and
were screened at 0.64 cm to remove fines. Shales of three differ-
ent richnesses were isolated by heavy media liquids gravitational
separation (9) and determined by Fischer assay to have an organic
content of 104 L/t (density >2.25 g cm^{-3}), 129 L/t (density
>1.65 g cm^{-3}), and 184 L/t (density <1.65 g cm^{-3}), respectively.

Mechanical pulverizing and sieving procedures reduced the particle size to 100 x 200 and 200 x 325 mesh, although the data presented here are largely for the former size range. The mineral and elemental composition as a function of shale richness were determined from X-ray diffraction measurements (Phillips APD-3500) and energy dispersive X-ray fluorescence data (Kevex Model 0700). Low-temperature ash samples were prepared using a 13.56 MHz radio frequency asher (LFE Corp., Model LTA 504).

The stepwise dissolution of the mineral matter phase was accomplished in a series of acid and ether extractions which are summarized in flow-chart form in Figure 1. All traces of physisorbed water were removed by vacuum drying (P=400 torr) at 85°C with continuous purging of nitrogen gas for approximately 24 h. Bitumen was then separated using the Soxhlet extraction procedure based on a 7:3 mixture of benzene:methanol.

The resulting bitumen-free fraction was extracted with 6N HCl under nitrogen at room temperature for about 24 h. During the HCl extraction, mechanical magnetic separation was used to remove any iron contamination which may have been introduced during the initial grinding phases. The HCl aqueous phase was further extracted with ether, having adjusted the pH at three different steps with NaOH:pH=1, 6.5, >11. All three ether extracts (i.e., acidic/neutral, neutral, and basic) were carefully dried at room temperature while being purged with nitrogen.

The solid phase resulting from the HCl extraction (i.e., bitumen, carbonate-free oil shale) was initially neutralized with distilled water to pH~5 and then dried at 85°C for about 24 h in a nitrogen atmosphere. The Soxhlet extraction procedure with benzene/methanol was repeated to assure the complete removal of physically trapped bitumen. The remaining shale was then extracted with a 3:1 mixture of 50% HF:6N HCl under nitrogen at room temperature for approximately 24 h. Ether extraction of the aqueous HF/HCl phase generated three different pH fractions as discussed above. The final step of the preparation procedure was another benzene/methanol extraction of the solid fraction (i.e., bitumen, carbonate, silicate-free oil shale) to remove physically trapped bitumen.

During various steps of the extraction procedure, samples were withdrawn for elemental analysis by DC arc emission spectroscopy (ARL Model 2100 Film 2m Emission Spectrograph) to verify the efficiency of the overall technique. The structural composition of the various filtrate fractions was characterized using both FTIR (Digilab FTS-20E) and NMR (FT80A, Varian Associates) spectroscopy. The infrared spectra were run on thin film samples using a KBr window. Particle size determinations of the preferentially treated solid fractions were obtained using a particle counter (Coulter Electronics, Inc., Model TAII) and confirmed by scanning electron microscopy data (JEOL, JSM-35C Model).
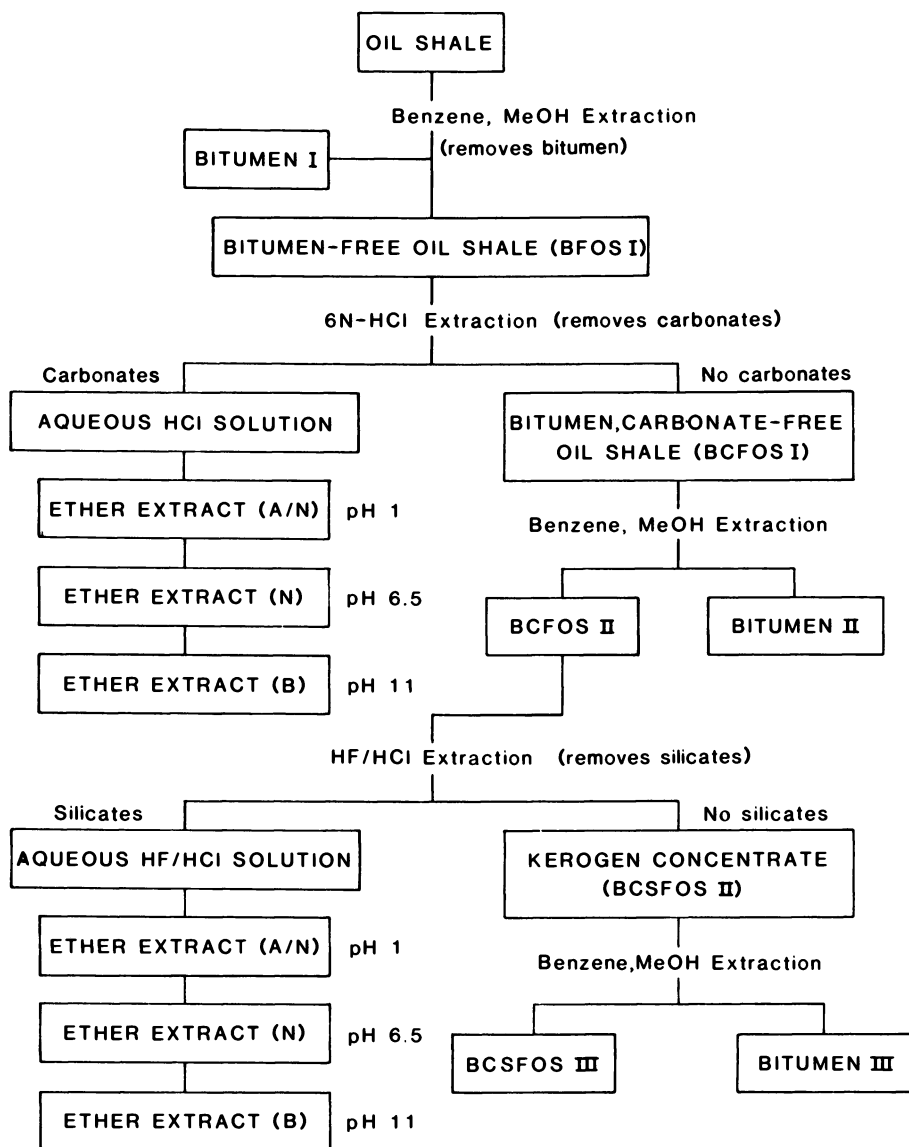
Figure 1. Preferential organic-mineral matter disassociation by chemical methods. Abbreviations: A/N, acidic/neutral; N, neutral; and B, basic.

Results and Discussion

Bulk Mineralogy and Elemental Composition

The composition of the original shale samples was determined to be approximately 13-23 wt% total organics based on elemental analysis of organic C, H, N, O, and S concentrations with the remaining 77-87 wt% consisting of various minerals. Tables I and II summarize the bulk mineralogy and elemental composition of the three different sample richnesses as well as the resulting low-temperature ash. The major minerals identified by X-ray diffraction include ankerite, dolomite, aragonite, calcite, quartz, albite, analcime, and illite. The specific types of mineral matter present do not vary with oil richness, although the relative concentrations of certain minerals are found to vary depending on the particular shale richness of these sets of samples. For example, it is observed that the concentrations of calcite and aragonite vary inversely with oil richness, whereas clay minerals (illite/smectite) and to some extent albite, follow a direct correlation between mineral and organic carbon content.

In general, the mineral concentrations in the low-temperature ash (LTA) increase proportionally with the amount of organics removed by the ashing procedure to within the accuracy of the X-ray diffraction measurements. The only exception to this is the clay mineral concentration which is found to be larger for the original oil shale than the low-temperature ashed shale. However, elemental analysis shows that the total concentrations of Al, Ca, and Si are relatively constant both before and after low-temperature ashing (see Table II). A possible explanation may be the collapse of the basal spacing of the clay minerals (e.g., smectites) due to oxidation of the organic compounds between these layers during low-temperature ashing. (10) However, removal of associated water could also cause layer collapse. The formation of organo-complexes of smectites is also a partial explanation for the direct correlation between the organic concentration and the clay mineral concentration observed by X-ray diffraction. It is also indicative of some mineral structure changes during the mild radio frequency (13.56 MHz, RF power <100 watts) low temperature ashing experiments.

Organic Matter Distribution

The bitumen fraction obtained from the first benzene/methanol Soxhlet extraction accounts for 11.8, 16.1, and 13.5 wt% of the total organics in the original shales for the 184, 129, and 104 L/t samples, respectively. These values are consistent with previous determinations of the bitumen content of Green River oil shales. (11)

Table I   Bulk mineralogy of Green River formation C-a Tract, Mahogany Zone, oil shale in weight percent

Sample Richness (L/t)		Analcime	Clay[a]	Quartz	Feldspar		Ankerite/ Dolomite	Calcite	Pyrite	TDI[b]	Trace
					Kspar	Albite					
104	Orig	14	8	14	6	5	30	14	<1	.34	Siderite
	LTA	18	7	13	8	9	29	14	<1	.44	Gypsum
129	Orig	12	10	16	<1	10	29	7	<1	.42	Gypsum
	LTA	19	7	14	<1	18	31	10	<1	.34	Aragonite
184	Orig	10	19	15	<1	13	20	2	2	.53	Marcasite
	LTA	14	8	17	<1	24	28	4	2	.75	

a   Clay minerals consist primarily of a mixed layer illite/smectite.
b   Total diffracting intensity, the sum of all fractions before normalization.

Table II   Bulk multielement analysis of Colorado oil shale
(C-a Tract, Mahogany Zone)

Sample Richness (L/t)	As[a] ppm	Al[b]	Ca[c]	Fe[c]	K[c]	Mn[c] ppm	P[c]	S[c]	Si[c]
		Wt%					wt%		
104 Orig	43	6.3	12.0	1.9	1.4	100	0.4	0.6	12.5
LTA	47	8.6	12.9	1.8	1.5	150	0.5	1.0	15.0
129 Orig	50	5.9	9.1	2.7	1.8	200	0.4	0.8	16.2
LTA	55	6.5	10.4	2.9	2.0	350	0.5	1.0	18.7
184 Orig	87	6.4	6.9	3.5	1.9	200	0.4	1.4	14.9
LTA	108	8.7	8.5	4.0	2.4	350	0.7	1.4	18.8

[a] INAA = Instrumental neutron activation analysis
[b] DRES = DC Arc Emission Spectroscopy
[c] XRF = X-ray fluorescence analysis

The HCl extraction preferentially separated carbonate minerals from the remaining mineral matter matrix.   As Table III indicates for the 184 L/t oil shale, approximately 99% of the Ca and approximately 96% of the Mg were removed as expected.   The bitumen- and carbonate-free fraction is also found to contain about 28% less Al which is probably associated with other mineral matter (e.g., albite and analcime) partially soluble in HCl.   (The rather large decrease in the Fe concentration from 3.7 wt% in the benzene/methanol treated oil shale to 1.2 wt% for the HCl treated shale is due to mechanical magnetic separation discussed in the experimental section and dissolution by HCl of minerals such as ankerite and siderite.)   The HCl extraction resulted in a weight loss of 28.6 wt%.   It is determined that at least 0.45 and 0.38 wt% of the total organics in the 104 and 184 L/t dried oil shale, respectively, are recoverable in the HCl/ether extracts and, thus, are intimately associated with carbonate minerals.   In addition, the results of the second benzene/ methanol Soxhlet extraction indicate that 3.40 and 3.65 wt% of the total organics which are bitumen in these two samples are released when the carbonate minerals are removed from the shale.

Table III Multielemental analysis (wt%) of original and treated
           Green River oil shale samples[a,b] (104 L/t sample)

Element	Original Oil Shale	Benzene/Methanol Treated Oil Shale	HCl-Treated Oil Shale	HF/HCl-Treated Oil Shale
Wt Fraction	100.0	97.1	68.6	29.6
Al	6.4	5.9	4.6	0.64
* As	87.1 ppm	88.1 ppm		
B	0.021	0.015	0.013	
Ba	0.11		0.08	0.05
Ca	5.1	5.2	0.04	0.04
Cr	0.03	0.03	0.01	0.01
Cu	0.003	0.004	0.003	0.003
Fe	3.6	3.7	1.2	0.96
K	1.9	2.0	1.2	0.23
Mg	4.4	4.5	0.18	0.17
Mn	0.083	0.074	0.013	0.006
Mo				0.005
Na	0.57	0.59	0.04	0.04
Ni	0.018	0.015	0.009	0.003
Si	15	15	14	0.62
Sr	0.08	0.07		0.01
Ti	0.28	0.30		0.07

---

[a] DC Arc Emission Spectroscopy, values given in wt%
[b] Mahogany Zone C-a Tract, 100 x 200 mesh oil shale
*   Instrumental Neutron Activation Analysis

     The HF/HCl extraction results in the removal of approximately
96% of the elemental Si present as well as approximately 90% of
the Al (see Table III). The total amount of HF/ether extracted
organics is at least 1.72 and 1.34 wt% of the total organic
content in the 104 and 184 L/t oil shale. Approximately 1.64 and
2.00 wt% of the total organics are trapped by the silicate miner-
als as determined by the results of the third benzene/methanol
Soxhlet extraction for the two different shale richnesses. The
above results are summarized in Table IV.
     In this study, an extraction approach to the problem of
attractive interactions in Green River (Mahogany Zone) oil shale
resulted in the preferential dissolution of both carbonate and
silicate minerals. As the results in Table IV indicate, the
interfacial organic layer between kerogen and the inorganic
mineral matrix was also simultaneously separated. Since the
majority of the bitumen was removed in the initial benzene/

Table IV   Organic matter distribution of treated oil shale
extracts[a] based on wt% of total organics

	104 GPT Oil Shale	129 L/t Oil Shale	184 L/t Oil Shale
Bitumen I	13.48	16.14	11.80
II	3.40	3.44	3.65
III	1.64	0.05	2.00
Total Bitumen	18.52	19.63	17.45
Carbonate Associated Organics			
Ether Extract I A/N	0.15	0.18	0.18
Ether Extract I N	0.21	0.19	0.13
Ether Extract I B	0.09	0.11	0.07
Total Extracts I	0.45	0.48	0.38
Silicate Associated Organics			
Ether Extract II A/N	1.33	0.26	0.50
Ether Extract II N	0.09	0.17	0.62
Ether Extract II B	0.30	0.02	0.22
Total Extracts II	1.72	0.45	1.34

---

[a]   Total organic concentrations based on elemental analysis are
determined to be 13.5, 16.2, 22.9 wt% for 104, 129, and
184 L/t oil shales, respectively.

methanol Soxhlet extraction step, these interfacial structures
associated with either carbonate or silicate minerals can be
considered to be a form of kerogen. Due to the influence of these
mineral bonding sites and their dissolution during the acid
treatment, the acid/ether extracted organic matter may have
slightly different properties than the bulk kerogen material.

It is determined that approximately four times more bitumen-
free organic matter appears to be associated with the silicate
mineral matrix than with carbonate minerals. (The anomalously low
results for the 129 L/t sample are being re-investigated.) This
is probably a lower bound, because of the inherent problems of
separating kerogen from the mineral matrix by acid leaching
methods. The spectroscopic data discussed in the next section
provide further insight into the composition of the kerogen-
carbonate/silicate interfacial layer and what types of interac-
tions may contribute to the binding forces in these oil shale
samples.

The benzene/methanol Soxhlet extraction data summarized in
Table IV indicate that 27 and 32 wt% of the bitumen for the 104
and 184 L/t oil shale is trapped by the inorganic mineral matrix

and thus, not accessible to removal in the initial Soxhlet extraction. The data also suggest that trapping of bitumen occurs to a greater extent by the carbonate mineral matrix. A previous study (3) of carboxylic acids in Green River oil shale bitumen has suggested that a strong interaction exists between these acids and the mineral matrix, particularly carbonate minerals. Further evidence for the coupling between minerals and bitumen facilitated by carboxylic acids is provided by the results of high pressure CO_2 disaggregation of Green River oil shale (4) and cation exchange experiments involving untreated and acid treated oil shale. (5) Although the bitumen fractions obtained in this study were not spectroscopically analysed for specific chemical constituents, the data summarized in Table IV indicate a strong interaction, including trapping, between bitumen and the carbonate mineral matrix in agreement with the previous studies.

Spectroscopic Analysis and Organic Matter Characterization

It is well established that certain organic compounds react readily with both hydrochloric and hydrofluoric acids to alter chemical/physical properties. For example, esters, amides, olefins, quinones, and alcohols undergo various hydrolysis, addition, and alkyl halide formation reactions in the presence of HCl. (12,13) In the case of HF, condensation reactions involving olefins and aromatic compounds occur readily. (13) Therefore, the intensity of several major IR bands corresponding to characteristic stretching and bending modes were monitored during the chemical extraction procedure (e.g., OH and C=C stretching vibrations). Since no substantial differences in the spectra were observed, it is concluded that insignificant chemical rearrangement occurred during the preferential disassociation procedure. Therefore, the results summarized in Table IV represent organic matter associated with either carbonate or silicate minerals as it naturally occurs at the interface between kerogen and the mineral matter matrix.

FTIR analysis of the various acid/ether extracted fractions indicates certain structural similarities as well as differences between the organic matter associated with carbonate minerals and that associated with silicate minerals (see Figure 2). The characterization of oil shale by FTIR is based on the assignment of several IR bands (14) and their respective absorbances (15) which are summarized in Table V. Both the oil shale ether extracts associated with carbonate and silicate minerals are found to contain insignificant concentrations of molecular water, alcohols, and aromatic compounds. The last observation is also consistent with NMR data to be discussed below. Although the assignment of the aryl-alkyl ether bands is somewhat uncertain, a definite trend among the spectra is observed. (16) Since the bands are not present in the HCl fractions but do occur in the HF/HCl extracts with the largest intensity for the pH 1 sample, a preferential silicate--aryl-alkyl ether association is suggested.
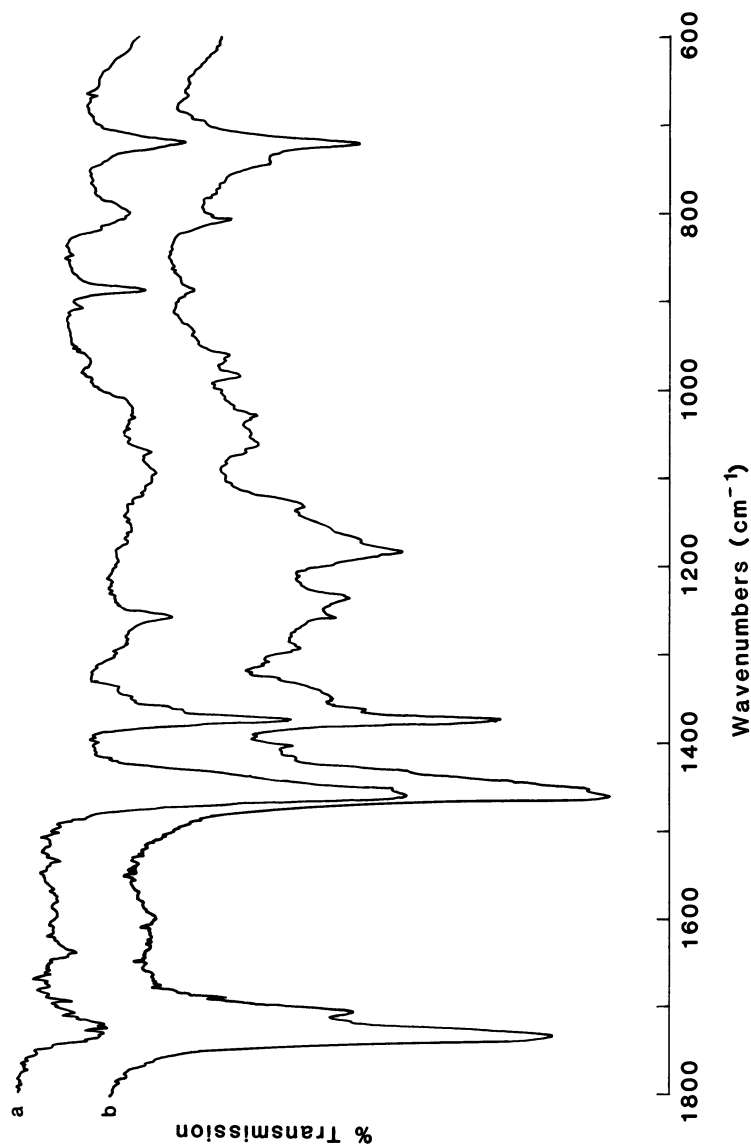
Figure 2. FTIR spectra of ether extracted (at pH 6.5) HCl (a) and HF/HCl (b) fractions (184 L/t sample).

It is determined that both groups of acid/ether extracted organics are predominantly paraffinic. The FTIR spectra indicate that the $[CH_3]/[CH_2]$ ratios in the series of ether extracts of the organics associated with silicate minerals increase with increasing pH: 0.40, 0.44, and 0.54. This seems to indicate the presence of more highly branched compounds and/or small molecules with increasing pH. By comparison, a ratio of 0.48 is determined for the neutral fraction of the HCl/ether extracted sample. These relatively high ratios are consistent with the high hydrogen content of Green River oil shales (atomic H/C ~1.5-1.6).

Table V   IR Band assignments

ν (cm^{-1})	Vibrational Mode
3430	OH stretch
3100-3000	CH stretch (aromatics)
2962	Asymmetric CH_3 stretch
2930	Asymmetric CH_2 stretch
2872	Symmetric CH_3 stretch
2860	Symmetric CH_2 stretch
1735	C=O stretch (esters)
1712	C=O stretch (ketones, aldehydes)
1630	C=O stretch (bridged quinones)
1620	C=C stretch
1455	Asymmetric CH_2 and CH_3 bend
1185	C-O stretch
1125, 1030	C-O vibration (aryl-alkyl ethers)
890	CH_2=C bend
870, 820, 750	Out of plane deformation aromatic CH
720	Skeletal vibration, straight chains $\geq$ 9 CH_2

Both the organics associated with carbonate minerals and those associated with silicate minerals contain long aliphatic chains as evidenced by the significant absorbance in these spectra at 720 cm^{-1}. However, the data indicate that relatively more of these chains are present with the organics associated with the silicate mineral group. Observation of this strong band is also attributed to the relatively high hydrogen content of the original samples.

The C=C stretching vibration is identified in the HCl extracts, although the intensity is approximately a tenth of the CH_3 symmetric bending vibration. This band disappears entirely in the HF/HCl extract spectra at all three pH's investigated. These results are in contrast to the data obtained by Spiro (2) for some Israeli oil shales using a similar procedure as that described in

this study. Spiro (2) reports relatively high absorbance ratios for C=C/CH$_3$, generally between 0.1 and 0.5. The higher values are predominantly identified with organics associated with silicates rather than with carbonate minerals as the results of this study would seem to indicate.

The band assigned to the CH$_2$=C bending mode is observed in both the HCl and HF/HCl spectra. The calculated concentration ratios CH$_2$=C/CH$_2$+CH$_3$ are fairly constant among the three HF pH samples, 0.002, <0.002, <0.002 in order of increasing pH, but a significantly larger ratio, 0.011, is obtained for the pH 6.5 HCl fraction. This further suggests a preferential association between olefinic hydrocarbons and carbonate minerals.

A distinct difference in the FTIR spectra of the HCl and HF/HCl samples is observed for those bands assigned to the C=O and C-O stretching vibrations of esters. Thus, a major distinction between the two acid/ether extracted organic groups appears to be the presence of relatively more ester-functional groups with those organics associated with silicate minerals. In addition, the data indicate relatively larger concentrations of ketones and aldehydes associated with silicate minerals. The results obtained by Spiro (2) concerning the ratio of IR intensities at 1710 cm^{-1} (C=O stretching) and 2980 cm^{-1} (C-H aliphatic) are inconsistent and are a function of the particular sample being studied. No correlation could be established between the 1710/2980 ratio and the origin of the organic matter, either terrestrial or marine.

In addition to FTIR analysis, the acid/ether extracted oil shale fractions were studied by NMR and complementary information obtained (see Table VI and Figure 3). The relative concentration of aromatic structures is found to be considerably larger for the original oil shale than for the organics isolated in the acid extracts and is consistent with FTIR data. The bitumen fraction separated in the initial benzene/methanol extraction contains an aromatic concentration substantially lower than that of the original sample but slightly larger than that of the HCl or HF/HCl extract fractions. It should be noted that distinct differences are observed between the proton spectra of this bitumen and the neutral organic fraction extracted with the silicate minerals (see Figures 3a and 3b). Therefore, the organic matter recovered from the ether extracts of the HCl and the HF/HCl mixtures is not residual bitumen which was not removed by the benzene/methanol Soxhlet extractions.

NMR and FTIR results indicate that both the organic matter associated with carbonate minerals and that associated with silicate minerals is predominantly of paraffinic composition. In addition, both groups contain approximately equal relative concentrations of aromatic structures. The latter result is in disagreement with Spiro's (2) data which indicate that the organic matter associated with silicates contains more aromatic as well as more polar structures as compared with the organics associated with carbonate minerals. This apparent difference in aromatic

Table VI ^{1}H-NMR Spectroscopic analysis

	Aromatic	Paraffinic
Total Organics in Oil Shale	~20%	~80%
H$_2$O Soluble Organics	<0.1%, mainly monoaromatics	>99%, some olefins, some polar (possibly ester)
Bitumen I	~5.2%, mono & diaromatics	94.8%, methyl, alkyl substituted paraffinic chains (>C$_{16}$), 2/3 paraffinic and 1/3 naphthenic
Carbonate Associated Organics[a]		
Ether Extract I, A/N	~3%, mainly monoaromatics	~97%, branched paraffins
Ether Extract I, N	~2%, mainly monoaromatics	~98%, branched paraffins some olefins
Ether Extract I, B	0.2%, mostly diaromatics	~99.8%, highest [CH$_3$]/[CH$_2$], some olefins
Silicate Associated Organics[a]		
Ether Extract II, A/N	~3%, mono & diaromatics	~97%, paraffinic chains (~C$_{10}$), some conjugated olefins
Ether Extract II, N	~1.8%, mainly monoaromatics	~98.2%, small molecules, regularly repeating structural type ~1% olefins
Ether Extract II, B	~1.8%, mainly monoaromatics	~98.2%, long-chain paraffins (~C$_{10}$), polar-functional groups

[a] Abbreviations: A/N - acidic/neutral, N - neutral, B - basic
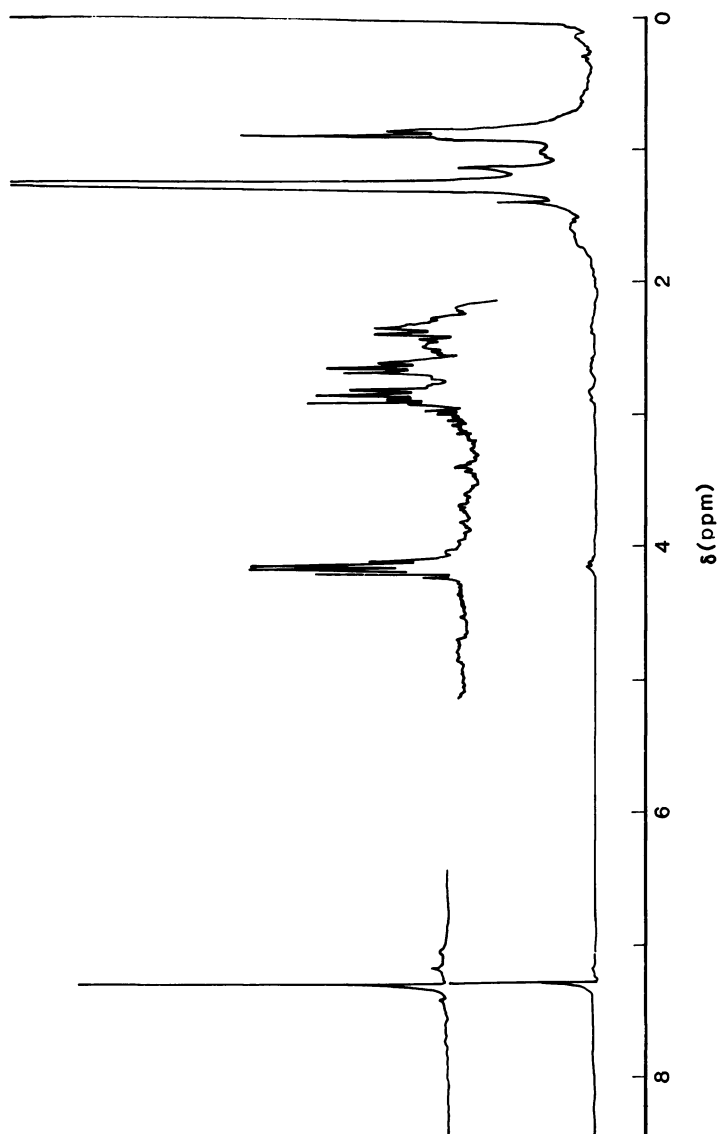
Figure 3a. ^{1}*H-NMR spectrum of neutral ether extracts of HF/HCl treated oil shale filtrate (184 L/t sample).*

δ(ppm)
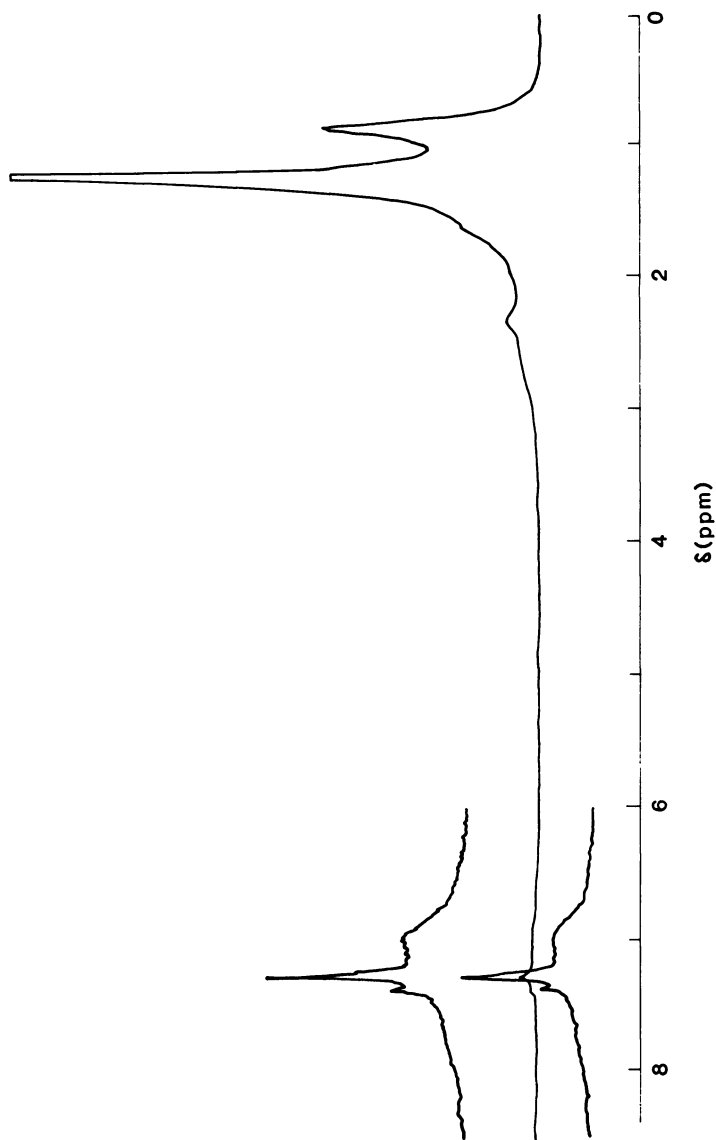
Figure 3b. ¹H-NMR spectrum of bitumen from 184 L/t Green River (Mahogany Zone) oil shale.

δ(ppm)

content between Colorado and Israeli oil shales and those discrepancies discussed above concerning the FTIR data may be the result of dissimilar mineralogical compositions and/or geochemical properties of the two oil shales. (17,18)

The paraffinic carbon composition is similar for both groups of acid/ether extracted organics as is the presence of mono- and diaromatic compounds. No significant pH effects are observed, although the basic HCl extract has a lower aromatic content than either the pH 1 or 6.5 fraction. The NMR data for the first bitumen fraction indicate that it is also predominantly paraffinic, in agreement with the earlier results of Spiro. (2)

Aliphatic molecule adsorption studies on clay minerals have demonstrated that the two major factors which affect adsorption, chain length and CH- activity, appear to act independently of each other. (19,20) It has been determined that chain lengths of up to 10 units strongly influence the adsorption process and that the lack of a high CH-activity can be overcome with additional CH_2 groups. As Table VI indicates, chain lengths of about C_{10} are identified with those organics associated with silicate minerals and branched paraffins having a high CH-activity are found to be associated with the carbonate mineral group.

Characterization of the HCl and HF/HCl extract fractions by FTIR and NMR spectroscopy indicate certain compositional similarities and differences between the organics associated with carbonate minerals and those associated with silicate minerals. These results appear to suggest an equal preference for chemical bonding as for physisorption and do not rule out one or the other type of interaction. However, physisorption of long-chained and branched paraffins would seem to be more likely than the formation of chemical bonds, although hydrogen bonding and other similar covalent or ionic interactions cannot be disregarded. Similarly, the presence of substantial concentrations of esters in the silicate-organic matter group suggests strongly bonded ester-silicate complexes, but physisorption may also be occurring. Therefore, although the data do not absolutely indicate chemical bonding versus physisorption, they do identify the relative concentrations of those organic species associated with either carbonate or silicate minerals, thereby suggesting certain types of interactions while predicting others to be rather unlikely. For example, the kerogen-carbonate mineral interaction may involve chemical bonding between olefinic functional groups and minerals such as $CaCO_3$ and $CaCO_3MgCO_3$, whereas aromatic structures are likely to be insignificant in kerogen-mineral matter bonding.

Particle Size Distribution

Further characterization of Mahogany Zone Green River oil shale involved the determination of the particle size distribution of the bitumen-, carbonate-, and silicate-free extract fractions

(see Table VII). The particle size of the original untreated oil
shale is found to range from 3 to 101 μm with about 80% of the
particles having a diameter between 40 and 80 μm. These values
are consistent with an initial mesh range of 100 x 200 or, equiva-
lently, apertures of 149 to 74 μm. Table VII indicates the
effects of the HCl and HF/HCl extractions on individual particle
size ranges. The difference between the bitumen-free and bitumen,
carbonate-free column is taken to be the carbonate mineral distri-
bution (positive population differences) and a residual matter
distribution (negative deltas). The residual distribution in-
cludes silicate minerals, kerogen, pyrite, and other insoluble
matter. Similarly, the silicate mineral distribution is derived
from positive differences between the bitumen, carbonate-free
populations and those of the kerogen concentrate (i.e., bitumen,
carbonate, and silicate-free fraction). The residual distribution
in this case consists primarily of kerogen and pyrite.

As the fifth column in Table VII shows, the carbonate mineral
distribution peaks between 3.2 and 4.0 μm and has a broad contri-
bution from 32.0 to 80.5 μm with a significant total population.
This bimodal distribution indicates that the carbonate minerals
are of essentially two different size ranges. The residual
distribution associated with the carbonate minerals is basically
characterized by a single peak between 4.0 and 10.1 μm. Since the
majority of the silicate minerals have a particle size between 4.0
and 10.1 μm (see sixth column of Table VII), the former residual
distribution is primarily of a silicate mineral composition. The
second residual distribution, that associated with silicate
minerals, is found to be bimodal, with the majority in the 3.2 to
4.0 μm range and a smaller percentage having a particle size
between 10.1 and 40.3 μm. Therefore, a reasonable estimate of the
kerogen matter particle size range appears to be both 3.2-4.0 μm
and 10.1 to 25.4 μm for these pulverized and screened 100 x
200 mesh samples.

Summary

The problem of organic-mineral matter bonding, particularly
that involving kerogen, although at first glance rather intract-
able, has been partially reduced in scale by the data presented
here. The chemical extraction technique outlined earlier proved
to successfully disassociate in a stepwise manner both carbonate
and silicate minerals from several oil shale samples of different
richness. The organic matter recovered subsequent to the initial
Soxhlet extraction was shown to be bitumen-free.

It was determined that approximately four times more bitumen-
free organic matter is associated with silicate minerals than with
carbonate minerals. The major structural constituent of the
various filtrate fractions was paraffinic compounds. However,
spectroscopic analysis indicated relatively larger concentrations
of olefins and branched paraffins with the acid/ether extracted

Table VII   Particle size distribution of preferentially
treated Colorado Colorado Green River oil shale
(184 L/t, 100 x 200 mesh sample)

Particle Size (μm)	Bitumen Free	Carbonate Free	Silicate Free	BF-CF[a]	CF-SF[b]
		(Population %)			
3.00-3.17	0	0	0	0	0
3.17-3.99	38.9	24.3	41.2	14.6	-16.9
3.99-5.03	22.2	23.6	21.6	-1.4	2.0
5.03-6.34	12.1	20.7	13.0	-8.6	7.7
6.34-7.99	7.7	21.0	8.9	-13.3	12.1
7.99-10.06	4.3	5.8	5.4	-1.5	0.4
10.06-12.68	2.4	1.7	3.4	0.7	-1.7
12.68-15.98	1.5	1.0	2.2	0.5	-1.2
15.98-20.13	1.2	0.7	1.5	0.5	-0.8
20.13-25.36	1.1	0.5	1.1	0.6	-0.6
25.36-31.95	1.2	0.4	0.8	0.8	-0.4
31.95-40.26	2.1	0.3	0.5	1.8	-0.2
40.26-50.72	2.3	0.2	0.2	2.1	0.0
50.72-63.90	1.8	0.1	0.1	1.7	0.0
63.90-80.51	1.0	0.0	0.0	1.0	0.0
80.51-101.44	0.1	0	0	0.1	0

[a]   Bitumen Free - Carbonate Free
[b]   Carbonate Free - Silicate Free

organics associated with the carbonate minerals. The silicate
mineral matrix was determined to interact with a bitumen-free
organic interfacial layer containing relatively more esters,
ketones, and long chain aliphatic compounds. In addition, trapp-
ing of bitumen-free organic matter was observed, particularly in
the case of the carbonate mineral matrix. These interactions
involving carbonate and silicate minerals are descriptive of the
binding forces in Green River oil shale as they pertain to the
interfacial layer between kerogen and the inorganic mineral
matrix.

Acknowledgments

Literature Cited

1.a. Aizenshtat, Z. Baedecker, M. J. and Kaplan, I. R. Geochim. et Cosmochim. Acta 1973, 37, 1881.

  b. Brown, F. S. Baedecker, M. J. Nissenbaum, A. and Kaplan, I. R. Geochim. et Cosmochim. Acta 1972, 36, 1185.

  c. Nissenbaum, A. Baedecker, M. J. and Kaplan, I. R. Geochim. et Cosmochim. Acta 1972, 36, 709.

2. Spiro, B. Chem. Geol. 1980, 31, 27.

3. Vandegrift, G. F. Wimans, R. E. Scott, R. G. and Horwitz, E. P. Fuel 1980, 59, 627.

4. Vangegrift, G. F. Wimans, R. E. and Horwitz, E. P. Fuel 1980, 59, 634.

5. Rouxhet, P. G. and Robin, P. L. Fuel 1978, 57, 533.

6. Jones, D. G. and Dickert, J. J. Amer. Inst. Chem. Eng. Symp. Ser. 1965, 61, 33.

7. Saxby, J. D. Chem. Geol. 1970, 6, 173.

8. Durand, B. and Nicaise, G. in "Kerogen-Insoluble Organic Matter from Sedimentary Rocks", Editions Technip, Paris, 1980, 35.

9. Larson, O. A. Schultz, C. W. and Michaels, E. L. in "Oil Shale, Tar Sands, and Related Materials", Am. Chem. Soc. Symp. Ser. 1981, 163, 139.

10. van Olphen, H. "An Introduction to Clay Colloid Chemistry", Second edition, John Wiley and Sons, New York, 1977; p. 67.

11. Yen, T. F. and Chilingarian, G. V. "Oil Shale", Elsevier Scientific, New York, 1976; p. 1.

12. Fieser, L. F. and Fieser, M. "Organic Chemistry", Third edition, Reinhold, New York, 1956, 1112.

13. Hickinbottom, W. J. "Reactions of Organic Compounds", Third edition, Longman, London, 1957, 608.

14. Bellamy, L. J. "The Infrared Spectra of Complex Molecules", Third edition, Chapman and Hall, New York, 1975.

15. Matkovsky, P. E. Belova, V. N. Brikenshtein, H. A. Dyachkovsky, F. S. Denisova, Z. A. and Kissin, Y. Yvsokomol. Soedim. 1975, A17, 2, 252.

16. Briggs, L. H. Cook, L. D. Fales, H. M. and Wielman, W. C. Anal. Chem. 1957, 29, 904.

17. Spiro, B. Geol. 1979, 25, 67.

18.a. Desborough, G. A. Pitman, J. K. and Huffman, C. Chem. Geol. 1976, 17, 13.

  b. Desborough, G. A. and Pitman, J. K. "Rocky Mountain Association of Geologists", 1974 Guidebook.

19. Hoffman, R. W. and Brindley, G. W. Geochim. et Cosmochim Acta 1960, 20, 15.

20. Allen, T. and Patel, R. M. J. Appl. Chem. 1970, 20, 165.

Mineral Reactions for Two Colorado Oil Shale Samples—A Comparison

LORINDA G. THOMPSON and WILLIAM J. THOMSON

Washington State University, Department of Chemical Engineering, Pullman, WA 99164-2710

Two Colorado oil shale samples; one from the Parachute Creek Member and the other from the C-a tract, were retorted, de-charred and then subjected to temperatures between 800 K and 1100 K in order to study the mineral reactions which take place. Comparisons between these two samples include the reversible nature of ankeritic dolomite and free calcite as well as the temperatures at which significant silication takes place. Results for the C-a tract samples indicated silication appears to take place in stages and that ankeritic dolomite decomposition can be prevented by relatively low CO_2 concentrations. Ankeritic dolomite and calcite decomposition rates were similar for the two samples and there was strong evidence that calcite recarbonation takes place via non-activated chemisorption of CO_2.

Second generation surface oil shale retorting processes will undoubtedly utilize the residual char on the spent shale leaving the retort. Whether this is done by combustion ([1]) or steam gasification ([2]) the temperatures will be sufficiently high that mineral reactions can occur to a significant extent. The more common mineral reactions include dolomite and calcite decomposition as well as solid-solid reactions between mineral carbonates and quartz to form various silicates. The latter reactions proceed at surprisingly fast rates in western shale even at mild temperatures (> 950 K). Since the grain sizes in western shales are on the order of 1-10µ ([3]), this high reactivity is probably due to the associated increase in mobility of the grains.

A knowledge of the mineral reaction rates is important to efficient oil shale processing because the decomposition reactions are highly endothermic and the reaction products can affect the disposal strategy for the shale ash. To date, the most extensive study of mineral reaction rates in western oil shale has been conducted by the oil shale group at Lawrence Livermore Laboratory (4,5). Using a 22 gallon per ton(GPT) oil shale sample from the Anvil Points area, they developed reaction rate expressions for dolomite and calcite decomposition as well as for the formation of silicates which were taken to be a reaction between quartz and calcite. Other investigators (6) however report only the formation of calcium-magnesium silicates.

Since it is usually assumed that western shale is similar when taken from the same horizontal strata, it was decided to investigate the mineral reactions which take place in an oil shale drawn from a deep core hole sample. The sample used was from the C-a tract in Colorado (designated "C-a"). Although, as shown in Table I, the elemental analyses of the C-a sample were similar to those for a sample from the Parachute Creek Member in western Colorado (designated "PCM"), X-ray diffraction data indicated that its dolomitic fraction more nearly resembled ankerite as opposed to dolomite. In addition, the total quantity of mineral carbonates was higher in the C-a sample. Also shown in Table I are data reported by Campbell (3) for a sample taken from the Anvil Points area.

Table I. Oil Shale Sample Data

	PCM	ANVIL (3)	C-a
ASSAY (Gallons per ton)	50	22	25
MINERAL % [a]			
DOLOMITE/ANKERITE	21	35.3	25
CALCITE	9	19.4	30
QUARTZ	–		26
SILICATES	–	41.0	14
ELEMENTAL % [a]			
Ca	10.2	–	12.3
Mg	3.4	–	3.5
Fe	2.8	–	2.5
Al	5.0	–	4.3
Na	2.6	–	2.0
K	1.7	–	1.7
Si	18.8	–	16.2

[a]Based on spent shale

Experimental

Figure 1 shows a schematic sketch of the experimental equipment. Approximately 1.5 g of spent shale (particle size = ~ 100 μ) were placed in a 400 mesh stainless steel basket which was suspended from a recording electrobalance which provided continuous gravimetric readings as the reactions proceeded. The reactor vessel was constructed of 310 stainless steel and placed in a 7.5 cm furnace capable of reaching temperatures as high as 1200 K. Any one or a mixture of gases could be metered to the reactor via a 3.2 mm sparge tube and provisions were made to sample the exit gases with on-line gas chromatography. Tracer tests indicated that the design of the sparge system effectively created an ideal back-mix state. Temperatures were monitored and controlled by means of two 1.6 mm shielded chromel-alumel thermocouples; one placed approximately 2 cm above the basket and the other placed 1 cm below the basket. Typically these two thermocouples read to within 4 K of each other.

Retorted shale samples were first de-charred at 700 K and then attempts were made to isolate the individual mineral reactions. While this was not too difficult in experiments conducted on the PCM sample, it posed a serious problem with the C-a sample. The problem is best understood by referring to the three sets of reactions which describe the primary mineral reactions occurring: the decomposition of ankeritic dolomite (Equation (1)), the reversible decompositon of calcite (Equation (2)), and the formation of silicates from calcite (Equation (3)).

$$CaMg_xFe_{1-x}(CO_3)_2 \longrightarrow CaO + xMgO + (1-x)\ FeO + 2CO_2 \quad (1)$$

$$CaCO_3 \rightleftharpoons CaO + CO_2 \quad (2)$$

$$CaCO_3 + MgO + SiO_2 \longrightarrow CaMg\ Silicates + CO_2 \quad (3)$$
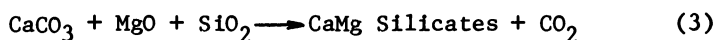
In all samples the presence of CO_2 could prevent calcite decomposition because of the reversible nature of (2). It was also found that the ankeritic dolomite in the C-a sample would not decompose (Equation (1)) below 925 K in the presence of CO_2. This minimum temperature for ankeritic dolomite decomposition was very close to the range where silication reactions were expected. Therefore, it was first necessary to study the silication reactions (Equation (3)) by raising the sample to the desired temperature (1000-1150 K) in the presence of CO_2. Ankeritic dolomite decomposition was investigated by measuring the decomposition rates of virgin samples in a CO_2-free environment at temperatures between 800 K and 925 K. Reversible calcite decomposition was then studied by recarbonating the CaO formed in Equation (1) and varying the CO_2 pressure as well as temperature.
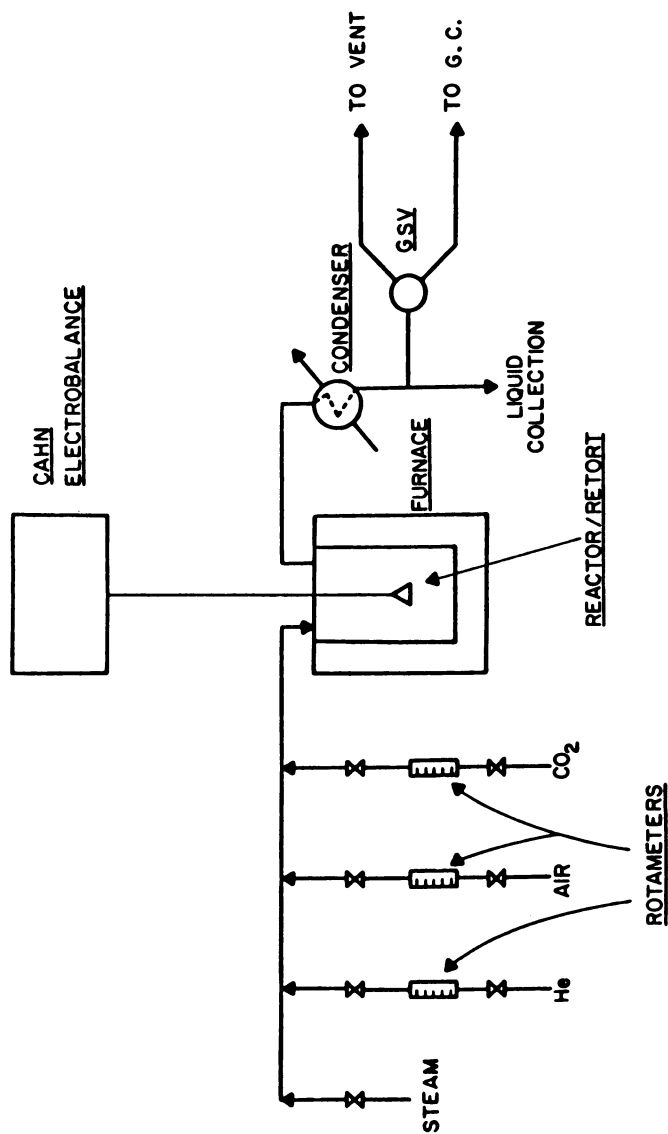
Figure 1. Schematic of thermogravimetric analysis system.

Results

Silication. Figure 2 shows the results obtained when a virgin
C-a sample was allowed to silicate in a CO_2 atmosphere at
temperatures between 1000 K and 1140 K. At 1000 K, silication
ceased after about 30% of the available CO_2 had been released.
That is, 30% of the mineral carbonates had been converted to
silicates. Interestingly, this "staging" effect proceeded as
the temperature was subsequently raised. It is possible that
this phenomenon is due to either the formation of different
silicates or, more likely, to the buildup of a silicate layer
around a reactant grain. The effect of temperatures in the
latter case would be to cause a dramatic increase in the diffu-
sivity of reactants through the layer since solid-solid
diffusion is known to be activated (7). However, attempts at
fitting the data to various grain diffusion models were not
successful and it may be that crystalline phase changes are
occurring as suggested by Huang et al (8). It is also interes-
ting that the silication reaction rates measured with the C-a
sample are approximately 20 times lower than predicted for the
Anvil Points sample (9).
   In one set of experiments a virgin sample was allowed to
decompose completely to the alkaline earth oxides and then
subjected to six cycles of recarbonation/decarbonation at
temperatures between 850 and 930 K. With each cycle there was a
successive reduction in the CO_2 uptake during recarbonation. It
is likely that this is due to irreversible silicate formation
from CaO since mass loss was not noted when the recarbonated
samples ($CaCO_3$) were held in a CO_2 environment at these tempera-
tures. This is somewhat surprising since CaO is normally
thought to silicate only at higher temperatures (6). Further
evidence for this hypothesis was obtained when, at the end of
the sixth cycle, the recarbonated sample was silicated in an
identical manner as the virgin sample described above. In this
case very similar staged plots were obtained but the rates were
reduced by over a factor of two. This would indicate that the
individual calcite grain activity is not uniform and the more
active sites produce CaO which preferentially silicate even at
low temperatures. The less active sites which recarbonate then
result in slower silication rates.

Ankerite/Calcite Decomposition. Since X-ray diffraction data
indicated that the ankeritic dolomite in the C-a sample was
closer to ankerite (x > .5 in Eq. (1)) than to dolomite (x <.3),
we shall refer to it as ankerite in the C-a sample and as
dolomite in the PCM sample.
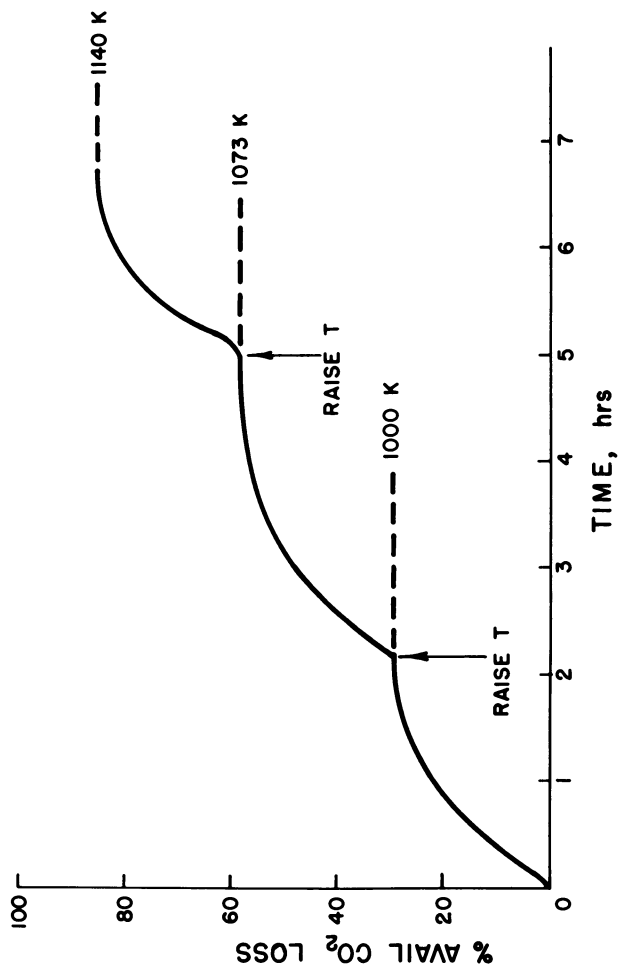
Figure 2. Weight loss due to silication (C-a sample).

Figure 3 is a comparison of first order decomposition plots for both ankerite and calcite in the C-a sample with that predicted by Soni and Thomson (12) for dolomite in the PCM sample. In both samples calcite decomposes at the same rate as the complete decomposition of ankerite (Eq (1)) at 850 K. However, it should be kept in mind that the data for calcite decomposition shown in Figure 3 is for calcite which was recarbonated from the CaO produced by Equations (1) and (2). Note also that the decomposition rates are about 30% lower in the C-a sample.

Based on past experience with the PCM sample, it was expected to be able to separate the ankerite decomposition into two steps.

$$CaMg_x Fe_{1-x}(CO_3)_2 \longrightarrow CaCO_3 + xMgO + (1-x)FeO + CO_2 \qquad (4)$$

$$CaCO_3 \rightleftharpoons CaO + CO_2 \qquad (2)$$
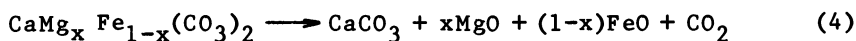
That is, since dolomite decomposition was unaffected by the presence of CO_2 and calcite decomposition can be prevented by a sufficient CO_2 over-pressure, Equation (4) was expected to prevail if ankerite decomposition was carried out at low temperatures (< 900 K) in a CO_2 environment. Figure 4 shows the results for ankerite decomposition carried out at two different temperatures with and without CO_2. Note that the presence of CO_2 completely prevents decomposition at 853 K and severely inhibits decomposition at 900 K.

However, when the temperature was raised to 933 K, ankerite decomposition was unaffected by the presence of CO_2. This afforded an opportunity to separate Reactions (4) and (2) but only in the narrow temperature range between 935 and 975 K (since 975 K was close to the minimum silication temperature). These results indicated that the rates of Equations (2) and (4) were almost identical and thus, if the reaction does proceed in two steps, the rate of (4) is the controlling step at these temperatures.

Figure 5 shows an Arrhenius plot for calcite and ankerite decomposition in the C-a sample. Although the rate constants are about equal at low temperatures, the higher activation energy for calcite (171 vs. 146 kJ/mole) produces rate constants which are 2.5 times higher for calcite than for ankerite at 925 K. Table II shows a comparison of the forward reaction rate constants for calcite decomposition for the three samples. All three have similar decomposition rate constants although Campbell and Burnham (9) report a higher activation energy for the Anvil Points shale.
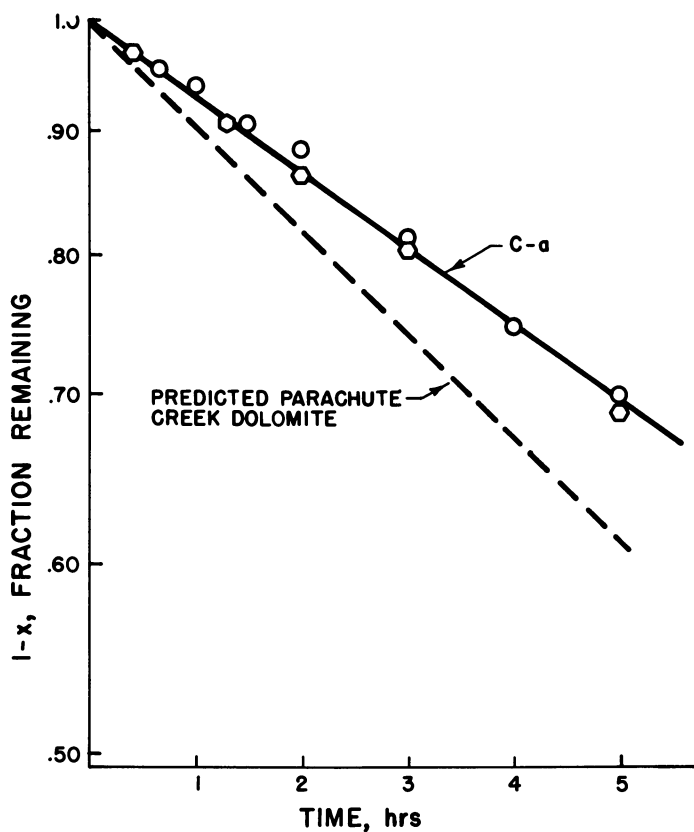
Figure 3. Mineral decomposition in He at 853 K. Key: ○, ankerite; and ○, calcite.
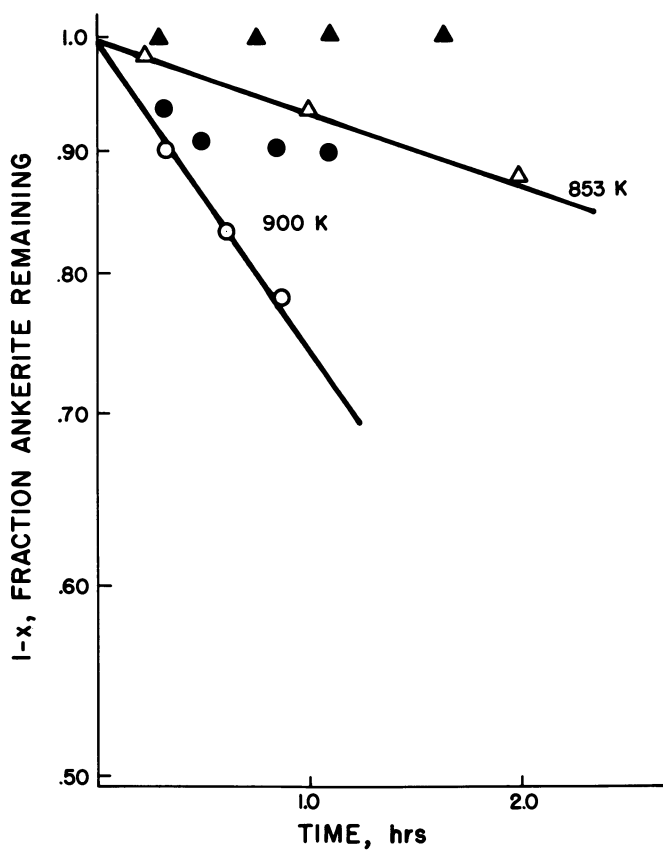
Figure 4. Decomposition of ankerite in the C-a sample. Key: ○ and △, CO₂ free; and ●
and ▲, 7% CO₂.
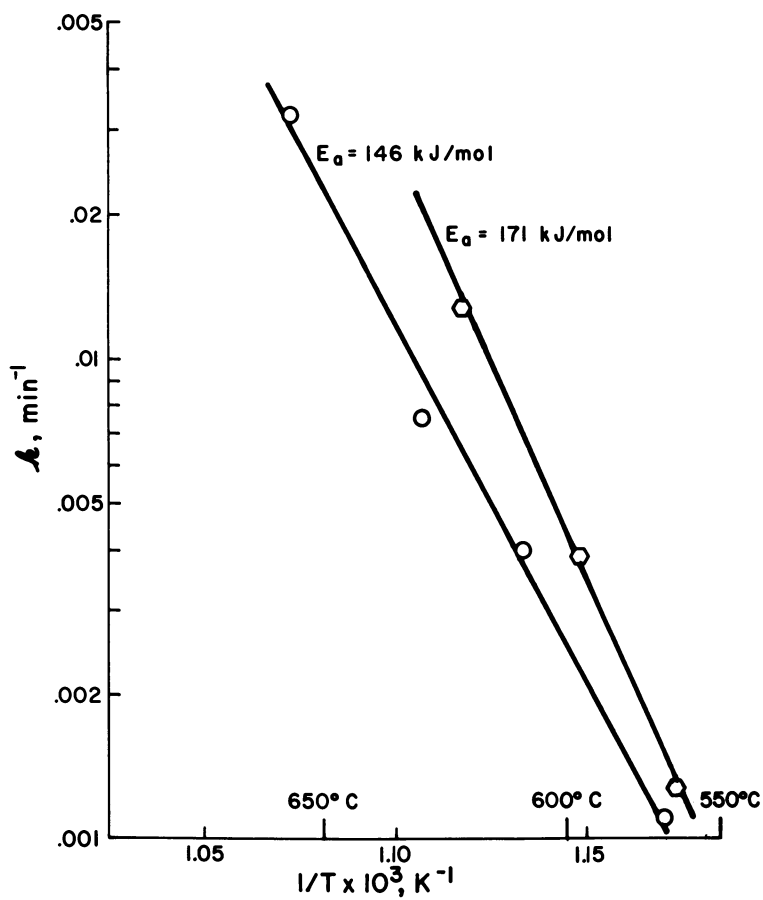
Figure 5.   Arrhenius plot: decomposition of ankerite (⊘) and calcite (◯) (C-a sample, He environment).

Table II. Comparison of Calcite Rate Parameters

$$CaCO_3 \underset{k_r}{\overset{k_f}{\rightleftharpoons}} CaO + CO_2$$
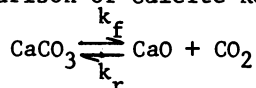
$$k_f = k^o_f \exp \left[-\frac{E_{f,r}}{RT} \right]$$

	E_f	k_f(at 853 K)
C-a	171 kJ/mol	0.0014 min^{-1}
PCM	171	0.0037
ANVIL PTS	242	0.0017

Reversible Calcite Decomposition. The reversible nature of cal-
cite decomposition was studied in both the PCM and C-a samples.
In the former this was achieved by carrying out the
decomposition at CO_2 pressures less than the equilibrium values.
In the latter, the calcite was decomposed to completion in a
CO_2-free atmosphere and then recarbonated at various CO_2 pres-
sures and temperatures. The data obtained with the PCM sample
were fit to the expression shown in Equation (5),

$$\frac{dX}{dt} = k_f \left[1 - \frac{X}{1-X} \frac{P_{CO_2}}{K_{eq}} \right] \qquad (5)$$

where X is the fraction calcite decomposed and K_{eq} is the
equilibrium constant. The rate constant and K_{eq} are given by
Equations (6) and (7).

$$k_f = 1.75 \times 10^6 \exp \left[\frac{-20,584}{T} \right] \qquad sec^{-1} \qquad (6)$$

$$K_{eq} = 6.2 \times 10^9 \exp \left[\frac{20,986}{T} \right] \qquad kPa^{-1} \qquad (7)$$

The recarbonation rates for the C-a sample are shown in
Figure 6 as a function of P_{CO_2} at 853 K. At each pressure the
initial data all follow a first order process and, moreover, the
slopes are directly proportional to P_{CO_2} . The latter indicates
that the recarbonation is initially first order with respect to
CO_2 as well as to the fraction CaO remaining. While the entire
recarbonation appears to be first order at P_{CO_2} = 2 kPa, note
that there is a significant departure from first order behavior
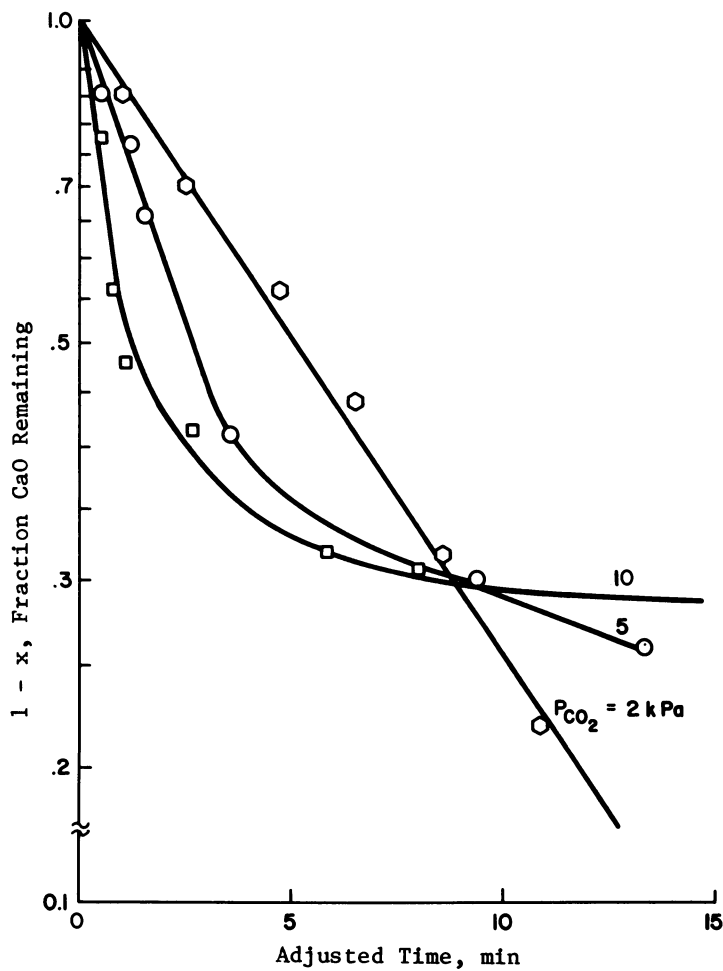
Figure 6. Effect of P_{CO_2} on calcite recarbonation (T = 853 K).

at higher CO_2 pressures. In fact, the departure occurs earlier and more abruptly as P_{CO_2} increases. A possible explanation for this behavior is that recarbonation takes place via a two-step mechanism; chemisorption of CO_2 on multiple CaO sites followed by chemical reaction to $CaCO_3$.

That is

$$CO_2 + nCaO \rightleftharpoons CO_2 \cdot [nCaO] \qquad\qquad (8)$$

$$CO_2 \cdot [nCaO] \rightleftharpoons CaCO_3 + (n-1)CaO \qquad\qquad (9)$$
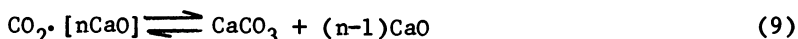
    This suggested mechanism is consistent with a number of observations made here and with previous work reported in the literature. For example it was found that recarbonation rates were relatively insensitive to temperature. This would indicate non-activated chemisorption and, as Fischbeck and Snaidt report (10), mineral recarbonation is often independent of temperature when the temperature dependencies of the decarbonation rate constant and the equilibrium constant are similar. This is exactly what is observed in western oil shales (Ref (9), Equations (6) and (7)). Previous work has also pointed to the role of chemisorption phenomena in mineral decomposition reactions. Spencer and Topley (11) have suggested that finely grained oxides can chemisorb H_2O as well as H_2 and Soni and Thomson (12) observed higher recarbonation rates when CO_2 was produced on the surface during oil shale char combustion.
    Further evidence that surface phenomenon is responsible for recarbonation is given in Figure 7 which compares recarbonation rates under identical conditions but with samples of a different history. Note that the sample which was subjected to five cycles of decarbonation-recarbonation, departs from first order behavior sooner and more drastically than the sample which had only been subjected to two cycles. While a virgin sample maintained first order behavior to higher conversions, it too exhibited a noticeable reduction in rate at higher conversions. Similar behavior has been noted in previous investigations of the decomposition of pure mineral carbonates and is usually referred to as "retention" (13). This has been attributed to the inability of some CaO sites to release strongly chemisorbed CO_2. Whatever the mechanism, the variation with decarbonation cycling indicates a change in surface structure and may be due to sintering and/or agglomeration of CaO sites.

Conclusions

    In comparing these shales, the most significant finding was that ankeritic dolomite decomposition could be prevented in the C-a sample below 930 K, with relatively low concentrations of CO_2. The enthalpy of reaction for Equation (4) is
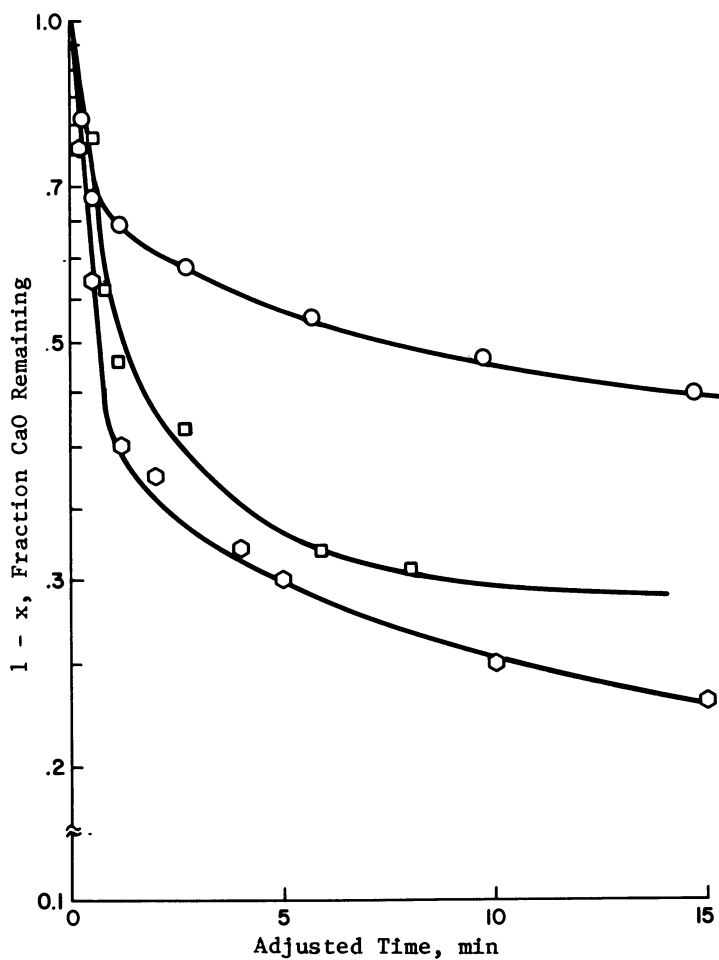
Figure 7. Effect of cycling on calcite recarbonation (T = 853 K, P_{CO_2} = 10 kPa). Key: ○, 5 cycles; □, 2 cycles; and ◯, virgin.

approximately 126 kJ/mole (3), which is an indication of the energy that could be saved while processing an oil shale of this nature.   It was also found that the activation energy for ankeritic dolomite decompostion was lower than that for calcite which may account for the apparent shift in the rate controlling step from Reaction (2) to Reaction (4) as temperatures were increased.

For all three of the shales, calcite decomposition rates in helium were similar. Reversible calcite studies with the C-a sample indicated that recarbonation takes place via chemisorption of CO_2.   The effects of "cycling" a sample on both subsequent recarbonation and silication suggests a loss of active sites, possibly by sintering. The lack of success in fitting the silication data to any solid state grain diffusion models, was yet another indication of the difficulty in predicting the behavior of these minerals. In all of the reactions studied it was apparent that the reaction rates were influenced by a combination of chemical kinetics, grain mobility, solid state crystalline behavior and chemisorption phenomena.

Acknowledgment

Literature Cited

1.   Hall, R.N., paper presented at National AIChE Meeting, Anaheim, CA., June 8, 1982.
2.   "Union Claims Boost in Shale-oil Technology", Oil & Gas J., 1974, 24, 26-7.
3.   Campbell, J. H., Lawrence Livermore Laboratory Rept. UCRL-52089, Pt. 2, 1978.
4.   Burnham, A. K., Stubblefield, C. T. and Campbell, J. H., Fuel, 1980, 59, 871.
5.   Burnham, A. K. and Koskinos, G. K., Lawrence Livermore Laboratory. Rept., UCID-18708, 1980.
6.   Park, Won C., Lindemanis, A. E. And Raab, G. A., In Situ.,1979, 3, 353.
7.   Schmalzried, H., "Solid State Reactions", Verlag Chemie, Academic Press, N.Y., 1974.
8.   Huang, C. S., Rogan, F. H. and Kun, Li, AIChE SYMP Ser., 77, #202, p. 1, 1982.
9.   Campbell, J. H. and Burnham, A. K., paper presented at AIChE National Mtg, Houston, TX, April 1-5, 1979.

10. Fischbeck, J. and Snaidt, R., Z. Electrochem., 1932, 38,
     p. 199.
11. Spencer, W. D. and Topley, B., J. Chem. Soc.,1929,
     p. 2633.
12. Soni, Y. and Thomson, W. J., I & Ec Proc. Des & Dev., 1979,
     p. 661.
13. Young, D. A., "Decomposition of Solids",Int. Encycl.
     Phys. Chem. & Chem. Phys., 1966, 1, Pergamon Press, NY.

Indigenous Mineral Matter Effects in Pyrolysis of Green River Oil Shale

K. M. JEONG and JOHN F. PATZER II

Gulf Research & Development Company, Pittsburgh, PA 15230

The effects of carbonate, silicate, and pyrite minerals on Green River oil shale pyrolysis were investigated using thermogravimetric analysis. Pyrolysis yields for raw oil shales increased with increasing organic carbon content of the oil shale, or, equivalently, with increasing silicate/carbonate ratio. Pyrite mineral effects were also found to increase with increasing silicate/carbonate ratio for the raw shales. Samples of carbonate-free and carbonate-, silicate-free shales were prepared by a preferential mineral extraction method. Pyrolysis yields and pyrite mineral effects were again found to be influenced by the presence of silicates. The results suggest that silicates contribute actively to the pyrolysis process through reactions with carbonates and through catalysis of organic decomposition and organic-pyrite interactions.

Conventional oil shale processing is based upon the thermal decomposition of kerogen and bitumen into various grades of oil products, gases, and carbonaceous residue. Historically, a variety of pyrolysis conditions, involving both above ground and in situ processing, have been used to obtain oil from shale. Numerous kinetic studies (1-6) have investigated the temperature and pressure effects on oil yield. Both isothermal and nonisothermal methods have been used. The studies have established an accepted decomposition mechanism which involves a series of consecutive reactions in which kerogen is first thermally converted to pyrobitumen. Pyrobitumen is a term used to describe the first, heavy kerogen decomposition product. The morphological resemblance of pyrobitumen to naturally occurring bitumen is unknown. Pyrobitumen and bitumen then generate volatile oils and gases and nonvolatile residual carbon. The physiochemical properties of oil shale undoubtedly influence the decomposition process.

A long history of speculation exists with regard to the con-
tribution of mineral constituents in oil shale to the kerogen and
bitumen decomposition process. The inorganic mineral matrix is
known to be intimately associated with the organic fraction (7),
both kerogen and bitumen, and therefore, is believed to affect the
conversion and release of oil products. Carlson (8) found that
the rate of kerogen conversion is related to the concentration of
inorganic matter in the shale, with the rate increasing with
increasing proportions of mineral matter. Carlson thus postulated
that the mineral matter was having a catalytic effect on the
kerogen conversion.

Previous thermogravimetric studies (9-11) on the influence of
mineral matter effects on kerogen conversion have focused on moni-
toring of the characteristic organic decomposition step of
specially prepared mixtures and the composition of the resulting
pyrolysates. In a study on the addition of various minerals to
kerogens prior to pyrolysis, Horsfield and Douglas (9) found that
increasingly acid minerals, in the order calcium carbonate, kaoli-
nite, bentonite, and alumina, lead to increasingly higher amounts
of lower molecular weight components in the pyrolysates. This
indicates a mineral matter-induced, acidic catalytic cracking
phenomenon taking place during the kerogen pyrolysis.

Espitalie, et al. (10) studied the pyrolysis of various kero-
gen types in mixtures with various minerals in addition to pyroly-
sis experiments on the source rocks for the kerogens. They
concluded that the minerals act as a heavy hydrocarbon trap, in
effect, limiting the possible yield of hydrocarbons from source
rocks. They also found that carbonate minerals have a lower
specific activity for the trapping phenomenon than do silicate
minerals.

Rostam-Abadi and Mickelson (11) studied the effects of pyrite
addition to both Eastern U.S. Devonian shales and Green River
shales. They found that a small amount of pyrite can cause a
sharp drop in the rate of kerogen decomposition. They also found
that the presence of pyrite results in a secondary decomposition
peak in the temperature range of 500-550°C, which follows the
primary kerogen decomposition peak in the temperature range of
about 400-500°C. Rostam-Abadi and Mickelson interpreted the
secondary peak as an interaction between the pyrite and kerogen
which lead to the formation of stable, char-forming thiophenic
structures during kerogen pyrolysis, resulting in a decreased rate
of of kerogen decomposition. The secondary decomposition peak was
believed due to partial pyrite decomposition.

Although the preceding observations seem to indicate definite
mineral matter influences on kerogen decomposition, extrapolation
of the results to actual oil shale processing is tenuous because a
physical mixture of kerogen and mineral matter, such as was used
in most of the previous work, is not likely to reproduce the exact
forms of physical structure or chemical bonding that exist in
indigenous oil shale.

The above studies provided the basis for this study on the effects of indigenous carbonate, silicate, and pyrite minerals on the pyrolysis of Green River and Eastern U.S. oil shales through thermogravimetric-differential thermogravimetric (TG-DTG) and thermogravimetric-mass spectroscopy (TG-MS) methods. The samples were prepared by a chemical extraction method which was shown to preferentially disassociate mineral components from the oil shale (12). In addition, the effect of oil shale richness, i.e., kerogen concentration, on pyrolysis yield was studied. Since the major mineral constituent not separated by the chemical extraction procedure was pyrite, a pyrite concentrate was prepared by standard density separation techniques from the carbonate/silicate-free kerogen concentrate. A silicate-induced pyrolysis effect, in conjunction with pyrite, is discussed based upon the TG-DTG data of the original and chemically extracted samples.

Experimental

Green River oil shale, obtained from the Mahogany zone of the C-a tract in Rio Blanco County, Colorado, was crushed to nominal 15 cm topsize and separated by standard density separation techniques (13,14) into nominal grades of 104, 129, and 184 liters per tonne (L/t). Each grade fraction was then further size-reduced to finer than 10 mesh and screened into different mesh size samples. The 100 to 200 mesh shale from each grade was used in the current experiments. Several experiments were also conducted using samples of Eastern U.S. shale obtained from Lewis County, Kentucky.

The chemical extraction procedure used to preferentially disassociate carbonate and silicate minerals is described elsewhere in this Symposium Series (12), and, thus, will be described only briefly here. The separation scheme is outlined in Figure 1. Initially, a bitumen-free oil shale is isolated by exhaustive Soxhlet extraction with a methanol/benzene mixture. A portion of the bitumen-free shale oil is then treated with HCl to produce a carbonate-, bitumen-free oil shale. Following Soxhlet extraction with benzene/methanol to remove carbonate-associated bitumens, a portion of the carbonate-, bitumen-free oil shale is then extracted with HF/HCl to produce a silicate-, carbonate-, bitumen-free shale. This shale is also Soxhlet extracted to remove silicate-associated bitumens. Finally, a portion of the silicate-, carbonate-, bitumen-free shale is separated by density into three fractions by sink/float techniques using both 15 wt% $ZnCl_2$ in distilled water and pure distilled water as immersion bath media.

TG-DTG measurements were made with a DuPont Model 951 thermogravimetric analyzer equipped with a 1091 disk memory. Weight loss data were obtained as a function of time and temperature. Samples were heated from room temperature to 900°C at a rate of 10°C/min. The purge gas was ultra-pure nitrogen, typically at

ORIGINAL OIL SHALE
|
BENZENE/MeOH EXTRACTION
|

BITUMEN FREE O.S.   BITUMEN I
|
6N HC1 EXTRACTION
(REMOVES CARBONATES)
|
CARBONATE–FREE O.S.
|
BENZENE/MeOH EXTRACTION
|

CARBONATE, BITUMEN   BiTUMEN II
FREE O.S.
|
50% HF/6N–HC1 EXTRACTION
(REMOVES SILICATES)
|
CARBONATE, SILICATE
FREE O.S.
|
BENZENE/MeOH EXTRACTION
|

CARBONATE, SILICATE   BITUMEN III
BITUMEN FREE O.S.
|
DENSITY SEPARATION WITH
DISTILLED WATER
|

SINK FRACTION   FLOAT FRACTION

Figure 1. Preferential mineral matter dissolution by chemical methods for oil shales.

100 ml/min. TG-MS data were obtained using a Cahn RH microbalance coupled to a Finnigan quadrapole mass spectrometer.

Results and Discussion

   Green River oil shale is a sedimentary rock consisting of finely laminated layers of marlstone interspersed with varying amounts of organic matter. These oil shales contain approximately 30-60 wt% carbonate minerals and 30-40 wt% silicate minerals. The bulk mineralogical composition of the starting 104, 129, and 184 L/t shales obtained from density separation were found to be fairly similar. The major minerals identified included analcime, clay, quartz, albite, ankerite/dolomite, and calcite. Elemental analysis of the three shales indicated that the organic matter stoichiometries were essentially identical. Thus, the density separation procedure appears to have isolated increasingly richer grades of shale without selectively altering the organic matter stoichiometry.
   Eastern U.S. oil shales are also sedimentary rocks. However, in contrast to Green River shales, the mineral constituents of Eastern U.S. shales are primarily silicates, with only about 1 wt% carbonate minerals. The bulk mineralogical composition of the Kentucky shale consisted primarily of quartz, illite and kaolinite, with some chlorite and pyrite. This is consistent with elemental analysis data which found the major mineral constituents to be Si, Al, Fe, and K. The elemental Ca concentration was less than 100 ppm.

Thermogravimetric Analysis of Untreated Shales. Figure 2 shows typical thermogravimetric data for the untreated 104, 129, and 184 L/t Green River oil shales and the Eastern U.S. oil shale. All of the weight loss data discussed in this paper were obtained at a heating rate of 10°C/ min. Differential analysis of the TG curves, DTG, indicates two major regions of volatile product release, peaking near 465 and 740°C, respectively. The majority of weight loss below 200°C is believed to be due to water evaporation.
   Traditionally, the DTG peak observed near 465°C has been assigned to organic carbon pyrolysis. Our TG-MS results, Figure 3, indicate that the organic matter release profile in the range 350 to 500°C, peaking near 430°C, is a broad mixture of C_{10}-C_{15} compounds which cannot be easily resolved into specific product identifications. Note that the temperatures associated with the TG-MS data are about 20 to 30°C lower than those for the TG-DTG experiments. This effect results from differences in instrumentation and does not reflect differences in pyrolysis. The potential contribution of silicate and carbonate minerals to the weight loss in this region was checked by separate TG of the major individual mineral constituents identified in the shale samples. The individual minerals showed insignificant thermal
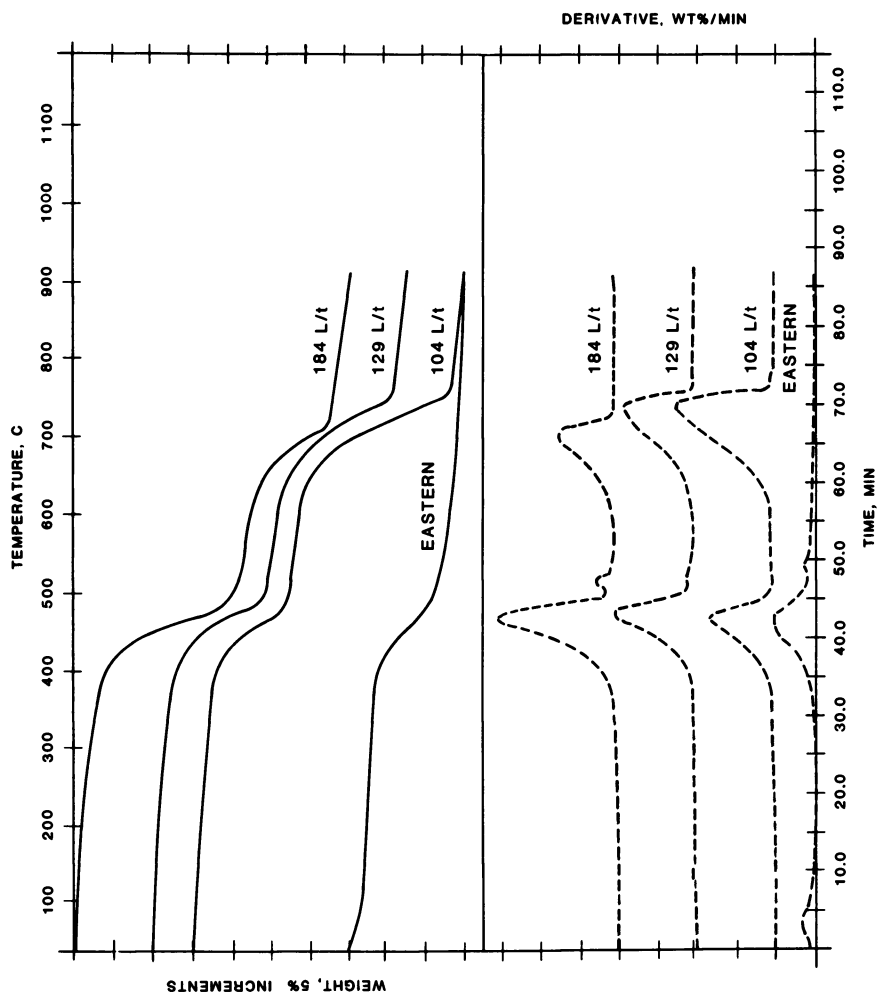
Figure 2. Thermogravimetric analysis of untreated Green River and eastern United States oil shales.
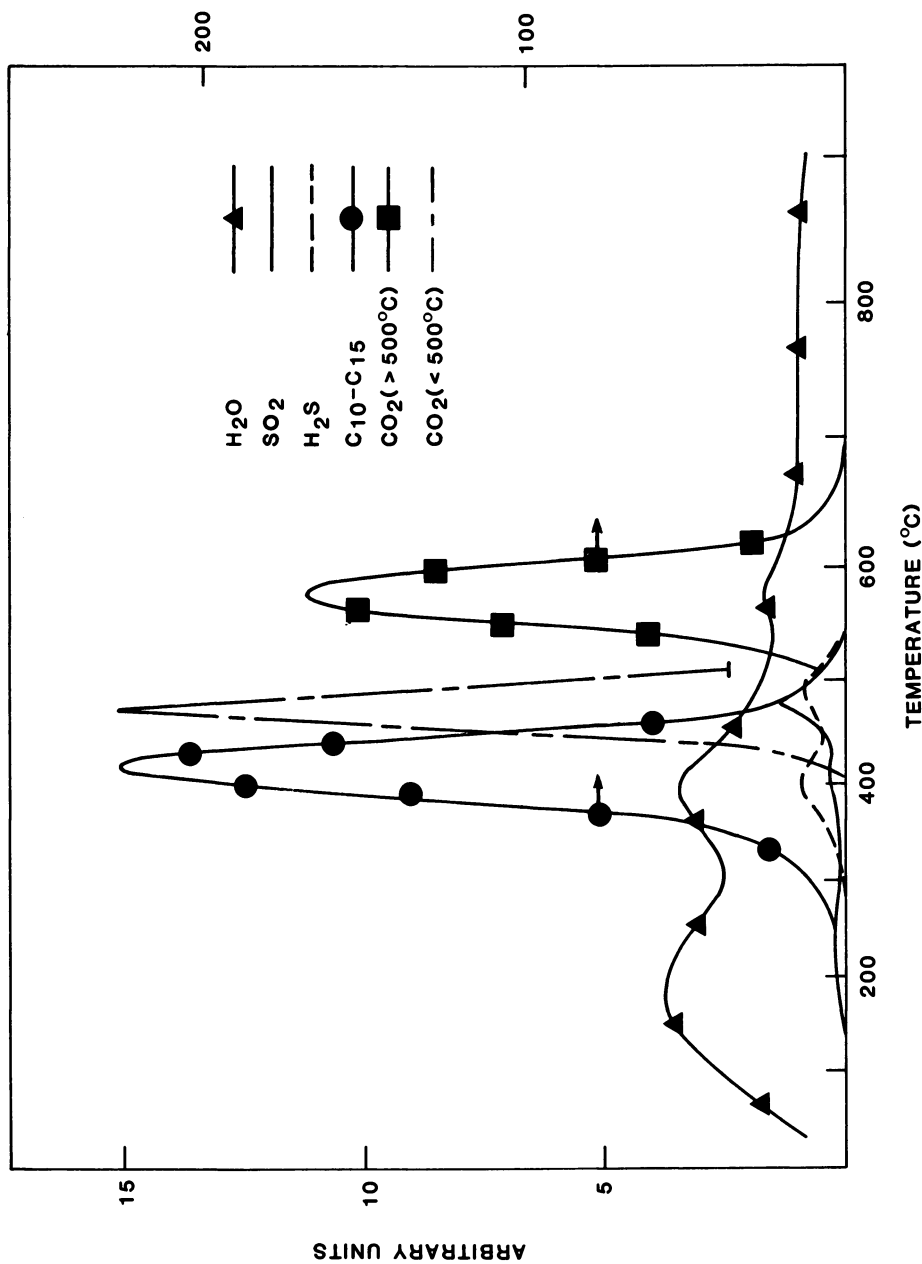
Figure 3. Thermogravimetric–mass spectroscopic analysis of 184 L/t untreated Green River oil shale.

decompositions over the temperature range 350 to 500°C, further supporting the traditional assignment of this DTG peak to organic matter pyrolysis.

The thermal decomposition of the carbonate minerals in Green River shales is reflected in the DTG maximum at 730 to 760°C in Figure 2. TG of pure calcite and dolomite show carbonate decomposition at 800°C and 730 to 780°C, respectively. The principle volatile product found by TG-MS in this temperature range was CO_2. These results are in agreement with Campbell (15), who found shale carbonate minerals undergo three major types of reactions in this region: (i) decomposition of dolomite to MgO, CO_2, and calcite; (ii) decomposition of calcite to CaO and CO_2; and (iii) reaction between calcite and silica to form calcium silicates.

The TG-DTG data correspond well with other available analytical data for the three samples. For example, the ratio of the weight loss in the organic evolution peak at 465°C to that of the CO_2 peak at 740°C increased from about 0.4 for the 104 L/t sample to about 1.5 for the 184 L/t sample. This trend is consistent with the relative organic carbon content of the two samples as well as the bulk mineralogy data which indicate that the 104 L/t sample has approximately 14 wt% calcite and 30 wt% dolomite versus less than 2 wt% calcite and 20 wt% dolomite for the 184 L/t sample. Carbonate carbon concentrations, as determined by acid leaching and evolved CO_2 titration, were found to be 4.8, 3.9, and 3.2 wt% for the 104, 129, and 184 L/t samples, respectively. These values correspond to expected weight losses in the TG carbonate decomposition region of approximately 18, 14, and 12 wt%, respectively, which compare well with observed weight losses of 21, 14, and 12 wt%, respectively.

DTG of a pyrite standard showed thermal decomposition over the temperature range 480 to 700°C, with the major weight loss occuring near 660°C. Although the pyrite concentration in the untreated oil shales was about 2 wt%, there is no clear indication in the DTG of these materials of any peak due to pyrite decomposition. The shales do, however, show evidence of a shoulder on the organic evolution peak, near 520°C. The TG-MS results for the 184 L/t shale show a definite evolution of SO_2 and H_2S occuring at about 500°C. Pyrite-organic matter reactions involving, for example, complexing of FeS_2 and elemental sulphur with aromatic and olefinic compounds are a potential explanation of this phenomenon. These results are in agreement with those of Rostam-Abadi and Mickelson (11) which were previously discussed. Similar mechanisms have been proposed for the effect of pyrites in coal pyrolysis and gasification (16).

Weight loss data determined from the TG curves are expressed in terms of the weight ratio of pyrolyzed organics from the TG experiment $(Or)^{TG}$ to the original organic content of the shale, (Or). This ratio is an expression of the net organic pyrolysis yield of the sample. Table I summarizes the pyrolysis yields determined for the 104, 129, and 184 L/t untreated shale samples.

The pyrolysis yield is observed to increase with shale organic content from 58.5 to 72.2 wt%. The increase in pyrolysis yield could be due to two factors: the mineral trapping phenomenon advanced by Espitalie, et al. (10) and a silicate-induced catalytic effect which will be discussed more fully. The organic decomposition temperature is reasonably constant for the three shales. The carbonate decomposition temperature, however, seems to be decreasing with increasing organic content. This probably reflects a changing dolomite/calcite ratio in the shales, as calcite decomposes at higher temperatures than does dolomite.

For comparison purposes, a sample of Eastern U.S. shale was also analyzed by TG-DTG. The absence of the characteristic carbonate decomposition peak in the 700-800°C temperature range is indicative of the lack of carbonate minerals in Eastern U.S. shales. The net organic pyrolysis yield, 47.6 wt%, Table I, is

Table I. Pyrolysis of Untreated Oil Shales[a]

Oil Shale	104 L/t	129 L/t	184 L/t	Eastern U.S.
Elem. Anal., wt%				
(C_c)	4.8	3.8	3.2	0.03
(C_o)	11.4	11.9	19.4	12.4
(Or)	14.2	14.8	24.1	--
X-ray Anal., wt%				
Carbonates	58	49	37	<1
Silicates	22	36	44	--
Pyrites	>1	>1	>2	3.4
TG Anal.				
$(C_c)^{TG}$, wt%	5.8	3.9	3.2	--
$(O_r)^{TG}$, wt%	8.3	9.8	17.4	5.9
$T_{o,max}$, °C	463	465	467	453
$T_{c,max}$, °C	758	733	729	--
TG. Pyr. Yield, wt%[c]				
Organics	58.5	66.2	72.2	47.6

[a] (C_c), (C_o), and (Or) represent carbonate carbon, organic carbon, and total organic concentration. For Green River oil shale: $(O_r) = (C_o)/0.805$ (23). TG superscript refers to TG measured quantities.

[b] $T_{o,max}$ and $T_{c,max}$ are the temperatures corresponding to the maximum in the DTG curve for the organic and the carbonate decomposition regions, respectively.

[c] Equal to 100 $(Or)^{TG}/(Or)$ Green River shales, 100 $(Or)^{TG}/(C_o)$ for Eastern U.S. shale.

substantially lower than that found for the Green River oil shales and is consistent with the lower H/C ratio and higher aromaticity (22) in the organic fraction. The lower maximum DTG pyrolysis temperature, 453°C, is possibly due to the absence of carbonate mineral bonding and, therefore, a lower enthalpy of reaction. The secondary peak near 520°C, indicative of pyrite-induced organic pyrolysis, is also observed in the DTG for the Eastern U.S. shale. The pyrite content of this shale is about 3 wt%.

TG-DTG Results of Treated Green River Oil Shale Fractions. The influence of the mineral matrix on the pyrolysis of Green River oil shale was investigated with the 184 L/t shale sample. In contrast with earlier studies (9-11), which were based upon the physical combination of mineral additives with oil shale and/or a kerogen concentrate, this study investigated the effects of the indigenous minerals through a procedure which selectively and sequentially removed various mineral constituents from the shale (12). The experimental procedure, outlined in Figure 1, produced the following six samples which were analyzed by TG: (A) a water-washed 184 L/t sample; (B) a bitumen-free sample; (C) a bitumen-, carbonate-free sample, (D) a bitumen-, carbonate-, silicate-free sample, i.e., kerogen concentrate, (E) a float fraction of the kerogen concentrate, and (F) a sink fraction of the kerogen concentrate. The thermogravimetric data are summarized in Table II. The TG-DTG curves for the six samples are shown in Figure 4.

Table II. Influence of the Mineral Matrix on Pyrolysis of Green River Oil Shale

Oil Shale	A	B	C	D	E	F
Elem. Anal., wt%						
(C_c)	2.9	3.1	0.2	0.2	0.2	0.2
(C_o)	20.5	19.3	25.7	66.6	66.6	65.3
(O_r)	25.5	24.0	31.9	82.7	82.8	81.1
X-ray Anal., wt%						
Carbonates	33	--	<1	0.8	0.2	0.6
Silicates	44	43	40	3.2	2.7	0.5
Pyrites	3.4	3.4	3.3	2.5	2.0	0.5
TG Anal., wt%						
$(C_c)^{TG}$, wt%	3.2	3.6	--	--	--	--
$(O_r)^{TG}$, wt%	15.3	14.8	20.8	47.6	56.7	45.7
$T_{o,max}$, °C	464	459	472	456	468	463
$T_{c,max}$, °C	724	704	--	--	--	--
TG Pyr. Yield, wt%						
Organics	60.0	61.7	65.2	57.6	68.5	56.4
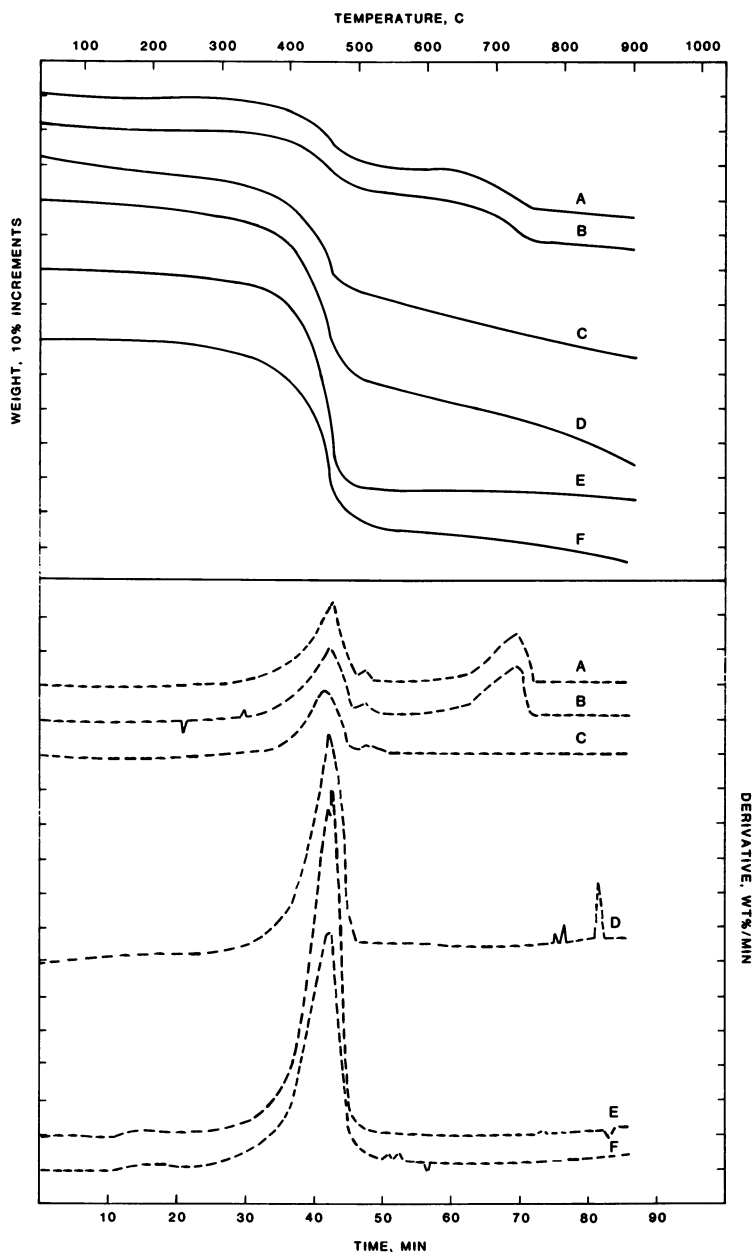
Figure 4. Thermogravimetric analysis of treated Green River oil shales. Key: A, water-washed 184 L/t; B, bitumen-free; C, bitumen- and carbonate-free; D, kerogen concentrate; E, kerogen concentrate float fraction; and F, kerogen concentrate sink fashion.

Sample A, the water-washed 184 L/t shale, is the raw shale against which comparisons on the effect of mineral constituents will be made. Contrary to initial expectations, the net pyrolysis yield after removal of the bitumen, Sample B, is observed to increase by 1.5 wt% with respect to that of Sample A. Although the bitumen component is generally believed to be pyrolyzed quantitatively, the kerogen component appears to be converted more effectively in the absence of bitumen. The secondary TG peak near 520°C, Figure 4, is still present for the bitumen-free sample. Thus, the peak is not associated with bitumen pyrolysis and is, therefore, by inference, associated with the bitumen-free kerogen component.

Removal of the carbonate minerals by HCl treatment, Sample C, resulted in a significant increase of 8.6 wt% in the net pyrolysis yield. The carbonate DTG maximum near 730°C is noticeably absent from the Sample C DTG curve, Figure 4. The postulated explanation of the increased yield of the bitumen-, carbonate-free shale is a combination of several factors. It appears that the carbonate minerals, thermochemically and/or kinetically, act to hamper the pyrolysis yield or possibly modify the mechanistic reaction pathway so as to yield a higher percentage of residual carbon. The observed increase in the pyrolysis yield is not due to the release of bitumen trapped by the carbonate minerals because such bitumens were removed by Soxhlet extraction prior to the TG analysis.

The decomposition of pure phase carbonate minerals has been extensively studied and reviewed (17). The influence of these minerals on oil shale pyrolysis kinetics has not been extensively studied, but the studies of Jukkola et al. (18) and Campbell (15) are notable. The results of both these studies indicate that the major calcite decomposition step is through reaction with silicate minerals in shale to produce Ca- and Ca-, Mg-silicates. The observed enhancement in pyrolysis yield after carbonate removal may be indicative of the catalytic role of silicate minerals in paraffinic and aromatic compound decompositions. In effect, an apparent preference for calcite-silicate interactions in raw shale limits silicate-catalyzed organic reactions which would presumably result in enhanced oil yields. It should be noted, however, that the silicate/carbonate ratio is increasing with net pyrolysis yield for the raw shales, Table I. This may reflect excess silicates becoming free to catalyze organic decomposition.

This proposed silicate mineral catalytic effect is further demonstrated by TG measurements of the kerogen concentrate, Sample D, which show a decrease in the net pyrolysis yield from 68.8 wt% for the bitumen-, carbonate-free Sample C to 57.6 wt% for the now silicate-free sample. These results suggest that the optimum pyrolysis oil yield is achieved for Green River oil shales which are carbonate-free, but still retain their original silicate mineral concentration or, possibly, an increased silicate concentration.

The positive effect of silicate minerals on oil shale pyroly- sis was not a priori predictable and its origin is difficult to quantify. However, one possible explanation involves the combined chemistry of silicate minerals, kerogen, and pyrite. It is known that pyrite can occur in the form of microcrystals coated with organic matter which aggregates together to form spherical fram- boids (19). It is proposed that organic decomposition at the pyrite-organic matter interface may be catalyzed by silicate minerals which act as an effective third body for the formation of thiophenic compounds. Liberation of the organic matter via pyrite decomposition and subsequent transformation would result in the observed oil yield trend. It has been shown that the reactions of S or H_2S with various organic molecules results in the formation of thiophenic structures as does the reaction of FeS_2 with organ- ics (20-21).

The catalytic effect of silica and aluminosilicates in sul- fur/organic reactions has been previously suggested in other chemical systems, but, to the authors' knowledge, has not been experimentally verified. A possible experimental observation of this interaction may be the 520°C DTG peak. Removal of the sili- cate minerals by HCl/HF extraction resulted in a significant reduction of the thermal decomposition process at this tempera- ture, as can be seen in Figure 4. Reproduction of the 520°C peak could only be obtained with substantial additions to the kerogen concentrate of a low temperature ash sample. In addition, an increase in the relative amount of weight loss at 520°C in compar- ison to the organic carbon decomposition was obtained by adding a fairly large amount of pyrite to Sample A.

The last step outlined in Figure 1 is the separation of the kerogen concentrate, Sample D, into sink-float fractions, samples E and F, respectively, by heavy media techniques (13,14) at a density of 1.145 g/mL. As seen in Figure 4, both fractions showed the typical organic matter decomposition at 460-470°C. As with the kerogen concentrate, Sample D, neither Sample E nor F exhibi- ted the 520°C peak associated with silicate catalytic activity.

The preceding observations suggest that indigenous silicate minerals contribute actively to oil shale pyrolysis. The sili- cates appear to react preferentially with carbonate minerals. Excess silicates, beyond the required amount for carbonate inter- actions, appear to catalyze the organic decomposition and organic- pyrite interaction. Indeed, the organic-pyrite interaction is not observed in the absence of sufficient silicates. These results are qualitative indications of trends which should be assessed in a more thorough and quantitative fashion.

Acknowledgment

Literature Cited

1. Haddadin, R. A.; Mizyet, F. A. <u>Ind. Eng. Chem. Process Des. Develop.</u> 1974, 13, 332.
2. Braun, R. L.; Rothman, A. J. <u>Fuel</u> 1975, 54, 129.
3. Herrell, A. J.; Arnold, C. <u>Thermochim. Acta</u> 1976, 17, 165.
4. Campbell, J. H.; Kuskinas, G.; Stout, N. <u>Fuel</u> 1978, 57, 372.
5. Noble, R. D.; Harris, H. G.; Tucker, W. F. <u>Fuel</u> 1981, 60, 573.
6. Thakur, D. S.; Nuttall, H. E.; Cha, C. Y. <u>ACS Fuel Chem. Preprints</u> 1982, 27(2), 131.
7. Tisot, P. R.; Murphy, W. I. R. <u>Chem. Engr. Prog. Symp. Ser.</u> 1965, 61(54), 25.
8. Carlson, A. J. <u>University of California Publications in Engineering</u> 1937, 3(6), 295.
9. Horsfield, B; Douglas, A. G. <u>Geochim. et Cosmochim. Acta.</u> 1980, 44, 1119.
10. Espitalie, J.; Nadee, M.; Tissot, B. <u>Am. Assn. Pet. Geol. Bull.</u> 1980, 64, 59.
11. Rostam-Abadi, M.; Mickelson, R. W. <u>AIChE 1981 Summer National Meeting</u> 1981, 16b, F9.
12. Jeong, K. M.; Kobylinski, T. P. This Symposium Series.
13. Larson, O. A.; Schultz, C. W.; Michaels, E. L. in "Oil Shale, Tar Sands, and Related Materials," Stauffer, H. C., Ed; ACS SYMPOSIUM SERIES No. 163, ACS:Washington, D.C., 1981; p. 139.
14. Patzer, J. F. <u>ACS Fuel Chem. Preprints</u> 1982, 27(2), 107.
15. Campbell, J. H. <u>UCRL-52089</u>, Part 2, Lawrence Livermore National Laboratory, 1979.
16. Attar, A. Fuel 1978, 57, 201.
17. Stern., K. H.; Weise, E. L. "High-Temperature Properties and Decomposition of Inorganic Salts, Part 2. Carbonates," Nat. Stand. Ref. Series, National Bureau of Standards, 1969.
18. Jukkola, E. E.; Denilauler, A. J.; Jenson, H. B.; Barnet, W. I.; Murphy, W. I. R. <u>Ind. Eng. Chem.</u> 1953, 45, 2711.
19. Durand. B. "Kerogen," Editions Technip, Paris, 1980.
20. Hartough, H. D. "Thiophene and Its Compounds," Interscience, New York, 1952.
21. Hartough, H. D.; Meisel, S. L. "Compounds with Condensed Thiophenic Rings," Interscience, New York, 1954.
22. Miknis, F. P.; Maciel, G. E. in "Fourteenth Oil Shale Symposium Proceedings," Gary, J.H., Ed.; Colorado School of Mines Press, Golden, 1981, p. 270.
23. Smith, J. W. U.S. Bur. Mines ROI 5725, 1961.

RECEIVED April 26, 1983

Effect of Mineral Species on Oil Shale Char Combustion

RALPH P. CAVALIERI and WILLIAM J. THOMSON

Washington State University, Department of Chemical Engineering, Pullman, WA 99164-2710

Six oil-shale samples with differing mineral compositions were retorted identically and the resulting char was subjected to combustion kinetic studies using TGA techniques. Elemental compositions were obtained using x-ray fluorescence. On shales with high concentrations of carbonates, mineral changes were effected by allowing partial decarbonation and/or silication to take place prior to the combustion studies. Combustion results are compared in terms of simple kinetic expressions and are discussed in the context of the mineral species present during initial combustion. Intrinsic rate constants were found to vary from one shale to another by a factor of ten. Catalytic activity was attributed to alkaline earth oxides formed by mineral carbonate decomposition of nahcolite and calcite.

In order to increase the energy efficiency of aboveground oil shale processes, the carbonaceous residue (char) remaining on retorted oil shale (spent shale) will either be combusted (1,2) or gasified (3). Although there is no great difficulty in combusting the char, it is important that combustion be carried out in a controlled fashion. Failure to do so can result in high temperatures (> 900 K) and the decomposition of mineral carbonates. These decomposition reactions are not only endothermic (4) but some of the products have the potential to cause environmental disposal problems (5).

Control of oil shale char combustion is more easily managed if there is a knowledge of how the rate of combustion depends on O_2 concentration and temperature. This motivation led to an earlier study (6) of the combustion kinetics of spent shale from the Parachute Creek Member in western Colorado. That study

provided evidence that one or more of the mineral species present in the shale acted as an oxidation catalyst. Consequently it was decided to follow up on that investigation by examining the combustion activity of other oil shales; specifically, those with differing elemental and/or mineral compositions.

Six oil shale samples were selected for evaluation and comparison: one from the Parachute Creek Member (PCM), one from a deep core sample in the C-a tract (C-a), two from the saline zone in western Colorado (S-A & S-B), one from the Geokinetics site in eastern Utah (GEOK) and one sample of Antrim shale from Michigan (ANT).

Experimental

The experimental thermogravimetric analysis (TGA) equipment was essentially identical to that described by Thompson and Thomson (7). However, in this study a larger reactor was employed (10 cm diameter vs. 7.5 cm) and the two thermocouples were positioned differently. In this case one was placed 2 cm above the shale and the other so that it barely missed touching the shale sample. The latter was used to monitor temperature excursions during the initial stage of combustion. The temperature difference between the surface of the shale and 2 cm above it rarely exceeded 10 K and then only for one to two minutes.

All of the shale samples were retorted in master batches and under identical conditions in a 2.5 cm diameter fixed bed retort. A nitrogen sweep gas at 100 scc/min was employed and the temperature was elevated at a rate of 5 K/min to a maximum temperature of 785 K at which point it was held for 1 hour. Table I shows the quantity of oil collected during retorting, the percentage of organic carbon on the spent shale and the percentage of some of the more important elements (obtained by x-ray fluorescence). Although there is a wide variation in the oil yields, we have previously shown (8) there to be no effect on the combustion activity of spent shale. However, it is interesting to note that the GEOK spent shale sample had nearly twice the organic carbon content of the PCM sample even though the two had similar oil yields.

Combustion tests were carried out by heating the sample to the desired temperature in a helium atmosphere and then exposing it to a pre-selected O_2 concentration by diluting air with helium. In some cases the samples were first subjected to high temperatures (800-1050 K) in either a helium or CO_2 atmosphere in order to effect changes in the mineral compositions and then cooled to the desired combustion temperature. Combustion activities were evaluated for O_2 partial pressures between 5 and 20 kPa and at temperatures between 700 and 825 K.
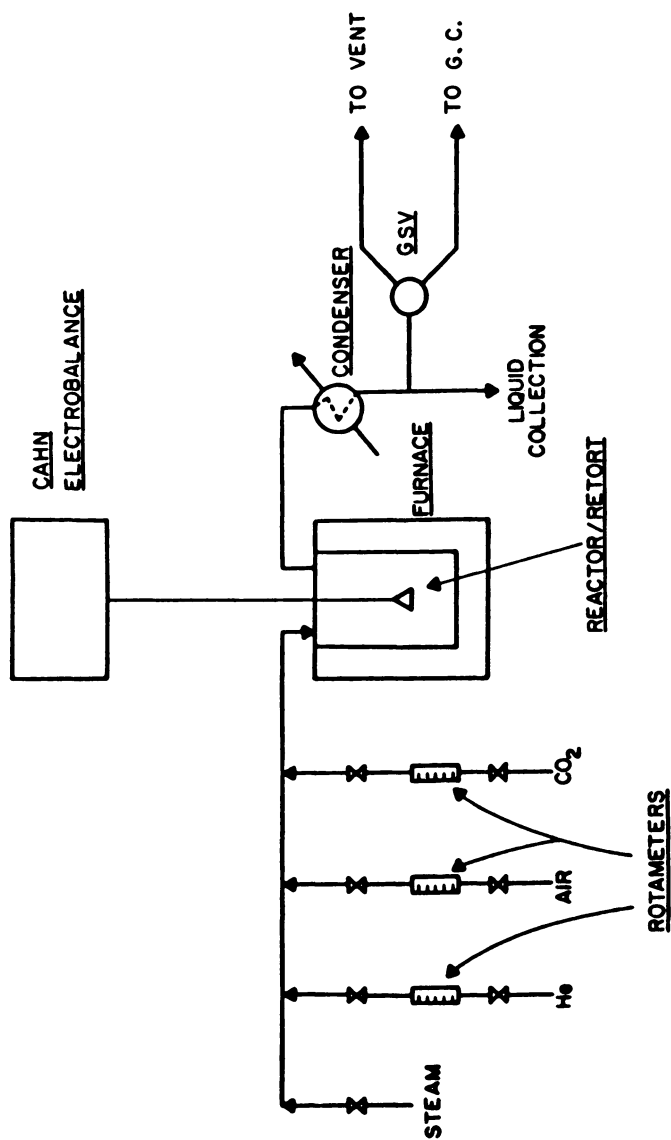
Figure 1. Schematic of thermogravimetric analysis equipment.

Table I. Composition of Spent Shale Samples

			Wt % Spent Shale						
Sample	GPT[a]	C[b]	Ca	Mg	Fe	Al	Na	K	Si
PCM	50	6.9	10.2	3.4	2.8	5.0	2.6	1.7	18.8
C-a	24	2.9	12.3	3.5	2.5	4.3	2.0	1.7	16.2
GEOK	44	12.0	15.2	4.3	3.1	4.8	2.3	2.0	19.6
S-A	30	3.8	8.4	3.6	3.1	6.3	2.8	2.1	22.3
S-B	40	3.9	1.0	1.0	5.6	10.9	0.4	1.7	30.2
ANT	11	5.7	0.7	1.2	5.4	8.3	0.4	3.4	31.0

[a] Gallons per ton raw shale
[b] Organic carbon spent shale

Analysis

The use of thermogravimetric analysis (TGA) apparatus to obtain kinetic data involves a series of trade-offs. Since we chose to employ a unit which is significantly larger than commercially available instruments (in order to obtain accurate chromatographic data), it was difficult to achieve time invariant O_2 concentrations for runs with relatively rapid combustion rates. The reactor closely approximated ideal back-mixing conditions and consequently a dynamic mathematical model was used to describe the time-varying O_2 concentration, temperature excursions on the shale surface and the simultaneous reaction rate. Kinetic information was extracted from the model by matching the computational predictions to the measured experimental data.

Because we used relatively large shale loadings (~1.5 g), we were careful to spread the shale over the basket in a relatively thin layer (~0.4 mm). Worst-case diffusional calculations indicated that diffusion resistance could be neglected and this was verified when experiments with half-loadings gave the same results as those with full 1.5 g loadings. Another factor of importance was the limitation of gas-solid mass transfer. Attempts were made to avoid this problem by using high gas flow rates. However, the maximum gas flow rates were dictated by the stability of the thermogravimetric readings. It was found that this flow rate was not sufficient to eliminate gas-solid mass transfer resistance for shales with the highest combustion rates. Again, the mathematical model was used in these cases to combine mass transfer and kinetic rates in order to extract the latter.

To illustrate the situation where gas-solid mass transfer plays an important role, Figure 2 shows the char combustion data

Figure 2. Mass transfer effects (GEOK, P_{O_2} = 10 kPa).

for the GEOK sample. Note that the higher temperature data do
not follow a straight line on a first order plot. The fact that
the lowest temperature run did follow a straight line and that
the low conversion data are similar at all temperatures, is a
clear indication of mass transfer problems. The downward trend
of the high conversion data is due to the shifting of the char
reaction order from zero (mass transfer controlled) to one
(kinetic controlled). As shown in our earlier work (6),
assuming first order with respect to both O_2 and char, the rate
is given by

$$r = \frac{k \, P_{O_2} \, C_c^o \, (1-X)}{1 + \dfrac{k \, C_c^o \, (1-X)}{k_m}}$$

where k is the kinetic rate constant, k_m is the mass transfer
coefficient, C_c^o is the initial char concentration and X is the
fraction char converted. Thus at low values of X, the right-
hand term in the denominator is dominant and the rate is zero
order with respect to char. At high values of X, the
denominator approaches 1.0 and the rate becomes first order.

The mass transfer coefficient was obtained from the low
conversion data in Figure 2 and when it was used in combination
with the first order assumption made above, excellent predic-
tions of the experimental data were obtained for all the shale
samples including those which were kinetically controlled
throughout. The model prediction is shown along with the
experimental data in Figure 2 for the high temperature run.

Rate Constants

As in our earlier work (6) the combustion reaction rate was
found to be first order with respect to both O_2 and char
content. Table II lists the apparent rate constants in terms of
the pre-exponential factor and the activation energy for all six
samples as well as comparative values at 700 K. The S-A sample
had the highest activity and has high concentrations of the
minerals dawsonite and nahcolite. Although these minerals will
have decomposed prior to combustion, the decomposition products
(Na_2CO_3, Al_2O_3) are present and, as will be shown, there is
strong evidence to indicate that the sodium acts as a catalyst.
It is also interesting that the activation energies are lowest
for the two shales (S-A and GEOK) with the highest rate con-
stants. It is tempting to attribute this result to catalytic
influences of the mineral matter but, in the case of the GEOK
sample, there is no separate evidence to suggest that the
minerals present at these low temperatures are, in any way,
catalytic.

Table II.   Kinetic Parameters

$$k = koEXP\left[\frac{-E}{RT}\right] \quad (kPa-min)^{-1}$$

Sample	ko x 10^{-7}	E^{a}	k (700K)
PCM	.025	97.07	.0140
C-a	18500.	147.9	.0168
GEOK	.00067	54.85	.054
S-A	.0031	50.04	.0571
S-B	.224	88.16	.0059
ANT	1.28	93.72	.013

[a] kJ/mol

Char combustion kinetics have been previously reported for Antrim shale by Rostam-Abadi and Mickelson (9). In that study the authors reported that the rate was second order with respect to the char remaining and that there was noticeable chemisorption of O_2. Attempts to fit our data for the Antrim shale to a second order rate expression were unsuccessful and, in all cases, the data appeared to follow first order kinetics. Although we did not have the precision to measure O_2 chemisorption, this phenomenon is consistent with our previous observations (6) of catalytic activity in those shales containing decomposed mineral carbonates. That is, the catalytic activity of CaO was attributed to its ability to chemisorb O_2. As will be discussed in more detail below, the Antrim shale sample did not contain such carbonates and no catalytic behavior was observed. However, the magnitude of the rate constants reported by Rostam-Abadi and Mickelson (9) are very similar to those measured here.

Finally it should be pointed out that the pre-exponential factor listed in Table II for the PCM sample, differs from the value we reported earlier (6). From our measurements of the actual shale temperature, we have discovered that the measured temperatures in the earlier study were in error. The values listed in Table II are now consistent with the reported measurements of Sohn and Kim (10).

Mineral Catalysis

Although a detailed x-ray diffraction analysis was not conducted as part of this study, some insight into the carbonate mineral behavior of the shales can be obtained by allowing the shales to decompose in an inert environment. Figure 3 shows the mass loss for the spent shales as the temperature was raised linearly at 2.7 ^{o}C/min in a helium purge stream. In the GEOK sample, only one large mass loss is apparent and this occurs at
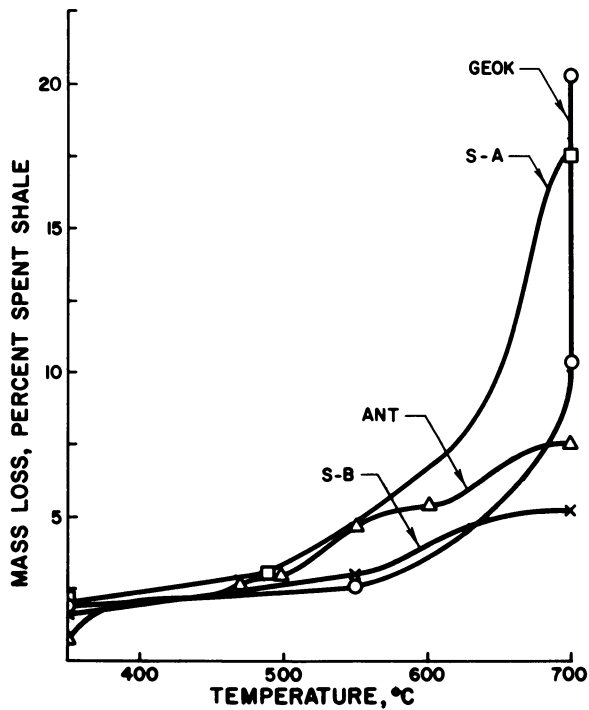
Figure 3. Mass loss due to mineral decomposition. Conditions: helium purge, heating rate = 2.7 K/min).

about 600 $^{\circ}$C. This is attributed to dolomite/calcite decomposition. There are two distinct mass loss occurrences with the ANT sample; one at 500 $^{\circ}$C and the other at 625 $^{\circ}$C. These are attributed to clay minerals which are typically found in devonian shale. The comparison between S-A and S-B is very interesting since there appears to be much less mineral decomposition in the S-B sample. The mass loss at 480°C in the S-A sample is attributed to dawsonite decomposition and the loss at 620°C is attributed to calcite decomposition. The S-B sample is low in dawsonite with its aluminum probably present in silicates. As can be seen from the elemental Ca measurements listed in Table I, it should be low in calcite as well.

One of the experiments which we conducted on the PCM sample was to thermally decompose the carbonate minerals (dolomite and calcite) to their oxides at 900 K according to reactions (1) and (2).

$$CaMg\ (CO_3)_2 \longrightarrow CaO + MgO + 2\ CO_2 \qquad (1)$$

$$CaCO_3 \rightleftharpoons CaO + CO_2 \qquad (2)$$
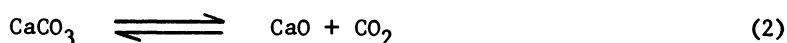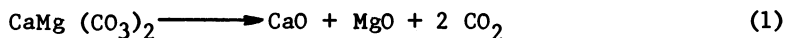
When the temperature was lowered to 700 K and the sample exposed to O_2, the observed combustion rate was ten times higher than when the carbonates were left intact. By process of elimination, the increased activity was attributed to the presence of CaO. In order to further investigate this phenomena, the same experiment was carried out with the C-a and the ANT sample. The C-a sample was chosen due to the fact that it contained more Ca than char on a molar basis. On the other hand, the ANT sample had a very low Ca content.

Figure 4 shows the comparative responses of the raw thermogravimetric readings when the decomposed samples were exposed to 10% O_2 at time = 0. Similar behavior was observed for the C-a and PCM samples; that is, the raw weight increased due to the recarbonation of CaO.

$$C + O_2 \longrightarrow CO_2 \qquad (3)$$

$$CaO + CO_2 \longrightarrow CaCO_3 \qquad (4)$$

Since the combustion rate is at least as fast as the recarbonation rate, the data in Figure 4 correspond to a combustion rate increase of about an order of magnitude in both samples. This also leads to the conclusion that the source of CaO does not appear to be important since most of it is produced from ankeritic dolomite in the C-a sample and over 30% from free calcite in the PCM sample. It should be pointed out that the weight change in PCM reached a maximum weight and then decreased due to the total recarbonation of the available CaO prior to
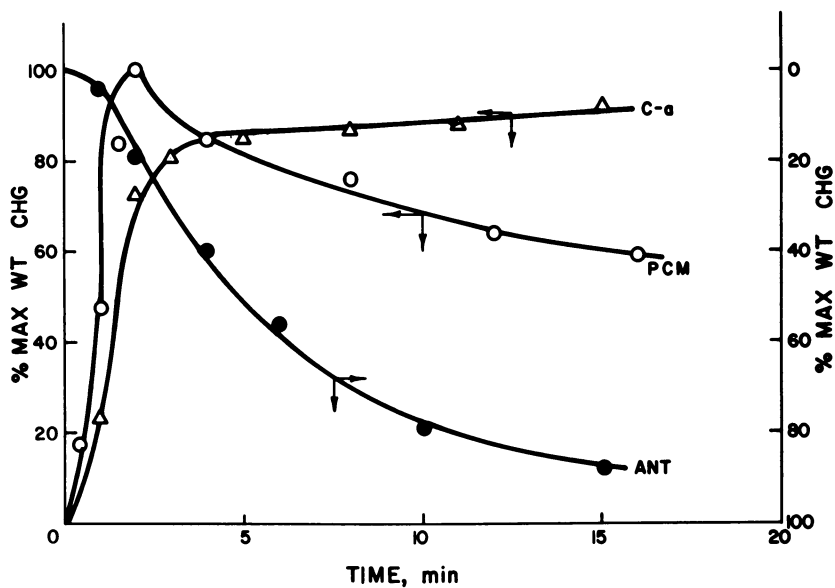
Figure 4. Oxidation after thermal pretreatment. Conditions: 700 K, P_{O_2} = k Pa).

complete combustion of the char. This was not the case for C-a which has more CaO than char. It is also interesting to note that the ANT sample, which has minimal Ca, did not experience a weight gain during combustion. In fact, the combustion rate was identical to that observed for ANT samples which had not been thermally pretreated. These results tend to support the hypothesis of CaO as a combustion catalyst.

Additional experiments were also run in order to examine the effects of water soluble mineral species on the combustion rate. Figure 5 shows first order plots for one S-B and two S-A samples. As pointed out earlier, the S-A and S-B samples are similar except for high concentrations of nahcolite and dawsonite in the former and it is this sample which had the highest combustion activity (Table II). Since it is possible to water leach sodium minerals, the S-A sample was subjected to water washing prior to combustion. After drying, the sample was combusted under identical conditions and, as can be seen from Figure 5, the combustion rate for the water washed S-A sample was identical to that observed with the S-B sample. In order to determine the elements removed during the water leaching process, the wash-water was analyzed using atomic absorption. Table III shows the results of these analyses for the S-A sample as well as for the S-B and GEOK samples. As expected, the S-A leachate was extremely high in Na. The fact that neither Ca nor Fe was leached from the S-A sample and that the GEOK sample showed no change in combustion rate despite similar K values points to the probable role of Na as an oxidation catalyst. This is not too surprising since it is well known that the Group I-a and, to a lesser extent, Group II-a elements are good gasification catalysts (11).

Table III. Elemental Analysis of Leachate Water

Concentrations - mg/g Spent Shale

SHALE	Na	K	Ca	Fe
S-A	21.7	0.24	0.0	0.0
S-B	0.15	0.05	0.49	0.0
GEOK	0.93	0.23	1.90	0.0

An attempt was also made to form silicates by allowing the mineral carbonates to react with the silica present in the shale to see if combustion activity would drop. Unfortunately it was necessary to maintain a CO_2 atmosphere during silication (to prevent the more favorable formation of CaO) which permitted the char to undergo CO_2 gasification.
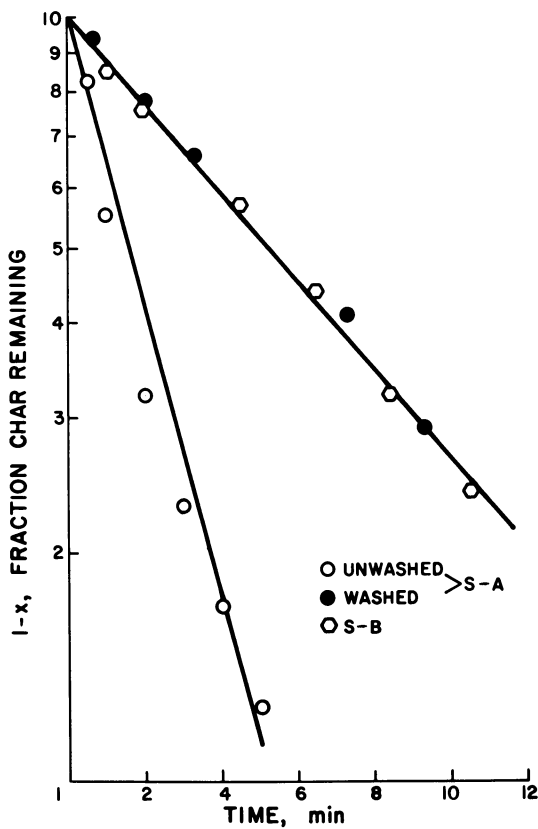
Figure 5. Effect of sodium removal on char combustion. Conditions: 700 K, P_{O_2} = 10 kPa).

$$CO_2 + C \rightleftharpoons 2CO \qquad (5)$$

As a result there was not enough char remaining to conduct combustion tests.

Conclusions

On the basis of the studies conducted here, it is readily apparent that the presence of minerals can drastically alter the reactivity of the residual char on spent oil shale. More detailed quantitative studies of the mineral compositions are necessary in order to be able to assess their importance under typical oil shale processing conditions and will be the subject of future manuscripts from this laboratory. However, at this time, there are several conclusions which can be made. First, the combustion of the char in all six of the shales followed first order kinetics with respect to the oxygen partial pressure and the char available. For the western shales this is in agreement with previous works which studied PCM and Anvil Points shales, but it does conflict with the results of Rostam-Abadi and Mickelson [9] who reported second order kinetics for Antrim shale. Secondly, we found that CaO has a catalytic effect on char combustion, most likely due to a chemisorption process. And finally we found that Na_2O, as derived from the thermal decomposition of nahcolite, has a pronounced catalytic effect on the char combustion rate of saline zone shale.

Acknowledgment

Literature Cited

1. Hall, R. N. paper presented at National AIChE Meeting, Anaheim, CA., June 8, 1982.
2. Griswold, C. and Duir, J. H., paper presented at National AIChE Meeting, Anaheim, CA., June 8, 1982.
3. "Union Claims Boost in Shale-oil Technology", 1974, 24, 26-7.
4. Campbell, J. H. Lawrence Livermore Laboratory, Rept. No. UCRL-52089 part 2, March 13, 1978.
5. Mavis. J. D. and Rosain, R. M. paper presented at National AIChE Meeting, Detroit, MI., August 16-19, 1981.
6. Soni, Y. and Thomson, W. J. I & EC Proc. Des. & Dev, 1979, 18, 661-7.
7. Thompson L. G. and Thomson, W. J. in this SYMPOSIUM SERIES.
8. Soni, Y. and Thomson, W. J. Proceedings of 11th Oil Shale Symposium, p. 364, April 1978.

9.   Rostam-Abadi, M. and Mickelson, R. W. paper presented at National AICHE Meeting, Anaheim, CA, June 7-10 1982.
10. Sohn, H. Y. and Kim, S. K. I & EC Proc. Des. & Dev, 1980, 19, 550-5.
11. Wen, W. Y. Catal. Rev.-Sci. Eng. 1980, 22, 1.